

Structural Diagnosis of Masonry Heritage: Contributions to Non-Destructive Testing, Structural Health Monitoring and Risk Assessment

Doctoral Thesis by:

Nirvan Makoond

Supervised by:

Luca Pelà

Climent Molins Borrell

Barcelona, November 2020

Thesis by compendium of publications

Doctoral programme in Construction Engineering



UNIVERSITAT POLITÈCNICA DE CATALUNYA
BARCELONATECH

Department of Civil and Environmental
Engineering



Structural Diagnosis of Masonry Heritage: Contributions to Non-Destructive Testing, Structural Health Monitoring and Risk Assessment

by

Nirvan Chandra Makoond

Doctoral thesis submitted in fulfilment of the requirements for the
Degree of Doctor of Philosophy in Construction Engineering

Supervisors:
Luca Pelà
Climent Molins Borrell

Barcelona, November 2020

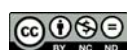
Thesis by compendium of publications

Thesis committee: Salvador Ivorra Chorro, Universidad de Alicante
Lluís Gil Espert, Universitat Politècnica de Catalunya
José Miguel Adam Martínez, Universitat Politècnica de València

Substitutes:
Rolando Antonio Chacon Flores, Universitat Politècnica de Catalunya
Alessandra Aprile, Università degli Studi di Ferrara



**UNIVERSITAT POLITÈCNICA
DE CATALUNYA
BARCELONATECH**



Content on this work is licensed under a Creative Commons license:
<https://creativecommons.org/licenses/by-nc-nd/4.0/>

Acknowledgements

First of all, I would like to express my sincere gratitude to both my supervisors, Climent Molins and Luca Pelà. Without their support, guidance, and trust, it is undeniable that the work presented in this thesis would not have been possible. I have learnt a lot from them, not only about engineering, but also about attitude and character. For me, they represent true role models, and I feel privileged to have had the opportunity to work with them over the last three and a half years.

Secondly, I would like to acknowledge the Agency for Management of University and Research Grants (*Agència de Gestió d'Ajuts Universitaris i de Recerca - AGAUR*) of the Government of Catalonia *Generalitat de Catalunya* and the European Social Fund for financing the predoctoral grant that allowed me to dedicate myself full-time to the research work presented in this thesis. This work has also benefited from additional financial support from the Spanish Ministry of Science, Innovation and Universities and the European Regional Development Fund through the SEVERUS project (Multilevel evaluation of seismic vulnerability and risk mitigation of masonry buildings in resilient historical urban centres, ref. num. RTI2018-099589-B-I00), from the Spanish Ministry of Economy and Competitiveness (Ministerio de Economía y Competitividad - MINECO) through the MULTIMAS project (Multiscale techniques for the experimental and numerical analysis of the reliability of masonry structures, ref. num. BIA2015-63882-P), from the City Council of Sant Cugat (Ajuntament de Sant Cugat) through a project aimed at monitoring the church of the monastery of Sant Cugat (Estudi de monitorització i seguiment de l'estructura de l'Església del Monestir de Sant Cugat, ref. num. C-10764), and from the Spanish Ministry of Education, Culture and Sports (Ministerio de Educación, Cultura y Deporte) through a project aimed at studying the structural condition of Mallorca Cathedral (Estudio, diagnóstico y peritación y en su caso planteamiento de actuaciones sobre el comportamiento constructivo-estructural de la catedral de Santa María, en la ciudad de Palma, isla de Mallorca (Balears), ref. num. 2/131400106ca-5/030300592 EF).

I also have to thank Pere Roca, for his positive outlook on my work, for the valuable discussion we have shared on Mallorca cathedral, and for providing me with many expert diagnosis reports which turned out to be an invaluable resource for the development of a significant component of this research. In retrospect, I am also very thankful for the dedication and passion he demonstrated when teaching us about the structural diagnosis of heritage structures during the SAHC Masters course several years ago. This is a comment which also extends to both of my supervisors as well as to the other great teachers of this course. Much of the knowledge I have been able to acquire on this topic is owed to them.

I am thankful to Daniel Alarcon for having been a good friend, for doing such a good job on the design and installation of the acquisition systems and sensors for the monitoring in Sant Cugat and Morrot, and for having taught me a lot on sensors and acquisition systems. I also extend my gratitude to Pau Trubat, for the coffees we have shared, and for helping me to get started with Linux shell commands to send computing jobs to the TITANI cluster. I am also grateful to Roger Ferré from CaminsTECH for checking my first script written in Bash and for always responding very promptly whenever we needed to modify the automatic checks of data collected by monitoring systems.

I also have to thank Tomàs Garcia and all the personnel of the LATEM laboratory at UPC for all the help they have given me with the experimental component of this work as well as for the preparation of specific items for different works on site. I would like to thank Robert and Jordi Cabrerizo in particular for always being kind, willing to help, and for being amongst my first Spanish teachers.

The submission of this thesis would not have been possible without the help and support of Rosa Olea from the Unitat de Suport a la gestió d'estudis de doctorat on all administrative matters.

I feel very lucky to have been able to share the past three and a half years with the amazing people of *Team Roca*: Larisa, Jorge, Belén, Philip, Savvas, Sara, Naveen, Camilla, and Chiara. These last years spent together

have only served to strengthen the already strong bonds I shared with Larisa and Jorge since going through the SAHC Masters together. It is unlikely that I would have been able to make it to Barcelona in 2017 without all the work done by Jorge to support our arrival before our integration in the research team. I have enjoyed so much the many conversations we have shared on masonry and on life. I also have to thank Jorge for being one of the first people to completely read the (long) manuscript I wrote on RISDiMaH. Larisa has been a cherished and trusted friend for many years, and I will always be indebted to her for making my transition to Spain so smooth, for teaching me Spanish, and for being the best flatmate one could ask for. Philip, thanks for being the best office-mate one could ask for. I will forever cherish our conversations. I do sincerely hope that the friendships forged with everyone in *Team Roca* will last until the end of my days.

A Eulàlia, Laia, Arnau, Àlicia i Alejandro, gràcies per haver estat una llar lluny de casa aquests darrers mesos.

I am grateful for having a friend such as Satyadhrik. Not only have our conversations about masonry helped me to improve the quality of my work, but our video calls have also been a great source of support. The frequent video calls I have shared with my childhood friends, Kaushal and Akshay, have also been a tremendous source of support.

I would also like to thank all members of my family. Whether your surname is Makoond, Maistry, Makoond-lall, Nepaul, Teker, or Bhageerutty, I love all of you and feel very privileged to have been born in such a loving and supportive family.

I also feel extremely privileged to have been blessed with amazing parents and an amazing sister. They have always prioritised education and the strong values they have given me have undoubtedly shaped the person I am today. They have always been there for me, and I have always been able to count on their unconditional love and support. I would like to extend a special thanks to my dad for always being keen to read my abstracts, introductions, and conclusions, and provide me with valuable suggestions on how to improve them.

Finally, I have to thank Irene, for reading my work, and for being my source of strength and my new reference point.

Abstract

A large number of established cultural heritage sites across the globe consist of masonry structures. The common responsibility to safeguard and protect such structures is now widely recognised, and an accurate evaluation of their current structural condition is often of paramount importance to ensure this. However, in many cases, recurrent uncertainties regarding material properties and the complex interaction among structural elements often makes the evaluation of structural safety a challenging task. As a consequence, there has been a considerable research effort on the development of methods and tools that can facilitate this task and experts responsible for the safety evaluation of unique masonry heritage structures today usually need to weigh information from various diagnosis activities before deciding the best course of action for preservation. Typical sources of valuable information are historical and in-situ surveys and inspections, minor and non-destructive testing (MDT and NDT), structural health monitoring (SHM), and structural analysis, among others. In a first instance, the research work presented in this thesis contributes to the enhancement of some key testing and SHM methods for the analysis of masonry structures. Specific topics dealing with materials testing, full-scale vibration testing, and static SHM are addressed. Subsequently, this is built upon to develop specific decision support tools that can assist decision-making for risk mitigation.

The research work performed in the field of materials testing involved an experimental study on the dynamic elastic properties of brick masonry constituents, which are known to differ from their static counterpart. Despite being a fundamental deformation property, experimentally determining the static elastic modulus in compression for brick masonry constituents remains a challenging task. This is mainly due to the difficulties linked to accurately measuring strains in the elastic deformation range of brittle materials. As a result, static modulus estimates usually show much larger dispersion than those involved in determining the dynamic elastic modulus. Although the static property is preferred for common structural verifications, the relationship between the two is yet to be well understood for typical brick masonry constituents. In fact, there are very few studies that evaluate the suitability of different techniques to estimate the dynamic elastic properties of these materials. As such, very little guidance is currently available on how to reliably estimate these properties for such materials. Following an experimental campaign to determine the dynamic elastic and shear moduli of a variety of brick masonry constituent materials, this research proposes a robust procedure based on the synergy of two non-destructive testing methods to reliably estimate these dynamic properties. In addition, an empirical expression to estimate the static elastic modulus of brick masonry constituents from its dynamic counterpart is also provided.

With respect to full-scale vibration testing, the present study deals specifically with masonry bell towers and the operational modal analysis (OMA) techniques used to extract modal parameters (natural frequencies, mode shapes, and damping ratios) from test acquisitions. Despite significant advances in system identification and modal analysis techniques, the accuracy of resulting modal parameter estimates from vibration tests are still highly dependent on test conditions, acquisition quality, and on the techniques employed for modal parameter estimation. In order to gain a better understanding on the actual effects of these factors in practice, this work first aimed to design a suitable acquisition system and program for the vibration testing of the bell tower of Seu Vella in Lleida, Catalonia. Two natural frequencies, including the fundamental one, could be clearly identified from the acquired vibration signatures. These results were used to calibrate a detailed finite element model of the structure and to estimate the effective dynamic elastic modulus of the material making up the tower. Several system identification and modal analysis techniques were investigated and the most suitable ones for identifying particular modal parameters under varying acquisition conditions are discussed.

The SHM component of this research was particularly focused on the analysis of data from static SHM systems which involve the continuous measurement of key slow-varying parameters over long time periods. Masonry heritage structures are often affected by slow irreversible deterioration mechanisms that can jeopardise structural stability in the foreseeable future. Static SHM has the potential to identify such mechanisms at a very early stage. This can greatly facilitate the implementation of adequate preventive and remedial measures which can be critical to ensure that such structures are preserved for generations to come. However,

since monitored parameters usually experience reversible seasonal variations of the same order of magnitude as changes caused by active mechanisms, identification of the latter is often a difficult task. This research presents a fully integrated automated data analysis procedure for complete static SHM systems utilising dynamic linear regression models to filter out the effects caused by environmental variations. The method does not only produce estimated evolution rates but also classifies monitored responses in pre-defined evolution states. The procedure has successfully been used to identify vulnerable areas in two important medieval heritage structures in Spain, namely the cathedral of Mallorca and the church of the monastery of Sant Cugat.

Following the presentation of the aforementioned specific research topics, all the previous findings in specific technical fields are built upon to elaborate multi-criteria decision-making (MCDM) tools meant to improve the objectivity, clarity, and transparency of decisions on the structural safety of masonry heritage. Due to the complexity of the problem and singular aspects of monuments, such decisions are challenging and often made solely on the basis of expert judgement. A systematic risk assessment procedure is proposed involving the computation of two MCDM indices to facilitate the decision-making process: an index related to the estimated risk of damage, and another to the uncertainty behind this estimation. Applications to several case studies are also included to demonstrate the usefulness of the proposed tools.

Resumen

Muchos sitios de patrimonio cultural en todo el mundo consisten en estructuras de mampostería. Para asegurar la preservación de tales estructuras, la evaluación precisa de su condición estructural es a menudo de suma importancia. Sin embargo, las incertidumbres recurrentes con respecto a las propiedades de los materiales, así como la compleja interacción entre los distintos elementos estructurales a menudo hacen que esta sea una tarea desafiante. Como consecuencia, ha habido un esfuerzo de investigación considerable en el ámbito del desarrollo de métodos y herramientas que puedan facilitar esta tarea, y los expertos responsables de la evaluación de estructuras de mampostería generalmente necesitan sopesar la información de diversos estudios de diagnóstico antes de decidir el mejor curso de acción para su conservación. Las fuentes típicas de información son fuentes históricas, inspecciones in situ, ensayos no destructivos, auscultación estructural (SHM, del inglés *Structural Health Monitoring*) y el análisis estructural, entre otros. En una primera instancia, el trabajo de investigación presentado en esta tesis contribuye a la mejora de algunos métodos clave para el análisis de estructuras de mampostería. Se abordan temas específicos relacionados con los ensayos de materiales, los ensayos de vibración de estructuras y el SHM. Posteriormente, esto conduce al desarrollo de herramientas específicas de apoyo a la toma de decisiones que pueden ayudar en la toma de decisiones para la mitigación de riesgos.

El trabajo de investigación realizado en el campo de los ensayos de materiales ha implicado un estudio experimental sobre las propiedades dinámicas elásticas de los componentes de mampostería de ladrillo, que se sabe que difieren de sus contrapartes estáticas. A pesar de ser una propiedad de deformación fundamental, la determinación experimental del módulo elástico estático en compresión para los componentes de la mampostería de ladrillo sigue siendo una tarea desafiante. Ello se debe principalmente a las dificultades inherentes en la medición precisa de las deformaciones en el rango de deformación elástica de materiales frágiles. Como resultado, las estimaciones del módulo estático muestran generalmente una dispersión mucho mayor que las involucradas en la determinación del módulo elástico dinámico. Aunque se prefiere la propiedad estática para las verificaciones estructurales comunes, la relación entre las dos aún no se comprende bien para los componentes típicos de mampostería de ladrillo. De hecho, existen muy pocos estudios que evalúen la idoneidad de diferentes técnicas para estimar las propiedades dinámicas elásticas de estos materiales. Como tal, actualmente hay muy poca orientación disponible sobre cómo estimar de manera fiable estas propiedades para dichos materiales. Tras una campaña experimental para determinar los módulos dinámicos elásticos y de corte de una variedad de ladrillos y morteros, esta investigación propone un procedimiento robusto basado en la combinación de dos métodos de ensayo no destructivos para estimar de manera fiable estas propiedades dinámicas. Además, también se proporciona una expresión empírica para estimar el módulo de elasticidad estático de los componentes de mampostería de ladrillo a partir de su contraparte dinámica.

Con respecto a ensayos de vibración de estructuras, el presente estudio considera específicamente campanarios de mampostería y las técnicas de análisis modal operacional (OMA, del inglés *Operational Modal Analysis*) utilizadas para extraer parámetros modales a partir de adquisiciones. A pesar de avances significativos en las técnicas de OMA, la precisión de las estimaciones resultantes de las pruebas de vibración aún depende en gran medida en las condiciones de la prueba, la calidad de la adquisición y las técnicas empleadas para la estimación de parámetros modales. Este trabajo tuvo como objetivo, en primer lugar, diseñar un sistema y programa de adquisición adecuados para ensayos de vibración del campanario de la Seu Vella en Lleida, Cataluña. Se investigaron varias técnicas de identificación de sistemas y de análisis modal y se discuten las más adecuadas para identificar parámetros modales particulares en diferentes condiciones de adquisición.

El componente de SHM de esta investigación se ha centrado en el análisis de datos de sistemas de SHM estáticos que implican la medición continua de parámetros clave de variación lenta durante largos períodos de tiempo. Las estructuras patrimoniales de mampostería a menudo se ven afectadas por mecanismos lentos de deterioro irreversible que pueden poner en peligro la estabilidad estructural en un futuro próximo.

El SHM estático tiene el potencial de identificar tales mecanismos en etapas tempranas. Ello puede facilitar enormemente la implementación de medidas preventivas y correctivas adecuadas que pueden ser críticas para asegurar que tales estructuras se preserven para las generaciones venideras. Sin embargo, dado que los parámetros monitoreados generalmente experimentan variaciones estacionales reversibles del mismo orden de magnitud que los cambios causados por mecanismos activos, la identificación de estos últimos es a menudo una tarea difícil. El Capítulo 5 de esta tesis presenta un procedimiento de análisis de datos automatizado totalmente integrado para sistemas completos de SHM estáticos que utilizan modelos de regresión lineal dinámica para filtrar los efectos causados por variaciones ambientales. El método no solo produce tasas de evolución estimadas, sino que también clasifica las respuestas monitoreadas en estados predefinidos de evolución. El procedimiento se ha utilizado con éxito para identificar áreas vulnerables en dos importantes estructuras patrimoniales medievales en España, a saber, la catedral de Mallorca y la iglesia del monasterio de Sant Cugat.

Finalmente, todos los hallazgos anteriores se utilizan para la elaboración de herramientas de toma de decisiones multicriterio (MCDM, del inglés *Muli-Criteria Decision-Making*) destinadas a mejorar la objetividad, claridad y transparencia de las decisiones de mitigación de riesgos para estructuras patrimoniales de mam-postería. Se propone un procedimiento sistemático de evaluación de riesgos que involucra el cálculo de dos índices MCDM: un índice relacionado con el riesgo estimado de daño y otro con la incertidumbre detrás de esta estimación. También se incluyen aplicaciones a varios casos de estudios para demostrar la utilidad de las herramientas propuestas.

Resum

Un gran nombre de llocs de patrimoni cultural consisteixen en estructures de maçoneria. La responsabilitat comuna de protegir aquestes estructures és ara àmpliament reconeguda i, sovint, és fonamental una avaluació acurada de la seva condició estructural actual per tal d'assegurar tal protecció. No obstant això, en molts casos, les incerteses recurrents en les propietats dels materials i la complexa interacció entre elements estructurals converteixen l'avaluació de la seguretat estructural en una tasca difícil. Com a conseqüència, hi ha hagut un considerable esforç investigador sobre el desenvolupament de mètodes i eines que puguin facilitar aquesta tasca, i els experts responsables de l'avaluació de la seguretat d'estructures del patrimoni de maçoneria necessiten normalment contrastar informació provinent de diverses activitats de diagnòstic abans de decidir les millors actuacions per a la seva preservació. Les fonts típiques d'informació són documents històrics, inspeccions in situ, assajos no destructius, monitorització de l'estructura (SHM, de l'anglès *Structural Health Monitoring*), i anàlisi estructural, entre altres. En una primera instància, el treball de recerca presentat en aquesta tesi contribueix a la millora d'alguns mètodes clau per a l'anàlisi d'estructures de maçoneria. S'aborden temes específics relacionats amb l'assaig de materials, assajos de vibració d'estructures i SHM. Posteriorment, això condueix al desenvolupament d'eines específiques de suport a la presa de decisions que poden ajudar en la presa de decisions per a la mitigació de riscos.

La recerca realitzada en el camp dels assajos de materials va implicar un estudi experimental de les propietats elàstiques dinàmiques de constituents de la fàbrica de maó, de les quals es coneix que difereixen de les estàtiques. Malgrat ser una propietat de deformació fonamental, la determinació experimental del mòdul elàstic estàtic a la compressió per a constituents de maçoneria de maó és encara una tasca desafiant. Això és principalment a causa de les dificultats vinculades a la forma exacta de mesurar tensions en el camp de deformació elàstic dels materials fràgils. Com a resultat, estimacions del mòdul estàtic mostren usualment una major dispersió que les estimacions obtingudes per al mòdul elàstic dinàmic. Tot i que la propietat estàtica és preferida per a verificacions estructurals comunes, encara cal entendre la relació entre la dues per a constituents de maçoneria de maó típics. De fet, hi ha molt pocs estudis que avaluin la idoneïtat de diferents tècniques per a estimar les propietats elàstiques dinàmiques d'aquests materials. Com a tal, actualment no hi ha gaires orientacions disponibles per a estimar de manera fiable aquestes propietats per a tals materials. Després d'una campanya experimental per a determinar el mòdul elàstic dinàmic i de cisalla d'una varietat de materials constituents de maçoneria de maó, aquest treball proposa un procediment robust basat en la combinació de dos mètodes d'assaig no destructiu per a una estimació fiable d'aquestes propietats dinàmiques. A més a més, també es proporciona una expressió empírica per estimar el mòdul elàstic estàtic de constituents de fàbrica del maó a partir del seu homòleg dinàmic.

Respecte als assajos de vibració, el present estudi tracta de campanars de maçoneria i de tècniques d'anàlisi modal operacional (OMA, de l'anglès *Operational Modal Analysis*) utilitzades per a extreure paràmetres modals (freqüències naturals, modes de vibració, i coeficients d'amortiment) a partir d'assajos d'adquisició. Malgrat avanços significatius en la identificació de sistemes i les tècniques d'anàlisi modal, la precisió d'estimacions de paràmetres modals resultants d'assajos de vibració d'estructures encara són altament dependents de les condicions de l'assaig, la qualitat de l'adquisició i les tècniques emprades per a l'estimació dels paràmetres modals. Per tal d'entendre millor els efectes reals d'aquests factors en la pràctica, aquest treball ha dissenyat un sistema d'adquisició adequat i un programa per a l'assaig de vibració del campanar de la Seu Vella a Lleida, Catalunya. Dues freqüències naturals, incloent la fonamental, van ser clarament identificats a partir de les vibracions adquirides. Aquests resultats es van utilitzar per a calibrar un model d'elements finits de l'estructura i per a estimar el mòdul elàstic dinàmic del material de la torre. Es van investigar diverses tècniques d'identificació de sistema i d'anàlisi modal, i es discuteixen les més adequades en diferents condicions d'assaig.

La part relacionada amb la monitorització en aquest treball s'ha enfocat particularment en l'anàlisi de dades obtingudes a partir de sistemes estàtics de SHM que consisteixen en la mesura contínua de paràmetres clau de variació lenta sobre períodes de temps llargs. Les estructures de patrimoni de maçoneria es veuen

sovint afectades per mecanismes de deteriorament irreversibles i lents que poden posar en risc l'estabilitat estructural en un futur pròxim. El SHM estàtic té el potencial d'identificar tals mecanismes en etapes primerenques. Això pot facilitar la implementació de mesures preventives i de rehabilitació adequades, les quals poden ser crítiques per assegurar que tals estructures siguin preservades per a futures generacions. Tot i això, donat que els paràmetres controlats experimenten variacions estacionals reversibles del mateix ordre de magnitud com els canvis causats per mecanismes actius, la identificació d'aquests mecanismes és sovint una tasca difícil. Aquesta tesi presenta un procediment plenament automatitzat per a l'anàlisi de dades per a sistemes de SHM estàtics, el qual utilitza models de regressió lineals dinàmics per filtrar els efectes causats per variacions ambientals. El mètode no només produeix una estimació de les taxes d'evolució, sinó que també classifica les respostes monitorejades en diferents estats d'evolució predefinitos. El procediment ha estat utilitzat amb èxit per a identificar àrees vulnerables en dos importants estructures de patrimoni medieval a Espanya: la catedral de Mallorca i l'església del monestir de Sant Cugat.

Finalment, totes les troballes anteriors s'utilitzen per a l'elaboració d'eines de presa de decisió multicriteri (MCDM, de l'anglès *Multi-Criteria Decision-Making*) destinades a millorar l'objectivitat, claredat i transparència de les decisions de mitigació de riscos per a estructures del patrimoni de maçoneria. Es proposa un procediment sistemàtic d'estimació de risc estructural que implica la computació de dos índexs MCDM: un índex relacionat amb el risc estimat de dany, i un altre relacionat amb la incertesa darrere d'aquesta estimació. Les aplicacions a diversos casos d'estudi també s'inclouen per demostrar la utilitat de les eines proposades.

Contents

Abstract	v
Resumen	vii
Resum	ix
Table of Contents	xiii
List of Figures	xv
List of Tables	xvii
I Research Summary	1
Abbreviations	3
1 Introduction	5
1.1 Background and motivation	5
1.2 Scope and objectives	7
1.3 Research dissemination	8
1.4 Outline	8
2 Literature review	11
2.1 Introduction	11
2.2 Dynamic elastic properties of brick masonry constituents	11
2.2.1 Selected techniques for estimating dynamic elastic properties	12
2.2.2 The relationship between static and dynamic elastic moduli	16
2.3 System identification and modal analysis	18
2.3.1 Data pre-processing	19
2.3.2 System identification techniques	19
2.3.3 Modal analysis of identified system models	20
2.4 Static SHM for masonry constructions	20
2.5 Risk assessment and decision-making	24
3 Materials testing	27
3.1 Introduction	27
3.2 Estimating dynamic elastic properties of masonry constituents	27
3.2.1 Experimental program	28
3.2.2 Results of dynamic tests	35
3.2.3 Proposed analysis procedure	39
3.3 Relationship between the static and dynamic elastic properties of brick masonry constituents	40
3.3.1 Experimental determination of static modulus	40
3.3.2 Results of static tests	46

3.3.3	Comparison and discussion	48
3.4	Summary	51
4	Full-scale vibration testing	53
4.1	Introduction	53
4.2	The bell tower of Seu Vella	53
4.3	Expected mode shapes and natural frequencies	54
4.3.1	Beam elements estimation	54
4.3.2	Solid elements estimation	56
4.4	Data acquisition	58
4.4.1	Sensors and data acquisition system	58
4.4.2	Location of accelerometers	59
4.4.3	Acquisitions	59
4.5	Modal parameter estimations	62
4.5.1	Pre-processing	62
4.5.2	System identification	63
4.5.3	Modal analysis of identified system models	65
4.5.4	Results and comparison with Finite Element (FE) model	66
4.5.5	Identification of higher frequency local modes	71
4.6	Dynamic action of bells	72
4.7	Summary	72
5	Structural health monitoring	75
5.1	Introduction	75
5.2	Data pre-processing	75
5.3	Previously applied data analysis methodologies	76
5.3.1	Linear and nonlinear regression of time-series	76
5.3.2	Preliminary evaluation of correlation with monitored environmental parameters	78
5.3.3	Filtering environmental effects using linear regression with selected predictors	78
5.4	Proposed analysis methodology	79
5.4.1	Filtering environmental effects using dynamic statistical models (ARX models)	80
5.4.2	Interpretation of results	84
5.5	Case studies	89
5.5.1	Mallorca cathedral	89
5.5.2	Monastery of Sant Cugat	92
5.6	Summary	98
6	Risk assessment and decision-making	101
6.1	Introduction	101
6.2	Risk assessment methodology	101
6.3	Standard questions for evaluating and updating indices	103
6.3.1	Essential questions	103
6.3.2	Optional questions	105
6.4	Level of knowledge index	105
6.5	Damage risk index	112
6.5.1	Damage vulnerability index	113
6.6	From risk assessment to decision making	119
6.7	Application to Mallorca cathedral	121
6.8	Application to other case studies	125
6.9	Summary	128
7	Conclusions	131
7.1	Summary	131
7.2	Main contributions	133
7.3	Suggestions for future work	134
	Appendices	137

A	Standard questions for risk assessment	139
A.1	Standardised Initial Expert Appraisal (SIEA)	140
A.1.1	Initial evaluation of level of knowledge and damage risk	140
A.1.2	Evaluation of which activities can best inform the assessment of damage vulnerability	142
A.2	Specific questions after structural analysis and structural health monitoring	145
A.3	Specific questions after evaluation of material properties	147
A.4	Specific questions after additional geometry and damage surveys	148
A.5	Specific questions after additional diagnosis activities for the assessment of material quality	149
A.6	Specific questions after in-situ tests of actual loading and boundary conditions	150
B	Answers to questions for case studies	151
B.1	Mallorca cathedral	152
B.1.1	Standardised Initial Expert Appraisal (SIEA)	152
B.1.2	Answers to questions at final “knowledge state”	157
B.2	Sant Cugat monastery	163
B.3	Tower from the remains of the castle of Lloberola	171
B.4	The church of Santa Maria de Guimerà	176
C	Risk assessment summaries for case studies	183
C.1	Mallorca cathedral	184
C.2	Sant Cugat monastery	186
C.3	Tower from the remains of the castle of Lloberola	188
C.4	The church of Santa Maria de Guimerà	190
	References	193
II	Publications	207
	Dynamic elastic properties of brick masonry constituents	209
	Relationship between the static and dynamic elastic modulus of brick masonry constituents	233
	Automated data analysis for static structural health monitoring of masonry heritage	255

List of Figures

1.1	Organisation of the thesis document.	9
2.1	Impulse Excitation of Vibration (IEV) test set-ups according to ASTM E1876 (ASTM, 2015). . .	13
2.2	Estimating dynamic elastic properties from IEV results according to ASTM E1876 (ASTM, 2015). . .	14
2.3	Ultrasonic Pulse Velocity (UPV) test set-up according to ASTM C597 (ASTM, 2010).	15
2.4	OMA workflow and common techniques for modal parameter extraction.	19
2.5	Examples of (a) peak picking and (b) FDD methods.	20
2.6	Examples of dynamic SHM from literature (Elyamani et al., 2017a; Lorenzoni et al., 2013). . . .	21
2.7	Examples of static SHM from literature (Ottoni; Blasi, 2015; Sánchez; Meli; Chávez, 2015). . . .	23
3.1	Markings made on every specimen prior to IEV testing.	30
3.2	IEV test set-ups.	30
3.3	Accelerometer mounting for IEV tests using scrim-backed adhesive tape.	31
3.4	Brick dimension measurement locations	31
3.5	Processing of acquired data during IEV tests	32
3.6	Locations of ultrasonic pulse travel time measurements across length.	34
3.7	Locations of ultrasonic pulse travel time measurements across width.	34
3.8	Measurement of ultrasonic pulse transit time across thickness.	34
3.9	Schematic representation of stresses in material during tests.	37
3.10	Variation of estimation of $E_{UPV,L}$ with ν for bricks from group I(a).	38
3.11	Variation of estimation of $E_{UPV,L}$ with ν for all bricks tested.	38
3.12	Proposed procedure for determining dynamic elastic properties.	39
3.13	Specimens cut from each handmade brick.	41
3.14	Loading scheme employed for tests to determine the static elastic modulus of specimens. . .	43
3.15	Experimental setup of static tests.	43
3.16	Example of an unsteady strain measurement deemed as being erroneous.	44
3.17	Example of an outlier among 3 strain measurements across different faces of a specimen. . . .	45
3.18	Prediction of static elastic modulus (E_{st}) from dynamic elastic modulus (E_{dy}).	50
3.19	Prediction errors of various existing expressions for estimating E_{st} from E_{dy}	51
4.1	The bell tower of Seu Vella.	54
4.2	Geometry (a) and boundary conditions (b) of the beam elements model.	54
4.3	Mode shapes predicted by beam elements model with $E=5.3$ GPa.	55
4.4	Solid elements model.	56
4.5	Mode shapes predicted by solid elements model with $E=5.3$ GPa.	57
4.6	Data acquisition system and connections on-site in the bell tower of La Seu Vella.	58
4.7	Location, positive acquisition direction, and pictures of accelerometers on-site.	59
4.8	Acquisition 2 and corresponding frequency domain transformation.	60
4.9	Acquisition 3 and corresponding frequency domain transformation.	60
4.10	Acquisition 4 and corresponding frequency domain transformation.	61
4.11	Acquisition 5 and corresponding frequency domain transformation.	61
4.12	Acquisition 6 and corresponding frequency domain transformation.	62
4.13	Example of a Singular Value Decomposition diagram.	64
4.14	Stabilisation diagram for Acquisition 4 model identified using pLSCE	65
4.15	Stabilisation diagram for Acquisition 4 model identified using SSIdat.	65
4.16	Points used for mode shape comparison.	67

4.17	Coordinate systems of models.	68
4.18	Estimated mode shapes (Mode 1)	69
4.19	Estimated mode shapes (Mode 6)	70
4.20	Local mode shape predicted by numerical model at 34.3 Hz.	71
5.1	Linear and nonlinear periodic models fitted to data.	76
5.2	Linear regression between structural and environmental parameters.	78
5.3	Filtering of temperature effect based on identified general linear trend.	79
5.4	Example of observed time lag between exterior and interior temperature.	83
5.5	Empirical distribution of ARX Residuals.	85
5.6	Static SHM: automated classification procedure	86
5.7	Static SHM: summary of classification tests	87
5.8	Proposed automated data analysis procedure for static SHM.	88
5.9	Modelling errors for the case of Mallorca cathedral.	90
5.10	Main outcomes from analysis of static SHM data of Mallorca cathedral.	91
5.11	SHM system installed in Sant Cugat monastery.	92
5.12	Tool for periodic verifications - Main window.	93
5.13	Tool for periodic verifications - Analysis interface.	94
5.14	Preliminary evaluation of correlation for the case of Sant Cugat monastery.	94
5.15	Previous structural interventions in Sant Cugat monastery.	95
5.16	Modelling errors for the case of Mallorca cathedral.	96
5.17	Main outcomes from analysis of static SHM data of Sant Cugat monastery.	97
5.18	Inclination trends of the bell tower of Sant Cugat monastery.	98
6.1	Proposed general risk assessment methodology.	102
6.2	Possible Level of Knowledge (LoK) concavity settings.	106
6.3	Criteria tree for LoK index.	107
6.4	Criteria tree for specific LoK sub-indicator on structural analysis and SHM.	108
6.5	Criteria tree for the Damage Risk (DR) index.	113
6.6	Value functions for questions in the Standardised Initial Expert Appraisal (SIEA).	114
6.7	Criteria tree for the Damage Vulnerability (DV) index.	115
6.8	Criteria tree for sub-indicator linked to the assessment of specific vulnerabilities.	116
6.9	Value functions for processed data from static SHM systems.	118
6.10	Decision matrix for using proposed indices.	121
6.11	Mallorca cathedral and investigations performed.	122
6.12	Initial and final LoK index values for Mallorca cathedral.	123
6.13	Initial and final DV index values for Mallorca cathedral.	124
6.14	Initial and final DR index values for Mallorca cathedral.	124
6.15	Case studies for risk assessment.	126
6.16	Landslide susceptibility around the church of Santa Maria de Guimerà (Palau et al., 2020).	127
C.1	RISDiMaH summary for Mallorca cathedral.	184
C.2	RISDiMaH summary for the church of the monastery of Sant Cugat.	186
C.3	RISDiMaH summary for the tower of Lloberola.	188
C.4	RISDiMaH summary for the church of Santa Maria de Guimerà.	190

List of Tables

1	Abbreviations.	3
2.1	Notable examples of static SHM systems installed in masonry cultural heritage structures. . .	22
3.1	Groups of brick types tested.	28
3.2	Groups of mortar types tested.	29
3.3	Final estimated dynamic elastic properties from IEV testing.	35
3.4	Estimated dynamic Young's modulus from UPV measurements across different directions. . .	35
3.5	Comparison of dynamic moduli across different specimen directions.	36
3.6	Comparison of dynamic Young's modulus from IEV and UPV measured across length.	37
3.7	Number of specimens used to evaluate static and dynamic elastic moduli	42
3.8	Comparison of average static and dynamic moduli across brick lengths.	46
3.9	Comparison of average static and dynamic moduli across brick widths.	47
3.10	Comparison of average static and dynamic moduli of mortar specimens.	47
3.11	Correlation matrix for combinations of E_{st} , E_{dy} , and ρ	48
3.12	Correlation matrix for combinations of E_{st} , E_{dy} , and f_c	49
3.13	Correlation matrix for combinations of E_{st} , E_{dy} , ρ , and f_c	49
4.1	Dimensions of beam elements.	55
4.2	Properties of beam elements model.	55
4.3	Predicted natural frequencies by beam elements model.	56
4.4	Properties of solid elements model.	56
4.5	Predicted natural frequencies by solid elements model.	57
4.6	Properties of accelerometers used for the vibration tests.	58
4.7	Description of different acceleration time-history acquisitions.	59
4.8	Estimated natural frequencies of mode 1.	66
4.9	Estimated natural frequencies of mode 6.	66
4.10	MAC for Mode 1 (Acquisition 2).	68
4.11	MAC for Mode 1 (Acquisition 4).	68
4.12	MAC for Mode 6 (Acquisition 5).	69
4.13	MAC for Mode 6 (estimates from all acquisitions using the pLSCF method).	70
4.14	Damping ratio estimates for Mode 1.	71
4.15	Damping ratio estimates for Mode 6.	71
4.16	Known information on the bells of the bell tower of Seu Vella.	72
5.1	Summary of initial estimates for nonlinear fitting procedure.	77
5.2	Ranges of ARX model orders tested using estimation data with a sampling period of 1 hour. . .	83
5.3	Structural sensors installed in Mallorca cathedral.	89
5.4	Estimated evolution rates after filtering for the case of Mallorca cathedral.	90
5.5	Structural sensors installed in Sant Cugat monastery.	92
5.6	Estimated evolution rates from direct fitting methods for the case of Sant Cugat monastery. .	95
5.7	Estimated evolution rates after filtering for the case of Sant Cugat monastery.	96
6.1	Pairwise comparisons and relative importance of diagnosis activity groups.	109
6.2	Pairwise comparisons and relative importance of different structural analysis aims.	112
6.3	Parameters of value functions for questions in the Standardised Initial Expert Appraisal (SIEA). 114	
6.4	Parameters of value functions for processed data from static SHM systems.	118

6.5	Possible diagnosis activities that can be suggested after risk assessment.	120
6.6	Initial and current automatic list of best activities for Mallorca cathedral.	125
6.7	Final index values for the structures studied as part of this research.	126
A.1.1	Questions to be answered during the first part of the SIEA.	140
A.1.2	Description of the significance of answers in the first part of the SIEA.	141
A.1.3	Ratings to be given during the second part of the SIEA (1).	142
A.1.4	Ratings to be given during the second part of the SIEA (2).	143
A.1.5	Description of the significance of ratings in the second part of the SIEA.	144
A.2.1	Questions on structural analysis and SHM.	145
A.2.2	Description of the significance of answers on structural analysis and SHM.	146
A.3.1	Questions on the estimation of material properties.	147
A.3.2	Description of the significance of answers on the estimation of material properties.	147
A.4.1	Questions on additional geometry and damage surveys.	148
A.4.2	Description of the significance of answers on additional geometry and damage surveys.	148
A.5.1	Questions on the assessment of material quality.	149
A.5.2	Description of the significance of answers on the assessment of material quality.	149
A.6.1	Questions on in-situ tests.	150
A.6.2	Description of the significance of answers on in-situ tests.	150
B.1.1	Answers to questions in the first part of the SIEA for Mallorca cathedral (1).	152
B.1.2	Answers to questions in the first part of the SIEA for Mallorca cathedral (2).	153
B.1.3	Ratings given in the second part of the SIEA for Mallorca cathedral (1).	154
B.1.4	Ratings given in the second part of the SIEA for Mallorca cathedral (2).	155
B.1.5	Ratings given in the second part of the SIEA for Mallorca cathedral (3).	156
B.1.6	Answers to questions on structural analysis for Mallorca cathedral.	157
B.1.7	Answers to questions on SHM for Mallorca cathedral.	158
B.1.8	Answers to questions on the estimation of material properties for Mallorca cathedral.	159
B.1.9	Answers to questions on additional geometry and damage surveys for Mallorca cathedral.	160
B.1.10	Answers to questions on the assessment of material quality for Mallorca cathedral.	161
B.1.11	Answers to questions on in-situ tests for Mallorca cathedral.	162
B.2.1	Answers to questions in the first part of the SIEA for Sant Cugat monastery (1).	163
B.2.2	Answers to questions in the first part of the SIEA for Sant Cugat monastery (2).	164
B.2.3	Ratings given in the second part of the SIEA for Sant Cugat monastery (1).	165
B.2.4	Ratings given in the second part of the SIEA for Sant Cugat monastery (2).	166
B.2.5	Ratings given in the second part of the SIEA for Sant Cugat monastery (3).	167
B.2.6	Answers to questions on structural analysis for Sant Cugat monastery.	168
B.2.7	Answers to questions on SHM for Sant Cugat monastery.	169
B.2.8	Answers to questions on the estimation of material properties for Sant Cugat monastery.	170
B.2.9	Answers to questions on additional geometry and damage surveys for Sant Cugat monastery.	170
B.2.10	Answers to questions on in-situ tests for Sant Cugat monastery.	170
B.3.1	Answers to questions in the first part of the SIEA for Lloberola tower (1).	171
B.3.2	Answers to questions in the first part of the SIEA for Lloberola tower (2).	172
B.3.3	Ratings given in the second part of the SIEA for Lloberola tower (1).	173
B.3.4	Ratings given in the second part of the SIEA for Lloberola tower (2).	174
B.3.5	Ratings given in the second part of the SIEA for Lloberola tower (3).	175
B.4.1	Answers to questions in the first part of the SIEA for the church of Santa Maria de Guimerà (1).	176
B.4.2	Answers to questions in the first part of the SIEA for the church of Santa Maria de Guimerà (2).	177
B.4.3	Ratings given in the second part of the SIEA for the church of Santa Maria de Guimerà (1).	178
B.4.4	Ratings given in the second part of the SIEA for the church of Santa Maria de Guimerà (2).	179
B.4.5	Ratings given in the second part of the SIEA for the church of Santa Maria de Guimerà (3).	180
B.4.6	Answers to questions on structural analysis for the church of Santa Maria de Guimerà.	181
C.1.1	Automatically generated list of best activities to perform for Mallorca cathedral.	185
C.2.1	Automatically generated list of best activities to perform for Sant Cugat monastery.	187
C.3.1	Automatically generated list of best activities to perform for the Lloberola tower.	189
C.4.1	Automatically generated list of best activities for Santa Maria de Guimerà church.	191

I

Research Summary

Abbreviations

The following abbreviations are used recurrently in this thesis.

Table 1: Abbreviations.

NDT	Non-Destructive Testing
IEV	Impulse Excitation of Vibration
UPV	Ultrasonic Pulse Velocity

OMA	Operational Modal Analysis
pLSCF	poly-reference Least Squares Complex Frequency domain identification
FDD	Frequency Domain Decomposition
SSI	Stochastic Subspace Identification
FE	Finite Element

SHM	Structural Health Monitoring
ARX	Auto-Regressive eXogenous (models)

MCDM	Multi-Criteria Decision-Making
SAW	Simple Additive Weighting
AHP	Analytic Hierarchy Process
DR	Damage Risk (index)
DV	Damage Vulnerability (index)
LoK	Level of Knowledge (index)
SIEA	Standardised Initial Expert Appraisal

1

Introduction

1.1. Background and motivation

Recent years have been marked by significant advances in analysis, inspection, testing, and monitoring techniques applied to the diagnosis of masonry heritage structures. Most of these developments are motivated by the fact that an accurate evaluation of the current structural condition is critical to ensure the survival of such structures. Despite these advances, the diagnosis of unique monuments still remains a challenging task. This is mainly due to the large number of uncertainties linked to the geometry of the structure, to the interaction among different parts, as well as to the mechanical, physical, and chemical properties of the material. To add to this complexity, the need to protect heritage value often prevents the extraction of a comprehensive set of samples to characterise the material. Modern standards for new structures conservatively account for such uncertainties, related to the structural scheme or to material characteristics, through the application of safety factors. Although this approach is adequate for new structures, where safety can be increased with modest increases in member size, it cannot be applied to heritage structures because requirements to improve capacity can lead to the loss of historic fabric or to changes in the original structural conception. Consequently, the principle of minimum intervention is preferred for heritage structures (ISCARSAH, 2005). This requires adopting a flexible and broad approach in order to be able to relate the remedial measures more clearly to the actual structural behaviour. In other words, faced with the impossibility of adopting a conservative approach, the diagnosis task is crucial, because the actual structural behaviour needs to be well understood to design appropriate remedial measures, if any.

As a result, the decision-making task on remedial measures becomes particularly difficult, since the very nature of the problem entails the need for an accurate diagnosis in the face of strict limitations on specimen extraction for testing. As a consequence of this challenge, there is a growing body of literature that has examined and evaluated the application of new technologies, minor destructive tests (MDT), and non-destructive testing (NDT) to facilitate the diagnosis of heritage structures. Such techniques can now be applied to provide information on a wide variety of aspects that are key to an accurate diagnosis. Applications exist to obtain more accurate representations of the geometry and damage (Van Genechten et al., 2008; Bevilacqua et al., 2018; Chiabrando et al., 2018), to estimate material properties (Pelà; Roca; Benedetti, 2015; Pelà et al., 2016b; Segura et al., 2019; Pelà; Roca; Aprile, 2016; Pelà; Roca; Aprile, 2018; Marastoni et al., 2017; Vasanelli et al., 2017; Garzón-Roca et al., 2013), to characterise material quality and variability (Hum-Hartley, 1978; Schuller, 2003; Binda; Maierhofer, 2006; Binda; Saisi, 2009; Valluzzi et al., 2018), to evaluate actual loading and boundary conditions (Schuller, 2003; Ivorra; Pallarés; Adam, 2011a; Ivorra; Giannoccaro; Foti, 2019; Bru et al., 2019; Russo; Spoldi, 2020), and even to monitor the structural response (Ramos et al., 2010; Elyamani et al., 2017a; Baeza et al., 2018; Lorenzoni et al., 2013; Ottoni; Blasi, 2015; Lorenzoni et al., 2016; Masciotta; Ramos; Lourenço, 2017; Cavalagli et al., 2019). Similarly, there is a considerable amount of literature on numerical modelling (D'Altri et al., 2020; Lourenço, 1998; Lourenço, 2002; Molins; Roca, 1998; D'Ayala, 2008; Zeman et al., 2008; Drougkas; Roca; Molins, 2015; Pelà; Cervera; Roca, 2011; Pelà; Cervera; Roca, 2013; Cervera et al., 2010; Saloustros; Cervera; Pelà, 2019) and other structural analysis tools (Roca et al., 2010; Block; Ochsendorf, 2007; Andreu; Gil; Roca, 2007; Heyman, 1995) that can be used to provide vital information for diagnosis and for accurately assessing the damage vulnerability of masonry heritage structures. As

a result, depending on cost limitations and on the complexity of the heritage structure, an expert responsible for structural diagnosis can nowadays choose from a wide variety of tools to inform decisions on further investigations or interventions. Subsequently, relevant information and results from all selected diagnosis activities should be used to assess the vulnerability of the structure.

Before making any recommendations on interventions or further investigation, experts also have to take into consideration other risk components not directly related to the vulnerability of the structure to damage. These include factors related to the exposure level, such as the cultural value associated to the structure, or to the hazard level, such as the probability of occurrence of a high intensity catastrophic event. This results in a complex decision problem involving multiple divergent criteria. Decisions requiring such assessment can often benefit from improved objectivity and transparency through the application of formal decision analysis and multi-criteria decision-making (MCDM) techniques (Miles, 1972; Edwards; Miles Jr.; Winterfeldt, 2007; Velasquez; Hester, 2013; Navarro; Yepes; Martí, 2019).

In fact, there are several examples in literature of applications of MCDM techniques for general vulnerability or risk assessment to facilitate decisions on preventive conservation at the urban or territorial scale (Ortiz; Ortiz, 2016; Tena; León, 2016; Ruiz-Jaramillo et al., 2019; Piñero et al., 2017; Dutta; Husain, 2009). The most popular methods involve the evaluation of seismic vulnerability (Benedetti; Benzoni; Parisi, 1988; Giovinazzi; Lagomarsino, 2004; Calvi et al., 2006; Vicente et al., 2011; D'Ayala; Speranza, 2003; Sangiorgio; Uva; Adam, 2020). Nowadays, results from such applications are even used in broader risk assessment frameworks to estimate losses in future earthquakes, to compare the impact on estimated loss of possible retrofitting solutions, and to plan emergency response (Calvi et al., 2006; Ferreira; Lourenço, 2019).

It is clear that risk assessment of masonry heritage structures at the territorial level has benefited greatly from the application of MCDM methods. In addition, it is undeniable that good decisions in conservation require the availability of appropriate information. This is evidenced by the development of integrated information systems based on well-defined concepts of preventive conservation to support risk management decisions for some UNESCO world heritage sites (Paolini et al., 2012; Heras et al., 2012; Heras et al., 2013). However, very few attempts have been made to apply decision analysis methods to assess the risk of structural damage in unique complex monuments. One of the main challenges to their application lies in the unique nature of each structure and the individual characteristics that shape their risk landscapes. Furthermore, as previously mentioned, the assessment of the damage vulnerability of unique monuments can be informed by a wide variety of diagnosis activities including NDT and structural health monitoring (SHM). Naturally, it is currently unfeasible to carry out many of these activities when conducting vulnerability assessment at a territorial scale. Consequently, most of the aforementioned methods developed for risk and vulnerability assessment at the territorial scale rely solely on information that can be obtained from technical visual inspections and geometry surveys. Therefore, because vulnerability is a key component of risk (UNGA, 2016), it can be expected that direct application of these methods for the risk assessment of a unique monument can only provide a very limited picture of the risk landscape that needs to be considered for decisions on preventive measures.

As such, any comprehensive risk assessment process for unique monuments should consider information from all relevant diagnosis activities carried out. This only adds to the difficulty of applying standard decision analysis methods since the suitability of different activities and the relative importance of the information they provide for global damage vulnerability assessment can change depending on the specific characteristics of different structures. Given the unique characteristics of individual monuments, any systematic application of MCDM techniques to assist decision-making on preventive conservation should be able to account for the fact that outcomes from various diagnosis activities will have a different impact on vulnerability assessment depending on specific conditions of each structure. It is also important to note that any assessment of safety can be seriously affected by the uncertainty attached to the data, laws, models, and assumptions used in the research (ISCARSAH, 2005). Therefore, in order to make better mitigation decisions, it is important to include information on the level of uncertainty in the assessment and decision-making process (Paolini et al., 2012). The recognition of uncertainty allows decision-makers to assess the limitations of available information and to take the best decision with respect to resource allocation for risk mitigation.

In light of the above, before addressing the development of decision support tools, the research presen-

ted in this thesis consisted in fulfilling a number of objectives related to certain specific technical fields that can contribute significantly to the structural diagnosis of masonry heritage. Specifically, topics of interest were identified related to materials testing, full-scale vibration testing, and SHM. An important motivation behind these tasks was to obtain a better understanding of practical issues related to different types of diagnosis activities that cannot be comprehended simply by reading the literature. The knowledge gained while achieving these objectives was then built upon to develop specific MCDM tools that can be applied to unique masonry heritage structures to assist experts in the evaluation of damage risk. Such tools are intended to improve objectivity, clarity, and transparency in the decision process and should be able to incorporate information from a wide range of diagnosis activities.

1.2. Scope and objectives

The research presented in this document is performed within the scope of structural risk assessment for masonry heritage. This is in itself a broad scope, which by definition involves interactions with many technical fields that can contribute to an accurate identification and characterisation of structural risk. For masonry heritage structures, relevant technical fields include building surveying, materials testing, in-situ testing, structural analysis, and structural health monitoring (SHM). In a first instance, the research work presented in this thesis aims to contribute to the enhancement of some key testing and SHM methods for the analysis of masonry structures. Specific topics dealing with materials testing, full-scale vibration testing, and static SHM are addressed. The specific objectives set relating to each of these fields are listed below.

Materials testing

- To develop a robust procedure for estimating the dynamic elastic properties of brick masonry constituents.
- To analyse the empirical relationship between the static and dynamic elastic moduli of brick masonry constituents.

Full-scale vibration testing

- To design a suitable acquisition system for the full-scale vibration testing of a masonry bell tower.
- To evaluate the efficiency of different system identification techniques for extracting modal parameters from acquired vibration signatures.

Structural health monitoring

- To develop an automated procedure for processing and analysing data from static SHM systems to facilitate the diagnosis of masonry heritage structures.

Following the achievement of these goals, the research aimed to develop useful multi-criteria decision-making (MCDM) tools to support risk management decisions. In this context, risk assessment refers to the identification, characterisation, and evaluation of the risk of structural damage occurring. Naturally, additional specific objectives also needed to be defined in order to achieve this final objective. These are listed below:

Risk assessment and decision-making

- To develop MCDM tools able to produce outputs that can concisely inform decision-makers on the risk of structural damage for a particular masonry heritage structure.
- To develop MCDM tools able to produce outputs that can concisely inform decision-makers on the level of knowledge used as a basis for risk assessment.
- To define a systematic risk assessment procedure, based on well-established principles of preventive conservation, within which proposed MCDM tools can be utilised.
- To propose a mechanism so that outputs of the MCDM tools can be automatically updated based on data collected by static SHM systems over time.

1.3. Research dissemination

The work presented in this thesis has resulted in the following scientific publications:

Articles in peer-reviewed international journals

1. MAKOOND, N.; PELÀ, L.; MOLINS, C., 2019. Dynamic elastic properties of brick masonry constituents. *Construction and Building Materials*. Vol. 199, pp. 756–770. ISSN 09500618. Available from DOI: 10.1016/j.conbuildmat.2018.12.071
2. MAKOOND, N.; CABANÉ, A.; PELÀ, L.; MOLINS, C., 2020a. Relationship between the static and dynamic elastic modulus of brick masonry constituents. *Construction and Building Materials*. Vol. 259, p. 120386. ISSN 09500618. Available from DOI: 10.1016/j.conbuildmat.2020.120386
3. MAKOOND, N.; PELÀ, L.; MOLINS, C.; ROCA, P.; ALARCÓN, D., 2020c. Automated data analysis for static structural health monitoring of masonry heritage structures. *Structural Control and Health Monitoring*. ISSN 1545-2255. Available from DOI: 10.1002/stc.2581

Conference papers and presentations in international conferences

- MAKOOND, N.; PELÀ, L.; MOLINS, C.; ROCA, P., 2020b. Static structural health monitoring and automated data analysis procedures applied to the diagnosis of a complex medieval masonry monastery. In: ZONTA, D.; HUANG, H. (eds.). *Sensors and Smart Structures Technologies for Civil, Mechanical, and Aerospace Systems 2020*. SPIE. ISBN 9781510635357. Available from DOI: 10.1117/12.2559837
- MAKOOND, N.; PELÀ, L.; MOLINS, C.; ROCA, P., 2021. Data analysis using ARX models applied to static structural health monitoring of the monastery of Sant Cugat. In: ROCA, P.; PELÀ, L.; MOLINS, C. (eds.). *Accepted for presentation in the 12th International Conference on Structural Analysis of Historical Constructions (SAHC 2020) to be held on September 29-30, and October 1, 2021*.

In addition, the following manuscript has also been submitted to a peer-reviewed international journal for consideration:

Manuscripts submitted for consideration to peer-reviewed international journals

- MAKOOND, N.; PELÀ, L.; MOLINS, C., 2020. A Risk Index for the Structural Diagnosis of Masonry Heritage (RISDiMaH). *Submitted for publication*

1.4. Outline

This document is composed of two parts. The first part is a collection of the main developments and results presented in the aforementioned publications. The second part includes the three accepted papers produced as part of this research. In this part, each paper follows its own numbering of sections, figures, equations, and references.

The first part of the document is organised in 7 chapters as follows:

- **Chapter 2** introduces the performed research by presenting a relevant **literature review** of the specific subject matters dealt with in Chapters 3 to 5, followed by an overview of the state-of-the-art in applying MCDM tools for the structural risk assessment of masonry heritage structures.
- **Chapter 3** presents the work developed as part of this research in the field of **materials testing**. This includes the development of a robust procedure for estimating the dynamic elastic properties of brick masonry constituents and the proposal of an empirical relationship for estimating the static elastic modulus of constituents from their dynamic counterpart.
- **Chapter 4** presents the work developed as part of this research on **full-scale vibration testing**. This involves designing a suitable acquisition system and planning the AVT of a medieval bell tower. It also presents a comparison of modal parameter estimates obtained through different system identification techniques under varying acquisition conditions.

- **Chapter 5** presents the work developed as part of this research in the field of **structural health monitoring**. This involves the development of an automated data analysis procedure for analysing data from static SHM systems to facilitate the diagnosis of masonry heritage structures. The efficacy of the proposed method for identifying vulnerable areas is demonstrated through applications to two important medieval heritage structures in Spain, namely the cathedral of Mallorca and the church of the monastery of Sant Cugat.
- **Chapter 6** presents the **risk assessment** procedure and MCDM tools developed as part of this research to support decisions on the structural safety of masonry heritage.
- Finally, **Chapter 7** concludes the first part of the document by summarising the main original contributions of the research and by outlining suggestions for future work.

Figure 1.1 summarises the organisation of the first part of the thesis and shows how the different chapters are connected to each other.

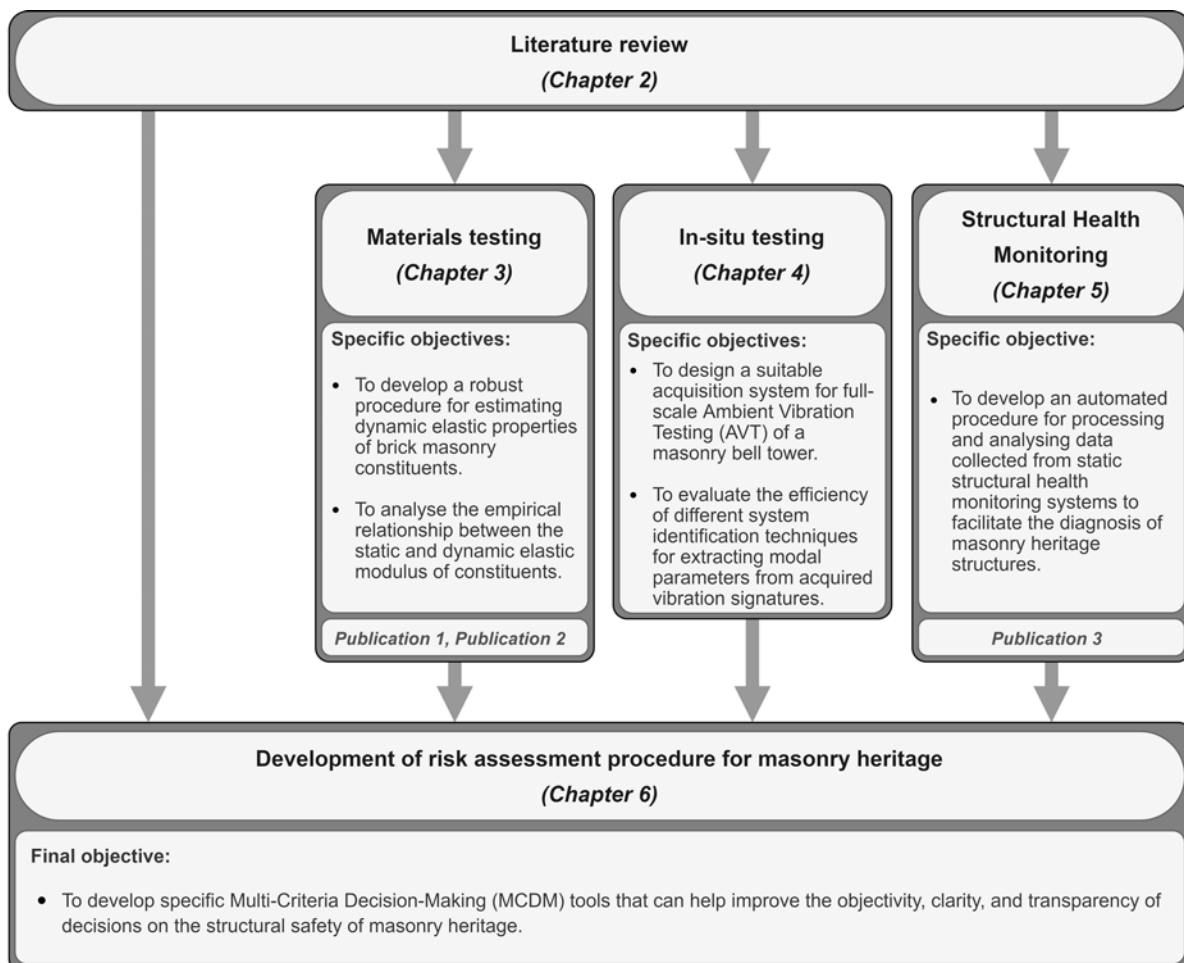


Figure 1.1: Organisation of the thesis document and how the main chapters relate to specific research objectives. Publication numbers refer to the numbered list of published articles in Section 1.3.

2

Literature review

2.1. Introduction

This chapter presents essential background information and theoretical concepts used as a basis for the research work developed in subsequent chapters. It is divided in four sections following this brief introduction. The first three present the state-of-the-art on the specific topics explored in the fields of materials testing (Section 2.2), in-situ testing (Section 2.3), and structural health monitoring (Section 2.4) respectively. The last section of the chapter (Section 2.5) aims to provide a general overview of MCDM methods that have previously been applied to facilitate the structural risk assessment of masonry heritage structures.

2.2. Dynamic elastic properties of brick masonry constituents

The work developed in the field of materials testing as part of this research consists of two parts. The first deals with the development of a robust procedure for estimating dynamic elastic properties of brick masonry constituents. The second part involves proposing an expression that can be used to estimate the static elastic modulus of typical brick masonry constituents from the dynamic one for practical applications.

Elastic constants of a material are fundamental properties that can be crucial for characterising the deformation behaviour of structural elements whether it is with respect to the design of new structures or for the assessment of existing ones.

Static elastic properties of masonry constituents are in general well understood. Indeed, a considerable amount of information is available in literature on the determination and estimation of such properties. For instance, the European Committee for Standardisation (CEN) has approved a European Standard on the determination of the static elastic modulus for natural stone since 2005 (CEN, 2005). Tests to determine static elastic properties rely mainly on measuring deformations while applying controlled loading. Hence, the modified application of recommendations from standards designed for other materials such as concrete is, at least in theory, relatively straightforward. As a consequence, several authors such as Binda et al. (Binda et al., 1996; Binda; Tiraboschi; Abbaneo, 1997; Binda; Tedeschi; Condoleo, 2006; Baronio et al., 2003), Oliveira et al. (Oliveira, 2000; Oliveira; Lourenço; Roca, 2000; Oliveira; Lourenço; Roca, 2007) and Pelà et al. (Pelà et al., 2016b) have explored testing procedures to determine these properties for masonry constituents and assemblages. Many of these studies have shown that although the theory behind the evaluation of static elastic properties is well understood, the scatter of results in experimental studies remains high in many cases, often due to the difficulties related to measuring deformations in the elastic range of brittle materials such as those typically used as constituents in brick masonry constructions. Nevertheless, a considerable amount of information is still available, not only on best testing practices, but also on the range of expected results for different types of bricks and mortar, as well as on the effects which can influence the estimates of static elastic properties for brick masonry constituents.

Dynamic elastic properties refer to the constants that define a material's behaviour in the elastic range

under vibratory conditions. When subjected to dynamic loading, experiments have shown that materials can feature a mechanical behaviour quite different from its static counterpart. A possible physical cause of this empirically known inequality between measured static and dynamic elastic moduli may be found in the different inelastic contributions to stress-strain which behave as a function of strain amplitude and frequency (energy and strain rate) (Mashinsky, 2003). Most of the studies available in literature focus on the relation between static and dynamic elastic properties of concrete (Takabayashi, 1954; Popovics, 1975; Swamy; Bandyopadhyay, 1975; Lydon; Balendran, 1986), or on that of rocks in a geomechanics context (Eissa; Kazi, 1988; Ciccotti; Mulargia, 2004; Martínez-Martínez; Benavente; García-del-Cura, 2012; Najibi et al., 2015; Fei et al., 2016). As such, although some authors, notably Totoev and Nichols (Totoev; Nichols, 1997; Nichols; Totoev, 1997), have explored this relationship for specific types of bricks, it is still not well understood.

The aforementioned work by Totoev and Nichols (Totoev; Nichols, 1997; Nichols; Totoev, 1997) includes the evaluation of the dynamic Young's modulus for specific types of bricks. However, the range of experimental techniques as well as the range of different constituents tested is rather limited, particularly when compared to the information available on static properties. Notably, the dynamic Young's modulus was only evaluated through means of longitudinal vibration tests and traditional ultrasonic pulse velocity (UPV) testing with longitudinal stress waves (P-waves). In such studies, the dynamic Poisson's ratio is assumed as being invariant from the quasi-static one, and no procedure is described for the experimental determination of the dynamic Poisson's ratio or shear modulus through torsional vibration tests. Although this is most likely a reasonable assumption, there is not sufficient information available in literature for this relationship to be well-established. In fact, studies available in literature involving the determination of dynamic Poisson's ratio or shear moduli, such as (Brotons et al., 2014) and (Dimter; Rukavina; Minažek, 2016), have only focused on very specific types of constituents. Moreover, although Totoev and Nichols (Totoev; Nichols, 1997; Nichols; Totoev, 1997) mention that UPV measurements can provide information on the isotropy of bricks, no detailed information is provided on the validity or correct interpretation of P-wave travel time readings for anisotropic cases. In such cases, wave propagation is not necessarily governed by the same simplified laws as in isotropic media and therefore evaluation of the dynamic modulus of elasticity using P-wave velocities alone can be quite unreliable. Finally, in order to carry out the longitudinal vibration tests, the specimens used by Totoev and Nichols had to be cut from whole bricks so that each resulting specimen had a greater ratio between the lateral dimensions and the length. Thus the non-destructive nature of the vibration tests were not fully exploited.

2.2.1. Selected techniques for estimating dynamic elastic properties

Dynamic elastic properties of materials can be calculated using data obtained from vibration tests or from the measured velocity of stress waves passing through the material. ASTM International has approved two of the most relevant existing standards on test methods that can be used to evaluate these properties, namely:

- A standard on the evaluation of the dynamic Young's Modulus, Shear Modulus and Poisson's ratio by Impulse Excitation of Vibration (IEV) for homogeneous elastic materials (ASTM, 2015).
- A standard for the determination of the propagation velocity of ultrasonic longitudinal stress waves through concrete which can be related to the material's dynamic elastic properties (ASTM, 2010).

Since dynamic properties are not evaluated directly but computed based on assumptions derived from the known behaviour of materials under specific conditions, the application of recommendations from standards is not so straightforward, particularly when they have been designed for different materials. The parameters being measured (wave travel time, frequency of vibration) often rely on many conditions which need to be understood and controlled carefully. This operation is necessary to be able to use the expressions relating measured parameters to material constants.

Two different techniques are employed by the aforementioned ASTM standards for estimating dynamic elastic properties, namely Impulse Excitation of Vibration (IEV) and Ultrasonic Pulse Velocity (UPV) testing. This subsection introduces the basic theory behind these techniques, highlighting important concepts that are essential for the correct interpretation of results derived from such procedures.

2.2.1.1. Impulse excitation of vibration (IEV) testing

It is known that specimens of elastic materials possess specific mechanical resonant frequencies that are determined by the elastic properties, mass, geometry of the test specimen, and boundary conditions imposed by the test set-up. The dynamic elastic properties of a material can therefore be computed if the geometry, mass, and mechanical resonant frequencies of a suitable test specimen of that material can be measured. Test set-ups that isolate specific resonance modes together with the processing of recorded vibration signals, allow these resonant frequencies to be determined. Specifications on specimen dimensions, test set-ups, expressions relating identified resonant frequencies to dynamic properties as well as other considerations are described thoroughly in the Standard Test Method for Dynamic Young's Modulus, Shear Modulus, and Poisson's Ratio by Impulse Excitation of Vibration released by ASTM International (ASTM, 2015).

The dynamic Young's modulus can be determined using the resonant frequency in either the flexural or the longitudinal mode of vibration. For the purpose of this study, the dynamic Young's modulus was only evaluated using the resonant frequency in the flexural mode because the ratios of dimensions of typical bricks means that the resonant frequency of the longitudinal mode would be much higher than that of the flexural mode. Since these frequencies were found to already be relatively high in the flexural mode, a quick estimate of the expected frequencies to be measured for the same Young's modulus in the longitudinal mode revealed that they would fall outside the range that could be accurately measured by the data acquisition system. The dynamic shear modulus is found using torsional resonant vibrations. To isolate the flexural mode of vibration, the ASTM standard (ASTM, 2015) states that the rectangular specimen should be supported along the width at a distance of $(0.224 \times Length)$ from either end of the length, as shown in Figure 2.1(a). On the other hand, to isolate the torsional mode, the rectangular specimen should be supported along the mid-points across the width and length as shown in Figure 2.1(b). Figure 2.1 also shows the recommended impact and sensor locations for each test. An important recommendation from (ASTM, 2015) is to place any direct contact transducers along the nodal lines which ensures minimal interference with the free-vibration of the specimen.

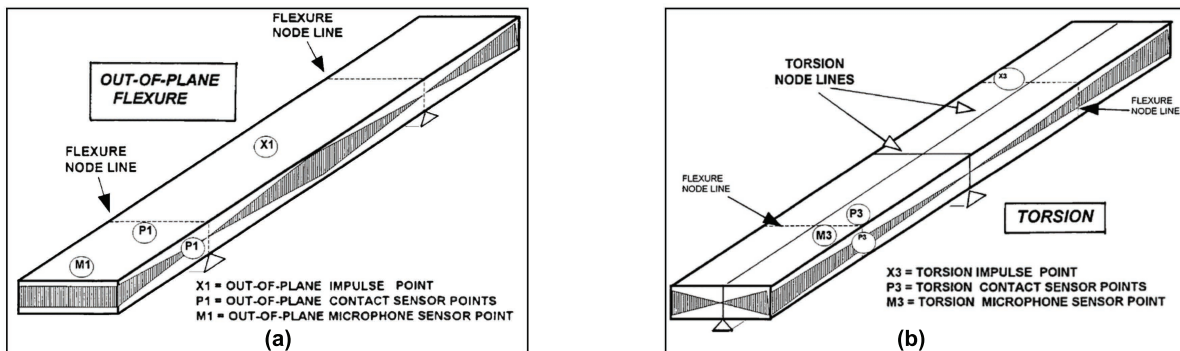


Figure 2.1: Specified IEV test set-ups including sensor and impact locations for isolating the flexural mode(a) and the torsional mode(b) of vibration according to ASTM E1876 (ASTM, 2015).

For the fundamental flexure frequency of a rectangular bar, the dynamic Young's modulus can be evaluated using Equation (2.1), whilst for the fundamental torsional frequency, the dynamic shear modulus can be computed using Equation (2.2).

$$E = 0.9465 \left(\frac{m f_f^2}{b} \right) \left(\frac{L^3}{t^3} \right) T_1 \quad (2.1)$$

$$G = \frac{4Lm f_t^2}{bt} [B/(1+A)] \quad (2.2)$$

Where E is the dynamic Young's modulus (Pa), m is the mass of the bar (g), b is the width of the bar (mm), L is the length of the bar (mm), t is the thickness of the bar (mm), f_f is the resonant frequency in flexure (Hz), T_1 is a correction factor dependent on Poisson's ratio as well as t and L , G is the dynamic shear modulus (Pa), f_t is the resonant frequency in torsion (Hz), B and A are correction factors dependent on b and t .

As we can see from Equation (2.2), the computation of the dynamic shear modulus from the measured torsional resonant frequency does not require knowledge of the dynamic Poisson's ratio. However, this unknown parameter is required for the evaluation of the T1 parameter in Equation (2.1). If isotropy is assumed, there exists a well known relationship between the Poisson's ratio, the Young's modulus and the shear modulus. Hence, for the isotropic case, the iterative procedure shown in Figure 2.2 can be used to find a suitable Poisson's ratio that will satisfy this relationship. In order for the iterative procedure to converge, a reasonable initial Poisson's ratio (ν_0) has to be selected. For all the specimens tested as part of this research, a ν_0 of 0.2 proved to be a good initial value to attain convergence.

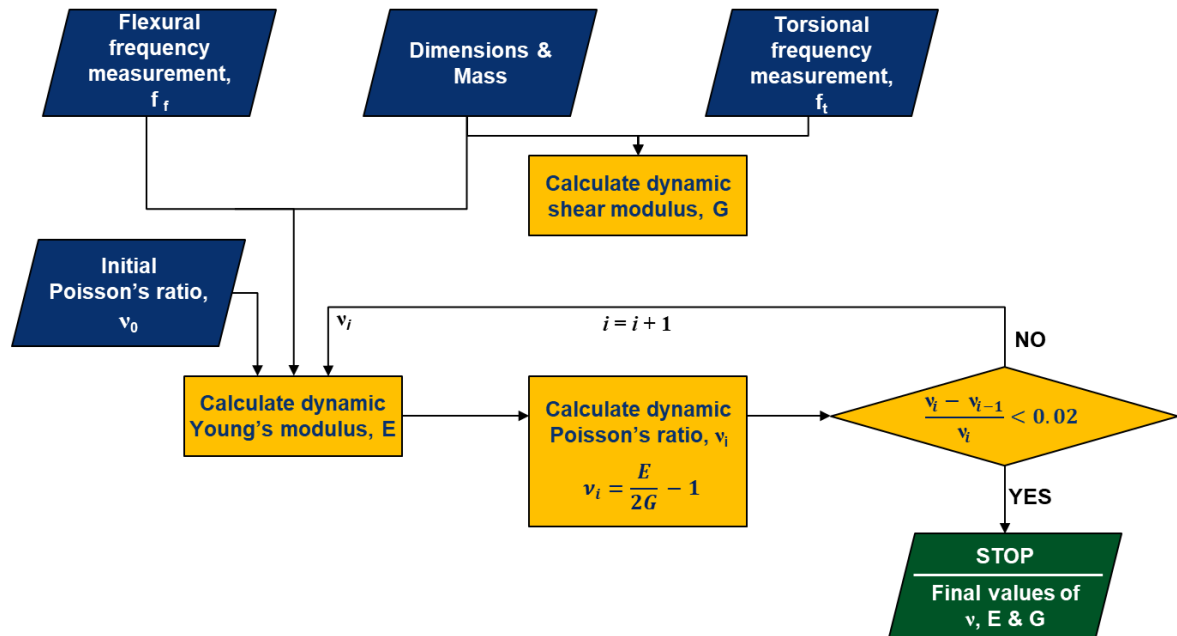


Figure 2.2: Procedure for estimating dynamic Young's modulus, shear modulus and Poisson's ratio from IEV test results according to ASTM E1876 (ASTM, 2015).

2.2.1.2. Ultrasonic pulse velocity (UPV) testing

Research on wave propagation in elastic solid materials dates back to the early 19th century (Achenbach, 1973). UPV testing makes use of elastic (or acoustic) waves which are in fact mechanical vibrations that propagate in gases, liquids and solids. Ultrasound corresponds to mechanical waves propagating at frequencies above the range of human hearing, which is conventionally considered as being limited to 20 kHz (Laugier; Haïat, 2011).

Although many different patterns of vibrational motion exist at the atomic level, in solids it can be said that two modes of bulk wave propagation exist that are most relevant to ultrasonic testing in the context of this research, namely:

- **Longitudinal waves:** Waves with particle displacement in the direction of wave propagation. These waves travel the fastest and are also known as compression waves or P-waves. The most accessible and commonly used electro-acoustical transducers in the construction industry produce waves primarily of this type (Bungey; Millard; Grantham, 1996).
- **Shear waves:** Also known as transverse waves, the direction of vibrations in these waves is normal to the direction of wave propagation (Nazarchuk; Skalskyi; Serhiyenko, 2017). Note that the direction of particle vibration is referred to as the polarization.

Wave propagation in isotropic media

The micro-structure of many engineering materials is formed from many randomly oriented grains which results in the mechanical properties being independent of direction on the macroscopic scale. These materials are therefore isotropic. In the case of ultrasonic wave propagation, when the wavelength is much greater

than the grain size, isotropic assumptions are quite valid (Lane, 2014). Under these circumstances, bulk waves propagate with equal velocity in every direction. Hence, in an infinite¹ isotropic material, wave energy may only propagate in two modes: longitudinal or shear. The equation of motion for an elastic isotropic solid can be decomposed into the following two wave equations relating the velocity of propagation of a longitudinal wave (c_l) and of a shear wave (c_s) to the material density ρ and the two constants used in Hooke's law for an elastic isotropic material (Young's Modulus, E , and Poisson's ratio, ν) (Rose, 1999; Lane, 2014).

$$c_l = \left(\frac{E(1-\nu)}{\rho(1+\nu)(1-2\nu)} \right)^{\frac{1}{2}} \quad (2.3)$$

$$c_s = \left(\frac{E}{2\rho(1+\nu)} \right)^{\frac{1}{2}} \quad (2.4)$$

However, if a wave encounters a boundary separating two media with different properties, part of the disturbance is reflected and part is transmitted into the second medium (Achenbach, 1973). Similarly, if a body has a finite cross-section which is comparable to the wavelength of the disturbance, waves can bounce back and forth between the bounding surfaces. Such circumstances can significantly increase the complexity of analysing the recorded wave signals and relating dynamic elastic properties of the material to travel time measurements. In many cases, this extra layer of complexity can be avoided by selecting the frequency of the signal generated by the ultrasonic transducer.

Standard test methods

UPV testing in the construction industry has traditionally been limited to P-wave measurements mainly used for inspection and quality control. As such, the most relevant standards for the purpose of this investigation only cover determination of the propagation velocity of ultrasonic longitudinal waves in hardened concrete (EN 12504-4:2004 (CEN, 2004) and ASTM C597 (ASTM, 2010)). Although the ASTM standard presents the relationship shown in Equation (2.3), it clearly states that the method should not be considered an adequate test for establishing compliance of the modulus of elasticity of field concrete with that assumed in the design. One of the reasons for this is that the relationship described in Equation (2.3) requires knowledge of the dynamic Poisson's ratio to determine the dynamic Young's modulus from the pulse velocity. Since the ASTM C597 standard is concerned only with determination of the velocity, it provides no indication of how to determine the Poisson's ratio.

The standard test method makes use of a pulse generator, a pair of electro-acoustical transducers, an amplifier, a time measuring circuit and a time display unit as shown in Figure 2.3.

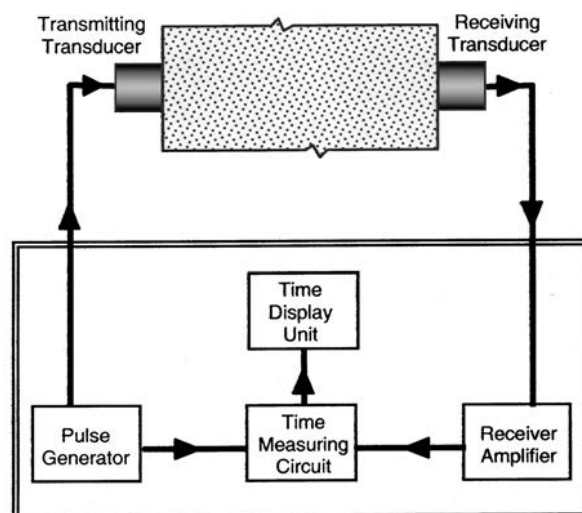


Figure 2.3: Ultrasonic Pulse Velocity (UPV) test set-up according to ASTM C597 (ASTM, 2010).

¹Note that in this context, infinite media means that boundaries have no influence on wave propagation (Rose, 2014).

It is stated that for best results, the transducers should be located directly opposite each other. The distance between centres of transducer faces must be measured, and the pulse velocity can then be calculated by dividing this distance by the pulse transit time measured using the apparatus as shown in Figure 2.3.

Wave propagation in anisotropic media

Previous research indicates that bricks formed by extrusion can exhibit a significant level of anisotropy (Fódi, 2011). Wave propagation in anisotropic media is substantially different from the isotropic case. The most significant difference is that elastic waves propagate with a velocity that depends on direction (Lane, 2014). Moreover, the number of independent constants which define the elastic behaviour of the material itself will be greater than 2 and will depend on the symmetry class or type of anisotropy assumed. Assuming an orthotropic material will result in 9 independent elastic constants while assuming transverse isotropy (material with a plane of isotropy) will result in 5. Furthermore, unlike the isotropic case, the wave modes are not necessarily pure modes as the particle vibration is neither parallel nor perpendicular to the propagation direction (Lane, 2014). In practice however, the anisotropic modes do show similarities to the isotropic modes and in these cases are referred to as quasi-longitudinal and quasi-shear. The quasi-shear modes are distinguished further by whether they are primarily horizontally (SH-waves) or vertically (SV-waves) polarized.

Christoffel's equations can be used to relate measured ultrasonic pulse velocities to the elastic constants. These expressions and related experimental procedures are not discussed here but a thorough description is given in (Rose, 1999). However, because the propagation of a wave along a specific plane does not depend on all the elastic constants used in the material definition, the experimental procedure has to include measurements across different planes. Moreover, the velocities of three wave modes (P-waves, SH-waves and SV-waves) need to be measured across each of these planes in order to determine the elastic constants. Hence, the full elastic characterisation of an anisotropic material cannot be directly determined using P-wave velocity measurements alone.

2.2.2. The relationship between static and dynamic elastic moduli

Since typical brick masonry constituents usually have negligible or very low tensile strengths, the elastic modulus in compression is often the most relevant material property related to elastic deformation.

As previously mentioned, experimental techniques that can be used to evaluate this property may be classified as static or dynamic. The former involves directly loading a specimen and measuring the corresponding change in strain. The static elastic modulus (E_{st}) is then computed by evaluating the slope of the experimental stress-strain curve in the elastic deformation range. On the other hand, as described in the preceding subsections, the dynamic elastic modulus (E_{dy}) can be derived from the measured resonant frequency of a specimen in a specific vibration test or from the measured velocity of a stress wave passing through the material. It is now well known that E_{st} can differ significantly from E_{dy} , with the latter generally being greater. It can be envisaged that this empirically known inequality arises mainly due to the fact that E_{dy} is measured at almost negligible stress levels compared to its static counterpart (Neville, 2011). However, studies have shown that this discrepancy is also due to the inherent heterogeneity of materials causing them to respond differently under cyclic or vibratory loading conditions (Neville, 2011; Philleo, 1955; Wesche; Manns, 1970; Bastgen; Hermann, 1977; Mashinsky, 2003).

For brittle materials, such as most typical brick masonry constituents, the static methods present significant challenges. Firstly, they are often very time consuming since they require gradually loading carefully prepared cylindrical or prismatic samples (Eissa; Kazi, 1988). Secondly, deformation magnitudes in the elastic range tend to be very low and can change relatively abruptly during loading due to the nature of the material (Binda; Tiraboschi; Abbaneo, 1997; Binda; Tedeschi; Condoleo, 2006; Baronio et al., 2003; Oliveira; Lourenço; Roca, 2007). Moreover, brick masonry constituents can contain noticeable heterogeneities that can significantly skew estimates of the deformation. Finally, most transducers that can be used to measure surface strains of such materials tend to be very sensitive to machine-specimen surface interaction (Binda et al., 1998). As such, it can be very difficult to obtain reliable measurements that reflect the actual elastic deformation of the material and the scatter of results is usually high, as evidenced in (Binda; Tiraboschi; Abbaneo, 1997; Binda; Tedeschi; Condoleo, 2006; Baronio et al., 2003; Oliveira; Lourenço; Roca, 2007; Pelà et al., 2016b).

Contrarily, the dynamic methods are much faster to execute and have the added benefit of being non-destructive. In addition, they do not suffer from the same limitation related to the difficulty of accurately capturing representative deformations. Therefore, as confirmed by the results presented in Section 3.2.2, most of the scatter in experimental results from such tests can usually be attributed to heterogeneity of the sample set rather than experimental error. However, for most common structural calculations, the statically determined modulus is preferred over that obtained by dynamic methods since the former is more representative of actual loading conditions. Given this fact, it is understandable why the correlation of these two parameters for brittle materials has received considerable attention, most notably for Portland cement concrete and for rocks.

Due to its widespread use as a construction material during the 20th century, a substantial research effort has been dedicated to better understanding the relationship between E_{dy} and E_{st} for concrete. In fact, in 1972, the empirical relationship shown below was even included in the now superseded British code of practice for the structural use of concrete (BSI, 1972).

$$E_{st} = 1.25E_{dy} - 19 \quad (2.5)$$

Where E_{st} and E_{dy} refer respectively to the static and the dynamic elastic modulus expressed in GPa .

It should be noted that this expression is not applicable for concretes with a cement content greater than 500 kg/m^3 or for lightweight concrete (Neville, 2011). To address this limitation, some researchers proposed the following expression for the latter (Swamy; Bandyopadhyay, 1975).

$$E_{st} = 1.04E_{dy} - 4.1 \quad (2.6)$$

A simpler general empirical relationship for concrete has also been proposed (Lydon; Balendran, 1986):

$$E_{st} = 0.83E_{dy} \quad (2.7)$$

As previously mentioned, the inherent material heterogeneity of concrete affects the two moduli (E_{st} and E_{dy}) in different ways. As such, studies have also been carried out in order to better understand how different material properties, such as compressive strength (f_c) or density (ρ_c), can influence the relationship between E_{st} and E_{dy} . As a result of this effort, it has been found that for concrete, the ratio of E_{st} to E_{dy} usually increases with increasing f_c (Takabayashi, 1954; Neville, 2011; Lee et al., 2017). Many researchers have also attempted to develop empirical relationships between E_{st} and E_{dy} that also incorporate other physical parameters. Although many of those ended up having a relatively limited range of applicability, one of the most useful expressions proposed for concrete does indeed suggest that the relation between E_{st} and E_{dy} is a function of density (Popovics, 1975):

$$E_{st} = \frac{446.09 \cdot E_{dy}^{1.4}}{\rho_c} \quad (2.8)$$

Where E_{st} and E_{dy} are once again to be specified in GPa and ρ_c is the density of hardened concrete in kg/m^3 .

Because of its relevance in the field of geomechanics, the relation between the static and dynamic elastic modulus of rocks has also received considerable attention (King, 1983; Heerden, 1987; Eissa; Kazi, 1988; Christaras; Auger; Mosse, 1994; Lacy, 1997; Horsrud, 2001; Ciccotti; Mulargia, 2004; Martínez-Martínez; Benavente; García-del-Cura, 2012; Brotons et al., 2014; Najibi et al., 2015; Fei et al., 2016; Brotons et al., 2016). Very detailed studies have been performed on certain specific types of rocks that have even allowed the influence of temperature and porosity on this relationship to be better understood (Brotóns et al., 2013; Brotons et al., 2014). However, the empirical relationships proposed by most authors are either applicable to only certain types of rocks or are valid for a limited elastic modulus range that tends to be greater than the elastic moduli of most typical brick masonry constituents. Of the several empirical relations available for rocks in the scientific literature, the following one proposed by Eissa and Kazi (Eissa; Kazi, 1988) could possibly lend itself to the case of brick masonry constituents since it was derived from a sample containing one of the most diverse set of rocks. Similarly to the expression proposed by Popovics for concrete (Equation (2.8)), the bulk density is also included as an explanatory variable in this relation.

$$\log_{10} E_{st} = 0.77 \log_{10}(\rho_r E_{dy}) + 0.02 \quad (2.9)$$

E_{st} and E_{dy} refer to the static and dynamic moduli of the rock in GPa while ρ_r refers to its bulk density in g/cm^3 .

Although the sample set used for the derivation of Equation (2.9) consists of a very diverse set of rocks, the compiled data used for the analysis also come from a wide variety of sources. It could therefore not be ensured that testing conditions have been kept constant for all specimens included in the analysis. It is well known that testing conditions can have a significant effect on the final estimated static or dynamic elastic modulus. A more recent study (Brotons et al., 2016), based on a dedicated experimental campaign on 33 specimens coming from 8 different igneous, sedimentary, and metamorphic rock types, proposes the following relationship instead.

$$E_{st} = 11.531 \rho_r^{-0.457} E_{dy}^{1.251} \quad (2.10)$$

With the static and elastic moduli expressed in GPa and the bulk density expressed in kg/m^3 .

The same authors also propose additional correlation models that incorporate total porosity and compressive strength of the rocks as additional explanatory variables. They report improved goodness of fit metrics with increasing level of complexity (Brotons et al., 2016).

In spite of the many empirical relationships proposed for concrete and rock, and despite the widespread use of brick masonry in construction, there exists very little research that attempts to explore this relationship for the case of brick masonry constituents. As previously stated, Totoev and Nichols do compare the static and dynamic moduli for some brick types (Totoev; Nichols, 1997; Nichols; Totoev, 1997), but no relationship is proposed for practical applications. As such, the relationship is still not well understood for the case of brick masonry constituents.

2.3. System identification and modal analysis

The work developed in the field of in-situ testing as part of this research specifically deals with the full-scale vibration testing of masonry bell towers. This involves the use of operational modal analysis (OMA) techniques to identify modal parameters (natural frequencies, associated mode shapes, and damping ratios) from recorded vibration signatures of the structure under investigation. The main difference between OMA and classical input-output experimental modal analysis (EMA) is that the type of input is considered as being a random process rather than a known force. As such, OMA can be performed without the need to apply and measure an artificial excitation. However, since OMA does not involve measurement of any input forces and relies solely on unmeasured ambient excitation, the mode shapes cannot be scaled in an absolute way and the frequency content of the excitation can be narrow-banded resulting in significant uncertainties. Hence, in some cases it is important to use different techniques for modal parameter extraction and compare the results in order to have a reasonable level of confidence on the estimates.

In general, it can be said that modal parameter extraction consists of the following 3 steps:

1. Data collection and pre-processing of the acceleration time-histories.
2. Identification of a linear system model.
3. Extraction of real modal parameters from the identified system.

There exists different system identification algorithms and techniques for modal parameter extraction that can be used in the context of OMA. Figure 2.4 summarises the general workflow as well as some of the most commonly used techniques for modal parameter extraction.

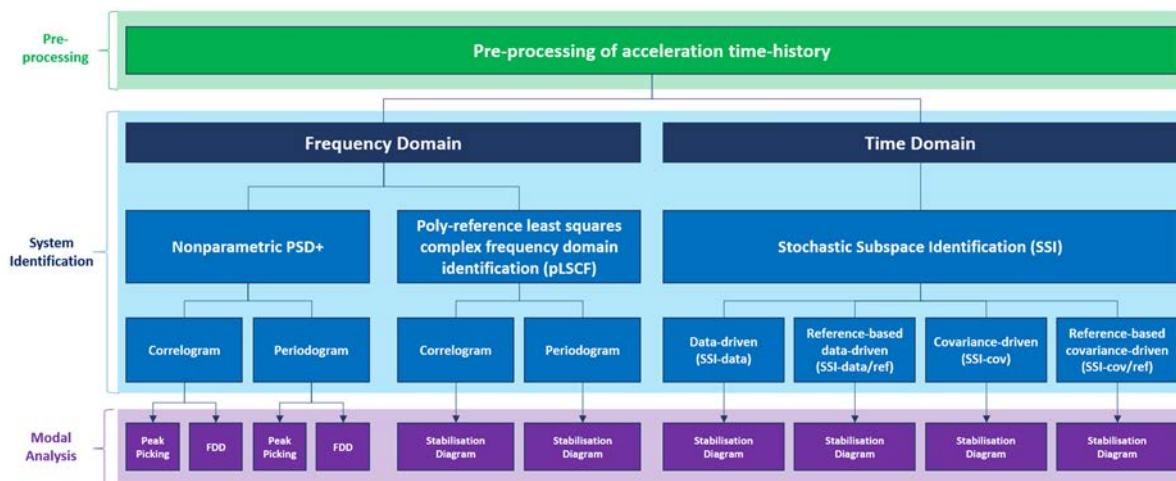


Figure 2.4: General workflow and common techniques for modal parameter extraction in the context of OMA.

2.3.1. Data pre-processing

Raw signals measured from accelerometers often have superimposed interference or excessive noise levels that may mask the required information. Moreover, they can lack certain characteristics required for display, recording, and transmission or further processing. It is for this reason that before attempting any system identification and subsequent modal analysis, some preliminary processing of the acceleration time-histories is usually required. The collection and pre-processing of data are not treated explicitly here, but an overview of standard techniques can be found in (Ewins, 2000; Maia; Montalvão e Silva, 1997; Heylen; Lammens; Sas, 1998).

2.3.2. System identification techniques

The different output-only system identification techniques introduced in Figure 2.4 are described briefly below:

- **Nonparametric PSD+ estimation:** In this identification method, the system model that will be identified is a Positive Power Spectral Density (PSD+) matrix at discrete frequency lines. The PSD+ between two channels is defined as the Fourier transform of the positive lags of the cross-correlation function (Reynders; Roeck, 2008). The natural frequencies can then be found by peak picking or Frequency Domain Decomposition (FDD).
- **Stochastic Subspace Identification (SSI):** Stochastic subspace identification methods involve modeling the dynamic behaviour of a vibrating structure as a discrete-time stochastic state-space model. For output-only cases, detailed knowledge of the excitation is replaced by the assumption that the system is excited by white noise.

In general, one main advantage of the SSI methods is that the only parameter that needs to be decided is the rank of the system. However, the resulting stabilisation diagrams after system identification used to extract modal parameters are not always clear. One of the reasons for this is that SSI, in most cases, will also predict false modes due to the algorithm itself as well as the excitation not satisfying the assumption of SSI that the input is zero mean white noise. Four commonly used variations of the SSI methods are shown in Figure 2.4. The algorithms behind each method are not discussed here; the reader can refer to (Reynders, 2012; Peeters; De Roeck, 1999; Peeters; De Roeck, 2001b) for a detailed description.

- **Poly-reference least squares complex frequency-domain identification (pLSCF):** This algorithm is a frequency-domain algorithm and therefore the first step of the algorithm is the estimation of the Positive Power Spectral Densities. Subsequently, a polyreference Least Squares Complex Frequency-domain algorithm is used to identify a Right Matrix Fraction Description model of the system (see (Reynders, 2012) for a more detailed description).

The main advantages of this method are that it is fast and yields much clearer stabilisation diagrams than the SSI methods. The main drawback of this method is that the damping estimates associated with

some stable poles decrease with increasing noise levels and this worsens for poorly excited modes.

2.3.3. Modal analysis of identified system models

Methods for extracting modal parameters from the system models identified using the techniques listed above are described briefly in this section:

- **Peak Picking and Frequency Domain Decomposition (FDD):** Peak Picking is one of the most intuitive of all available modal analysis techniques. It involves simply selecting peaks from the average normalised power spectral density (ANPSD) as shown in Figure 2.5 (a).

FDD involves plotting the singular values of the PSD matrix (obtained by adding the estimated PSD+ and its complex conjugate). The modal parameters can then be estimated by picking the peaks in the highest singular value(s). Note that for well-separated modes, only the highest singular value should be considered whereas for closely separated modes, other singular values should be considered as well. An example FDD plot is shown in Figure 2.5 (b). Note that neither the peak picking method nor the FDD method allow damping to be estimated directly.

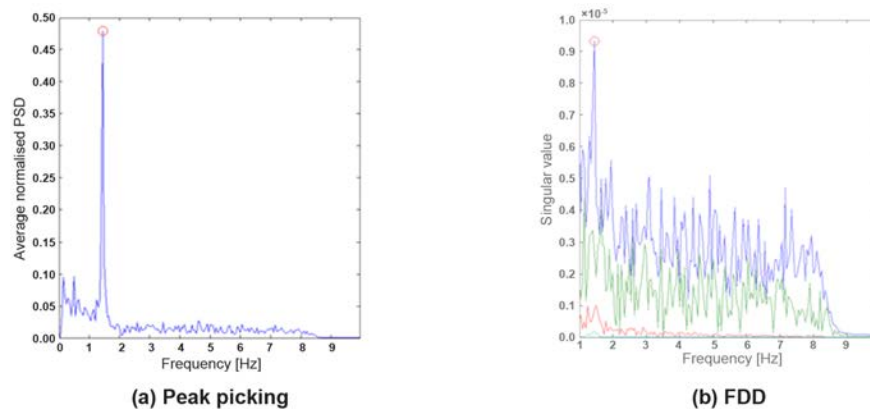


Figure 2.5: Examples of (a) peak picking and (b) FDD methods.

- **Stabilisation diagrams:** Stabilisation diagrams are representations of modal parameters identified using the pLSCF or SSI methods (see Figure 2.4). They allow the qualitative distinction of parameters that are stable for models of increasing order (points over the same vertical alignment) which are the modes with structural significance. The other parameters are numerical modes used to model the noise that exists in measured data.

Hence, using a stabilisation diagram, the estimation of any mode can be judged qualitatively from the continuity of the stabilisation column. Moreover, the estimation of any mode can also be judged quantitatively from the values of the modal phase collinearity (MPC), the modal phase (MP) and the modal phase difference (MPD). Values of MPC, MP and MPD close to 1, 0° and 0° respectively represent a more accurate estimation of the selected mode.

2.4. Static SHM for masonry constructions

A large number of the established cultural heritage sites worldwide are made of masonry and the common responsibility to safeguard them for future generations is now widely recognized. Although many of these old buildings prove their structural soundness by surviving to the present time in relatively good condition, many have suffered from considerable damages caused either by natural or man induced events throughout their history. In order to ensure their survival, an accurate evaluation of their current structural condition is often of paramount importance. However, recurrent uncertainties regarding material properties and the complex interaction among structural elements often makes the evaluation of their structural safety challenging, despite recent advances in structural analysis, inspection, testing, and monitoring techniques.

Structural health monitoring (SHM), which aims to gain knowledge of the integrity of in-service structures by monitoring damage sensitive features, can prove to be a very useful tool to better comprehend underlying causes of damage in structures. This is particularly true for heritage structures since the extraction of

a comprehensive set of samples for laboratory testing is often not feasible due to the heritage value of the structure. Moreover, excessive extensive interventions are undesirable in such cases due to the need to respect authenticity and “a correct diagnosis is [thus] indispensable for a proper evaluation of safety and for rational decisions on any treatment measures to be adopted” (ISCARSAH, 2005). Data from SHM can thus prove to be extremely valuable, particularly when ongoing deterioration mechanisms are still present.

In general, monitoring strategies to be applied can be categorised as static or dynamic. As shown in Figure 2.6, dynamic monitoring is oriented to the characterisation and control of dynamic properties such as natural frequencies, mode shapes and damping ratios (Elyamani et al., 2017a; Aras; Altay, 2015; Bassoli et al., 2018; Ivorra; Giannoccaro; Foti, 2019; El-Attar; Saleh; Zaghaw, 2005; Russo; Spoldi, 2020). Static monitoring is aimed at the continuous measurement of slow-varying parameters over a long period (Lorenzoni, 2013). Due to the slow progression of parameters of interest and because the data is largely influenced by seasonal cycles, monitoring periods of at least 2 years are usually required for meaningful conclusions to be derived from the data when it comes to static monitoring. In fact, due to the inability of commonly used analysis techniques to consider several factors and quantify uncertainties related to the analysis, longer monitoring periods are often required to establish a satisfactory level of confidence on resulting conclusions. Although recent research has focused more on data analysis for dynamic monitoring (Shi; Worden; Cross, 2016; Barontini et al., 2018; Khoa et al., 2018; Mario Azzara et al., 2018; Cabboi; Gentile; Saisi, 2017; Deraemaeker; Worden, 2018), presumably due to the fact that this monitoring strategy enables the extraction of useful information about the structure as a whole in a short time period, it must be said that masonry heritage structures are most often affected by slow ongoing deterioration mechanisms that are not easily identifiable. As such, static monitoring appears to be particularly appealing.

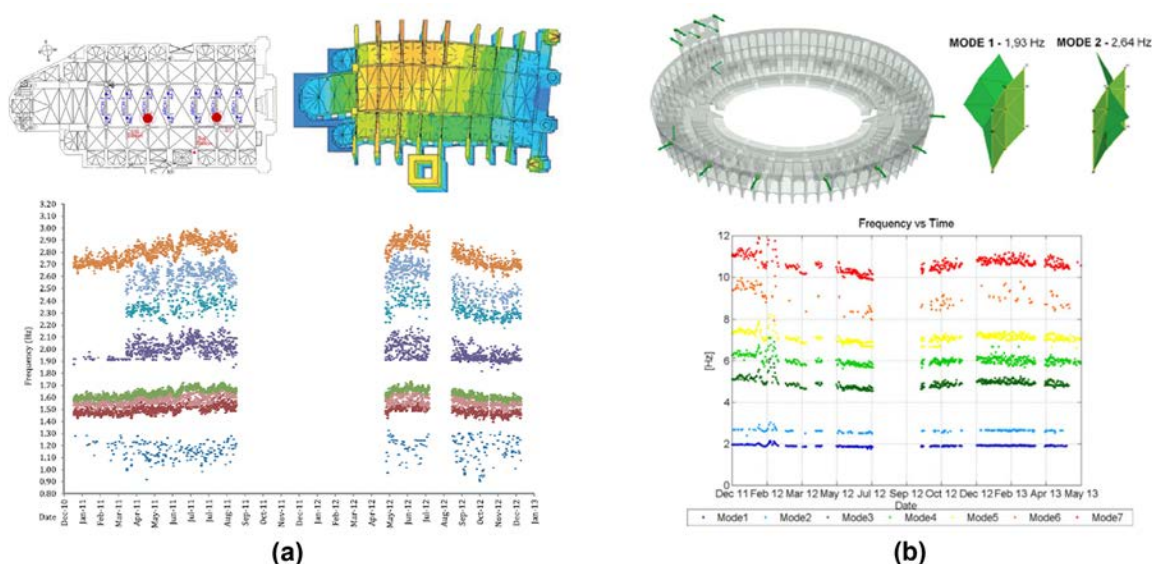


Figure 2.6: Examples of dynamic SHM from literature: (a) Mallorca cathedral (Elyamani et al., 2017a) and (b) the Roman Arena of Verona (Lorenzoni et al., 2013).

Since unreinforced masonry is characterised by a very low tensile strength, cracking is probably the most common pathology visible in masonry structures of the built cultural heritage. Because structural integrity can be impaired if cracks remain active, crack monitoring has emerged as one of the most important basic parameters in long-term heritage SHM systems (Baeza et al., 2018). Since lateral displacements or rigid rotations of key elements can also severely compromise structural performance, the inclination of such elements and distances between them are the other structural parameters that are most often also of interest.

In the case of static SHM, it is essential to remove any anomalies present in the data that are not caused by a physical phenomena related to structural behaviour before any further analysis can be carried out. These often appear as "spikes" in sensor data (Cornelis; Peeters, 2014) and can originate from several sources such as capacitive or inductive noise in the analog signal path, communication errors (Halfpenny, 2008) or undesired external interactions with the sensor. The initial interpretation task then involves the identification of either a stationary or an evolutionary condition from the recorded data of each monitored response. Al-

though this might appear simple in theory, in actual practice it proves to be difficult (Baraccani et al., 2017), given that features monitored for their sensitivity to damage are also sensitive to changes caused by environmental and operational conditions. In fact, it can even be said that this is a major issue prohibiting the extension of SHM technologies to structures in operation in the real world (Worden et al., 2007).

Nevertheless, there exists a number of data normalisation techniques that can be used to separate measurements relevant to structural damage from those associated with the environmental variation of the system (Sohn, 2007). In fact, there are several examples of static monitoring systems applied to masonry cultural heritage structures as shown in Table 2.1 and Figure 2.7. As shown, some recent static SHM systems have also been used in conjunction with ambient vibration testing (AVT) and/or dynamic monitoring (see Figure 2.7(b)). Examples of structures where such systems have been used include the monastery of J eronimos in Lisbon (Masciotta et al., 2016b), the Roman Arena (Lorenzoni et al., 2013) and the stone tomb of Cansignorio della Scala (Gaudini et al., 2008) in Verona as well as the Anime Sante church in L'Aquila (Russo, 2013).

Many of the above-mentioned investigations have relied on two basic procedures for the analysis and interpretation of the data collected from the static monitoring system. The first of which involves carrying out a simple linear regression from the recorded evolution of structural parameters such as crack widths and inclinations (response variables). If an underlying trend is found, the slope of the trend line allows the rate at which the phenomena in question is progressing to be estimated. The second procedure involves examining the correlation between temperature variations and the evolution of each response variable. In certain cases (Bartoli; Chiarugi; Gusella, 1996; Rossi; Rossi, 2015), analyses have attempted to remove the underlying periodicity present in crack width evolutions by examining the autocorrelation function of the signal and subtracting a sinusoidal function containing the signal's main period. Although it is true that a periodic sinusoid component fitted to the data is likely to contain the main seasonal behaviour, this theoretical formulation does not explicitly address the effect that measured environmental parameters (predictors) such as temperature or humidity have on the variation of monitored structural parameters. As such, careful implementation is required to avoid components not necessarily caused by seasonal variations from also being removed from the original signal during this processing step. Moreover, in this era of climate change, seasonal variations are becoming less predictable. Therefore it can no longer be assumed that their effects can always be accurately modelled by a regular periodic function.

Table 2.1: Notable examples of static SHM systems installed in masonry cultural heritage structures.

Structure	Monitoring start	No. of years*	No. of instruments	Combined with dynamic tests?
Santa Maria del Fiore - <i>Opera del Duomo system</i> (Bartoli; Chiarugi; Gusella, 1996; Ottoni; Blasi, 2015)	1955	55	22	No
Santa Maria del Fiore - <i>ISMES system</i> (Bartoli; Chiarugi; Gusella, 1996; Ottoni; Blasi, 2015)	1987	20	150	No
Basilica of San Marco (Rossi; Rossi, 2015)	1991	3.5	23	No
Metropolitan Cathedral in Mexico City (S�anchez; Meli; Ch�avez, 2015)	1994	10	38	Yes
Basilica S. Maria Gloriosa dei Frari (Rossi; Rossi, 2015)	2003	3.6	11	No
Cathedral of Modena (Baraccani et al., 2015)	2003	9	22	No
"Regina Montis Regalis" Basilica of Vicoforte (Ceravolo et al., 2017)	2004	10	133	No
Monastery of Jer�onimos (Masciotta et al., 2016b)	2005	9	10	Yes
Roman Arena of Verona (Lorenzoni et al., 2013)	2011	> 4	24	Yes
Church of the Major Seminary of Comillas (Blanco et al., 2018)	2012	5	67	No

* Minimum number of monitoring years (as reported in literature).

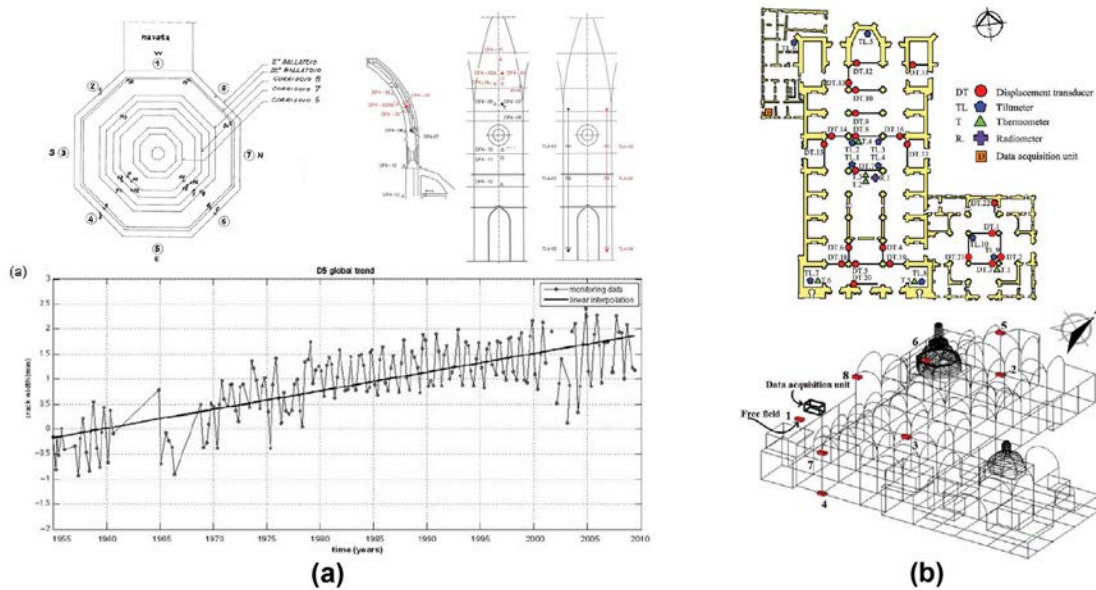


Figure 2.7: (a) Example from literature of two static SHM systems installed in the dome of Santa Maria del Fiore Dome in Florence, Italy. The evolution of the crack widths recorded by one of the oldest instruments is shown since the start of monitoring in 1955 (Ottoni; Blasi, 2015). (b) Example from literature of combined static and dynamic SHM (Sánchez; Meli; Chávez, 2015).

In order to provide a systematic way of dealing with seasonal changes, a simple method based on the evaluation of reference quantities was proposed (Baraccani et al., 2017). In fact, this method can be considered as one aiming to solve the well-studied problem of identifying directionality from a time series, whereby directionality is defined as asymmetry in time (Lawrance, 1991). As such, although it has been successfully applied to analyse data in a few heritage structures (Baraccani et al., 2017; Baraccani et al., 2014), like many methods developed to detect directionality in other fields of study (Mansor et al., 2016), it cannot explicitly consider the effect of measured predictors on the response parameters.

Some authors have intentionally searched for methods that do not require the measurement of environmental variables, arguing that with approaches having this requirement, all factors influencing the parameters of interest must also be monitored and understood in order to have reasonable confidence in any model prediction capability (Cross; Worden; Chen, 2011). As a consequence, a method based on finding a stationary linear combination among monitored responses, known as cointegration, has been successfully applied to eliminate the adverse influence of environmental changes from dynamic SHM data whilst maintaining sensitivity to structural damage (Cross; Worden; Chen, 2011). However, although such combinations can often be found between two identified natural frequencies, the local nature of response variables in static SHM systems means that finding such combinations can be difficult. Recently, an enhancement of the cointegration approach has been proposed making it more suitable to confronting cases when nonlinear relations between system responses exist (Shi; Worden; Cross, 2016). However, since it is based on a Bayesian machine learning approach known as Gaussian process regression, it requires a training period that does not contain any data corresponding to damage (Shi; Worden; Cross, 2016). In fact, this is also a requirement of many other sophisticated analysis methods that have been applied to damage detection in the presence of environmental variability from dynamic SHM data. These include negative selection (Barontini et al., 2018), other machine learning techniques (Worden et al., 2007; Khoa et al., 2018) as well as those based on linear and kernel principal component analysis (PCA) (Reynders; Wursten; Roeck, 2014; Mario Azzara et al., 2018; Cabboi; Gentile; Saisi, 2017) or on the Mahalanobis squared-distance (Deraemaeker; Worden, 2018). This is a difficult requirement when it comes to static SHM systems for masonry heritage structures since the damage phenomena of interest very often relate to very slow and long processes which have begun long before any decision on monitoring could be taken. Moreover, for such cases, previous studies have shown that temperature is clearly one of the most influential environmental factors contributing to the seasonal variations of the local response parameters being monitored. As such, since temperature monitoring can easily be included in any modern monitoring system with very little additional cost, the current research will focus on a method which takes advantage of measured predictors.

One of the simplest approaches which explicitly takes measured environmental variables into consideration was used for filtering out the effect of temperature from crack widths monitored as part of the static monitoring system in the dome of Santa Maria del Fiore (Ottoni; Blasi, 2015). The method attempts to remove the periodicity of the response variable caused by the predictor by simply subtracting the corresponding effect from the identified general linear trend found between the two. A key assumption behind this method is that a linear relationship exists between the selected structural and environmental parameters even if this is not always an adequate representation. Moreover, it can be assumed that due to the thermal inertia of the material, among other factors, the crack width at any point in time will in fact depend not only on the current temperature but also on previous ones. Another limitation of this method is that only a single predictor can be used to filter out the environmental variability of the response variable.

Nevertheless, meaningful conclusions on the state of the structure in question could still be derived from the data of all the previously mentioned static monitoring systems. Indeed, these examples show that static SHM can prove to be a powerful tool with respect to the diagnosis of heritage structures. It must be said however, that in every case, expertise and previous experience of the interpreter still play a vital role in the ability to draw conclusions from the processed data. Moreover, most of the procedures that have been applied to the analysis of data from static SHM systems of heritage structures provide no means of adequately quantifying the uncertainties or understanding the confidence levels associated to the estimated trends.

Utilising statistical black box models could prove to be an appealing alternative to remove the effects of environmental factors on measurements since they can exploit a large number of observations to reconstruct dependencies between recorded parameters. In particular, dynamic linear regression models able to represent response variables when they depend linearly on their own rate of change, on the rate of change of predictors as well as on the present value of the predictors appear to be ideal. Although there exists some examples (Peeters; De Roeck, 2001a; Ramos et al., 2010; Kita; Cavalagli; Ubertini, 2019) which make use of such models to filter out environmental effects on the evolution of natural frequencies extracted from dynamic monitoring systems, application to static SHM systems has been very limited. In fact, one of the only examples available in literature involves application to the monitoring of a crack on frescos present in Battuti Hall of Conegliano cathedral (Lorenzoni et al., 2016). In this case, a Single Input-Single Output (SISO) model that comprehends an Auto-Regressive output and an eXogenous input (ARX) was used. Unlike the case of simple linear regression, the dynamic nature of these regression models mean that they are well suited to model complex environmental effects such as those due to thermal inertia.

Although the quality criteria presented in previous research (Peeters, 2000; Peeters; De Roeck, 2001a; Lorenzoni et al., 2016) can facilitate the choice of adequate ARX model orders, a systematic methodological procedure for the implementation of such models to the analysis of data from complete masonry heritage static SHM systems is still missing from literature. Moreover, to the best of the authors knowledge, Multiple Input-Single Output (MISO) ARX models incorporating both interior and exterior temperatures as predictors have not yet been applied to the case of static SHM systems. Utilising such models could theoretically allow the identified models to better represent the environmental variability imposed on the response variables since they would be able to incorporate effects caused by thermal gradients. In addition, it should also be noted that despite the theoretical advantages of this method over some of the more traditional analysis techniques, applications to large data sets from whole networks of sensors in complex heritage structures is still lacking in literature. It is only through such applications that a well-defined systematic procedure can be developed to move from the analysis results to the diagnosis of the structure as a whole.

2.5. Risk assessment and decision-making

As stated in the introduction, there are several examples in literature of applications of multi-criteria decision-making (MCDM) techniques for general vulnerability or risk assessment to facilitate decisions on preventive conservation at the urban or territorial scale (Ortiz; Ortiz, 2016; Tena; León, 2016; Ruiz-Jaramillo et al., 2019; Piñero et al., 2017; Dutta; Husain, 2009). Although these proposed MCDM tools all differ in terms of the specific criteria they employ, they all share some common points. Firstly, they are all indicator-based and rely on one of the simplest and most widely used MCDM techniques known as simple additive weighting (SAW). This technique consists in the addition of normalised criteria scores weighted by corresponding relevance factors

defined in a previous step. The popularity of this technique stems from its very simple and transparent calculation procedure and from the fact that it is very intuitive for decision-makers. Naturally, this simplicity comes at the price of strong assumptions on the decision problem that need to be considered carefully. The additive value model behind SAW means that attributes are assumed to be preferentially independent. This means that preference regarding the value of one attribute is not influenced by the values of other attributes at the same hierarchy level of the decision problem (Yoon; Hwang, 1995; Dyer, 2005). In addition to this, SAW can only deal with maximising positive defined criteria, meaning that any minimising criteria need to be properly converted to maximising ones (Navarro; Yepes; Martí, 2019; Velasquez; Hester, 2013). In spite of these limitations, successful applications of the technique for prioritisation of preventive conservation at the territorial level is a clear indicator that it can be adapted to provide meaningful insights for decisions on heritage structures. Some authors have even attempted to complement their proposed index representing global damage risks with a decay model to predict the service life and the evolution of maintenance costs over time (Tena; León, 2016).

With respect to masonry structures, although there are some examples of MCDM applications for the assessment of general damage vulnerability at a territorial scale, applications that have had the greatest success in terms of widespread use in practice specifically involve the evaluation of seismic vulnerability. This is a direct consequence of the increase in losses caused by natural catastrophes in the last few decades and the subsequent need to assess and prioritise vulnerability among large stocks of existing buildings in earthquake-prone regions. In one of the earliest applications of MCDM techniques to this problem, the seismic vulnerability is expressed through a Vulnerability Index computed from 10 key attributes using SAW (Benedetti; Benzoni; Parisi, 1988). The choice of the specific attributes as well as the index formulation are based on a vast set of post-earthquake damage observations together with expert judgements. This method and adaptations of it have been applied extensively in Italy in the past few decades (Calvi et al., 2006). Another interesting application, known as the Macroseismic Method (Giovinazzi; Lagomarsino, 2004), employs vulnerability curves derived for different standard vulnerability classes and building typologies using fuzzy set theory and post-earthquake damage data. The curves relate a standard measure of seismic intensity to physical damage and are introduced as a function of a single vulnerability index. This vulnerability index can be refined using a seismic behaviour modifier and a regional factor. The seismic behaviour modifier is constructed using SAW. A hybrid method has also been proposed that utilises components from both aforementioned methods for the seismic vulnerability assessment of masonry structures in a historical city centre in Portugal (Vicente et al., 2011). Based on available data, changes were also made to attributes and weights of the index developed for use in Italy. This method has also been adapted and applied to other historical city centres. The same method has been further modified for the seismic vulnerability assessment of vernacular architecture (Ortega et al., 2019). In this case, two different approaches were employed for determining the relative weights between attributes. The first involved performing multiple linear regression on results from an extensive parametric study using numerical models. The second approach was based on expert opinion collected through a survey designed to be processed using the Analytic Hierarchy Process (AHP), a popular decision analysis method (Saaty, 1990; Navarro; Yepes; Martí, 2019; Velasquez; Hester, 2013). This method has also been used by some researchers to consider artistic and architectural value in a seismic vulnerability assessment approach based on the analysis of macro-elements (Sangiorgio; Uva; Adam, 2020).

In many natural-hazard-prone areas, the assessment of seismic risk alone might not be sufficient for the prioritisation of disaster risk reduction and resilience-enhancing strategies. To address this, some researchers have recently proposed a multi-hazard risk prioritisation index for cultural heritage assets which was calibrated and applied to 25 heritage buildings in the Philippines (Sevieri et al., 2020). The computation of the index relies on data collected through a standard rapid-visual-survey form. Two separate risk prioritisation indices related to the seismic and wind hazard are first computed. Both make use of SAW with weights determined using the AHP. In this particular application (Sevieri et al., 2020), the multi-hazard risk prioritisation index was calculated as the Euclidian norm of the vector with single-hazard prioritisation indices as components. This means that the single-hazard risk indices need to have the same range of variation and that the multi-hazard risk index will be characterised by a different range. Nevertheless, the authors do mention that combination weights can be used instead of the Euclidean norm because the relative effect on the built environment of two different catastrophic events can change completely depending on the return period considered.

On another note, as a result of the large heterogeneity across the global masonry building stock together with the potential complexity of the diagnosis task, there have been very few attempts at developing systematic diagnosis decision support tools for masonry structures. Two notable tools have been developed which guide the user to possible causes of observed damage from visual inspections (Van Balen, 1996; De Vent, 2011). Both methods can be considered as expert systems that rely on extensive damage databases together with the systematization of expert diagnostic knowledge through hierarchical decision trees. One of these methods, initially named *Masonry Damage Diagnostic System*, was designed specifically for evaluating the possible causes of degradation in brick masonry structures (Van Balen, 1996), and could even incorporate laboratory results to refine the diagnosis. One of the aims behind this inclusion was to prove the interest of different analysis types and to stimulate the use of proper diagnosis activities. Applications of this expert system have produced very satisfactory results and revealed that the increase of systematisation in the diagnosis process forces users to think through the problem and facilitates the collection of information from different partners and experts in a structured way (Van Balen, 1996). This diagnostic system was later expanded to include more materials, like plasters and natural stone, and renamed *Monument Damage Diagnosis System* (Hees; Naldini; Lubelli, 2009). Another notable system worth mentioning, called *Doctor House* (Bernat; Gil, 2013), was developed for the more general diagnosis of pathologies of structural elements. Although these expert systems can help in the identification of specific damage causes, they cannot take into consideration information from structural analysis, SHM, or NDT. Moreover, the diagnosis task addressed by such expert systems is only a preliminary task before safety and subsequent vulnerability assessment.

The methods, mechanisms, and criteria employed by the indices and expert systems described in this section have all been considered during the development of the tools proposed as part of this research. Nevertheless, it must be said that the proposed approach is inherently different from all those described here.

3

Materials testing

3.1. Introduction

The research work carried out on materials testing first involved the development of a robust procedure for estimating the dynamic elastic properties of brick masonry constituents (Section 3.2). Subsequently, estimates obtained using the proposed procedure were used to establish an empirical relation between the dynamic and static elastic moduli of such materials (Section 3.3).

3.2. Estimating dynamic elastic properties of masonry constituents

The main aim of this part of the research is to assess the applicability of a combined procedure based on two non-destructive techniques to experimentally determine both the dynamic Young's modulus and shear modulus of brick masonry constituents. The two chosen methods are UPV testing with P-waves and IEV testing. The theory behind these two methods, as well as the respective procedures for the estimation of the dynamic elastic properties, are described in Section 2.2.1. The two techniques were selected not only because of the simplicity and speed of their application, but also because they make use of equipment that is nowadays widely used in the construction industry and hence relatively accessible. UPV testing with P-wave transducers is commonly used for non-destructive quality control of concrete while accelerometers and data acquisition systems required for IEV testing are used for dynamic response testing and monitoring of many structures, such as bridges and towers. Moreover, the research also aims to test whole brick specimens since this would allow these methods to be applied to recently manufactured bricks as well as to those extracted from existing constructions. For the dynamic tests, mortar specimens were also cast in moulds having dimensions of a standard brick ($290 \times 140 \times 40 \text{ mm}^3$).

Different types of bricks and mortars were explored in order to derive useful ranges of results for different masonry typologies. Although an effort has been made to include specimens of varied quality and porosity in the sample set to appropriately validate testing protocols and analysis procedures, explicitly defining the relationship between porosity or chemical composition of the materials to the dynamic elastic properties is beyond the scope of this research. Previous studies available in literature such as (Asmani et al., 2001) and

Parts of this chapter have been published in:

- MAKOOND, N.; PELÀ, L.; MOLINS, C., 2019. Dynamic elastic properties of brick masonry constituents. *Construction and Building Materials*. Vol. 199, pp. 756–770. ISSN 09500618. Available from DOI: 10.1016/j.conbuildmat.2018.12.071
- MAKOOND, N.; CABANÉ, A.; PELÀ, L.; MOLINS, C., 2020a. Relationship between the static and dynamic elastic modulus of brick masonry constituents. *Construction and Building Materials*. Vol. 259, p. 120386. ISSN 09500618. Available from DOI: 10.1016/j.conbuildmat.2020.120386

(García, 2018) address these relationships more directly for specific types of materials (alumina ceramics and specific stones).

As a result, a robust methodology, combining information from both UPV and IEV testing, for the determination of dynamic elastic properties of typical brick masonry constituents is proposed.








3.2.1. Experimental program

The experimental campaign was carried out at the Laboratory of Technology of Structures and Building Materials of the Universitat Politècnica de Catalunya (UPC-BarcelonaTech). This subsection presents information about the material components, the preparation of the specimens and the dynamic testing procedures.

3.2.1.1. Materials tested

7 different groups of solid bricks were tested in order to investigate different types of materials, both used in existing and new constructions. 5 of these groups (I(a), I(b), III, V(a) and V(b)) consisted of handmade bricks formed by moulding. Of these, 2 groups (I(a) and I(b)) consisted of solid terracotta bricks, tested after production, before use in any construction project. On the other hand, group III bricks have been extracted from an industrial complex built in the early 20th century, part of Barcelona's industrial heritage. Bricks from group V(a) and V(b) were extracted from a typical residential building located in Rambla de Catalunya, a street in the centre of Barcelona. It should be noted that the UPV testing procedure for specimens from group V(b) consisted of less measurements (more detail is given in Section 3.2.1.3). The 2 groups of solid bricks manufactured using a conventional extrusion process (II and IV) were both tested before use in any construction project. The type of bricks from group II have been used to build timber vaults in an ongoing construction project in Barcelona. Finally, bricks from group IV are manufactured using an automated process and are compliant with the EN 771-1:2011 standard (CEN, 2011). A brief summary of the different groups tested is given in Table 3.1.

Table 3.1: Groups of brick types tested.




Group	Specimen labels	Manufacturing	Year	f_{cn}^* [MPa]	Average bulk density [kg/m ³]	Average measured dimensions [mm ³]	Sample view
I(a)	1 - 7	Handmade in moulds	2017	16.1 ± 16%	1,781 ± 1%	40 × 147 × 306	
I(b)	T1 - T6	Handmade in moulds	2015	17.0 ± 15%	1,768 ± 3%	40 × 146 × 306	
II	SF1 - SF5	Conventional extrusion	2016	40.0 ± 16%	1,655 ± 0.3%	38 × 141 × 291	
III	FC1 - FC3	Handmade in moulds	1903	8.0 ± 17%	1,598 ± 5%	43 × 144 × 294	
IV	A1 - A6	Conventional extrusion	2018	53.2 ± 8%	1,673 ± 0.4%	40 × 132 × 272	
V(a)	RC6,RC8	Handmade in moulds	1930	8.3 ± 43%	1,720 ± 1%	40 × 145 × 291	
V(b)	W2L1 - W2L5, W2L7	Handmade in moulds	1930	10.7 ± 15%	1,718 ± 1%	43 × 145 × 294	

* Reference normalised compressive strength for corresponding brick type obtained by testing bricks in accordance with the European standard EN 772-1 (CEN, 2010).

Two different types of mortar, which can be considered as being at either end of the range of stiffness encountered in typical brick masonry structures, were prepared and tested. The first mortar type consisted

of a hydraulic lime weakened by adding recycled limestone filler to the mixture in order to match mechanical properties more representative of mortars found in historical constructions (MB and MIIB) (Segura et al., 2020). For both mortars MB and MIIB, 50% of the powder volume was replaced by the limestone filler. The main difference between specimens from these two groups is that those from group MB were unmoulded 5 days after initial casting whereas those from group MIIB were unmoulded after 14 days. This change was implemented because specimens from group MB were found to be too fragile at the time of unmoulding (Makoond; Pelà; Molins, 2019). Specimens from group MB were tested 32 days after initial casting while MIIB specimens were tested after 27 days. The second mortar type considered consisted of a typical cement mortar used in new constructions (MC). This type of mortar was chosen because it can serve as a good control sample, not only due to the many studies that have been carried out on the properties of Portland cement mixes, but also because it is relatively easy to prepare homogeneous and isotropic specimens from this material. Since several studies (Boulay et al., 2013; Ramesh; Azenha; Lourenço, 2019) reveal that such mixes have usually already gained between 85-90% of their stiffness after just 4 days, it was deemed suitable to test MC specimens after 14 days. Key characteristics of the different mortar specimen groups tested are summarised in Table 3.2.

Table 3.2: Groups of mortar types tested.

Group	Specimen labels	Mix proportions (by weight)	f_{cn}^* (28 days) [MPa]	Average bulk density [kg/m ³]	Average measured dimensions [mm ³]	Sample view
MB	MB1 - MB5	Lime : filler : water 1 : 0.64 : 0.37	2.3 ± 6%	1,776 ± 2%	41 × 139 × 290	
MIIB	MIIB1 - MIIB8	Lime : filler : water 1 : 0.64 : 0.37	2.0 ± 12%	1,932 ± 1%	42 × 139 × 290	
MC	MC1 - MC5	Cement : sand : water 1 : 3.2 : 0.33	48.8 ± 5%	2,183 ± 1%	41 × 139 × 291	

* Reference normalised compressive strength for corresponding mortar type obtained by testing prismatic specimens in accordance with the European standard EN 1015-11 (CEN, 2019).

3.2.1.2. Impulse excitation of vibration testing

Testing equipment

For each IEV test, a suitable data acquisition system able to record the vibrations of the specimen was required so that the resonant frequency could then be extracted from the resulting acceleration-time history. The data acquisition system designed for these tests consisted of a lightweight (25 g) triaxial integrated circuit piezoelectric accelerometer (PCB 356B18), a signal conditioner (PCB 482A16) and an embedded real-time controller (cRIO-9064) equipped with a vibration input module (NI-9234). During testing, the real-time controller was connected to a laptop equipped with a program specifically created for these acquisitions using the LabVIEW 2016 programming environment (National Instruments, 2016).

Specimen preparation

It is clear from Equation (2.1) that the accuracy of the estimated dynamic elastic modulus is highly dependent on the regularity of the specimen and the uncertainty related to its dimensions. For instance, since the thickness and length variables in the modulus equation have an exponent of 3, an error of 1% in these dimensions would result in an error of 3% in the estimated modulus. Hence, in order to reduce the variations in dimensions within each specimen, the surfaces of brick specimens were polished in order to regularise the faces.

It is important to note that moisture content of the specimens can have an effect on the observed resonant frequency and hence on the estimated dynamic elastic properties. In order to control this parameter, all specimens were dried before testing at 120°C in a drying oven until the mass was constant as recommended in (ASTM, 2001).

Preparation of specimens also entailed marking the lines along which each specimen should be supported during testing to isolate the fundamental flexural and torsional modes. Finally, the impact and sensor

locations were also marked as shown in Figure 3.1 in order to facilitate mounting of the sensor and ensure consistent impulse excitations.

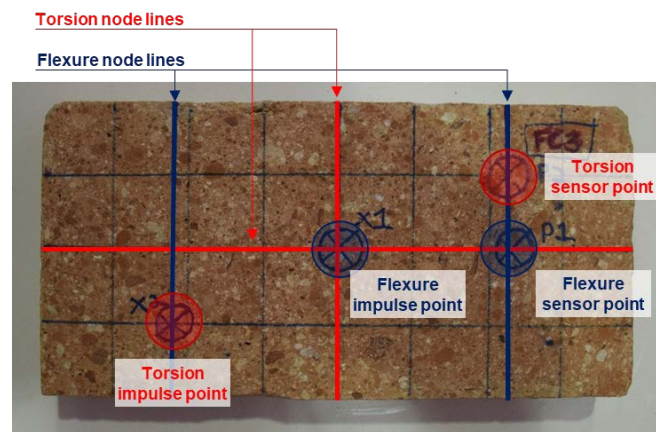


Figure 3.1: Markings made on every specimen prior to IEV testing.

Test set-up

Simple custom rigid supports were fabricated in order to isolate the flexural and torsional modes. For all tests, the supports were placed on isolation pads in order to prevent ambient vibrations from being picked up by the accelerometer. The supports were metallic and had a sharp edge in contact with the specimen along the nodal lines. The supports can be seen in Figure 3.2 which also shows the test set-ups used for flexural (a) and torsional (b) IEV tests on whole bricks.

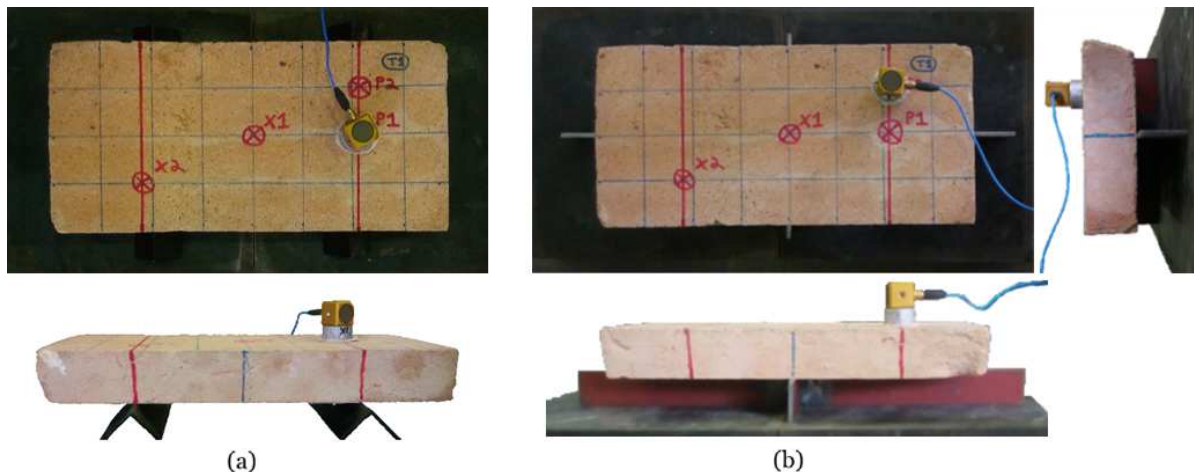


Figure 3.2: (a) Test set-up for flexural IEV test (view from top and front). (b) Test set-up for torsional IEV test (view from top, front and side).

For all tests on bricks, the accelerometer was fixed using an adhesive mounting technique via a lightweight (18 g) aluminium mounting plate fixed to the brick's surface using a 2-component cold curing superglue. This ensured adequate vibration transmissibility while also reducing any mass loading effects (see Figure 3.2). Although this technique proved to impart very little damage on most bricks, removal of the mounting plate did cause some loss of material from the surface of many bricks. This loss of material proved to be quite significant in the case of the fragile MB Mortars. Since one of the secondary aims of this research campaign is to keep the specimens as intact as possible for further testing, a less intrusive mounting method was desirable, particularly for the more fragile lime mortar specimens. Hence, a different mounting technique was tested which involved fixing the accelerometer on the surface of the specimen using scrim-backed adhesive tape as shown in Figure 3.3. Naturally, this technique further reduces any mass loading effects since the mass of the adhesive tape is much lower than that of the mounting plate. However, since it is a less commonly used mounting technique than the aforementioned one, the adequacy of its vibration transmissibility had to be verified for the purpose of these tests. In order to achieve this, a comparative study was carried out between the two mounting methods on all the specimens from the MB mortar group. The observed resonant

frequency was found to differ by less than 1.2% across all the specimens. Hence, the mounting technique with the scrim-backed adhesive tape was used to test all mortar specimens to avoid any further damage to the specimens.

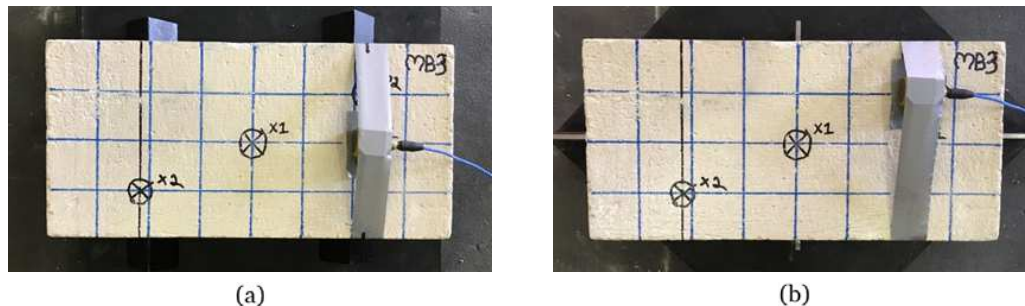


Figure 3.3: Accelerometer mounting using scrim-backed adhesive tape for (a) flexural test set-up and (b) torsional test set-up of IEV tests.

Another important consideration before testing any specimens involves selecting an appropriate sampling frequency to be used for all the tests. Based on the capabilities of every element of the data acquisition system, a sufficiently high sampling frequency must be chosen to prevent any aliasing. This requires an estimation of the expected resonant frequencies that need to be measured. In the case of the specimens tested for this research campaign, the observed resonant frequencies varied from 586 Hz to 1794 Hz for the flexural tests and from 746 Hz to 2099 Hz for the torsional tests. A sampling frequency of 20 kHz was used for all the IEV tests.

Testing procedure

Before actually executing the vibration tests, the mass and dimensions of each specimen had to be determined accurately for consequent computation of the dynamic elastic properties. The mass was determined using an electronic balance with a resolution of 0.5 g, satisfying the requirement stipulated in the ASTM standard for all specimens tested (0.1% of the specimen mass (ASTM, 2015)). Each dimension was taken as the average of multiple readings along each of them at the locations shown in Figure 3.4. These measurements were taken with a Vernier caliper with a precision of 0.02 mm. The multiple measurements were not only used to compute the average dimensions but also to quantify the variation in dimensions of the specimens. The coefficients of variation of all dimensions of all specimens were found to be less than 2% except for 6 specimens which had coefficients of variations of less than 4% for the measured thickness dimensions.

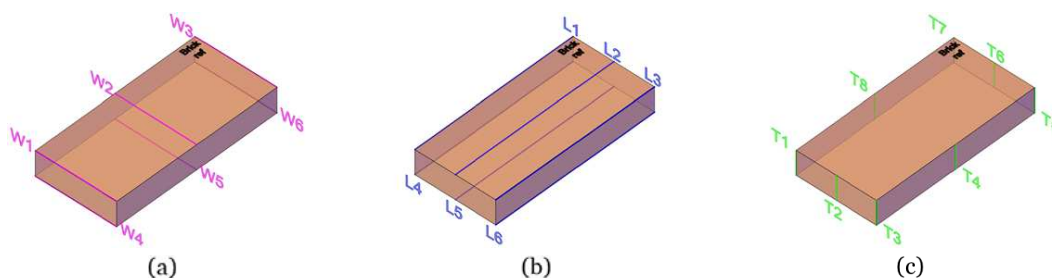


Figure 3.4: Locations of the 20 measurements taken with a Vernier caliper for every specimen tested under IEV. (a) 6 measurements of the length taken for every specimen. (b) 6 measurements of the width taken for every specimen. (c) 8 measurements of the thickness taken for every specimen.

Once the set-ups described in the previous section have been prepared, the IEV tests simply involve applying an impulse at the specified location using an impact tool which satisfies the requirements stated in (ASTM, 2015). In practice, the size and geometry of the tool depends on the size and weight of the specimen and the force needed to produce vibration. In the case of the bricks, one of the most important considerations was to ensure that the impact was not too strong for the higher amplitudes of the recorded signals not to fall outside the measurable range of the accelerometer (± 5 g).

For each IEV test, the vibration signals were recorded whilst the specimen was impacted several times (see Figure 3.5). An appropriate feature extraction procedure needed to be implemented in order to extract

the resonant frequency from the acceleration-time histories. It should be noted that one of the requirements from the ASTM standard (ASTM, 2015) is to determine the resonant frequency as the average of five consecutive readings which lie within 1% of each other. Because of this requirement, it was essential to be able to estimate the resonant frequency during testing itself. Hence, the Frequency Domain Decomposition (FDD) technique was used, because it does not only allow fast estimation of the resonant frequency but also exploits the data recorded from the 3 channels of the tri-axial accelerometer for improved accuracy. A custom script for processing the files generated by the LabVIEW acquisition program and subsequently carrying out FDD analysis was created in the MATLAB[®] computing environment (MathWorks, [n.d.]) by modifying the original FDD script by (Farshchin, 2015). This process is summarised in Figure 3.5.

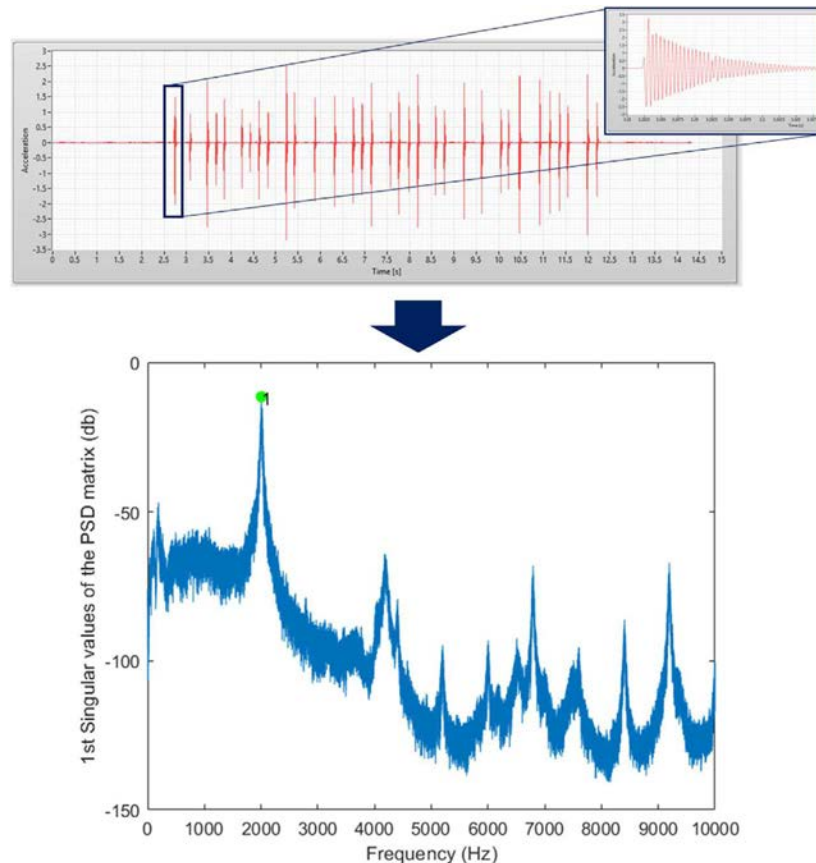


Figure 3.5: Top: Acceleration-time history for a single IEV test (with a zoom-in of a single impulse shown). Bottom: Selection of peak during FDD process.

Once the resonant frequencies were extracted, Equations (2.1) and (2.2) could be used to estimate the dynamic Young's modulus and shear modulus respectively. The iterative procedure described in Section 2.2.1.1 was used to estimate the dynamic Poisson's ratio and update the dynamic Young's modulus accordingly.

3.2.1.3. Ultrasonic pulse velocity testing

Testing equipment

The ultrasonic pulse travel times were recorded using a PROCEQ Pundit[®] PL-200 commercial ultrasonic testing instrument (PROCEQ, 2014). This equipment incorporates a pulse generator, receiver amplifier and time measuring circuit into one unit with a touch-screen display that can be used to view the waveform of recorded signals and pulse travel time in real-time. Different transducers can be used with this instrument, each of which is better suited for different applications.

The selection of the appropriate transducer is largely dependent on grain size and on the dimensions of the test object. The frequency of the transducer should be chosen so that the resulting ultrasonic pulse has a wavelength smaller than the minimum lateral dimension of the test specimen but at least twice as large as the grain size (PROCEQ, 2014). Since the wavelength is dependent on the velocity of propagation

(wavelength equals velocity divided by frequency), the selection of an appropriate transducer before testing the material is not so straightforward. It is known that the ultrasonic pulse velocity in concrete ranges from 3000 m/s to 5000 m/s (PROCEQ, 2014). Most materials tested as part of this campaign are characterised by lower velocities. In fact, the observed velocities vary from 1132 m/s (Type V(b) brick) to 4270 m/s (CM Mortar). A pair of 250 kHz transducers was used for all the UPV tests carried out as part of this research, resulting in wavelengths ranging from 5 mm to 17 mm. These wavelengths are all smaller than 38 mm, the smallest thickness encountered across all specimens. Although this range of wavelengths can also be considered as being greater than the average grain size of the materials under test, in some cases, the specimens contained significant heterogeneities such as voids or aggregates that are larger than the aforementioned wavelength range. Moreover, the specimens characterised by lower ultrasonic pulse velocities also turn out to be the most heterogeneous. This results in a greater likelihood of scattering affecting the reliability of the results for these specimens, since the wavelengths of the ultrasonic pulses are smaller while the effective grain size can be considered as being larger due to the heterogeneities. Taking multiple readings at different locations can help to improve the reliability of results in such cases.

Treatment of specimens

Besides using a coupling gel between the transducers and the material during testing, the surfaces of the bricks were polished beforehand to ensure a smooth surface and hence prevent excessive loss of signal due to inadequate acoustic coupling. Since all the mortar specimens were cast in specifically designed moulds, their surfaces were adequately smooth and no further polishing was carried out.

As is the case for IEV tests, moisture content of the specimens is another factor that can influence UPV results. Hence, to control this parameter, all measurements were made on oven-dried specimens which had been allowed to stabilise to room temperature.

The final preparation step before executing the UPV tests involved marking the locations through which the velocity will be measured in order to be able to accurately position the transducers and measure the corresponding path lengths. A 4×8 grid of equal divisions on the largest faces of each specimen was used to locate all path lengths across the length, width and thickness (see Figure 3.1).

Testing procedure

Before carrying out any UPV tests, masses and dimensions measured for the IEV tests were used to compute the densities of specimens which are required to evaluate dynamic Young's moduli using Equation (2.3).

All measurements of pulse transit times were carried out using direct transmission with the transducers arranged directly opposite each other, widely considered as the optimum configuration for accurate pulse velocity determination. Using the UPV evaluated in this way into Equation (2.3) can be considered as giving a very localised estimate of the elastic properties since the velocity is only representative of the path along which the pulse travelled. Since it is known that many types of brick masonry constituents can have a significant level of heterogeneity, and even anisotropy in some cases, it is important to determine the pulse velocity at multiple locations and even across different directions before utilising them to evaluate the elastic constants describing the overall material behaviour. For the purpose of this research, three different variables were defined to describe the elastic moduli computed from multiple pulse velocities evaluated across the three different directions of each brick-sized specimen (length, width, and thickness). They will hereafter be referred to as $E_{UPV,L}$, $E_{UPV,W}$, and $E_{UPV,T}$.

For the UPV tests across the length and width of specimens, the reported pulse transit time at a single location was taken as the average of five consecutive readings with a coefficient of variation of less than 2% to reduce the effect of any measurement errors. The pulse transit time was measured at 3 locations across the length as shown in Figure 3.6 and 3 locations across the width as shown in Figure 3.7. The path lengths at these locations were measured using a Vernier caliper and the pulse velocity was computed by dividing the path length by the transit time. $E_{UPV,L}$ was then computed from Equation (2.3) using the average of the computed velocities from the 3 length locations specified and the Poisson's ratio estimated from the IEV tests. $E_{UPV,W}$ was computed using exactly the same procedure but using the velocities computed from the transit times and path lengths measured across the width.

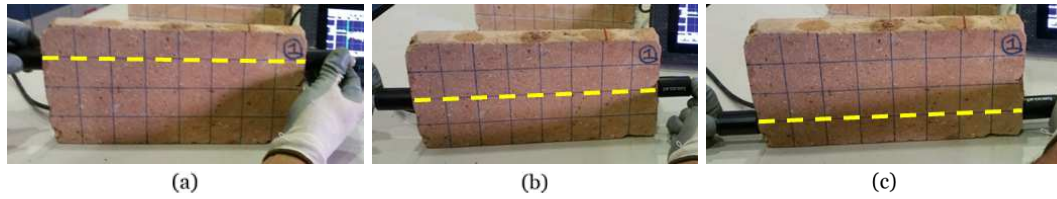


Figure 3.6: Locations of ultrasonic pulse travel time measurements across length: (a) Top quarter, (b) Middle, (c) Bottom quarter.

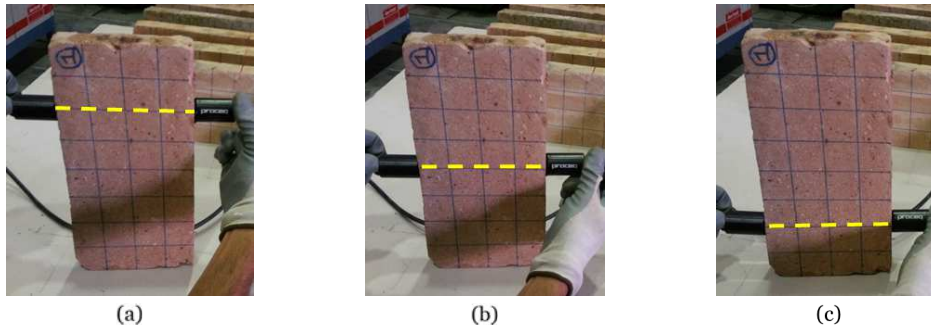


Figure 3.7: Locations of ultrasonic pulse travel time measurements across width: (a) Top quarter, (b) Middle, (c) Bottom quarter

Specimens from group V(b) were tested before the methodology described herein had been developed. As such, for specimens from group V(b), the transit time was only measured at the middle location across the length and the width. Moreover, no measurements of pulse transit times were taken across the thickness of specimens from this group.

For all other specimens, the procedure used for computing $E_{UPV,T}$ differed from that used for $E_{UPV,L}$ and $E_{UPV,W}$. Due to the shorter distance of the path length, it was expected that the effect of heterogeneities and scattering would be more significant. As such, the pulse transit time across the thickness was measured at 32 different locations on the face of each specimen as shown in Figure 3.8.

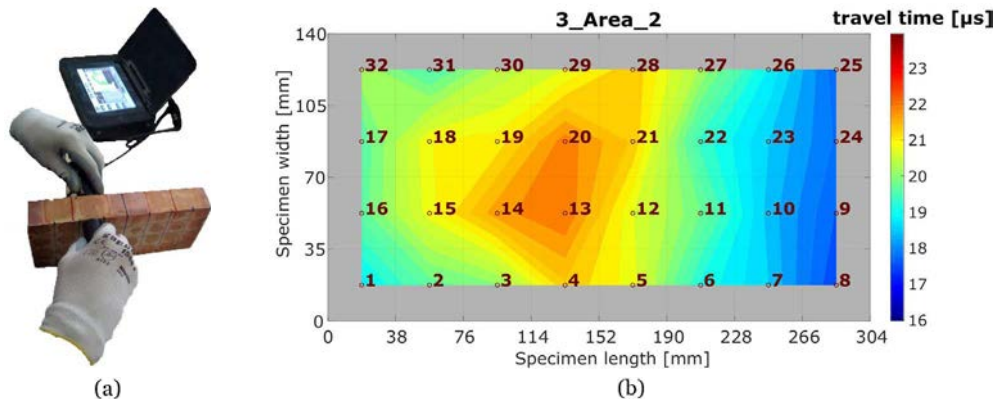


Figure 3.8: (a) Measurement of ultrasonic pulse transit time across thickness. (b) Example of an ultrasonic travel time colour map generated from 32 measurements over the face of each specimen.

The 32 measurements were used to generate travel time contour maps that could also be used to assess the heterogeneity of each specimen. In order to minimise the effect of measurement errors, two consecutive sets of 32 readings were taken for each specimen and corresponding readings that differed by more than 2% were eliminated from any further computation. Since taking 32 measurements of path length was both time-consuming and impractical (parts at the centre of specimens were difficult to access to measure accurately), the pulse velocity was computed by dividing the average of the 8 thickness measurements taken as part of the IEV procedure by the average of the 32 measurements of pulse transit times. $E_{UPV,T}$ was then computed for each specimen from this computed velocity and using the Poisson's ratio estimated from IEV testing.

3.2.2. Results of dynamic tests

As described in Section 2.2.1.1, the dynamic Young's modulus (E_{IEV}), shear modulus (G_{IEV}) and Poisson's ratio (ν_{IEV}) for each specimen were computed from the measured mass, dimensions and fundamental frequencies by direct application of Equations (2.1) and (2.2) through the procedure described in Figure 2.2. The average of these results for each specimen group are presented in Table 3.3. As can be expected, in the case of bricks, the specimens produced by extrusion (groups II and IV) have higher values of dynamic Young's and shear moduli. This is because they are generally of higher quality and less porous than the bricks handmade in moulds and therefore exhibit a more stiff elastic behaviour. Similarly, the more modern cement mortar specimens appear to be much more stiff than the weaker lime mortars.

Table 3.3: Final estimated dynamic elastic properties from IEV testing.

Specimen Group	Number of Specimens tested	Average values					
		E_{IEV} [MPa]	coeff. of variation	G_{IEV} [MPa]	coeff. of variation	ν_{IEV} [MPa]	coeff. of variation
35		Units					
I(a)	7	7,882	15%	3,530	15%	0.12	14%
I(b)	6	7,931	17%	3,628	17%	0.09	41%
II	5	18,313	1%	7,240	1%	0.26	7%
III	3	7,107	13%	3,309	10%	0.07	31%
IV	6	15,505	1%	5,733	1%	0.35	5%
V(a)	2	5,475	8%	2,525	5%	0.08	31%
V(b)	6	4,068	30%	1,965	29%	0.03	70%
21		Mortar					
MB	5	3,987	10%	1,811	9%	0.10	16%
MIIB	8	4,269	6%	1,886	6%	0.12	24%
MC	8	28,954	5%	11,417	3%	0.27	8%

In addition to the estimates of the dynamic properties from IEV tests, dynamic Young's moduli for every specimen were also computed using Equation (2.3) from the average ultrasonic pulse velocity across different directions, derived as described in Section 3.2.1.3. This results in three estimates of the dynamic Young's modulus from UPV tests for every specimen, corresponding to its three main dimensions ($E_{UPV,L}$, $E_{UPV,W}$, and $E_{UPV,T}$). The average of these results for each specimen group are presented in Table 3.4.

Table 3.4: Estimated dynamic Young's modulus from UPV measurements across different directions.

Specimen Group	Number of Specimens tested	Average values					
		$E_{UPV,L}$ [MPa]	coeff. of variation	$E_{UPV,W}$ [MPa]	coeff. of variation	$E_{UPV,T}$ [MPa]	coeff. of variation
35		Units					
I(a)	7	7,837	18%	8,241	19%	5,764	20%
I(b)	6	7,938	13%	8,189	15%	5,979	17%
II	5	13,756	4%	15,199	4%	8,924	5%
III	3	7,305	2%	8,717	7%	8,016	15%
IV	6	9,157	8%	7,109	8%	12,035	8%
V(a)	2	5,498	4%	6,336	7%	5,754	14%
V(b)	6	4,604	35%	5,538	22%	-	-
21		Mortar					
MB	5	4,527	6%	5,686	7%	6,230	7%
MIIB	8	4,887	16%	6,486	4%	6,123	2%
MC	8	28,601	4%	30,125	6%	29,236	4%

One of the most useful applications of the estimated dynamic Young's moduli across different directions is to evaluate if the specimens are actually isotropic. As such, a comparison of the relative scatters between these estimated properties for every specimen group is summarised in Table 3.5. The scatters are normalised to $E_{UPV,L}$ which can be considered the most reliable estimate from UPV tests carried out as part of this research. This is due to the fact that it is computed from the pulse velocity determined across the largest dimension of the specimens, hence minimising the effects of localised heterogeneities as well as those of measurement errors.

As described in Section 3.2.1.3, the 32 measurements of pulse transit time across the thickness cover almost the whole area over the two largest opposing faces of each specimen. Hence, for each set of readings, the maximum variation of the pulse transit times measured across the thickness ($\Delta t_T = t_{T,max} - t_{T,min}$) can provide an indication of the level of heterogeneity for each specimen. As mentioned in Section 3.2.1.3, two consecutive sets of readings were taken for each specimen. Therefore the representative maximum variation of each specimen ($\Delta t_{T,spec}$) was taken as the average of $\Delta t_{T,1}$ and $\Delta t_{T,2}$. Similarly, the representative average measured pulse transit time of each specimen ($\bar{t}_{T,spec}$) was taken as the average of $\bar{t}_{T,1}$ and $\bar{t}_{T,2}$. In order to allow adequate comparisons between specimens, a unitless heterogeneity measure for each specimen (HM_{spec}) was computed as follows:

$$HM_{spec} = \frac{\Delta t_{T,spec}}{\bar{t}_{T,spec}} \quad (3.1)$$

Subsequently, the heterogeneity measure for a specimen group (HM_{Group}) was computed as the average of the HM_{spec} values of all specimens belonging to that group. These values are presented in Table 3.5.

Table 3.5: Comparison of dynamic Young's modulus from UPV measurements across different directions and heterogeneity measure for each specimen group.

Specimen Group	Number of Specimens tested	Average values			HM_{Group}
		$\frac{E_{UPV,L} - E_{UPV,W}}{E_{UPV,L}}$	$\frac{E_{UPV,L} - E_{UPV,T}}{E_{UPV,L}}$	$\frac{E_{UPV,W} - E_{UPV,T}}{E_{UPV,L}}$	
35		Units			
I(a)	7	-5%	26%	32%	24%
I(b)	6	-3%	25%	28%	22%
II	5	-10%	35%	46%	10%
III	3	-19%	-10%	10%	26%
IV	6	22%	-31%	-54%	8%
V(a)	2	-15%	-5%	11%	26%
V(b)	6	-20%	-	-	-
21		Mortar			
MB	5	-26%	-38%	-12%	16%
MIIB	8	-33%	-25%	7%	11%
MC	8	-5%	-2%	3%	9%

The comparisons in Table 3.5 reveal that the bricks produced by extrusion (groups II and IV) display a higher level of anisotropy since the relative scatters between estimated dynamic Young's moduli for different directions were consistently greater for specimens from these two groups. It should be noted that the average values of the relative scatters between the estimated dynamic Young's moduli for specific directions also appear to be significant for some of the other specimen groups tested (I(a), I(b), MB, MIIB). However, there are much greater variations in these relative scatters among individual specimens from these groups when compared to the variations among the specimens from groups II and IV. This can be expected due to the greater homogeneity of the bricks manufactured by extrusion, confirmed by the significantly lower group heterogeneity measures (see Table 3.5). It is clear to see that although the comparison of estimated dynamic Young's moduli from ultrasonic P-wave velocities in different directions can provide some information on the inherent anisotropy of the material, it can be misleading and hence requires very careful interpretation. Moreover, as described in Section 2.2.1.2, the wave modes are not necessarily pure modes in anisotropic media. Therefore, the ratios of the estimated dynamic moduli from P-wave velocities between different directions do not

necessarily reflect the actual ratios between elastic constants of the material. In fact, for the anisotropic case, estimating the dynamic elastic modulus from traditional ultrasonic P-wave testing alone can definitely be considered as being unreliable.

Comparing the dynamic Young's modulus evaluated from IEV testing with that evaluated from UPV testing with P-waves across the length of the specimens can be considered a more robust way of evaluating the reliability of the results from UPV testing. In theory, the stresses developed during testing with these two methods should be resisted across the same material direction as illustrated in Figure 3.9. Table 3.6 presents the relative scatter between E_{IEV} and $E_{UPV,L}$ for each specimen group.

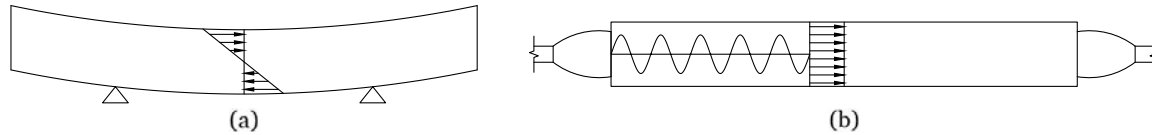


Figure 3.9: Schematic representation of stresses in material during flexural IEV test (a) and during UPV testing across length (b).

Table 3.6: Comparison of dynamic Young's modulus from IEV and UPV measured across length.

Specimen Group	Number of Specimens tested	Average values				
		E_{IEV} [MPa]	coeff. of variation	$E_{UPV,L}$ [MPa]	coeff. of variation	$\frac{E_{IEV}-E_{UPV,L}}{E_{IEV}}$
35		Units				
I(a)	7	7,882	15%	7,837	18%	1%
I(b)	6	7,931	17%	7,938	13%	-0.1%
II	5	18,313	1%	13,756	4%	25%
III	3	7,107	13%	7,305	2%	-3%
IV	6	15,505	1%	9,157	8%	41%
V(a)	2	5,475	8%	5,498	4%	-0.4%
V(b)	6	4,068	30%	4,604	35%	-13%
21		Mortar				
MB	5	3,987	10%	4,527	6%	-14%
MIIB	8	4,269	6%	4,887	16%	-14%
MC	8	28,954	5%	28,601	4%	1%

From Table 3.6, it is clear that the differences between E_{IEV} and $E_{UPV,L}$ are significantly greater for specimens from group II and IV when compared to the differences for specimens from any other group of constituent materials tested. This suggests that values of dynamic Young's modulus evaluated from UPV testing only with P-waves is unreliable for bricks produced by extrusion due to their apparent anisotropy. Hence, the comparison of E_{IEV} and $E_{UPV,L}$ has brought us to the same conclusion as the comparison of the dynamic Young's moduli estimated from ultrasonic compression wave velocities across different directions. However, in this case, the disagreement between E_{IEV} and $E_{UPV,L}$ is much more apparent and the comparison does not lend itself to misinterpretation. From a more general perspective, it is clear that the bricks manufactured through an extrusion process (groups II and IV) show the smallest coefficients of variation. As previously discussed, one of the main reasons for this is that they are characterised by greater homogeneity.

For results from IEV testing, the estimates of dynamic Poisson's ratio generally have greater coefficients of variation, indicating that the evaluation of this parameter is more sensitive to heterogeneities and to changes in testing conditions (see Table 3.3). Nevertheless, for specimens characterised by a more marked isotropic behaviour, it can be said that IEV testing can provide reliable estimates of the dynamic Poisson's ratio. In fact, most specimen groups have a coefficient of variation of 31% or less for this parameter with the exception of groups I(b) and V(b). Even so, it should be noted that the average estimated value of the dynamic Poisson's ratio was quite low for both these groups of specimens. Hence, the 41% and 70% coefficients of variation among specimens from group I(b) and V(b) respectively, relate to variations of only 0.04 and 0.02 respectively in the estimated Poisson's ratio. The value of the dynamic Poisson's ratio determined for the cement mortar

is significantly higher than that of the lime mortar and of the brick specimens handmade in moulds.

One of the main advantages of reliably estimating the dynamic Poisson's ratio using IEV testing, is that it can provide a value for a previously unknown parameter in Equation (2.3), used to compute the dynamic Young's modulus from the experimentally evaluated ultrasonic compression wave velocity. In order to assess the benefit gained from this information, a sensitivity study was carried out between the assumed dynamic Poisson's ratio and the evaluated dynamic Young's modulus for all brick specimens. If no information is known on the Poisson's ratio, it can be assumed that this value can fall anywhere within the range of values determined from IEV testing across all brick specimens tested as part of this research. Hence, the sensitivity study includes Poisson's ratios ranging from 0.01 to 0.37. The results of this study for $E_{UPV,L}$ are shown first only for bricks from group I(a) (Figure 3.10) and subsequently for all brick specimen groups (Figure 3.11).

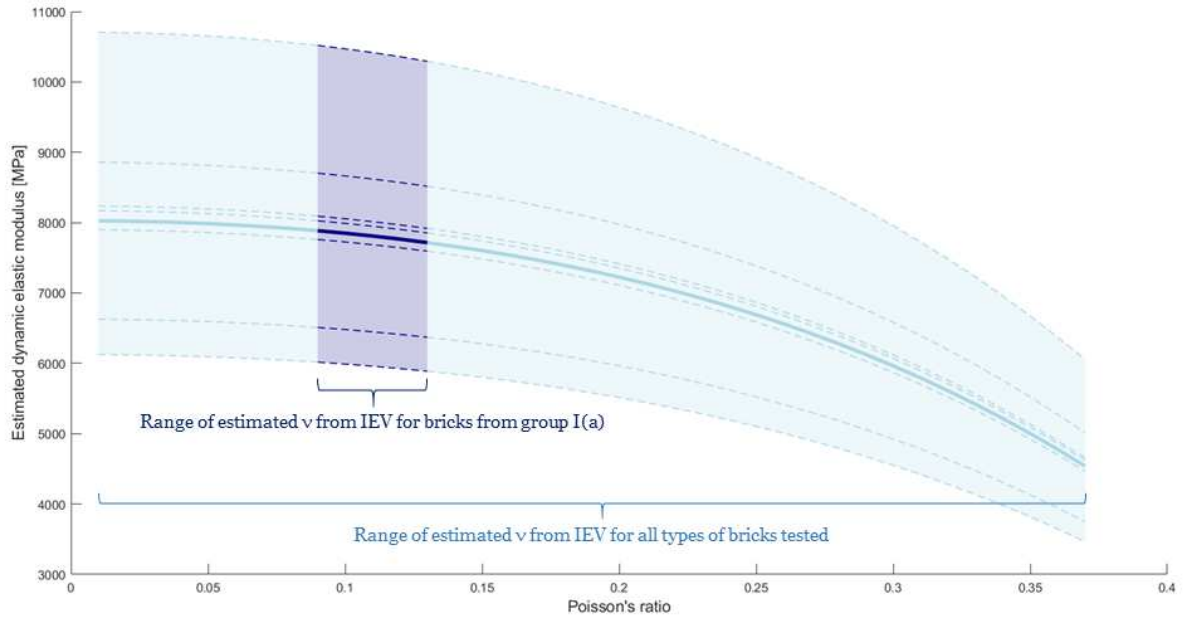


Figure 3.10: Variation of estimation of $E_{UPV,L}$ with ν for bricks from group I(a).

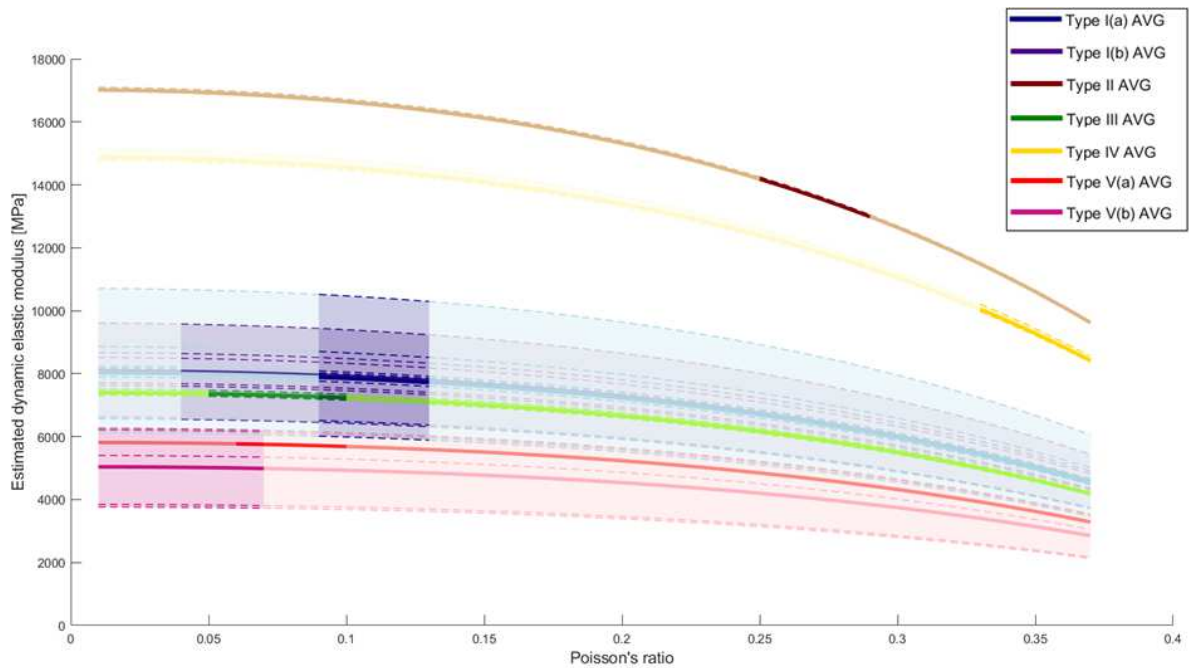


Figure 3.11: Variation of estimation of $E_{UPV,L}$ with ν for all bricks tested as part of this experimental campaign. Areas shaded with a lighter colour refer to the range of estimated ν across all the types of bricks tested. Areas shaded with a darker colour refer to the range of estimated ν for a specific group.

A similar trend across an equivalent range of values as shown for $E_{UPV,L}$ was observed for the sensitivity studies of $E_{UPV,W}$ and $E_{UPV,T}$. It is clear to see that using the information on the dynamic Poisson's ratio obtained from IEV testing can contribute to a significant improvement in the estimation of the dynamic Young's modulus from UPV testing. In fact, the sensitivity study revealed that using the Poisson's ratios only within the range estimated from IEV testing for each specific brick specimen group reduced the maximum variation in the estimated dynamic Young's modulus from 50% to a maximum of 3.6%.

It should be noted that although the coefficients of variation for the computed Poisson's ratio are lowest for the bricks produced by extrusion (see Table 3.3), the estimated values of this parameter for these types of bricks are unreliable. The main reason for this is that bricks manufactured from an extrusion process usually exhibit a certain level of anisotropy. As previously discussed, results from the tests carried out as part of this research confirm this anisotropic character. Since a fundamental assumption behind the analytical expression used for the computation of Poisson's ratio from IEV results is isotropy, these values cannot be considered reliable estimates. Nevertheless, the values of dynamic shear modulus evaluated from the torsional IEV tests do not depend on Poisson's ratio and therefore still provide a good representation of how the material behaves in the orientation in which it was tested. Although the expression relating the measured flexural resonant frequency to the dynamic Young's modulus (Equation (2.1)) contains a correction factor dependent on Poisson's ratio, the final estimated value is very insensitive to changes in Poisson's ratio. In fact, a simple sensitivity study showed that this parameter has a maximum variation of less than 1.74% for any specimen over the whole range of estimated Poisson's ratios across all specimen groups. Hence, it can be said that IEV testing also provides a good representation of the dynamic Young's modulus of anisotropic bricks when acting against out-of-plane flexural loads.

3.2.3. Proposed analysis procedure

Based on all the experimental methods described in detail in Sections 3.2.1.2 and 3.2.1.3, a summary of the recommended analysis procedure for obtaining reliable estimates of the dynamic elastic properties of brick masonry constituents is shown in Figure 3.12.

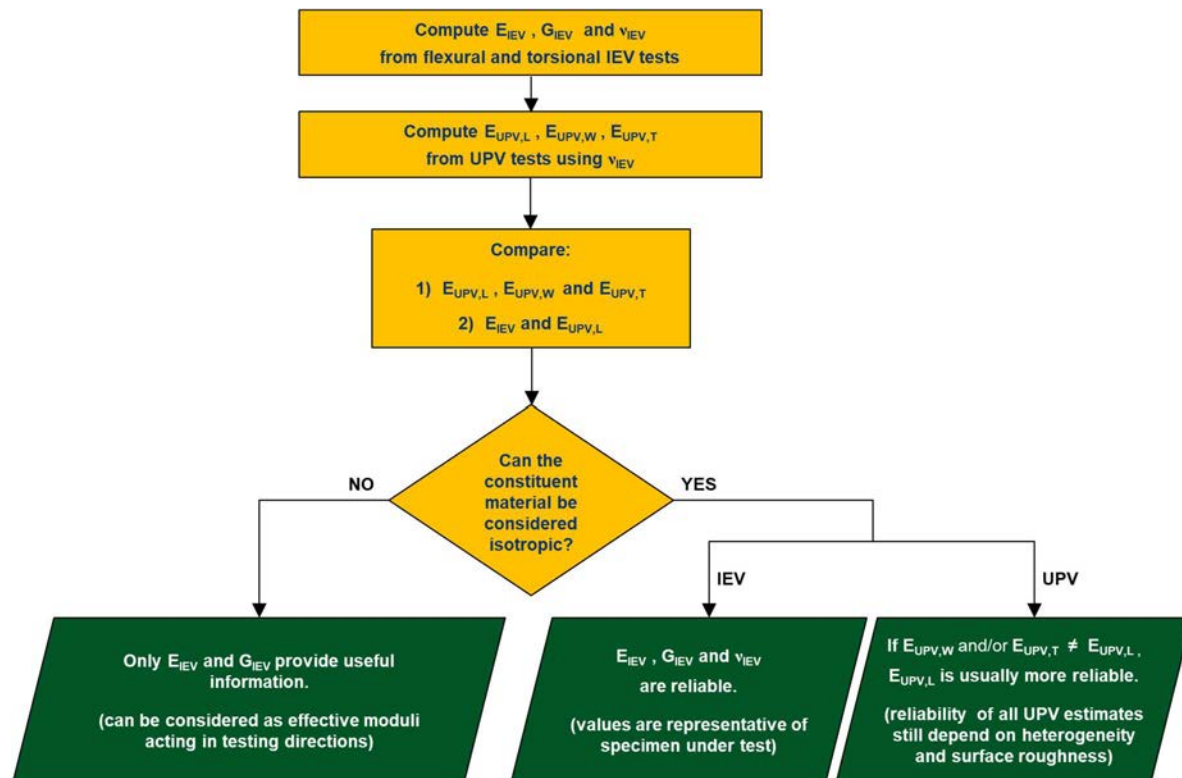


Figure 3.12: Summary of the proposed procedure for determining dynamic elastic properties of brick masonry constituents.

As can be seen from Figure 3.12, the first step of the analysis process involves computing E_{IEV} , G_{IEV} , and ν_{IEV} from the results of IEV tests conducted as described in Section 3.2.1.2. Following this, the resulting ν_{IEV} is used in the computation of $E_{UPV,L}$, $E_{UPV,W}$, and $E_{UPV,T}$ from ultrasonic pulse velocities measured across different dimensions of each specimen as described in Section 3.2.1.3. The average values for each group of specimens representing a particular type of brick or mortar can then be obtained. All subsequent analysis can be carried out with these representative average values. Once these values have been obtained, it is important to assess if any of the brick or mortar types being tested exhibit a significant level of anisotropy in order to evaluate the reliability of the obtained results. If there are significant relative scatters (>30%) between $E_{UPV,L}$, $E_{UPV,W}$ and $E_{UPV,T}$ as well as a significant relative scatter (>20%) between E_{IEV} and $E_{UPV,L}$ then the material under test can be said to be anisotropic. If this is the case, only the dynamic Young's modulus (E_{IEV}) and the dynamic shear modulus (G_{IEV}) computed from results of IEV testing provide a good representation of the behaviour of the material in the respective testing orientations. On the other hand, if the material exhibits a predominantly isotropic behaviour, in theory, all the dynamic elastic material properties evaluated from IEV and UPV testing can be considered reliable. However, since the reliability of UPV estimates depend strongly on heterogeneity and surface roughness, if $E_{UPV,W}$ and/or $E_{UPV,T}$ differ from $E_{UPV,L}$, the latter parameter can be considered as being more reliable in most cases.

The application of this analysis process can be illustrated with two simple examples. Taking the case of the cement mortar tested as part of this research (group MC), the relative scatters between $E_{UPV,L}$, $E_{UPV,W}$ and $E_{UPV,T}$ are all of 5% or less and the relative scatter between E_{IEV} and $E_{UPV,L}$ is of only 1%. In this case, it is clear that the material is isotropic and all the estimated dynamic elastic properties can be considered reliable. On the contrary, for the type of bricks belonging to group II, the relative scatter between $E_{UPV,L}$ and $E_{UPV,T}$ is 35% while that between $E_{UPV,W}$ and $E_{UPV,T}$ is 46%. Furthermore, the relative scatter between E_{IEV} and $E_{UPV,L}$ turned out to be 25%. For these bricks, all properties estimated from UPV tests as well as the value of ν_{IEV} cannot be considered reliable. Nevertheless, E_{IEV} is still representative of the dynamic Young's modulus when out-of-plane flexural loads are acting on this type of brick while G_{IEV} still provides a good representation of the response of bricks of this type to torsional loads (in the same orientation as the bricks were tested).

3.3. Relationship between the static and dynamic elastic properties of brick masonry constituents

The main aim of this part of the research is to propose an expression that can be used to estimate the static elastic modulus of typical brick masonry constituents from the dynamic one for practical applications. In order to achieve this, an experimental campaign was carried out to estimate the static elastic moduli of the same materials described in Section 3.2.1.1, whose dynamic elastic moduli had already been estimated. It should be noted that the static tests were not performed by the author of this thesis, but by another researcher as part of a broader investigation.

This section first presents the procedures used for the experimental determination of the static elastic moduli of all the specimens. The static elastic moduli are then compared to the dynamic ones evaluated for the same specimens. Finally, the suitability of several empirical expressions developed for rocks and concrete are assessed before proposing one to be used for typical brick masonry constituents.

3.3.1. Experimental determination of static modulus

3.3.1.1. Specimen preparation for static tests

Static tests from which the elastic moduli are to be evaluated involve fixing the applied stress at lower levels than the compressive strength for fixed intervals during testing. Hence, prior knowledge of the approximate compressive strengths of the specimens from each group is required before executing the tests.

In the case of bricks, while the dynamic tests described in Section 3.2 were executed on whole bricks, those used for the static tests consisted of $40 \times 40 \times 80 \text{ mm}^3$ prisms cut out from the same bricks. Before cutting these out, the two opposing largest faces of the bricks were polished so that each brick had a uniform

thickness of 40 mm. Since handmade bricks formed by moulding can be reasonably approximated as being isotropic (Fódi, 2011), it can be assumed that for each specimen group, the average compressive strength evaluated across the brick lengths should correspond to that evaluated across the widths. As such, for specimen groups I(a), I(b), III, and V(a), a $40 \times 40 \times 80 \text{ mm}^3$ prism across the width was cut out from each brick to estimate the compressive strength according to the procedure in (CEN, 2010) (see (c) in Figure 3.13). The reference compressive strength (f_{cn}) for each group was then taken as the average of the ones estimated from these prisms. As shown in Figure 3.13, three more $40 \times 40 \times 80 \text{ mm}^3$ prisms were cut out across the width of each remaining brick to evaluate the static elastic modulus across the width ($E_{st,W}$), while three equally sized prisms were cut across the length to evaluate the modulus in that direction ($E_{st,L}$).

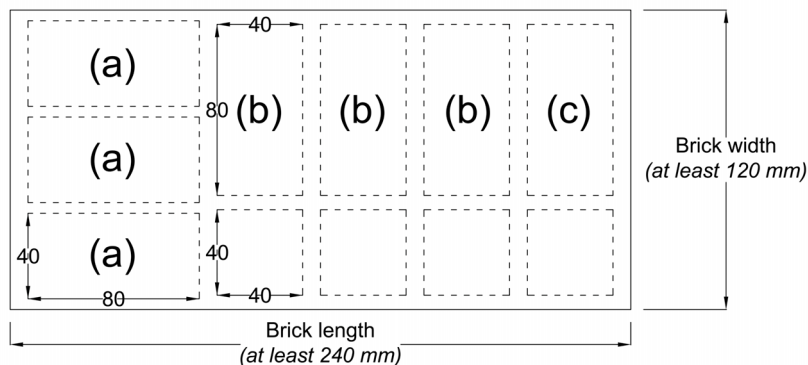


Figure 3.13: Specimens cut from each handmade brick. (a) Specimens used for estimating static elastic modulus across length. (b) Specimens used for estimating static elastic modulus across width. (c) Specimen used for estimating compressive strength.

It should be noted that one of the prisms across the width of a brick from group V(a) was damaged and therefore only 2 specimens could be used to evaluate $E_{st,W}$ for that particular brick. Furthermore, although bricks from group V(b) were also formed by moulding, the same specimens shown in Figure 3.13 were not cut out from each brick. This is due to the fact that $40 \times 100 \times 100 \text{ mm}^3$ prisms had already been cut from these bricks to evaluate their compressive strengths according to (CEN, 2010) as part of a previous experimental campaign. Naturally, the compressive strength evaluated from the previous campaign was taken as the representative strength for each brick from this group. However, this meant that less remaining area was available from each brick to extract specimens for the evaluation of elastic moduli. As such, only $40 \times 40 \times 80 \text{ mm}^3$ prisms across the length were cut from each brick. Although the number of specimens that could be cut out from each brick varied, it was ensured that at least 2 were extracted from each to calculate $E_{st,L}$. As described in greater detail in Section 3.2.3, only the dynamic elastic modulus across the length is available for bricks produced by extrusion (groups II and IV). Hence, only $E_{st,L}$ is included in this study for these bricks. These were also derived from tests carried out on $40 \times 40 \times 80 \text{ mm}^3$ specimens cut out across the length of each brick. Table 3.7 shows the number of specimens of each group used for both the static and dynamic tests.

Given that bricks are most often loaded in compression across their thickness, the choice of investigating the relationship between static and dynamic modulus across the width and length of bricks might appear counter-intuitive. Particularly when the procedure described in Section 3.2.3 allows for the estimation of dynamic elastic moduli of bricks handmade in moulds across their thickness. However, since this study mainly aims to better understand the relationship between static and dynamic moduli, this choice was made to ensure that only reliable estimates that reflect the actual material behaviour are compared. As stated in Section 2.2.2, for typical brittle brick materials, measuring surface strains in the elastic range can be a very challenging task with several possible sources of error. The impact of these errors on the final estimated value of the static elastic modulus is likely to be significantly greater if the strains are measured over a shorter gauge length. Since the polished bricks tested as part of this research were at most 40 mm thick, only very short gauge lengths were available to measure strains across this dimension. In fact, the coefficients of variation of static elastic moduli estimated from strain measurements across the lengths and widths of bricks already proved to be significantly greater than those estimated from dynamic methods (see Section 3.3.2), despite the fact that they allowed strain measurements over a longer gauge length. Moreover, the dynamic modulus across the thickness is not available for the anisotropic bricks produced by extrusion. As such, elastic moduli estimated across the thickness of bricks were not included in this study.

Before testing, the surfaces of all the cut prismatic brick specimens were polished and regularised to ensure uniform loading and to reduce possible sources of error in deformation measurements. Since moisture content of the specimens can alter the deformation behaviour of these materials, all specimens were dried at 120 °C in a drying oven until the mass was constant prior to testing.

With respect to mortars included in this study, all specimens for the static tests were prepared in standard $40 \times 40 \times 160 \text{ mm}^3$ prismatic moulds. Naturally, they were cast at the same time as the specifically moulded brick-shaped specimens used to estimate the dynamic elastic moduli. The standard prismatic specimens were tested to evaluate both the compressive strength and the static elastic modulus. The number of specimens used to evaluate both the static and dynamic moduli for each group of mortars tested is summarised in Table 3.7.

Table 3.7: Number of specimens available for evaluating the dynamic and static elastic moduli for groups of bricks and mortars tested.

Group	I(a)	I(b)	II	III	IV	V(a)	V(b)	MB	MIIB	MC
Number of (brick-sized) specimens for dynamic tests	7	6	5	3	6	2	6	5	8	5
Number of specimens for static tests	42	36	15	18	18	11	16	3	3	6

3.3.1.2. Experimental procedure for static tests

The stress-strain relationship of brittle materials, such as typical brick masonry constituents, usually reveals a certain degree of non-linearity even at stress levels well below their ultimate strength. This can be attributed to microcracks (Zimmerman, 1985) and creep effects (Neville, 2011). Due to this inherent non-linearity, different definitions of the static elastic modulus have been proposed for such materials depending on how the latter is calculated. It is possible to find a *tangent modulus* at any point on the stress-strain curve, but this will only apply to loading levels in the vicinity of the point at which the modulus was calculated and is therefore of little practical significance. The *chord modulus* taken as the slope of the line connecting two specific points on the stress-strain curve is usually preferred since it is more representative of the material behaviour under actual loading conditions of interest. It should be noted that since the first point used for the computation of the chord modulus is usually at a very low stress level, some books (Neville, 2011), articles (Binda; Tiraboschi; Abbaneo, 1997; Baronio et al., 2003) and even standards (CEN, 2013) have come to refer to it as a *secant modulus*.

Naturally, since the secant modulus will depend on the two points chosen to compute it, it is important to select them carefully. To the best of the authors' knowledge, no standards exist for the determination of the static elastic modulus of brick masonry constituents. However, some guidance for the selection of appropriate nominal stress levels can be found from the European Standards for the determination of the static moduli of elasticity of concrete (EN 12390-13:2013) (CEN, 2013) and natural stone (EN 14580:2005) (CEN, 2005), as well as in the standard for the determination of the compressive strength of masonry (EN 1052-1:1998) (CEN, 1998). All these standards recommend to use a nominal upper stress level at a third of the estimated compressive strength (f_c). However, they differ in their recommendation for the nominal lower stress level at which the strain should be evaluated for the computation of the static elastic modulus. Whilst the standard for concrete recommends a nominal lower level between 10% and 15% of f_c , that for natural stone recommends one corresponding to approximately 2% of f_c . Based on these recommendations, for the static tests carried out as part of this research, the nominal upper stress level (σ_b) was set as approximately equal to 30% of the representative compressive strength for each specimen group. The nominal lower stress level (σ_a) was set as approximately equal to 10% of the representative compressive strength for each group. The latter value was chosen because the measured strains at lower stress values approached the minimum resolution of the strain transducer for some of the specimens with low compressive strengths.

To eliminate some of the creep effects and to allow the extension pieces of the transducers to settle at fixed points on the material, it is vital to subject each specimen to cycles of pre-loading up to the nominal upper stress level. Standards (CEN, 2013) and (CEN, 2005) suggest to carry out three loading cycles and to determine the stabilised secant modulus based on the third cycle. This procedure was thus adopted for all

the tests carried out to determine the static elastic modulus of the brick masonry constituents, resulting in the loading scheme shown in Figure 3.14. As shown, the load was held constant for 60 s at the nominal upper and lower stress levels. The final increasing branch of the loading scheme after the third cycle was implemented to verify the continuity of the slope of the stress-strain curve beyond σ_b .

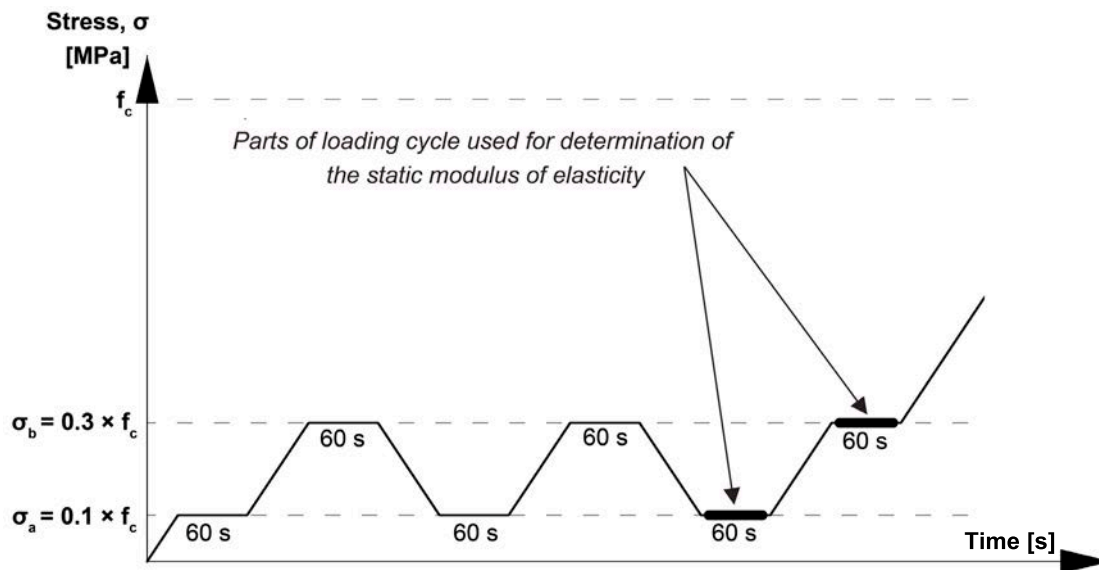


Figure 3.14: Loading scheme employed for tests to determine the static elastic modulus of specimens.

It should be noted that specimens from group I(a) were tested before the final testing protocol was developed. For tests on these specimens, σ_a was set at 5% of f_c instead of 10%.

The experimental procedure thus involved applying a compressive load according to the loading scheme shown in Figure 3.14 while recording vertical strain measurements across the surface of three faces using a gauge length of 50 mm as shown in Figure 3.15. The remaining face of each specimen was equipped with a transducer to record horizontal strains during testing for a different study. A custom adjustable frame was designed and built to quickly and securely hold all the transducers in position without inhibiting their measuring ability.

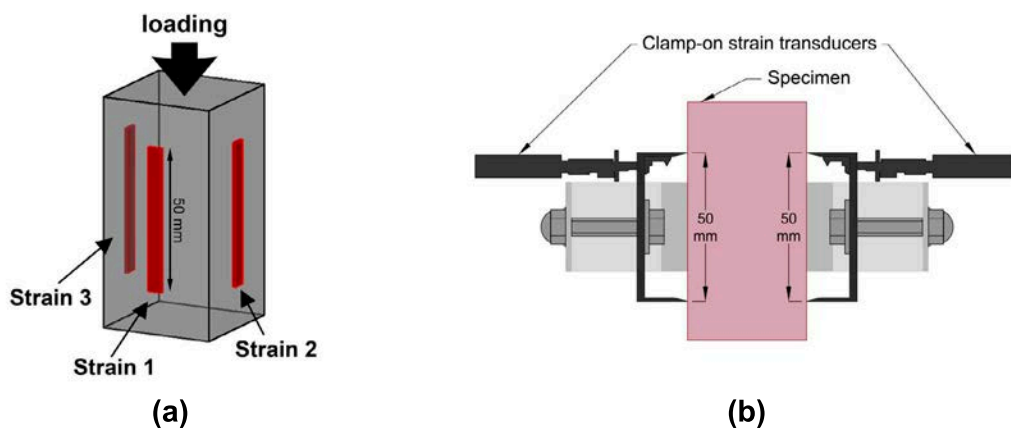


Figure 3.15: (a) Schematic diagram showing locations at which strain was measured during testing of each specimen. (b) Cross-section across clamp-on strain transducers placed on opposing faces of a specimen.

All tests were carried out with load control while measurements were recorded with a sampling rate of 5 Hz. A load cell with a maximum compression force of 200 kN was used for all tests except for those on lime mortar specimens. These were tested using a load cell with a maximum capacity of 10 kN. During the cyclic loading procedure, loads were applied with a constant velocity of 0.25 kN/s in between successive

nominal levels. As shown in Figure 3.15, clamp-on strain transducers with an effective minimum resolution of approximately $0.013 \mu\text{m}/\text{mm}$ were used to measure strains during all tests.

3.3.1.3. Derivation of static elastic modulus from raw data

Once the experiments were completed, the compression loads recorded during each test were converted to stresses through division by the cross-sectional area of the specimen. Data points corresponding to the parts of the third loading cycle held at the nominal lower (σ_a) and upper (σ_b) stress levels were then extracted from all the stress and strain measurements. In order to ensure that there were no inconsistencies during loading and that the stresses were effectively held at the nominal levels, the coefficients of variation among extracted data points corresponding to each specific level were verified. Since they never exceeded 0.25%, the loading of all the specimens was deemed as being consistent with the scheme shown in Figure 3.14 and the mean stress recorded during the period for which the loading was held at a nominal level was taken as the central tendency.

Similarly, each representative measured strain value corresponding to a nominal stress level was computed as the mean of the strains recorded during the period for which the stress was held at that level. However, since surface strain measurements of brittle materials are prone to error, two important verifications were carried out to ensure erroneous measurements were not included in the computation of the elastic modulus. First, measurements from a specific strain transducer for a particular test were discarded if the magnitude of the mean strain for a nominal stress level was lower than the minimum resolution of the transducer ($0.013 \mu\text{m}/\text{mm}$). Measurements smaller than this hardware limitation can actually be considered as being equivalent to not registering any strain. Second, measurements from a specific strain transducer for a particular test were also discarded if the coefficient of variation among extracted data points corresponding to the same nominal level exceeded 1%. This requirement was established to identify apparent sudden changes of strain that were recorded while the applied load was kept constant, such as the one shown in Figure 3.16.

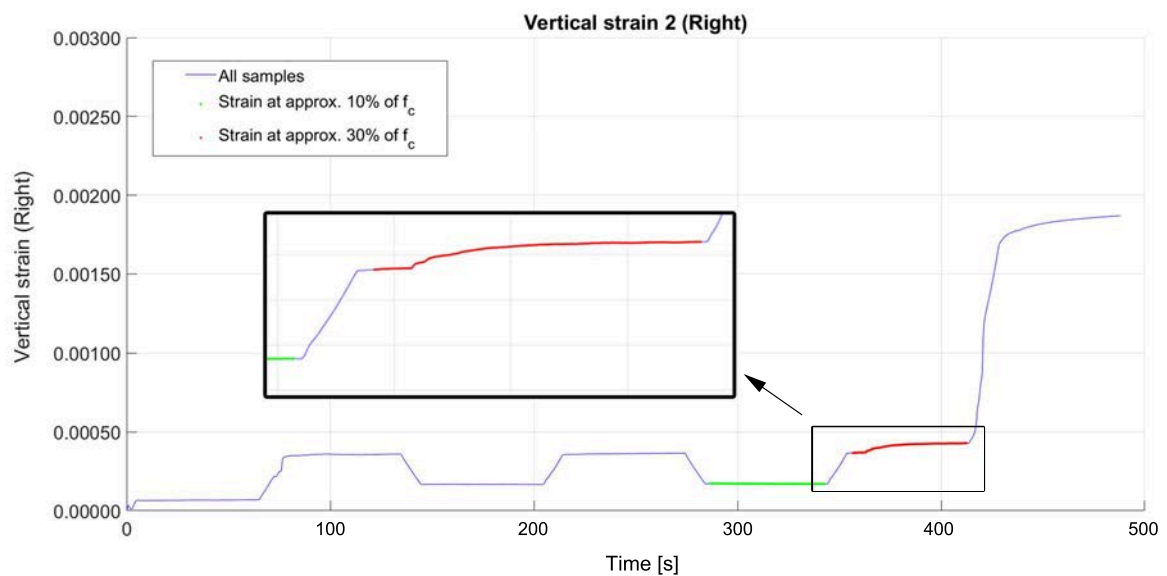


Figure 3.16: Example of an unsteady strain measurement deemed as being erroneous.

This cross-check of the experimental readings is introduced in this research as it proves to be of paramount importance in experimental tests evaluating the deformation characteristics of masonry components. Identifying and eliminating such erroneous values, mostly due to possible contact problems between the strain transducer and the specimen's surface, can have a significant effect on the accuracy of the final estimates of the static elastic modulus. In this case, as a result of the filtering procedure described in the previous paragraph, out of the 168 specimens tested, at least one strain measurement was discarded from 22 specimens.

Once these erroneous strain values were eliminated, the strain difference between the nominal upper and lower stress levels was computed for each strain transducer for every test. The mean of the three vertical

strain changes measured across different faces of each specimen then needs to be computed before E_{st} can be estimated. Naturally, in case one or more of the strain measurements across a particular face had been deemed to be erroneous, they have to be excluded from the computation of the mean strain change. However, before proceeding with the estimation of E_{st} , for some of the specimens still left with three non-erroneous strain measurements, a clear outlier could be identified as shown in Figure 3.17. These outliers most likely occurred due to the presence of very localised heterogeneities close to the surface across which the strain was being measured and are therefore not representative of the true material behaviour. Hence, although the treatment of outliers is rarely straightforward, in this particular case, it can be deemed that a better estimate of the actual E_{st} can be obtained by excluding such outliers from the data set.

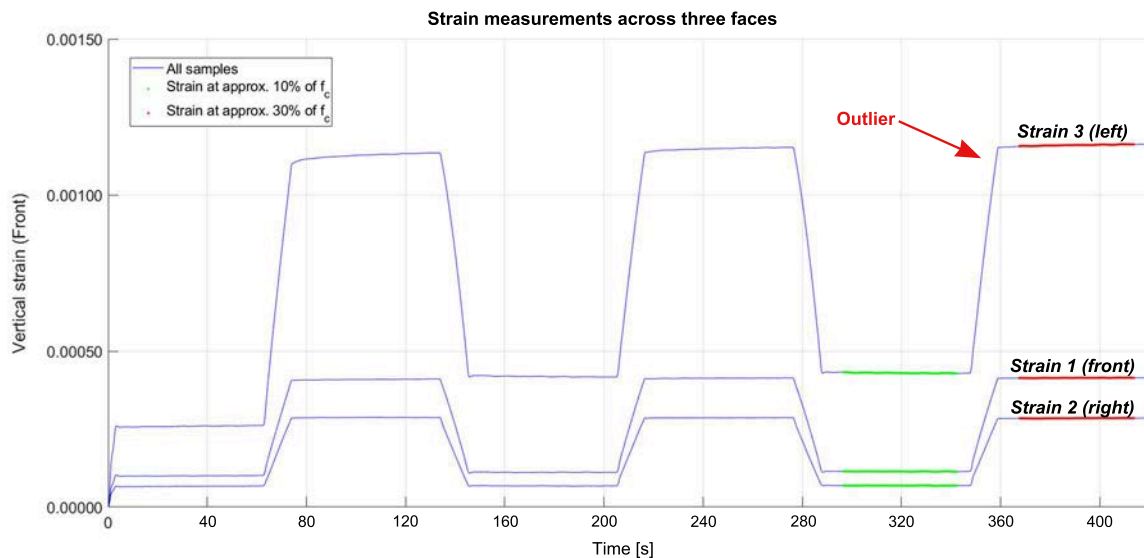


Figure 3.17: Example of an outlier among 3 strain measurements across different faces of a specimen.

Although there exists several statistical procedures to deal with outliers in data sets, many of them are not effective when only a small number of observations are available. As such, most common methods would not perform well for the case of the measured strain changes since only 3 observations are available. However, a well-known procedure, known as Dixon's Q test (Dean; Dixon, 1951), has been developed specifically for such cases. It relies on the computation of a Q ratio for each observation as follows:

$$Q = \frac{x_n - x_{n-1}}{\omega} \quad (3.2)$$

Where x_n is the observation for which the Q ratio is being computed, x_{n-1} is the nearest neighbour of x_n and ω is the range of the set of observations defined as the difference between the largest and the smallest observation.

The conventional implementation of the Q test involves excluding observations with Q ratios greater than tabulated rejection thresholds corresponding to a specific confidence level assuming a normally distributed population. As can be seen from Equation (3.2), the Q ratio is normalised by the range which is considered as one of the most efficient measures of dispersion for a small number of observations (Dean; Dixon, 1951). It is therefore based solely on the relative distances between observations irrespective of the magnitude of the range. As a result, the test tends to penalise outliers more strictly in a less dispersed sample. This is a disadvantage in the case of the measured strain changes since the desired outcome is to exclude an outlier that differs significantly from the other measurements in terms of magnitude rather than excluding one that differs relatively more than the others within a small range.

To overcome this limitation, for each set of measured strain changes, the magnitude of the dispersion (measured by the range) was compared to the magnitude of the central tendency (measured by the mean). If the range was found to be greater than 75% of the mean value, the observation with the greatest Q ratio, computed as shown in Equation (3.2), was excluded from the data set. Using this procedure, a single outlying

value for the strain change was excluded for 10 of the 168 specimens tested as part of this research.

Subsequently, the static elastic modulus E_{st} of each tested specimen was computed using the following expression:

$$E_{st} = \frac{\overline{\sigma_b} - \overline{\sigma_a}}{\epsilon_{diff}^*} \quad (3.3)$$

Where $\overline{\sigma_a}$ and $\overline{\sigma_b}$ refer to the mean stresses recorded during the third loading cycle at the lower and upper nominal levels respectively while ϵ_{diff}^* refers to the mean strain change measured between the two nominal stress levels across 3 different specimen faces excluding any identified outliers or erroneous values.

3.3.2. Results of static tests

For each brick, the average value of static elastic moduli of specimens extracted across the brick length was taken to represent the static elastic modulus of the brick across its length ($E_{st,L}$). Similarly, the average static elastic modulus of specimens extracted across a brick's width was taken as the static elastic modulus of the brick across its width ($E_{st,W}$). Each one of these values were compared to the most reliable corresponding dynamic elastic modulus (E_{dy}) of the same brick, which had previously been estimated using impulse excitation of vibration (IEV) or ultrasonic pulse velocity (UPV) methods (see Section 3.2). As previously described, estimates of the dynamic elastic modulus obtained using IEV are more reliable and representative of the elastic modulus of the entire specimen when compared to UPV estimates. Hence, values estimated using IEV were utilised for the comparison of elastic moduli across a brick's length and for mortar specimens. Nevertheless, it is worth mentioning that there is generally a good agreement between UPV and IEV estimates for isotropic constituent materials as described in Section 3.2. Since the IEV methods utilised cannot provide estimates for the dynamic elastic modulus across a brick's width (see Section 3.2), UPV estimates were used for comparison to $E_{st,W}$.

For all specimen groups consisting of handmade bricks formed in moulds, except group V(b) (see Section 3.3.1.1), both $E_{st,L}$ and $E_{st,W}$ were computed. Due to their anisotropic nature, no dynamic elastic modulus across the width of bricks produced by extrusion was available for comparison (specimen groups II and IV). Therefore, $E_{st,W}$ of these bricks could not be used to better understand the relationship between E_{st} and E_{dy} . This resulted in a data set containing 35 pairs of E_{st} and E_{dy} estimates across brick lengths and 18 across brick widths. The average values of $E_{st,L}$ and $E_{st,W}$ for each specimen group are summarised in Tables 3.8 and 3.9 along with the average dynamic modulus values corresponding to the same specimen group and material direction.

Table 3.8: Comparison of average static ($E_{st,L}$) and dynamic (E_{IEV}) elastic modulus measured across brick lengths.

Specimen group	Static		Dynamic*		$\frac{E_{st}}{E_{dy}}$
	$E_{st,L}$ [MPa]	coeff. of variation	E_{IEV} [MPa]	coeff. of variation	
I(a)	6,287	27%	7,882	15%	0.798
I(b)	7,920	22%	7,931	17%	0.999
II	16,081	7%	18,313	1%	0.878
III	5,996	22%	7,107	13%	0.844
IV	13,249	16%	15,505	1%	0.855
V(a)	5,572	7%	5,475	8%	1.018
V(b)	4,736	28%	4,068	30%	1.164

* Determined according to the procedure reported in Section 3.2.

Table 3.9: Comparison of average static ($E_{st,W}$) and dynamic ($E_{UPV,W}$) elastic modulus measured across brick widths.

Specimen group	Static		Dynamic*		$\frac{E_{st}}{E_{dy}}$
	$E_{st,L}$ [MPa]	coeff. of variation	$E_{UPV,W}$ [MPa]	coeff. of variation	
I(a)	5,504	23%	8,241	19%	0.668
I(b)	7,563	21%	8,189	15%	0.924
II	-	-	-	-	-
III	6,051	18%	8,717	7%	0.694
IV	-	-	-	-	-
V(a)	5,389	23%	6,336	7%	0.851
V(b)	-	-	-	-	-

* Determined according to the procedure reported in Section 3.2.

In contrast, for mortars, a single average E_{st} is taken from all the tested prisms belonging to a specimen group. Thus only 3 new pairs of E_{st} and E_{dy} estimates are added to the data set containing 53 pairs of estimates from different brick specimens. The E_{st} values are shown together with the dynamic elastic modulus for the corresponding mortar type in Table 3.10.

Table 3.10: Comparison of average static (E_{st}) and dynamic (E_{IEV}) modulus of mortar specimen groups.

Specimen group	Static		Dynamic*		$\frac{E_{st}}{E_{dy}}$
	$E_{st,L}$ [MPa]	coeff. of variation	E_{IEV} [MPa]	coeff. of variation	
MB	2,696	8%	3,987	10%	0.676
MIIB	2,666	29%	4,269	6%	0.625
MC	27,167	8%	28,954	5%	0.938

* Determined according to the procedure reported in Section 3.2.

As can be expected, the coefficient of variation (CV) of E_{st} is significantly greater than that of the corresponding E_{dy} for almost all specimen groups. Nonetheless, the CV between specimens for E_{dy} can be seen to be marginally greater than that of E_{st} in 3 cases, namely for MB mortars and for groups V(a) and V(b) when the modulus is evaluated across brick lengths. In these cases, the CV of E_{dy} tends to be only 1% or 2% higher than that of E_{st} . It should also be noted that many specimens from these particular groups were found to have a relatively high level of heterogeneity and much of the dispersion between estimated moduli values can be attributed to this (see Section 3.2.2). In contrast, for the remaining specimen groups, the coefficients of variation among specimens for E_{st} are twice as large on average as those for E_{dy} . In fact, the greatest relative difference between these coefficients of variation occurs for one of the most homogeneous specimen groups (group IV). This is a clear indication of the increased difficulty and propensity for error of the static tests.

In terms of the magnitudes of the elastic moduli, with the exception of $E_{st,L}$ for specimen groups V(a) and V(b), the representative static elastic modulus of a specimen group is found to be always lower than its dynamic counterpart. This is in agreement with the trend generally observed in previous studies of this relationship for rocks and concrete, as already described in Section 2.2.2. In fact, for both group V(a) and group V(b), the relative difference between E_{st} and E_{dy} is smaller than the coefficient of variation associated to either value. This shows that the estimate of the difference between the two material properties is smaller than the dispersion related to the measurement of either one. As such, although exceptional observations for which $\frac{E_{st}}{E_{dy}}$ ratios greater than 1 have been reported for the case of rocks (Eissa; Kazi, 1988), in this case, it can be said that these occurrences cannot be deemed significant and do not reflect the true relationship between these two properties.

If individual specimens are analysed, the estimated static elastic modulus is greater than the dynamic one for 11 of the 56 pairs of E_{st} and E_{dy} available for comparison. However, it should be noted that 7 of the 11 specimens are from group V(a) or V(b). Moreover, it should be noted that, even for individual specimens, the

ratio $\frac{E_{st}}{E_{dy}}$ is very close to 1 for most cases.

Based on the 42 pairs of E_{st} and E_{dy} values available for handmade bricks formed by moulding, simple linear regression with the intercept fixed at 0 reveals that 0.85 is a reasonable estimate of the $\frac{E_{st}}{E_{dy}}$ ratio for such bricks. The same procedure reveals that 0.87 is a good estimate of this ratio for bricks produced by extrusion based on the 11 data points available. These preliminary observations suggest that a suitable relationship can be found for both bricks produced by extrusion and for those handmade in moulds. As such, they were analysed as a single data set in an attempt to better understand the underlying relationship between static and dynamic elastic moduli for such materials. The 2 pairs of E_{st} and E_{dy} values available for lime mortar specimens suggest an average $\frac{E_{st}}{E_{dy}}$ ratio of 0.65 for this material. On the other hand, MC specimens tested as part of this research suggest a $\frac{E_{st}}{E_{dy}}$ ratio of 0.94, which is in good agreement with findings from previous studies on Portland cement-based mixes (Swamy; Bandyopadhyay, 1975). The two available data points for lime mortars and the single one of cement mortar certainly cannot be used for in-depth studies specifically on these respective material types. However, it was deemed beneficial to evaluate how well they agree with a general relationship for brittle constituent materials typically used in brick masonry constructions. As such, they were also included in the data set analysed in the following section.

3.3.3. Comparison and discussion

Previous studies (Popovics, 1975; Eissa; Kazi, 1988; Brotons et al., 2014; Brotons et al., 2016) have already established that including material compressive strength, density and even porosity can lead to improved prediction capability of correlation models. However, given the variability of the sample set in terms of chemical composition and manufacturing process, it is unclear as to whether or not including them as explanatory variables can limit the range of practical applications significantly. Hence, in order to evaluate this, a correlation study was carried out between different combinations of explanatory variables that can be included in the prediction model (see Tables 3.11 and 3.12). Such a study was also carried out previously in order to assess which combinations of material density and dynamic modulus to use for the prediction of the static elastic moduli of rocks (Eissa; Kazi, 1988). It is achieved by computing the Pearson correlation coefficient ($R_{X,Y}$) between different combinations of dependent and explanatory variables, as shown in Equation (3.4). This coefficient is a dimensionless measure of linear dependence that can vary between -1 and +1, with absolute values closer to unity indicating a better correlation. The sign of the coefficient indicates the type of correlation. A negative sign indicates that an increase of one parameter leads to a decrease of the other whereas a positive sign indicates that the increase of one leads to an increase of the other.

$$R_{X,Y} = \frac{cov(X, Y)}{\sigma_X \cdot \sigma_Y} \quad (3.4)$$

Where $R_{X,Y}$ is the Pearson correlation coefficient between the variables X and Y , $cov(X, Y)$ is the covariance between them and σ_X and σ_Y are their respective standard deviations.

First, the same explanatory variable combinations explored in (Eissa; Kazi, 1988) for rocks were tested on the sample set of brick masonry constituents. As shown in Table 3.11, this involves various combinations of the material density (ρ) and the dynamic elastic modulus (E_{dy}).

Table 3.11: Correlation matrix for various combinations of static (E_{st}) and dynamic (E_{dy}) moduli and density (ρ) of brick masonry constituents.

Variables	E_{dy}	$\log_{10} E_{dy}$	ρ	$\rho\sqrt{E_{dy}}$	ρE_{dy}	$\sqrt{\rho E_{dy}}$	$\log_{10} \rho E_{dy}$	$\rho \log_{10} E_{dy}$	$\frac{E_{dy}}{\rho}$	$\sqrt{\frac{E_{dy}}{\rho}}$
E_{st}	0.97	0.89	0.10	0.94	0.96	0.95	0.89	0.70	0.94	0.92
$\log_{10} E_{st}$	0.92	0.92	-0.05	0.88	0.88	0.91	0.91	0.60	0.92	0.93

Previous studies have shown that the compressive strength of the material can influence the relation between static and dynamic elastic moduli for concrete (Neville, 2011; Takabayashi, 1954; Lee et al., 2017) and rocks (Brotons et al., 2016). It was therefore deemed relevant to assess the suitability of including it as an

explanatory variable for the case of brick masonry constituents. As such, as shown in Table 3.12, a correlation study was also carried out involving the same configurations as shown in Table 3.11 but substituting the material density with its compressive strength (f_c).

Table 3.12: Correlation matrix for various combinations of static (E_{st}) and dynamic (E_{dy}) moduli and compressive strength (f_c) of brick masonry constituents.

Variables	E_{dy}	$\log_{10} E_{dy}$	f_c	$f_c \sqrt{E_{dy}}$	$f_c E_{dy}$	$\sqrt{f_c E_{dy}}$	$\log_{10} f_c E_{dy}$	$f_c \log_{10} E_{dy}$	$\frac{E_{dy}}{f_c}$	$\sqrt{\frac{E_{dy}}{f_c}}$
E_{st}	0.97	0.89	0.84	0.90	0.93	0.93	0.87	0.86	-0.32	-0.32
$\log_{10} E_{st}$	0.92	0.92	0.85	0.87	0.87	0.91	0.92	0.85	-0.43	-0.42

Since some researchers (Brotons et al., 2016) have reported improved correlation for some rock types when increasing levels of complexity are added to the prediction expressions, the suitability of including both ρ and f_c was also carried out. This was achieved by substituting ρ with $\rho \cdot f_c$ in all the configurations tested in (Eissa; Kazi, 1988) before calculating the correlation coefficients. The outcome is summarised in Table 3.13.

Table 3.13: Correlation matrix for various combinations of static (E_{st}) and dynamic (E_{dy}) moduli with density (ρ) and compressive strength (f_c) of brick masonry constituents.

Variables	E_{dy}	$\log_{10} E_{dy}$	$\rho \cdot f_c$	$\rho \cdot f_c \sqrt{E_{dy}}$	$\rho \cdot f_c \cdot E_{dy}$	$\sqrt{\rho \cdot f_c \cdot E_{dy}}$	$\log_{10} (\rho \cdot f_c \cdot E_{dy})$	$(\rho \cdot f_c) \log_{10} E_{dy}$	$\frac{E_{dy}}{\rho \cdot f_c}$	$\sqrt{\frac{E_{dy}}{\rho \cdot f_c}}$
E_{st}	0.97	0.89	0.87	0.93	0.94	0.94	0.87	0.89	-0.33	-0.33
$\log_{10} E_{st}$	0.92	0.92	0.86	0.87	0.85	0.91	0.92	0.86	-0.43	-0.41

As can be seen from Tables 3.11, 3.12 and 3.13, of all the explored combinations, the strength of the linear correlation is strongest directly between E_{st} and E_{dy} . Although it is clear that there is still a relatively strong linear correlation between f_c and E_{st} or $\rho \cdot f_c$ and E_{st} , none of the explored combinations with E_{dy} contribute to strengthening its linear correlation with E_{st} . As previously mentioned, this is most likely due to the variability of the sample set which reflects the diversity of typical brick masonry constituents. Different mortars have distinct chemical compositions and can harden through different setting reactions. Bricks can differ greatly according to the manufacturing process and ingredients from which they are made. Given this variability, and recognising that the heterogeneity of materials affect the static and dynamic moduli in different ways, it cannot be expected that there exists a single relation between the two moduli based on physical behaviour. However, the high value of the correlation coefficient between E_{st} and E_{dy} is a promising indicator that there exists a linear empirical relationship between the two that could be useful for many practical applications.

As such, simple linear regression was carried out between measured values of E_{st} and E_{dy} to identify the unknown parameters of the relationship between the two. To prevent the proposed model from predicting zero or negative values of the static elastic modulus from positive measured values of the dynamic one, the intercept was fixed as 0. This left the slope as the only unknown parameter to be identified through the regression. As a result of this procedure, the following expression is proposed to estimate the static elastic modulus of brick masonry constituents from measurements of the dynamic one.

$$E_{st} = 0.87E_{dy} \quad (3.5)$$

Where E_{st} and E_{dy} refer to the static and dynamic moduli measured in consistent units.

Despite the simplistic nature of the proposed expression, the measured data are in very good agreement with its predictions. In fact, although the sample of measured dynamic elastic moduli ranges more than 26 *GPa* (from 2.7 *GPa* to 29 *GPa*), the entire 95% prediction interval of the proposed relation spans only 4.6 *GPa* (see Figure 3.18). In spite of this, it is worth noting that specifically for the weakened hydraulic lime mortar used as part of this study, using a $\frac{E_{st}}{E_{dy}}$ ratio of 0.65 is recommended instead of the general proposed relationship.

It is clear to see that the proposed relationship is extremely close to one of the simplest and oldest empirical expressions proposed for concrete (Lydon; Balendran, 1986). This relation suggests that the static modulus is approximately equivalent to $0.83E_{dy}$. As such, although it is unlikely that a single relation between E_{st} and E_{dy} for brittle materials can be developed based on physical behaviour, it is undeniable that there are many similarities in the relation of these properties for such materials. Hence, several existing relationships proposed for concrete and rocks were tested on the data set containing 56 pairs of measured E_{st} and E_{dy} for various brick masonry constituents. Most of these are shown in Figure 3.18.

Although several metrics were used to assess the accuracy of the models, the standard error of the estimate (σ_e) is probably the one that is most easily interpreted since it is expressed in the units of the measurements. This parameter indicates approximately how large prediction errors are for your data set and is computed as follows.

$$\sigma_e = \sqrt{\frac{\sum_{i=1}^n (Y_i - Y_i')^2}{n - k - 1}} \quad (3.6)$$

Where Y_i refer to actual measurements of E_{st} while Y_i' refer to model predictions. With n equal to the number of data sample points and k equal to the number of explanatory variables used in the model, $n - k - 1$ represents the number of degrees of freedom available for the computation of the error metric.

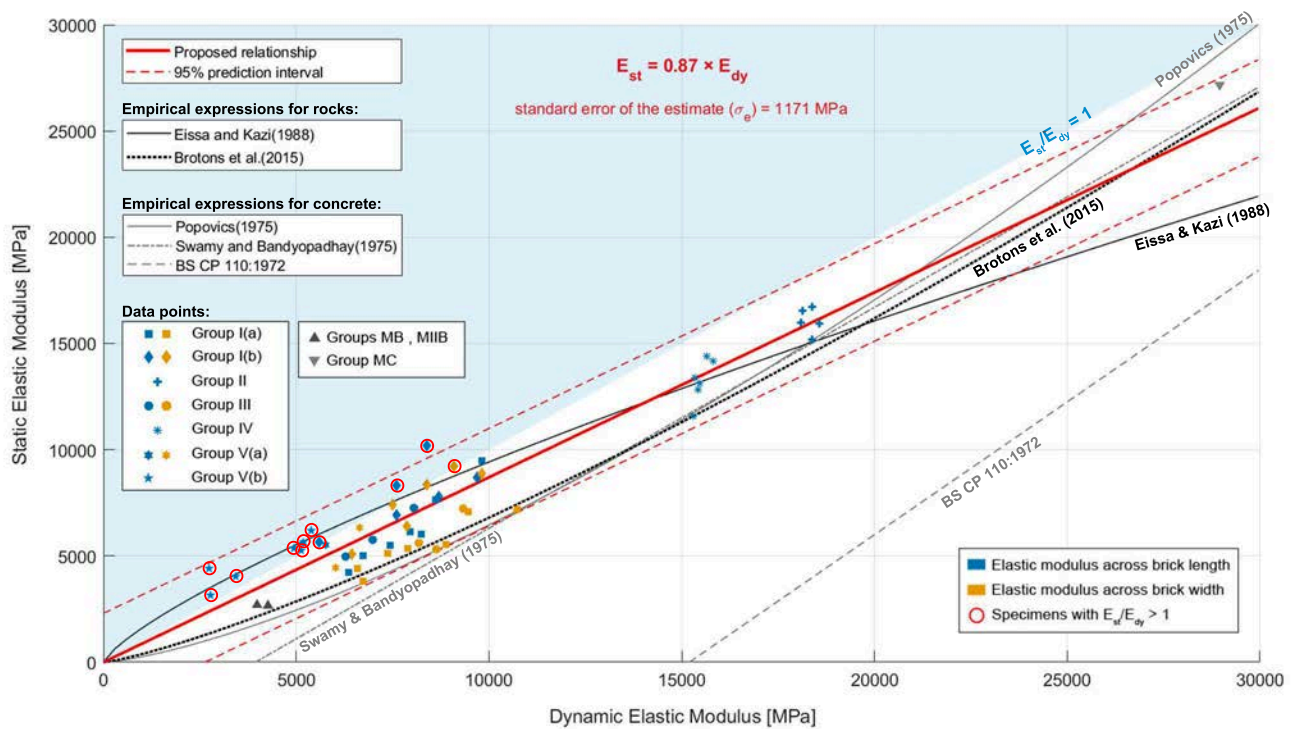


Figure 3.18: Prediction of static elastic modulus (E_{st}) from dynamic elastic modulus (E_{dy}).

The final standard prediction errors for the different models used to predict E_{st} from E_{dy} are shown in Figure 3.19. It can be seen that the proposed simple empirical expression results in the smallest error. The second most accurate model is clearly that proposed by Lydon and Balendran (1986) (Lydon; Balendran, 1986). This is expected since it has the same form as the proposed single-parameter model with only a slight variation in the magnitude of the parameter. However, having been developed for concrete, the expression proposed by Lydon and Balendran was estimated from specimens with much higher stiffness. The closeness of the two identified models thus suggests that these simple expressions have a large range of applicability which can be very useful for practical applications. The least well-performing models appear to be linear ones developed for concrete that include a non-zero intercept. Although these work well for specific types of concrete, they are clearly not suitable for lower stiffness brittle materials such as the ones tested as part of this research. That being said, specifically for the cement mortar tested as part of this research, the expression proposed by

Swamy and Bandyopadhyay (1975) for lightweight concrete (Swamy; Bandyopadhyay, 1975) provides a better estimate of the measured static elastic modulus when compared to the proposed relationship. Although the nonlinear models that incorporate density are able to better represent the relation between E_{st} and E_{dy} for some small ranges of stiffness, it is clear that over the entire range of specimens tested, they are less accurate than the simpler proposed model. Finally, the nonlinear models developed for rocks appear to be more applicable to the case of brick masonry constituents than the one developed for concrete. This is most likely due to the fact that the variability usually encountered in a sample of rocks more closely matches the variability of typical brick masonry constituents than that of concrete.

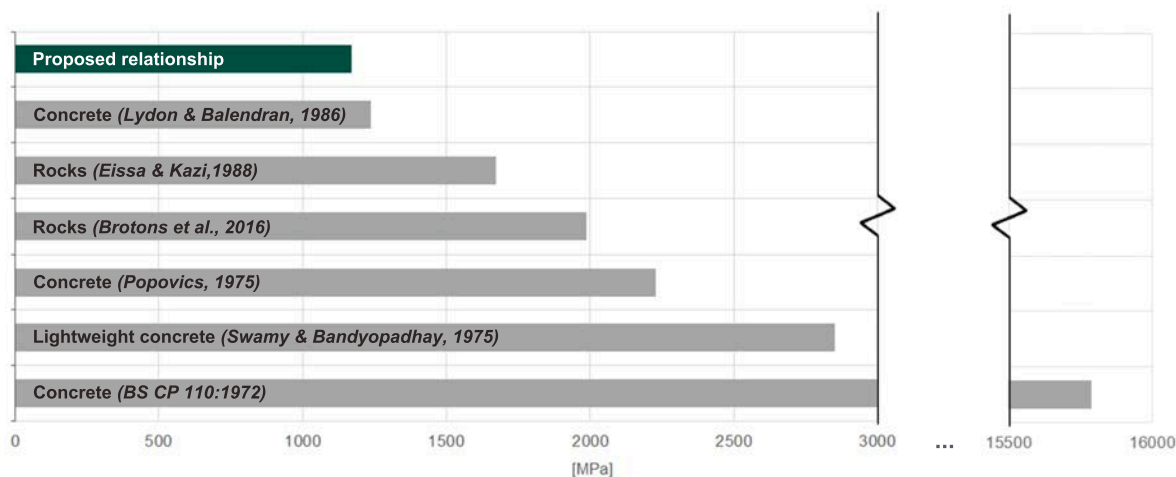


Figure 3.19: Prediction errors of various existing expressions for estimating E_{st} from E_{dy}

3.4. Summary

The research carried out in materials testing has proposed a robust procedure based on the synergy of two approaches, namely Impulse Excitation of Vibration (IEV) and Ultrasonic Pulse Velocity (UPV) testing for the determination of the dynamic elastic properties of brick masonry constituents. The influence of testing conditions and other factors specific to brick masonry constituents have been evaluated to assess the applicability of these techniques. At the same time, methods to mitigate possible sources of error have been explored and as a result, clear practical provisions have been given concerning every step of the procedure from testing protocols to the interpretation of results. Moreover, in order to derive meaningful ranges of results for different masonry typologies, the experimental program has explored different types of bricks and mortars. The tests have considered hydraulic lime mortar, cement mortar, new bricks manufactured using either hand-made moulding or extrusion, and existing bricks extracted from heritage buildings in Barcelona, Spain.

The proposed methodology can be applied to whole brick specimens as well as to specifically-cast mortar specimens. In the case of whole brick specimens, these can be recently manufactured or extracted from existing constructions. In the latter scenario, the methods described in this chapter cannot be considered as being fully non-destructive since they implicitly require the extraction of bricks from the structure. Nevertheless, both methods can be used to test extracted bricks without causing any further significant damage to the material, allowing the same bricks to be re-used or to undergo further testing. In the case of mortar specimens, since they have to be cast to specific dimensions, the proposed testing procedures are not suitable for testing mortar already present in existing masonry structures. However, the procedures can be applied to test freshly-cast mortar either for use in new constructions or intended for repair works. The results obtained from the present investigation show that the two methods (IEV and UPV) can provide reliable estimates of the actual dynamic elastic properties of typical brick masonry constituents.

For isotropic constituent materials, one of the main advantages of the proposed procedure lies in using the dynamic Poisson's ratio derived from IEV tests to improve the accuracy of the dynamic Young's modulus evaluated from conventional UPV tests based on the transmission of P-waves. Since UPV tests are simpler

and faster to execute when compared to IEV tests, a possible application of this procedure could involve determination of the dynamic Poisson's ratio using IEV testing on a selected number of specimens together with characterisation of the dynamic Young's modulus using UPV testing on a larger sample size. In the case of existing single-leaf walls, this procedure may even be extended to in-situ UPV tests on bricks.

Results from the experiments reveal that bricks produced by a conventional extrusion procedure exhibit a significant level of anisotropy. In this case, the estimation of the dynamic Young's modulus from traditional UPV tests is not reliable since the propagation of ultrasonic waves is not governed by the same simplified rules as in isotropic media. The procedure involving the combined information from flexural and torsional IEV tests to evaluate the dynamic Poisson's ratio is also not applicable to such bricks since it relies on the fundamental assumption of isotropy. Nevertheless, IEV tests can still provide estimates of effective dynamic elastic moduli which define the behaviour of brick specimens when subjected to flexural or torsional loading.

An extension of the research presented herein may explore testing procedures involving ultrasonic shear wave transducers to better characterise the dynamic elastic behaviour of anisotropic bricks. Theoretically, such transducers could also be used to directly evaluate the dynamic Poisson's ratio of isotropic constituents. However, it should be noted that accurately determining the arrival time of the shear wave can prove to be especially difficult, particularly when testing materials with significant heterogeneities and rough surfaces.

The research has also proposed an empirical expression that can be used to estimate the static elastic modulus of typical brick masonry constituents from the dynamic modulus. Since the estimation of the latter parameter can be executed more quickly and reliably, the proposed expression can be used in a wide range of practical applications. To ensure that the expression would be meaningful for different masonry typologies, the tests have considered hydraulic lime and cement mortar, new bricks manufactured either by hand-made moulding or extrusion, and bricks extracted from heritage buildings in Barcelona, Spain.

Several combinations of explanatory variables were investigated before selecting the final model. Nonetheless, simply expressing the static elastic modulus as a ratio of the dynamic one appears to be most effective over the range of materials tested. This most probably arises due to the large variability of brick masonry constituents in terms of isotropy, heterogeneity, chemical composition, and manufacturing process. It is undeniable that incorporating other explanatory variables such as density or compressive strength would lead to more accurate models for specific types of brick masonry constituents. However, the proposed expression has proven to be applicable to a wide range of constituent materials with sufficient accuracy for many practical applications.

The most useful application of the proposed expression is that it provides a means to obtain very quick estimates of the static elastic modulus from whole bricks in a laboratory setting with minimal specimen preparation. This can save considerable time when compared to the tedious and lengthy cyclic static tests usually required to estimate this property. For bricks handmade in moulds, the study also revealed that the same expression can be applied to estimate the static elastic modulus across both the length or the width of bricks. Hence, although tests across other dimensions were not explicitly included in this study, it is deemed reasonable to assume that the proposed expression can be used together with appropriate dynamic tests to quickly estimate the static elastic modulus across the thickness of bricks formed by moulding. In addition, for the case of single-leaf brick masonry walls, the proposed relationship can be used together with ultrasonic pulse velocity (UPV) testing to quickly estimate the static modulus of elasticity of bricks in-situ. In fact, the same procedure would even allow the estimation of the static elastic modulus of mortar in-situ if some very thick joints can be identified. Since conventional UPV testing with compression waves is not valid for anisotropic material, such an in-situ procedure cannot be directly extended to the case of walls built with bricks produced by extrusion.

The proposed empirical expression has been calibrated based on an accurate control over the measurements of the static modulus, as they usually exhibit higher scattering due to the relevant technical complexity of the tests. Although the applicability of the same suggested empirical expression cannot be ensured for materials differing significantly from those included in this research, the study has provided a general experimental methodology that may be replicated in the laboratory to derive alternative relationships.

4

Full-scale vibration testing

4.1. Introduction

This part of the research work first involved designing a suitable acquisition system and plan for the full-scale vibration testing of a masonry bell tower. In addition, another objective set was to evaluate the efficiency of different system identification techniques for extracting modal parameters from the acquired vibration signatures. The subject of this study is the bell-tower of Seu Vella, located in the historical city of Lleida in Catalonia, and dating back to the 14th century.

Ultimately, through the vibration testing and estimation of modal parameters, the investigation aims to characterise the dynamic behaviour of the bell tower. The effect of different bell swinging systems and ringing schemes on the dynamic behaviour was also of interest since it was planned that the bell ringing systems would be changed in the near future.

The assessment procedure involved:

- Full-scale vibration testing.
- Extraction of modal parameters (natural frequencies, mode shapes, and damping ratios) using different operational modal analysis (OMA) techniques.
- Finite element (FE) analysis, correlation with experimental results, and model updating to estimate an effective global elastic modulus for the material of the tower.

A brief description of the bell tower and its geometry is first given (Section 4.2) before presenting the numerical models employed as well as their initial predictions of the tower's dynamic behaviour (Section 4.3). The testing equipment, sensor locations, and acquisitions made are then described (Section 4.4). Subsequently, the specific data processing steps applied are presented before discussing the modal parameter estimates and the calibration of numerical models (Section 4.5). Finally, a brief discussion on the dynamic actions of different bell-ringing systems is given (Section 4.6) before summarising the main conclusions from this part of the work (Section 4.7).

4.2. The bell tower of Seu Vella

The bell tower of Seu Vella forms part of a historical complex that also includes a church, a cloister, and a canonical house. Although the historical complex consists of different parts built over different periods of time, there was a particularly notable construction effort in the second half of the 14th century that lasted up to the first third of the 15th century. It is during this time that the bell tower was built in the south-west corner of the cloister. The tower measures more than 60 m in height and has an octagonal shape in plan as shown in Figure 4.1. The diameter of the fourth floor, where the bell used for striking the hours (Silvestra) is housed, is smaller than the lower floors (see Figure 4.1).

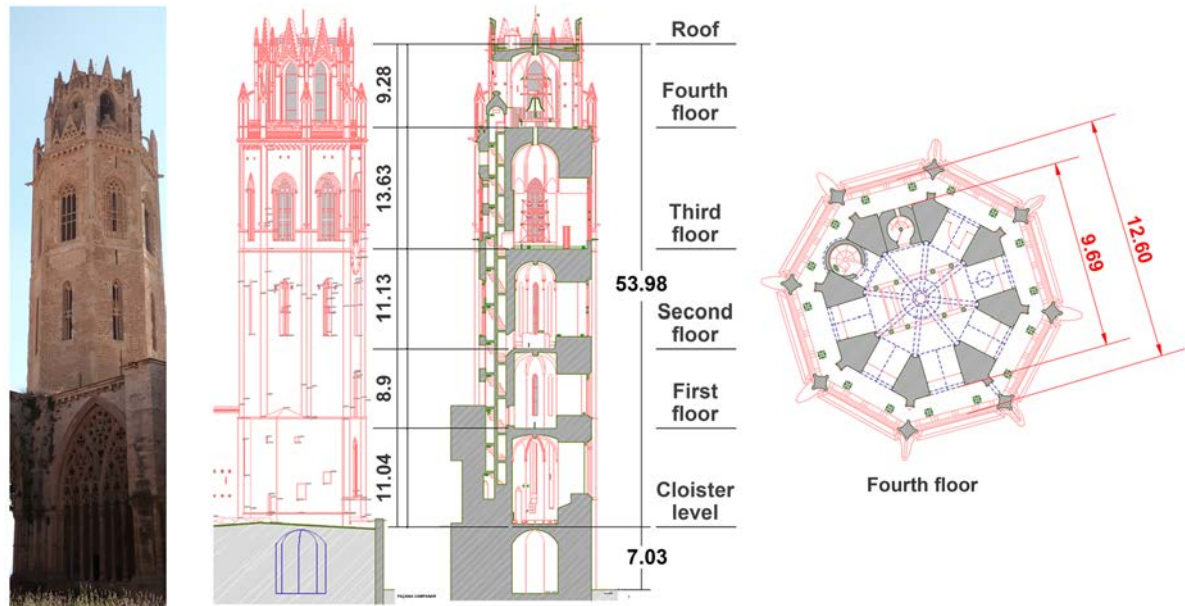


Figure 4.1: A picture of the bell tower from inside the cloister and the main dimensions of the tower (all dimensions in metres).

4.3. Expected mode shapes and natural frequencies

In order to decide the location of the accelerometers and design the acquisition system for the full-scale vibration testing, some preliminary analyses were carried out to predict the expected mode shapes.

4.3.1. Beam elements estimation

A simple FE model idealising the tower with two hollow octagonal beam elements with an isotropic homogeneous linear elastic material was first created to obtain an idea of the mode shapes that could be expected. This analysis was carried out using Autodesk Robot Structural Analysis 2017 (Autodesk, 2017). The geometry of the model and the boundary conditions are shown in Figure 4.2.

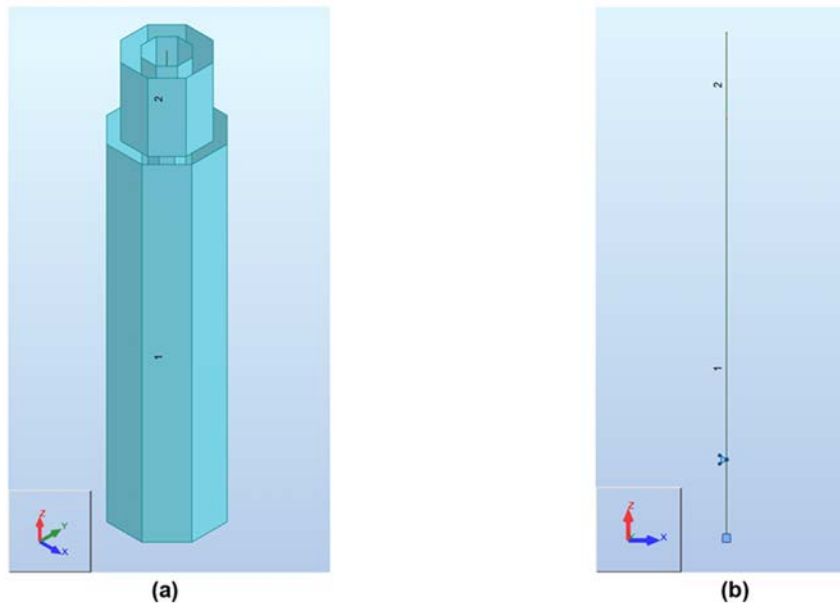


Figure 4.2: Geometry (a) and boundary conditions (b) of the beam elements model.

The base of the tower was assumed as fixed at the ground level of the cloister (see Figure 4.1), and an additional horizontal constraint was added to account for the connection of the tower to the cloister (see

Figure 4.2). In order to account for the presence of openings and the staircase, reduced diameters were used to reduce the stiffness of the beam elements. The final dimensions used for the beam elements are shown in Table 4.1.

Table 4.1: Dimensions of beam elements.

Beam element	Outer diameter [m]	Thickness [m]	Height [m]
1	11.6	4	44.70
2	8.59	2	9.28

It is known that La Seu Vella was built using two types of sandstone, namely Piedra Floresta and Piedra Vinaixa (González, 2006). Modern sandstones of this type from Lleida are known to have densities around 2300 kg/m³ (Stone Contact, 2017). Since it was observed that the mortar joints of the bell tower are relatively thin, it can be assumed that the density of the stone is a good estimate of the equivalent density of the masonry assemblage. As such, the density of the material model used for the beam elements simulation was set at 2300 kg/m³. The resulting model had a total mass of 11,157 metric tonnes (see Table 4.2). Poisson's ratio for different types of sandstone can vary significantly within the range from 0.05 to 0.40 (Gercek, 2007). Since no information was available on the Poisson's ratio of the material making up the bell tower, a value of 0.2 was assumed to be a reasonable estimate (it should be mentioned that the resulting analysis was not very sensitive to changes of Poisson's ratio within an acceptable range). No information was available on the dynamic elastic modulus of the masonry assemblage. The analysis was carried out with different values of the dynamic elastic modulus until the predicted frequencies were in good agreement with the experimentally obtained natural frequencies. The expected natural frequencies and mode shapes for a dynamic elastic modulus of 5.3 GPa are shown in Figure 4.3 and Table 4.3.

Table 4.2: Properties of beam elements model.

Density [kg/m ³]	2300
Total mass of model [metric tonnes]	11,157
Elastic modulus [GPa]	Predicted modes shown for a modulus 5.3 GPa
Poisson's ratio	0.2

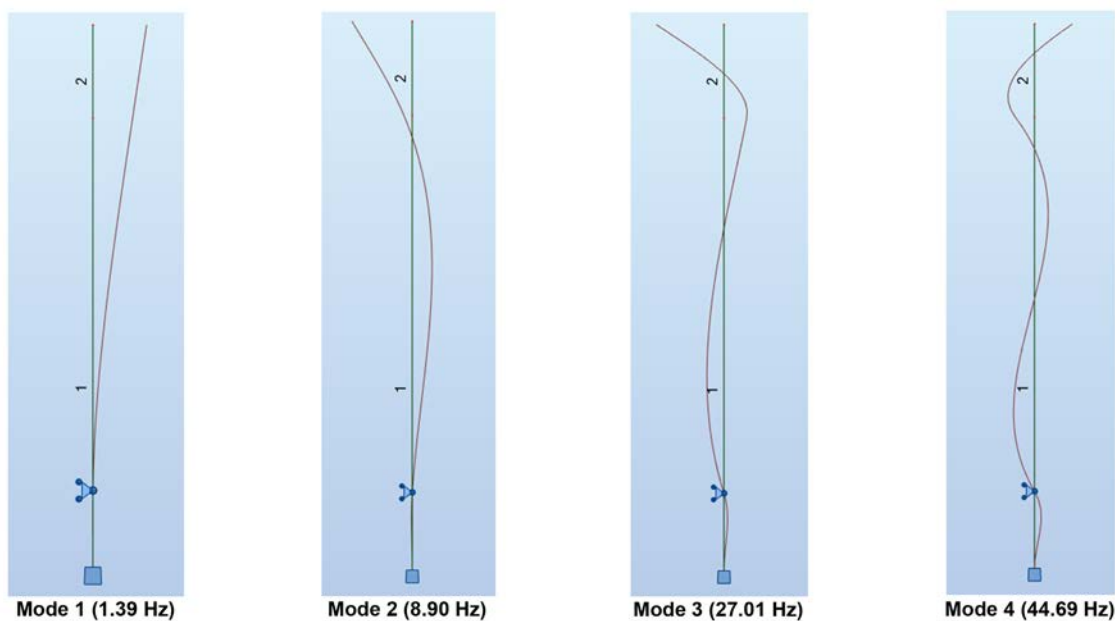


Figure 4.3: Mode shapes predicted by beam elements model with $E=5.3$ GPa.

Table 4.3: Natural frequencies and percentage mass participation for each mode predicted by beam elements model with the elastic modulus taken as 5.3 GPa.

Mode	1	2	3	4
Frequency [Hz]	1.39	8.9	27.01	44.69
Effective mass participation	50.6%	12.7%	5.7%	3.8%

4.3.2. Solid elements estimation

It is clear that the beam elements model relies on many assumptions to idealise the behaviour of the tower. For instance, the openings and the connection to the cloister can only be accounted for in an approximate manner. Moreover, this model fails to take into consideration many three-dimensional aspects that could have a significant effect on the stiffness of the tower and subsequently on the predicted mode shapes and frequencies. Hence, a more detailed three-dimensional model made up of solid tetrahedral elements was created to obtain estimates that rely on fewer assumptions. This model will be calibrated to the experimentally identified modes. The commercial software DIANA FEA Release 10.1 (DIANA FEA BV, 2016) was used to carry out this analysis. Based on available plans and elevations, the geometry shown in Figure 4.4(a) was created using 228,246 tetrahedral elements.

As was the case for the beam elements model, the base was assumed as fixed at the ground level of the cloister. The connection of the tower to the two cloister walls was modelled using horizontal constraints where visible connections exist in the real structure as shown in Figure 4.4(b). As can be seen from Figure 4.4, part of the cloister walls was included in the model in order to represent the connection more accurately. The same linear elastic material properties used for the beam elements model was used for this three-dimensional model. The properties of the model are summarised in Table 4.4.

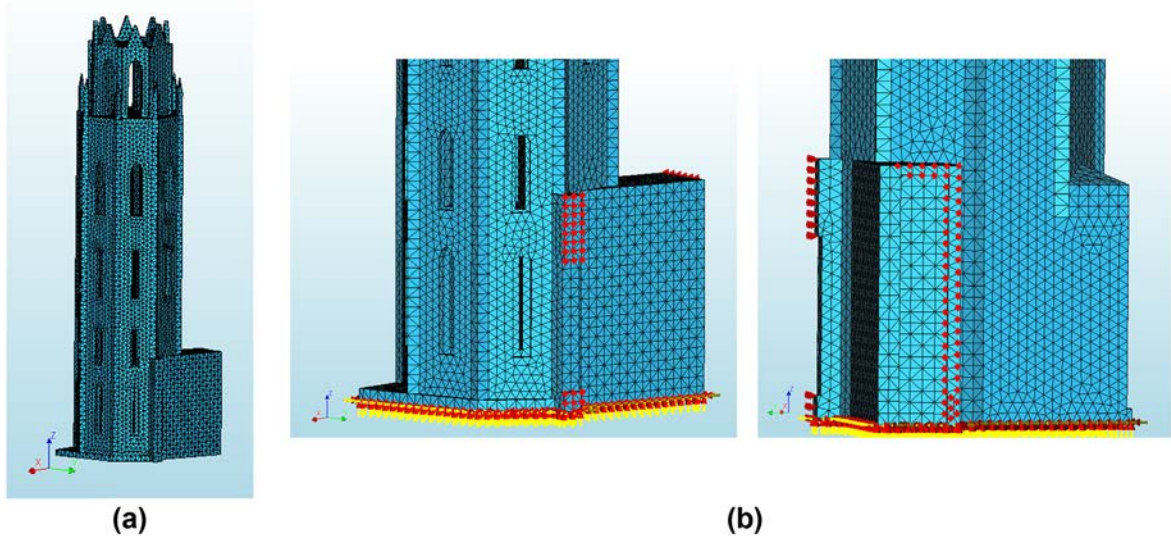


Figure 4.4: (a) Three-dimensional geometry of solid elements model and (b) imposed constraints to model connection between tower and cloister walls.

Table 4.4: Properties of solid elements model.

Density [kg/m ³]	2300
Mass of tower [metric tonnes]	11,156
Mass of cloister walls [metric tonnes]	786
Total mass of model [metric tonnes]	11,942
Elastic modulus [GPa]	Predicted modes shown for a modulus 5.3 GPa
Poisson's ratio	0.2

As can be seen from Table 4.4, the mass of the tower itself is very close to the mass of the beam elements model. This is an indication that the diameter reduction was a good approximation of the stiffness reduction caused by openings. However, the mass of the entire solid elements model is greater than that of the beam elements model, mostly due to the cloister walls.

Once again, the analysis was carried out with different values of the modulus of elasticity and the model was calibrated according to the experimentally acquired natural frequencies. The mode shapes and natural frequencies predicted by this model with the elastic modulus set at 5.3 GPa are shown in Figure 4.5.

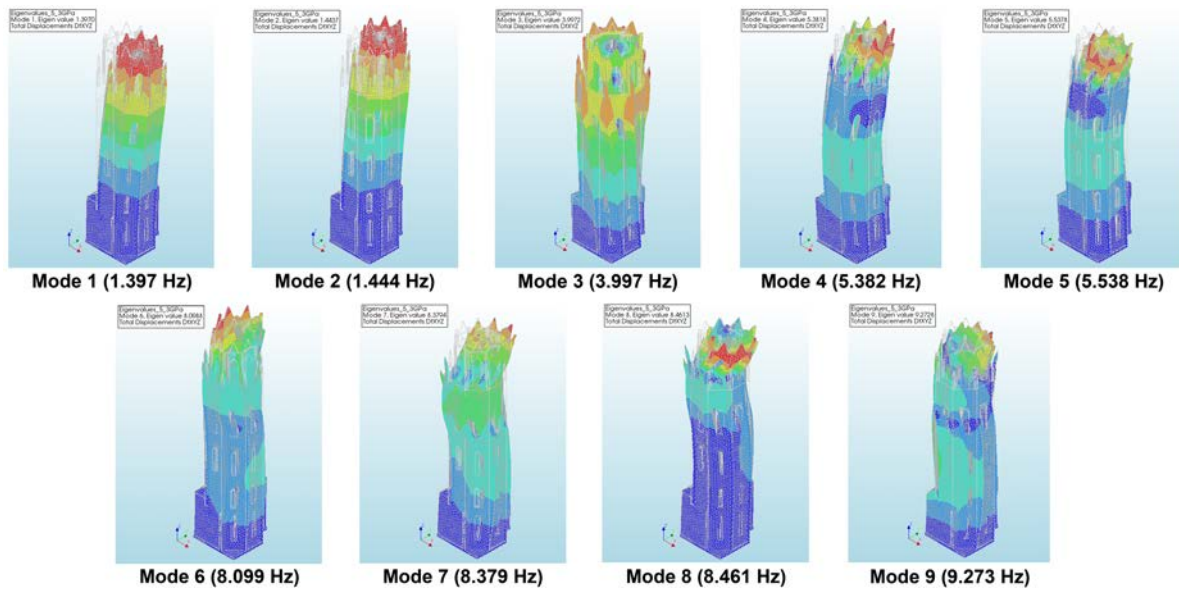


Figure 4.5: Mode shapes predicted by solid elements model with $E=5.3$ GPa.

Table 4.5: Natural frequencies and percentage mass participation for each mode predicted by solid elements model with the elastic modulus taken as 5.3 GPa.

Mode	Frequency [Hz]	Effective mass participation	Description
1	1.40	13.1%	1st bending mode along x-direction (SE-NW)
2	1.44	12.9%	1st bending mode along y-direction (NE-SW)
3	4.00	13.1%	Torsional mode
4	5.38	5.2%	2nd bending mode along y-direction (NE-SW)
5	5.54	5.6%	2nd bending mode along x-direction (SE-NW)
6	8.10	5.4%	Torsional mode
7	8.38	8.8%	Mostly bending along y-direction (NE-SW)
8	8.46	3.1%	Torsional mode mostly involving upper section.
9	9.27	4.3%	Torsional mode

The results from this analysis show that the beam elements model provides a good estimation of the frequency of the first bending mode. Nevertheless, it is clear from Figure 4.5 and Table 4.5 that the three-dimensional model is able to predict certain real modes such as the closely spaced 2nd bending mode (1.444 Hz) and the torsional 3rd mode (3.997 Hz) which the simplified beam elements model is unable to predict due to its two-dimensional nature. Moreover, the model contains much more information particularly with respect to the actual mode shapes.

Finally, this model can also predict higher frequency local modes. Although in most cases such natural frequencies are not of interest with respect to the global behaviour of the structure, they can be relevant, particularly when there are concentrated dynamic loads acting in a particular region of the structure. This is discussed in detail in Section 4.5.5.

4.4. Data acquisition

4.4.1. Sensors and data acquisition system

The main components of the data acquisition system used for vibration testing consisted of three integrated circuit piezoelectric accelerometers, a four-channel signal conditioner (PCB 482A16) that allows the gain to be adjusted ($\times 1$, $\times 10$, or $\times 100$), and an embedded real-time controller (cRIO-9064) equipped with a vibration input module (NI-9234). Power was supplied to the system through a constant current power supply. This, together with the signal conditioner ensured constant current excitation to the sensors, which is required for proper operation. The real-time controller was connected to a laptop, equipped with a programme specifically designed for this data acquisition. In addition to simultaneously recording the acceleration time-histories from all three sensors, the programme allowed visualisation of the acceleration time-history in real-time and visualisation of the corresponding power spectrum immediately after acquisition on the laptop's display. The programme used for the data acquisition was created using NI LabVIEW 2016 (National Instruments, 2016). The data acquisition system that was installed on-site is shown in Figure 4.6. The characteristics of the 3 accelerometers used are summarised in Table 4.6.

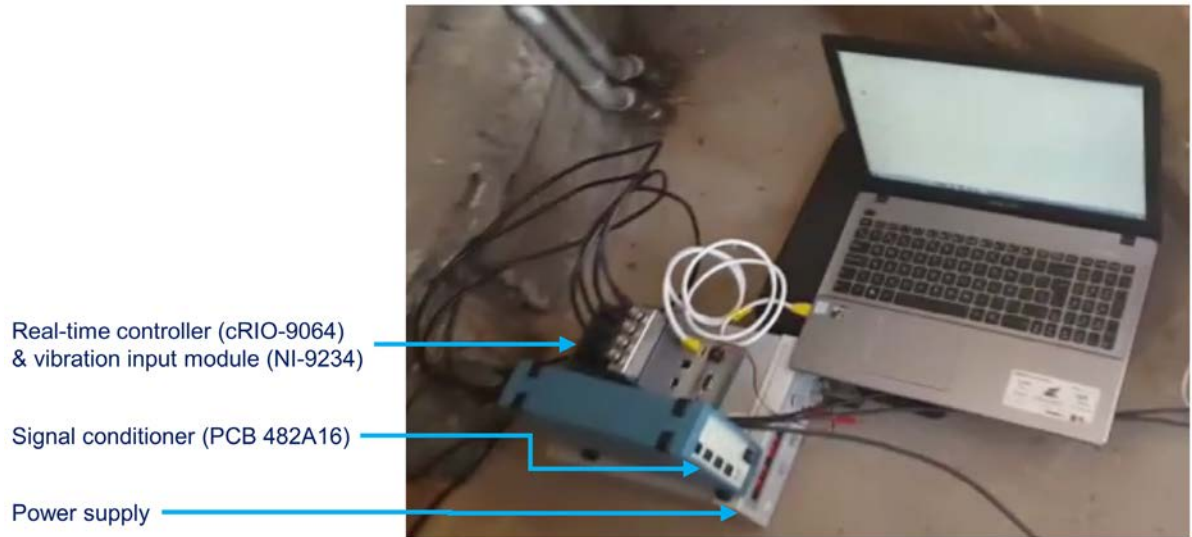


Figure 4.6: Data acquisition system and connections on-site in the bell tower of La Seu Vella.

Table 4.6: Properties of accelerometers used for the vibration tests.

Name	PT1	PU1	PU2
Model number	482C15	393A03	393C
Type	Piezoelectric	Piezoelectric	Piezoelectric
Uniaxial/ Triaxial	Triaxial	Uniaxial	Uniaxial
Mass [g]	25	210	885
Frequency range [Hz]	0.5 to 3000 ($\pm 5\%$) 0.3 to 5000 ($\pm 10\%$)	0.5 to 2000 ($\pm 5\%$) 0.3 to 4000 ($\pm 10\%$)	0.01 to 1200 ($\pm 5\%$) 0.03 to 4000 ($\pm 10\%$)
<i>Broadband Resolution [g]</i>	0.00005	0.00001	0.0001
<i>Spectral Noise (1 Hz) [$\frac{g}{\sqrt{Hz}}$]</i>	0.0000114	0.000002	-
<i>Spectral Noise (100 Hz) [$\frac{g}{\sqrt{Hz}}$]</i>	0.0000012	0.0000002	-
Effective Resolution [g]	0.00005	0.00001	0.0001
Measurement range [g]	± 5	± 5	± 2.5

4.4.2. Location of accelerometers

Based on the expected mode shapes, the three piezoelectric accelerometers were placed in the locations shown in Figure 4.7. The Triaxial accelerometer (PT1) was placed on top of the roof of the fourth floor and the positive x and y directions were oriented as shown in Figure 4.7. PU1 was placed on the exterior façade of a wall of the fourth floor with the positive direction oriented outwards while PU2 was placed on the interior façade of the wall of the third floor with the positive direction oriented inwards. All three accelerometers were placed more or less in-line on the same side with the axis of acquisition oriented approximately in the same direction. Naturally, the only acquisition along a different axis was perpendicular to this axis and was being recorded by the Triaxial accelerometer at the top.

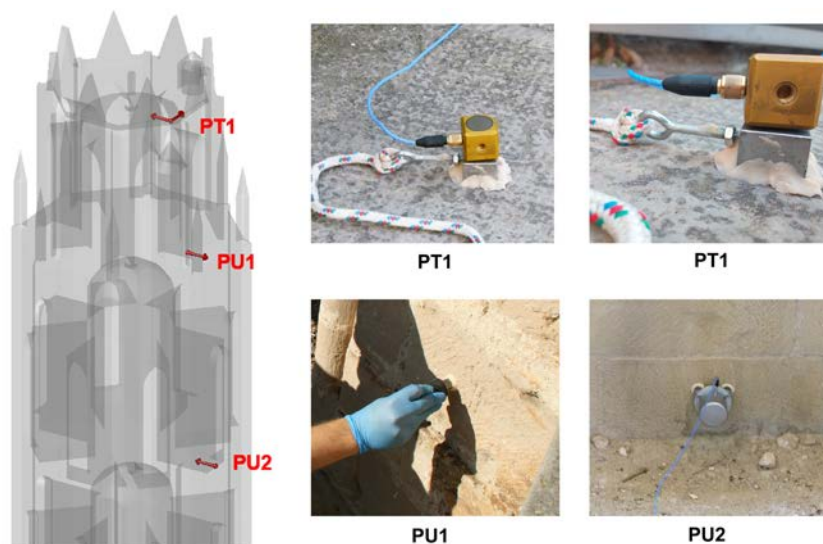


Figure 4.7: Location, positive acquisition direction, and pictures of accelerometers on-site.

As can be seen in the pictures in Figure 4.7, adhesive mounting was used to fix the sensors with a two-part glue via a mounting base. This mounting method creates a stiff connection that allows adequate vibration transmissibility. Moreover, this mounting configuration also ensures minimal sensitivity deviation in the frequency range of interest.

4.4.3. Acquisitions

As summarised in Table 4.7, different acceleration acquisitions were taken under different excitation conditions. All acquisitions were recorded with a sampling frequency of 200 Hz.

Table 4.7: Description of different acceleration time-history acquisitions.

Acquisition	Duration [mm:ss]	Description	Peak acceleration in y direction [m/s^2] (see Figure 4.17(b))
Acquisition 1	00:47	Test	0.59
Acquisition 2	06:40	Random ringing of the five liturgical bells (Third floor) - Bells swinging	0.99
Acquisition 3	06:16	Ambient vibrations	0.10
Acquisition 4	10:00	Only one of the liturgical bells ringing (Third floor) - Bell swinging	1.06
Acquisition 5	15:00	Silvestra ringing (Fourth floor) - Hammer impact on bell	0.35
Acquisition 6	12:51	Ambient vibrations	0.16

The first acquisition consisted only of a short test to verify that the data acquisition system was functioning properly and that the data could be extracted. Hence, this data was not processed further for modal parameter estimation. The unprocessed acceleration time-histories of the four channels and the corresponding frequency domain transformations for Acquisitions 2 to 6 are shown in Figures 4.8 to 4.12.

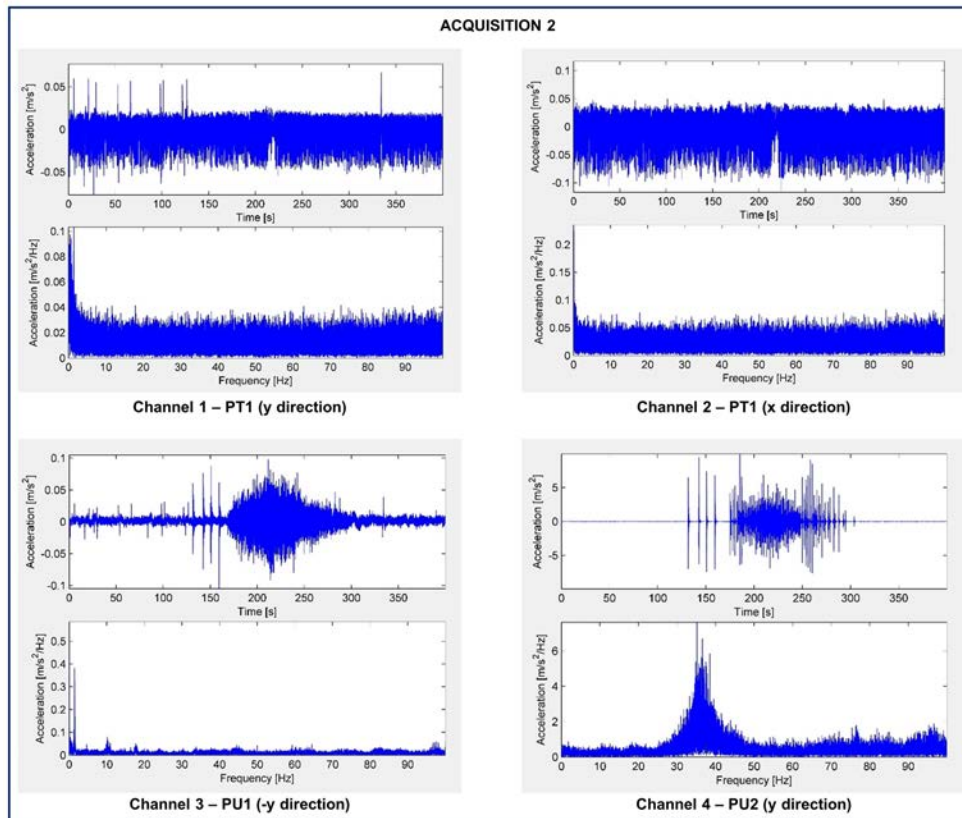


Figure 4.8: Acquisition 2 raw acceleration time-history and corresponding frequency domain transformation.

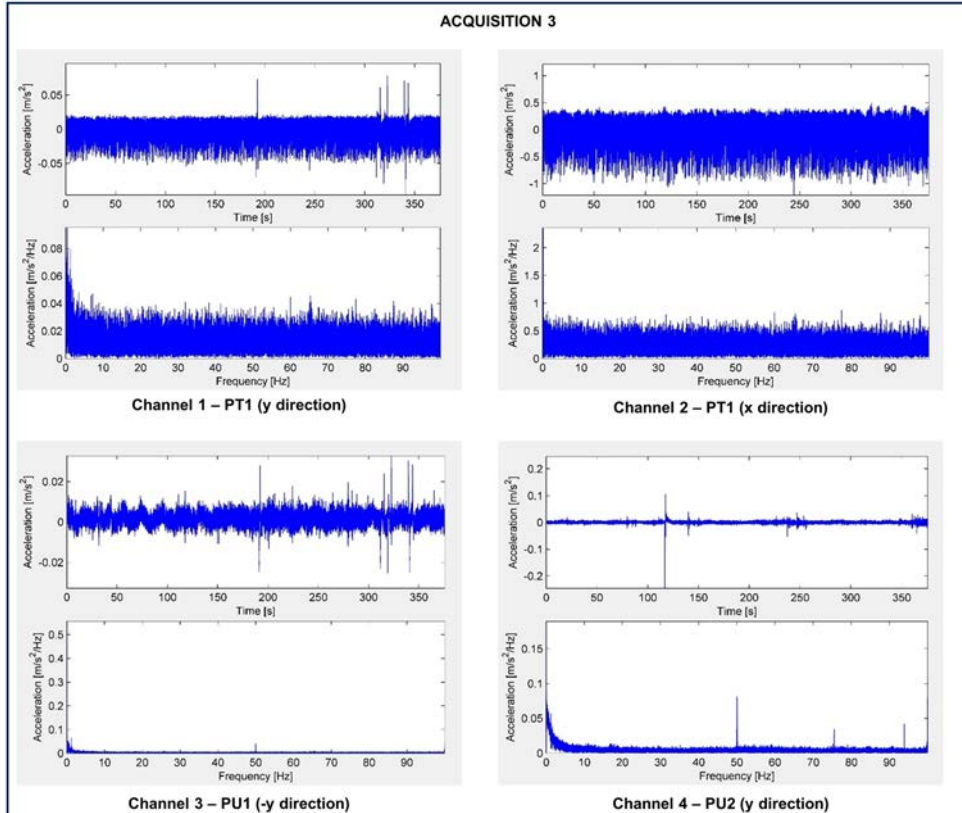


Figure 4.9: Acquisition 3 raw acceleration time-history and corresponding frequency domain transformation.

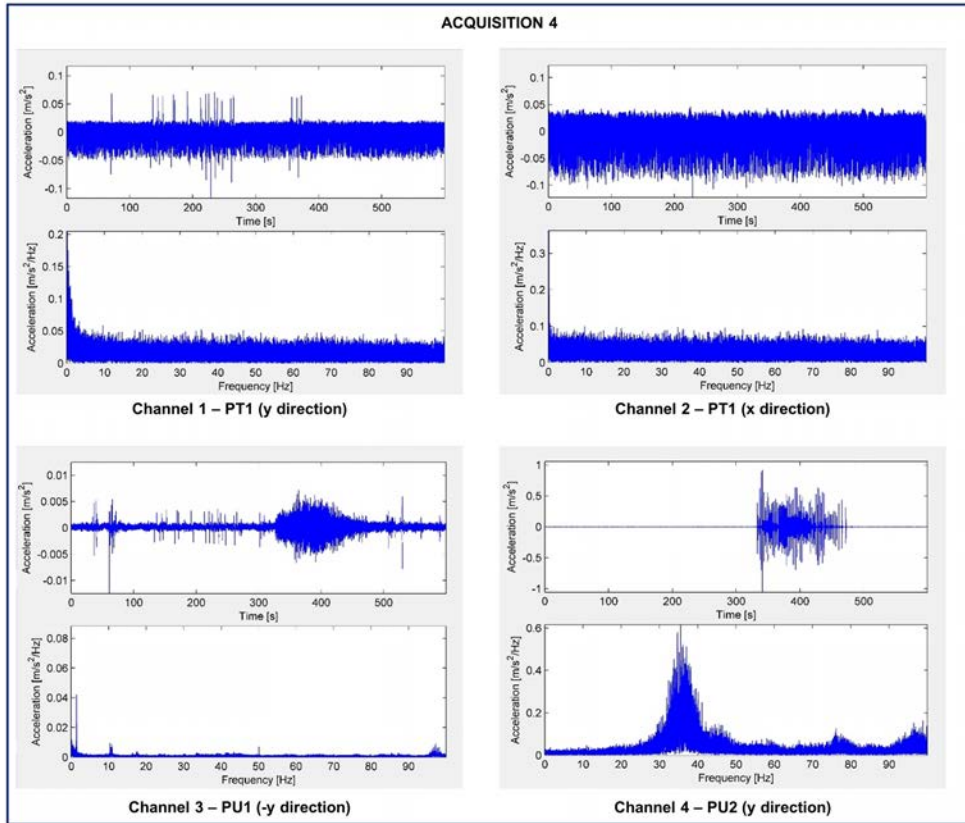


Figure 4.10: Acquisition 4 raw acceleration time-history and corresponding frequency domain transformation.

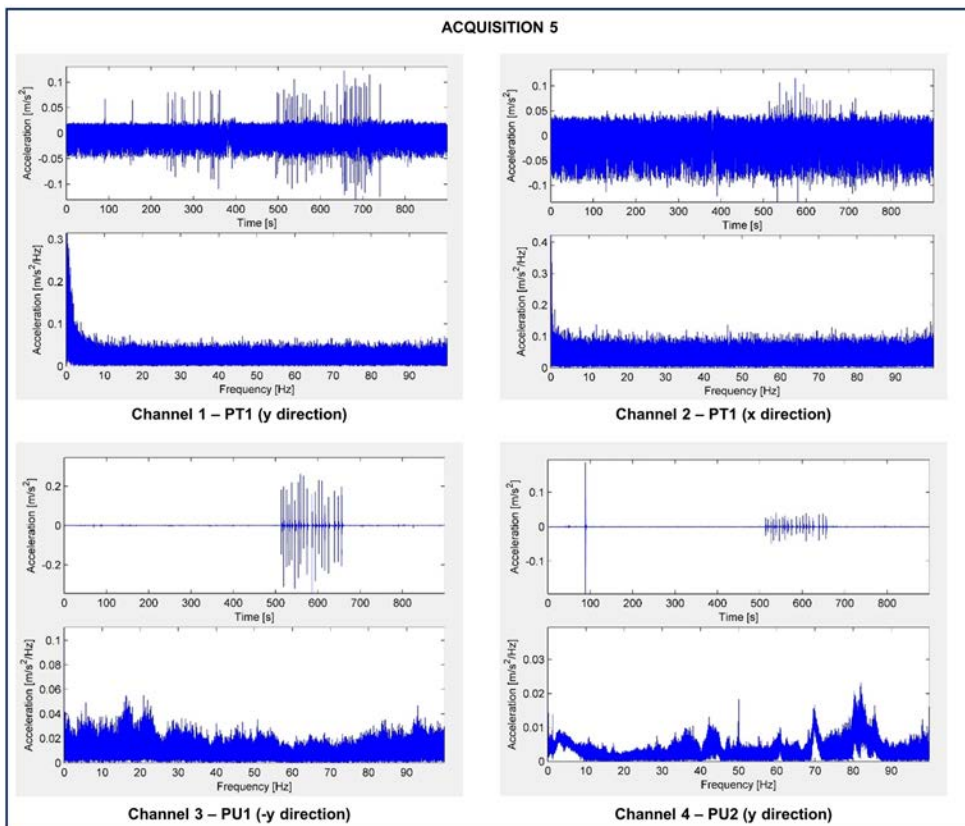


Figure 4.11: Acquisition 5 raw acceleration time-history and corresponding frequency domain transformation.

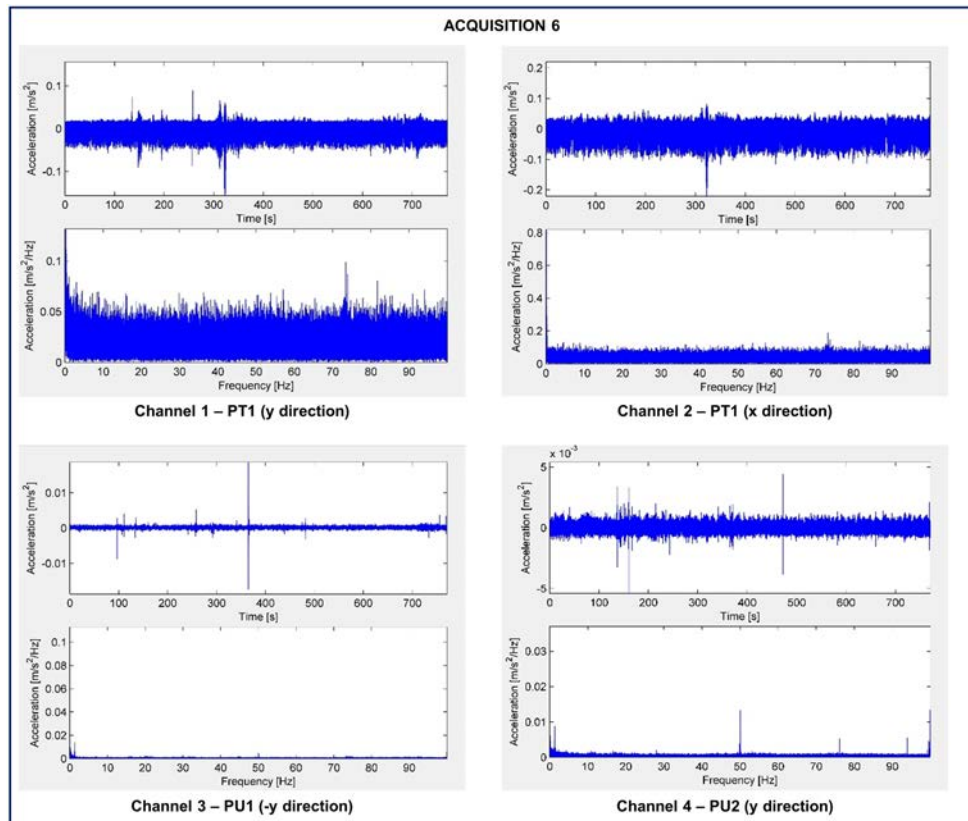


Figure 4.12: Acquisition 6 raw acceleration time-history and corresponding frequency domain transformation.

By observing these acceleration time-histories, it is clear that the signal-to-noise ratio appears to be better for channels 3 and 4 (accelerometers PU1 and PU2). This could be expected since the specifications of the triaxial accelerometer (PT1) indicate a higher spectral noise level (see Table 4.6).

4.5. Modal parameter estimations

The results obtained from the procedures described in Section 2.3 and the calibration of the numerical models are described in this section. The most important data processing steps applied are also briefly discussed. The pre-processing, system identification, and modal parameters extraction was carried out using MACEC 3.2 (Reynders; Schevenels; De Roeck, 2011), a toolbox for the MATLAB computing environment.

4.5.1. Pre-processing

As described in Section 2.3, it is usually beneficial to implement some preliminary processing to raw signals before performing system identification in order to reduce the effect of superimposed interference and excessive noise. For the purposes of this investigation, all signals were subjected to the following pre-processing:

- (i) **Offset removal**, to correct signals that had an offset from zero.
- (ii) **Decimation** with a factor of 10. When the sampling frequency is too high with respect to the bandwidth of interest, it may result in high-frequency disturbance in the data above the frequency band of interest. Using decimation, one may resample the data by selecting every j^{th} sample from the original data sequence. If the original sampling frequency was f_s , the decimated data sequence is sampled with a frequency of f_s/j . To prevent Aliasing (appearance of ambiguous signals in the time domain that are much lower in frequency than the signal being sampled), a digital anti-aliasing filter with a cut-off frequency of $f_s/2j$ must be applied. This means that only natural frequencies less than 10 Hz can be identified. Since the primordial goal is to identify the lower natural frequencies which are relevant

for the global behaviour of the structure. This decimated data sequence was preferred for this initial analysis. Another advantage of decimation is that it reduces the time of processing a signal.

- (iii) **High pass filter** with a frequency value of 0.1Hz. This was carried out to remove disturbances at very low frequencies.

4.5.2. System identification

4.5.2.1. Nonparametric Positive Power Spectral Density (PSD+) estimation

Two known methods for calculating the PSD+ matrix were investigated, the correlogram method and the periodogram method.

The **correlogram method** calculates the PSD+ by first estimating the correlation function through averaging and then taking the discrete Fourier transform (Reynders; Schevenels; De Roeck, 2011). The only parameter that needs to be specified is the number of time lags. For larger time lag values, there are less data points available for averaging, which makes the correlation estimates less accurate. However, the downside to smaller time lags is that they worsen the frequency resolution of the resulting PSD+ estimate. For this study, the correlogram approach with a time lag of 400 samples was found to provide satisfactory results and was used for all acquisitions. This resulted in a frequency resolution of 0.05 Hz.

The **periodogram method** calculates the PSD+ by dividing the available raw time data into blocks, doubling the length of each block by adding zeros, taking the Fourier transform for each block, multiplying all outputs with the Hermitian transpose of the reference outputs for each frequency, and averaging the result over all blocks (Reynders; Schevenels; De Roeck, 2011). This method relies on two user-specified parameters, the number of blocks that the raw time data will be divided into and the time window parameter, which equals the ratio between the length of one block and the length of the rectangular time window used for noise reduction. Greater values of the time window parameter results in a smoother PSD+ curve and hence a reduced noise level. However, increasing the time window parameter by 2 results in a larger frequency resolution by a factor of 2. The periodogram method was used with a different number of blocks for each acquisition so that the resulting window length was of 400 samples. This method proved to give very similar or the same result as the correlogram method for the different acquisitions. Hence, only the correlogram results are presented in this chapter.

4.5.2.2. Stochastic subspace identification (SSI)

The following four SSI methods were investigated for this study. The algorithms behind each method are not discussed here; the reader can refer to (Reynders, 2012) and (Peeters; De Roeck, 1999) for more detailed descriptions of the methods employed.

- **Covariance-driven stochastic subspace identification (SSI-cov)**

In this realisation algorithm, the raw time-histories of the output measurements, gathered in a block Hankel matrix, are converted to covariances between outputs in a block Toeplitz matrix. The decomposition (singular value decomposition) of this resulting matrix reveals the order of the system and allows the identification problem to be solved for the modal parameters.

- **Data-driven stochastic subspace identification (SSI-data)**

As is the case for SSI-cov, the raw time-histories of the output measurements are gathered in a block Hankel matrix. However, the key step of this subspace algorithm is projecting the row space of the future outputs into the row space of the past outputs. This projection is computed using QR-factorisation. The decomposition of the resulting matrix reveals the order of the system and allows the identification problem to be solved.

- **Reference-based covariance-driven stochastic subspace identification (SSI-cov/ref)**

The key difference between SSI-cov and SSI-cov/ref is that SSI-cov/ref only needs the covariances between the outputs and a limited set of selected reference channels instead of the covariances between all outputs. This makes the reference-based method less time-consuming. Moreover, if the channels showing the best signal-to-noise ratio are chosen as references, it can result in a more accurate estimation of the modal parameters (provided all the modes are present in the data of the reference channels).

- **Reference-based data-driven stochastic subspace identification (SSI-data/ref)**

The key difference between SSI-dat and SSI-dat/ref is that instead of projecting the row space of future outputs into the row space of all past outputs, SSI-dat/ref only projects the row space of future outputs into the row space of the past reference outputs. Once again, this makes the reference-based method less time-consuming and if the channels showing the best signal-to-noise ratio are chosen, the method can also lead to predictions that are more accurate (provided all the modes are present in the data of the reference channels).

As previously stated, only the system order (i) needs to be specified. Higher values of i usually yield more accurate system estimates. Reynders and Roeck describe how the choice of i is connected to the relationship between the sampling frequency and the lowest frequency of interest (Reynders; Roeck, 2008). Specifically, it is recommended that i be at least greater than the sampling frequency divided by twice the lowest frequency of interest. For the case of this investigation, that value is 71. It was found that initial values of i of 150 or 200 usually yielded good results.

In order to choose the final system order to be used for the analysis, the singular values (of the projection matrix for SSI-dat and of the block Toeplitz matrix for SSI-cov) were calculated using an expected system order of 150 or 200. The plot shown in Figure 4.13 could then be visualised. For noiseless data, the system order equals the number of nonzero singular values. For noisy data, the noise causes some singular values to be different from zero (their values are usually very low). After visualising the singular value decomposition diagram, a suitable system order was chosen which contains most of the nonzero singular values. For example, a system order of 400 was chosen for the acquisition shown in Figure 4.13.

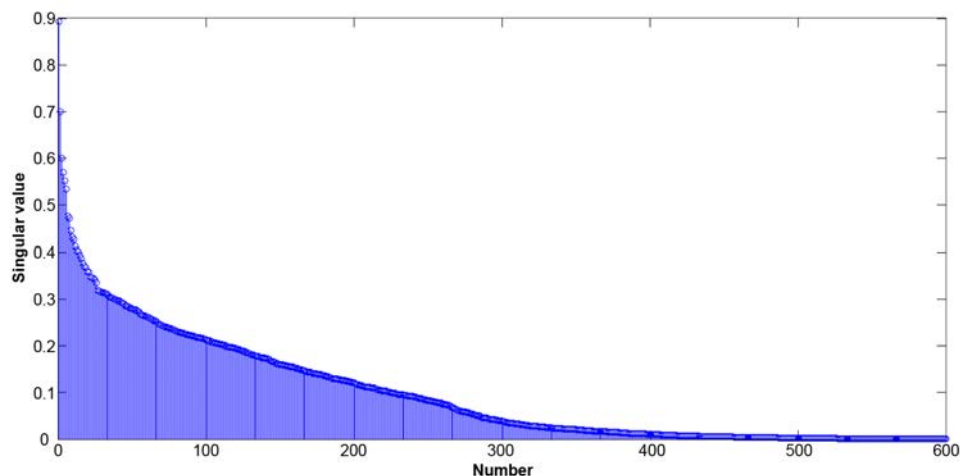


Figure 4.13: Example of a Singular Value Decomposition diagram.

When using the SSI methods with reference channels, the outputs from accelerometers PU1 and PU2, placed on the fourth and third floor respectively, were used as reference channels since they appeared to exhibit a better signal-to-noise ratio in most cases.

The covariance-driven SSI methods proved to be very time consuming and for the acquisitions for which they were attempted, did not provide additional information in comparison to the data-driven methods. Hence, only results from the data-driven SSI methods are presented in this chapter.

4.5.2.3. Operational poly-reference least squares complex frequency domain identification (pLSCF)

This algorithm is a frequency-domain algorithm and therefore the first step of the algorithm is the estimation of the Positive Power Spectral Densities. The same parameters used to estimate the PSD+ for peak picking or FDD were used. Subsequently, the only parameter that needs to be specified is the polynomial order. Polynomial orders of 100 or 150 were found to yield adequate results (note that the system order equals the matrix polynomial order times the number of references – 4 in this case).

4.5.3. Modal analysis of identified system models

4.5.3.1. Peak Picking and Frequency Domain Decomposition (FDD)

Both peak picking and FDD allow modes of structural significance to be extracted from previously computed PSD+ matrices. Although, theoretically, the FDD method allows for the accurate separation of closely separated modes, it was not always the case for the analyses of the bell tower of Seu Vella, most probably due to significant noise levels in the acquired data. In most cases, the ANPSD (used for peak picking) depicted the 1st mode more clearly than the singular values of the PSD+ matrix (used for FDD). It is important to note that neither the peak picking method nor the FDD method allow damping to be estimated.

4.5.3.2. Stabilisation diagrams

As stated in Section 2.3, stabilisation diagrams are representations that allow the distinction of modal parameters that are stable for models of increasing order (represented by points over the same vertical alignment). They can be employed to extract modes of structural significance from systems identified using the pLSCF or SSI methods.

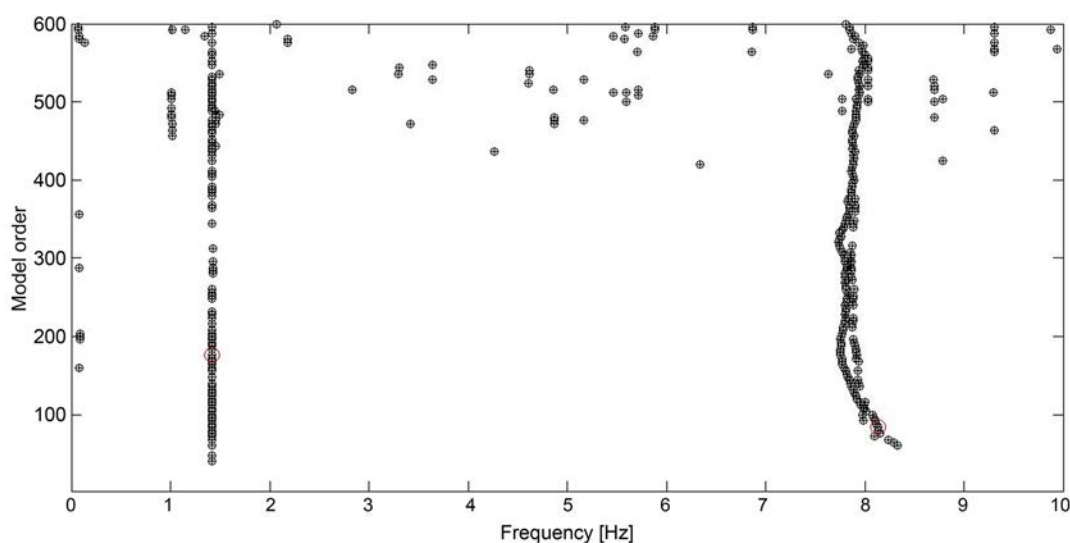


Figure 4.14: Stabilisation diagram for Acquisition 4 model identified using pLSCF.

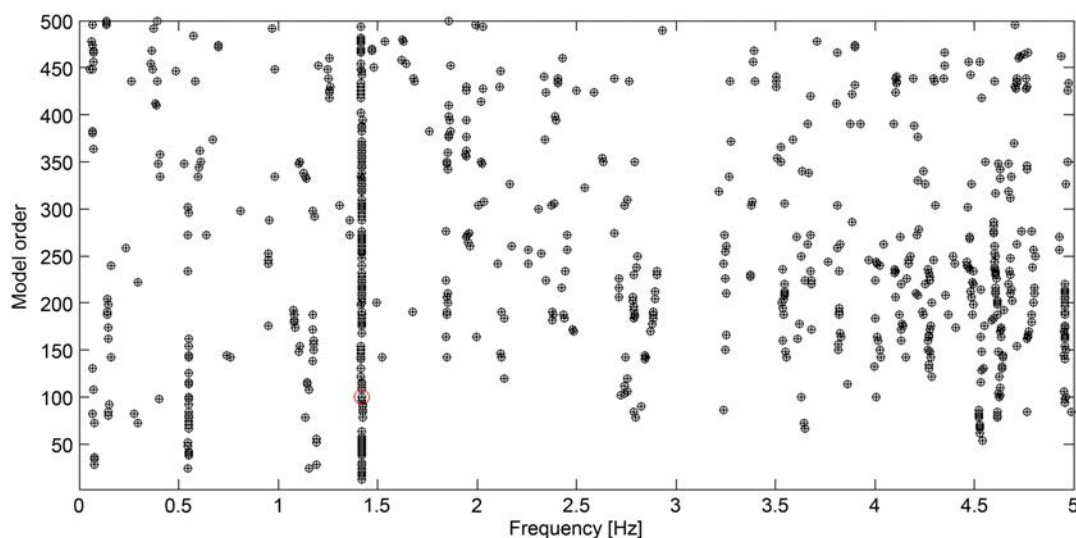


Figure 4.15: Stabilisation diagram for Acquisition 4 model identified using SSIdat.

In general, from the acquisitions analysed as a part of this study, the pLSCF methods yielded clearer stabilisation diagrams than the SSI methods (see Figures 4.14 and 4.15). This is expected, particularly given the

nature of the acquisitions and the observed noise levels. Nevertheless, it should be noted that damping estimates associated to stable modes identified using pLSCF tend to decrease with increasing noise levels, and that this worsens for poorly excited modes. In fact, as presented in Section 4.5.4, for the resonance modes identified as part of this study, the damping ratios predicted using the pLSCF methods were consistently lower than those estimated using SSI methods. The damping ratios estimated using the SSI methods can be considered as being more reliable.

It should be noted that clearer stabilisation diagrams could possibly be obtained using the SSI methods if longer acquisitions are recorded. This will not only cause variance errors of modal parameters to decay, but also result in an excitation with a more broad-banded frequency range over the length of the acquisition. The latter can contribute to clearer stabilisation diagrams because SSI methods rely on the assumption that the input is zero mean white noise.

4.5.4. Results and comparison with Finite Element (FE) model

In order to distinguish real modes from numerical modes and for more confident modal parameter estimation, both the natural frequencies and mode shapes estimated from the acquired acceleration time-histories were compared to results from the solid elements model. The model was calibrated and the effective global dynamic elastic modulus was estimated as 5.3 GPa. Two modes could be identified, namely Mode 1 and Mode 6 as predicted by the FE model with solid elements.

4.5.4.1. Natural frequencies

The natural frequencies estimated from all the identification methods and the different acquisitions are summarised in Tables 4.8 and 4.9.

Table 4.8: Estimated natural frequencies of mode 1. The coefficient of variation (CV) is shown both for estimates from different methods using the same acquisition data and for estimates obtained from different acquisitions.

MODE 1 - Natural frequency estimates [Hz]								
FEM		FDD	PP	SSIdat	SSIdat/ref	pLSCF	Average	CV
1.397	Acquisition 2	1.45	1.45	1.43	1.44	1.44	1.44	0.6%
	Acquisition 3	-	1.35	-	-	-	1.35	-
	Acquisition 4	1.40	1.40	1.42	1.43	1.42	1.41	0.9%
	Acquisition 5	-	-	-	-	-	-	-
	Acquisition 6	-	1.35	-	-	-	1.35	-
	AVERAGE							1.39

Table 4.9: Estimated natural frequencies of mode 6. The coefficient of variation (CV) is shown both for estimates from different methods using the same acquisition data and for estimates obtained from different acquisitions.

MODE 6 - Natural frequency estimates [Hz]								
FEM		FDD	PP	SSIdat	SSIdat/ref	pLSCF	Average	CV
8.099	Acquisition 2	-	-	-	-	8.04	8.04	-
	Acquisition 3	-	-	-	-	8.16	8.16	-
	Acquisition 4	-	-	-	-	8.13	8.13	-
	Acquisition 5	-	-	8.10	8.21	8.21	8.17	0.6%
	Acquisition 6	-	-	8.11	-	8.10	8.11	0.1%
	AVERAGE							8.12

It is clear that the first mode is more easily identified when bells are swinging (Acquisitions 2 and 4). It can also be observed that the frequencies estimated when five liturgical bells were swinging randomly (Acquisition 2) are slightly higher than those estimated when a single bell was swinging (Acquisition 4). In fact, it is likely that the first two bending modes have been identified here. As the solid elements model predicts, the first two modes have very close frequencies that are very much in agreement with those estimated from

the vibration recordings. Moreover, although the first two modes represent bending in different directions, the model also suggests that the first two modes have very similar mode shape vectors along the axis where three acquisition points were available (when scaled so that the PT1 component has a value of 1). Therefore, with only one (relatively noisy) acquisition point in the perpendicular direction, it becomes very difficult to differentiate the first two modes from this acquisition setup for this particular case.

From Table 4.8, it can also be observed that the natural frequency estimated under ambient vibrations only (Acquisitions 3 and 6) are slightly lower. In fact, the identification under these ambient conditions was not so straightforward. In the case of both acquisitions 3 and 6, there was a very clear peak at 1.25 Hz followed by a less obvious one at 1.35 Hz in the average normalised power spectral density (ANPSD). However, none of the more sophisticated techniques revealed an easily distinguishable mode at either of these frequencies. Since the estimated mode shape vectors were in better agreement with those predicted by the solid elements model in the case of the peak at 1.35 Hz, it was decided that this was a better estimate of the first mode.

The estimations resulting from Acquisition 5 suggest that ringing the large bell, Silvestra, by striking it with a hammer does not excite the first bending modes significantly more than under ambient conditions. In fact, the first modes could not be estimated clearly using any of the techniques attempted as part of this investigation. Clearly, the first bending modes are excited much more significantly by swinging bells that impose a dynamic horizontal load on the structure, such as is the case for Acquisitions 2 and 4. However, the 6th mode could be estimated more easily in this case. While for most of the acquisitions (Acquisitions 2,3 and 4) this mode could only be estimated using the pLSCF method, for Acquisition 5, the mode could also be estimated using two SSI methods. Moreover, considering all the acquisitions made, the mode shape vector corresponding to Mode 6 estimated from Acquisition 5 showed much better agreement with the one predicted by the solid elements model.

It should also be noted that the 6th mode could be identified quite clearly from Acquisition 6 by using the SSIdat method. Although the excitation conditions during Acquisition 3 were similar to those during Acquisition 6, the SSIdat method was not able to identify the 6th mode in this case. This could be due to the much longer acquisition time of Acquisition 6. Since the expressions for the standard deviation of modal parameters contains the term $\frac{1}{\sqrt{N}}$ with N being the number of available data samples, it is known that variance errors decay as N increases (Reynders, 2012).

4.5.4.2. Mode shapes

Most of the mode shapes estimated from different methods as part of this study were complex mode shapes. Before being able to compare them to the mode shapes predicted by the FE model, they had to be converted to real valued ones. As previously stated, mode shapes cannot be scaled in an absolute way using pure OMA as is the case here. Therefore, all mode shapes were scaled so that the mode shape vector component of Channel 1 (PT1 – y direction) was equal to 1. In addition to this, only the direction for which there were 3 points was compared since there was only one channel in the perpendicular direction.

Three points corresponding to the locations of the accelerometers were selected on the solid elements model as shown in Figure 4.16.

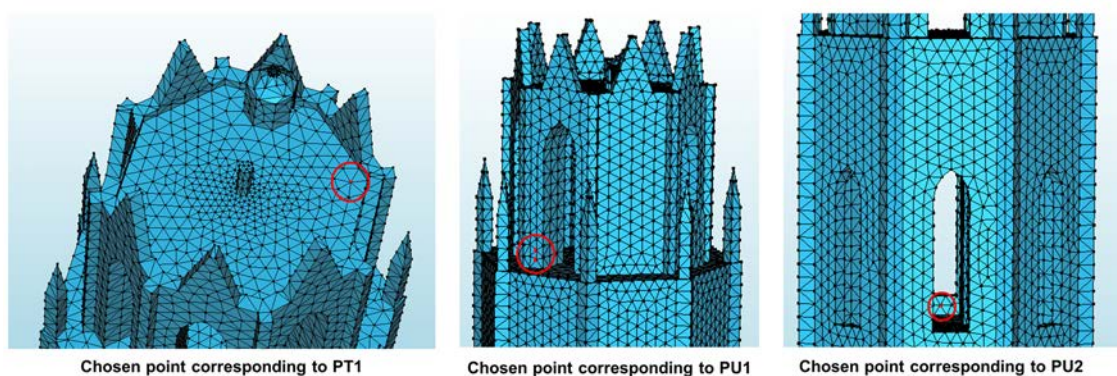


Figure 4.16: Points used for mode shape comparison.

The predicted mode shape displacements were then transformed to the simplified coordinate system used for modal parameter estimation (see Figure 4.17).

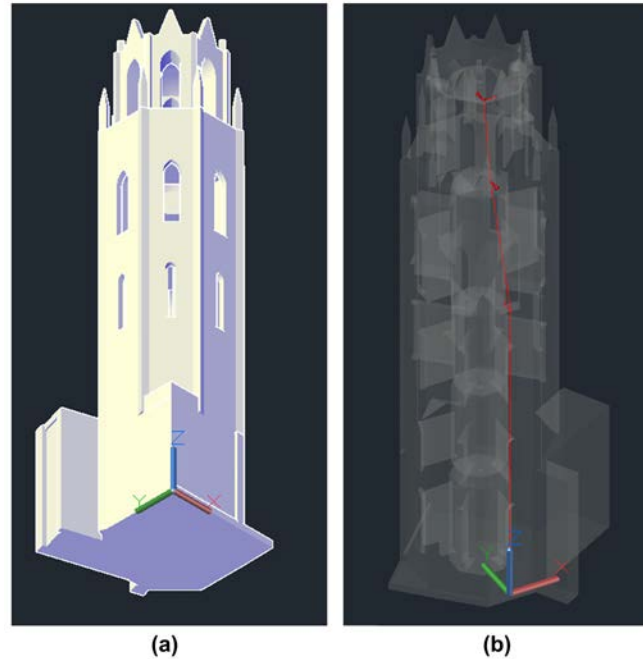


Figure 4.17: (a) Coordinate system of finite element model. (b) Coordinate system used for modal parameter estimation.

The Modal Assurance Criterion (MAC) between different mode shape vectors was computed to quantitatively compare mode shapes estimated from different acquisitions, obtained using different techniques, and predicted by FE modelling. The MAC is defined as a scalar constant relating the degree of consistency (linearity) between two modal vectors. It takes on values from zero - representing no consistent correspondence, to one - representing a consistent correspondence (Allemang, 2003).

For the first mode, the MAC values for Acquisitions 2 and 4 are summarised in Tables 4.10 and 4.11 respectively.

Table 4.10: MAC for Mode 1 (Acquisition 2).

	FEM	FDD	PP	SSIdat	SSIdat/ref	pLSCF
FEM		0.93	0.93	0.68	0.60	0.98
FDD	0.93		0.96	0.77	0.70	0.94
PP	0.93	0.96		0.59	0.51	0.89
SSIdat	0.68	0.77	0.59		0.99	0.80
SSIdat/ref	0.60	0.70	0.51	0.99		0.73
pLSCF	0.98	0.94	0.89	0.80	0.73	

Table 4.11: MAC for Mode 1 (Acquisition 4).

	FEM	FDD	PP	SSIdat	SSIdat/ref	pLSCF
FEM		0.70	0.78	0.98	0.98	0.99
FDD	0.70		0.99	0.80	0.81	0.78
PP	0.78	0.99		0.86	0.87	0.85
SSIdat	0.98	0.80	0.86		1.00	1.00
SSIdat/ref	0.98	0.81	0.87	1.00		1.00
pLSCF	0.99	0.78	0.85	1.00	1.00	

In both cases, the mode shape vector closest to the prediction from the solid elements model was ob-

tained using the pLSCF method.

For Acquisition 4, the time domain methods provide estimated mode shapes that are significantly closer to the prediction from the solid elements model when compared to those obtained from non-parametric frequency domain methods (Peak Picking and FDD). However, for Acquisition 2, it is interesting to note that the more sophisticated time domain methods result in estimates that are much less consistent with the FE prediction when compared to the frequency domain methods. Since the 5 bells on the third floor were swinging randomly during Acquisition 2, it is likely that this disparity arises from the fact that the excitation did not satisfy the assumption of SSI that the input is zero mean white noise. In fact, closer inspection of the estimated mode shape vectors reveals that the disparity occurs mostly due to the sign of the component of the mode shape vector corresponding to PU2, the uniaxial accelerometer placed on the third floor. In fact, the magnitudes of the components of the mode shape vector estimated using SSIdat are in fact closer to those predicted by the solid elements model when compared to those estimated using PP, FDD, and even pLSCF for this case.

For Acquisitions 3 and 6, the 1st mode could only be estimated using the Peak Picking method. When compared to the mode shape predicted by the solid elements model, the estimated mode shapes from Acquisition 3 has a MAC of 0.57 whereas that estimated from Acquisition 6 has a MAC of 0.60.

Figure 4.18 shows the estimated shape of the 1st mode from each acquisition which showed the best agreement with the one predicted by the solid elements model. It is clear that the best estimate arises from Acquisition 4 during which a single bell on the third floor was swinging.

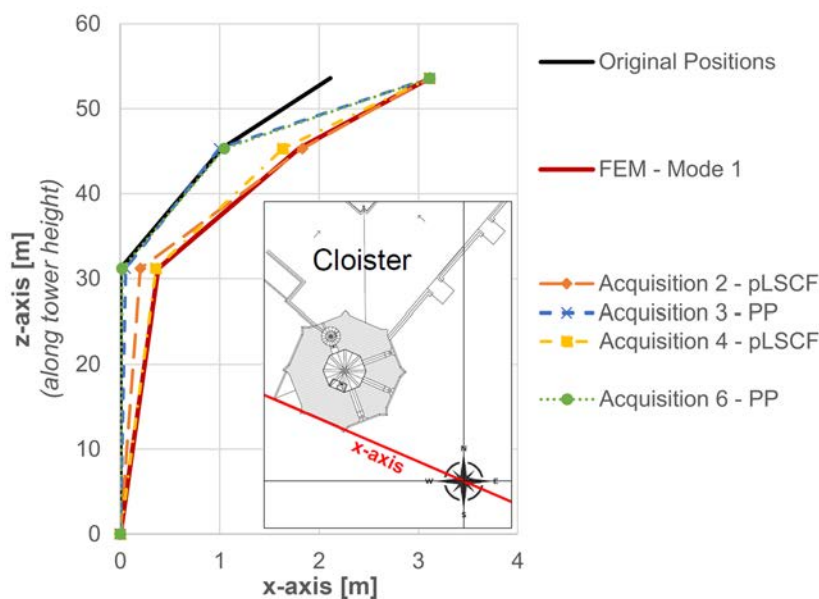


Figure 4.18: Comparison of estimated mode shapes for Mode 1 from different acquisitions. The same displacement component has been used to scale all mode shapes to allow a fair comparison.

For the 6th mode, the MAC values for Acquisition 5 are summarised in Table 4.12. Once again, the estimated mode shape most consistent with the prediction from the solid elements model was obtained using the pLSCF method.

Table 4.12: MAC for Mode 6 (Acquisition 5).

	FEM	SSIdat	SSIdat/ref	pLSCF
FEM		0.83	0.79	0.93
SSIdat	0.83		1.00	0.97
SSIdat/ref	0.79	1.00		0.96
pLSCF	0.93	0.97	0.96	

For Acquisition 6, both the SSIdat and the pLSCF method resulted in estimated mode shapes with a MAC value of 0.79 when compared to the prediction from the solid elements model, with the pLSCF estimate being slightly more consistent with the FE model. From all the other acquisitions (Acquisition 2, 3, and 4), this mode could only be estimated using the pLSCF method. The MAC values comparing the estimated mode shapes from all acquisitions using the pLSCF method to the prediction from the solid elements model are summarised in Table 4.13. The predicted mode shape for Mode 6 by the solid elements model is compared to the corresponding estimated mode shape from each acquisition that best matches it in Figure 4.19.

It is clear that the mode shape most consistent with the solid elements model was estimated from Acquisition 5.

Table 4.13: MAC for Mode 6 (estimates from all acquisitions using the pLSCF method).

	Acquisition 2 (pLSCF)	Acquisition 3 (pLSCF)	Acquisition 4 (pLSCF)	Acquisition 5 (pLSCF)	Acquisition 6 (pLSCF)
FEM	0.66	0.79	0.79	0.93	0.79

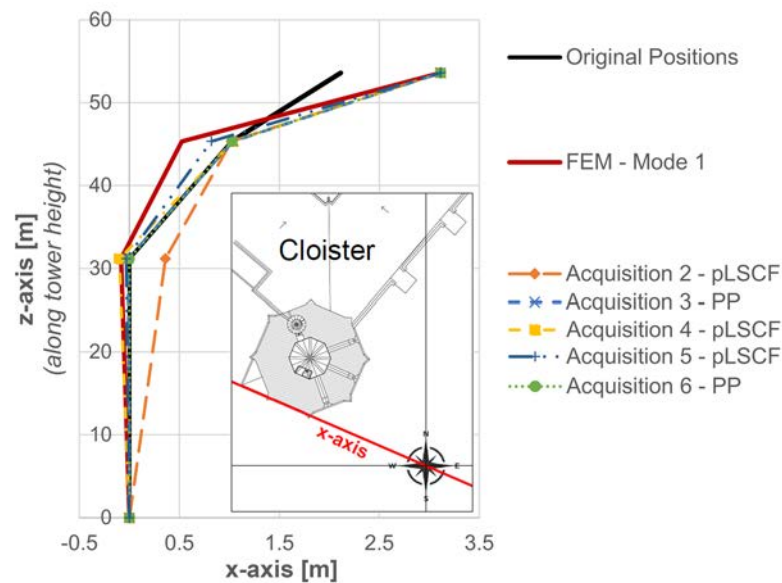


Figure 4.19: Comparison of estimated mode shapes for Mode 6 from different acquisitions. The same displacement component has been used to scale all mode shapes to allow a fair comparison.

4.5.4.3. Damping ratios

Damping ratios could only be estimated using SSI and pLSCF methods. The estimates of damping ratio identified using these methods from all acquisitions are summarised in Table 4.14 for Mode 1 and Table 4.15 for Mode 6.

The low damping ratio estimated for Mode 1 is characteristic to masonry bell towers. The estimates from the different methods are generally in good agreement with a standard deviation of approximately 0.3%. This suggests that the estimate is a rather accurate one. The consequence of such a low damping ratio (0.61%) is that it can cause a high dynamic amplification factor when the excitation frequencies from the swinging bells come close to one of the tower's natural frequencies (Ivorra; Pallarés; Adam, 2011b). The damping ratio estimates for Mode 6 are significantly higher and the fact that the standard deviation is quite significant (15.2%) indicates that they are less accurate estimates.

It can be observed that the damping ratios predicted using the pLSCF method tend to be lower than those estimated using the SSI methods. This difference can be attributed to the nature of the pLSCF method itself and can be expected to increase with increasing noise levels. The effect is particularly dramatic for the damping ratio associated to Mode 1 and estimated from Acquisition 2.

Table 4.14: Damping ratio estimates for Mode 1. The coefficient of variation (CV) is shown both for estimates from different methods using the same acquisition data and for estimates obtained from different acquisitions.

MODE 1 - Damping ratio estimates [%]					
	SSIdat	SSIdat/ref	pLSCF	Average	CV
Acquisition 2	0.63	1.06	0.14	0.61	61.6%
Acquisition 3	-	-	-	-	-
Acquisition 4	0.64	0.62	0.56	0.61	5.6%
Acquisition 5	-	-	-	-	-
Acquisition 6	-	-	-	-	-
AVERAGE				0.61	0.3%

Table 4.15: Damping ratio estimates for Mode 6. The coefficient of variation (CV) is shown both for estimates from different methods using the same acquisition data and for estimates obtained from different acquisitions.

MODE 1 - Damping ratio estimates [%]					
	SSIdat	SSIdat/ref	pLSCF	Average	coeff. of variation
Acquisition 2	-	-	7.18	7.18	-
Acquisition 3	-	-	7.48	7.48	-
Acquisition 4	-	-	8.61	8.61	-
Acquisition 5	9.51	11.86	11.03	10.8	9.0%
Acquisition 6	8.11	-	8.1	8.11	0.1%
AVERAGE				8.44	15.2%

4.5.5. Identification of higher frequency local modes

The original acceleration-time histories were decimated by a factor of 10 and consequently natural frequencies greater than 10 Hz were not investigated in-depth. Nevertheless, the original frequency domain transformations of the data from the uniaxial accelerometer on the third floor (PU2) suggest that there could be a natural mode of vibration at approximately 35 Hz which was noticeably excited during Acquisitions 2 and 4, when the bells on the third floor were swinging (see Figures 4.8 and 4.10). Although such modes are usually not very important for the global structural behaviour, their excitation could potentially have significant effects on certain local members. It is in fact interesting to observe that the calibrated solid elements model predicts a natural mode of vibration at 34.3 Hz with the shape shown in Figure 4.20.

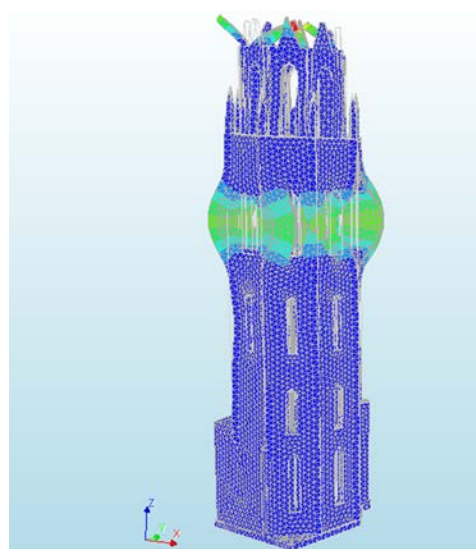


Figure 4.20: Local mode shape predicted by numerical model at 34.3 Hz.

Despite only involving a mass participation of 1.16%, it is possible that this vibration mode is excited when bells on the third floor are swinging. More in-depth analysis can be carried out to better understand such resonance modes if they are of interest in specific cases.

4.6. Dynamic action of bells

The swinging of bells on belfries is a classical problem in structural dynamics. Swinging bells can be classified according to the system which controls their movement. In general, three common swinging systems exist: the Central European, English, and Spanish systems (Ivorra et al., 2006). Each system presents some singular characteristics of frequency and oscillation that give rise to different forces that are variable in time on their supporting structures. Only the Central European and Spanish systems will be discussed here since they are the only ones relevant for the bells of the tower of Seu Vella.

In the Central European system, the bells tilt on their axis up to a maximum swing angle with no counterweight. This system can be highly unbalanced and as such are usually located inside a tower with structures specifically designed to that effect (Ivorra et al., 2006).

On the other hand, in the Spanish system, a counterweight provides a high level of balance and the bells rotate continuously in the same direction (Ivorra et al., 2006).

All the liturgical bells of the bell tower of la Seu Vella found on the third floor originally used to swing according to the Spanish system. However, the bell ringing system was modified in the past so that, at present, they swing according to the Central European system with a maximum swing angle of 80°. Moreover, the bell striking the hours, Silvestra, has also been modified to swing according to the Central European system. Previous studies, notably (Ivorra et al., 2006), clearly show that this can exert considerably more significant horizontal dynamic loads on the structure.

Naturally, in order to quantify this effect, the dynamic forces due to the bells of La Seu Vella (listed in Table 4.16) must first be computed. Analytical models exist to estimate these dynamic forces for a specific bell and they rely on knowledge of the bell's weight, the distance from the bell's centre of gravity to the rotation axis, and the moment of inertia of the bell (Heyman; Threlfall, 1976; Ivorra et al., 2006; Ivorra; Giannoccaro; Foti, 2019).

Table 4.16: Known information on the bells of the bell tower of Seu Vella.

Bell	Description	Weight [kg]	Diameter [cm]	Bronze Height [cm]
Meuca		96	55	53
Marieta I		190	69	61
Crist	Liturgical bells (third floor)	244	75	65
Puríssima		368	86	78
Bàrbara		496	95	83
Mònica	Bell for striking quarter-hours (fourth floor)	408	89	75
Silvestra	Bell for striking the hours (fourth floor)	4632	200	148

4.7. Summary

The results of the operational modal analysis (OMA) carried out on the bell tower of Seu Vella indicate that its first natural frequency can be considered as being 1.39 Hz. In addition to this, the 6th mode was estimated as having a frequency of 8.09 Hz from the recorded acquisitions. A detailed three-dimensional finite element (FE) model of the structure was also calibrated based on estimates derived from the OMA. According to the calibration of this linear elastic model, the material making up the bell tower can be considered as having a global dynamic elastic modulus of 5.3 GPa.

Moreover, the analysis also allowed the damping ratio corresponding to the first mode of vibration to be estimated as 0.61%. Such a low damping ratio can cause a high dynamic amplification factor if the excitation frequencies of the swinging bells come close to this natural frequency. With respect to swinging bells, previous studies clearly show that a bell swinging according to the Central European system tends to impose much greater horizontal dynamic loads when compared to one swinging according to the Spanish system.

Following this investigation, the effect of different bell ringing systems can be compared quantitatively by analysing the inertia forces caused by different swinging systems, characterising the dynamic nature of these forces, and computing the possible dynamic amplification factors of these loads.

Several acquisitions corresponding to distinct excitation conditions were processed using several different modal parameter estimation techniques as part of this study. From all the system identification methods explored, the operational poly-reference least squares complex domain identification (pLSCF) method proved to be fairly robust at being able to identify modes of structural significance under various excitation and noise conditions. In fact, for modes identified as part of this study, the mode shapes estimated using pLSCF were consistently in better agreement with predictions from the FE model compared to those predicted by other techniques, including the more time-consuming time-domain methods. However, it is important to note that the damping ratio estimates from pLSCF proved to be less reliable than those obtained from the time-domain methods.

In fact, it must be said that the modal parameter estimates obtained from the time-domain methods could prove to be significantly different if longer acquisitions with a better signal-to-noise ratio were taken. Specifically, the signal-to-noise ratio could be improved by not placing any accelerometer on the roof since that makes recordings susceptible to being affected by local vibration modes of the roof itself. Another improvement that could be made to the testing procedure itself involves placing at least one additional accelerometer to capture vibrations perpendicular to the main axis of acquisition used for this investigation. This could help to separate identification estimates of the first two bending modes that appear to be very closely spaced in terms of frequency. More accelerometers can also be strategically placed to identify higher order modes such as the torsional one. Such measures can lead to a significant increase in the confidence levels associated to the estimated modal parameters.

5

Structural health monitoring

5.1. Introduction

This part of the research work aims to develop a holistic automated procedure for the processing and analysis of data collected by static SHM systems. The proposed procedure consists of two parts. The first includes steps on how to implement models comprehending an **Auto-Regressive** output and an **eXogenous** input (ARX) to filter out environmental variability for entire static SHM systems installed in masonry heritage structures. The second part includes further processing steps to facilitate the interpretation of results from the first part of the procedure for the overall diagnosis of the structure being monitored.

Before presenting analysis methodologies, a brief overview of key data pre-processing procedures applicable to static SHM of heritage structures is presented (Section 5.2). The aim of this section is not to give an exhaustive overview of all the pre-processing possibilities but rather to present key steps that although are not directly related to the analysis procedure are essential for the accuracy of the analysis results. Following this section, a series of simple and intuitive methods that have previously been applied to analyse data from static SHM of masonry heritage structures are presented (Section 5.3). The proposed methodology utilising ARX models is then elaborated (Section 5.4). Every methodology described is then applied to data from two case studies (Section 5.5), namely the cathedral of Mallorca (monitored from 2003 to 2008) and the church of the monastery of Sant Cugat close to Barcelona (ongoing monitoring since 2017). For the latter case, a user-friendly tool developed in the MATLAB computing environment is currently used to quickly and easily update analysis results as new data is received from the monitoring system. This tool is presented in Section 5.5.2 together with the results from applying the proposed procedure to this case study. For both case studies, a comparison of the outcomes that can be derived from the proposed procedure to those obtained from the more intuitive methods presented is also carried out. The results reveal that the proposed automated data analysis procedure can greatly facilitate the prognosis of masonry heritage structures.

5.2. Data pre-processing

When it comes to static SHM of masonry heritage structures, two stages of pre-processing are normally implemented before any further analysis is carried out. Since raw signals from sensors come in a variety of forms such as voltage, current, resistance or frequency, the first pre-processing stage consists in converting these signals to meaningful physical units as well as correcting the readings to account for thermal expansion of the materials making up the sensors. It is convenient to automatically program this pre-processing stage at the

Parts of this chapter have been published in:

- MAKOOND, N.; PELÀ, L.; MOLINS, C.; ROCA, P.; ALARCÓN, D., 2020c. Automated data analysis for static structural health monitoring of masonry heritage structures. *Structural Control and Health Monitoring*. ISSN 1545-2255. Available from DOI: 10.1002/stc.2581

level of the data logger itself. The second pre-processing stage involves removing any anomalies present in the data that are not caused by a physical phenomena related to the structural behaviour. These often appear as "spikes" in sensor data (Cornelis; Peeters, 2014) and can originate from several sources such as capacitive or inductive noise in the analog signal path, communication errors (Halfpenny, 2008) or undesired external interactions with the sensor. With respect to the case studies forming part of this research, on rare occasions where such spikes were identified, the data points related to the anomaly were deleted and replaced with corresponding values based on linear interpolation of neighbouring non-anomalous values. This was considered an acceptable approach for the case of static SHM because it can be expected that anomalies will be scarce due to the high quality of modern sensors and cables, combined with the comparatively low sampling rate of such systems (samples usually collected every 15 min or every hour). Moreover, any complex procedure to detect and remove anomalies will incur an additional risk of eliminating data that could provide valuable information on the evolution of the response variables in question. Nevertheless, it must be said that since anomaly detection from time series is an important problem with applications in many fields (Chakraborty et al., 2018), there exist several techniques that can be applied to automate their identification and removal, including some that have been used for other types of SHM systems (Halfpenny, 2008; Cornelis; Peeters, 2014).

5.3. Previously applied data analysis methodologies

5.3.1. Linear and nonlinear regression of time-series

The most intuitive analysis methodology applied to static SHM involves fitting each data set to a linear trend line using ordinary least squares regression, as shown in Figure 5.1. The slope of the identified trend line is then used as an estimate of the evolution rate of the structural parameter in question. Although this method has been used successfully in the past to assess ongoing damage mechanisms in several heritage structures (Russo, 2013; Masciotta et al., 2016a; Sánchez; Meli; Chávez, 2015; Ottoni; Blasi, 2015), it can easily be biased by asymmetry caused by the position of the monitoring period in relation to seasonal cycles. Moreover, since it involves fitting a straight-line to an evolution which is clearly not linear, it provides no means of assessing the quality of the fit.

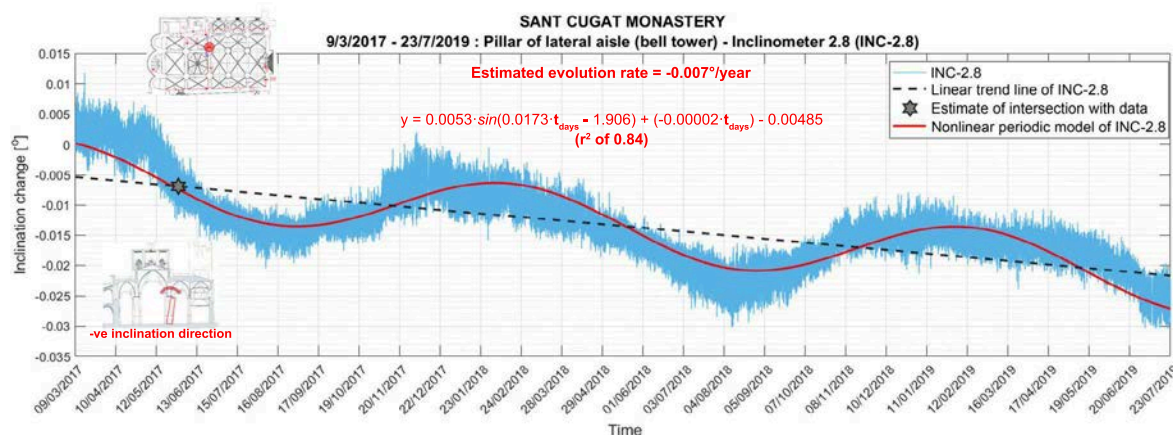


Figure 5.1: Linear and nonlinear periodic model fitted to data. An estimate of the first intersection point of the data with the fitted linear trend is shown in the figure.

A more appropriate approach to the problem involves evaluating the underlying trend of each response variable after subtracting a sinusoidal function containing the signal's main period. Several methods can be used for identifying such a sinusoidal function. In the context of this research, a method previously employed for analysing data from the static SHM system installed in Mallorca cathedral from 2003 to 2008 was employed. The method makes use of the Levenberg-Marquardt algorithm (Moré, 1978) to solve the nonlinear least squares problem of fitting the data from each sensor to the following nonlinear function comprising of a periodic component ($A \sin(Pt - \phi)$) and a linear one ($Bt + C$).

$$y = A \sin(Pt - \phi) + Bt + C \quad (5.1)$$

Where y is the monitored structural parameter of interest, t is time while A , P , ϕ , B , and C are unknowns

found using the Levenberg-Marquardt algorithm. Note that A , P and $\frac{\phi}{P}$ correspond respectively to the amplitude, period and phase shift of the periodic component of the function while B and C correspond respectively to the slope and y-intercept of the straight line component.

Hence, after the fitting procedure, the evolution of each response variable is modelled by a nonlinear periodic function, as shown in Figure 5.1. The resulting value of B from Equation (5.1) is then an estimate of the evolution rate of the monitored structural parameter after removing the identified sinusoidal component containing the signal's main period.

However, it must be said that as with many nonlinear fitting algorithms, the Levenberg-Marquardt algorithm is susceptible to converging at a local minimum rather than a global one. Hence, particularly when dealing with large data sets acquired over long time periods, adequate convergence was found to rely heavily on setting appropriate initial estimates of the unknown parameters. In this case, a good initial estimate of the amplitude can be obtained directly from the data while the main period can be expected to relate to the duration of a tropical year (approximately 365.24 days (Meeus; Savoie, 1992)). Initial estimates of the remaining parameters can be obtained using results from the linear regression procedure. A summary of adequate initial estimates for all the unknown parameters in Equation (5.1) is given in Table 5.1.

As shown, the initial value of the coefficient related to phase shift relies on an estimate of the position of the first intersection point with the straight line fit. This was obtained by subtracting the identified linear trend from the raw data and identifying the first two points between which there was a change of sign. Linear interpolation between these two points provided an estimate of the time to the first intersection point. In order to avoid intersection points caused by higher frequency fluctuations not representative of the seasonal period, this procedure was carried out after removing higher frequency components from the data using a multi-level wavelet decomposition with Symlet Wavelets (Daubechies, 1992; Donoho; Johnstone, 1994). An example of the estimated intersection point is shown in Figure 5.1.

Table 5.1: Summary of initial estimates specified for each response variable for the nonlinear fitting procedure.

Parameter in Eqn. (5.1)	Initial estimate
A	$A_0 = \frac{\max(y_i) - \min(y_i)}{2}$, where y_i refers to the vector containing all the values of the response variable recorded over the whole monitoring period.
P	$P_0 = \frac{2\pi}{365.242}$, if the 24 h day is used as the base unit of the duration vector.
ϕ	$\phi_0 = P_0 \times$ Estimated position of the first intersection point of data with straight line fit (see Figure 5.1)
B	$B_0 =$ Slope of trendline identified from linear regression
C	$C_0 =$ y-intercept of trendline identified from linear regression

A significant improvement of this method compared to linear regression lies in the fact that it attempts to model the actual nonlinear behaviour of the response variable. Selected metrics can thus be used to assess the quality of the fit and to reject trend estimates when the nonlinear periodic model cannot represent the evolution of the structural parameter. Two simple metrics were found to be particularly useful for this purpose. The first one being the well-known coefficient of determination (r^2) defined in Equation (5.2).

$$r^2 = \left[\frac{\text{COV}(\hat{y}, y)}{\sigma_{\hat{y}} \cdot \sigma_y} \right]^2 \quad (5.2)$$

Where \hat{y} is a vector containing all predicted response values computed from Equation (5.1), y is a vector containing all measured response values, and $\sigma_{\hat{y}}$ and σ_y are their respective standard deviations. r^2 ranges from 0 to 1, with a value closer to 1 indicating a better fit (Asuero; Sayago; González, 2006).

Based on the results from the case studies forming part of this research, it is recommended to dismiss evolution rates when the method yields a coefficient of determination lower than 0.6. The other useful metric was found to be the percentage by which the final identified period differs from 365.24 days. The rationale being that since seasonal cycles rely on the movement of the sun, if the periodic component is to represent them, it should have a period close to the duration of a tropical year. As such, if the final identified period is found to differ by more than 25% from 365.24, the estimated evolution trend should be rejected.

Despite this improvement, the method still fails to explicitly assess the effect that measured environmental parameters have on the measured structural parameters. As such, the estimates can be significantly biased by underlying trends or irregular changes in environmental parameters. Once again, this makes it difficult to decide which thresholds reflect an actual evolutionary or stationary condition.

5.3.2. Preliminary evaluation of correlation with monitored environmental parameters

It is clear that variations of environmental parameters, notably changes in temperature, are the root cause of reversible seasonal changes experienced by most masonry structures. Since some of these parameters can easily be monitored, taking advantage of such measurements to filter-out their effect from the evolution of structural parameters can definitely provide an improvement on the method presented in Section 5.3.1.

Before attempting any procedure using actual measurements of environmental parameters, it is important to determine which ones have the greatest influence on the evolution of each response. This can be achieved by computing the Pearson correlation coefficient ($R_{X,Y}$) between measured environmental and structural parameters. As described by equation (5.3) below, this coefficient between two random variables X and Y , with standard deviations of σ_X and σ_Y respectively, can be understood as a normalised version of covariance and hence represents a dimensionless measure of their linear dependence.

$$R_{X,Y} = \frac{cov(X, Y)}{\sigma_X \cdot \sigma_Y} \quad (5.3)$$

$R_{X,Y}$ can vary between -1 and +1 with absolute values closer to unity indicating a better correlation (Asuero; Sayago; González, 2006). The sign of the coefficient indicates the type of correlation. A negative sign means that an increase of one parameter leads to a decrease of the other while a positive one signals the opposite. Hence, following this preliminary evaluation, monitored environmental parameters showing the strongest influence on structural ones can be chosen for the subsequent analyses presented in the following sections.

5.3.3. Filtering environmental effects using linear regression with selected predictors

One method which explicitly considers measured environmental parameters (predictors) relies on the assumption that their effect on responses can be represented by a perfectly linear model. The two unknown parameters of such a model can be identified through simple linear regression between recorded values of each response and the chosen predictor as shown in Figure 5.2.

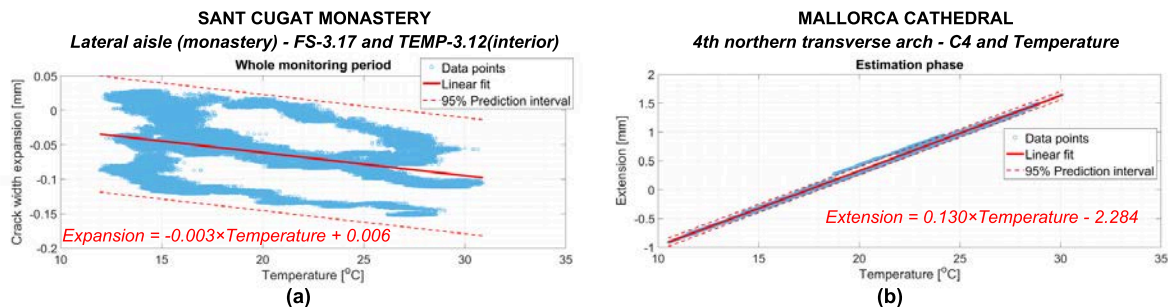


Figure 5.2: (a) Example of linear regression between crack width expansion and temperature over whole monitoring period. (b) Example of linear regression between the monitored span of an arch and temperature over an estimation phase of one year.

Due to the simplistic nature of the assumed relationship, it is clear that effects caused by structural mechanisms of interest can influence the identified linear models. Hence, one can argue that using data only from a single seasonal cycle for the regressions will provide the most suitable models. On the other hand, since the relationship between some predictors and responses change over several seasonal cycles, it can also be argued that data from the entire monitoring period can better represent their dependency. Hence, models are identified for both cases (listed below) and the results are then compared. In fact, the differences between them are used in the proposed classification procedure to evaluate the evolutionary state of monitored responses.

1. **Linear filter (i):** Linear regression between selected predictor and response variable using data from the entire monitoring period.

2. **Linear filter (ii):** Linear regression between selected predictor and response variable using data only from a full calendar year (this period will hereafter be referred to as the estimation phase).

Following the regression procedure, measured values of each selected predictor are substituted into the corresponding linear model to simulate changes of the structural parameter caused by the environmental one. Since variations experienced by structural parameters can be considered as the result of a series of phenomena, the actual measurements of the latter are then filtered by simply subtracting the simulated effect, as shown in Figure 5.3. Estimates of the underlying annual evolution rates ($ER_{lin(i)}$ and $ER_{lin(ii)}$) are then obtained by carrying out simple regressions of these filtered residuals.

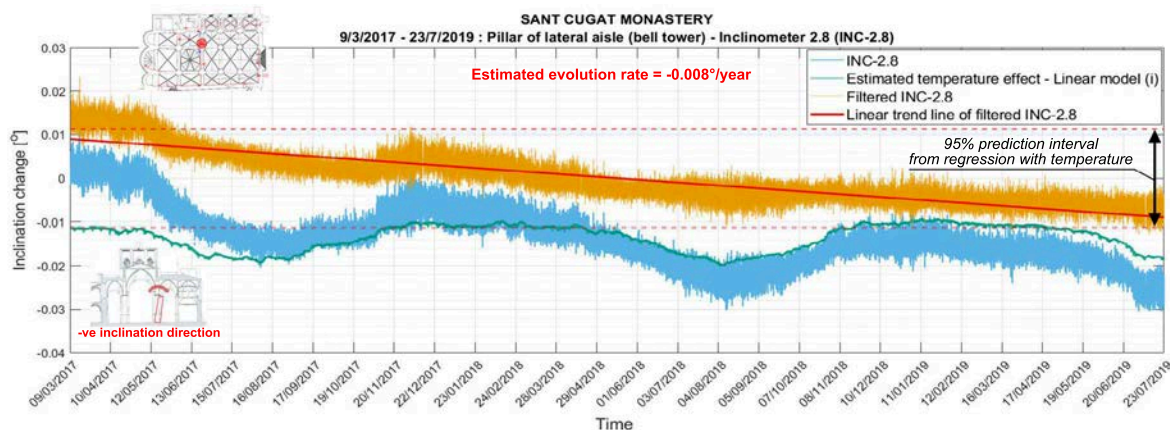


Figure 5.3: Filtering of temperature effect based on identified general linear trend.

A significant advantage of this method when compared to the previous two is that it explicitly uses measured predictors and hence allows an assessment of how well each linear model can predict the relationship between environmental and structural parameters using common error metrics. In fact, if the residuals are assumed to be normally distributed when no significant structural mechanism is present, a prediction interval representing a specific level of confidence can be obtained based on the dispersion of residuals. This can prove extremely useful for the interpretation of results since it is expressed in the same units as the monitored structural parameter.

5.4. Proposed analysis methodology

Although it is clear that simple linear models can provide a good representation of the relationship between environmental and structural parameters (Figure 5.2(b)), in many cases, it fails to represent the relationship adequately (Figure 5.2(a)). One of the main reasons for this is the fact that the simplistic nature of the model cannot take into consideration certain effects influencing the system it aims to describe, such as those due to thermal inertia.

Hence the proposed automated data analysis methodology developed as part of this research consists of two parts. The first part aims to improve upon the method presented in Section 5.3.3 by exploiting dynamic regression models to describe the relationship between selected predictors and structural parameters more reliably. The process can be applied to a complete SHM system and includes a procedure for estimating model orders that are best suited for system identification, as well as provisions to deal with irregularly sampled and missing data.

The second part of the methodology aims to facilitate the interpretation of the predicted evolution rates after the filtering process. This is achieved by classifying the state of each monitored structural parameter based on the evaluated underlying trend and the level of uncertainty associated to the models describing its relationship with selected environmental parameters. Since the linear models described in Section 5.3.3 are clearly adequate for certain cases, the classification procedure also takes advantage of predictions from this method. Hence, a preliminary step to the proposed data analysis procedure involves carrying out all the analysis methods presented in Section 5.3.

5.4.1. Filtering environmental effects using dynamic statistical models (ARX models)

The procedure of utilising ARX models for evaluating any underlying trends present in response variables involves selecting suitable model orders by adopting some quality criteria. The coefficients of the ARX models can then be estimated using QR factorization (Björck, 1967) based on measurements collected during an estimation phase. In order for the model to capture most of the reversible components caused by environmental effects during a complete seasonal cycle, the estimation phase should ideally span at least 1 full year. Once this model has been estimated and validated, it can be used together with data collected after the estimation phase to simulate responses based on measured predictors. The residuals obtained by subtracting the simulated behaviour from its recorded counterpart then allows changes related to irreversible structural damage to be distinguished from reversible ones caused by varying environmental conditions.

As its name suggests, an Auto-Regressive with eXogenous input (ARX) model utilises measured values of past outputs together with those of past and current or delayed predictors to describe the dynamics of a system. The single-input single-output (SISO) form of the ARX model has the following structure:

$$\hat{y}(t) + a_1 y(t-1) + \dots + a_{na} y(t-na) = b_1 x^{env}(t-nk) + \dots + b_{nb} x^{env}(t-nb-nk+1) + e(t) \quad (5.4)$$

Where $\hat{y}(t)$ is the predicted response at time t , $e(t)$ is the white-noise disturbance value, na and nb are the and exogenous orders of the ARX model, and nk is the delay. Specifically, na and nb refer respectively to the number of past samples of the response and predictor variables used for identification and nk is the number of samples of the predictor variable that occur before the predictor starts influencing the response. Hence $y(t-1)\dots y(t-na)$ refer to the previous responses on which the current one depends, while $x^{env}(t-nk)\dots x^{env}(t-nb-nk+1)$ refer to the previous and delayed predictors on which the current response depends. The multiple-input single-output (MISO) form of an ARX model has the same structure as that described by Equation (5.4) but with additional parameters to incorporate any number of additional predictors. Therefore, for each new predictor incorporated in the model, a new exogenous order and delay has to be specified.

The first step of the filtering procedure involves selecting which measured environmental variables will be used as predictors for the representation of the dynamic system as an ARX model. Two possible candidates that are commonly monitored as part of SHM systems are temperature and relative humidity. It can be expected that temperature will have the greatest influence on the evolution of the response variable. Since relative humidity measurements were available in addition to temperature ones for one of the case studies forming part of this research, the results from the preliminary evaluation of correlation described in Section 5.3.2 were compared. Indeed, the results reveal that for every monitored structural parameter, the linear correlation is stronger with temperature than with relative humidity. In fact, for almost every response investigated as part of the two case studies, the dependency on temperature is clearly visible when examining daily fluctuations. Hence, SISO ARX models with temperature as the sole predictor constitute the most basic ARX model that should be identified for every monitored response. If temperature is recorded at more than one location (for instance in the interior and at the exterior of the structure), the data from the temperature sensor showing the greatest Pearson correlation coefficient with the response should be used as the predictor in the SISO ARX model.

Recent years have been marked by a significant increase in the ability of modern computers to exploit large amounts of data for system identification. As such, in addition to the SISO ARX models described in the previous paragraph, the proposed data analysis methodology also incorporates the use of MISO ARX models to filter out seasonal variations when multiple suitable environmental parameters are monitored. Naturally, the decision of which environmental parameters to include in the models has to be addressed. It is undeniable that the presence of moisture in the masonry fabric can significantly alter its mechanical behaviour (Amde; Martin; Colville, 2007; Sathiparan; Rumeshkumar, 2018; Witzany; Cejka; Zigler, 2010) and hence influence the response of structures. However, the design of an adequate acquisition protocol for the monitoring of parameters representative of the water absorption phenomena can be a challenging task, particularly for large complex masonry structures (Moropoulou et al., 2019). Some authors have attempted to include measured relative humidity on-site as a predictor in a MISO ARX model in an attempt to filter out moisture related effects from natural frequencies being monitored through a dynamic monitoring system (Ramos et al., 2010). Although it was clear that water absorption had a notable effect in this case due to observed changes of the

natural frequencies at the beginning of rainy seasons, the inclusion of this predictor provided no improvement in the model's ability to describe the environmental variability. This can be attributed to the fact that measurements made by humidity sensors on the exterior of walls actually reflect the level of moisture in the air and not in the masonry. For this reason, the proposed methodology does not include MISO ARX models with relative humidity as a predictor, even if it is good practice to monitor it in most SHM systems. However, it was envisaged that temperature gradients between interior and exterior temperature could significantly influence the dynamics of the system. Since both are often recorded as part of modern SHM systems, it is recommended to utilise MISO ARX models that incorporate both as predictors to characterise the environmental influence on the evolution of monitored structural responses. Nevertheless, the proposed methodology can be extended to include any monitored environmental parameters causing reversible variations of structural responses such as the moisture content in the masonry or the level of water in the foundation soil. The latter can be monitored with piezometers and the former could possibly be monitored by humidity sensors placed at different locations both along the thickness of masonry walls and at different levels of the structure (Ramos, 2007). However, it should be noted that in some cases, particularly for masonry structures with an interior leaf made of lime concrete, moisture diffusion can produce a redistribution of stresses over several centuries (Ferretti; Bažant, 2006) which can even be the root cause of a slow irreversible deterioration mechanism. Similarly, changes in water table levels can sometimes cause significant differential settlements over long time periods resulting in the activation of a progressive damage mechanism (Toll et al., 2012; De-Jong, 2016). Under such circumstances, it would be undesirable to include these monitored parameters as predictors in the MISO ARX model at the filtering stage since the trends they induce can be essential for an accurate diagnosis of the structure.

Once predictors to be used in the ARX models have been selected, the next step of the procedure involves extracting data from the estimation phase. This represents the data set for which the errors between the model output and the measured response will be minimised. In most cases it is perfectly adequate to take data collected during the first complete year as the estimation data. However, if there are significant periods for which data is missing during the first year of monitoring, it is recommended to consider any period lasting one year which has the least amount of missing data as the estimation phase.

It is key to adequately condition the estimation phase data before carrying out any system identification. Besides converting raw signals from sensors to meaningful physical units and removing clear anomalies, another procedure which can be useful to implement involves resampling the data. This is particularly useful to reduce the computational cost of system identification in cases for which the data is sampled at a high rate. Since the damage phenomena of interest typically progresses slowly over many years, if the SHM system samples data at intervals shorter than an hour, noticeable savings in terms of computational cost can be achieved by increasing the sampling interval to an hour without any significant loss of accuracy in terms of the predicted evolution rates. Naturally, after using the ARX models to simulate the environmental effect, the data will have to be upsampled back to the original sampling rate so that the residuals can be computed from the measured values of the response variables in the same way they were for the method described in Section 5.3.3. Upsampling is a lossless procedure and hence straightforward application of spline interpolation (De Boor, 1978) can safely be used for this purpose. However, for the downsampling procedure, great care has to be taken to prevent aliasing and avoid distorting the original signal excessively. To prevent aliasing, a low-pass anti-aliasing filter should be implemented before the resampling procedure. The question then arises as to which interpolation method will prove to be both robust and accurate in representing the original signal. Three different methods were tested as part of this research: Linear interpolation using 2 neighbouring points as well as piecewise cubic (Fritsch; Carlson, 1980) and spline interpolation (De Boor, 1978), both of which use 4 neighbouring points. Linear interpolation resulted in the smallest maximum and mean errors for data from all the 16 sensors tested. In every case, the mean error was several orders of magnitude smaller than the minimum resolution of the sensor and the maximum error smaller than the greatest daily variation experienced by the sensor. As such, it was concluded that using linear interpolation for downsampling is most adequate. Although most modern data loggers will accurately provide data at a uniformly sampled rate, analysing data collected from more archaic systems could create a need for system identification from irregularly sampled data. Since such data is not easily handled by discrete-time model identification techniques (Garnier; Wang, 2008), it is recommended to resample the data to a uniform rate using the same procedure described in this paragraph before carrying out system identification in such cases.

A particular characteristic of ARX models is that the equation error is modelled as being a zero-mean white process with unknown variance (Diversi; Guidorzi; Soverini, 2010). In fact, the noise model is coupled to the identified parameters of the response variable and hence the only unknown parameter related to noise that needs to be solved for during the identification process is the variance of the noise term. Although this means that the noise and the dynamics of the system cannot be modelled independently, the simplicity of the scheme creates no stability problems in optimal predictors and allows unbiased estimates of the parameters by means of least squares. However, it is crucial to remove the mean from both the response and predictor data before carrying out system identification to avoid an offset term in Equation (5.4). In fact, it is good practice to normalise the input and output data for this system identification task (Peeters, 2000). Therefore, for each estimation data set, the result after removing the mean should also be divided by the standard deviation. It is important to store both the means and the standard deviations, since it is instrumental to transform all the identified ARX models back to the engineering units of the original data.

Before carrying out system identification using the normalised data sets, a choice needs to be made on the delay to be specified. If the environmental and structural parameters are acquired simultaneously, it is perfectly adequate to simply assume a delay of 0 in most cases. This is particularly true when the environmental parameter is temperature, as is the case for the recommended ARX models for the static SHM case. However, in some cases, the model could benefit from a short dead time occurring before the first predictor it uses to simulate the current response. In order to evaluate the most suitable delays for each response, the proposed procedure includes a quick delay estimation computation based on the comparison of ARX models with orders of 8, evaluated for different delays spanning from 0 to 48 hours. As can be expected, out of the 44 ARX models estimated for the case studies (28 SISO and 16 MISO models), the delay estimation computation suggested that a delay of 0 was most appropriate for most of the cases. Moreover, only delays of up to 12 hours were suggested for the 12 cases for which it was deemed that a dead time would be suitable.

The last step remaining before estimating the parameters of the ARX models involves specifying appropriate auto-regressive and exogenous model orders. In essence, these control the duration in the past that is considered by each model to predict responses since it defines the number of past samples used for prediction. Choosing the right combination of model orders is no straightforward task but this can greatly influence the quality of the final models. For instance, it is likely that responses being significantly affected by a structural mechanism would benefit more from a higher auto-regressive order while those influenced by complex environmental phenomena would benefit more from higher exogenous model orders. Hence, a systematic procedure was developed as part of this research to select suitable combinations of model orders for each response from a pre-defined range. The procedure involves dividing the estimation data of each response equally to form an estimation and a validation subset. Models for each of the structures defined by the pre-defined range are then estimated using the estimation subset. The loss functions are then computed for these models when applied to the validation subset. The loss function (V) refers to the error that is minimised by the least-squares method during system identification. As shown by Equation (5.5), it can be defined as the normalized sum of squared prediction errors.

$$V = \frac{1}{N} \sum_{k=1}^N e_k^2 \quad (5.5)$$

Where N is the number of measurements, k is the time step and e_k are prediction errors defined as the measured response minus the predicted one.

Following the computation of loss functions, the structure resulting in the lowest error when applied to the validation data set is specified for each response. The parameters of these models with known structures can then be estimated using all the data from the estimation phase. A significant benefit of the order selection procedure is that it relies on loss functions computed on validation subsets and hence the final ARX models already inherently include a process that helps ensure that they are useful not only for the estimation data, but also for new data from subsequent phases of the monitoring period. However, the task of defining the range of model orders that need to be tested still needs to be addressed. Since it was expected that one of the main benefits stemming from the dynamic nature of ARX models would be their ability to consider thermal inertia effects, an investigation was carried out on the required model orders that would theoretically be able to encompass most of the effects of this physical phenomena. In general, the thermal inertia of a building envelope causes two noticeable differences between external and internal temperature fluctuations:

a decrement of the amplitude and a time lag between the two (Verbeke; Audenaert, 2018). Previous research reveals that the duration of these thermal lags rely heavily on the thermophysical properties of wall elements and that lags of approximately 12 hours can be observed from experiments on brick masonry walls with a thickness of less than 30 cm (Ulgen, 2002). It can be expected that thermal inertia effects will be substantially different in masonry heritage structures as they can be characterised by massive external walls that are often thicker than 1 m. Based on measurements from one of the case studies, most of the time lags between external and internal temperature appear to last less than a day. However, as can be seen in 5.4, in some extreme cases, time lags lasting several days could be identified.

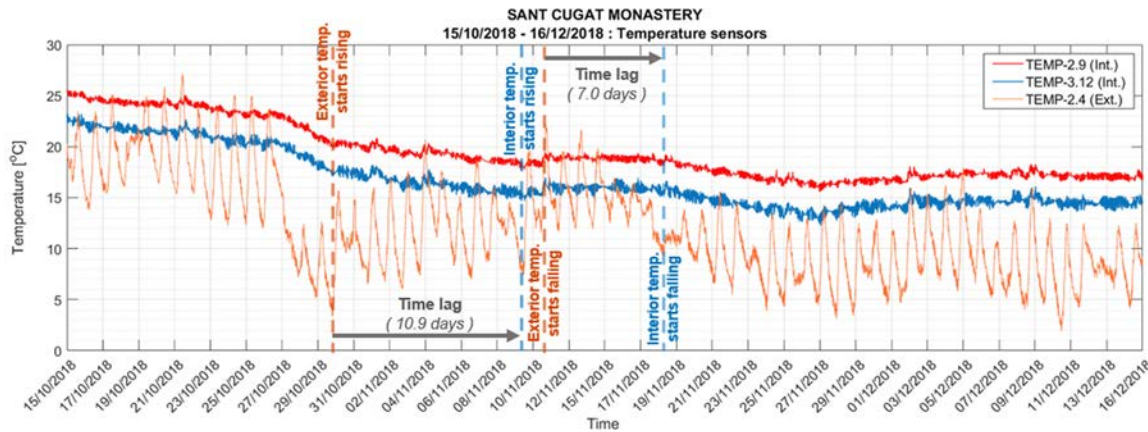


Figure 5.4: Example of observed time lag between exterior and interior temperature in Sant Cugat monastery.

Based on these observations, the ranges listed in Table 5.2 were tested as part of this research. If the acquisition was made at a higher rate, the estimation data was resampled to a sampling period of 1 hour. The results from all the ranges tested reveal that it is important to specify a lower limit in the range to prevent the model structure determined by the order selection procedure from being overly dependent on only past responses or predictors. A lower limit corresponding to at least four days is recommended. It was also found that specifying a larger range leads to more accurate final models even if the upper limit of the range is unchanged. For instance, specifying a pre-defined range of 4 to 10 days yielded more accurate models than specifying one of 8 to 10 days. Of course, the final range selected is largely dependent on the computational expense that can be spared. Due to the nature of the computation, it is highly recommended to condition its implementation to take advantage of the parallel computing capabilities of modern computers. The proposed method involves carrying out the same procedure on all sensors of SHM systems that monitor a structural parameter and does not require any intermediate values computed from the data of other sensors. Hence, the model order selection procedure as well as the subsequent parameter estimation procedure can be carried out in parallel for all sensors. Effectively, this means that the procedure can be extended to systems with a larger number of sensors without any additional expense in terms of wall-clock time provided that a sufficient number of parallel running nodes are available to carry out the computation.

Table 5.2: Ranges of ARX model orders tested using estimation data with a sampling period of 1 hour.

Corresponding duration [days]		SISO ARX - model orders tested		MISO ARX - model orders tested	
Lower limit	Upper limit	Lower limit	Upper limit	Lower limit	Upper limit
1	4	24	96	24	96
4	6	96	144	96	144
8	10	192	240	192	240
4	10	96	240	96	240
4	15	96	360	-	-
5	20	120	480	-	-
5	25	120	600	-	-

If the estimation data is resampled to a sampling period of 1 hour and the full model estimation procedure is implemented in parallel for all sensors, the maximum ranges listed in Table 5.2 are recommended for SISO models and MISO ones with 2 predictors. For analysing the data from the two case studies, the maximum time taken to undergo the full procedure to estimate the parameters of ARX models with these suggested

ranges was 22 hours for the SISO models and 70 hours for the MISO models. This was deemed to be reasonable since the models only need to be estimated once. They can then be used to give updated predictions from new data within seconds.

Once the final models have been identified for each monitored response, they can be used to simulate the expected responses from new measurements of predictors. It is very important to highlight the distinction made between simulation and prediction in the realm of system identification since one of the greatest advantages of using ARX models for the analysis of static SHM systems stems from this difference. It is clear from Equation (5.4) that both past responses and predictors are used to describe the dynamics of the system. The data from both are therefore used during the estimation phase. However, there are two ways of generating a model response: it can be predicted or simulated. Prediction involves computing the model response at a particular point in time using values of measured predictors and past responses. Simulation on the other hand, involves computing the model response using only measured predictors. Effectively, this means that although the model is able to account for changes that are likely due to structural mechanisms through the parameters associated to past responses, it is also able to exclude those when computing the expected response by only using terms of the model that correspond to predictors. This is ideal for the case of static SHM since it is often impossible to isolate a period of time during which the relationship between environmental predictors and structural responses can be considered as being completely isolated and free from effects caused by active structural mechanisms. Any evolution trend is then estimated by carrying out a regression of the residuals obtained by subtracting the simulated environmental effect of the responses from their measured values.

Two different goodness-of-fit measures were used to compare the effectiveness of the linear, SISO ARX, and MISO ARX models in representing the relationship between predictors and responses: the previously described coefficient of determination (r^2) and 1.96 times the standard error of the estimate (σ_e) (Smith, 2012). This standard error metric is computed from residuals as shown in Equation (5.6).

$$\sigma_e = \sqrt{\frac{\sum_{i=1}^n (y_i - \hat{y}_i)^2}{n - k - 1}} \quad (5.6)$$

Where y_i refer to actual measurements of structural responses while \hat{y}_i refer to model predictions. With n equal to the number of data sample points and k equal to the number of explanatory variables used in the model, $n - k - 1$ represents the number of degrees of freedom available for the computation of the error metric.

$1.96\sigma_e$ can therefore be interpreted as a typical distance of measured data points from model predictions. It was specifically chosen to evaluate the effectiveness of different models because it is used to define the 95% prediction interval from a normally distributed sample and because it is in the same units as the responses. In all cases, these were computed from the measured and simulated values of responses over the time period used to estimate the model. As will be seen in Section 5.5, for almost all of the 28 responses monitored as part of the two case studies, the ARX models were able to represent the environmental variation much more accurately than the linear models.

5.4.2. Interpretation of results

As a result of the analyses presented in Sections 5.3.3 and 5.4.1, an estimated filtered evolution rate is obtained for each response variable. In fact, since these methods aim to directly model the relationship between environmental and structural parameters, the standard error of the estimate computed from residuals for each model over the estimation phase represents a certain level of confidence in the model's ability to predict variations of the response. Since such metrics are in the same units as the response, they can be compared directly to evaluate the level of certainty associated to the estimated filtered evolution rates. In order to provide a systematic way of doing so, the current research proposes a multi-step classification approach based on comparing results obtained from the methods presented in Sections 5.3.3 and 5.4.1 through a series of 5 logical tests (see Figure 5.6). Two key values obtained from the most extensive ARX-based procedure used are employed in every test: the filtered annual evolution rate (ER_{ARX}) and 1.96 multiplied by the standard error of the estimate computed over the estimation phase ($1.96\sigma_{e-ARX}$). The approach can be programmed so that in addition to the predicted rates, a label is automatically assigned to each monitored response. Based on the outcomes of the tests, each response is classified in one of the following four categories:

1. **Stationary:** Monitored parameters showing a clear stationary trend outside reversible variations caused by environmental parameters.
2. **Evolutionary:** Monitored parameters showing a clear evolutionary trend outside reversible variations caused by environmental parameters.
3. **Apparently stationary:** Monitored parameters showing a stationary trend but for which there still is a rather large uncertainty associated to the estimation of the trend.
4. **Apparently evolutionary:** Monitored parameters showing an evolutionary trend but for which there still is a rather large uncertainty associated to the estimation of the trend.
5. **Inconclusive:** Monitored parameters for which no clear conclusion can be made on its evolutionary state from the available monitoring data alone.

The first test of the classification procedure aims to identify responses which clearly show a stationary trend. Since classifying a response as stationary when it is experiencing an active trend can have dangerous consequences, relatively strict conditions have been established for this test. Specifically, $1.96\sigma_{e-ARX}$ must be lower than 5 times the minimum effective resolution of the sensors and $2ER_{ARX}$ (the estimated evolution over two years) must be lower than 0.005 units. In addition to these two requirements, this test includes another requirement based on the normality of the residuals. This stems from the understanding of a truly stationary time-series as one that can be represented by a model with Gaussian errors (Mansor et al., 2016). Hence, it can be said that if the residuals after the filtering process are normally distributed, the model has been able to capture most of the environmental variability, and the response does not contain any underlying trend caused by active structural mechanisms. Naturally, in order for this requirement to be incorporated in an automated procedure, one has to quantify the degree of normality of the residuals. There exist many different tests to verify if observations are from a normal population and most of them rely on computing a test statistic and a critical value. The latter is usually dependent on the sample size and a chosen significance level. The hypothesis that the sample belongs to a normal population is then rejected or accepted based on the relationship between the test statistic and the critical value. In the case of data from static SHM, the sample size is usually very large since it contains data sampled every hour over several years. Moreover, the dynamics of the system are often very complex making it difficult for any model to eliminate all reversible effects perfectly. As such, the sample set containing residuals will almost always fail to satisfy most established normality tests irrespective of the chosen significance level. Nevertheless, it is clear that in some cases, the residuals can be well represented by a normal distribution (see Figure 5.5).

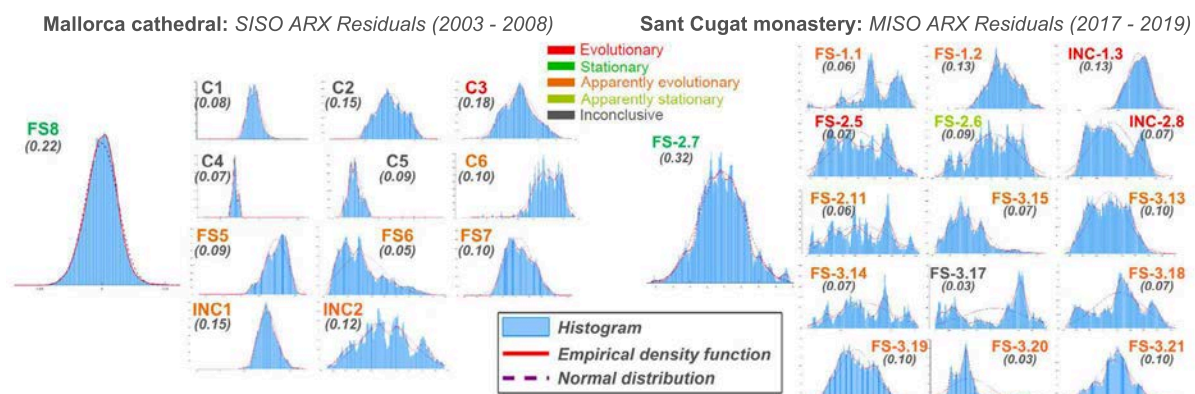


Figure 5.5: Empirical distribution of ARX Residuals for responses forming part of case studies. Values of the adapted Lilliefors ratio for the case of static SHM is also shown. The colour of the sensor name relates to the final estimated condition according to the proposed classification procedure.

Hence, a modified normality test based on the Lilliefors Test (Lilliefors, 1967) was developed for this purpose. As is the case for the original test, the test-statistic ($kstat$) is computed by finding the maximum deviation of the empirical cumulative distribution function (CDF) from the CDF of a normal distribution with the same mean and standard deviation as the sample data set. The original test rejects the hypothesis of normality if the test statistic is greater than the critical value. Hence the sample is said to be from a normal distribution if the ratio of the critical value over the test statistic is greater than or equal to 1. In contrast to

the original test, the modified one proposes a fixed critical value of 0.005 and requires the computation of an adapted Lilliefors ratio equivalent to $\frac{0.005}{k_{stat}}$. These ratios computed for the residuals obtained from the most extensive ARX-based procedures applied to the responses forming part of the case studies, are shown in Figure 5.5. Based on these observed ratios, it is suggested that for the case of static SHM, residuals that have an adapted Lilliefors ratio greater than 0.2 can be considered as being normally distributed. Hence, responses that satisfy this requirement together with the first two presented at the start of this paragraph can be considered as being stationary.

The second test aims to identify responses that clearly show an evolutionary trend. Hence, the estimated evolution rate should be significant in comparison to the error associated to modelling the environmental variation and this error should be sufficiently small. It must be noted that in certain cases, if a structural parameter is particularly responsive to changes in environmental conditions, it can experience large reversible variations. In such cases, even if the ARX model is able to accurately simulate the seasonal variations, the value of $1.96\sigma_{e-ARX}$ might still be significant in comparison to the minimum effective resolution of the sensor. In order to avoid penalising the accuracy of the model in such cases, a small value of $1.96\sigma_{e-ARX}$ was defined as the maximum between 5 times the minimum effective resolution of the sensor and 20% of the average maximum daily variation experienced by all sensors in the SHM system measuring the same type of response. If the residuals satisfy this requirement and $2ER_{ARX}$ is greater than $1.96\sigma_{e-ARX}$, the response is classified as evolutionary.

The subsequent tests are not as rigorous as the first two but intend to utilise most of the useful information obtained from the various proposed analysis procedures to provide an informed estimate of the condition of each structural response being monitored. The third test classifies a response as apparently stationary if $1.96\sigma_{e-ARX}$ is less than 0.05 and $2ER_{ARX}$ is less than $0.4 \times 1.96\sigma_{e-ARX}$. Test 4 relies on three requirements to classify a response as apparently evolutionary: $1.96\sigma_{e-ARX}$ must be less than 0.2, $2ER_{ARX}$ must be greater than $0.4 \times 1.96\sigma_{e-ARX}$ and the Pearson correlation coefficient computed between the response and relevant temperature records must be greater than 0.6. The rationale being that a response is most likely evolutionary if its relationship with temperature can be well represented by a linear approximation and the predicted trend after filtering out simulated environmental effects is significant in relation to the error associated to this simulation. The final test relies on a comparison between the estimated evolution rates from all methods attempting to directly filter out reversible effects caused by measured predictors ($ER_{lin(i)}$, $ER_{lin(ii)}$, $ER_{SISO-ARX}$ and if applicable $ER_{MISO-ARX}$). The test classifies the response as apparently evolutionary if the estimated rates from all these methods agree to within 25% (normalised to the lowest evolution rate for each response) and if $2ER_{ARX}$ is greater than $0.45 \times 1.96\sigma_{e-ARX}$. A greater requirement is imposed on the evolution rate in comparison to Test 4 because there is less physical meaning associated to this test. Although a response can satisfy both Test 4 and Test 5, Test 3 has been designed to be mutually exclusive from these two. Figure 5.6 presents a summary of the overall classification procedure while the tests it employs are summarised in Figure 5.7.

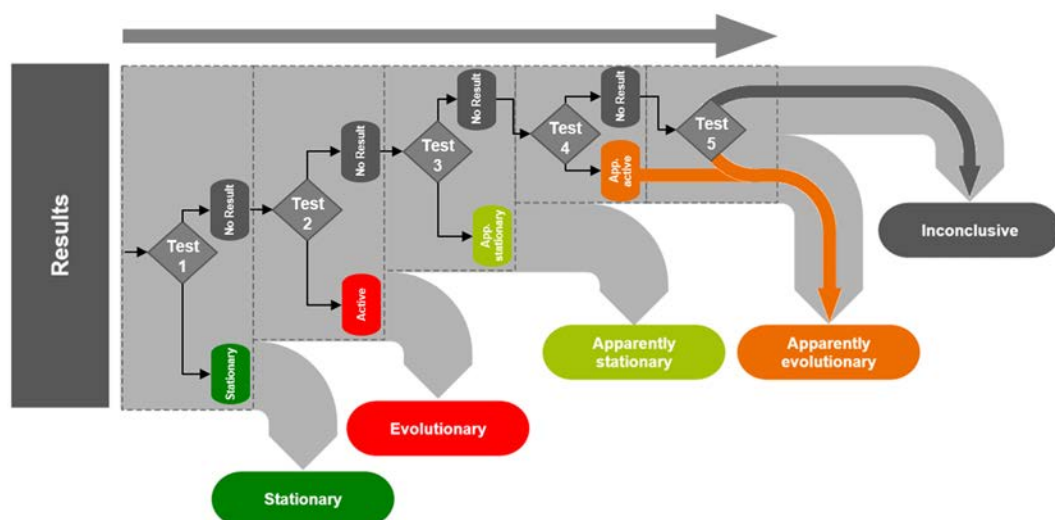


Figure 5.6: Automated classification procedure for interpretation of results after filtering effect of environmental variability.

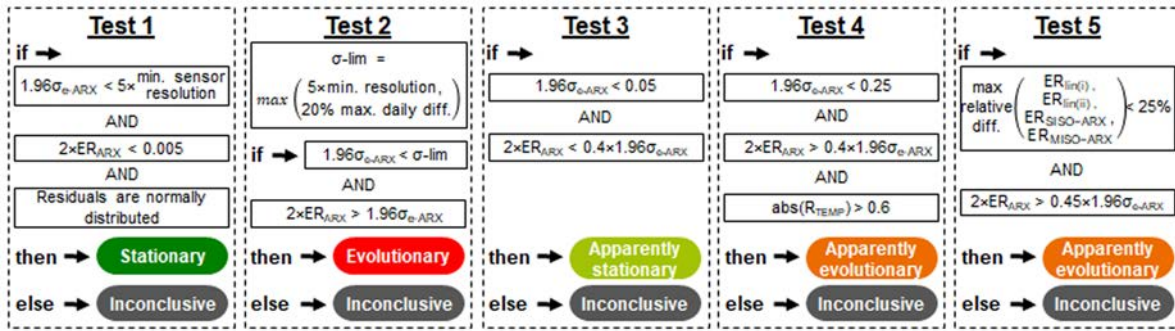


Figure 5.7: Summary of tests used by automated classification procedure.

As shown in Figure 5.6, if Tests 1, 2 or 3 are satisfied, the results related to that particular response does not undergo any further tests since it would already have been assigned a label. If a response fails all tests, it is classified as inconclusive. One of the main advantages of the classification procedure is that it can greatly facilitate how the estimated evolution rates should be prioritised during the prognosis. Basically, the possible underlying mechanisms related to responses classified as "Evolutionary" should be investigated first followed by those labelled as "Apparently evolutionary" that show the greatest ratio between ER_{ARX} and $1.96\sigma_{e-ARX}$. Responses labelled as "Inconclusive" often require an extended period of monitoring in order to shed more light on their actual state. Of course, longer monitoring periods will also help develop a greater level of certainty on any diagnosis made from the data analysis, particularly if the cause of some estimated trends cannot be explained.

The complete proposed automated procedure for analysing records of a monitored structural parameter is summarised in a flowchart on the next page (Figure 5.8).

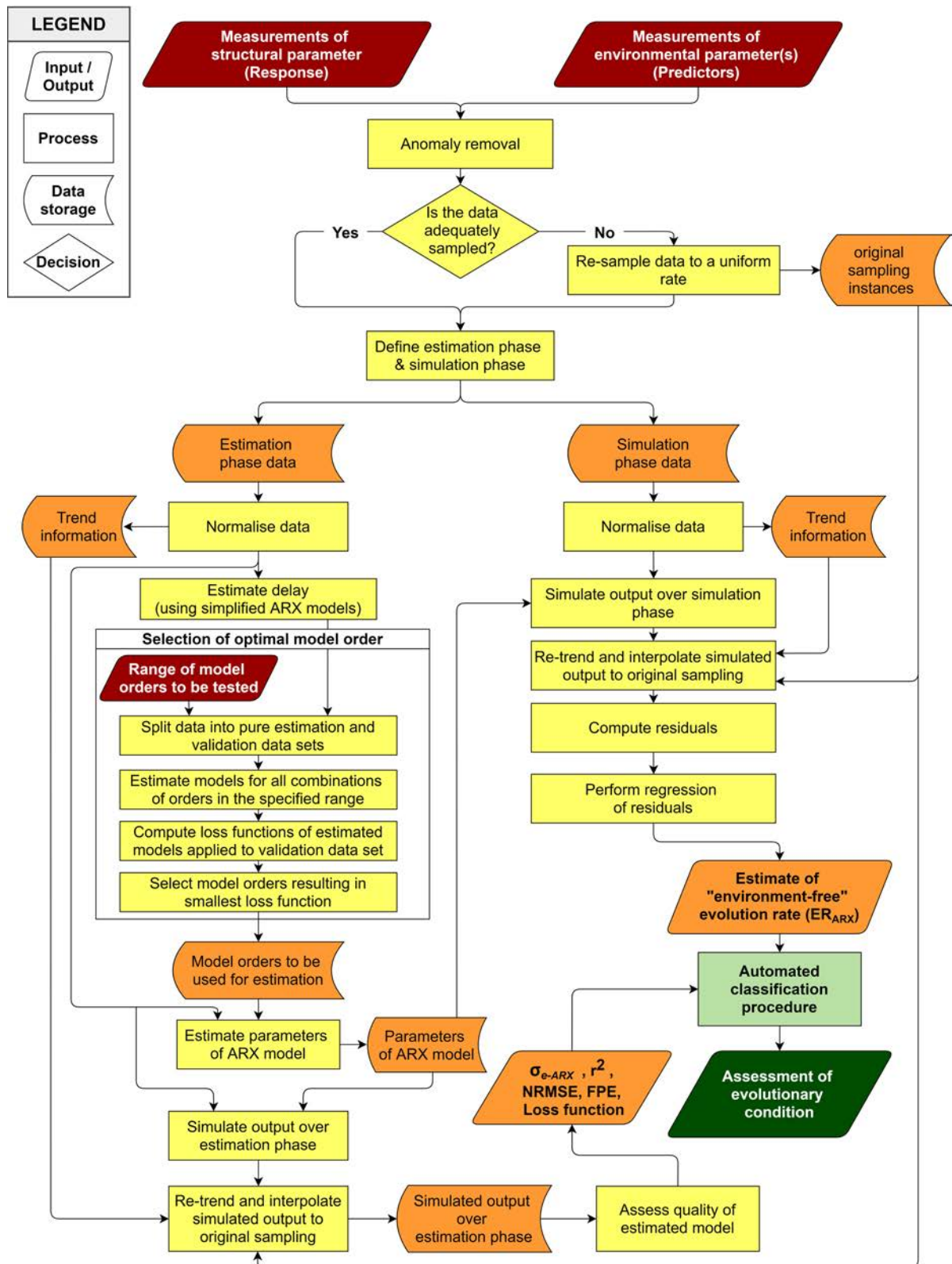


Figure 5.8: Procedure for the implementation of ARX models to filter out the effect of measured environmental parameters and assess the evolutionary condition of a monitored structural parameter.

5.5. Case studies

The two case studies forming part of this research consist of medieval churches and cathedrals. Such structures were usually built over very long time periods and still represent some of the most daring and complex examples of masonry design. The first case study, the cathedral of Santa Maria in Palma de Mallorca, was built progressively from the apse to the façade over a period of 300 years, from 1306 to 1600 (Pelà et al., 2016a). The cathedral boasts grand proportions and presents many structurally audacious aspects. The most daring of which probably is the slenderness of the columns (Elyamani et al., 2017a), reaching a ratio of 14.2 in some areas while the value encountered in other Gothic cathedrals usually ranges from 7 to 9 (Roca et al., 2013). For all these reasons, it represents one of the most emblematic monuments of the Catalan Gothic Style. The second case study, the monastery of Sant Cugat, is located in Sant Cugat del Vallès, Catalonia. The monastery is composed of a cloister and a church, with the latter being the main focus of the study. The masonry structure at the site today consists of various parts built over different time periods, mostly from the mid-12th century to the 15th century. The interaction between different parts results in a complex overall structural behaviour, adding to the difficulty of the diagnosis.

5.5.1. Mallorca cathedral

5.5.1.1. SHM system and results

A five-year monitoring system was installed in the cathedral in 2003 to better understand the complex behaviour of the structure and to identify any active mechanisms possibly contributing to its deterioration. In addition to temperature and humidity sensors, the system consisted of 6 convergence extensometers monitoring changes in the distance between two points, four crackmeters monitoring changes in crack widths and two inclinometers monitoring changes of inclination of key elements. The convergence extensometers and crackmeters had a resolution of 0.01 mm while the inclinometers had an effective resolution of 0.001°. Table 5.3 describes the location of every sensor monitoring a structural parameter and the total duration of useful data collected by each one over the five-year monitoring period. The predicted evolution rates from methods based on directly fitting time series to selected models are also shown in Table 5.3. The location of the sensors together with the final estimated evolutionary condition are also shown in Figure 5.10.

Table 5.3: Summary of structural sensors used in the SHM system installed in Mallorca cathedral and estimated evolution rates from methods based on directly fitting time series to selected models.

Sensor	Location	Years of data	Type	Units	Evolution rate [unit/year]	
					Linear regression	Nonlinear regression
C1	4th central transverse arch	1.2	Extensometer	mm	0.17	-
C2	4th central transverse arch	4.9	Extensometer	mm	0.05	-
C3	4th southern transverse arch	4.8	Extensometer	mm	0.10	0.09
C4	4th northern transverse arch	3.7	Extensometer	mm	0.12	0.06
C5	8th southern longitudinal arch	2.8	Extensometer	mm	0.02	0.05
C6	8th northern longitudinal arch	4.2	Extensometer	mm	0.07	0.06
FS5	Southern wall - 8th bay	4.2	Crackmeter	mm	0.01	0.01
FS6	Southern wall - 8th bay	4.2	Crackmeter	mm	-0.05	-0.04
FS7	Central nave - 6th bay	4.2	Crackmeter	mm	0.06	0.08
FS8	Central nave - 7th bay	4.2	Crackmeter	mm	0.00	0.00
INC1	4th pillar (central nave - south)	2.3	Inclinometer	°	0.000	0.013
INC2	Interior main façade	1.9	Inclinometer	°	0.036	0.034

The evolution rate predicted for convergence extensometer C1 from the periodic model was disregarded because the identified period varied by more than 45% from the duration of a tropical year. On the other hand, that of convergence extensometer C2 was disregarded because it had a very poor correlation with the data (coefficient of determination of 0.19) indicating that the evolution of the data could clearly not be well represented by the nonlinear periodic model. Despite the greater sophistication of the nonlinear model, it can be seen that the estimated evolution rates between these two methods are in good agreement for certain cases, notably for convergence extensometers C3 and C6, for crackmeter FS5 and for inclinometer INC2.

Before discussing the estimated evolution rates predicted by the methods presented in Sections 5.3.3 and 5.4.1, a comparison of how well the linear and ARX models are able to represent the relationship between responses and predictors is presented in Figure 5.9. It is clear that the ARX models are better suited to represent the environmental variation in almost every case.

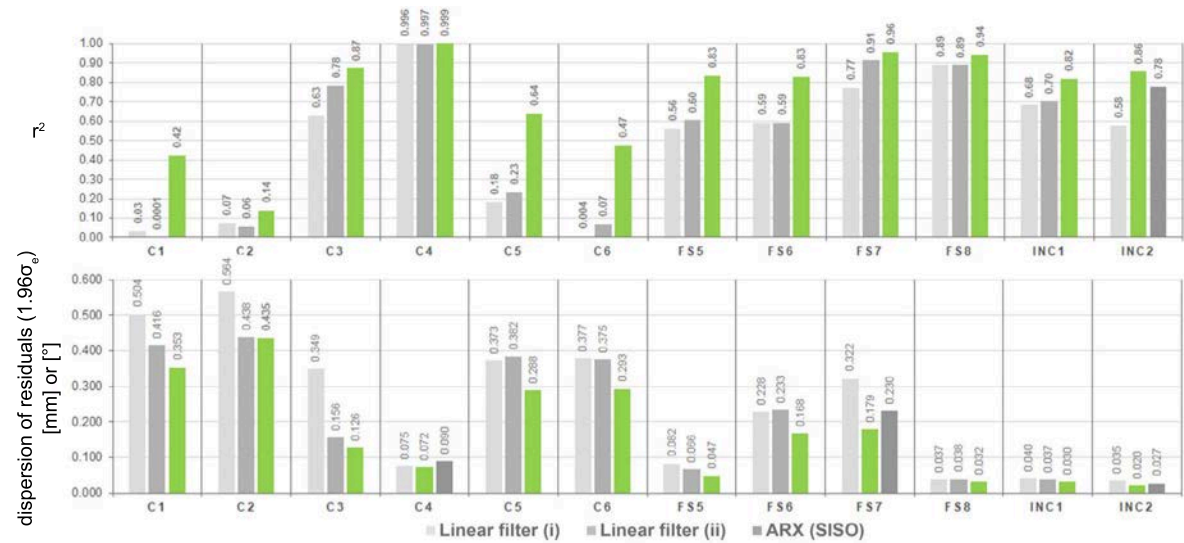


Figure 5.9: Coefficient of determination (r^2) and dispersion of residuals ($1.96\sigma_e$) between simulated and measured responses in Mallorca cathedral.

The evolution rates estimated after filtering the simulated environmental effect using linear and ARX models are presented in Table 5.4. The estimated condition of each response using the procedure described in Section 5.4.2 is also shown in the table and illustrated in Figure 5.10.

Table 5.4: Comparison of estimated evolution rates for monitored structural parameters of Mallorca cathedral from methods filtering out simulated effect of measured environmental parameters.

Sensor	Units	Estimate of annual evolution rate [unit/year]			Estimated condition
		Linear filter (i)	Linear filter (ii)	SISO ARX filter	
C1	mm	0.123	0.163	0.056	Inconclusive
C2	mm	0.055	0.054	0.057	Inconclusive
C3	mm	0.081	0.088	0.077	Evolutionary
C4	mm	0.017	0.016	0.002	Inconclusive
C5	mm	0.007	0.003	0.014	Inconclusive
C6	mm	0.074	0.068	0.068	App. Evolutionary
FS5	mm	0.010	0.009	0.011	App. Evolutionary
FS6	mm	-0.036	-0.036	-0.040	App. Evolutionary
FS7	mm	0.083	0.082	0.050	App. Evolutionary
FS8	mm	0.002	0.002	0.002	Stationary
INC1	°	0.007	0.007	0.007	App. Evolutionary
INC2	°	0.028	0.026	0.031	App. Evolutionary

The results indicate that the convergence extensometer placed across the southern transverse arch of the 4th bay is clearly experiencing an increasing trend of approximately 0.08 mm/year. The simpler methods considered also predict rates which are in good agreement with this. It can also be observed that the crackmeter placed across a crack in the vault of the central nave in the 7th bay is clearly stationary outside cyclic seasonal variations. Although there is a greater level of uncertainty associated to other estimated trends, the apparent evolutionary trend shown by the inclinometer monitoring the inclination of the front façade (INC2) deserves

particular attention because despite being the sensor with the shortest duration of useful data (1.2 years), it shows a significant trend after the effect of temperature has been filtered out and the residuals from the models used for the filtering process have a relatively low scatter. In fact, it very nearly satisfies the condition to be classified as "Evolutionary" according to the procedure described in Section 5.4.2. Once again, evolution rates predicted by simpler methods are also in good agreement with the final one. The trend exhibited by this sensor corresponds to an outward inclination of the façade.

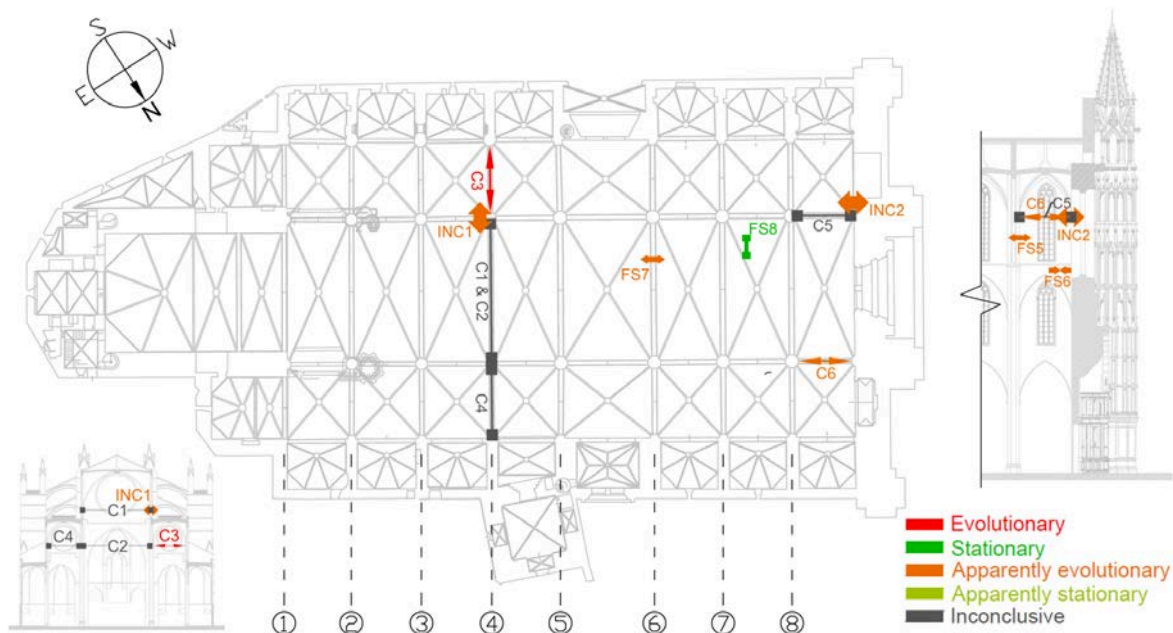


Figure 5.10: Main outcomes from analysis of static SHM data of Mallorca cathedral.

5.5.1.2. Prognosis

The opening trend across the southern transverse arches of Mallorca cathedral has been addressed in a previous study (Pelà et al., 2016a) and can be attributed to a slow ongoing deformation caused by an unbalanced thrust during the construction process. The study, based on a time-dependent finite element analysis able to account for the creep behaviour of masonry, showed that the use of temporary ties during the construction process could clearly contribute to the structure's stability. The model used to represent the creep behaviour of masonry was calibrated based on a deformation rate of 0.1 mm/year between 543 and 548 years after construction (corresponding to the monitoring period) and concluded that under such conditions, this deformation would not have stabilised for a long period of time after construction. However, the research did indicate that if the model was calibrated for lower deformation rates, it could be shown that the phenomena would stabilise in a shorter time period.

The analysis of the monitoring data also reveals that the façade could be experiencing an outward inclination. The structure has already historically faced problems related to the main façade since the previous one was dismantled and reconstructed during the 19th century due to a worrying inclination. In fact, the out-of-plumb of the previous façade is recorded to have increased by 10 cm from the mid-17th century to the beginning of the 19th century. It should also be mentioned that a technical report based on an inspection carried out by the Spanish Institute of Cultural Heritage in 2012 (IPCE, 2012) reports the presence of transverse cracks across the vault of the main entrance. Such damage would be consistent with problems related to the detachment of the façade. Moreover, an outward tilting of the façade would also be consistent with the apparent evolutionary trends derived for the convergence extensometer C6 and the crackmeters FS5 and FS7. However, it must also be said that it is unlikely that the entire façade is tilting outward as a rigid block because the magnitude of the estimated evolution rate is relatively high and hence such a phenomenon would have become clearly visible at a much earlier stage. It is more likely that only the upper part of the façade is experiencing an outward rotation with a rotating centre at a height between sensors FS5 and FS6. This would also explain the apparent underlying closing trend revealed for the crack monitored by FS6. These observations

suggest that the façade is still being affected by an active mechanism and that further investigation could definitely shed more light on its true nature.

5.5.2. Monastery of Sant Cugat

5.5.2.1. SHM system

In order to investigate the root cause of several visible structural pathologies, a long-term static SHM system consisting of 14 crackmeters, 2 inclinometers, 3 thermistors and 3 humidity sensors was installed in the church of the monastery, as shown in Figure 5.11.

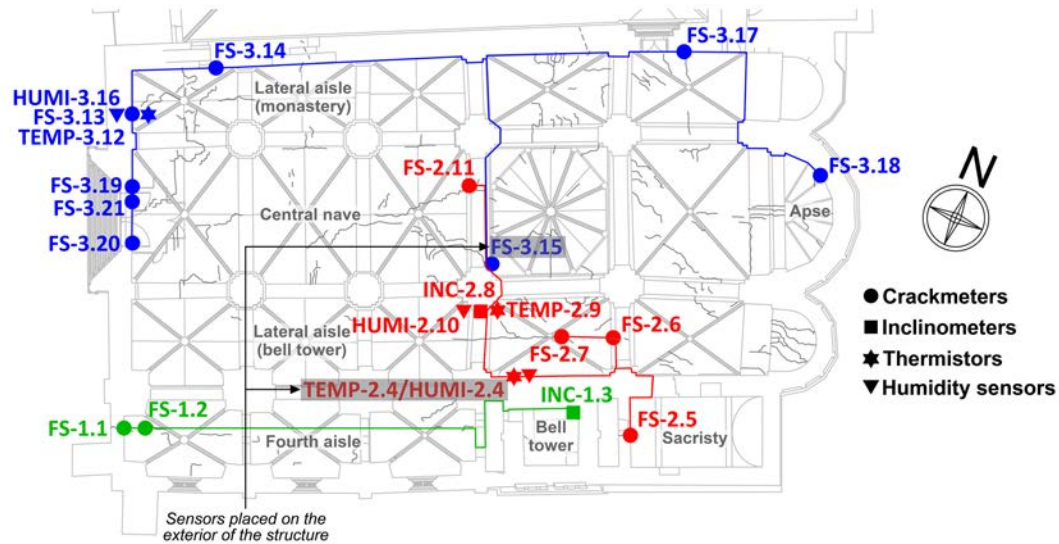


Figure 5.11: Plan view showing position of sensors and layout of structural health monitoring system installed in the church of the monastery of Sant Cugat. A different colour is assigned to each group of sensors connected to the same data logger or expansion module.

Table 5.5: Summary of structural sensors used in the SHM system installed in Sant Cugat monastery together with the total duration of useful data collected up to 28/10/2020.

Sensor	Location	Duration of useful data [years]	Type
FS-1.1	Fourth aisle	3.6	Crackmeter
FS-1.2		3.6	Crackmeter
INC-1.3	Bell tower	3.6	Inclinometer
FS-2.5	Sacristy	3.6	Crackmeter
FS-2.6	Lateral aisle (bell tower)	3.6	Crackmeter
FS-2.7		3.6	Crackmeter
INC-2.8		3.6	Inclinometer
FS-2.11	Central nave	3.6	Crackmeter
FS-3.15	Central nave (exterior)	3.6	Crackmeter
FS-3.13	Lateral aisle (monastery)	3.6	Crackmeter
FS-3.14		3.6	Crackmeter
FS-3.17		3.6	Crackmeter
FS-3.18	Apse	3.6	Crackmeter
FS-3.19	Interior front façade	2.9	Crackmeter
FS-3.20		2.9	Crackmeter
FS-3.21	Lintel main entrance	2.5	Crackmeter

Most of the sensors have been installed since March 2017 except the two crackmeters placed beneath the rose window (installed in December 2017) and the one placed in the lintel of the main entrance (installed

in April 2018). In this case, the crackmeters and inclinometers have minimum resolutions of 0.003 mm and 0.002° respectively. A summary of all the structural sensors of the system is given in Table 5.5. Although the system is still actively collecting data, the results presented in this chapter were based on the data collected up to 28/10/2020. As such, Table 5.5 also shows the duration of useful data collected by each sensor up to this date.

5.5.2.2. Tool for periodic updating of analysis

All the processing steps and analysis methodologies described in Sections 5.2, 5.3, and 5.4 have been implemented in an easy-to-use MATLAB tool that can be used to download files containing updated data from the sensors installed in the monastery of Sant Cugat. These files are uploaded daily from the data acquisition system in place on-site via a wireless network to a remote server from which the MATLAB tool can download the files.

The tool consists of two interfaces which the user can interact with to carry out several tasks. The Main window which appears upon running the application is shown in Figure 5.12.

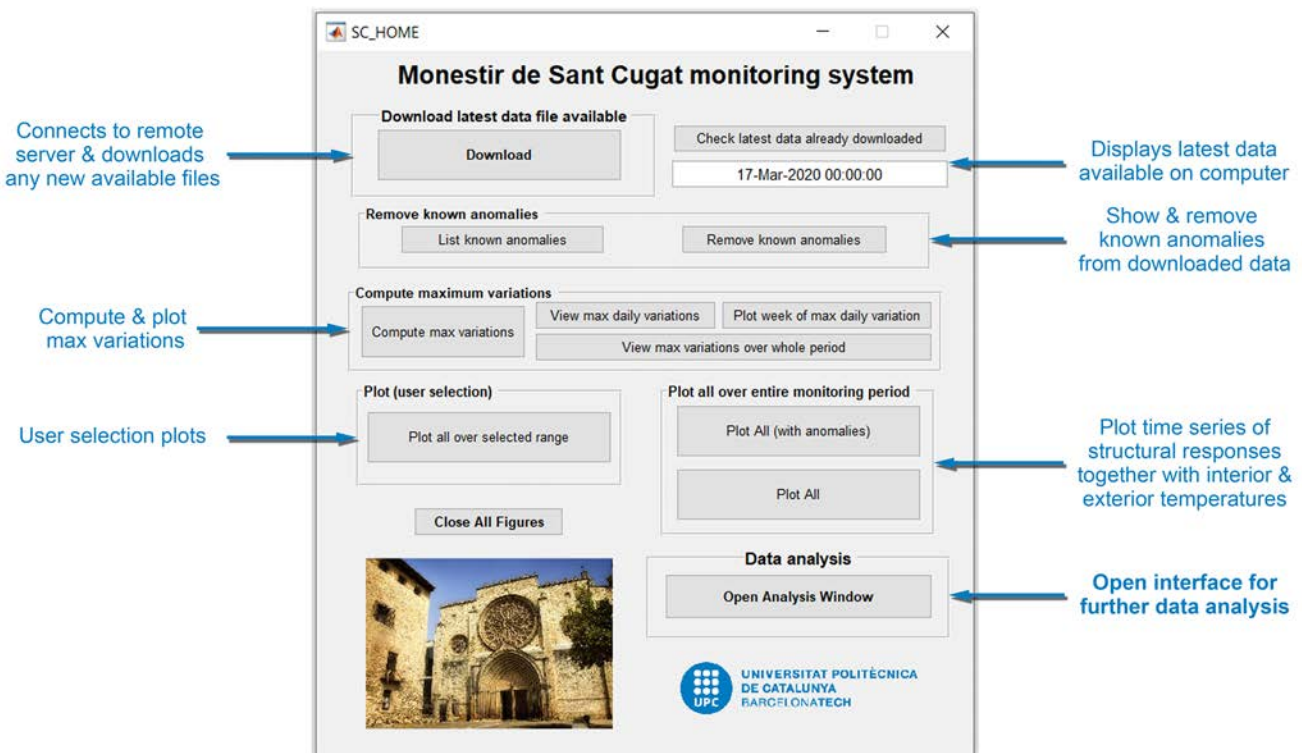


Figure 5.12: Main window of the application used to carry out periodic verifications of data from the monitoring system installed in the monastery of Sant Cugat.

From the Main window, the user can verify the latest data stored on the user's system, download any new data available from the remote server, remove known anomalies from the data, compute maximum variations of each response which can be used for comparison to established thresholds, and create different plots showing the evolution of the acquired data.

The Analysis window shown in Figure 5.13 can also be launched from the Main window. From this window, all the analysis procedures described from Sections 5.3 and 5.4 can be executed. The user can then choose to extract or visualise any updated results within minutes.

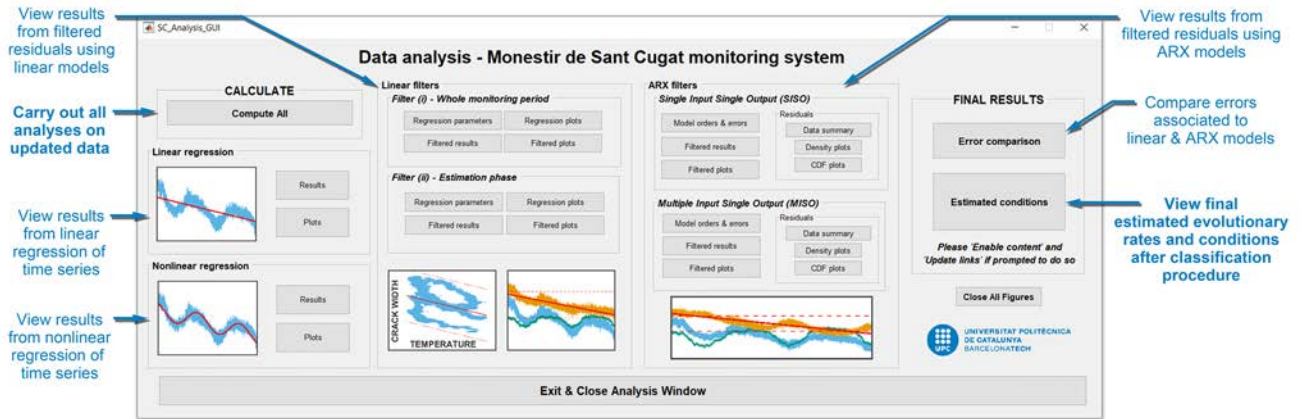


Figure 5.13: Analysis interface of the application used to carry out periodic verifications of data from the monitoring system installed in the monastery of Sant Cugat.

5.5.2.3. Initial observations from correlation with temperature

As stated in 5.3.2, computing the Pearson correlation coefficient ($R_{X,Y}$) between measured environmental and structural parameters can help identify the most suitable environmental parameters to use as predictors in models representing the dependence of a structural response on environmental fluctuations.

$R_{X,Y}$ values between temperature and each structural response monitored in the monastery of Sant Cugat are shown in Figure 5.14. For each response, the preliminary evaluation of correlation was carried out with exterior temperatures recorded by the thermistor placed outside the structure, as well as with interior temperatures recorded by the nearest thermistor placed inside the structure.

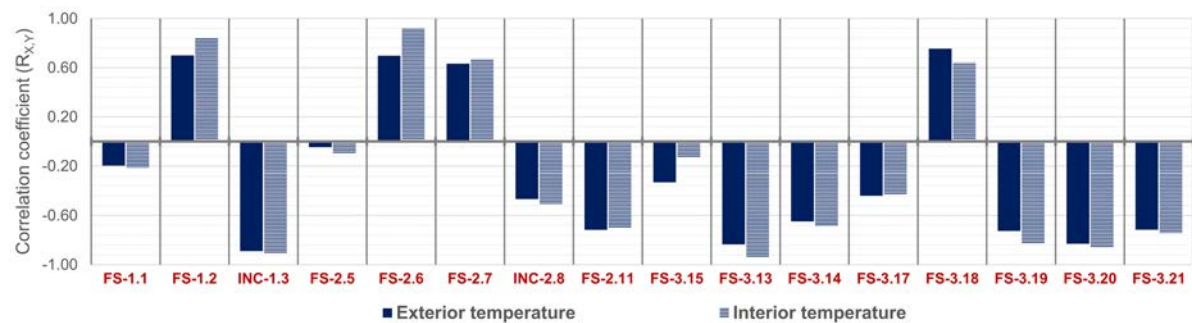


Figure 5.14: Correlation coefficients computed over the entire monitoring period up to 28/10/2020 between structural parameters and temperatures monitored in Sant Cugat moastery.

Both inclinometers have a strong negative correlation with temperature. This indicates that both the bell tower and the pillar at the southwest corner of the cimborio tend to incline towards the south when temperatures increase.

As expected, most monitored crack widths exhibit a negative correlation with temperature. This is the expected behaviour since increasing temperatures cause materials to expand thus reducing crack widths and vice versa. However, four of the monitored cracks show a positive correlation with temperature. It is possible that the unexpected thermal response of some of these cracks is linked to the structural intervention that was completed in 1996 (SAPIC, 1996). This activity involved inserting several tie rods in the southern part of the church, as shown in Figure 5.15. If these elements were actively working, an increase in temperature would cause an expansion of the tie rod and a subsequent loss in tension, which could induce the opening of cracks. This type of response has been observed previously in a masonry tower as reported by (Saisi; Gentile; Ruccolo, 2016). In addition to the insertion of tie rods, the structural intervention of 1995-1996 also involved consolidation with a heavily reinforced concrete overlay of the gothic vaults of the fourth and lateral aisle on the side of the bell tower (see Figure 5.15). The expansion of the reinforcement during increasing temperatures can exert a force on the concrete and subsequently on the masonry. This effect can also contribute to the positive correlation observed between temperatures and the crack widths monitored by FS-1.2, FS-2.6 and FS-2.7.

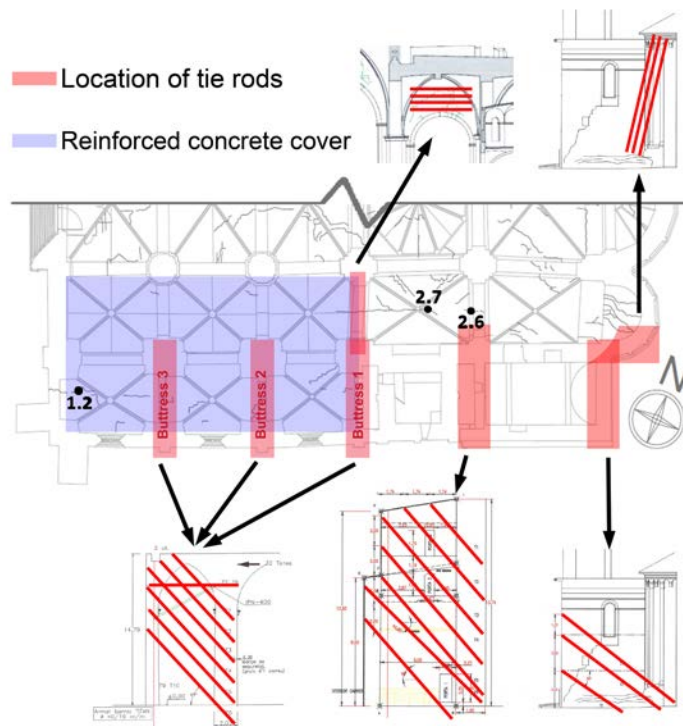


Figure 5.15: Structural interventions completed in 1996 in the southern part of the church, with the position of some sensors monitoring cracks which exhibit a positive correlation with temperature.

5.5.2.4. Main results

The estimated evolution rates for all monitored structural parameters in the monastery of Sant Cugat from methods based on directly fitting time series to selected models are shown in Table 5.6.

Table 5.6: Comparison of estimated evolution rates for monitored structural parameters in the monastery of Sant Cugat from methods based on directly fitting time series to selected models (based on data up to 28/10/2020).

Sensor	unit	Estimate of annual evolution rate [unit/year]	
		Linear regression	Nonlinear regression
FS-1.1	mm	0.098	0.097
FS-1.2	mm	0.004	0.004
INC-1.3	°	-0.003	-0.003
FS-2.5	mm	0.031	0.031
FS-2.6	mm	0.002	0.002
FS-2.7	mm	0.001	0.001
INC-2.8	°	-0.005	-0.005
FS-2.11	mm	0.058	0.060
FS-3.15	mm	0.006	-
FS-3.13	mm	-0.013	-0.008
FS-3.14	mm	-0.015	-0.014
FS-3.17	mm	-0.045	-0.045
FS-3.18	mm	0.020	0.020
FS-3.19	mm	-0.201	-0.119
FS-3.20	mm	-0.055	0.002
FS-3.21	mm	0.087	0.089

The evolution rate predicted for crackmeter FS-3.15 was disregarded because it had a poor correlation with the data (coefficient of determination of 0.40) indicating that the evolution of the data could not be well represented by the nonlinear periodic model. Despite the greater complexity of the nonlinear model, it is clear that the estimated evolution rates between the two methods are in good agreement for many cases, notably for crackmeters FS-2.5, FS-3.17, and FS-3.18 and for inclinometer INC-1.3.

As for the previous case study, a comparison of the errors between measured responses and those simulated from linear and ARX models during their respective estimation phases was carried out in order to evaluate the ability of each model type to represent the dependency of structural parameters on environmental ones (see Figure 5.16). In this case, it is possible to see the added benefit of using both interior and exterior temperature as predictors in the ARX models since the MISO models outperform the SISO ones for almost all monitored responses despite the fact that they have lower model orders.

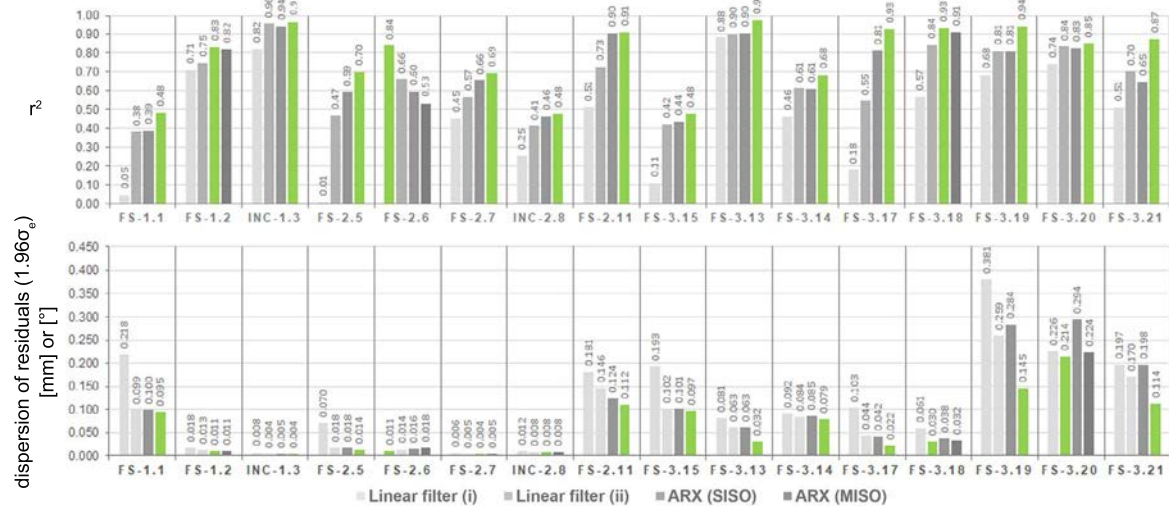


Figure 5.16: Coefficient of determination (r^2) and dispersion of residuals ($1.96\sigma_e$) between simulated and measured responses in Sant Cugat monastery.

Before stating the main conclusions with respect to the diagnosis of the church's structural condition, the evolution rates estimated using methods described in Sections 5.3.3 and 5.4.1 as well as the evolutionary states evaluated from the procedure elaborated in Section 5.4.2 are summarised in Table 5.7 and Figure 5.17.

Table 5.7: Comparison of estimated evolution rates for monitored structural parameters of Sant Cugat monastery from methods filtering out the simulated effect of measured environmental parameters (based on data up to 28/10/2020).

Sensor	Units	Estimate of annual evolution rate [unit/year]				Estimated condition
		Linear filter (i)	Linear filter (ii)	SISO ARX filter	MISO ARX filter	
FS-1.1	mm	0.099	0.099	0.100	0.106	App. Evolutionary
FS-1.2	mm	0.004	0.004	0.004	0.004	App. Evolutionary
INC-1.3	°	-0.003	-0.003	-0.003	-0.003	Evolutionary
FS-2.5	mm	0.031	0.031	0.030	0.032	Evolutionary
FS-2.6	mm	0.000	0.000	0.000	-0.001	App. Stationary
FS-2.7	mm	0.002	0.002	0.002	0.002	Stationary
INC-2.8	°	-0.005	-0.005	-0.005	-0.006	Evolutionary
FS-2.11	mm	0.063	0.063	0.066	0.073	App. Evolutionary
FS-3.15	mm	0.008	0.008	0.009	0.009	Inconclusive
FS-3.13	mm	-0.011	-0.011	-0.010	-0.006	App. Stationary
FS-3.14	mm	-0.015	-0.014	-0.015	-0.013	Inconclusive
FS-3.17	mm	-0.045	-0.045	-0.043	-0.035	Inconclusive
FS-3.18	mm	0.018	0.018	0.012	0.021	App. Evolutionary
FS-3.19	mm	-0.142	-0.144	-0.133	-0.095	App. Evolutionary
FS-3.20	mm	-0.015	-0.004	-0.030	0.012	Inconclusive
FS-3.21	mm	0.089	0.090	0.078	0.092	App. Evolutionary

The outcome of the analysis indicates that 3 of the monitored parameters are experiencing significant evolutionary trends outside the cyclic seasonal variations: the inclination of the bell tower (INC-1.3) as well as that of one of the pillars of the cimborio (INC-2.8) on the side of the bell tower towards the south and the opening of the crack in the Sacristy. All methods filtering out the simulated effect of environmental parameters predict very similar rates for these 3 trends. In fact for the inclination of the pillar of the cimborio, which shows the greatest predicted rate out of the two inclinations, methods based solely on fitting the time series to selected models also predict similar rates as those evaluated through the more sophisticated approaches. The same can be said about the crack in the Sacristy. As will be discussed in the next section, it is likely that these trends are being caused by the same phenomenon.

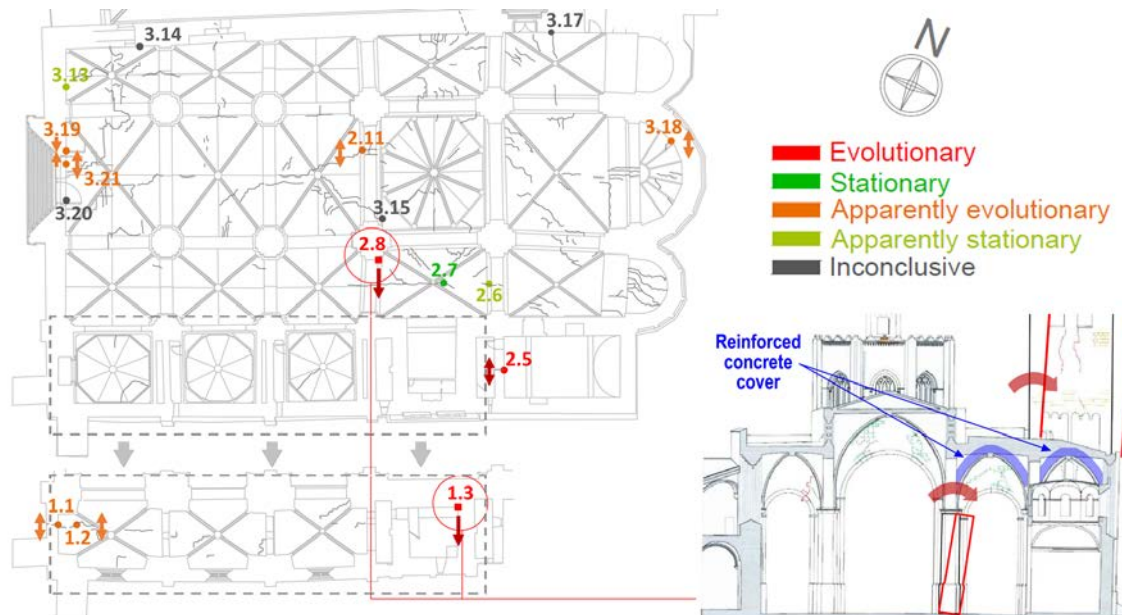


Figure 5.17: Main outcomes from analysis of static SHM data of Sant Cugat monastery.

The results also reveal that the monitored crack across the vault of the lateral aisle appears to be stationary. It is interesting to note that in both case studies, the monitored parameter showing the most stationary trend corresponds to a crack in a vault. This is most probably due to the flexibility of vaults in comparison to other stiffer structural members and hence their increased ability to deform without suffering significant irreversible damage.

It can also be seen that the highest evolutionary rates are predicted for cracks in the interior of the front façade below the rose window. One of these monitored cracks appears to be experiencing a closing trend outside seasonal variations. Since cracks are inherently caused due to the material experiencing tensile stresses, closing trends indicate that the behaviour of the structure has changed since the formation of the crack which initially had to be opening. However, for all monitored cracks below the rose window, it must be said that the magnitude of observed trends are comparable to that of the errors associated to the models used to filter out the effect of temperature.

5.5.2.5. Prognosis

The first conclusion that can be made from the analysis of the monitoring data so far is related to the effect of the bell tower on the rest of the elements. The measurements of the inclinometer on the wall of the bell tower suggest an outward leaning trend of $0.003^\circ/\text{year}$ outside seasonal variations. The fact that the crack in the western wall of the sacristy appears to be opening at a rate of $0.032 \text{ mm}/\text{year}$ is consistent with this movement since this wall is intrinsically tied to the bell tower. It also indicates that this outward rotation is most likely starting from a considerably low point (below the point at which the crack is already opening in the sacristy). Moreover, it is likely that the observed outward movement of the pillar supporting the cimborio is linked to this outward movement of the bell tower. All of these observations are consistent with the history of the construction of the structure since most of it was built in the 14th Century while the bell tower was only completed in the 18th Century, when an arch joining the then incomplete bell tower and the cimborio

was also dismantled. It appears that the addition of this part of the structure is still having an active effect, even today. The main body of the bell tower has a total height of approximately 29m and if this whole part was rotating outwards as a rigid block, the measured inclination would reflect an outward leaning of approximately 1.5cm every 10 years at the top of this block. In fact, recent topographic and laser scan surveys of the bell tower's geometry reveal that its southern and eastern wall have inclinations of up to 1.5% (Ajuntament de Sant Cugat, 2019b) corresponding to a net displacement of 52 cm from the vertical position at the top of the main body of the tower (see Figure 5.18). This strengthens the findings from the analysis of the monitoring data and suggests that a structural intervention could be required in the future to prevent further deterioration due to this mechanism.

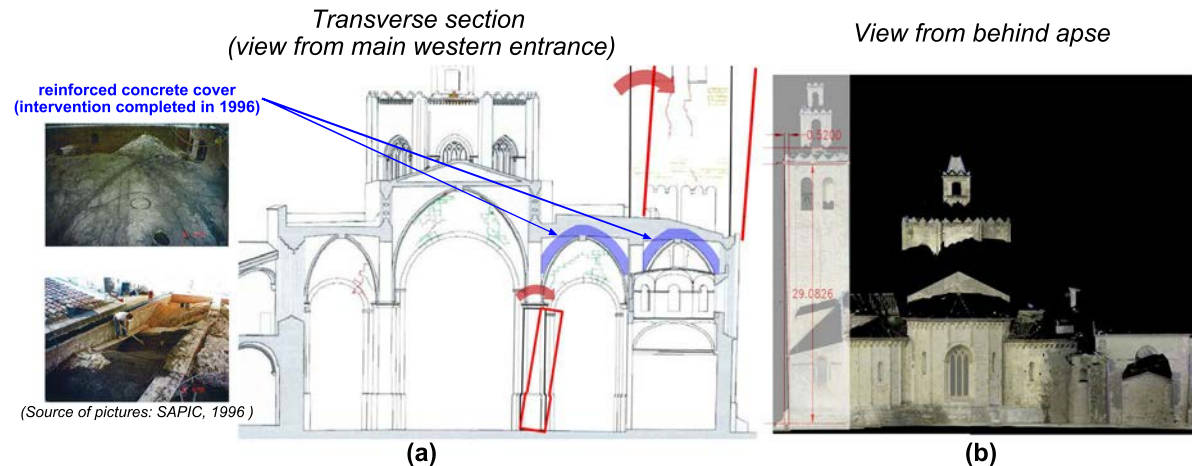


Figure 5.18: (a) Observed inclination trends and location of reinforced concrete cover added in 1995-1996. (b) Measured inclination of the bell tower of Sant Cugat with (all measurements shown in m) (Ajuntament de Sant Cugat, 2019b).

Finally, the magnitude of the variations experienced by cracks below the rose window indicate that they deserve particular attention. However, since these cracks have been monitored for a shorter period of time and the fact that restoration works were being carried out on this part of the structure during the start of the monitoring period means that an acceptable level of confidence cannot yet be associated to any of the observed trends. An extended monitoring period is recommended before any suitable conclusions can be made on possible mechanisms affecting this area.

5.6. Summary

This part of the research has presented an integrated approach for the data analysis of static structural health monitoring (SHM) of masonry heritage structures. The proposed methodology utilises dynamic linear regression models, which can consider multiple predictors to filter out the reversible seasonal variations experienced by most structural parameters of interest. These models are able to attribute components of a current response caused by past ones when estimating the parameters of the model but can then disregard these components when simulating the effect only caused by environmental predictors. This is ideal for the case of static SHM since active structural mechanisms of interest have often begun long before any decision on monitoring could be made and it is thus impossible to define a period of time for which the relationship between structural and environmental parameters are isolated. In fact, the first part of the proposed method could also be used to filter out environmental effects on the evolution of natural frequencies recorded by dynamic monitoring systems. However, it is worth mentioning that in the case of masonry heritage structures, rather than attempting to detect very slow deterioration mechanisms, the dynamic monitoring strategy is most often oriented towards assessing the effectiveness of repairs, identifying significant changes in boundary conditions, or towards the early identification of more pronounced damage characterised by a faster evolution rate. The nature of these objectives facilitates the application of several sophisticated analysis procedures because it simplifies the task of defining an adequate training period. As a result, several procedures including machine learning approaches, negative selection and principal component analysis could prove to be more efficient for the analysis of data from dynamic SHM systems.

The static SHM strategy is clearly well suited to identify slow-varying underlying trends in each monitored

parameter. However, in most cases, cost and technical limitations only allow a very limited number of parameters to be monitored at specific location points. As a result, it can be very challenging to extract general conclusions on the global structural response. Given this inherent difficulty, one of the main advantages of the proposed methodology over previously applied ones is that it does not only provide estimated evolution rates of the monitored parameters but also evaluates their evolutionary state and classifies them accordingly. The classification is based on the estimated rates and the errors of the models used to represent the relationship between structural and environmental parameters. This can greatly help to identify areas that should be prioritised during the diagnosis of the structure and to extract meaningful conclusions on the relationship between different monitored parameters. In addition, the entire procedure can be fully automated and once implemented, can provide up to date analysis results as the monitoring period increases. In fact, an extension of the current research would be to assess if the trends of the residuals estimated after the proposed filtering of environmental effects change over longer monitoring periods. If they do, using higher order polynomial models to describe the trend could reveal whether or not a particular evolutionary state is stabilising or not.

The usefulness of the method has clearly been demonstrated through the application to two case studies. In both cases, outcomes of the proposed automatic procedure helped to identify vulnerable areas in important heritage structures. The results also reveal that simpler methods are often able to predict evolution rates rather accurately. This explains why such methods have been used successfully in the past for the accurate diagnosis of structures. However, such methods are not always accurate and provide very little means of assessing the reliability of results, whereas the proposed methodology is more robust and gives clear indications related to the reliability of results.

6

Risk assessment and decision-making

6.1. Introduction

This chapter elaborates the proposed solutions that specifically address the final objective of this thesis, which is to develop useful multi-criteria decision-making (MCDM) tools to support decisions on the structural safety of masonry heritage.

Two indices are proposed that can be used to gauge the level of knowledge on the actual structural condition and the associated damage risks. The input data for computing both indices is derived from answers to standard questions that need to be completed by the expert responsible for structural diagnosis. Questions used to feed the indices include essential and optional ones. Essential questions need to be answered following the initial history, geometry, and damage survey. Since optional questions relate to the outcome of specific diagnosis activities, they can only be answered if these are carried out. Both indices are computed using simple additive weighting (SAW) based on specifically designed hierarchical trees of the criteria that influence the level of knowledge and the damage risk. A novel modification is proposed to allow the relative importance of information from different activities to change depending on ratings and rankings that have to be provided as answers to certain essential questions. Naturally, for the index values to be meaningful and useful for decision-making, they have to be evaluated within the framework of a systematic risk assessment procedure based on well-defined scientific principles.

A proposal for such a risk assessment procedure is first presented to provide a general understanding of the mechanisms used to compute and update index values (Section 6.2). Subsequently, a brief description is given of the standard questions whose answers are the main input to both indices (Section 6.3). The specific criteria and hierarchical structures of the level of knowledge (Section 6.4) and damage risk (Section 6.5) indices are then elaborated. Following this explanation, one of the most useful outcomes for decision-making from applying the proposed risk assessment methodology is shown (Section 6.6). This involves the automatic generation of a list of relevant diagnosis activities ordered according to their remaining possible contribution to the level of knowledge index. A decision grid with ranges of the proposed indices is also presented in the same section to demonstrate how the method can help improve objectivity and clarity in the decision process. An application to a complex case-study, the cathedral of Mallorca in Spain, is then presented (Section 6.7) before showcasing several other applications (Section 6.8). Finally, the main conclusions of this part of the research are summarised in Section 6.9.

6.2. Risk assessment methodology

In the context of this research, risk assessment refers to the identification, characterisation, and evaluation of the risk of structural damage occurring in a unique masonry heritage structure. The main aim of such a procedure is to determine the most suitable course of action for best preserving the structure. Given the particular characteristics of these structures and the need for minimum intervention, it is now widely accepted that the best form of therapy is a preventive conservation approach, whereby structural condition, risks, and

threats are periodically monitored (ICOMOS, 2003; ISCARSAH, 2005; Paolini et al., 2012; Heras et al., 2013; Van Balen, 2017). Within the proposed risk assessment framework, as previously mentioned, key indices are introduced to monitor the estimated level of risk and the level of knowledge on the structural condition. The proposed risk assessment methodology has thus been designed to allow these indices to be updated easily after any diagnosis activity or intervention is performed.

As summarised in Figure 6.1, the proposed methodology involves a standardised initial expert appraisal (SIEA) that needs to be completed by the professional responsible for structural risk assessment after an initial desk study and inspection have been carried out.

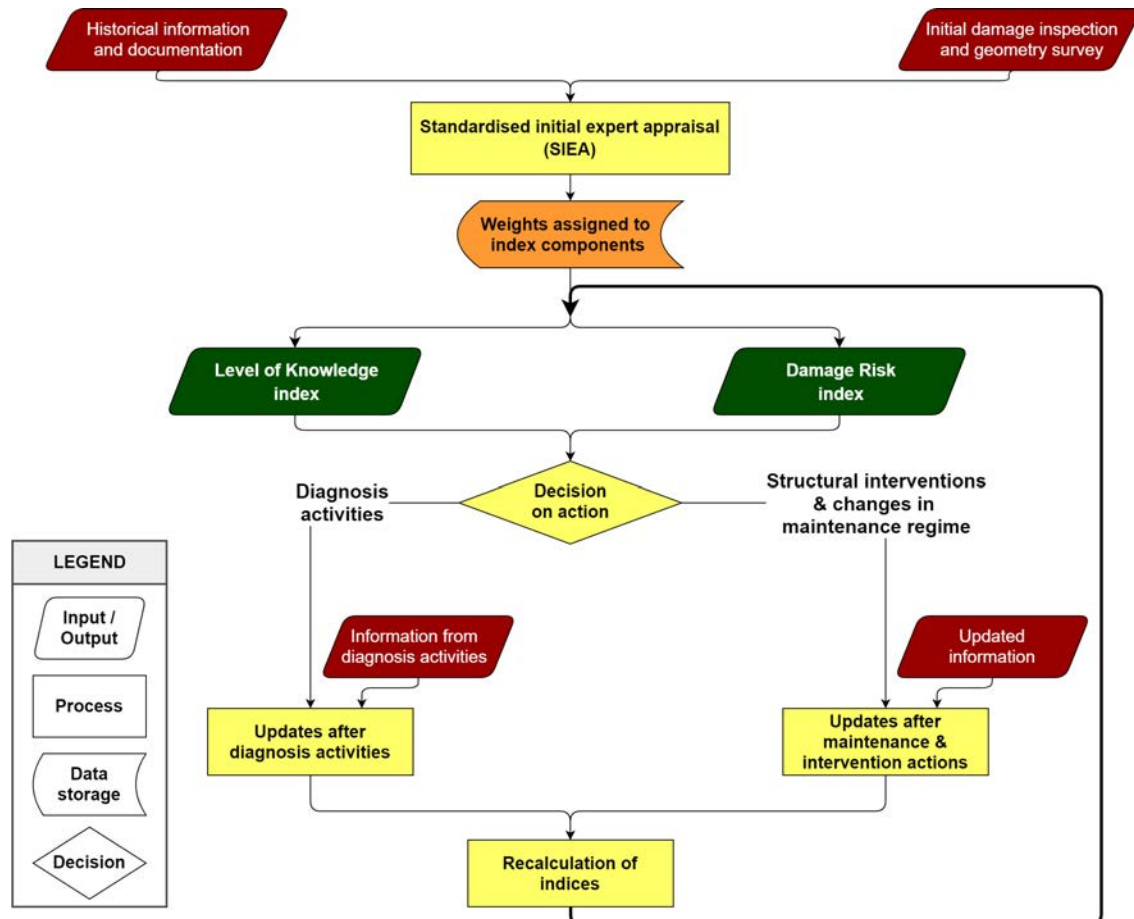


Figure 6.1: Proposed general risk assessment methodology.

Before the SIEA, all relevant available documents should be gathered and analysed to produce reliable information about the structural history of the building. In addition, an initial inspection should be carried out to identify the most important signs of decay and damage, to formulate initial hypotheses on potential active deterioration phenomena, and to decide whether there are immediate risks requiring urgent action. This inspection can also include measurements to obtain a general idea of key dimensions. The initial understanding of the structure provided by these activities can then be used to give an appropriate direction to subsequent investigations.

The SIEA has thus been designed in two parts. The first contains a standard set of questions requiring answers in the form of ratings that can be used to provide an initial understanding of the damage risk and the level of knowledge on the structural condition. The second part requires the expert to rank structural analysis goals and to rate the potential value of information that can be obtained from different research activities for assessing damage vulnerability. All rankings and ratings provided are then used to define weights among criteria and to compute initial values for two standard indices: the Level of Knowledge (LoK) index and the Damage Risk (DR) index. The actual components and structure of these two indices are described in detail in

Sections 6.4 and 6.5.

Once the initial values of the indices are evaluated, the expert has to make a decision on the best course of action to safeguard the cultural and historical value of the structure as a whole. Possible decision alternatives usually include performing further diagnosis activities for a more complete and reliable assessment of vulnerability, performing structural interventions based on the current level of knowledge, or implementing an improved maintenance programme. As such, answers to standard questions have to be given or updated after each diagnosis activity or intervention is performed in order to update the LoK and DR index values accordingly. A brief description of all standard questions included as part of the proposed methodology is given in Section 6.3, while a detailed explanation of how to update index values after performing different types of activities is given in Section 6.6. Of course, following risk assessment, the decision may be that no action is required. If this is the case, the values of the LoK and DR indices remain unchanged until a re-evaluation is deemed necessary.

6.3. Standard questions for evaluating and updating indices

This section provides a brief overview of all standard questions that can be used to evaluate and update the LoK and DR indices. These questions can be broadly categorised as essential or optional. Answers to essential questions are required to compute initial values of the indices and therefore need to be provided during the standardised initial expert appraisal (SIEA). Answers to optional questions provide relevant information for risk assessment from various diagnosis activities. As such, specific relevant questions only need to be answered after a particular diagnosis activity has been performed. It is important to note that all questions have been arranged according to the logical order for which it would be most convenient for the user to answer them, and not according to the structure of the LoK and DR indices.

6.3.1. Essential questions

The individual questions that need to be answered during the two parts of the SIEA are not listed here but can be found in Appendix A.1, together with explanations of the possible range of answers.

6.3.1.1. Initial evaluation of level of knowledge and damage risk

The first part of the SIEA consists of 11 questions that require answers in the form of ratings. As previously mentioned, these are used to compute the initial values of the LoK and DR indices. Some of these questions consist of more than one part. Specifically, answers from the 4 parts of question 1 are used to establish the level of knowledge in terms of historical information and documentation. Questions 2 and 3 provide information on the level of knowledge in terms of geometry and damage mapping. Question 4 is related to the assessment of material quality from visual inspections and consists of two parts: the first informs the LoK index while the second informs the DR index. The remaining questions in the first part of the SIEA are all used in the computation of the DR index. Question 5 provides information on the level of exposure in terms of cultural value and potential loss. Questions 6 and 7 provide information on the damage vulnerability linked respectively to poor maintenance and to the need for urgent action. Question 8 is used to represent the expert's initial assessment of the damage vulnerability to slowly evolving progressive collapse mechanisms. Questions 9 and 10 are related to earthquakes and other catastrophic events respectively. They provide information on the hazard level and on the vulnerability to these specific hazards. Finally, question 11 involves assessing the fire hazard.

6.3.1.2. Assessing the importance of different diagnosis activities

As previously mentioned, rankings and ratings provided in the second part of the SIEA are used to define the weights assigned to specific components of the LoK and DR indices. This allows the hierarchical structure of the two indices to be modified based on singular characteristics of different monuments. Since the two indices are used to describe the decision problem within the proposed risk assessment methodology, this weight-setting procedure enables meaningful insights to be drawn even if the methodology is applied to different structures with unique characteristics. The hierarchical structures of the two indices and the procedure used to establish weights from the provided ratings are described in greater detail in Sections 6.4 and 6.5.

This part of the SIEA consists of 8 questions (12 to 19), all of which are made up of several parts. The first and second parts of question 12 determine whether the vulnerability to earthquakes or other catastrophic events are explicitly considered in the assessment. If the decision is taken to include the vulnerability to these specific hazards, they will have to be assessed and ratings will have to be provided to define the possible contribution of different structural analysis and monitoring tools to the level of knowledge on these specific vulnerabilities. If the decision is taken to exclude a specific vulnerability, it will not be explicitly considered when evaluating the global damage vulnerability. However, it is worth noting that the hazard related to earthquakes and other catastrophic events will still be included in the global risk assessment. The third part of question 12 then involves ranking the following 3 possible aims of structural analysis according to their importance for global damage vulnerability characterisation:

1. Structural analysis aimed at better understanding the vulnerability to progressive collapse.
2. Structural analysis aimed at better understanding the vulnerability to earthquakes.
3. Structural analysis aimed at better understanding the vulnerability to other catastrophic events.

The assigned ranks are then used to determine the relative importance that these 3 aims are given in the vulnerability component of the DR index. Naturally, if the vulnerability to earthquakes or to other catastrophic events has already been excluded from the analysis in the first two parts of question 12, only the remaining relevant aims need to be ranked. If both have already been excluded, only the vulnerability to progressive collapse is considered. The vulnerabilities to specific hazards are treated separately in the proposed assessment procedure mainly because they can differ significantly. For instance, a structure can prove to have adequate capacity to withstand its normal working loads while still being extremely vulnerable to suffering damage during an earthquake. In addition, this separation is also implemented because the suitability of different structural analysis and monitoring tools for diagnosis can change depending on the specific vulnerability under evaluation.

Once a decision has been made on including the vulnerability to specific hazards in the risk assessment, ratings have to be provided to evaluate the suitability of specific diagnosis activities. The information from several different types of activities can be included in the proposed risk assessment procedure. Diagnosis activities are grouped together according to the type of information they can provide, ratings are used to assign weights among activities within a group based on their possible contribution to the level of knowledge on damage vulnerability. Specifically, 5 groups of activities have been identified:

- Structural analysis and SHM
- Activities involving the evaluation of specific mechanical, physical, or chemical properties of materials
- Geometry and damage surveys
- Activities to characterise material quality and variability
- Activities to evaluate actual loading and boundary conditions in-situ

Although the choice of grouping structural analysis and SHM together might appear counter-intuitive as they are often executed separately, it stems mainly from the fact that these two types of activities can be combined in many different ways to provide complimentary information on the capacity and response of a monument to specific structural actions. As such, they were grouped together to allow the expert performing risk assessment to adjust the relative importance of information from specific structural analysis and SHM activities depending on the particular characteristics of the structure. Question 13 thus involves rating different structural analysis and SHM activities based on the extent to which it can help assess the structure's vulnerability to progressive collapse. Activities that need to be rated include: evaluating the loads supported by different members (load report), graphic statics and limit analysis, finite element (FE) modelling, dynamic SHM, and static SHM. Each activity can be rated as 0, 1 or 2. Activities that are rated as 0 will not be considered in the risk assessment. This choice can be made if the information that an activity can provide is deemed irrelevant or if the cost of performing an activity is already known to be too high for a given project. Conversely, activities that are deemed essential or that can contribute significantly to the vulnerability assessment should be rated as 2. Finally, activities that can only complement the vulnerability assessment should be rated as 1.

For question 13, if limit analysis procedures or FE modelling are given a rating which is greater than 0, the rating attributed to the load report is automatically fixed at 1 because evaluating the loading scenario is a necessary preliminary step before performing limit analysis or FE modelling. If the vulnerability to earthquakes and other catastrophic events are included in the risk assessment, the value of different structural analysis and SHM activities for assessing these specific vulnerabilities also needs to be evaluated. This is achieved by rating activities listed in questions 14 and 15. With the exception of the load report, the same activities listed in question 13 are included in these two questions. The same rating scale is also used.

In fact, the same scale is used to rate the different activities in other groups. Tests for estimating material properties need to be rated in question 16, possible geometry and damage mapping activities need to be rated in question 17, and activities linked to the characterisation of material quality and variability need to be rated in question 18. Finally, ratings need to be assigned in question 19 for different in-situ activities that can be used to evaluate actual loading and boundary conditions.

6.3.2. Optional questions

Once the essential questions from the standardised initial expert appraisal (SIEA) have been completed, the LoK and DR indices need to be updated every time an additional diagnosis activity is performed. To achieve this, the proposed risk assessment framework includes specific questions related to many possible diagnosis activities (see Appendix A). Of course, the answers to these questions only need to be completed or updated after relevant activities have been performed. The answers provided are then used to re-evaluate the LoK and DR index values as described in Sections 6.4 and 6.5.

The optional questions are organised according to the 5 identified activity groups listed in Section 6.3.1.2. These questions are not listed here but can be found in Appendices B to E, together with explanations of the possible range of answers. In general, each question relates to a specific diagnosis activity and consists of several parts. In most cases, each question specifically consists of at least one part used for evaluating the LoK index, and at least another part used for evaluating the DR index.

However, optional questions related to additional geometry and damage surveys only consist of a single part used to update the LoK index based on the effectiveness of the activities in addressing the lack of knowledge on geometry and damage. Naturally, the global ratings given during the first part of the SIEA on the level of knowledge on geometry (question 2) and existing damage (question 3) need to be updated after any of the geometry and damage mapping activities are carried out. Relevant vulnerability ratings provided in the first part of the SIEA can also be updated if the new information on geometry and damage changes the initial perception of vulnerability.

It is also worth mentioning that the proposed framework includes distinct optional questions for structural analysis and SHM activities aimed at better understanding the vulnerability to progressive collapse mechanisms, to earthquakes, and to other catastrophic events. In addition, for the case of static SHM, both the LoK and DR indices can be periodically updated after an initial configuration by taking advantage of processed results from the methodology described in Chapter 5.

6.4. Level of knowledge index

All answers to questions related to the level of knowledge are provided in the form of a rating ranging from 0 to 5, with 0 representing no information and 5 representing the highest possible level of knowledge. Each rating can be provided as any rational number within this range and will eventually be combined into a single LoK index to facilitate the decision-making process. The questions have been designed so that ratings represent the comprehensiveness of the different types of research activities performed. Generally, as more and more relevant in-depth investigations are carried out, the uncertainty associated to vulnerability assessment should decrease. As such, the index is intended to inform decision-makers on the general level of uncertainty related to the vulnerability assessment, with a higher level of knowledge indicating less uncertainty. Based on applications to case studies, it can be considered that final LoK index values ranging from 0 to 1.5 represent a low level of knowledge while values between 3 to 5 represent a high level of knowledge. Therefore, index values from 1.5 to 3 suggest a moderate level of knowledge on damage vulnerability.

At this stage, it is relevant to highlight a particular feature of the process behind safety evaluation. When no information is available on a structure, significant improvements can often be made to the understanding of vulnerability through the acquisition of a few key pieces of information and using simplified analysis methods. However, as the general level of knowledge increases, further reducing the uncertainty associated to the vulnerability assessment typically requires more and more effort. In other words, as our understanding of a structure improves, identifying damage causes or quantifying capacity with even greater accuracy usually requires employing even more sophisticated methods and acquiring even more data. This learning effect can be considered in the computation of the LoK index value by transforming the original ratings to a suitable score using an ascending concave value function (see Figure 6.2). Effectively, due to the decreasing slope of such a function, a small increase from a low rating causes a greater increase in the transformed score when compared to the same increment added to a higher rating.

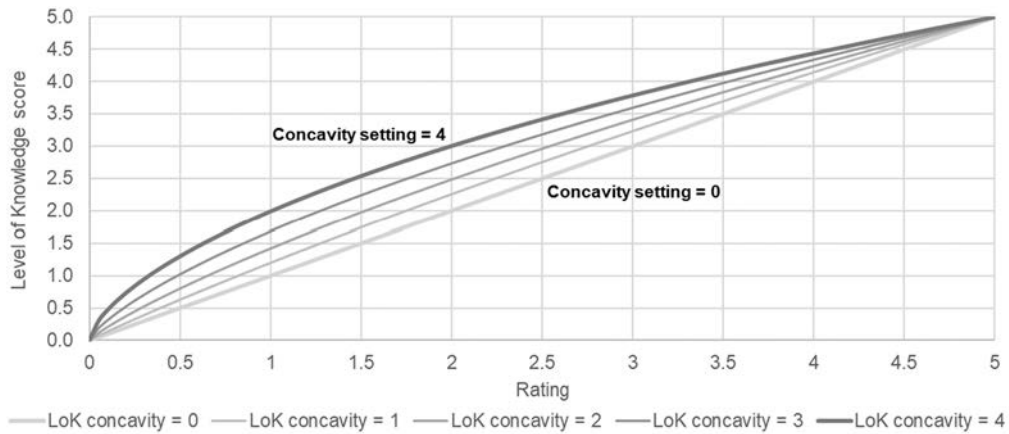


Figure 6.2: Possible settings to adjust the transformation of ratings given as answers to questions into scores used for computing the value of the LoK index.

As described in Section 6.5, similar value functions are also employed in the computation of the DR index to convert answers from specific questions into homogenised scores. As such, a single expression that depends on a few parameters is defined for all value functions employed within the risk assessment framework. The parameters can be modified so that the curvature of the function can be adjusted to best represent the relationship between the original units of the answer and the homogenised score used for computing the final index value. The general value function employed in this research is shown in Equation (6.1). It has been adapted from the one proposed as part of a method known as MIVES (Aguado et al., 2012; Josa et al., 2020), which was initially developed for sustainability assessment.

$$S_i(X_i) = K_i \cdot \left[1 - \exp \left(-m_i \left(\frac{|X_i - X^*|}{n_i} \right)^{A_i} \right) \right] + S_{min} \quad (6.1)$$

$$K_i = \frac{S_{max} - S_{min}}{1 - \exp \left(-m_i \left(\frac{|X_{max} - X_{min}|}{n_i} \right)^{A_i} \right)} \quad (6.2)$$

Where S_i represents each homogenised score that will be combined to compute the LoK index value and X_i refers to each rating provided to update the LoK index. K_i is a factor that can be used to scale the range of the resulting index score. It is computed as shown in Equation (6.2). In this case, the LoK index has a range which can vary from 0 (S_{min}) representing no knowledge at all to 5 (S_{max}) representing very comprehensive knowledge. X_{max} and X_{min} are the maximum and minimum possible rating values, which are also 5 and 0 for all LoK questions. X^* can be either X_{min} or X_{max} depending on if the answer is a maximising positive defined criteria or not. In the case of the LoK index, because all questions have been set so that a higher rating represents a higher level of knowledge, $X^* = X_{min}$. The constants m_i and n_i can be used to modify the geometry of the value function and they have been set at 1 and 20 for the function used to transform all answers related to the level of knowledge. Finally, A_i is a shape factor that defines approximately whether the curve is concave ($A_i < 1$), close to a straight line ($A_i \approx 1$), or whether it is convex or S-shaped ($A_i > 1$). In the case of the LoK index, the expert completing the SIEA can choose between five different concavity settings to

best reflect the learning curve associated with the particular structure of interest. If the LoK concavity is set to 0, the ratings provided as answers to questions are directly combined to compute the index. Otherwise, the four other settings included in the framework are shown in Figure 6.2. They correspond to substituting the values of 0.95, 0.85, 0.75 and 0.65 for A_i in Equation (6.1).

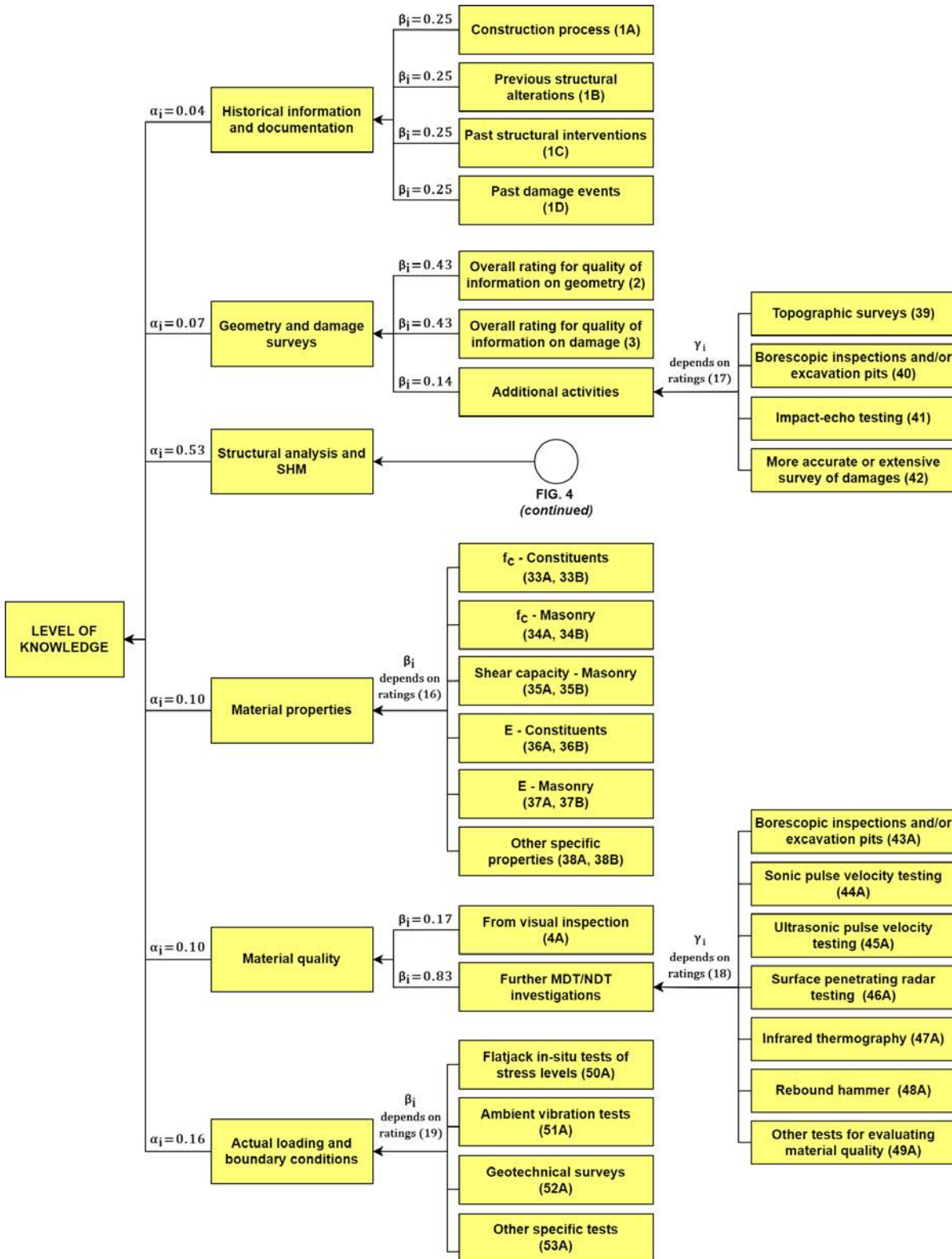


Figure 6.3: Criteria tree for the index representing the general level of knowledge on damage vulnerability. The relevant question references are shown in brackets at the end of each branch. Parameters α_i , β_i , and γ_i refer to relevant weights that need to be applied to criteria at the first, second, and third hierarchical level respectively.

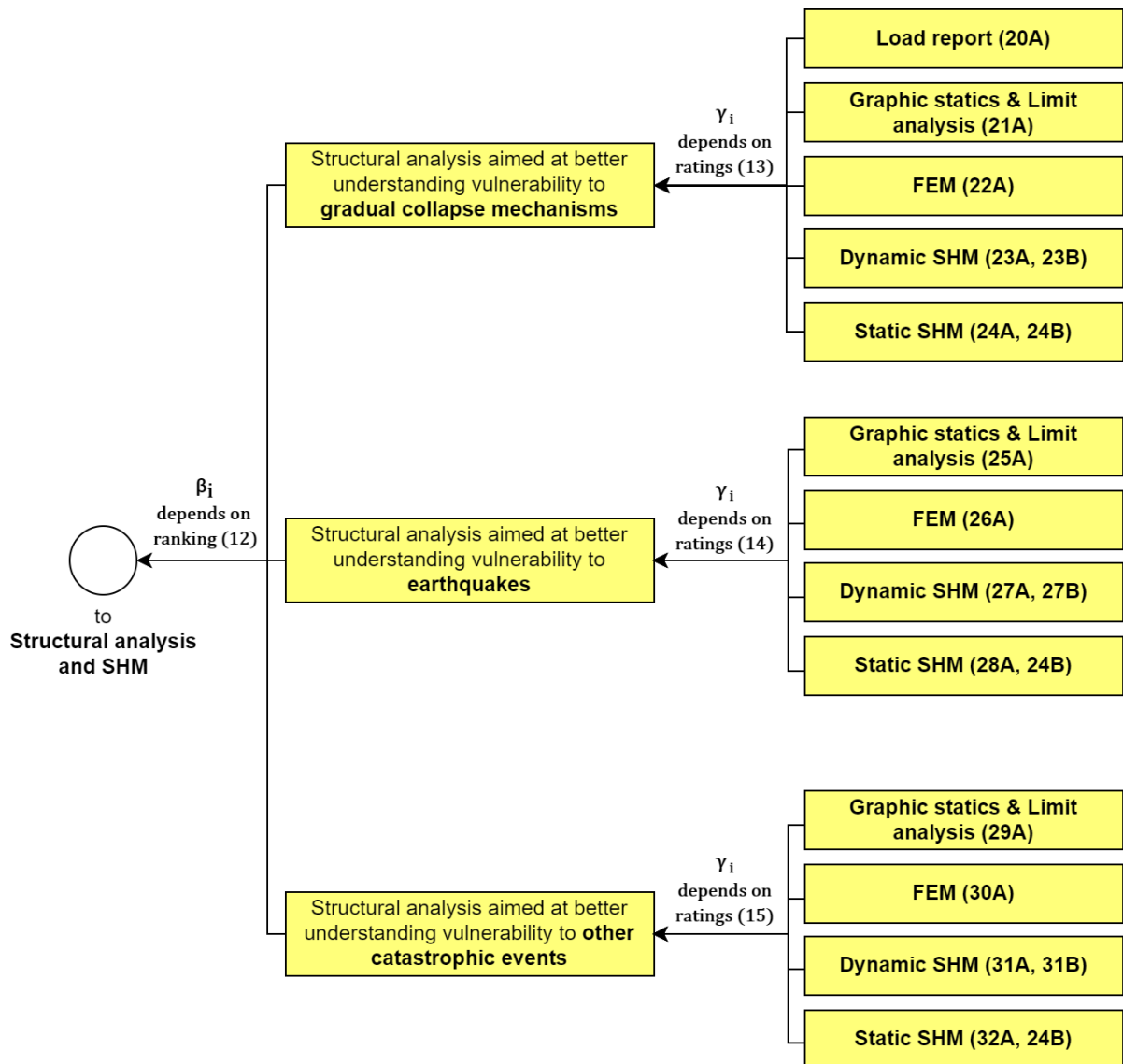


Figure 6.4: Criteria tree for the level of knowledge sub-indicator related to information from structural analysis and SHM. The relevant question references are shown in brackets at the end of each branch. Parameters β_i and γ_i refer to relevant weights that need to be applied respectively to criteria at the second and third hierarchical level of the global level of knowledge index.

As shown in Figures 6.3 and 6.4, most of the branches forming the hierarchical structure of the LoK index end on a criteria which depends on the rating from a single question. In such cases, the value function can simply be applied directly to the rating before proceeding with the computation of the index. However, when it comes to the experimental characterisation of specific material properties, the value used to represent the comprehensiveness of relevant investigations is taken as the mean of two ratings (see Figure 6.3): one related to the confidence level of estimates and another to the coverage area of the investigation. Similarly, in the case of static or dynamic SHM, the value used to represent the comprehensiveness of investigations is also taken as the mean of two ratings: one related to coverage area and another to monitoring duration (see Figure 6.4). In both cases, the value function is applied on the mean of the two relevant ratings. In the case of static SHM, the monitoring duration is taken directly as the number of years. This is then converted to a suitable level of knowledge rating using an ascending concave value function designed so that the rating varies between 0 to 5 as the monitoring duration increases from 0 to 15 years. In particular, the transition from a low to a moderate level of knowledge (corresponding approximately to a rating of 1.5) occurs after 2.4 years while the transition from a moderate to a high one (rating of 3) occurs after 6.6 years. The value function providing such a transformation can be represented by Equation (6.1) with $X^* = X_{min} = 0$, $X_{max} = 15$, $m_i = 2$, $n_i = 100$ and $A_i = 0.75$.

Once the answers to the standard questions are converted to homogenised scores that can reflect the level of knowledge on the structural condition, they are combined according to the hierarchical structure shown in Figure 6.3 using simple additive weighting (SAW). Relevant diagnosis activities are grouped according to the type of information they can provide for evaluating the structural condition of a masonry heritage structure. As shown, the relative weights among these groups at the first level of the hierarchical structure are constant. This is because a strong assumption behind the LoK index is that the relative importance among these groups remains unchanged in terms of the information they can provide for global vulnerability assessment. For instance, structural analysis is definitely considered as being of considerable importance since it is the only activity able to provide direct quantitative estimates of safety levels. It is able to achieve this by evaluating both demand and capacity through the use of mathematical models.

As previously mentioned in Section 6.3.1.2, SHM activities are grouped together with structural analysis because of the diverse ways in which they can be combined to provide information on damage causes, as well as on the structural response and capacity. The fact that they are grouped together allows the expert responsible for risk assessment to rate the importance of structural analysis and SHM activities relative to each other based on foreseeable combined applications that are appropriate for the unique characteristics of a monument. As shown in Figure 6.3, the remaining identified activity groups include the analysis of historical information and available documentation, activities related to capturing the actual geometry and damage, evaluating specific material properties, characterising material quality and variability, and performing in-situ tests to determine actual loading and boundary conditions.

For the computation of the global LoK index, appropriate relevance factors are needed to represent the relative importance of information that can potentially be derived from each group of activities. In order to reduce the subjectivity involved in this task, a popular procedure in the realm of decision analysis known as the Analytic Hierarchy Process (AHP) (Saaty, 1990) was employed. This procedure allows an analyst to conduct a rational and consistent assessment of weights by first establishing pairwise comparisons among parameters under consideration at the same hierarchy level. A well-defined fundamental scale ranging from 1 to 9 must be used to evaluate the intensity of the importance of each parameter over another. According to the scale, 1 is used if two parameters are of equal importance whereas 9 is used to define the extreme importance of one parameter over another. The AHP then allows weights to be obtained for each parameter based on solving an eigenvalue problem after collecting the individual comparison scores into a matrix. The pairwise comparison matrix constructed for evaluating the weights among different activity groups is shown in Table 6.1, together with the resulting priority vector containing the relative weights attributed to each group. An additional benefit of using the AHP for determining weights is that a procedure is defined for verifying the consistency of the pairwise judgements provided (Alonso; Lamata, 2006; Saaty, 1990). The verification first involves computing a consistency index, which is a function of the largest eigenvalue calculated as a solution of the AHP and the rank of the judgement matrix. Once this index is computed, a ratio is found by dividing it by a random consistency index. The latter is the average consistency index of a large number of randomly generated reciprocal matrices. If the final consistency ratio is smaller than 10%, the weights can be considered as being logically sound (Saaty, 1990). It was ensured that this consistency condition was satisfied for all AHP comparisons used as part of this research.

Table 6.1: Pairwise comparison matrix and resulting priority vector containing the weights assigned to the importance of information from different activity groups for the global level of knowledge.

	A	B	C	D	E	F	Priority Vector
A. Historical info. & docs.	1	1/3	1/7	1/4	1/4	1/4	4%
B. Geometry & damage	3	1	1/6	1/2	1/2	1/3	7%
C. Structural analysis & SHM	7	6	1	6	6	6	53%
D. Material properties	4	2	1/6	1	1	1/2	10%
E. Material quality	4	2	1/6	1	1	1/2	10%
F. In-situ conditions	4	3	1/6	2	3	1	16%

As shown in Table 6.1 and Figure 6.3, structural analysis and SHM are very important when compared to any other activity group. This is partly due to the ability of some structural analysis methods to provide

quantitative estimates of safety levels and also partly due to the large breadth and depth of information that such methods can provide for vulnerability assessment. As a result, following the application of the AHP, more than half of the contribution to the LoK index relies on information from structural analysis and SHM activities.

The second most influential group for the computation of the LoK index involves in-situ tests to evaluate actual loading and boundary conditions. Such tests are often specifically designed or adapted to investigate specific unknown parameters that are deemed to be of interest for vulnerability assessment. In addition, they are often the only possible way of obtaining key information on real conditions that can prove to be vital for validating models used to better understand the structural condition and associated safety levels. This explains why this activity group is given moderate importance over all other groups except structural analysis and SHM.

The next two most influential activity groups are related to the estimation of material properties and to the characterisation of material quality and variability. Both groups of activities end up contributing 10% to the LoK index following the AHP. In fact, these two activity groups can provide complimentary information as both activity types possess characteristics suitable to address some weaknesses of the other. Tests to estimate material properties, particularly mechanical parameters, can provide key information for structural analysis. However, it is often unfeasible to test enough specimens so that the sample provides a good representation of the variability of material properties in different parts of a structure. In contrast, although several NDT methods used for characterising material quality can cover large areas of the structure, they are usually limited in terms of the information they can provide on the strength and deformation properties of the material. Nevertheless, performing activities categorised in these two groups are often the only way of obtaining information on materials that can be indispensable for an accurate vulnerability assessment.

Following the activities linked to material characterisation, geometry and damage surveys are the next biggest contributors to the LoK index. It is undeniable that accurate representations of a structure's geometry and damage are key to an accurate vulnerability assessment. Reliable information on these aspects of a heritage structure are not only required for many different types of analyses and for validating models, but it also forms much of the basis for the development of initial hypotheses on possible causes of damage and for early decisions on the most suitable activities for further investigations. However, as a greater level of sophistication is applied to improve vulnerability assessment, information on geometry and visible damage often becomes mostly useful for planning tests, to accurately represent real conditions in sophisticated analyses, and for validating results. In other words, when the level of knowledge on damage vulnerability is moderate or high, significant further improvements normally cannot be attained only by performing more geometry and damage surveys. This explains why the relative importance assigned to this group of activities is relatively low.

Finally, information from the historical survey has been assigned the lowest weight in the first level of the hierarchical structure of the LoK index. This choice does not absolutely mean that the historical survey is a superfluous activity that may be omitted in the studies of conservation of the built heritage, as it definitely constitutes the essential preliminary stage of the scientific method (ISCARSAH, 2005). However, the choice of a lower weight is partly due to the limited reliability of historical sources. As a result, information needs to be critically assessed and assumptions often need to be made when interpreting it (ISCARSAH, 2005). Furthermore, useful documents have often been prepared for purposes other than structural engineering, meaning that relevant technical information might be missing or incorrect. In addition, much like information on the structure's geometry, information acquired through a historical survey often cannot contribute directly to improving an already high level of knowledge on damage vulnerability.

As shown in Figures 6.3 and 6.4, many of the weights among criteria at subsequent levels depend on the ratings provided during the second part of the SIEA (see Section 6.3.1.2). Exceptions to this are criteria related to historical information and documentation, to the actual geometry and visible damage, and to the material quality. This is because some of the information contributing to the weighted score linked to these activity groups are taken from answers provided during the first part of the SIEA. In fact, for the score representing the level of knowledge in terms of historical information, all relevant ratings are provided during the SIEA. Of course, these can be modified if new information becomes available, but this does not affect the hierarchical structure of the index. As shown in Figure 6.3, four scores are used for computing the combined score linked

to historical information. These are related to the comprehensiveness and quality of information available on the construction process, on past damage events and on previous structural alterations and interventions. Because information from any of these aspects can be equally pertinent for vulnerability assessment, equal weights are assigned to each in the computation of the LoK index.

With respect to the weighted score linked to the level of knowledge on geometry and visible damage, it is influenced mostly by the global ratings provided by the expert responsible for geometry and damage surveys. These ratings are initially provided during the first part of the SIEA (questions 2 and 3) but have to be updated after carrying out any activities involving the acquisition of information on geometry or damage. Clearly, if such activities are deemed to be relevant during the second part of the SIEA, it reveals an identified lack of knowledge. To account for activities carried out to address this gap, the score representing the level of knowledge on geometry and damage depends on a third criteria derived as a weighted total of the scores representing the comprehensiveness of information from specific additional activities (see Figure 6.3). Specifically, both of the global ratings on geometry and damage contribute 43% to the final weighted score linked to this activity group, while the remaining 14% is based on additional activities that are deemed relevant. These weights correspond to the outcome of applying the AHP after attributing equal importance to the two global ratings and giving both moderate importance over the information from additional activities. If all such activities are deemed as being irrelevant during the second part of the SIEA, the score related to geometry and damage depends only on the two global ratings with equal importance assigned to each.

The weighted score representing the level of knowledge on material quality depends on two criteria. The first reflects how well the material quality could be evaluated from visual inspections and the second represents the comprehensiveness of further investigations. Because results from MDT and NDT procedures for evaluating material quality can be much more informative when compared to the limited evaluation that can be made from visual inspections, 83% of the level of knowledge score for material quality relies on the comprehensiveness of MDT and NDT investigations while only 17% is attributed to the visual inspection conditions. This corresponds to a strong importance attributed to further investigations in an AHP context. As is the case for additional activities related to geometry and damage, if all further investigations on material quality are deemed to be irrelevant during the SIEA, the level of knowledge on material quality depends only on the conditions of visual inspections.

For all remaining activity groups, the relative weights among relevant criteria at subsequent levels of the hierarchical structure depend only on rankings and ratings provided during the second part of the SIEA. For activity groups related to the estimation of material properties and the evaluation of in-situ conditions, the score for each group is directly based on the weighted sum of scores representing the level of knowledge for individual activities (see Figure 6.3). As mentioned in Section 6.3.1.2, the importance of the information that each individual activity can provide for global vulnerability assessment is rated as either 0, 1 or 2 depending on its possible contribution. The relative weight attributed to activities rated as 0 is set to 0, meaning that information from the activity is no longer taken into consideration for risk assessment. The weights of remaining activities connected to a single parent criteria are then simply computed from the ratings provided as shown in Equation (6.3).

$$\gamma_i = \frac{r_i}{\sum_{i=1}^n r_i} \quad (6.3)$$

Where γ_i refers to the weight attributed to the score related to the individual activity i when computing the score of the parent criteria connected to n activities. On the other hand, r_i refers to the rating attributed to the importance of information from activity i during the SIEA (0, 1 or 2).

It should be noted that if the ratings of all individual activities connected to a single parent criteria are set to 0, the weight attributed to their parent criteria is also set to 0. This eliminated weight is then redistributed proportionally among remaining criteria connected to the same branch at the corresponding level.

As shown in Figure 6.4, the hierarchical structure leading to the level of knowledge score for structural analysis and SHM has been designed to account for the fact that these activities can be planned for investigating the vulnerability to specific hazards. As described in Section 6.3.1.2, the weights attributed to each of

the three possible aims (understanding the vulnerability to progressive collapse, earthquakes, or other catastrophes) depend on how they are ranked in the third part of question 12 during the SIEA. The specific aim ranked first is given a weight of 72% while the one ranked second is given a weight of 21%. The aim deemed as being least important is therefore attributed a weight of 8%. These were derived using the AHP from the pairwise comparison matrix shown in Table 6.2. The weights of the individual structural analysis and SHM activities connected to each specific aim are then computed using Equation (6.3) from the ratings provided in the SIEA.

Table 6.2: Pairwise comparison matrix and resulting priority vector containing the weights reflecting the importance assigned to different aims of structural analysis and SHM (1: understanding the vulnerability to progressive collapse, 2: to earthquakes, and 3: to other catastrophes) based on how they were ranked.

Rank	1	2	3	Priority Vector
1	1	4	8	72%
2	1/4	1	3	21%
3	1/8	1/3	1	8%

Once all of the weights have been determined, the final LoK index value can then simply be computed using equation Equation (6.4).

$$LoK\ index = \sum_{i=1}^N \alpha_i \cdot \beta_i \cdot \gamma_i \cdot S_{LoK,i} \quad (6.4)$$

Where $S_{LoK,i}$ refers to the score of a particular criteria at the end of one of the branches of the hierarchical structure shown in Figure 6.3. The parameters α_i , β_i and γ_i refer to the weights that need to be applied at every level. For their assessment, see Figures 6.3 and 6.4, Table 6.1, and Equation 6.3. Of course, if a criteria is found at the end of a branch ending after the second level, γ_i should be considered as 1 (see Figure 6.3). N refers to the number of individual criteria that are ultimately considered for the computation of the index. This number can change depending on how many activities are deemed as being irrelevant during the SIEA. If information from all possible activities are considered, $N = 41$.

The value of the LoK index should initially be computed after the SIEA. Following this, every time a diagnosis activity or intervention is performed, the appropriate ratings should be modified and the LoK index should be computed again (see Figure 6.1). In this way, the LoK index can help inform decision-makers on the uncertainty associated to vulnerability assessment within a dynamic process following the preventive conservation approach.

6.5. Damage risk index

As previously mentioned, the risk of interest for this research is that of a masonry heritage structure suffering from structural damage. Naturally, the most important requirement for a meaningful assessment of this risk is an appropriate diagnosis of the structural condition leading to an accurate evaluation of vulnerability. Nevertheless, as stated in the introduction, when deciding the best course of action to preserve such structures, experts have to consider hazard and exposure according to agreed-upon definitions in the context of disaster risk (UNGA, 2016). The final damage risk is therefore defined as being a function of vulnerability, hazard, and exposure, as shown in Figure 6.5.

The damage risk (DR) index can vary from 1 representing the lowest possible risk level to 5 representing the highest. This means that all the criteria used to define it also need to be homogenised to this scale. Unlike the LoK index, the DR index can never be 0. This condition is set to facilitate the interpretation of index values for decision-making and to reflect the fact that there will never be a situation with absolutely no risk in the case of unique heritage structures.

Although the vulnerability component is analysed thoroughly as part of this research, the hazard and exposure components rely on recurrent criteria that are normally considered when making recommendations for mitigating the risk of structural damage. As such, they serve mainly to amplify or contract the resulting vulnerability score based on hazard and exposure conditions. It can therefore often be useful when making

decisions to also directly examine the vulnerability component as a damage vulnerability (DV) index in its own right.

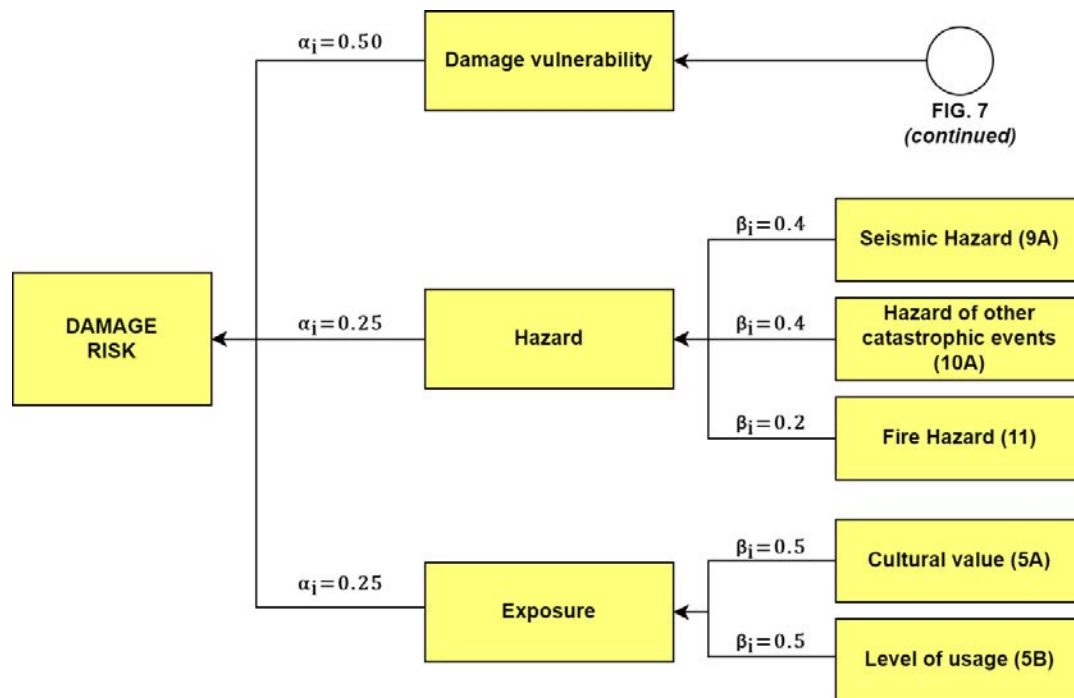


Figure 6.5: Criteria tree for the damage risk index. The relevant question references are shown in brackets at the end of each branch. Parameters α_i and β_i refer to relevant weights that need to be applied to criteria at the first and second hierarchical level respectively.

Despite the simplified approach employed to estimate the actual hazard and exposure level, they play a key role in defining the possible mitigation measures that can be employed. As such, they contribute 25% each to the final value of the DR index, while the value of the DV index determines the remaining 50%. In an AHP context, this is equivalent to giving damage vulnerability a slight importance over hazard and exposure while giving them equal importance amongst themselves.

All the information required to compute the scores related to hazard and exposure are provided during the first part of the SIEA. The final score linked to exposure depends on two ratings related to the cultural value and the potential loss based on the level of usage. In this case, the range of each possible rating has been designed so that no transformation is needed before combining them using additive weighting. As shown in Figure 6.5, equal importance is assigned to the two ratings. The final hazard score depends on three criteria related to the intensity and probability of occurrence of fires, of earthquakes, and of other catastrophic events. With respect to the seismic hazard, the only information that needs to be supplied during the SIEA is the peak ground acceleration (PGA) with a 10% probability of being exceeded in 50 years. Very good estimates of this value for any region in the world can easily be obtained using an online interactive map (Pagani et al., 2018). The value function shown in Figure 6.6(d) is then used to transform the supplied acceleration value to a hazard score ranging from 1 to 5. The function can be defined using Equation (6.1) with the parameters shown in Table 6.3, and has been calibrated to be in good agreement with the hazard levels shown in (Global Seismic Hazard Assessment Program (GSHAP), 1999). As shown, the function transforms any PGA from 0.2 m/s^2 to 4 m/s^2 into a hazard score ranging from 1 to 5. It is implemented as a conditional formula so that any PGA below 0.2 m/s^2 is attributed a score of 1 while one greater than 4 m/s^2 is scored as 5. For the remaining two hazard components, their scores are taken directly as the ratings provided during the SIEA.

6.5.1. Damage vulnerability index

In addition to providing information on the hazard and exposure level, answers to questions from the first part of the SIEA also provide pertinent information for initial damage vulnerability assessment. These include ratings related to material quality, to the level of maintenance, to the need for urgent action, and to initial evaluations of the vulnerability to specific hazards.

Because it is much more intuitive to grade material quality on an ascending scale, the answer provided during the SIEA on this aspect consists of a rating that can vary from 1 to 5 to reflect increasing levels of material quality and homogeneity. Naturally, this needs to be converted to a suitable homogenous vulnerability score before it can be considered in the DV index. This is achieved using the descending value function shown in Figure 6.6(a), defined by substituting the parameters shown in Table 6.3 into Equation (6.1).

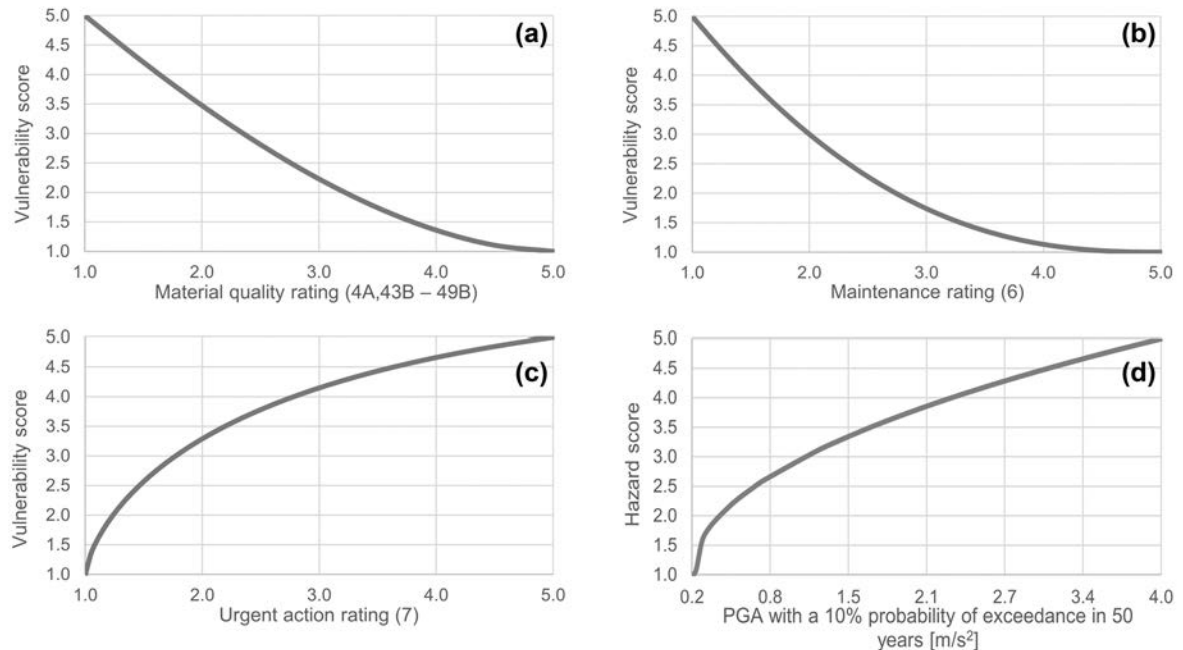


Figure 6.6: Value functions converting answers given in the first part of the SIEA to relevant homogenised scores to be combined in the DR index. The functions shown apply to material quality ratings (a), the maintenance rating (b), the urgent action rating (c), and the measure of seismic hazard (d).

Table 6.3: Parameters used in Equation (6.1) to derive value functions for specific answers provided in the first part of the SIEA.

	X^*	X_{min}	X_{max}	m_i	n_i	A_i
Material quality (4A, 43B-49B)	X_{max}	1	5	1	10	1.8
Maintenance (6)	X_{max}	1	5	1	10	2.5
Urgent action (7)	X_{min}	1	5	1	2	0.7
Acceleration - seismic hazard (9A)	X_{min}	0.2	4	0.5	200	0.5

After inspecting and evaluating material quality, it can be very difficult to draw meaningful conclusions on the vulnerability of the structure if the material is deemed to be of moderate or moderately high quality. However, identifying clear signs of poor material quality and degradation has definitive implications for vulnerability, and this should be reflected with a high vulnerability score attributed to this criteria. This effect is accounted for through the choice of a convex shape for the descending value function related to this criteria as shown in Figure 6.6(a). Within the proposed framework, material quality is also graded according to an ascending scale after further MDT or NDT investigations have been carried out (questions in A.5). As such, the same value function is also applied to relevant material quality ratings after further investigations following the SIEA. In fact, it can be said that such an effect also holds true when evaluating the state of maintenance, whereby very poor conditions have a more pronounced effect on vulnerability. Within the proposed risk assessment methodology, two ratings have to be provided during the SIEA on the state of maintenance. The first rating is intended to represent the actual maintenance condition whereas the second one is meant to indicate the suitability of the current maintenance plan to address relevant pathologies. The final maintenance rating is then taken as the mean of these two. As is the case for the material quality rating, a convex descending value function is also employed to transform this rating into a vulnerability score. However, as shown in Figure 6.6 and Table 6.3, different parameters are proposed for this criteria so that the curvature is better suited to the range of the maintenance condition rating.

The SIEA question on the need for urgent action consists of two parts. The response to the first part determines whether or not there is a need for urgent action. If the expert believes there is such a need, the second part of the question determines the extent of possible damage if no action is taken. Therefore, only the rating provided in this second part is used in the computation of the DV index. Because the need for urgent action is by definition associated to a high level of risk, an ascending concave value function with a very pronounced curvature is used to transform the corresponding rating into a homogenised vulnerability score (see Figure 6.6(c)). In addition, in case the need for urgent action is identified, the homogenised score linked to it contributes to 90% of the final DV index value (see Figure 6.7). These two measures ensure that the final DV and DR index values are high even if only a small fraction of the structure is likely to be affected if no urgent action is taken. If it is deemed that no urgent action is required, the weight attributed to the urgent action criteria is set to 0 and the eliminated weight is redistributed proportionally among the remaining criteria in the first level of the hierarchical structure of the DV index.

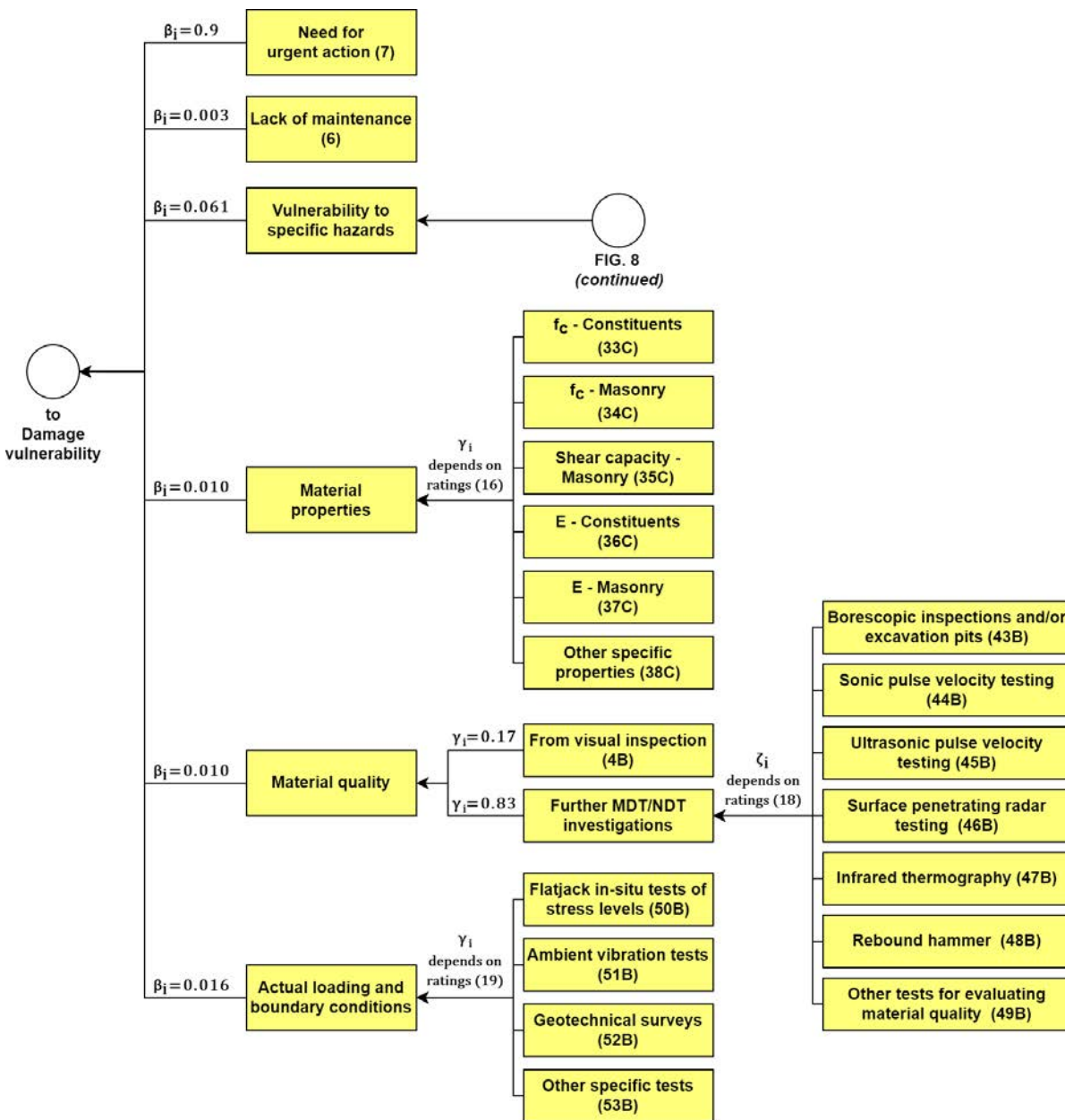


Figure 6.7: Criteria tree for the damage vulnerability index. The relevant question references are shown in brackets at the end of each branch. Parameters β_i , γ_i , and ζ_i refer to relevant weights that need to be applied to criteria at the second, third, and fourth hierarchical level of the global damage risk index respectively.

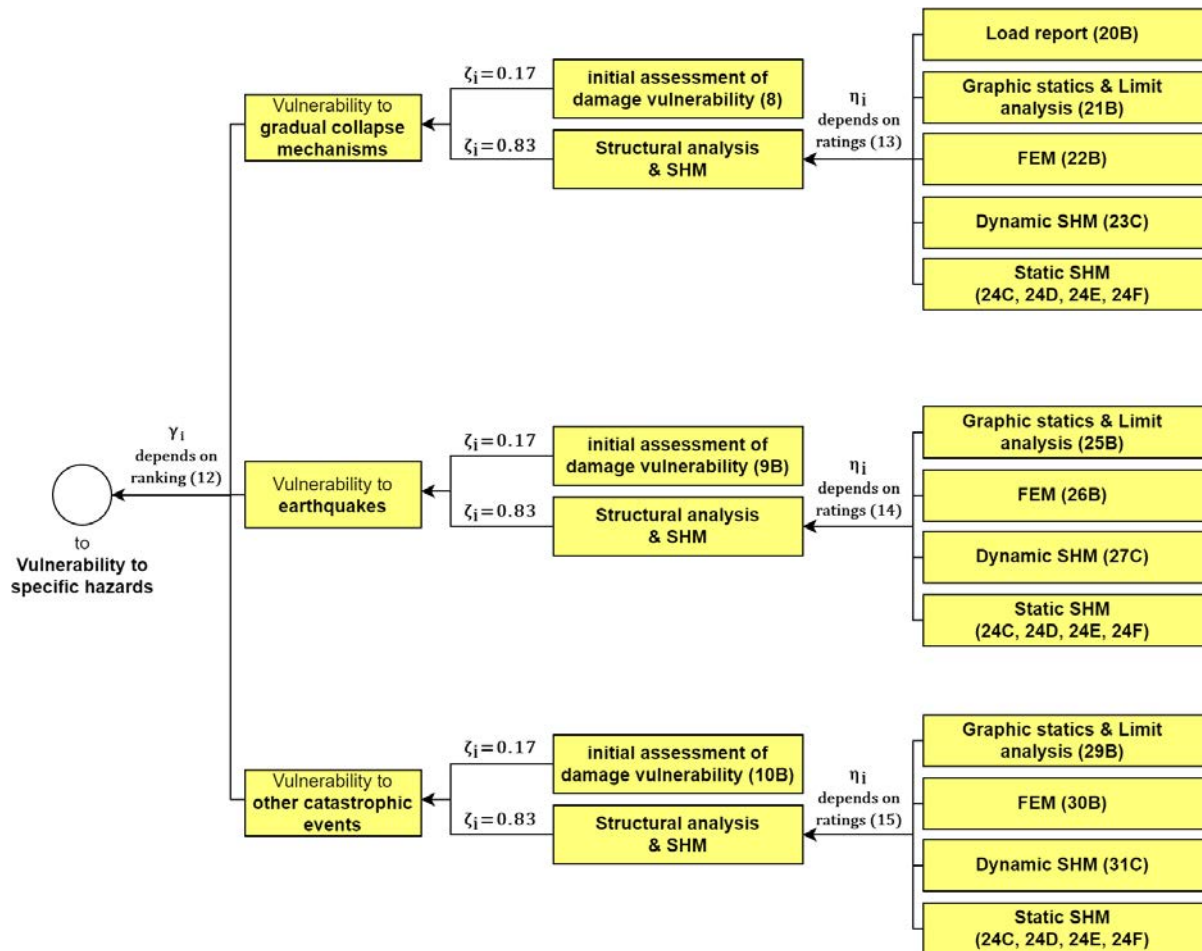


Figure 6.8: Criteria tree for the sub-indicator linked to the assessment of specific vulnerabilities. The relevant question references are shown in brackets at the end of each branch. Parameters γ_i , ζ_i , and η_i refer to relevant weights that need to be applied to criteria at the third, fourth, and fifth hierarchical level of the global damage risk index respectively.

In fact, at any level of the DV index, if no information is available on a particular criteria, the weight attributed to it is set to 0 and the eliminated weight is redistributed proportionally among all remaining criteria at the same level connected to the same parent criteria. This axiom is established for the DV index because the best estimate of damage vulnerability can always only be based on available information and investigations carried out. This is in stark contrast to the mechanism behind the LoK index whereby no information from a particular activity deemed as being relevant represents a lack of knowledge. As such, as described in Section 6.4, the weights among different criteria at different levels of the LoK index can only change if the rankings and ratings provided in the second part of the SIEA are changed.

For cases not requiring urgent action, much of the hierarchical structure of the DV index can be explained in terms of the structure of the LoK index. It is clear that information on the material or from in-situ tests of actual conditions are invaluable to inform structural analysis methods and to ensure that mathematical models employed provide an accurate representation of reality. In addition, they can also often provide some indications on the general vulnerability to damage. However, unlike structural analysis and SHM, most of these activities cannot be tailored to specifically evaluate the vulnerability to distinct hazards. This explains why the vulnerability criteria scores associated to material properties, material quality, and in-situ tests are combined in the first level of the DV index, as shown in Figure 6.7. The weights assigned to each of these three groups are the same as that assigned to the corresponding groups when computing the LoK index. As described in Section 6.4, this is because the weights are assigned in the LoK index based on the possible information that each activity group can provide for global damage vulnerability assessment. In fact, the consistency between the two indices is vital for them to provide meaningful insights when used jointly for decision-making. As such, for these three activity groups, the subsequent hierarchical levels have the same structural organisation as the corresponding parts of the LoK index and weights which depend on ratings

provided in the second part of the SIEA are computed in a similar way. However, as previously mentioned, in the case of the DV index, if no information is available on a particular criteria, its relevance factor is set to 0 and weight redistribution is carried out at that level. Of course, answers to questions related to damage vulnerability are used to compute the criteria scores instead of those relating to the level of knowledge.

According to the activity groups defined in this research, since the contribution of material characterisation and in-situ tests have already been considered, the remaining criteria in the first level of the DV index must be based on historical information, geometry and damage surveys, structural analysis, and SHM. Excluding the special case of the need for urgent action, which has already been addressed, the remaining criteria include the maintenance condition and the outcome of specific studies carried out to evaluate the vulnerability to specific hazards (see Figure 6.7). As such, to maintain the consistency with the LoK index, the sum of the weights of these two criteria in the first level of the DV index must be equal to the sum of the weights attributed to the aforementioned remaining activity groups in the LoK index. This corresponds to a total weight of 64% that has to be divided between the two criteria. Although the maintenance condition can definitely play an important role in defining the rate of change related to decay and deterioration processes, it is seldom the true underlying cause of these processes. In most circumstances, the true cause of these can be related to environmental effects and mechanical actions. In the context of this research, a better understanding of the effects of these underlying causes is considered as being much more significant for an accurate vulnerability assessment. As such, when no urgent action is required, only 3% of the DV index value is determined by the criteria representing the damage vulnerability linked to a lack of maintenance (see Fig. 6.7). This represents 5% of the 64% left to be distributed after considering the contribution of material characterisation activities and tests of in-situ conditions.

Consequently, 61% of the DV index value relies on evaluations of the damage vulnerability to specific hazards. This criteria in turn depends on individual assessments of the vulnerability to progressive collapse mechanisms, to earthquakes, and to other catastrophic events. As shown in Figure 6.8, the weights assigned to each of these depend on the responses and rankings provided in question 12 of the SIEA. As described in Section 6.4, the first, second, and third ranked specific vulnerabilities are attributed weights of 72%, 21%, and 8% respectively. Naturally, if the choice is made during the SIEA to exclude the vulnerability to a specific hazard from the assessment, weights are redistributed proportionally among the remaining specific vulnerabilities based on how they have been ranked. As shown in Figure 6.8, each of the three identified specific vulnerabilities relies on an initial assessment and on the conclusions that could be drawn from the application of structural analysis and SHM. Because the initial assessment is made on the basis of historical information and data collected through geometry and damage surveys, the weights assigned to these specific activity groups in the LoK index can be used to derive the weight that needs to be assigned to the initial assessment component of each specific vulnerability. In the LoK index, the combined weight of the activity groups related to historical information and geometry and damage surveys amounts to 11% (see Table 6.1). This represents 17% of the sum of the combined weight of these two activity groups with structural analysis and SHM in the LoK index. Therefore, as shown in Figure 6.8, 17% of the score of each criteria related to a specific vulnerability is attributed to the initial assessment while the remaining 83% are based on the conclusions from structural analysis and SHM. The weight attributed to each activity contributing to each structural analysis and SHM criteria is then derived using the ratings provided during the SIEA in a similar way as it is done for the LoK index.

The vulnerability score attributed to each specific initial assessment comes directly from relevant ratings given during the first part of the SIEA. The range of each rating has been designed so that no additional transformation is needed to convert it into a homogeneous vulnerability score before it can be compounded into the DV index.

In fact, the range of most ratings used to compute the DV and DR indices have been designed so that they can be directly compounded without requiring an additional transformation. Exceptions include the four questions from the first part of the SIEA shown in Figure 6.6, all questions providing a material quality rating, and processed results from static SHM. For the latter, as mentioned in Section 6.3.2, the proposed risk assessment methodology can take advantage of results from the automated data analysis procedure described in (Makoond et al., 2020c) to automatically update the DV index. Four key processed results are utilised for this purpose: the percentage of monitored parameters classified as evolutionary and the average growth rate

of monitored crack widths, distances, and inclinations classified at least as apparently evolutionary. If the automated data analysis procedure is not used, reasonable estimates for these values have to be provided to update the DV index. These four processed results are then converted to a homogenised vulnerability score according to the value functions shown in Figure 6.9. These have been constructed based on observations made from the monitoring of 18 crack widths, 6 distances, and 4 inclinations in two complex medieval structures (Makoond et al., 2020c). The duration of available monitoring data from these sensors varied between 2 to 5 years, and the data acquired have already been used to draw meaningful conclusions for the vulnerability assessment of the two structures. In addition, the value function for transforming monitored inclinations has been designed so that a vulnerability score of 5 is attributed to an inclination that would correspond to an apex displacement of 0.15 m after 10 years of a 10 m block experiencing rigid rotation. On the other hand, a score of 1 is attributed to an inclination corresponding to an apex displacement of 0.01 m after 10 years with the same assumptions. All the value functions used for transforming static SHM results can be defined by substituting the parameters listed in Table 6.4 into Equation (6.1). They are all implemented as conditional functions so that all original responses lower than X_{min} (see Equation (6.1)) are given a vulnerability score of 1 while all responses greater than X_{max} (see Equation (6.1)) are given a score of 5.

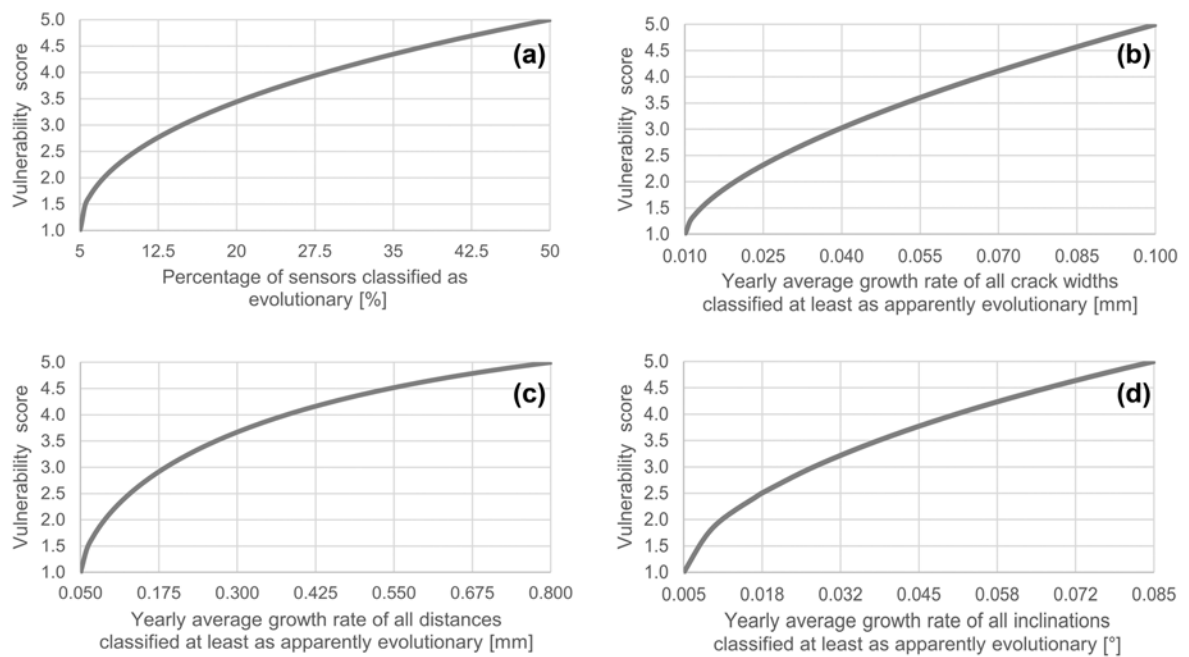


Figure 6.9: Value functions converting processed results from static SHM to homogenised vulnerability scores to be combined in the damage vulnerability index. Specifically, the functions shown are used to transform the percentage of sensors classified as evolutionary (a) and the average growth rate of monitored crack widths (b), distances (c), and inclinations (d).

Table 6.4: Parameters used in Equation (6.1) to derive value functions for converting processed results from static SHM into vulnerability scores.

	X^*	X_{min}	X_{max}	m_i	n_i	A_i
Percentage evolutionary (24C)	X_{min}	5	50	1	600	0.5
Crack widths (24D)	X_{min}	0.01	0.1	0.5	200	0.62
Distances (24E)	X_{min}	0.05	0.8	8	10	0.65
Inclinations (24F)	X_{min}	0.005	0.085	4	6	0.6

The final homogenised vulnerability score based on information from static SHM is computed as a weighted sum with 50% attributed to the score related to the percentage of monitored parameters classified as evolutionary while the remaining 50% is distributed equally among the scores linked to crack widths, distances, and inclinations.

Once all relevant inputs have been converted to homogenised scores, the DV index can be simply com-

puted as shown in Equation (6.5).

$$DV\ index = \sum_{i=1}^N \beta_i \cdot \gamma_i \cdot \zeta_i \cdot \eta_i \cdot S_{DV,i} \quad (6.5)$$

Where $S_{DV,i}$ refers to the score of a particular criteria at the end of one of the branches of the hierarchical structure shown in Figures 6.7 and 6.8, while β_i , γ_i , ζ_i and η_i refer to the weights that need to be applied at every level. If a criteria is found at the end of a branch ending after the first level, γ_i , ζ_i and η_i should be considered as 1. Similarly, if a criteria is found at the second level, ζ_i and η_i should be considered as 1 while only η_i should be considered as 1 for criteria found at the third level. N refers to the number of individual criteria that are ultimately considered for the computation of the index. This can change depending on what diagnosis activities have actually been carried out. If all the possible diagnosis activities identified are used, $N = 36$.

Once the DV index has been computed, the DR index can be simply calculated through a weighted sum of the DV index value and the scores related to the Hazard and Exposure levels using the weights shown in Figure 6.5.

6.6. From risk assessment to decision making

A significant advantage of the proposed risk assessment methodology is that it allows a systematic updating of the risk assessment every time a relevant risk mitigation action is taken. This can include a temporary emergency intervention, more permanent structural interventions, an improvement to the maintenance plan, or even specific measures taken to reduce the fire hazard. The methodology also relies on a systematic process for updating the risk assessment after performing diagnosis activities aimed at better characterising damage vulnerability. In both cases, the update is achieved through answers to standard questions that must be provided by the expert responsible for risk assessment. These answers are then used to update the two key indices proposed to facilitate the decision-making task: one related to the level of knowledge on damage vulnerability and the other to the estimated risk level.

For the case of diagnosis activities, only questions relating to the particular activities carried out need to be answered. These will normally consist of one part to evaluate the comprehensiveness of the investigations, and another related to estimated vulnerability levels. An exception to this is the case of static SHM. In this case, after an initial configuration, both indices can be periodically updated automatically by taking advantage of processed results from the methodology described in (Makoond et al., 2020c).

After an improved maintenance plan has been implemented, the response to the question on maintenance condition provided in the SIEA needs to be updated. Similarly, after specific measures are taken to reduce the fire hazard, only the single response to the question on this aspect must be updated. If an emergency intervention is carried out, the response to the SIEA question on the need for urgent action needs to be updated. In addition, ratings provided in the SIEA as initial assessments of the perceived vulnerability also need to be updated to reflect the new safety level. These must also be updated every time any structural intervention is carried out. These specific evaluations of the vulnerability to progressive collapse mechanisms, to earthquakes, and to other catastrophic events are based on available historical information and on geometry and damage surveys. In fact, both the level of knowledge and damage vulnerability ratings associated to all diagnosis activities previously performed must be updated to reflect what is known about the new structural condition. This means that the LoK score of a previously applied diagnosis activity can return to 0 if it provides absolutely no information on the new condition of a strengthened structure. As such, the value of the LoK index can decrease after interventions have been carried out. This aspect of the proposed methodology is meant to encourage the design of interventions whose efficiency can be verified and evaluated through rigorous scientific methods.

Because questions that need to be answered can vary depending on the situation and on previous answers, it is vital that the computation and consultation of the indices be implemented as a user-friendly interactive computer programme. This strategy will greatly facilitate data entry, and allows necessary updates to be made with ease after relevant actions have been carried out.

A very useful output of such a program can be a list of relevant diagnosis activities ordered according to their possible contribution to the global level of knowledge. These possible contributions can change depending on the initial evaluation made by the expert and on activities that have already been carried out. Because of the way the LoK index is computed, the possible contribution of any activity considered can easily be calculated. The maximum possible increase of the final LoK index value that can be caused by performing a diagnosis activity can be calculated as the remaining homogenised LoK score that can be attributed to the activity multiplied by all the relevant weights at every level connecting it back to the final index value. The possible contribution of that particular activity is then obtained by dividing this maximum possible increase by the difference between the maximum LoK index value and the current index value. Table 6.5 shows the values of this possible contribution if an LoK score of 0 is attributed to each activity and equal ratings are assigned to all of them during the SIEA.

Table 6.5: Diagnosis activities that can be listed according to their remaining possible contribution to the level of knowledge on damage vulnerability.

Diagnostic activity	Activity group	Possible contribution to level of knowledge indicator*
Graphic statics & Limit analysis	Structural analysis & SHM	11.2%
Finite Element Modelling		11.2%
Dynamic SHM		11.2%
Static SHM		11.2%
Load report		8.2%
Flatjack in-situ tests of stress levels	Actual loading & boundary conditions	4.0%
Ambient vibration tests		4.0%
Geotechnical surveys		4.0%
Other specific in-situ tests		4.0%
More information on Geometry	Geometry & damage surveys	3.7%
More information on Damage		3.3%
Compressive strength - Constituents	Material properties	1.7%
Compressive strength - Masonry		1.7%
Shear capacity - Masonry		1.7%
Elastic modulus - Constituents		1.7%
Elastic modulus - Masonry		1.7%
Other material properties		1.7%
Pits/inspections	Material quality	1.2%
Sonic pulse velocity testing		1.2%
Ultrasonic pulse velocity testing		1.2%
Surface penetrating radar		1.2%
Infrared thermography		1.2%
Rebound hammer		1.2%
Other tests of material quality		1.2%

* If equal weights are assigned among activities at each category level during the Standardised Initial Expert Appraisal (SIEA).

It can be helpful for the expert performing risk assessment to consult this dynamic list after updating index values to ensure that the importance attributed to key activities are in line with what can be expected. This can even be used as a basis for fine-tuning provided ratings. Eventually, the list can prove to be useful for selecting the most suitable methods for further investigations and for communicating why particular diagnosis activities are being recommended. It can also provide valuable information to inform cost-benefit analyses. Some diagnosis activities such as SHM can be quite expensive and almost always require some form of cost-benefit analysis before their implementation. However, although costs can be estimated accurately, it can be very difficult to obtain quantitative information on the expected benefits. The potential contribution to the LoK index can serve this purpose. Of course, since the indices are only meant to be approximate tools to help inform decision-makers, the specific needs of each case should be considered and the decisions on

the best research activities to conduct should not be based only on the index values.

The main aim of the two indices computed as part of the proposed risk assessment methodology is to help decision-makers to evaluate the current level of risk and the uncertainty associated to this estimation. The proposed approach thus promotes risk mitigation decisions that make efficient use of resources. The decision matrix shown in Figure 6.10 demonstrates how the two indices can be used jointly to decide on the best course of action for preserving a masonry heritage structure. Indicative ranges of the LoK and DR indices are also shown. Because the DV index is more sensitive to changes in the evaluation of the structural condition, decision-makers can also choose to jointly examine the LoK and DV indices in a similar fashion before making a decision. Once again, it is important to stress that the proposed methodology is not designed with the aim of automating decisions. The proposed decision grid can therefore not be used blindly without properly understanding the assumptions behind the computation of the indices.

Level of knowledge	High (3 - 5)	Low magnitude of risk with low uncertainty. No action is often acceptable.	Prioritise risk mitigation strategies by cost-benefit analysis.	Highest priority for strengthening and risk mitigation.
	Medium (1.5 - 3)	Low magnitude of risk with moderate uncertainty. Action may not be necessary.	More detailed risk analysis can be considered. Cost-benefit analysis of relevant diagnosis activities is recommended.	Very high priority for risk mitigation. Cost-benefit analysis of mitigation strategies and diagnosis activities is recommended.
	Low (0 - 1.5)	Requires research to ascertain that the assessment is correct, but low priority.	High priority for research if dealing with complex structures. For simpler structures, specific identified interventions may be relevant.	Highest priority for research. Cost-benefit analysis of relevant diagnosis activities is recommended. Short-term mitigation may be required.
		(1 - 2)	(2 - 4)	(4 - 5)
		Low	Medium	High
		Damage risk (or vulnerability)		

Figure 6.10: Decision matrix adapted from (Paolini et al., 2012) demonstrating how the proposed indices can be used to facilitate decisions.

6.7. Application to Mallorca cathedral

A complex case study has been chosen to demonstrate the usefulness of the proposed risk assessment methodology. The cathedral of Santa Maria in Palma de Mallorca (Figure 6.11) can definitely be considered as one of the most remarkable monuments built in the so-called Catalan Gothic style. It boasts grand proportions and structurally audacious piers with slenderness ratios that can be twice that of many comparable Gothic cathedrals. Having been built over a period of 300 years, the cathedral has a very complex structural scheme consisting of the interaction of several different parts. It has been the subject of numerous studies and scientific investigations of relevance for characterising damage risk and has in part been chosen as a case study because both the details and conclusions of these studies are well reported in literature (González et al., 2008; Roca et al., 2007; Roca et al., 2008; Roca et al., 2010; IPCE, 2012; Roca et al., 2013; Pelà et al., 2016a; Elyamani et al., 2017a; Elyamani et al., 2017b; Elyamani; Roca, 2018). In addition, data collected from a static SHM system over a period of 5 years from 2003 to 2008 has already been processed using the automated data analysis procedure presented in Chapter 5. As such, results from this application could seamlessly be incorporated into the risk assessment through the procedure described in Sections 6.4 and 6.5.1.

In the case of Mallorca cathedral, much is known on the construction process, on previous structural alterations, and on past damage events thanks to extensive historical research (González et al., 2008; Elyamani; Roca, 2018). Similarly, a substantial amount of information is available on existing damages as well on the geometry. This includes reports from visual inspections (IPCE, 2012), surveys of the most important pathologies, as well as master plan drawings (González et al., 2008; Elyamani; Roca, 2018). The basic information on damage and geometry has been further improved over the years with more accurate or in-depth invest-

igations. In the case of geometry, these investigations have included pits in the roof to reveal a system of masonry walls supporting the terrace floor slab (Roca et al., 2008), as well as additional topographic and photogrammetry surveys (Roca et al., 2013; Pelà et al., 2016a). Various structural analysis methods have also been applied for the diagnosis and safety evaluation of the structure, including graphic statics analyses to evaluate the stability of a transverse bay (Roca et al., 2010; Elyamani; Roca, 2018), kinematic limit analysis to evaluate the seismic capacity (Elyamani; Roca, 2018), and several sophisticated FE modelling approaches to assess the vulnerability to both progressive collapse and earthquakes (Roca et al., 2010; Roca et al., 2013; Pelà et al., 2016a; Elyamani et al., 2017b). In addition to the previously mentioned static monitoring system, two different dynamic SHM systems have been installed in the structure, one in 2005 (Roca et al., 2008) and the other in 2010 (Elyamani et al., 2017a). Several investigations have also been carried out to better understand the material quality and variability in several parts of the structure. This includes seismic tomography, surface penetrating radar investigations, thermography investigations, pits in the roof, and the extraction of a core to reveal the inner composition of a buttress (Roca et al., 2008; Elyamani; Roca, 2018). Several investigations have also been carried out to better characterise the actual loading and boundary conditions in-situ. This includes ambient vibration tests used mainly to validate numerical models (Roca et al., 2008; Elyamani et al., 2017a), soil investigations using geophysical techniques, and in-situ determination of work stresses using the hole drilling technique (Roca et al., 2008). With respect to material properties, microscopy and diffractometry analyses performed on samples of constituents allowed the identification of different masonry types corresponding to different construction stages (Roca et al., 2008). However, with respect to mechanical parameters, the determination of the average material strength has proved to be very difficult due to the risks associated with possible in-situ tests, as well as the inability of extracting large enough specimens (Roca et al., 2008). Nevertheless, information about the global stiffness could be obtained by calibrating models with dynamic tests performed in-situ (Roca et al., 2008).

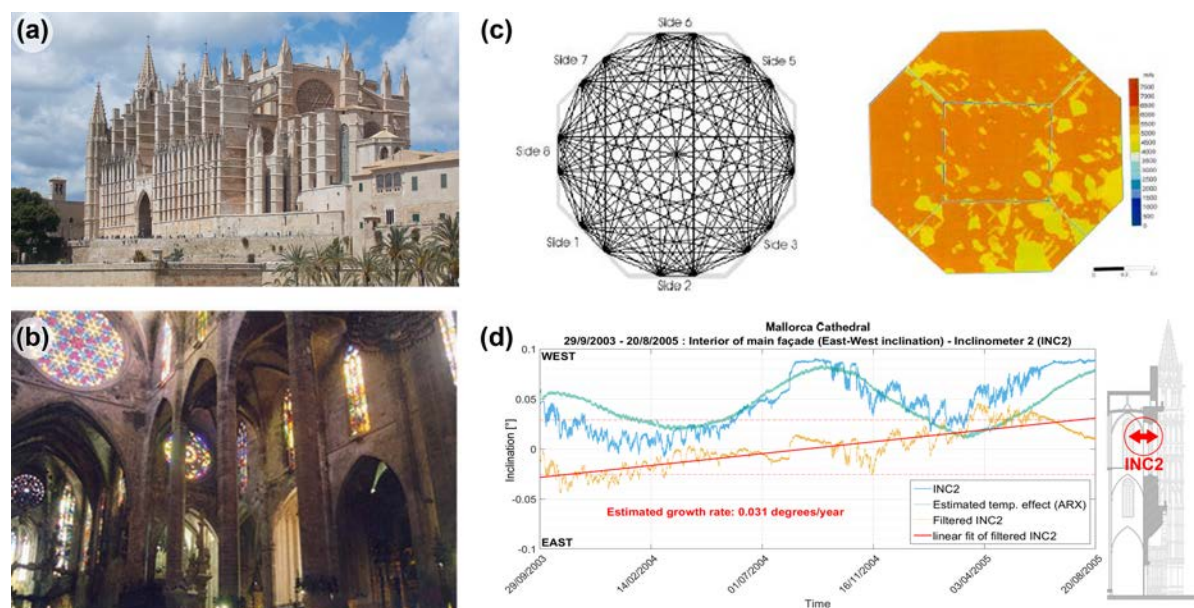


Figure 6.11: (a) Exterior view of Mallorca cathedral. (b) Interior view of Mallorca cathedral (Pelà et al., 2016a). (c) Sonic tomography of piers (Roca et al., 2008). (d) Recorded time series of inclination monitored as part of static SHM system installed in 2003. Filtering of simulated reversible environmental effects and estimation of underlying evolution rate is also shown.

Although the aforementioned diagnosis activities have been carried out at different points in time, two “knowledge states” have been defined for the purpose of risk assessment to best demonstrate the application of the proposed methodology and to facilitate the interpretation of results:

1. **Initial state:** This state is meant to be representative of the level of knowledge that will typically be available for the risk assessment performed when completing the standardised initial expert appraisal (SIEA). As such, it is assumed that information is only available from historical information and from initial geometry and damage surveys. With respect to geometry, it is assumed that only information from the historical construction master plan drawings are available in this state.
2. **Final state:** This state is meant to be representative of the current level of knowledge on the structural

condition. As such, all the information sources are considered and the final index values depend on SIEA questions as well as on relevant optional questions related to the aforementioned diagnosis activities.

All ratings used to compute the initial and final index values are provided alongside the corresponding questions in the Appendix B.1. Answers from the SIEA used to compute the initial index values can be found in Section B.1.1, whereas all answers or updates used to compute the final index values are shown in Section B.1.2. A level of knowledge (LoK) concavity setting of 2 (see Section 6.4) was used for computing the LoK indices. The scores of all sub-indicators related to a particular index are always shown using a custom radial diagram such as the ones shown in Figure 6.12. In such diagrams, each sector refers to a sub-indicator used to compute the final index value. The central angle of each sector represents its weight in the index, whereas its individual radius shows its score.

The initial and final values of the LoK index for Mallorca cathedral are shown in Figure 6.12 together with the LoK scores for each diagnosis activity group. The custom diagrams shown in Figure 6.12 are clearly an effective means of transmitting meaningful information on the general level of knowledge used as a basis for risk assessment. In this case, a clear message that can be conveyed through the interpretation of the diagrams is that the current level of knowledge is high for most important aspects of safety evaluation, but that accurate estimation of relevant material properties remains a challenge. In addition, the clear increase in the index value from the initial state can clearly be appreciated, showing how all the diagnosis activities carried out over the years have contributed to a shift from a low level of knowledge on the structural condition to a high one.

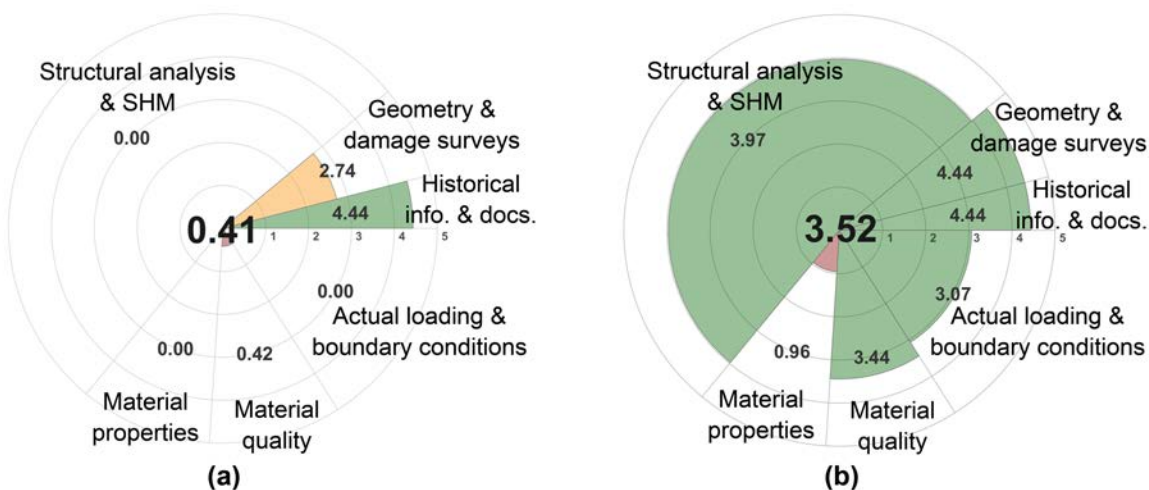


Figure 6.12: Initial (a) and final (b) values of the level of knowledge (LoK) index for Mallorca cathedral. The LoK scores for each diagnosis activity group are also shown.

With respect to damage vulnerability, preliminary assessments based solely on visual inspections and historical information could definitely lead to the conclusion that there are possible risks of experiencing damage caused by progressive collapse mechanisms. This is mainly due to the significant deformations of the piers and the presence of cracks at the base of columns. However, most structural analysis techniques applied to investigate the safety of the representative bay structure have revealed that significant further damage of critical sections linked to slow deterioration mechanisms is not likely to occur, at least not in the very near future (Roca et al., 2013; Pelà et al., 2016a; Elyamani; Roca, 2018). In addition, NDT has revealed the solid nature and high material quality of the inner core of piers (Roca et al., 2008). With respect to the vulnerability to earthquakes, some studies show possible signs of weakness in the longitudinal direction. While it remains true that investigations of seismic capacity indicate a very safe condition, particularly in the transverse direction (Roca et al., 2013), results from detailed dynamic FE modelling do indicate that the capacity is lower in the longitudinal direction (Elyamani et al., 2017a; Elyamani; Roca, 2018). Moreover, during a far epicentre earthquake in 2005, records from the earliest dynamic monitoring system installed in the cathedral revealed that the building experienced a certain excitation of its fundamental vibration mode with the largest acceleration amplitudes occurring in the longitudinal direction (Roca et al., 2007). It should also be noted that studies attempting to better understand the seismic capacity of the cathedral using limit analysis show that

the most likely collapse mechanisms are linked to an outward rotation of the main façade (Roca et al., 2010; Elyamani; Roca, 2018). To add to this fact, recent analysis of static monitoring data indicate that there is possibly an underlying evolutionary trend related to the outward rotation of part of the façade (Makoond et al., 2020c). As such, it can be said that although there are no clear signs of a definite vulnerability to the probable seismic loads that can be expected in the region, the combination of aforementioned observations certainly suggest some specific, albeit localised, vulnerabilities.

Even if only individual ratings related to specific activities have been provided, most of the general conclusions described in the previous paragraph can clearly be appreciated by examining the differences between the initial and final damage vulnerability (DV) index diagrams shown in Figure 6.13. Specifically, there has been a significant decrease in the estimated vulnerability to slowly evolving progressive collapse mechanisms and a very slight increase in the estimated vulnerability to earthquakes.

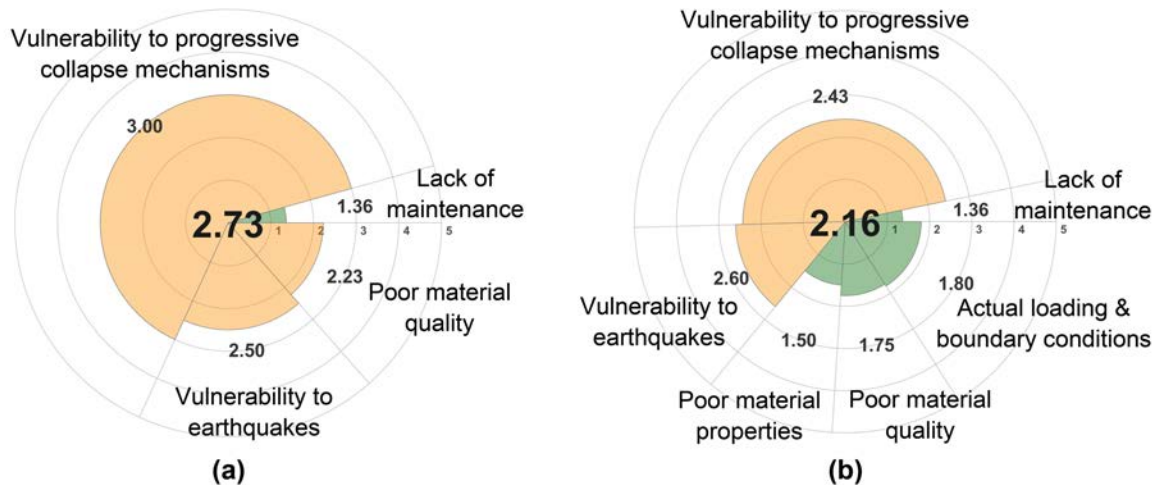


Figure 6.13: Initial (a) and final (b) values of the damage vulnerability (DV) index for Mallorca cathedral. The scores for the first level of vulnerability components are also shown.

The initial and final damage risk (DR) index values for Mallorca cathedral are shown in Figure 6.14. Despite the significant decrease in estimated vulnerability, it is clear that the score linked to the exposure component of the DR index adequately fulfils the function of maintaining a more moderate risk level due to the potential loss and the high cultural value associated to this structure.

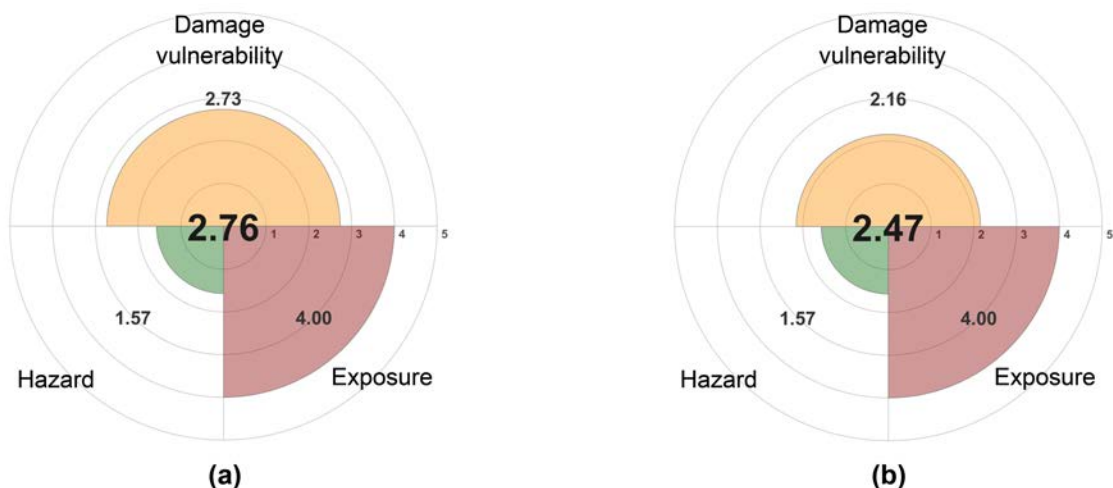


Figure 6.14: Initial (a) and final (b) values of the damage risk (DR) index for Mallorca cathedral. The scores for the first level of risk components are also shown.

The changes in the dynamic list of best activities (see Section 6.6) from the initial state to the final one are shown in Table 6.6. Some of the most suitable activities suggested at the different stages are along the

lines of what can be expected. At the initial stage, versatile structural analysis tools able to evaluate diverse loading scenarios can contribute significantly to the level of knowledge. Because a vast array of such methods have already been applied comprehensively to the study of Mallorca cathedral, it can be deemed reasonable that SHM has more potential at this stage to further improve the understanding of specific vulnerabilities. However, it is very important to note that this list is not based on actual specific hypotheses that need to be investigated by the activity. Such hypothesis and the uncertainty linked to their formulation need to be the most important considerations before the final decision on any investigation is made. Feasibility and associated costs are also very important considerations which cannot be ignored.

Table 6.6: Initial and current list of best diagnosis activities to perform in Mallorca cathedral according to the possible contribution of the activity to the level of knowledge (LoK) index.

Initial list of best activities after SIEA		Current list of best activities	
Diagnostic activity	Possible contribution to remaining LoK index	Diagnostic activity	Possible contribution to remaining LoK index
Finite Element Modelling	15.5%	Static SHM	19.0%
Graphic statics & Limit analysis	13.4%	Flatjack in-situ stress tests	9.0%
Static SHM	13.4%	Dynamic SHM	8.6%
Dynamic SHM	9.9%	Compressive strength - Masonry	8.5%
Ambient vibration tests	5.8%	Shear capacity - Masonry	8.5%
Geotechnical surveys	5.8%	Other specific in-situ tests	6.5%
Load report	5.6%	Finite Element Modelling	4.6%
Sonic pulse velocity testing	3.0%	Compressive strength - Constituents	4.2%
Surface penetrating radar	3.0%	Elastic modulus - Constituents	4.2%
Flatjack in-situ stress tests	2.9%	Graphic statics & Limit analysis	4.1%
Other specific in-situ tests	2.9%	Pits/inspections	3.3%
Compressive strength - Masonry	2.7%	Ambient vibration tests	2.7%
Shear capacity - Masonry	2.7%	Geotechnical surveys	2.7%
More information on Geometry	1.9%	Sonic pulse velocity testing	2.2%
More information on Damage	1.6%	More information on Damage	1.8%
Pits/inspections	1.5%	Surface penetrating radar	1.4%
Infrared thermography	1.5%	Elastic modulus - Masonry	1.3%
Compressive strength - Constituents	1.4%	More information on Geometry	0.9%
Elastic modulus - Constituents	1.4%	Infrared thermography	0.7%
Elastic modulus - Masonry	1.4%	Other material properties	0.6%
Other material properties	1.4%	Load report	0.6%

The application of the risk assessment methodology to this case study demonstrates how its key outputs can help form a good overview of the general risk situation by considering the combined effect of individual insights drawn from different activities. It also ensures that most relevant criteria are taken into consideration when defining the global risk of damage.

6.8. Application to other case studies

Besides the application to the very complex case of Mallorca cathedral, three additional case studies are presented to demonstrate how the risk assessment methodology can function under varying conditions of risk, complexity, and information availability.

The specific ratings used to compute the initial and final index values are not shown here but are provided alongside the corresponding questions in Appendix B. Unlike the case of Mallorca cathedral, no initial “knowledge states” were defined for these case studies and all index scores reflect the evaluation based on the latest information available at the time of performing the risk assessment. A detailed summary of the results for all case studies is presented in Appendix C. This includes a breakdown of the scores of criteria at the first hierarchical level of the respective indices and the automatically generated list of best diagnosis activities to perform according to the possible remaining contribution to the LoK index. The case studies are shown in Figure 6.15 along with their relative locations with respect to the city of Barcelona and the cathedral of Mallorca.

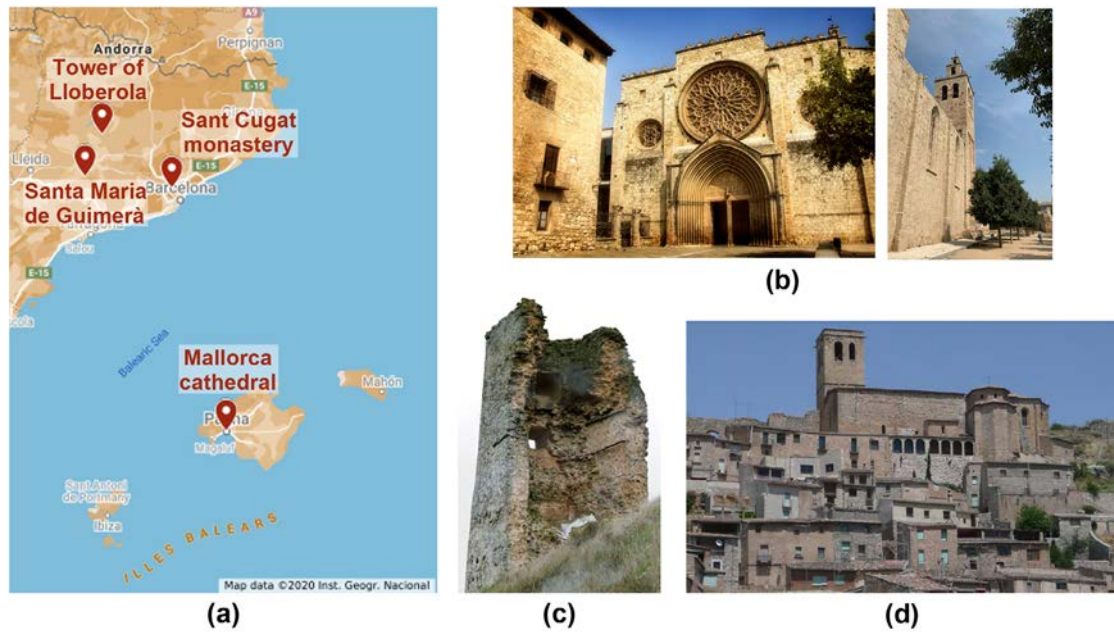


Figure 6.15: (a) Map showing location of case studies. (b) Sant Cugat monastery. (c) Tower from the remains of the castle of Lloberola (Molins, 2018). (d) Church of Santa Maria de Guimerà (Molins; Roca, 2018).

The first case study, the church of the monastery of Sant Cugat, is currently equipped with a static SHM system which has been installed since 2017 (Section 5.5). It is also a complex structure since it consists of different parts built over different periods, mostly from the mid-12th century to the 15th century. It has already been presented as a case study in the SHM component of this research (Chapter 5), and has been the subject of several other studies (Garcia Ramonda et al., 2015; Ajuntament de Sant Cugat, 2019a). This knowledge and information combined with on-site visual inspections form the basis used for the risk assessment of this particular case study. The remaining case studies include a medieval tower from the remains of Lloberola castle and the 14th century church of Santa Maria de Guimerà. The risk assessment for these two structures were performed solely based on expert diagnosis reports of their structural condition (Molins, 2018; Molins; Roca, 2018).

The resulting LoK and DR index values for all the case studies after risk assessment are summarised in Table 6.7. The values of the first level components of the DR index are also shown.

Table 6.7: Final index values for the structures studied as part of this research.

Case study	Level of Knowledge	Damage Vulnerability	Hazard	Exposure	Damage Risk	Curent state and recommendations
Mallorca cathedral	3.52	2.16	1.57	4.00	2.47	Structure has adequate capacity to withstand most foreseeable loads in the near and mid-term future. However, further research is needed to better understand if there is an active deterioration mechanism linked to the outward rotation of part of the facade.
Sant Cugat monastery	1.75	2.44	1.57	3.50	2.49	Structure has adequate capacity to withstand most foreseeable loads in the near future. However, there is definitely an active deterioration mechanism linked to the outward rotation of the bell tower. Further research needed to better understand true cause.
Torre Lloberola	0.51	3.92	1.46	2.00	2.83	Structural intervention in 2017 addressed most urgent needs. However, interventions definitely required to ensure stability in the long-term.
Santa Maria de Guimerà	1.03	3.73	2.07	2.00	2.88	Some works of urgent character required. However, vulnerabilities behind this need are relatively localised.

A substantial amount of information is available for the case of the church of Sant Cugat monastery, including more than 3 years of static monitoring data (see Appendices B and C). In general, it can be said that the structure is in good condition and that there are no significant immediate threats to the global structural integrity. However, as described in Chapter 5, recent analysis of monitoring data has confirmed that there is currently an active mechanism linked to the outward rotation of the bell tower. Although the estimated evolution rates do not represent an alarming situation at present, it is undeniable that further study is required to better understand the true cause and nature of this mechanism, and to design adequate interventions to limit possible negative consequences it may have for structural integrity. In fact, several in-situ investigations are already planned to be carried out on this structure, which should lead to an increased level of knowledge for risk assessment.

Of all the case studies considered, the tower from the remains of Lloberola castle definitely represents the structure with the simplest geometrical arrangement. Given the simpler nature of the structure, it can be said that initial investigations contribute more towards exhaustive knowledge when compared to the more complex case studies presented in this section. As such, while the LoK concavity setting was set at 2 for all the other case studies, it was set at 4 for this particular case in order to account for this effect (see Section 6.4). In this case, the main sources of available information were detailed analyses of historical sources and of visible damages (Molins, 2018). Although it is evident that this structure has suffered from severe deterioration, it must be highlighted that the most urgent matters have been addressed by a recent intervention. Nevertheless, the measures implemented cannot be considered as being sufficient to ensure long-term safety. As such, the vulnerability level can still be considered as being rather high, particularly considering the long run. It should also be mentioned that since no visitors are currently able to visit the structure (to the best of the author's knowledge), the exposure level of this particular structure has been considered as being relatively low compared to the other case studies (see Table 6.7).

In addition to detailed analyses of historical sources and damages, results from graphic statics analysis of a typical section of the main nave was also available for the case of the church of Santa Maria de Guimerà (Molins; Roca, 2018). For this particular case, the particular location and situation of the structure prompted an investigation into the landslide susceptibility in the area. This information is available with a resolution of 30 m for the entire region of Catalonia thanks to the work of (Palau et al., 2020). It is known that historic masonry churches can suffer significant damages due to landslides, as evidenced in (Ferrero et al., 2020). As shown in Figure 6.16, the susceptibility to landslides turned out to be "Moderate" in the precise location of the church, with several adjoining grid cells showing a "High" susceptibility. As a result, this case is the only one for which the specific vulnerability of the structure to other catastrophic events (see Sections 6.4 and 6.5) was explicitly included in the risk assessment (see Appendices B and C). Nevertheless, it must be said that the surrounding urban landscape and the fact that a retaining structure was recently reconstructed reduce the hazard of a landslide affecting the precise location of the church.

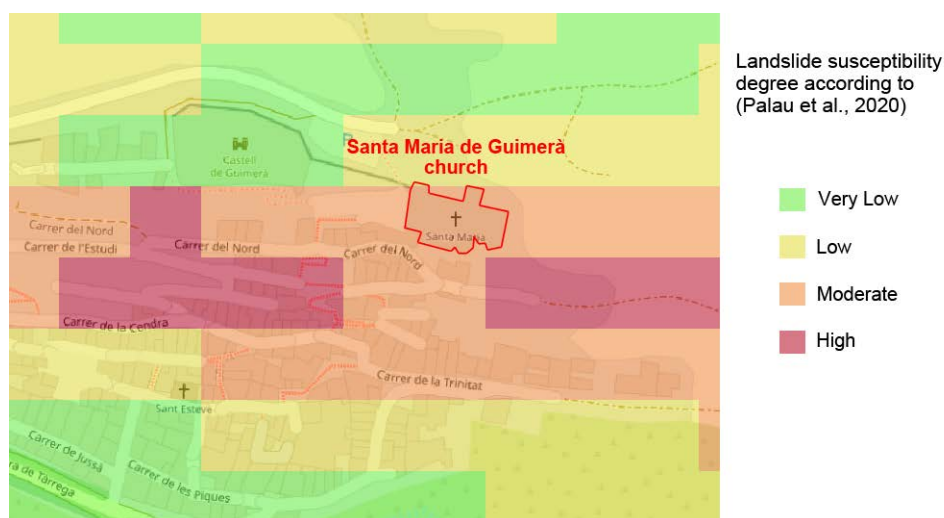


Figure 6.16: Landslide susceptibility around the church of Santa Maria de Guimerà (Palau et al., 2020).

With respect to damage vulnerability, it must be said that the church of Santa Maria de Guimerà is generally in a poor state of conservation with certain specific matters requiring immediate attention. The first action required involves adequate control of the lateral thrust imposed by the vaults and arches. This involves the removal of a reinforced concrete cover which possibly exists above the vaults and waterproofing of the roof along with adequate drainage design to prevent rainwater ingress. Another required intervention that can be considered as urgent involves the stabilisation of an external wall which is in a precarious equilibrium state and clearly susceptible to collapse. Although it does not form part of the structure of the church itself, debris from the collapse of this wall could cause significant damage to the church. In addition to these urgent needs, several other interventions could be required to ensure long-term stability. Static structural health monitoring of specific parameters could allow certain phenomena to be better ascertained before making definitive decision on the most suitable interventions required.

In general, it can be said that the index values provide adequate representations of the main conclusions that can be drawn from the risk assessment of the case studies. The LoK indices adequately convey the depth and sophistication of the analyses forming the basis of the risk assessment, and the vulnerability and risk index values are in line with what can be expected based on the descriptions elaborated in previous paragraphs. Nevertheless, it is important to recall that the main purpose of the indices is not to automate decisions but rather to ensure that a thorough and rigorous thought process is behind recommendations, to inform decision makers as concisely and clearly as possible, and to facilitate communication among relevant stakeholders.

That being said, in addition to the useful insights presented by the indices and their accompanying custom radial diagrams (see Appendix C), the automatically generated lists of best activities (see Appendix C) are also in-line with what can be expected and can also provide additional useful insights. Of course, the choice of which action to perform (if any) must ultimately be based on the specific needs of each structure and cannot be based only on the proposed generalised index formulation.

Specifically, it can be seen that static SHM is very highly ranked in all the case studies. This stems mainly from the fact that it is a powerful and adaptable tool that can provide useful information to better understand a wide range of structural phenomena. In fact, static SHM turns out to be ranked at the top of the list of possible diagnosis activities for two of the four cases included in this thesis. In the case of the tower of Lloberola, it is surpassed by FE modelling. This is due to the simpler geometry of the structure, which means that the development of useful models can be expected to be more straightforward. In the case of the church of the monastery of Sant Cugat, static SHM is surpassed by several diagnosis activities. This is definitely due to the fact that a relatively comprehensive system is already installed in the structure and has been providing useful and reliable data since more than 3 years. It is interesting to see that most of the diagnosis activities that can now contribute more to the LoK index score, such as FE modelling and AVT, are also activities that can directly be used to better understand the phenomena related to the bell tower, which is the main source of concern for this structure.

Of course, in cases for which it is already previously known that cost and technical limitations significantly reduce the potential usefulness of a particular activity, the relative importance of information from that particular activity in the index structures can be reduced through appropriate ratings in the second part of the SIEA. This was implemented for the case of FE modelling for the church of Santa Maria de Guimerà due to the complexity of the structure and of boundary conditions.

Finally, it can be observed that the need for more information on existing damage is recurrently found at the bottom of the list of best diagnosis activities as a consequence of the availability of expert damage analyses for the cases studied.

6.9. Summary

This research has proposed a systematic methodology for the risk assessment of masonry heritage structures which relies on the computation of two key indices representing the estimated risk level and the level of knowledge on which the estimation is based. Both indices have been developed using well-established multi-criteria decision-making (MCDM) procedures and have been expressly designed to improve the ob-

jectivity behind decisions on the preservation of unique masonry heritage structures. These indices should be re-evaluated every time the risk assessment needs to be updated. Most of the information required for the computation of the indices have to be supplied by the expert responsible for risk assessment in the form of standard answers to standard questions. Furthermore, the risk assessment procedure and the assumptions behind the computation of the indices are based on current best practices for the analysis, conservation, and structural restoration of architectural heritage. As such, it is specifically designed so that a dynamic risk assessment is performed, promoting the application of minimum interventions based on a strong scientific basis.

Three main novelties are linked to the proposed risk assessment methodology. The first is that it proposes decision-making tools in the form of standard indices able to consider information from a diverse set of diagnosis activities including structural analysis, structural health monitoring (SHM), damage surveys, material characterisation tests, non-destructive testing (NDT), and specific in-situ tests. The second is that it allows the expert responsible for risk assessment to tailor the hierarchical tree structures defining the indices according to the unique characteristics of a heritage structure. This is achieved through a systematic hierarchy re-structuring procedure based on rankings and ratings provided by the expert during an initial standardised appraisal. This needs to be carried out after performing a site visit and analysing available historical information. The third novelty lies in the possibility of automatically updating the index values based on data collected using static SHM systems. This is achieved by taking advantage of processed results from the automated data analysis procedure presented in Chapter 5.

However, it is very important to highlight that the proposed procedure is not meant to automate decisions, but rather to support decision-makers and to inform them as clearly and usefully as possible. In fact, for the final indices to provide meaningful insights, it is essential that answers to the standard questions are provided by a professional with sufficient experience and knowledge on the structural diagnosis of masonry heritage structures.

It is envisaged that besides helping decision-making, standard outputs proposed as part of the procedure have the potential to facilitate the communication of key aspects behind recommendations to non-technical stakeholders. While it is clear that risk mitigation measures for masonry heritage structures need to be based on solid scientific evidence and findings, it is often important for non-technical stakeholders to be involved in the decision process. As such, indices which can easily be explained in terms of a decision grid can help communicate the most important technical points for decisions. The communication can be further enhanced with standard outputs, such as radial diagrams showing the composition of index values or dynamic lists of best activities based on their possible contribution to the level of knowledge indicator. In a similar fashion, the proposed risk assessment procedure can be employed to streamline collaboration among experts with different sub-fields of specialisation by providing them with a common framework to share insights on the comprehensiveness of different investigations and on pertinent information for the evaluation of damage risk.

The proposed risk assessment framework can also be seen as an initial step towards incorporating relevant technical aspects related to structural damage into broader decision support systems for heritage. Such integrated systems could eventually help in addressing the increasing need to consider criteria related to sustainability, energy efficiency, and socio-economic impacts for decision-making on heritage.

7

Conclusions

7.1. Summary

As masonry heritage structures become older, it is undeniable that the need to manage their deterioration becomes increasingly important. This coupled with the increased awareness of our common responsibility to safeguard cultural heritage has led to great innovation in the development of techniques and procedures for structural diagnosis. As a result, several complementary activities are often employed nowadays to perform the diagnosis of complex heritage structures. An initial component of the research involved investigations and applications related to certain specific relevant technical fields. This initial work, involving materials testing, full-scale vibration testing, and structural health monitoring (SHM), provided a better understanding of many practical issues which were taken into consideration during the subsequent development of decision support tools. Despite significant advances in specific techniques and the clear need to consider information from diverse diagnosis activities for decision-making, there has been very little research effort on the development of robust decision analysis methods for choosing the best course of action for preservation. This research represents an original contribution that makes use of decision analysis to support the structural risk assessment of unique masonry heritage structures.

Besides describing essential theoretical concepts required for the correct interpretation of results presented in subsequent chapters, *Chapter 2* also briefly summarises the state-of-the-art in relevant topics and motivates the research presented in this thesis.

The review of existing literature revealed that the information available on the dynamic elastic properties of brick masonry constituents is scarce despite their widespread use as construction materials. Furthermore, the relationship between the static and dynamic elastic modulus, which is already used in practical applications for testing rocks and concrete, is yet to be well understood for these constituent materials. The research presented in *Chapter 3* aims to address this gap through an experimental study of the dynamic elastic properties of typical brick masonry constituents. After a rigorous analysis of the obtained results, a robust procedure involving the combined use of Ultrasonic Pulse Velocity (UPV) testing and Impulse Excitation of Vibration (IEV) testing is proposed for the estimation of dynamic elastic and shear moduli of brick masonry constituents. In addition, the research also explored the empirical relationship between the static and elastic moduli of the materials considered for the experimental campaign. The efficiency of several existing expressions for rocks and concrete were evaluated, before proposing an empirical expression to estimate the static elastic modulus of brick masonry constituents from the dynamic modulus.

This thesis also includes a study on the full-scale vibration testing of masonry bell towers and operational modal analysis (OMA) techniques used to extract modal parameters (natural frequencies, mode shapes, and damping ratios) from test acquisitions. A literature review revealed that system identification and modal analysis for OMA is a well established field and that there have been significant advances towards the accurate estimation of natural frequencies, mode shapes, and damping ratios from recorded vibration signatures. In general, after performing some basic pre-processing tasks on collected data, OMA involves the identification of a suitable system model from the acquired data, and the extraction of modal parameters that characterise

the dynamic behaviour of a structure. A summary of the reviewed OMA techniques is provided in Chapter 2. Naturally, given the nature of the task, the accuracy of resulting estimates are still highly dependent on test conditions and acquisition quality. **Chapter 4** presents the application of all the reviewed OMA techniques to the case of the bell tower of Seu Vella in Lleida, Catalonia. Two natural frequencies, including the fundamental one, could be clearly identified from the acquired vibration signatures. These results were used to calibrate a detailed finite element (FE) model of the structure and to estimate the effective dynamic elastic modulus of the material making up the tower. Based on the analyses performed as part of this research, the operational poly-reference least squares complex domain identification (pLSCF) method proved to be the most robust for the correct estimation of the natural frequencies and associated mode shapes. However, the damping estimates provided by time-domain methods appear to be more reliable.

With respect to SHM, it is safe to say that there is sufficient evidence to show that static monitoring can prove to be a powerful tool for the diagnosis of heritage structures. This monitoring strategy is particularly suitable for the early identification of slow ongoing deterioration mechanisms. However, the influence of fluctuating environmental parameters is reported to be a recurrent challenge for the interpretation of results. This problem has been the subject of several studies, and the combined use of monitored environmental parameters and dynamic linear regression models appear to be a promising solution. Auto-Regressive eXogenous-input (ARX) models appear to be particularly appealing, with several examples demonstrating their effectiveness for filtering out variations driven by environmental changes from the time series of estimated natural frequencies as part of dynamic SHM investigations. However, the application of such models to static SHM systems has been very limited. In particular, applications to large data sets from whole networks of sensors in complex heritage structures are still lacking in literature. As such, the research presented in **Chapter 5** proposes a fully automated data analysis procedure for static SHM that not only filters out reversible components driven by changing environmental parameters from measurements, but also classifies monitored parameters into predefined evolutionary states. ARX models are employed in the first part of the proposed procedure while estimated evolutionary rates and metrics representing modelling uncertainties and errors are considered in the latter. The complete procedure has been successfully applied to analyse the data collected from two systems installed in important heritage structures in Spain, namely the cathedral of Mallorca and the monastery of Sant Cugat. In both cases, the proposed methodology allowed the identification of active deterioration mechanisms of interest for the preservation of the structures.

Finally, the work presented in **Chapter 6** specifically addresses the proposal of a systematic procedure for assessing the risk of structural damage in masonry heritage structures, and the development of multi-criteria decision-making (MCDM) tools that can be used within the assessment procedure. With respect to masonry heritage, most of the MCDM techniques reported in literature deal with the assessment of vulnerability or risk at the territorial scale. In particular, methods specifically developed for the assessment of seismic vulnerability have had the greatest success in terms of widespread use in practice. Most of these existing methods for vulnerability or risk assessment are indicator-based and employ one of the simplest and most popular MCDM techniques known as simple additive weighting (SAW). Moreover, all reviewed existing methods only consider information from technical visual inspections and geometry surveys in the assessment of damage risk or vulnerability. Although this is suitable for risk assessments at territorial scale that involve a large number of buildings, it is definitely an important weakness for the risk assessment of unique masonry heritage structures since activities such as non-destructive testing (NDT) and SHM can represent key sources of valuable information. As such, the MCDM tools proposed as part of this research have been expressly designed to explicitly consider relevant information from many applicable diagnosis activities including structural analysis, NDT, and SHM. Two specific MCDM indices are proposed to concisely inform decision-makers on the estimated risk of structural damage (DR index) and on the level of knowledge (LoK index) used as a basis for this estimation. It is important to highlight that the proposed indices are not meant to be used for automating decisions but rather to support decision-makers and to inform them as clearly and as usefully as possible. Most of the information required for the computation of the indices have to be supplied in the form of standard answers to standard questions by the expert(s) performing risk assessment. Two types of standard questions are used for the computation of indices: essential questions and optional ones. According to the proposed assessment methodology, the essential questions must be answered after an initial desk study and inspection have been carried out. Based on these initial answers, the MCDM indices can already present useful indications on the estimated risk of damage and the uncertainty behind this estimation. An important set of essential questions are also specifically designed to gauge the relative usefulness of

different diagnosis activities for the structure under evaluation. Answers to these questions are employed to automatically modify the weights between criteria to ensure that the MCDM indices can still provide meaningful insights for different structures despite their unique characteristics. The optional questions relate to specific diagnosis activities and must only be answered to update index values after such activities have been performed. For the special case of data from static SHM systems, the proposed risk assessment methodology allows the LoK and DR index values to be automatically updated from the results of the automated data analysis procedure presented in Chapter 5. Naturally, answers to relevant questions must be updated every time a new diagnosis activity or intervention is carried out. Through this dynamic process, the proposed risk assessment methodology aims to promote a preventive approach to conservation which strives for minimum interventions based on a strong scientific basis. The methodology has been applied to several case studies to demonstrate its ability to provide useful insights for decisions.

7.2. Main contributions

The originality of the present work lies mainly in the following contributions:

Materials testing

- The development of a robust experimental procedure based on the synergy of two approaches for the determination of dynamic elastic properties of brick masonry constituents. The two techniques employed by the procedure are Ultrasonic Pulse Velocity (UPV) testing and Impulse Excitation of Vibration (IEV) testing. Clear practical provisions have been given concerning every step of the procedure.
- The proposal of an empirical expression that can be used to estimate the static elastic modulus of typical brick masonry constituents from the dynamic one. This expression can have a wide range of practical applications since the latter can be estimated more quickly and reliably but the former is preferred for many common structural verifications.

Structural health monitoring

- The development of a fully integrated and automated procedure for analysing data from complete static structural health monitoring (SHM) systems installed in masonry heritage structures. The proposed procedure can be seen as consisting of two parts. The first part employs dynamic linear regression models to filter out reversible seasonal variations from the records of monitored structural parameters of interest. The second part relies on a series of logical tests to classify monitored structural parameters into predefined evolutionary states in order to facilitate the diagnosis task. The usefulness of the automated procedure has been clearly demonstrated through its ability to help identify vulnerable areas in two important medieval heritage structures in Spain, namely the cathedral of Mallorca and the church of the monastery of Sant Cugat.

Risk assessment and decision-making

- The proposal of standard MCDM indices for the structural risk assessment of masonry heritage. An important novelty of the proposed indices lies in their ability to consider information from a diverse set of diagnosis activities including structural analysis, SHM, damage surveys, material characterisation tests, NDT, and specific in-situ tests.
- The development of a process allowing an expert responsible for risk assessment to tailor the hierarchical structures defining the proposed indices according to the unique characteristics of a heritage structure. This is achieved through a systematic hierarchy re-structuring procedure based on rankings and ratings provided by the expert during an initial standardised appraisal.
- The development of a process to automatically update the proposed indices based on data collected using static SHM systems. This is achieved by taking advantage of processed results from the automated data analysis procedure which constitutes the main contribution of this research in the field of structural health monitoring.

7.3. Suggestions for future work

As a consequence of the research presented in this thesis, the following investigations can be suggested as further work:

- The development of testing procedures making use of ultrasonic shear wave transducers to better characterise the dynamic elastic behaviour of bricks produced by extrusion which present an anisotropic character. Theoretically, such transducers could also be used to directly evaluate the dynamic Poisson's ratio of isotropic constituents. However, it should be noted that accurately determining the arrival time of the shear wave can prove to be especially difficult, particularly when testing materials with significant heterogeneities and rough surfaces.
- The extension of the proposed procedure for estimating dynamic elastic properties of brick masonry constituents to the case of stone masonry, which represents a material often used in historical constructions. This would involve adapting the test procedures and analysis steps for particular anisotropy and heterogeneity characteristics of stone. In addition, the shape and size of specimens could also be modified based on practical and experimental considerations related to testing stone.
- The evaluation of the relationship between static and dynamic elastic properties for different types of stone commonly used for construction in different geographic areas. Although detailed studies have been performed on this relationship for specific types of stones, there still exist several types of stone for which it is not well understood. In many geographical areas, stones from the same common quarries have often been used recurrently in the past for construction throughout the region. Studying the relationship between static and dynamic elastic modulus of stones found in such quarries could therefore contribute to more accurate structural analysis for a large number of structures. In addition, if these studies are performed after the method proposed in this thesis for brick masonry constituents has already been adapted to the case of stone, it should lead to a more accurate representation of the relationship between static and dynamic parameters.
- Assessment of the dynamic interaction between swinging bells and the tower of Seu Vella. This first involves evaluating the horizontal dynamic forces that would be produced by the swinging bells for different relevant swing angles and velocities. Subsequently, the identified resonant frequencies and calibrated numerical model presented in this thesis could be used to estimate dynamic amplification factors and to better understand the influence of bell harmonics on the structural response. Results from such analyses would allow the formulation of specific recommendations on swing angles and velocities that minimise the interaction between bell harmonics and the resonant modes of the tower.
- Investigations on the relation between the structural response of masonry structures and different environmental parameters besides temperature through long-term structural health monitoring (SHM) data. The data analysis procedures presented in this thesis provide the necessary tools to better understand the relationship between monitored structural parameters and any environmental parameter for which data is available. This is a very interesting possibility since access to data on a wide range of climatic factors at several locations around the world are becoming more and more readily available thanks to the advent of technology. As such, for situations whereby the effect of specific climatic factors such as wind or rain could be of relevance to structural safety, the methods presented in this thesis could be employed to better characterise and to monitor these effects.
- The application of more sophisticated methods to classify monitored parameters in static SHM systems according to their underlying evolutionary state. Although the efficiency of the proposed classification procedure has been demonstrated through the application to case studies, attempting to address the problem through other techniques, such as those based on artificial intelligence, could lead to more accurate and efficient results.
- Development and testing of a user-friendly interface for utilising the proposed risk assessment method and MCDM indices. This is crucial for the proposed method to be useful in practice.

- The design of standardised forms for different common masonry structural typologies to ensure adequate consideration of specific criteria in the proposed MCDM indices.
- Employing the proposed risk assessment framework for education. Although it is often relatively straightforward to evaluate whether students are able to carry out structural calculations correctly, it can be difficult to evaluate their ability to collect information from different sources to make appropriate recommendations under conditions of uncertainty. However, this is a skill which is always required for evaluating risk in real life applications. In this regard, using the proposed assessment methodology when carrying out integrated projects could be a means of obtaining some insight into the thought process of students.
- Further application, validation, and improvement of the multi-criteria decision-making (MCDM) indices proposed as support tools for decisions on the structural safety of masonry heritage. Given the strong assumptions on which the employed decision models are based, such tools usually become more effective after widescale application. As such, more applications to diverse masonry heritage structures are required to further validate and improve the proposed tools. In addition, given the structured organisation of criteria forming the basis of the tools, further applications would in fact also represent a data collection exercise on the determinants of decisions on heritage. If a sufficiently high number of risk assessments are performed, the collected data could be analysed by means of exploratory factor analysis or other artificial intelligence-based methods such as decision tree algorithms to reveal important trends and determinants behind decisions on heritage.
- The application of more sophisticated multi-attribute decision models to the risk assessment of masonry heritage. As stated in this thesis, the simple additive weighting (SAW) technique employed in this research for the development of MCDM indices relies on strong assumptions of independence among criteria (or attributes). If a specific risk assessment task can be framed as a choice between a series of well defined alternatives, several models based on multi-attribute utility theory (MAUT) can be applied towards identifying the optimal choice. Some of these models, such as partial or total decomposition models, are able to deal with attributes which are not independent. The use of such models could allow for a more accurate representation of (parts of) the decision problem addressed by this research. In addition, if sufficient data is available, the possibility of applying multi-attribute expected utility models to the risk assessment of masonry heritage could be explored. Such models are able to represent the choice alternatives as uncertain parameters. This approach could eliminate the need for a separate level of knowledge index as proposed by this research since the uncertainty behind the best choice alternative would be explicitly represented by the decision model. Naturally, the use of such models requires that the attributes be defined as random variables rather than deterministic values. As such, a large amount of data or a sufficiently strong theoretical basis must be available to justify the probability distributions assigned to all criteria.
- Expansion of the proposed risk assessment framework to include other criteria. Finally, because it involves the structured organisation of criteria relevant for decisions, the developed risk assessment framework has the potential of eventually being further expanded so that relevant technical aspects related to structural damage can be incorporated into a broader decision support system for heritage that also includes sustainability criteria related to environmental and socio-economic impacts.

Appendices

Appendix A: Standard questions for risk assessment

Appendix B: Answers to questions for case studies

Appendix C: Risk assessment summary for case studies

A

Standard questions for risk assessment

A.1. Standardised Initial Expert Appraisal (SIEA)

A.1.1. Initial evaluation of level of knowledge and damage risk

Table A.1.1: Questions to be answered during the first part of the SIEA. Answers are used to evaluate initial value of indicators related to the level of knowledge and the damage risk.

Question ref.	Question	Answer range
<i>Historical information and documentation (level of knowledge)</i>		
1	Please rate the quality and comprehensiveness of information available on the following topics:	
1A	The construction process.	(0 - 5)
1B	Historical structural alterations.	(0 - 5)
1C	Past structural interventions.	(0 - 5)
1D	Past damage events (Fires, earthquakes, destructive events).	(0 - 5)
<i>Geometry & damage surveys (level of knowledge)</i>		
2	Please rate the quality and quantity of information available on the geometry of the structure.	(0 - 5)
3	Please rate the accuracy and comprehensiveness of information available for damage analysis.	(0 - 5)
<i>Initial material quality (level of knowledge and damage vulnerability)</i>		
4A	Please rate the level of accessibility to all the different materials of the structural system during visual inspections?	(0 - 5)
4B	How would you rate the overall integrity and quality of the masonry material based on visual inspections?	(1-5)
<i>Exposure</i>		
5A	Please rate the level of exposure in terms of the cultural value that the structure represents.	(1-5)
5B	Please rate the level of exposure in terms of usage and potential loss.	(1-5)
<i>Lack of maintenance (damage vulnerability)</i>		
6A	How would you describe the state of maintenance of the structure?	(1-5)
6B	Please rate the suitability of the current maintenance plan to address visible pathologies.	(1-5)
<i>Need for urgent action (damage vulnerability)</i>		
7A	Are there clear signs that urgent action is required to stabilise the structure?	0 or 1
7B	How much of the structure is likely to be affected if no urgent action is taken	(1-5)
<i>Progressive collapse mechanisms (damage vulnerability)</i>		
8	Based on available historical information, damage inspections, and reasonable engineering judgement, please rate the perceived susceptibility of the structure to experience significant damage due to progressive collapse mechanisms.	(1-5)
<i>Earthquakes (hazard and damage vulnerability)</i>		
9A	What is the peak ground acceleration with a 10% probability of exceedance in 50 years? [m/s^2]	$\geq 0 m/s^2$ (1-5)
9B	Based on the information available about past performance to historical earthquakes, as well as the evidence on the structure in terms of damage, please rate how concerning is the perceived vulnerability of the structure to earthquakes.	(1-5)
<i>Other catastrophic events (hazard and damage vulnerability)</i>		
10A	Please rate the hazard of other catastrophic events in terms of their potential intensity and frequency of occurrence?	(1-5)
10B	Based on available historical information, damage inspections, and reasonable engineering judgement, please rate how concerning is the perceived vulnerability of the structure to other potential catastrophic events.	(1-5)
<i>Fire hazard</i>		
11	Please rate the fire hazard in terms of possible sources of ignition, available fuel and potential for fire to spread.	(1-5)

Table A.1.2: Description of the significance of the different values that can be attributed to each question in the first part of the SIEA.

Question ref.	Range description
<i>Historical information and documentation (level of knowledge)</i>	
1A - 1D	0: No information; 1: Very Poor; 2: Poor; 3: Fair; 4: Good; 5: Excellent
<i>Initial geometry & damage surveys (level of knowledge)</i>	
2	0: No geometrical information; 1: Limited, possibly unreliable, idea of general dimensions; 2: Measurements of some key dimensions, no verification of inclinations; 3: Measurements of most key dimensions, some inclination verifications; 4: Comprehensive set of measurements and/or drawings, some investigations on dimensions of hidden elements; 5: Comprehensive reliable set of drawings, comprehensive knowledge on dimensions of hidden elements
3	0: No visual inspection, no information on damage; 1: Many critical areas could not be inspected, no damage summary; 2: Many critical areas could be inspected, some damage summary or mapping; 3: Most critical areas could be inspected, good damage mapping; 4: All critical areas could be inspected, mapping of most significant damages; 5: All areas could be inspected, comprehensive mapping of all significant cracks and damages
<i>Initial material quality (level of knowledge and damage vulnerability)</i>	
4A	0: No visual inspection carried out; 1: Very poor. Many critical areas are not accessible, structural elements have complex multi-leaf morphologies, very heterogenous material.; 2: Poor. Many critical areas are not accessible, structural elements have multi-leaf morphologies, heterogenous material; 3: Moderate. Many critical areas are accessible, structural elements have multi-leaf morphologies, mostly homogeneous material; 4: Good. Most critical areas are accessible, structural elements have single-leaf morphologies, mostly homogeneous material; 5: Very good. All areas are accessible, simple single-leaf wall morphologies, very homogenous material
4B	1: Very poor quality, large variability. Material clearly vulnerable to more damage; 2: Poor quality ; 3: Moderate quality; 4: High quality; 5: Very high quality, very uniform material
<i>Exposure</i>	
5A	1-2: Listed in regional or provincial heritage registers; 2-4: Listed in national heritage register; 5: UNESCO World Heritage site
5B	1: Very low number of visitors and very low potential value of loss; 2: Low number of visitors and low potential value of loss; 3: Moderate number of visitors and moderate potential value of loss; 4: High number of visitors and high potential value of loss; 5: Very high number of visitors and very high potential value of loss
<i>Lack of maintenance (damage vulnerability)</i>	
6A	1: Poor; 2: Fair; 3: Good; 4: Very good; 5: Excellent
6B	1: Minimal maintenance; 2: Irregular and unorganised maintenance plan; 3: Maintenance plan addresses only some pathologies; 4: Maintenance plan appropriate for most visible pathologies; 5: Comprehensive and detailed tailored maintenance plan
<i>Need for urgent action (damage vulnerability)</i>	
7A	0: No; 1: Yes
7B	1: A tiny fraction; 2: A small fraction; 3: A moderate fraction; 4: A substantial fraction; 5: All or most of the structure
<i>Progressive collapse mechanisms (damage vulnerability)</i>	
8	1: Very low (good condition, minimal damages); 2: Low; 3: Medium; 4: High; 5: Very high (major damages implying stability problems)
<i>Earthquakes (hazard and damage vulnerability)</i>	
9A	Specific value function
9B	1: Very low; 2: Low; 3: Moderate; 4: High; 5: Very high
<i>Other catastrophic events (hazard and damage vulnerability)</i>	
10A	1: Very low hazard; 2: Low hazard; 3: Moderate hazard; 4: High hazard; 5: Very high hazard
10B	1: Very low; 2: Low; 3: Medium; 4: High; 5: Very high
<i>Fire hazard</i>	
11	1: Very low hazard; 2: Low hazard; 3: Moderate hazard; 4: High hazard; 5: Very high hazard

A.1.2. Evaluation of which activities can best inform the assessment of damage vulnerability

Table A.1.3: Ratings to be given in the second part of the SIEA. They are used to assign weights to the contribution of different diagnosis activities to the level of knowledge indicator.

Question ref.	Question	Answer range
<i>Ranking the importance of vulnerability to specific hazards for global vulnerability assessment</i>		
12A	Should earthquakes be included in the vulnerability assessment?	0 or 1
12B	Should other catastrophic events be included in the vulnerability assessment?	0 or 1
12C	Please rank the following possible 3 aims of structural analysis according to their importance for global damage vulnerability characterisation:	
12C(i)	Structural analysis aimed at better understanding vulnerability to progressive collapse mechanisms	1,2 or 3
12C(ii)	Structural analysis aimed at better understanding vulnerability to earthquakes	1,2 or 3
12C(iii)	Structural analysis aimed at better understanding vulnerability to other identified catastrophic events	1,2 or 3
<i>Structural analysis and structural health monitoring - Progressive collapse mechanisms</i>		
13	Please rate to what extent information from the following diagnosis activities can help assess the structure's vulnerability to progressive collapse mechanisms.	
13A	Load report	0,1 or 2
13B	Graphic statics & Limit analysis	0,1 or 2
13C	FEM	0,1 or 2
13D	Dynamic SHM	0,1 or 2
13E	Static SHM	0,1 or 2
<i>Structural analysis and structural health monitoring - Earthquakes</i>		
14	Please rate to what extent information from the following diagnosis activities can help assess the structure's vulnerability to earthquakes	
14A	Graphic statics & Limit analysis	0,1 or 2
14B	FEM	0,1 or 2
14C	Dynamic SHM	0,1 or 2
14D	Static SHM	0,1 or 2
<i>Structural analysis and structural health monitoring - Other catastrophic events</i>		
15	Please rate to what extent information from the following diagnosis activities can help assess the structure's vulnerability to other catastrophic events	
15A	Graphic statics & Limit analysis	0,1 or 2
15B	FEM	0,1 or 2
15C	Dynamic SHM	0,1 or 2
15D	Static SHM	0,1 or 2

Table A.1.4: Ratings to be given in the second part of the SIEA. They are used to assign weights to the contribution of different diagnosis activities to the level of knowledge indicator.

Question ref.	Question	Answer range
<i>Material properties</i>		
16	Please rate to what extent information from the following activities can help assess the structure's damage vulnerability	
16A	Experimental characterisation of compressive strengths of constituents	0,1 or 2
16B	Experimental characterisation of compressive strength of masonry	0,1 or 2
16C	Experimental characterisation of shear load-bearing capacity of masonry	0,1 or 2
16D	Experimental characterisation of elastic moduli of constituents	0,1 or 2
16E	Experimental characterisation of elastic modulus of masonry	0,1 or 2
16F	Experimental characterisation of chemical composition and/or other specific material properties	0,1 or 2
<i>Additional geometry and damage mapping activities</i>		
17	Please rate to what extent the following activities can help improve the level of knowledge on the existing geometry and damage	
17A	Topographic surveys (including laser scanning, photogrammetry, or equivalent)	0,1 or 2
17B	Borescope inspections and/or excavation pits	0,1 or 2
17C	Impact-echo testing	0,1 or 2
17D	More accurate or extensive survey of damages	0,1 or 2
<i>Additional diagnostic activities for assessment of material quality (MDT/NDT)</i>		
18	Please rate to what extent the following activities can help to assess the material quality	
18A	Borescope inspections and/or excavation pits	0,1 or 2
18B	Sonic pulse velocity testing (including tomography)	0,1 or 2
18C	Ultrasonic pulse velocity testing	0,1 or 2
18D	Surface penetrating radar testing	0,1 or 2
18E	Infrared thermography	0,1 or 2
18F	Rebound hammer	0,1 or 2
18G	Other specific tests for evaluating material quality and condition	0,1 or 2
<i>In-situ evaluation of actual loading and boundary conditions</i>		
19	Please rate to what extent information from the following activities can help assess the structure's damage vulnerability	
19A	Flatjack in-situ tests of stress levels	0,1 or 2
19B	Ambient vibration tests	0,1 or 2
19C	Geotechnical surveys	0,1 or 2
19D	Other specific tests	0,1 or 2

Table A.1.5: Explanation of possible ratings to be given in .

Question ref.	Range description
<i>Ranking the importance of vulnerability to specific hazards for global vulnerability assessment</i>	
12A, 12B	1: The vulnerability to earthquakes (or other catastrophic events) is explicitly considered in the assessment. Ratings will have to be given on the possible contribution of different structural analysis and monitoring tools to the level of knowledge on this vulnerability;
	0: Earthquakes (or other catastrophic events) are not considered in the vulnerability assessment. The hazard of earthquakes and other catastrophic events is still included in the risk assessment. No ratings will have to be given on the possible contribution of different structural analysis and monitoring tools to the level of knowledge on the vulnerability to earthquakes (or other catastrophic events).
12C(i) - 12C(iii)	1: Most important aim for global damage vulnerability characterisation.
	2: Second most important aim for global damage vulnerability characterisation.
	3: Least important aim for global damage vulnerability characterisation.
<i>Structural analysis, structural health monitoring and additional diagnosis activities</i>	
13A - 13E, 14A - 14D, 15A - 15D, 16A - 16F, 17A - 17D, 18A - 18G, 19A - 19D	0: Irrelevant / Not considered in risk analysis; 1: Can complement; 2: Can contribute significantly / Essential

A.2. Specific questions after structural analysis and structural health monitoring

Table A.2.1: Questions that need to be answered to update indicators of level of knowledge and damage vulnerability after structural analysis or structural health monitoring has been carried out.

Question ref.	Question	Answer range
<i>Load report</i>		
20A	How much of the loads needed for a comprehensive evaluation were calculated?	(0 - 5)
20B	Are there areas with concerning high loading levels?	(1 - 5)
<i>Graphic statics and limit analysis</i>		
21A, 25A*,29A†	What proportion of identified cases of interest were evaluated?	(0 - 5)
21B, 25B*,29B†	Are there potential cases with a precarious equilibrium?	(1 - 5)
<i>Finite element modelling</i>		
22A, 26A*,30A†	What proportion of identified loading scenarios of interest were investigated?	(0 - 5)
22B, 26B*,30B†	Do the simulations reveal that parts of the structure could be vulnerable to foreseeable loading conditions?	(1 - 5)
<i>Dynamic structural health monitoring</i>		
23A, 27A*,31A†	What proportion of dynamic parameters of interest have been monitored?	(0 - 5)
23B, 27B*,31B†	Is the monitoring duration suitable to observe the phenomena of interest?	(0 - 5)
23C, 27C*,31C†	Are there signs that parts of the structure could be vulnerable to foreseeable loading conditions?	(1 - 5)
<i>Static structural health monitoring</i>		
24A, 28A*,32A†	What proportion of parameters of interest have been monitored?	(0 - 5)
24B*†	How many years of monitoring data are available to date?	≥ 0 years (0 - 5)
24C*†	What percentage of sensors are classified as evolutionary?	≥ 0% (1 - 5)
24D*†	What is the yearly average growth rate of all monitored crack widths classified as apparently evolutionary or evolutionary? [mm]	≥ 0 mm (0 - 5)
24E*†	What is the yearly average growth rate of all monitored distances classified as apparently evolutionary or evolutionary? [mm]	≥ 0 mm (0 - 5)
24F*†	What is the yearly average growth rate of all monitored inclinations classified as apparently evolutionary or evolutionary? [°]	≥ 0 ° (0 - 5)

* Structural analysis aimed at better understanding vulnerability to earthquakes.

† Structural analysis aimed at better understanding vulnerability to other catastrophic events.

Table A.2.2: Description of the significance of the different values that can be attributed to each specific question related to structural analysis or structural health monitoring.

Question ref.	Range description
<i>Load report</i>	
20A	0: No load report; 1: A minuscule fraction; 2: A tiny fraction; 3: A small fraction; 4: A substantial fraction; 5: All or most of the relevant loads
20B	1: None; 2: A few potential areas; 3: Several potential areas / Definitely in at least one area; 4: Definitely in some areas; 5: Definitely in several areas
<i>Graphic statics and limit analysis</i>	
21A, 25A*,29A [†]	0: No limit analysis; 1: A minuscule fraction; 2: A tiny fraction; 3: A small fraction; 4: A substantial fraction; 5: All or most of the relevant cases
21B, 25B*,29B [†]	1: None; 2: A few potential cases; 3: Several potential cases / At least one definitive case; 4: Some definitive cases; 5: Several definitive cases
<i>Finite element modelling</i>	
22A, 26A*,30A [†]	0: No FEM; 1: a minuscule fraction; 2: a tiny fraction; 3: a small fraction; 4: a substantial fraction; 5: All or most of the relevant scenarios
22B, 26B*,30B [†]	1: None; 2: A few potential cases; 3: Several potential cases / At least one definitive case; 4: Some definitive cases; 5: Several definitive cases
<i>Dynamic structural health monitoring</i>	
23A, 27A*,31A [†]	0: No dynamic SHM; 1: a minuscule fraction; 2: a tiny fraction; 3: a small fraction; 4: a substantial fraction; 5: All or most of the relevant parameters
23B, 27B*,31B [†]	0: No dynamic SHM; 1: Absolutely not; 2: With a great deal of uncertainty; 3: With moderate uncertainty; 4: With little uncertainty; 5: With minimal uncertainty
23C, 27C*,31C [†]	1: None; 2: A few potential indications; 3: Several potential indications / At least one definitive indication; 4: Some definitive indications; 5: Several definitive indications
<i>Static structural health monitoring</i>	
24A, 28A*,32A [†]	0: No static SHM; 1: a minuscule fraction; 2: a tiny fraction; 3: a small fraction; 4: a substantial fraction; 5: All or most of the relevant parameters
24B* [†]	Specific value function
24C* [†]	Specific value function
24D* [†]	Specific value function
24E* [†]	Specific value function
24F* [†]	Specific value function

* Structural analysis aimed at better understanding vulnerability to earthquakes.

† Structural analysis aimed at better understanding vulnerability to other catastrophic events.

A.3. Specific questions after evaluation of material properties

Table A.3.1: Questions that need to be answered to update indicators of level of knowledge and damage vulnerability after experimental evaluation of material properties.

Question ref.	Question	Answer range
<i>Experimental characterisation of compressive strengths of constituents</i>		
33A	How would you rate the overall confidence level of the estimated compressive strengths?	(0 - 5)
33B	What proportion of the areas of interest have been covered by the current and previous investigations?	(0 - 5)
33C	Are there potential estimates indicating worryingly low strengths?	(1 - 5)
<i>Experimental characterisation of compressive strength of masonry</i>		
34A	How would you rate the overall confidence level of the estimated compressive strengths?	(0 - 5)
34B	What proportion of the areas of interest have been covered by the current and previous investigations?	(0 - 5)
34C	Are there potential estimates indicating worryingly low strengths?	(1 - 5)
<i>Experimental characterisation of shear load-bearing capacity of masonry</i>		
35A	How would you rate the overall confidence level of the estimated capacity?	(0 - 5)
35B	What proportion of the areas of interest have been covered by the current and previous investigations?	(0 - 5)
35C	Are there potential estimates indicating worryingly low strengths?	(1 - 5)
<i>Experimental characterisation of elastic moduli of constituents</i>		
36A	How would you rate the overall confidence level of the estimated moduli?	(0 - 5)
36B	What proportion of the areas of interest have been covered by the current and previous investigations?	(0 - 5)
36C	Are there potential stiffness estimates indicating material degradation?	(1 - 5)
<i>Experimental characterisation of elastic modulus of masonry</i>		
37A	How would you rate the overall confidence level of the estimated moduli?	(0 - 5)
37B	What proportion of the areas of interest have been covered by the current and previous investigations?	(0 - 5)
37C	Are there potential stiffness estimates indicating material degradation?	(1 - 5)
<i>Experimental characterisation of composition and/or other specific properties</i>		
38A	How would you rate the overall confidence level of the estimated properties?	(0 - 5)
38B	What proportion of the areas of interest have been covered by the current and previous investigations?	(0 - 5)
38C	Do some of the estimated properties suggest an increased vulnerability of the material to degradation or damage?	(1 - 5)

Table A.3.2: Description of the significance of the different values that can be attributed to each specific question related to experimental evaluation of material properties.

Question ref.	Range description
33A, 34A, 35A, 36A, 37A, 38A	0: No tests; 1: Not confident at all; 2: Slightly confident; 3: Somewhat confident; 4: Fairly confident; 5: Completely confident
33B, 34B, 35B, 36B, 37B, 38B	0: No tests; 1: a minuscule fraction; 2: a tiny fraction; 3: a small fraction; 4: a substantial fraction; 5: All or most of the relevant areas
33B, 34C, 35C, 36C, 37C, 38C	1: None; 2: A few potential ones; 3: Several potential ones / Definitely at least one; 4: Definitely some; 5: Definitely several

A.4. Specific questions after additional geometry and damage surveys

Table A.4.1: Questions that need to be answered to update indicators of level of knowledge and damage vulnerability after additional geometry and damage surveys.

Question ref.	Question	Answer range
<i>Topographic surveys</i>		
39	What proportion of the possible areas of interest have been covered by the current and previous topographic surveys?	(0 - 5)
2	Please update the global rating of the level of knowledge on the geometry of the structure	(0 - 5)
<i>Borescope inspections and/or excavation pits</i>		
40	What proportion of the possible areas of interest have been covered by the current and previous investigations?	(0 - 5)
2	Please update the global rating of the level of knowledge on the geometry of the structure	(0 - 5)
<i>Impact-echo testing</i>		
41	What proportion of the possible areas of interest have been covered by the current and previous impact-echo tests?	(0 - 5)
2	Please update the global rating of the level of knowledge on the geometry of the structure	(0 - 5)
<i>More accurate or extensive survey of damages</i>		
42	What proportion of the possible areas of interest have been covered by the current and previous investigations?	(0 - 5)
3	Please update the global rating of the level of knowledge on existing damages	(0 - 5)
<i>Option to update initial damage vulnerability assessment</i>		
8	Based on available historical information, damage inspections, and reasonable engineering judgement, please rate the perceived susceptibility of the structure to experience significant damage due to progressive collapse mechanisms.	(1 - 5)
9B	Based on the information available about past performance to historical earthquakes, as well as the evidence on the structure in terms of damage, please rate how concerning is the perceived vulnerability of the structure to earthquakes.	(1 - 5)
10B	Based on available historical information, damage inspections, and reasonable engineering judgement, please rate how concerning is the perceived vulnerability of the structure to other potential catastrophic events.	(1 - 5)

Table A.4.2: Description of the significance of the different values that can be attributed to each specific question related to additional geometry and damage surveys.

Question ref.	Range description
39, 40, 41, 42	0: No additional surveys, inspections or tests; 1: A minuscule fraction; 2: A tiny fraction; 3: A small fraction; 4: A substantial fraction; 5: All of the relevant areas
2, 3, 8, 9B, 10B	See Table A.1.2

A.5. Specific questions after additional diagnosis activities for the assessment of material quality

Table A.5.1: Questions that need to be answered to update indicators of level of knowledge and damage vulnerability after carrying out activities involving the assessment of material quality.

Question ref.	Question	Answer range
<i>Boreoscope inspections and/or excavation pits</i>		
43A	What proportion of the possible areas of interest have been covered by the current and previous investigations?	(0 - 5)
43B	How would you rate the overall integrity and quality of the masonry material based on the investigations?	(1 - 5)
<i>Sonic pulse velocity testing (including tomography)</i>		
44A	What proportion of the possible areas of interest have been covered by the current and previous investigations?	(0 - 5)
44B	How would you rate the overall integrity and quality of the masonry material based on the outcome of the pulse velocity tests?	(1 - 5)
<i>Ultrasonic pulse velocity testing</i>		
45A	What proportion of the possible areas of interest have been covered by the current and previous investigations?	(0 - 5)
45B	How would you rate the overall integrity and quality of the masonry material based on the outcome of the pulse velocity tests?	(1 - 5)
<i>Surface penetrating radar testing</i>		
46A	What proportion of the possible areas of interest have been covered by the current and previous investigations?	(0 - 5)
46B	How would you rate the overall integrity and quality of the masonry material based on the outcome of the radar tests?	(1 - 5)
<i>Infrared thermography</i>		
47A	What proportion of the possible areas of interest have been covered by the current and previous investigations?	(0 - 5)
47B	How would you rate the overall integrity and quality of the masonry material based on the outcome of the thermography tests?	(1 - 5)
<i>Rebound hammer</i>		
48A	What proportion of the possible areas of interest have been covered by the current and previous investigations?	(0 - 5)
48B	How would you rate the overall integrity and quality of the masonry material based on the outcome of the rebound tests?	(1 - 5)
<i>Other specific tests for evaluating material quality and condition</i>		
49A	What proportion of the possible areas of interest have been covered by the current and previous investigations?	(0 - 5)
49B	How would you rate the overall integrity and quality of the masonry material based on the outcome of the tests?	(1 - 5)

Table A.5.2: Description of the significance of the different values that can be attributed to each specific question related to the assessment of material quality.

Question ref.	Range description
43A, 44A, 45A, 46A, 47A, 48A, 49A	0: No tests; 1: A minuscule fraction; 2: A tiny fraction; 3: A small fraction; 4: A substantial fraction; 5: All or most of the relevant areas
43B, 44B, 45B, 46B, 47B, 48B, 49B	1: Very poor quality, large variability; 2: Poor quality ; 3: Moderate quality; 4: High quality; 5: Very high quality, very uniform material

A.6. Specific questions after in-situ tests of actual loading and boundary conditions

Table A.6.1: Questions that need to be answered to update indicators of level of knowledge and damage vulnerability after carrying out in-situ tests of actual loading and boundary conditions.

Question ref.	Question	Answer range
<i>Flatjack in-situ tests of stress levels</i>		
50A	What proportion of the possible areas of interest have been covered by the current and previous investigations?	(0 - 5)
50B	Are there many areas with concerning high stress levels?	(1 - 5)
<i>Ambient vibration tests</i>		
51A	What proportion of the dynamic parameters of interest have been covered by the current and previous investigations?	(0 - 5)
51B	Are there signs that parts of the structure could be vulnerable to foreseeable loading conditions?	(1 - 5)
<i>Geotechnical surveys</i>		
52A	What proportion of investigations required for a comprehensive characterisation of the soil-structure interaction effects have been carried out?	(0 - 5)
52B	Are there signs of possible active mechanisms or specific vulnerabilities related to soil-structure interaction or to site effects?	(1 - 5)
<i>Other specific tests</i>		
53A	What proportion of identified parameters of interest have been covered by the current and previous investigations?	(0 - 5)
53B	Are there signs that parts of the structure could be vulnerable to foreseeable loading conditions?	(1 - 5)

Table A.6.2: Description of the significance of the different values that can be attributed to each specific question related to in-situ tests of actual loading and boundary conditions.

Question ref.	Range description
50A, 51A, 52A, 53A	0: No tests; 1: A minuscule fraction; 2: A tiny fraction; 3: A small fraction; 4: A substantial fraction; 5: All or most of the relevant areas
50B, 51B, 52B, 53B	1: None; 2: A few potential indications; 3: Several potential indications / At least one definitive indication; 4: Some definitive indications; 5: Several definitive indications

B

Answers to questions for case studies

B.1. Mallorca cathedral

B.1.1. Standardised Initial Expert Appraisal (SIEA)

Table B.1.1: Answers to questions in the first part of the SIEA for Mallorca cathedral (1).

Question ref.	Question	Answer range	Answer for Mallorca	Comments
<i>Historical information and documentation (level of knowledge)</i>				
1	Please rate the quality and comprehensiveness of information available on the following topics:			
1A	The construction process.	(0 - 5)	4.5	
1B	Historical structural alterations.	(0 - 5)	4	Extensive historical research (Domenge and many others)
1C	Past structural interventions.	(0 - 5)	4.5	
1D	Past damage events (Fires, earthquakes, destructive events).	(0 - 5)	4	
<i>Geometry & damage surveys (level of knowledge)</i>				
2	Please rate the quality and quantity of information available on the geometry of the structure.	(0 - 5)	2.5	Historical masterplan drawings
3	Please rate the accuracy and comprehensiveness of information available for damage analysis.	(0 - 5)	3	Documents from Herráez & Domenge
<i>Initial material quality (level of knowledge and damage vulnerability)</i>				
4A	Please rate the level of accessibility to all the different materials of the structural system during visual inspections?	(0 - 5)	2	Complex structure
4B	How would you rate the overall integrity and quality of the masonry material based on visual inspections?	(1-5)	3	Masonry mostly of very good quality, particularly for important structural elements.
<i>Exposure</i>				
5A	Please rate the level of exposure in terms of the cultural value that the structure represents.	(1-5)	4	Very important structure; Protected cultural site of national interest (BCIN). Many tourists; Emblematic monument of Mallorca.
5B	Please rate the level of exposure in terms of usage and potential loss.	(1-5)	4	
<i>Lack of maintenance (damage vulnerability)</i>				
6A	How would you describe the state of maintenance of the structure?	(1-5)	3	
6B	Please rate the suitability of the current maintenance plan to address visible pathologies.	(1-5)	4	

Table B.1.2: Answers to questions in the first part of the SIEA for Mallorca cathedral (2).

Question ref.	Question	Answer range	Answer for Mallorca	Comments
<i>Need for urgent action (damage vulnerability)</i>				
7A	Are there clear signs that urgent action is required to stabilise the structure?	0 or 1	0	
7B	How much of the structure is likely to be affected if no urgent action is taken	(1-5)	NA	
<i>Progressive collapse mechanisms (damage vulnerability)</i>				
8	Based on available historical information, damage inspections, and reasonable engineering judgement, please rate the perceived susceptibility of the structure to experience significant damage due to progressive collapse mechanisms.	(1-5)	3	Deformed shape of columns, arches, and vaults. Vertical cracks at the base of some columns.
<i>Earthquakes (hazard and damage vulnerability)</i>				
9A	What is the peak ground acceleration with a 10% probability of exceedance in 50 years? [m/s^2]	$\geq 0 m/s^2$ (1-5)	$0.4 m/s^2$ (1.9)	
9B	Based on the information available about past performance to historical earthquakes, as well as the evidence on the structure in terms of damage, please rate how concerning is the perceived vulnerability of the structure to earthquakes.	(1-5)	2.5	Has survived moderate intensity earthquakes in the past, with some parts rebuilt or strengthened after some of them.
<i>Other catastrophic events (hazard and damage vulnerability)</i>				
10A	Please rate the hazard of other catastrophic events in terms of their potential intensity and frequency of occurrence?	(1-5)	1	Not in a zone historically affected by high intensity hurricanes and cyclones; No landslides.
10B	Based on available historical information, damage inspections, and reasonable engineering judgement, please rate how concerning is the perceived vulnerability of the structure to other potential catastrophic events.	(1-5)	1	Most expected hazards such as storms are not likely to cause more damage than a moderate intensity earthquake.
<i>Fire hazard</i>				
11	Please rate the fire hazard in terms of possible sources of ignition, available fuel and potential for fire to spread.	(1-5)	2	Rating given mainly due to presence of flammable wooden elements.

Table B.1.3: Ratings given in the second part of the SIEA for Mallorca cathedral (1).

Question ref.	Question	Answer range	Answer for Mallorca	Comments
<i>Ranking the importance of vulnerability to specific hazards for global vulnerability assessment</i>				
12A	Should earthquakes be included in the vulnerability assessment?	0 or 1	1	
12B	Should other catastrophic events be included in the vulnerability assessment?	0 or 1	0	Low hazard.
12C	Please rank the following possible 3 aims of structural analysis according to their importance for global damage vulnerability characterisation:			
12C(i)	Structural analysis aimed at better understanding vulnerability to progressive collapse mechanisms	1,2 or 3	1	
12C(ii)	Structural analysis aimed at better understanding vulnerability to earthquakes	1,2 or 3	2	
12C(iii)	Structural analysis aimed at better understanding vulnerability to other identified catastrophic events	1,2 or 3	NA	
<i>Structural analysis and structural health monitoring - Progressive collapse mechanisms</i>				
13	Please rate to what extent information from the following diagnosis activities can help assess the structure's vulnerability to progressive collapse mechanisms.			
13A	Load report	0,1 or 2	1	
13B	Graphic statics & Limit analysis	0,1 or 2	2	
13C	FEM	0,1 or 2	2	
13D	Dynamic SHM	0,1 or 2	1	
13E	Static SHM	0,1 or 2	2	
<i>Structural analysis and structural health monitoring - Earthquakes</i>				
14	Please rate to what extent information from the following diagnosis activities can help assess the structure's vulnerability to earthquakes			
14A	Graphic statics & Limit analysis	0,1 or 2	1	
14B	FEM	0,1 or 2	2	
14C	Dynamic SHM	0,1 or 2	2	
14D	Static SHM	0,1 or 2	1	

Table B.1.4: Ratings given in the second part of the SIEA for Mallorca cathedral (2).

Question ref.	Question	Answer range	Answer for Mallorca	Comments
<i>Structural analysis and structural health monitoring - Other catastrophic events</i>				
15	Please rate to what extent information from the following diagnosis activities can help assess the structure's vulnerability to other catastrophic events			
15A	Graphic statics & Limit analysis	0,1 or 2	NA	
15B	FEM	0,1 or 2	NA	
15C	Dynamic SHM	0,1 or 2	NA	
15D	Static SHM	0,1 or 2	NA	
<i>Material properties</i>				
16	Please rate to what extent information from the following activities can help assess the structure's damage vulnerability			
16A	Experimental characterisation of compressive strengths of constituents	0,1 or 2	1	
16B	Experimental characterisation of compressive strength of masonry	0,1 or 2	2	
16C	Experimental characterisation of shear load-bearing capacity of masonry	0,1 or 2	2	
16D	Experimental characterisation of elastic moduli of constituents	0,1 or 2	1	
16E	Experimental characterisation of elastic modulus of masonry	0,1 or 2	1	
16F	Experimental characterisation of chemical composition and/or other specific material properties	0,1 or 2	1	
<i>Additional geometry and damage mapping activities</i>				
17	Please rate to what extent the following activities can help improve the level of knowledge on the existing geometry and damage			
17A	Topographic surveys (including laser scanning, photogrammetry, or equivalent)	0,1 or 2	2	
17B	Borescopic inspections and/or excavation pits	0,1 or 2	0	
17C	Impact-echo testing	0,1 or 2	0	
17D	More accurate or extensive survey of damages	0,1 or 2	2	

Table B.1.5: Ratings given in the second part of the SIEA for Mallorca cathedral (3).

Question ref.	Question	Answer range	Answer for Mallorca	Comments
<i>Additional diagnostic activities for assessment of material quality (MDT/NDT)</i>				
18	Please rate to what extent the following activities can help to assess the material quality			
18A	Borescopic inspections and/or excavation pits	0,1 or 2	1	
18B	Sonic pulse velocity testing (including tomography)	0,1 or 2	2	
18C	Ultrasonic pulse velocity testing	0,1 or 2	0	
18D	Surface penetrating radar testing	0,1 or 2	2	
18E	Infrared thermography	0,1 or 2	1	
18F	Rebound hammer	0,1 or 2	0	
18G	Other specific tests for evaluating material quality and condition	0,1 or 2	0	
<i>In-situ evaluation of actual loading and boundary conditions</i>				
19	Please rate to what extent information from the following activities can help assess the structure's damage vulnerability			
19A	Flatjack in-situ tests of stress levels	0,1 or 2	1	
19B	Ambient vibration tests	0,1 or 2	2	
19C	Geotechnical surveys	0,1 or 2	2	
19D	Other specific tests	0,1 or 2	1	

B.1.2. Answers to questions at final “knowledge state”

Table B.1.6: Answers to questions on structural analysis for Mallorca cathedral.

Question ref.	Question	Answer range	Answer for Mallorca	Comments
<i>Load report</i>				
20A	How much of the loads needed for a comprehensive evaluation were calculated?	(0 - 5)	4.75	
20B	Are there areas with concerning high loading levels?	(1 - 5)	3	
<i>Graphic statics and limit analysis</i>				
21A, 25A*,29A†	What proportion of identified cases of interest were evaluated?	(0 - 5)	4.5, 3.5*	Graphic static analyses to evaluate stability of a transverse bays (Rubio, Maynou); *Kinematic analyses to evaluate seismic capacity of expected mechanisms (Coutinho)
21B, 25B*,29B†	Are there potential cases with a precarious equilibrium?	(1 - 5)	2, 2.5*	Further damage due to slow progressive mechanisms not likely (transverse direction); *Most mechanisms verify for expected demand but capacity is lowest in longitudinal direction; *Most critical mechanisms related to outward rotation of façade
<i>Finite element modelling</i>				
22A, 26A*,30A†	What proportion of identified loading scenarios of interest were investigated?	(0 - 5)	4.5, 4*	FEM with creep behaviour of masonry; *Non-linear dynamic FEM (Roca, Pelà, Elyamani, Clemente)
22B, 26B*,30B†	Do the simulations reveal that parts of the structure could be vulnerable to foreseeable loading conditions?	(1 - 5)	2, 2.5*	Further damage due to gradual mechanisms not likely (transverse direction); *Capacity adequate for expected demand but capacity lower in longitudinal direction

* Structural analysis aimed at better understanding vulnerability to earthquakes.

† Structural analysis aimed at better understanding vulnerability to other catastrophic events.

Table B.1.7: Answers to questions on SHM for Mallorca cathedral.

Question ref.	Question	Answer range	Answer for Mallorca	Comments
<i>Dynamic structural health monitoring</i>				
23A, 27A*,31A†	What proportion of dynamic parameters of interest have been monitored?	(0 - 5)	3, 4*	Two dynamic monitoring campaigns: 2005 & 2010 (1.36 years of useful data from 2010 monitoring) (Roca, Elyamani, Caselles)
23B, 27B*,31B†	Is the monitoring duration suitable to observe the phenomena of interest?	(0 - 5)	3, 3*	
23C, 27C*,31C†	Are there signs that parts of the structure could be vulnerable to foreseeable loading conditions?	(1 - 5)	3, 3*	During a far epicentre earthquake in 2005, building experienced excitation of fundamental frequency with greatest amplitudes in longitudinal direction
<i>Static structural health monitoring</i>				
24A, 28A*,32A†	What proportion of parameters of interest have been monitored?	(0 - 5)	3, 1*	Static SHM data collected over a period of 5 years from 2003 to 2008.
24B*†	How many years of monitoring data are available to date?	≥ 0 years (0 - 5)	3.5 yrs (2.0)	
24C*†	What percentage of sensors are classified as evolutionary?	$\geq 0\%$ (1 - 5)	8% (2.14)	
24D*†	What is the yearly average growth rate of all monitored crack widths classified as apparently evolutionary or evolutionary? [mm]	≥ 0 mm (0 - 5)	0.034 mm (2.76)	
24E*†	What is the yearly average growth rate of all monitored distances classified as apparently evolutionary or evolutionary? [mm]	≥ 0 mm (0 - 5)	0.073 mm (1.74)	
24F*†	What is the yearly average growth rate of all monitored inclinations classified as apparently evolutionary or evolutionary? [$^{\circ}$]	$\geq 0^{\circ}$ (0 - 5)	0.019 $^{\circ}$ (2.5)	

* Structural analysis aimed at better understanding vulnerability to earthquakes.

† Structural analysis aimed at better understanding vulnerability to other catastrophic events.

Table B.1.8: Answers to questions on the estimation of material properties for Mallorca cathedral.

Question ref.	Question	Answer range	Answer for Mallorca	Comments
<i>Experimental characterisation of elastic modulus of masonry</i>				
37A	How would you rate the overall confidence level of the estimated moduli?	(0 - 5)	2	
37B	What proportion of the areas of interest have been covered by the current and previous investigations?	(0 - 5)	4	
37C	Are there potential stiffness estimates indicating material degradation?	(1 - 5)	2	Estimated by calibrating FEM models using results of AVT (Roca)
<i>Experimental characterisation of composition and/or other specific properties</i>				
38A	How would you rate the overall confidence level of the estimated properties?	(0 - 5)	4	Chemical composition analysis by microscopy and diffractometry on samples from different parts of the structure
38B	What proportion of the areas of interest have been covered by the current and previous investigations?	(0 - 5)	4	(Vendrell); Allowed identification of different masonry types corresponding to different construction stages.
38C	Do some of the estimated properties suggest an increased vulnerability of the material to degradation or damage?	(1 - 5)	1	

Table B.1.9: Answers to questions on additional geometry and damage surveys for Mallorca cathedral.

Question ref.	Question	Answer range	Answer for Mallorca	Comments
<i>Topographic surveys</i>				
39	What proportion of the possible areas of interest have been covered by the current and previous topographic surveys?	(0 - 5)	4.5	Photogrammetry of the entire structure.
2	Please update the global rating of the level of knowledge on the geometry of the structure	(0 - 5)	4.5	
<i>More accurate or extensive survey of damages</i>				
42	What proportion of the possible areas of interest have been covered by the current and previous investigations?	(0 - 5)	4	Inspection and reports (Roca & IPCE).
3	Please update the global rating of the level of knowledge on existing damages	(0 - 5)	4	
<i>Option to update initial damage vulnerability assessment</i>				
8	Based on available historical information, damage inspections, and reasonable engineering judgement, please rate the perceived susceptibility of the structure to experience significant damage due to progressive collapse mechanisms.	(1 - 5)	-	
9B	Based on the information available about past performance to historical earthquakes, as well as the evidence on the structure in terms of damage, please rate how concerning is the perceived vulnerability of the structure to earthquakes.	(1 - 5)	-	
10B	Based on available historical information, damage inspections, and reasonable engineering judgement, please rate how concerning is the perceived vulnerability of the structure to other potential catastrophic events.	(1 - 5)	-	

Table B.1.10: Answers to questions on the assessment of material quality for Mallorca cathedral.

Question ref.	Question	Answer range	Answer for Mallorca	Comments
<i>Borescope inspections and/or excavation pits</i>				
43A	What proportion of the possible areas of interest have been covered by the current and previous investigations?	(0 - 5)	1	Pits in the roof; Core to reveal inner composition of buttress (Roca).
43B	How would you rate the overall integrity and quality of the masonry material based on the investigations?	(1 - 5)	3	Light infill above vaults removed and replaced by system of masonry walls and pottery; Inner material of buttresses is a poor and easily workable limestone.
<i>Sonic pulse velocity testing (including tomography)</i>				
44A	What proportion of the possible areas of interest have been covered by the current and previous investigations?	(0 - 5)	3.5	Seismic tomography of columns (Roca, Clapes, Caselles)
44B	How would you rate the overall integrity and quality of the masonry material based on the outcome of the pulse velocity tests?	(1 - 5)	4	Columns are solid.
<i>Surface penetrating radar testing</i>				
46A	What proportion of the possible areas of interest have been covered by the current and previous investigations?	(0 - 5)	4	Extensive study of walls and buttresses (Roca, Clapes, Caselles).
46B	How would you rate the overall integrity and quality of the masonry material based on the outcome of the radar tests?	(1 - 5)	4	Revealed inner filling and thin joints of outer layer of buttresses; Revealed solid nature of clerestory walls.
<i>Infrared thermography</i>				
47A	What proportion of the possible areas of interest have been covered by the current and previous investigations?	(0 - 5)	4	Thermography monitoring (14 days in winter, 16 days in summer) with a large coverage (Elyamani)
47B	How would you rate the overall integrity and quality of the masonry material based on the outcome of the thermography tests?	(1 - 5)	3	Evidence of some thermal inertia in summer.

Table B.1.11: Answers to questions on in-situ tests of actual loading and boundary conditions for Mallorca cathedral.

Question ref.	Question	Answer range	Answer for Mallorca	Comments
<i>Ambient vibration tests</i>				
51A	What proportion of the dynamic parameters of interest have been covered by the current and previous investigations?	(0 - 5)	4	Several tests able to identify global resonant modes (Roca, Elyamani, Caselles)
51B	Are there signs that parts of the structure could be vulnerable to foreseeable loading conditions?	(1 - 5)	2	AVTs were mainly designed to calibrate numerical models. No clear signs of vulnerability identified.
<i>Geotechnical surveys</i>				
52A	What proportion of investigations required for a comprehensive characterisation of the soil-structure interaction effects have been carried out?	(0 - 5)	4	Extensive geophysical investigations (Clapes, Caselles, Roca)
52B	Are there signs of possible active mechanisms or specific vulnerabilities related to soil-structure interaction or to site effects?	(1 - 5)	1.5	Almost all foundations rest on rock except a small part.
<i>Other specific tests</i>				
53A	What proportion of identified parameters of interest have been covered by the current and previous investigations?	(0 - 5)	1	Hole drilling to evaluate stress levels (Roca).
53B	Are there signs that parts of the structure could be vulnerable to foreseeable loading conditions?	(1 - 5)	2	

B.2. Sant Cugat monastery

Table B.2.1: Answers to questions in the first part of the SIEA for the church of Sant Cugat monastery (1).

Question ref.	Question	Answer range	Answer for Sant Cugat	Comments
<i>Historical information and documentation (level of knowledge)</i>				
1	Please rate the quality and comprehensiveness of information available on the following topics:			
1A	The construction process.	(0 - 5)	4.5	Extensive historical research.
1B	Historical structural alterations.	(0 - 5)	4.5	
1C	Past structural interventions.	(0 - 5)	4	
1D	Past damage events (Fires, earthquakes, destructive events).	(0 - 5)	4	
<i>Geometry & damage surveys (level of knowledge)</i>				
2	Please rate the quality and quantity of information available on the geometry of the structure.	(0 - 5)	3.5	Master plan drawings (2000); Use of laser scanner to measure inclination of bell tower and southern façade.
3	Please rate the accuracy and comprehensiveness of information available for damage analysis.	(0 - 5)	3.5	Mapping of most major cracks and main pathologies available; Some areas can be difficult to access to inspect regularly.
<i>Initial material quality (level of knowledge and damage vulnerability)</i>				
4A	Please rate the level of accessibility to all the different materials of the structural system during visual inspections?	(0 - 5)	2	Complex structure; Different parts built over different periods; Uncertainties on inner composition of structural elements.
4B	How would you rate the overall integrity and quality of the masonry material based on visual inspections?	(1-5)	3	Masonry quality can vary.
<i>Exposure</i>				
5A	Please rate the level of exposure in terms of the cultural value that the structure represents.	(1-5)	3.5	Protected cultural site of national interest (BCIN).
5B	Please rate the level of exposure in terms of usage and potential loss.	(1-5)	3.5	Many tourists; Valuable art; Important monastery in Catalunya.
<i>Lack of maintenance (damage vulnerability)</i>				
6A	How would you describe the state of maintenance of the structure?	(1-5)	3	
6B	Please rate the suitability of the current maintenance plan to address visible pathologies.	(1-5)	4	

Table B.2.2: Answers to questions in the first part of the SIEA for the church of Sant Cugat monastery (2).

Question ref.	Question	Answer range	Answer for Sant Cugat	Comments
<i>Need for urgent action (damage vulnerability)</i>				
7A	Are there clear signs that urgent action is required to stabilise the structure?	0 or 1	0	
7B	How much of the structure is likely to be affected if no urgent action is taken	(1-5)	NA	
<i>Progressive collapse mechanisms (damage vulnerability)</i>				
8	Based on available historical information, damage inspections, and reasonable engineering judgement, please rate the perceived susceptibility of the structure to experience significant damage due to progressive collapse mechanisms.	(1-5)	2	Problems with southern façade in the past; Could have been partly addressed by intervention in 1995-1996 (SAPIC, 1996).
<i>Earthquakes (hazard and damage vulnerability)</i>				
9A	What is the peak ground acceleration with a 10% probability of exceedance in 50 years? [m/s^2]	$\geq 0 m/s^2$ (1-5)	$0.4 m/s^2$ (1.9)	
9B	Based on the information available about past performance to historical earthquakes, as well as the evidence on the structure in terms of damage, please rate how concerning is the perceived vulnerability of the structure to earthquakes.	(1-5)	2.5	No documentary evidence of significant damages due to earthquakes; Several earthquakes are known to have struck Catalonia between 1427 and 1429.
<i>Other catastrophic events (hazard and damage vulnerability)</i>				
10A	Please rate the hazard of other catastrophic events in terms of their potential intensity and frequency of occurrence?	(1-5)	1	Not in a zone historically affected by high intensity hurricanes and cyclones; No landslides.
10B	Based on available historical information, damage inspections, and reasonable engineering judgement, please rate how concerning is the perceived vulnerability of the structure to other potential catastrophic events.	(1-5)	1	Most expected hazards such as storms are not likely to cause more damage than a moderate intensity earthquake.
<i>Fire hazard</i>				
11	Please rate the fire hazard in terms of possible sources of ignition, available fuel and potential for fire to spread.	(1-5)	2	

Table B.2.3: Ratings given in the second part of the SIEA for the church of Sant Cugat monastery (1).

Question ref.	Question	Answer range	Answer for Sant Cugat	Comments
<i>Ranking the importance of vulnerability to specific hazards for global vulnerability assessment</i>				
12A	Should earthquakes be included in the vulnerability assessment?	0 or 1	1	
12B	Should other catastrophic events be included in the vulnerability assessment?	0 or 1	0	Low hazard.
12C	Please rank the following possible 3 aims of structural analysis according to their importance for global damage vulnerability characterisation:			
12C(i)	Structural analysis aimed at better understanding vulnerability to progressive collapse mechanisms	1,2 or 3	1	
12C(ii)	Structural analysis aimed at better understanding vulnerability to earthquakes	1,2 or 3	2	
12C(iii)	Structural analysis aimed at better understanding vulnerability to other identified catastrophic events	1,2 or 3	NA	
<i>Structural analysis and structural health monitoring - Progressive collapse mechanisms</i>				
13	Please rate to what extent information from the following diagnosis activities can help assess the structure's vulnerability to progressive collapse mechanisms.			
13A	Load report	0,1 or 2	1	
13B	Graphic statics & Limit analysis	0,1 or 2	2	
13C	FEM	0,1 or 2	2	
13D	Dynamic SHM	0,1 or 2	1	
13E	Static SHM	0,1 or 2	2	
<i>Structural analysis and structural health monitoring - Earthquakes</i>				
14	Please rate to what extent information from the following diagnosis activities can help assess the structure's vulnerability to earthquakes			
14A	Graphic statics & Limit analysis	0,1 or 2	1	
14B	FEM	0,1 or 2	2	
14C	Dynamic SHM	0,1 or 2	2	
14D	Static SHM	0,1 or 2	1	

Table B.2.4: Ratings given in the second part of the SIEA for the church of Sant Cugat monastery (2).

Question ref.	Question	Answer range	Answer for Sant Cugat	Comments
<i>Structural analysis and structural health monitoring - Other catastrophic events</i>				
15	Please rate to what extent information from the following diagnosis activities can help assess the structure's vulnerability to other catastrophic events			
15A	Graphic statics & Limit analysis	0,1 or 2	NA	
15B	FEM	0,1 or 2	NA	
15C	Dynamic SHM	0,1 or 2	NA	
15D	Static SHM	0,1 or 2	NA	
<i>Material properties</i>				
16	Please rate to what extent information from the following activities can help assess the structure's damage vulnerability			
16A	Experimental characterisation of compressive strengths of constituents	0,1 or 2	1	
16B	Experimental characterisation of compressive strength of masonry	0,1 or 2	2	
16C	Experimental characterisation of shear load-bearing capacity of masonry	0,1 or 2	2	
16D	Experimental characterisation of elastic moduli of constituents	0,1 or 2	1	
16E	Experimental characterisation of elastic modulus of masonry	0,1 or 2	1	
16F	Experimental characterisation of chemical composition and/or other specific material properties	0,1 or 2	1	
<i>Additional geometry and damage mapping activities</i>				
17	Please rate to what extent the following activities can help improve the level of knowledge on the existing geometry and damage			
17A	Topographic surveys (including laser scanning, photogrammetry, or equivalent)	0,1 or 2	2	Measuring the inclination of pillars could be relevant.
17B	Borescopic inspections and/or excavation pits	0,1 or 2	2	Investigations on the foundations of the bell tower.
17C	Impact-echo testing	0,1 or 2	0	
17D	More accurate or extensive survey of damages	0,1 or 2	0	

Table B.2.5: Ratings given in the second part of the SIEA for the church of Sant Cugat monastery (3).

Question ref.	Question	Answer range	Answer for Sant Cugat	Comments
<i>Additional diagnostic activities for assessment of material quality (MDT/NDT)</i>				
18	Please rate to what extent the following activities can help to assess the material quality			
18A	Borescopic inspections and/or excavation pits	0,1 or 2	1	
18B	Sonic pulse velocity testing (including tomography)	0,1 or 2	2	
18C	Ultrasonic pulse velocity testing	0,1 or 2	0	
18D	Surface penetrating radar testing	0,1 or 2	1	
18E	Infrared thermography	0,1 or 2	1	
18F	Rebound hammer	0,1 or 2	0	
18G	Other specific tests for evaluating material quality and condition	0,1 or 2	0	
<i>In-situ evaluation of actual loading and boundary conditions</i>				
19	Please rate to what extent information from the following activities can help assess the structure's damage vulnerability			
19A	Flatjack in-situ tests of stress levels	0,1 or 2	1	
19B	Ambient vibration tests	0,1 or 2	2	Particularly bell tower.
19C	Geotechnical surveys	0,1 or 2	2	
19D	Other specific tests	0,1 or 2	1	Dynamic tests to evaluate actual tension in ties across the cimborio

Table B.2.6: Answers to questions on structural analysis for the church of Sant Cugat monastery.

Question ref.	Question	Answer range	Answer for Sant Cugat	Comments
<i>Load report</i>				
20A	How much of the loads needed for a comprehensive evaluation were calculated?	(0 - 5)	4	
20B	Are there areas with concerning high loading levels?	(1 - 5)	3	
<i>Graphic statics and limit analysis</i>				
21A, 25A*,29A†	What proportion of identified cases of interest were evaluated?	(0 - 5)	4, 3.5*	Limit analysis of a typical bay (across all four aisles & considering different scenarios for the 4th bay); *Kinimatic analysis of possible collapse mechanisms (Garcia Ramonda et al., 2015).
21B, 25B*,29B†	Are there potential cases with a precarious equilibrium?	(1 - 5)	2, 2*	Further damage due to slow progressive mechanisms not likely (transverse direction); Equilibrium of southern façade may be precarious based on some possible scenarios; *Most mechanisms verify for expected demand; *Façade most vulnerable of the scenarios considered.

* Structural analysis aimed at better understanding vulnerability to earthquakes.

† Structural analysis aimed at better understanding vulnerability to other catastrophic events.

Table B.2.7: Answers to questions on structural health monitoring for the church of Sant Cugat monastery.

Question ref.	Question	Answer range	Answer for Sant Cugat	Comments
<i>Static structural health monitoring</i>				
24A, 28A*,32A†	What proportion of parameters of interest have been monitored?	(0 - 5)	4, 2*	Data from 09/03/2017 (for most sensors) up to 28/10/2020.
24B*†	How many years of monitoring data are available to date?	≥ 0 years (0 - 5)	3.6 yrs (2.0)	
24C*†	What percentage of sensors are classified as evolutionary?	$\geq 0\%$ (1 - 5)	19% (3.37)	
24D*†	What is the yearly average growth rate of all monitored crack widths classified as apparently evolutionary or evolutionary? [mm]	≥ 0 mm (0 - 5)	0.061 mm (3.81)	
24E*†	What is the yearly average growth rate of all monitored distances classified as apparently evolutionary or evolutionary? [mm]	≥ 0 mm (0 - 5)	NA	
24F*†	What is the yearly average growth rate of all monitored inclinations classified as apparently evolutionary or evolutionary? [$^{\circ}$]	$\geq 0^{\circ}$ (0 - 5)	0.004 ^o (1.0)	

* Structural analysis aimed at better understanding vulnerability to earthquakes.

† Structural analysis aimed at better understanding vulnerability to other catastrophic events.

Table B.2.8: Answers to questions on the estimation of material properties for the church of Sant Cugat monastery.

Question ref.	Question	Answer range	Answer for Sant Cugat	Comments
<i>Experimental characterisation of composition and/or other specific properties</i>				
38A	How would you rate the overall confidence level of the estimated properties?	(0 - 5)	4	Chemical composition of materials (Vendrell).
38B	What proportion of the areas of interest have been covered by the current and previous investigations?	(0 - 5)	2	
38C	Do some of the estimated properties suggest an increased vulnerability of the material to degradation or damage?	(1 - 5)	1	

Table B.2.9: Answers to questions on additional geometry and damage surveys for the church of Sant Cugat monastery.

Question ref.	Question	Answer range	Answer for Sant Cugat	Comments
<i>Topographic surveys</i>				
39	What proportion of the possible areas of interest have been covered by the current and previous topographic surveys?	(0 - 5)	3	Use of laser scanner to measure inclination of bell tower and and southern façade.

Table B.2.10: Answers to questions on in-situ tests for the church of Sant Cugat monastery.

Question ref.	Question	Answer range	Answer for Sant Cugat	Comments
<i>Geotechnical surveys</i>				
52A	What proportion of investigations required for a comprehensive characterisation of the soil-structure interaction effects have been carried out?	(0 - 5)	2.5	Geophysical investigations (1992) - SPT; Inspection of foundations.
52B	Are there signs of possible active mechanisms or specific vulnerabilities related to soil-structure interaction or to site effects?	(1 - 5)	3	

B.3. Tower from the remains of the castle of Lloberola

Table B.3.1: Answers to questions in the first part of the SIEA for the tower from the remains of the castle of Lloberola (1).

Question ref.	Question	Answer range	Answer for Lloberola tower	Comments
<i>Historical information and documentation (level of knowledge)</i>				
1	Please rate the quality and comprehensiveness of information available on the following topics:			
1A	The construction process.	(0 - 5)	4	Substantial historical information. Knowledge of some restorations with missing documentation and incomplete information. Better information on past events could have revealed causes of important cracks.
1B	Historical structural alterations.	(0 - 5)	4	
1C	Past structural interventions.	(0 - 5)	3	
1D	Past damage events (Fires, earthquakes, destructive events).	(0 - 5)	3.5	
<i>Geometry & damage surveys (level of knowledge)</i>				
2	Please rate the quality and quantity of information available on the geometry of the structure.	(0 - 5)	4.5	Detailed geometry survey using laser scanner; Relatively simple geometrical arrangement.
3	Please rate the accuracy and comprehensiveness of information available for damage analysis.	(0 - 5)	4	Detailed photographic survey including all major cracks and some minor ones (Molins).
<i>Initial material quality (level of knowledge and damage vulnerability)</i>				
4A	Please rate the level of accessibility to all the different materials of the structural system during visual inspections?	(0 - 5)	3.5	Relatively simple geometry; All sides accessible; Multi-leaf morphology but can see interior leaf in some parts.
4B	How would you rate the overall integrity and quality of the masonry material based on visual inspections?	(1-5)	2	
<i>Exposure</i>				
5A	Please rate the level of exposure in terms of the cultural value that the structure represents.	(1-5)	3	Protected cultural site of national interest (BCIN).
5B	Please rate the level of exposure in terms of usage and potential loss.	(1-5)	1	No visitors.
<i>Lack of maintenance (damage vulnerability)</i>				
6A	How would you describe the state of maintenance of the structure?	(1-5)	2	Specific recommendations for improved maintenance (Molins).
6B	Please rate the suitability of the current maintenance plan to address visible pathologies.	(1-5)	4	

Table B.3.2: Answers to questions in the first part of the SIEA for the tower from the remains of the castle of Lloberola (2).

Question ref.	Question	Answer range	Answer for Lloberola tower	Comments
<i>Need for urgent action (damage vulnerability)</i>				
7A	Are there clear signs that urgent action is required to stabilise the structure?	0 or 1	0	Intervention in 2017 addressed the most urgent aspects well.
7B	How much of the structure is likely to be affected if no urgent action is taken	(1-5)	NA	
<i>Progressive collapse mechanisms (damage vulnerability)</i>				
8	Based on available historical information, damage inspections, and reasonable engineering judgement, please rate the perceived susceptibility of the structure to experience significant damage due to progressive collapse mechanisms.	(1-5)	4	Many significant cracks; Some parts susceptible to partial collapse; Stabilisation works of 2017 not sufficient to guarantee long-term safety.
<i>Earthquakes (hazard and damage vulnerability)</i>				
9A	What is the peak ground acceleration with a 10% probability of exceedance in 50 years? [m/s^2]	$\geq 0 m/s^2$ (1-5)	$0.5 m/s^2$ (2.2)	
9B	Based on the information available about past performance to historical earthquakes, as well as the evidence on the structure in terms of damage, please rate how concerning is the perceived vulnerability of the structure to earthquakes.	(1-5)	4.5	
<i>Other catastrophic events (hazard and damage vulnerability)</i>				
10A	Please rate the hazard of other catastrophic events in terms of their potential intensity and frequency of occurrence?	(1-5)	1	Not in a zone historically affected by high intensity hurricanes or cyclones.
10B	Based on available historical information, damage inspections, and reasonable engineering judgement, please rate how concerning is the perceived vulnerability of the structure to other potential catastrophic events.	(1-5)	2.5	Most expected hazards are not likely to cause more damage than a moderate intensity earthquake.
<i>Fire hazard</i>				
11	Please rate the fire hazard in terms of possible sources of ignition, available fuel and potential for fire to spread.	(1-5)	1	No obvious ignition sources and very few flammable materials.

Table B.3.3: Ratings given in the second part of the SIEA for the tower from the remains of the castle of Lloberola (1).

Question ref.	Question	Answer range	Answer for Lloberola tower	Comments
<i>Ranking the importance of vulnerability to specific hazards for global vulnerability assessment</i>				
12A	Should earthquakes be included in the vulnerability assessment?	0 or 1	1	
12B	Should other catastrophic events be included in the vulnerability assessment?	0 or 1	0	Low hazard.
12C	Please rank the following possible 3 aims of structural analysis according to their importance for global damage vulnerability characterisation:			
12C(i)	Structural analysis aimed at better understanding vulnerability to progressive collapse mechanisms	1,2 or 3	1	
12C(ii)	Structural analysis aimed at better understanding vulnerability to earthquakes	1,2 or 3	2	
12C(iii)	Structural analysis aimed at better understanding vulnerability to other identified catastrophic events	1,2 or 3	NA	
<i>Structural analysis and structural health monitoring - Progressive collapse mechanisms</i>				
13	Please rate to what extent information from the following diagnosis activities can help assess the structure's vulnerability to progressive collapse mechanisms.			
13A	Load report	0,1 or 2	1	Evaluation of possible stress levels.
13B	Graphic statics & Limit analysis	0,1 or 2	1	The study of some possible mechanisms could provide better insight on safety condition.
13C	FEM	0,1 or 2	2	Investigation of possible settlement scenarios that could have caused observed cracks.
13D	Dynamic SHM	0,1 or 2	1	
13E	Static SHM	0,1 or 2	2	
<i>Structural analysis and structural health monitoring - Earthquakes</i>				
14	Please rate to what extent information from the following diagnosis activities can help assess the structure's vulnerability to earthquakes			
14A	Graphic statics & Limit analysis	0,1 or 2	2	Kinematic mechanisms (triangular sections delimited by large cracks)
14B	FEM	0,1 or 2	2	Different scenarios with horizontal loads.
14C	Dynamic SHM	0,1 or 2	2	
14D	Static SHM	0,1 or 2	1	

Table B.3.4: Ratings given in the second part of the SIEA for the tower from the remains of the castle of Lloberola (2).

Question ref.	Question	Answer range	Answer for Lloberola tower	Comments
<i>Structural analysis and structural health monitoring - Other catastrophic events</i>				
15	Please rate to what extent information from the following diagnosis activities can help assess the structure's vulnerability to other catastrophic events			
15A	Graphic statics & Limit analysis	0,1 or 2	NA	
15B	FEM	0,1 or 2	NA	
15C	Dynamic SHM	0,1 or 2	NA	
15D	Static SHM	0,1 or 2	NA	
<i>Material properties</i>				
16	Please rate to what extent information from the following activities can help assess the structure's damage vulnerability			
16A	Experimental characterisation of compressive strengths of constituents	0,1 or 2	1	
16B	Experimental characterisation of compressive strength of masonry	0,1 or 2	2	
16C	Experimental characterisation of shear load-bearing capacity of masonry	0,1 or 2	2	
16D	Experimental characterisation of elastic moduli of constituents	0,1 or 2	1	Possibly useful for micro-modelling or discrete element modelling.
16E	Experimental characterisation of elastic modulus of masonry	0,1 or 2	1	Useful for macro-modelling.
16F	Experimental characterisation of chemical composition and/or other specific material properties	0,1 or 2	1	
<i>Additional geometry and damage mapping activities</i>				
17	Please rate to what extent the following activities can help improve the level of knowledge on the existing geometry and damage			
17A	Topographic surveys (including laser scanning, photogrammetry, or equivalent)	0,1 or 2	0	Near-complete information available from previous laser scan.
17B	Borescopic inspections and/or excavation pits	0,1 or 2	1	Possible investigation of masonry under stone mound; Uncertainties regarding foundations of eastern wall.
17C	Impact-echo testing	0,1 or 2	0	
17D	More accurate or extensive survey of damages	0,1 or 2	0	

Table B.3.5: Ratings given in the second part of the SIEA for the tower from the remains of the castle of Lloberola (3).

Question ref.	Question	Answer range	Answer for Lloberola tower	Comments
<i>Additional diagnostic activities for assessment of material quality (MDT/NDT)</i>				
18	Please rate to what extent the following activities can help to assess the material quality			
18A	Borescopic inspections and/or excavation pits	0,1 or 2	0	To evaluate integrity of masonry in different parts of the structure.
18B	Sonic pulse velocity testing (including tomography)	0,1 or 2	2	
18C	Ultrasonic pulse velocity testing	0,1 or 2	0	Could provide useful information on nature of rising damp phenomenon.
18D	Surface penetrating radar testing	0,1 or 2	0	
18E	Infrared thermography	0,1 or 2	1	
18F	Rebound hammer	0,1 or 2	0	
18G	Other specific tests for evaluating material quality and condition	0,1 or 2	0	
<i>In-situ evaluation of actual loading and boundary conditions</i>				
19	Please rate to what extent information from the following activities can help assess the structure's damage vulnerability			
19A	Flatjack in-situ tests of stress levels	0,1 or 2	0	Some of the most important damages have possibly been caused by differential settlements in the past.
19B	Ambient vibration tests	0,1 or 2	1	
19C	Geotechnical surveys	0,1 or 2	2	
19D	Other specific tests	0,1 or 2	0	

B.4. The church of Santa Maria de Guimerà

Table B.4.1: Answers to questions in the first part of the SIEA for the church of Santa Maria de Guimerà (1).

Question ref.	Question	Answer range	Answer for Santa Maria de Guimerà	Comments
<i>Historical information and documentation (level of knowledge)</i>				
1	Please rate the quality and comprehensiveness of information available on the following topics:			
1A	The construction process.	(0 - 5)	4.5	Substantial historical information
1B	Historical structural alterations.	(0 - 5)	4.5	
1C	Past structural interventions.	(0 - 5)	3	Evidence of restorations with limited information (uncertain if reinforced concrete cover exists over vaults)
1D	Past damage events (Fires, earthquakes, destructive events).	(0 - 5)	3	Better information on past events could have revealed causes of important cracks.
<i>Geometry & damage surveys (level of knowledge)</i>				
2	Please rate the quality and quantity of information available on the geometry of the structure.	(0 - 5)	3	Main dimensions and deformed shape.
3	Please rate the accuracy and comprehensiveness of information available for damage analysis.	(0 - 5)	4	Detailed photographic survey including all major cracks and pathologies (Molins).
<i>Initial material quality (level of knowledge and damage vulnerability)</i>				
4A	Please rate the level of accessibility to all the different materials of the structural system during visual inspections?	(0 - 5)	2.5	Complex geometry; Multi-leaf wall morphologies.
4B	How would you rate the overall integrity and quality of the masonry material based on visual inspections?	(1-5)	2	Likely to have been severely affected by water ingress and humidity during its lifetime.
<i>Exposure</i>				
5A	Please rate the level of exposure in terms of the cultural value that the structure represents.	(1-5)	2	Listed in heritage register but with no special protection status.
5B	Please rate the level of exposure in terms of usage and potential loss.	(1-5)	2	
<i>Lack of maintenance (damage vulnerability)</i>				
6A	How would you describe the state of maintenance of the structure?	(1-5)	1	Specific recommendations for improved maintenance (Molins).
6B	Please rate the suitability of the current maintenance plan to address visible pathologies.	(1-5)	4	

Table B.4.2: Answers to questions in the first part of the SIEA for the church of Santa Maria de Guimerà (2).

Question ref.	Question	Answer range	Answer for Santa Maria de Guimerà	Comments
<i>Need for urgent action (damage vulnerability)</i>				
7A	Are there clear signs that urgent action is required to stabilise the structure?	0 or 1	1	
7B	How much of the structure is likely to be affected if no urgent action is taken	(1-5)	2.5	
<i>Progressive collapse mechanisms (damage vulnerability)</i>				
8	Based on available historical information, damage inspections, and reasonable engineering judgement, please rate the perceived susceptibility of the structure to experience significant damage due to progressive collapse mechanisms.	(1-5)	3	Deformed shape of columns, arches, and vaults. Vertical cracks at the base of some columns.
<i>Earthquakes (hazard and damage vulnerability)</i>				
9A	What is the peak ground acceleration with a 10% probability of exceedance in 50 years? [m/s^2]	$\geq 0 m/s^2$ (1-5)	$0.4 m/s^2$ (1.9)	
9B	Based on the information available about past performance to historical earthquakes, as well as the evidence on the structure in terms of damage, please rate how concerning is the perceived vulnerability of the structure to earthquakes.	(1-5)	3.5	
<i>Other catastrophic events (hazard and damage vulnerability)</i>				
10A	Please rate the hazard of other catastrophic events in terms of their potential intensity and frequency of occurrence?	(1-5)	2	In a zone with a moderate landslide susceptibility. However, surrounding urban landscape and recently re-built retaining structure lower hazard at the church's location.
10B	Based on available historical information, damage inspections, and reasonable engineering judgement, please rate how concerning is the perceived vulnerability of the structure to other potential catastrophic events.	(1-5)	3.5	A landslide could cause some damage.
<i>Fire hazard</i>				
11	Please rate the fire hazard in terms of possible sources of ignition, available fuel and potential for fire to spread.	(1-5)	2.5	Some flammable (wooden) objects; Some clearly flammable objects left unsupervised in porch on southern side.

Table B.4.3: Ratings given in the second part of the SIEA for the church of Santa Maria de Guimerà (1).

Question ref.	Question	Answer range	Answer for Santa Maria de Guimerà	Comments
<i>Ranking the importance of vulnerability to specific hazards for global vulnerability assessment</i>				
12A	Should earthquakes be included in the vulnerability assessment?	0 or 1	1	
12B	Should other catastrophic events be included in the vulnerability assessment?	0 or 1	1	
12C	Please rank the following possible 3 aims of structural analysis according to their importance for global damage vulnerability characterisation:			
12C(i)	Structural analysis aimed at better understanding vulnerability to progressive collapse mechanisms	1,2 or 3	1	
12C(ii)	Structural analysis aimed at better understanding vulnerability to earthquakes	1,2 or 3	3	
12C(iii)	Structural analysis aimed at better understanding vulnerability to other identified catastrophic events	1,2 or 3	2	
<i>Structural analysis and structural health monitoring - Progressive collapse mechanisms</i>				
13	Please rate to what extent information from the following diagnosis activities can help assess the structure's vulnerability to progressive collapse mechanisms.			
13A	Load report	0,1 or 2	1	
13B	Graphic statics & Limit analysis	0,1 or 2	2	
13C	FEM	0,1 or 2	1	Many challenges foreseen for the creation of useful models given complexity of structure and boundary conditions.
13D	Dynamic SHM	0,1 or 2	1	
13E	Static SHM	0,1 or 2	2	
<i>Structural analysis and structural health monitoring - Earthquakes</i>				
14	Please rate to what extent information from the following diagnosis activities can help assess the structure's vulnerability to earthquakes			
14A	Graphic statics & Limit analysis	0,1 or 2	2	Study of possible collapse mechanisms (earthquakes). Many challenges foreseen for the creation of useful models given complexity of structure and boundary conditions.
14B	FEM	0,1 or 2	1	
14C	Dynamic SHM	0,1 or 2	2	
14D	Static SHM	0,1 or 2	2	

Table B.4.4: Ratings given in the second part of the SIEA for the church of Santa Maria de Guimerà (2).

Question ref.	Question	Answer range	Answer for Santa Maria de Guimerà	Comments
<i>Structural analysis and structural health monitoring - Other catastrophic events</i>				
15	Please rate to what extent information from the following diagnosis activities can help assess the structure's vulnerability to other catastrophic events			
15A	Graphic statics & Limit analysis	0,1 or 2	2	Study of possible collapse mechanisms (land-slides). Many challenges foreseen for the creation of useful models given complexity of structure and boundary conditions.
15B	FEM	0,1 or 2	1	
15C	Dynamic SHM	0,1 or 2	1	
15D	Static SHM	0,1 or 2	2	
<i>Material properties</i>				
16	Please rate to what extent information from the following activities can help assess the structure's damage vulnerability			
16A	Experimental characterisation of compressive strengths of constituents	0,1 or 2	1	
16B	Experimental characterisation of compressive strength of masonry	0,1 or 2	2	
16C	Experimental characterisation of shear load-bearing capacity of masonry	0,1 or 2	2	
16D	Experimental characterisation of elastic moduli of constituents	0,1 or 2	0	
16E	Experimental characterisation of elastic modulus of masonry	0,1 or 2	1	
16F	Experimental characterisation of chemical composition and/or other specific material properties	0,1 or 2	1	
<i>Additional geometry and damage mapping activities</i>				
17	Please rate to what extent the following activities can help improve the level of knowledge on the existing geometry and damage			
17A	Topographic surveys (including laser scanning, photogrammetry, or equivalent)	0,1 or 2	1	More accurate geometry surveys can help.
17B	Borescopic inspections and/or excavation pits	0,1 or 2	2	To better ascertain geometry of foundations.
17C	Impact-echo testing	0,1 or 2	0	
17D	More accurate or extensive survey of damages	0,1 or 2	1	

Table B.4.5: Ratings given in the second part of the SIEA for the church of Santa Maria de Guimerà (3).

Question ref.	Question	Answer range	Answer for Santa Maria de Guimerà	Comments
<i>Additional diagnostic activities for assessment of material quality (MDT/NDT)</i>				
18	Please rate to what extent the following activities can help to assess the material quality			
18A	Borescopic inspections and/or excavation pits	0,1 or 2	2	Verify the presence of a reinforced concrete cover above vaults; Better understand composition of some structural elements.
18B	Sonic pulse velocity testing (including tomography)	0,1 or 2	1	
18C	Ultrasonic pulse velocity testing	0,1 or 2	0	To evaluate integrity of masonry in different parts of the structure.
18D	Surface penetrating radar testing	0,1 or 2	0	
18E	Infrared thermography	0,1 or 2	0	
18F	Rebound hammer	0,1 or 2	0	
18G	Other specific tests for evaluating material quality and condition	0,1 or 2	0	
<i>In-situ evaluation of actual loading and boundary conditions</i>				
19	Please rate to what extent information from the following activities can help assess the structure's damage vulnerability			
19A	Flatjack in-situ tests of stress levels	0,1 or 2	1	Some of the most important damages may have been caused by differential settlements.
19B	Ambient vibration tests	0,1 or 2	1	
19C	Geotechnical surveys	0,1 or 2	2	
19D	Other specific tests	0,1 or 2	0	

Table B.4.6: Answers to questions on structural analysis for the church of Santa Maria de Guimerà.

Question ref.	Question	Answer range	Answer for Santa Maria de Guimerà	Comments
<i>Load report</i>				
20A	How much of the loads needed for a comprehensive evaluation were calculated?	(0 - 5)	3.5	
20B	Are there areas with concerning high loading levels?	(1 - 5)	3	
<i>Graphic statics and limit analysis</i>				
21A, 25A*, 29A†	What proportion of identified cases of interest were evaluated?	(0 - 5)	3, 0*, 0†	Graphic statics analysis of a typical section of the nave.
21B, 25B*, 29B†	Are there potential cases with a precarious equilibrium?	(1 - 5)	3.5, NA*, NA†	Analysis reveals that the thrust imposed by the vaults and arches could be slightly high.

* Structural analysis aimed at better understanding vulnerability to earthquakes.

† Structural analysis aimed at better understanding vulnerability to other catastrophic events.

C

Risk assessment summaries for case studies

C.1. Mallorca cathedral

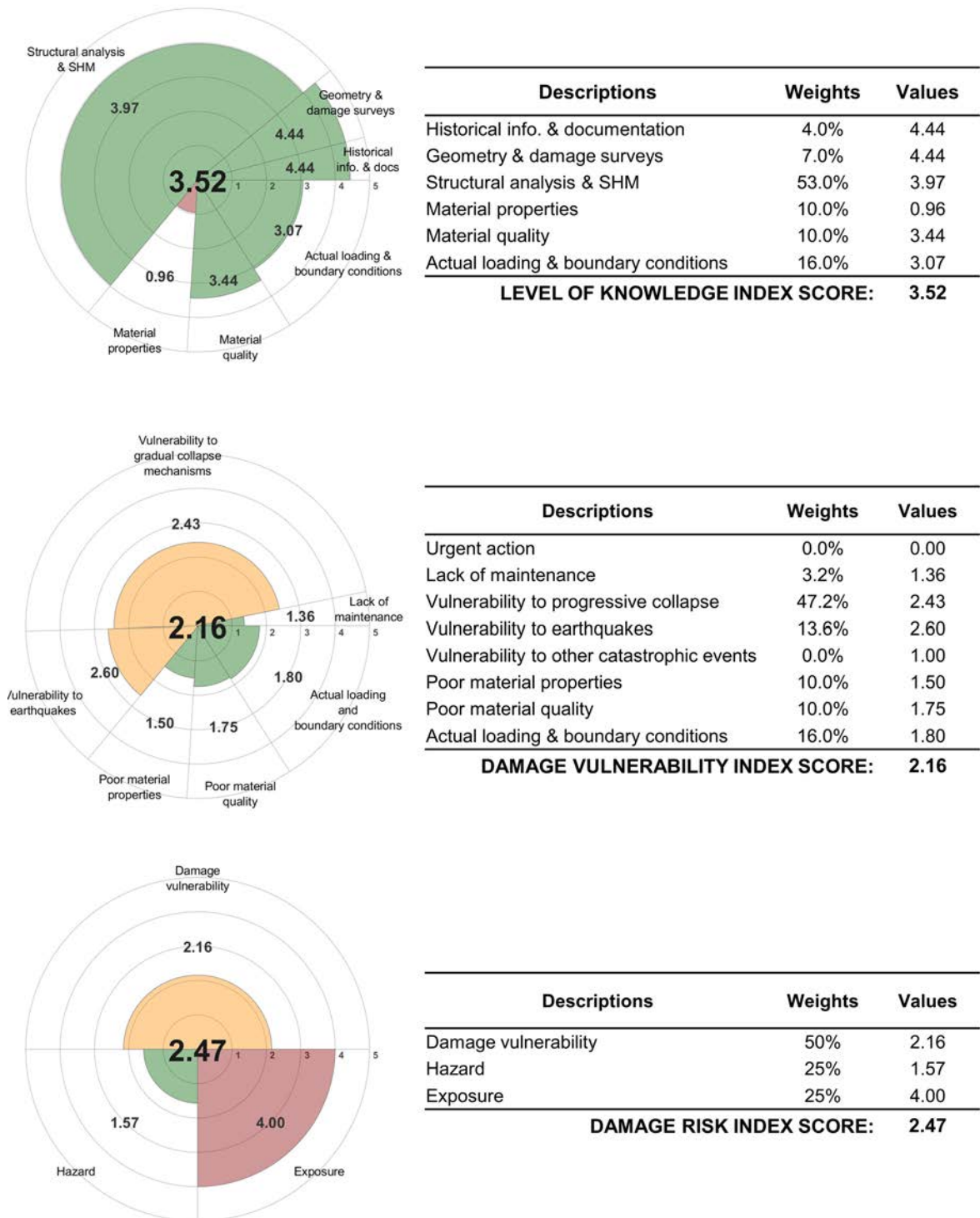


Figure C.1: RISDiMaH summary for Mallorca cathedral.

Table C.1.1: Automatically generated list of best activities to perform for Mallorca cathedral.

Activity	Category	Possible contribution to remaining LoK
Static SHM	Structural analysis & SHM	19.0%
Flatjack in-situ stress tests	Other in-situ tests	9.0%
Dynamic SHM	Structural analysis & SHM	8.6%
Compressive strength - Masonry	Material properties	8.5%
Shear capacity - Masonry	Material properties	8.5%
Other specific tests	Other in-situ tests	6.5%
Finite Element Modelling	Structural analysis & SHM	4.6%
Compressive strength - Constituents	Material properties	4.2%
Elastic modulus - Constituents	Material properties	4.2%
Graphic statics & Limit analysis	Structural analysis & SHM	4.1%
Pits/inspections	Material quality	3.3%
Ambient vibration tests	Other in-situ tests	2.7%
Geotechnical surveys	Other in-situ tests	2.7%
Sonic pulse velocity testing	Material quality	2.2%
More information on Damage	Geometry and Damage mapping	1.8%
Surface penetrating radar	Material quality	1.4%
Elastic modulus - Masonry	Material properties	1.3%
More information on Geometry	Geometry and Damage mapping	0.9%
Infrared thermography	Material quality	0.7%
Other material properties	Material properties	0.6%
Load report	Structural analysis & SHM	0.6%

C.2. Sant Cugat monastery

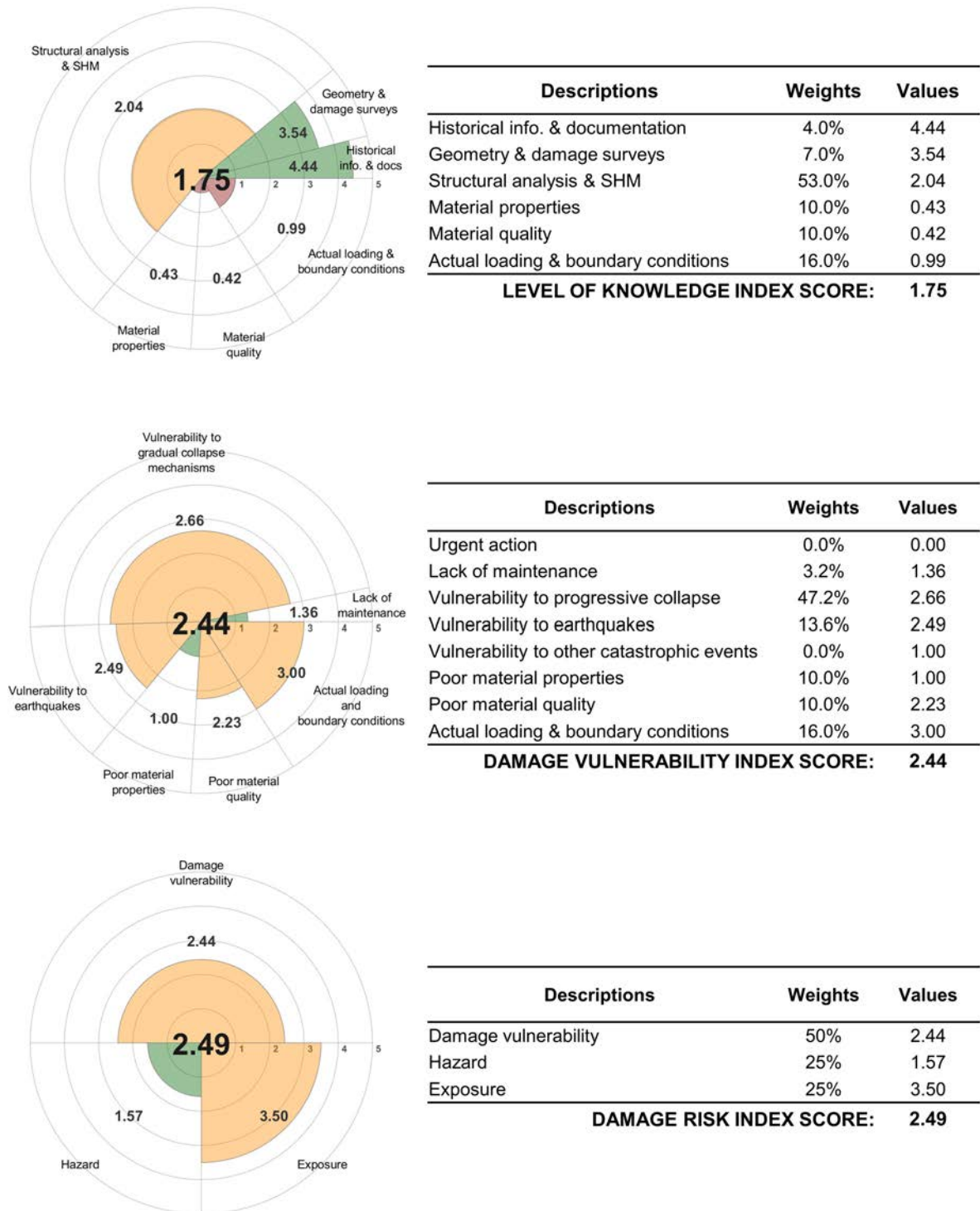
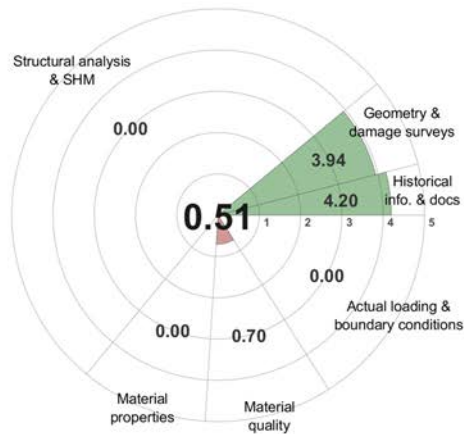


Figure C.2: RISDiMaH summary for the church of the monastery of Sant Cugat.

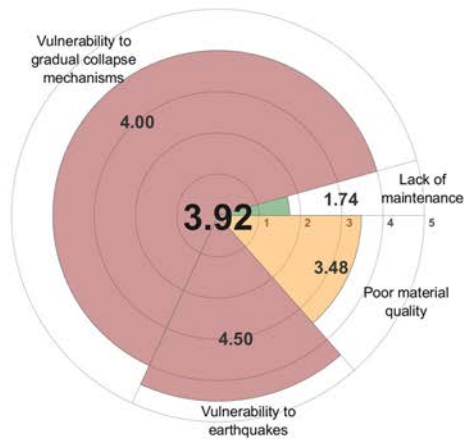
Table C.2.1: Automatically generated list of best activities to perform for the church of the monastery of Sant Cugat.

Activity	Category	Possible contribution to remaining LoK
Finite Element Modelling	Structural analysis & SHM	21.9%
Dynamic SHM	Structural analysis & SHM	14.0%
Ambient vibration tests	Other in-situ tests	8.2%
Static SHM	Structural analysis & SHM	6.8%
Sonic pulse velocity testing	Material quality	5.1%
Graphic statics & Limit analysis	Structural analysis & SHM	4.4%
Flatjack in-situ stress tests	Other in-situ tests	4.1%
Other specific tests	Other in-situ tests	4.1%
Compressive strength - Masonry	Material properties	3.8%
Shear capacity - Masonry	Material properties	3.8%
Geotechnical surveys	Other in-situ tests	3.3%
Pits/inspections	Material quality	2.6%
Surface penetrating radar	Material quality	2.6%
Infrared thermography	Material quality	2.6%
More information on Geometry	Geometry and Damage mapping	2.1%
Compressive strength - Constituents	Material properties	1.9%
Elastic modulus - Constituents	Material properties	1.9%
Elastic modulus - Masonry	Material properties	1.9%
Load report	Structural analysis & SHM	1.2%
More information on Damage	Geometry and Damage mapping	1.1%
Other material properties	Material properties	0.6%

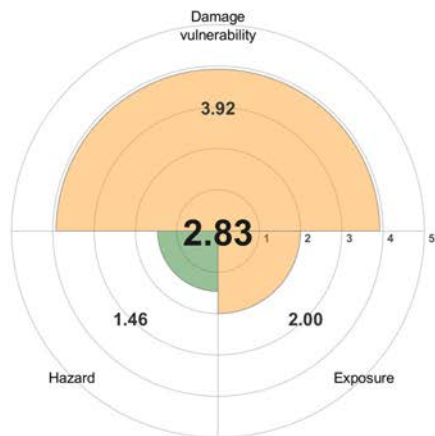
C.3. Tower from the remains of the castle of Lloberola



Descriptions	Weights	Values
Historical info. & documentation	4.0%	4.20
Geometry & damage surveys	7.0%	3.94
Structural analysis & SHM	53.0%	0.00
Material properties	10.0%	0.00
Material quality	10.0%	0.70
Actual loading & boundary conditions	16.0%	0.00
LEVEL OF KNOWLEDGE INDEX SCORE:		0.51



Descriptions	Weights	Values
Urgent action	0.0%	0.00
Lack of maintenance	4.3%	1.74
Vulnerability to progressive collapse	63.8%	4.00
Vulnerability to earthquakes	18.3%	4.50
Vulnerability to other catastrophic events	0.0%	2.50
Poor material properties	0.0%	0.00
Poor material quality	13.5%	3.48
Actual loading & boundary conditions	0.0%	0.00
DAMAGE VULNERABILITY INDEX SCORE:		3.92



Descriptions	Weights	Values
Damage vulnerability	50%	3.92
Hazard	25%	1.46
Exposure	25%	2.00
DAMAGE RISK INDEX SCORE:		2.83

Figure C.3: RISDiMaH summary for the tower of Lloberola.

Table C.3.1: Automatically generated list of best activities to perform for the tower from the remains of the castle of Lloberola.

Activity	Category	Possible contribution to remaining LoK
Finite Element Modelling	Structural analysis & SHM	16.9%
Static SHM	Structural analysis & SHM	15.0%
Geotechnical surveys	Other in-situ tests	11.9%
Graphic statics & Limit analysis	Structural analysis & SHM	10.3%
Dynamic SHM	Structural analysis & SHM	10.3%
Load report	Structural analysis & SHM	6.6%
Sonic pulse velocity testing	Material quality	6.2%
Ambient vibration tests	Other in-situ tests	5.9%
Infrared thermography	Material quality	3.1%
Compressive strength - Masonry	Material properties	2.8%
Shear capacity - Masonry	Material properties	2.8%
Compressive strength - Constituents	Material properties	1.4%
Elastic modulus - Constituents	Material properties	1.4%
Elastic modulus - Masonry	Material properties	1.4%
Other material properties	Material properties	1.4%
More information on Geometry	Geometry and Damage mapping	1.3%
More information on Damage	Geometry and Damage mapping	0.4%

C.4. The church of Santa Maria de Guimerà

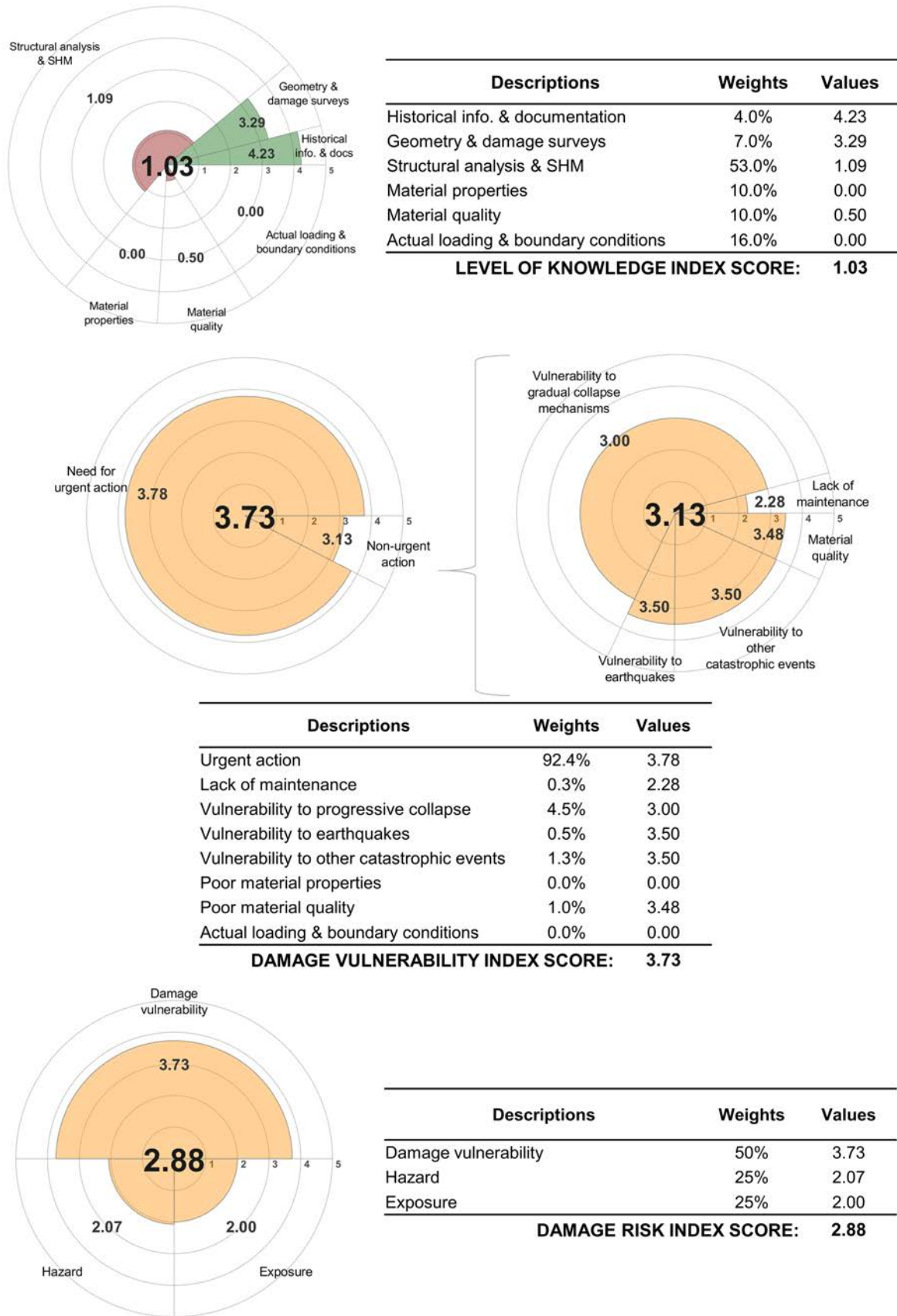


Figure C.4: RISDiMaH summary for the church of Santa Maria de Guimerà.

Table C.4.1: Automatically generated list of best activities to perform for the church of Santa Maria de Guimerà.

Activity	Category	Possible contribution to remaining LoK
Static SHM	Structural analysis & SHM	19.7%
Dynamic SHM	Structural analysis & SHM	10.6%
Graphic statics & Limit analysis	Structural analysis & SHM	10.4%
Geotechnical surveys	Other in-situ tests	10.1%
Finite Element Modelling	Structural analysis & SHM	9.9%
Pits/inspections	Material quality	7.0%
Flatjack in-situ stress tests	Other in-situ tests	5.0%
Ambient vibration tests	Other in-situ tests	5.0%
Compressive strength - Masonry	Material properties	3.6%
Shear capacity - Masonry	Material properties	3.6%
Sonic pulse velocity testing	Material quality	3.5%
More information on Geometry	Geometry and Damage mapping	2.1%
Compressive strength - Constituents	Material properties	1.8%
Elastic modulus - Masonry	Material properties	1.8%
Other material properties	Material properties	1.8%
Load report	Structural analysis & SHM	1.6%
More information on Damage	Geometry and Damage mapping	0.9%

References

- ACHENBACH, J. D., 1973. *Applied mathematics and Mechanics*. Vol. 16, Wave propagation in elastic solids. ISBN 0720403251. ISSN 00442267. Available from DOI: 10.1002/zamm.19920720607.
- AGUADO, A.; CAÑO, A. del; CRUZ, M. P. de la; GÓMEZ, D.; JOSA, A., 2012. Sustainability Assessment of Concrete Structures within the Spanish Structural Concrete Code. *Journal of Construction Engineering and Management*. Vol. 138, no. 2, pp. 268–276. ISSN 0733-9364. Available from DOI: 10.1061/(ASCE)CE.1943-7862.0000419.
- AJUNTAMENT DE SANT CUGAT, 2019a. *Informe tècnic: Comprovació de la verticalitat de la torre del campanar i la façana sud del monestir*.
- AJUNTAMENT DE SANT CUGAT (SANT CUGAT CITY COUNCIL), 2019b. *Informe tècnic: Comprovació de la verticalitat de la torre del campanar del monestir (Measurement of the inclination of the bell tower of the monastery)*.
- ALLEMANG, R. J., 2003. The modal assurance criterion - Twenty years of use and abuse. *Sound and Vibration*. Vol. 37, no. 8, pp. 14–21. ISBN 1541-0161. ISSN 15410161. Available from DOI: 10.1016/j.chemgeo.2006.02.014.
- ALONSO, J. A.; LAMATA, M. T., 2006. Consistency in the Analytic Hierarchy Process: A New Approach. *International Journal of Uncertainty, Fuzziness and Knowledge-Based Systems*. Vol. 14, no. 04, pp. 445–459. ISSN 0218-4885. Available from DOI: 10.1142/S0218488506004114.
- AMDE, A. M.; MARTIN, J. V.; COLVILLE, J., 2007. The Effects of Moisture on Compressive Strength and Modulus of Brick Masonry. In: *13th International Brick and Block Masonry Conference*. Amsterdam.
- ANDREU, A.; GIL, L.; ROCA, P., 2007. Computational Analysis of Masonry Structures with a Funicular Model. *Journal of Engineering Mechanics*. Vol. 133, no. 4, pp. 473–480. ISSN 0733-9399. Available from DOI: 10.1061/(ASCE)0733-9399(2007)133:4(473).
- ARAS, F.; ALTAY, G., 2015. Seismic evaluation and structural control of the historical Beylerbeyi Palace. *Structural Control and Health Monitoring*. Vol. 22, no. 2, pp. 347–364. ISSN 15452255. Available from DOI: 10.1002/stc.1677.
- ASMANI, M.; KERMEL, C.; LERICHE, A.; OURAK, M., 2001. Influence of porosity on Young's modulus and poisson's ratio in alumina ceramics. *Journal of the European Ceramic Society*. Vol. 21, no. 8, pp. 1081–1086. ISBN 0955-2219. ISSN 09552219. Available from DOI: 10.1016/S0955-2219(00)00314-9.
- ASTM INTERNATIONAL, 2001. *Annual Book of ASTM Standards*. C 1259 - Standard Test Method for Dynamic Young's Modulus, Shear Modulus, and Poisson's Ratio for Advanced Ceramics by Impulse Excitation of Vibration. No. January 1999.
- ASTM INTERNATIONAL, 2010. *Annual Book of ASTM Standards*. Vol. 04, C597 - Standard Test Method for Pulse Velocity Through Concrete. No. 02. ISBN 9996758001. Available from DOI: 10.1520/C0597-09.
- ASTM INTERNATIONAL, 2015. *Annual Book of ASTM Standards*. E1876 - Standard Test Method for Dynamic Young's Modulus, Shear Modulus, and Poisson's Ratio by Impulse Excitation of Vibration. Available from DOI: 10.1520/E1876-15.
- ASUERO, A. G.; SAYAGO, A.; GONZÁLEZ, A. G., 2006. The Correlation Coefficient: An Overview. *Critical Reviews in Analytical Chemistry*. Vol. 36, no. 1, pp. 41–59. ISSN 1040-8347. Available from DOI: 10.1080/10408340500526766.
- EL-ATTAR, A. G.; SALEH, A. M.; ZAGHW, A. H., 2005. Conservation of a slender historical Mamluk-style minaret by passive control techniques. *Structural Control and Health Monitoring*. Vol. 12, no. 2, pp. 157–177. ISSN 1545-2255. Available from DOI: 10.1002/stc.54.
- AUTODESK, 2017. *User's Guide: Robot Structural Analysis Professional 2017*.

- BAEZA, F.; IVORRA, S.; BRU, D.; VARONA, F., 2018. Structural Health Monitoring Systems for Smart Heritage and Infrastructures in Spain. In: OTTAVIANO, E.; PELLICCIO, A.; GATTULLI, V. (eds.). *Mechatronics for Cultural Heritage and Civil Engineering*. Springer International Publishing, Vol. 92, pp. 271–294. Intelligent Systems, Control and Automation: Science and Engineering. ISBN 978-3-319-68645-5. Available also from: <http://link.springer.com/10.1007/978-3-319-68646-2>.
- BARACCANI, S.; PALERMO, M.; AZZARA, R. M.; GASPARINI, G.; SILVESTRI, S.; TROMBETTI, T., 2017. Structural Interpretation of Data from Static and Dynamic Structural Health Monitoring of Monumental Buildings. *Key Engineering Materials*. Vol. 747, pp. 431–439. ISBN 9783035711646. ISSN 1662-9795. Available from DOI: 10.4028/www.scientific.net/KEM.747.431.
- BARACCANI, S.; SILVESTRI, S.; GASPARINI, G.; PALERMO, M.; TROMBETTI, T.; SILVESTRI, E.; LANCELLOTTA, R.; CAPRA, A., 2015. A Structural Analysis of the Modena Cathedral. *International Journal of Architectural Heritage*. Vol. 10, no. 2-3, p. 15583058.2015.1113344. ISSN 1558-3058. Available from DOI: 10.1080/15583058.2015.1113344.
- BARACCANI, S.; TROMBETTI, T.; PALERMO, M.; GASPARINI, G.; SILVESTRI, S.; DIB, A., 2014. A Methodology of Analysis for a Critique Interpretation of the Data Acquired from Monitoring Systems of Historical Buildings. In: *7th European Workshop on Structural Health Monitoring*.
- BARONIO, G.; BINDA, L.; TEDESCHI, C.; TIRABOSCHI, C., 2003. Characterisation of the materials used in the construction of the Noto Cathedral. *Construction and Building Materials*. Vol. 17, no. 8, pp. 557–571. ISSN 09500618. Available from DOI: 10.1016/j.conbuildmat.2003.08.007.
- BARONTINI, A.; MASCIOTTA, M. G.; RAMOS, L. F.; MENDES, P. A.; LOURENÇO, P. B., 2018. Application of a bio-inspired anomaly detection algorithm for unsupervised SHM of a historic masonry church. In: *10th International Masonry Conference (10th IMC)*. Milan, Italy.
- BARTOLI, G.; CHIARUGI, A.; GUSELLA, V., 1996. Monitoring Systems on Historic Buildings: The Brunelleschi Dome. *Journal of Structural Engineering*. Vol. 122, no. 6, pp. 663–673. ISSN 0733-9445. Available from DOI: 10.1061/(ASCE)0733-9445(1996)122:6(663).
- BASSOLI, E.; VINCENZI, L.; D'ALTRI, A. M.; MIRANDA, S. de; FORGHIERI, M.; CASTELLAZZI, G., 2018. Ambient vibration-based finite element model updating of an earthquake-damaged masonry tower. *Structural Control and Health Monitoring*. Vol. 25, no. 5, e2150. ISSN 15452255. Available from DOI: 10.1002/stc.2150.
- BASTGEN, K. J.; HERMANN, V., 1977. Experience made in determining the static modulus of elasticity of concrete. *Matériaux et Constructions*. Vol. 10, no. 6, pp. 357–364. ISSN 0025-5432. Available from DOI: 10.1007/BF02473733.
- BENEDETTI, D.; BENZONI, G.; PARISI, M. A., 1988. Seismic vulnerability and risk evaluation for old urban nuclei. *Earthquake Engineering & Structural Dynamics*. Vol. 16, no. 2, pp. 183–201. ISSN 00988847. Available from DOI: 10.1002/eqe.4290160203.
- BERNAT, E.; GIL, L., 2013. Aided Diagnosis of Structural Pathologies with an Expert System. *Advances in Structural Engineering*. Vol. 16, no. 2, pp. 379–393. ISSN 1369-4332. Available from DOI: 10.1260/1369-4332.16.2.379.
- BEVILACQUA, M. G.; CAROTI, G.; PIEMONTE, A.; TERRANOVA, A. A., 2018. Digital Technology and Mechatronic Systems for the Architectural 3D Metric Survey. In: *Mechatronics for Cultural Heritage and Civil Engineering*, pp. 161–180. Available from DOI: 10.1007/978-3-319-68646-2_7.
- BINDA, L.; FACCHINI, M.; MIRABELLA ROBERTI, G.; TIRABOSCHI, C., 1998. Electronic speckle interferometry for the deformation measurement in masonry testing. *Construction and Building Materials*. Vol. 12, no. 5, pp. 269–281. ISSN 09500618. Available from DOI: 10.1016/S0950-0618(98)00009-9.
- BINDA, L.; MAIERHOFER, C., 2006. Strategies for the Assessment of Historic Masonry Structures. In: *In-situ evaluation of historic wood and masonry structures (NSF/RILEM Workshop)*. Prague, pp. 37–56.
- BINDA, L.; TEDESCHI, C.; CONDOLEO, P., 2006. Characterisation of Materials Sampled From Some My S'on Temples. In: *7th International Congress on Civil Engineering*.
- BINDA, L.; TIRABOSCHI, C.; MIRABELLA ROBERTI, G.; BARONIO, G.; CARDANI, G., 1996. *Measuring masonry material properties: detailed results from an extensive experimental research Part I: Tests on masonry components. (Report 5.1 Politecnico di Milano)*.

- BINDA, L.; SAISI, A., 2009. Application of NDTs to the diagnosis of Historic Structures. In: *NDTCE' 09 Non-Destructive Testing in Civil Engineering*. Nantes, pp. 43–69. Available also from: <https://www.ndt.net/article/ndtce2009/papers/1005.pdf>.
- BINDA, L.; TIRABOSCHI, C.; ABBANEO, S., 1997. Experimental Research to Characterise Masonry Materials. *Masonry International*. Vol. 10. Available also from: <https://www.masonry.org.uk/downloads/experimental-research-to-characterise-masonry-materials/>.
- BJÖRCK, Å., 1967. Solving linear least squares problems by Gram-Schmidt orthogonalization. *BIT*. Vol. 7, no. 1, pp. 1–21. ISSN 0006-3835. Available from DOI: 10.1007/BF01934122.
- BLANCO, H.; BOFFILL, Y.; LOMBILLO, I.; VILLEGAS, L., 2018. An integrated structural health monitoring system for determining local/global responses of historic masonry buildings. *Structural Control and Health Monitoring*. Vol. 25, no. 8, e2196. ISSN 15452255. Available from DOI: 10.1002/stc.2196.
- BLOCK, P.; OCHSENDORF, J., 2007. Thrust network analysis: A new methodology for three-dimensional equilibrium. *Journal of the International Association for Shell and Spatial Structures*. Vol. 48, no. 155, pp. 167–173. ISSN 1028365X.
- BOULAY, C.; STAQUET, S.; AZENHA, M.; DERAEMAERKER, A.; CRESPINI, M.; CARETTE, J.; GRANJA, J.; DELSAUTE, B.; DUMOULIN, C.; KARAIKOS, G., 2013. Monitoring elastic properties of concrete since very early age by means of cyclic loadings, ultrasonic measurements, natural resonant frequency of composite beam (EMM-ARM) and with smart aggregates. In: *VIII International Conference on Fracture Mechanics of Concrete and Concrete Structures, FraMCoS-8*. No. March.
- BRITISH STANDARDS INSTITUTION (BSI), 1972. *BS CP 110-1:1972; Code of practice for the structural use of concrete; Part 1: Design, materials and workmanship*. ISBN 0 580 07488 9. Available also from: <http://shop.bsigroup.com/en/ProductDetail/?pid=00000000010197621>.
- BROTONS, V.; TOMÁS, R.; IVORRA, S.; GREDEAGA, A., 2014. Relationship between static and dynamic elastic modulus of calcarenite heated at different temperatures: the San Julián's stone. *Bulletin of Engineering Geology and the Environment*. Vol. 73, no. 3, pp. 791–799. ISBN 9781138001497. ISSN 1435-9529. Available from DOI: 10.1007/s10064-014-0583-y.
- BROTONS, V.; TOMÁS, R.; IVORRA, S.; GREDEAGA, A.; MARTÍNEZ-MARTÍNEZ, J.; BENAVENTE, D.; GÓMEZ-HERAS, M., 2016. Improved correlation between the static and dynamic elastic modulus of different types of rocks. *Materials and Structures*. Vol. 49, no. 8, pp. 3021–3037. ISSN 1359-5997. Available from DOI: 10.1617/s11527-015-0702-7.
- BROTÓN, V.; TOMÁS, R.; IVORRA, S.; ALARCÓN, J. C., 2013. *Engineering Geology*. Vol. 167, Temperature influence on the physical and mechanical properties of a porous rock: San Julian's calcarenite. Elsevier. ISSN 00137952. Available from DOI: 10.1016/j.enggeo.2013.10.012.
- BRU, D.; IVORRA, S.; BETTI, M.; ADAM, J. M.; BARTOLI, G., 2019. Parametric dynamic interaction assessment between bells and supporting slender masonry tower. *Mechanical Systems and Signal Processing*. Vol. 129, pp. 235–249. ISSN 08883270. Available from DOI: 10.1016/j.ymsp.2019.04.038.
- BUNGEY, J. H.; MILLARD, S. G.; GRANTHAM, M. G., 1996. *Testing of Concrete in Structures*. ISBN 0203487834.
- CABBOI, A.; GENTILE, C.; SAISI, A., 2017. From continuous vibration monitoring to FEM-based damage assessment: Application on a stone-masonry tower. *Construction and Building Materials*. Vol. 156, pp. 252–265. ISSN 09500618. Available from DOI: 10.1016/j.conbuildmat.2017.08.160.
- CALVI, G. M.; PINHO, R.; MAGENES, G.; BOMMER, J. J.; RESTREPO-VÉLEZ, L. F.; CROWLEY, H., 2006. Development of Seismic Vulnerability Assessment Methodologies over the Past 30 Years. *ISSET Journal of Earthquake Technology, Paper No. 472*. Vol. 43, no. 3, pp. 75–104. ISSN 0972-0405.
- CAVALAGLI, N.; KITA, A.; FALCO, S.; TRILLO, F.; COSTANTINI, M.; UBERTINI, F., 2019. Satellite radar interferometry and in-situ measurements for static monitoring of historical monuments: The case of Gubbio, Italy. *Remote Sensing of Environment*. Vol. 235, no. June, p. 111453. ISSN 00344257. Available from DOI: 10.1016/j.rse.2019.111453.
- CERAVOLO, R.; DE MARINIS, A.; PECORELLI, M. L.; ZANOTTI FRAGONARA, L., 2017. Monitoring of masonry historical constructions: 10 years of static monitoring of the world's largest oval dome. *Structural Control and Health Monitoring*. Vol. 24, no. 10, e1988. ISSN 15452255. Available from DOI: 10.1002/stc.1988.

- CERVERA, M.; PELÀ, L.; CLEMENTE, R.; ROCA, P., 2010. A crack-tracking technique for localized damage in quasi-brittle materials. *Engineering Fracture Mechanics*. Vol. 77, no. 13, pp. 2431–2450. ISSN 00137944. Available from DOI: 10.1016/j.engfracmech.2010.06.013.
- CHAKRABORTY, G.; KAMIYAMA, T.; TAKAHASHI, H.; KINOSHITA, T., 2018. An Efficient Anomaly Detection in Quasi-Periodic Time Series Data—A Case Study with ECG. In: *Time Series Analysis and Forecasting. ITISE 2017. Contributions to Statistics*. Springer, Cham, pp. 147–157. Available from DOI: 10.1007/978-3-319-96944-2_10.
- CHIABRANDO, F.; DONATO, V.; LO TURCO, M.; SANTAGATI, C., 2018. Cultural Heritage Documentation, Analysis and Management Using Building Information Modelling: State of the Art and Perspectives. In: *Mechatronics for Cultural Heritage and Civil Engineering*, pp. 181–202. Available from DOI: 10.1007/978-3-319-68646-2_8.
- CHRISTARAS, B.; AUGER, F.; MOSSE, E., 1994. Determination of the moduli of elasticity of rocks. Comparison of the ultrasonic velocity and mechanical resonance frequency methods with direct static methods. *Materials and Structures*. Vol. 27, no. 4, pp. 222–228. ISSN 0025-5432. Available from DOI: 10.1007/BF02473036.
- CICCOTTI, M.; MULARGIA, F., 2004. Differences between static and dynamic elastic moduli of a typical seismogenic rock. *Geophysical Journal International*. Vol. 157, no. 1, pp. 474–477.
- CORNELIS, B.; PEETERS, B., 2014. Online Bayesian spike removal algorithms for structural health monitoring of vehicle components. In: *Eurodyn 2014: Proceedings of the 9th International Conference on Structural Dynamics*. Porto, pp. 2295–2301. ISBN 978-972-752-165-4. ISSN 2311-9020.
- CROSS, E. J.; WORDEN, K.; CHEN, Q., 2011. Cointegration: a novel approach for the removal of environmental trends in structural health monitoring data. *Proceedings of the Royal Society A: Mathematical, Physical and Engineering Sciences*. Vol. 467, no. 2133, pp. 2712–2732. ISSN 1364-5021. Available from DOI: 10.1098/rspa.2011.0023.
- D'ALTRI, A. M.; SARHOSIS, V.; MILANI, G.; ROTS, J.; CATTARI, S.; LAGOMARSINO, S.; SACCO, E.; TRALLI, A.; CASTELLAZZI, G.; MIRANDA, S. de, 2020. Modeling Strategies for the Computational Analysis of Unreinforced Masonry Structures: Review and Classification. *Archives of Computational Methods in Engineering*. Vol. 27, no. 4, pp. 1153–1185. ISSN 1134-3060. Available from DOI: 10.1007/s11831-019-09351-x.
- D'AYALA, D.; SPERANZA, E., 2003. Definition of Collapse Mechanisms and Seismic Vulnerability of Historic Masonry Buildings. *Earthquake Spectra*. Vol. 19, no. 3, pp. 479–509. ISSN 8755-2930. Available from DOI: 10.1193/1.1599896.
- D'AYALA, D. F., 2008. Numerical Modelling of Masonry Structures. In: *Structures & Construction in Historic Building Conservation*. Oxford, UK: Blackwell Publishing Ltd, pp. 151–172. Available from DOI: 10.1002/9780470691816.ch9.
- DAUBECHIES, I., 1992. *Ten Lectures on Wavelets*. Society for Industrial and Applied Mathematics. ISBN 978-0-89871-274-2. Available from DOI: 10.1137/1.9781611970104.
- DE BOOR, C., 1978. *A Practical Guide to Splines*. Springer-Verlag New York. ISBN 978-0-387-95366-3.
- DE VENT, I., 2011. *Prototype of a diagnostic decision support tool for structural damage in masonry*. ISBN 9789085707608. Available also from: <http://resolver.tudelft.nl/uuid:e9a3a2f9-16b5-4b22-a1f4-6511f3543f6e>. PhD thesis. TU Delft.
- DEAN, R. B.; DIXON, W. J., 1951. Simplified Statistics for Small Numbers of Observations. *Analytical Chemistry*. Vol. 23, no. 4, pp. 636–638. ISSN 0003-2700. Available from DOI: 10.1021/ac60052a025.
- DEJONG, M., 2016. Settlement effects on masonry structures. In: *Structural Analysis of Historical Constructions: Anamnesis, diagnosis, therapy, controls - Proceedings of the 10th International Conference on Structural Analysis of Historical Constructions, SAHC 2016*, pp. 449–456.
- DERAEMAEKER, A.; WORDEN, K., 2018. A comparison of linear approaches to filter out environmental effects in structural health monitoring. *Mechanical Systems and Signal Processing*. Vol. 105, pp. 1–15. ISSN 0888-3270. Available from DOI: 10.1016/J.YMSSP.2017.11.045.
- DIANA FEA BV, 2016. *DIANA FEA (Release 10.1) User's Manual*. Delft.

- DIMTER, S.; RUKAVINA, T.; MINAŽEK, K., 2016. Estimation of elastic properties of fly ash-stabilized mixes using nondestructive evaluation methods. *Construction and Building Materials*. Vol. 102, pp. 505–514. ISSN 09500618. Available from DOI: 10.1016/j.conbuildmat.2015.10.175.
- DIVERSI, R.; GUIDORZI, R.; SOVERINI, U., 2010. Identification of ARX and ARARX Models in the Presence of Input and Output Noises. *European Journal of Control*. Vol. 16, no. 3, pp. 242–255. ISSN 09473580. Available from DOI: 10.3166/ejc.16.242-255.
- DONOHO, D. L.; JOHNSTONE, I. M., 1994. Ideal Spatial Adaptation by Wavelet Shrinkage. *Biometrika*. Vol. 81, no. 3, p. 425. ISSN 00063444. Available from DOI: 10.2307/2337118.
- DROUGKAS, A.; ROCA, P.; MOLINS, C., 2015. Analytical micro-modeling of masonry periodic unit cells – Elastic properties. *International Journal of Solids and Structures*. Vol. 69-70, pp. 169–188. ISSN 00207683. Available from DOI: 10.1016/j.ijso1str.2015.04.039.
- DUTTA, M.; HUSAIN, Z., 2009. An application of Multicriteria Decision Making to built heritage. The case of Calcutta. *Journal of Cultural Heritage*. Vol. 10, no. 2, pp. 237–243. ISSN 12962074. Available from DOI: 10.1016/j.culher.2008.09.007.
- DYER, J. S., 2005. MAUT — Multiattribute Utility Theory. In: *Multiple Criteria Decision Analysis: State of the Art Surveys*. New York: Springer-Verlag, pp. 265–292. ISBN 978-0-387-23081-8. Available from DOI: 10.1007/0-387-23081-5_7.
- EDWARDS, W.; MILES JR., R.; WINTERFELDT, D. von, 2007. *Advances in decision analysis : from foundations to applications*. Cambridge University Press. ISBN 9780521863681.
- EISSA, E.; KAZI, A., 1988. Relation between static and dynamic Young's moduli of rocks. *International Journal of Rock Mechanics and Mining Sciences & Geomechanics Abstracts*. Vol. 25, no. 6, pp. 479–482. ISBN 0148-9062. ISSN 01489062. Available from DOI: 10.1016/0148-9062(88)90987-4.
- ELYAMANI, A.; CASELLES, O.; ROCA, P.; CLAPES, J., 2017a. Dynamic investigation of a large historical cathedral. *Structural Control and Health Monitoring*. Vol. 24, no. 3, e1885. ISSN 15452255. Available from DOI: 10.1002/stc.1885.
- ELYAMANI, A.; ROCA, P., 2018. One century of studies for the preservation of one of the largest cathedrals worldwide: a review. *Scientific Culture*. Vol. 4, no. 2, pp. 1–24. Available from DOI: 10.5281/zenodo.1214557.
- ELYAMANI, A.; ROCA, P.; CASELLES, O.; CLAPES, J., 2017b. Seismic safety assessment of historical structures using updated numerical models: The case of Mallorca cathedral in Spain. *Engineering Failure Analysis*. Vol. 74, pp. 54–79. ISSN 13506307. Available from DOI: 10.1016/j.engfailana1.2016.12.017.
- EUROPEAN COMMITTEE FOR STANDARDIZATION (CEN), 1998. *EN 1052-1. Methods of test for masonry - Part 1: Determination of compressive strength*.
- EUROPEAN COMMITTEE FOR STANDARDIZATION (CEN), 2004. *EN 12504-4. Testing concrete — Part 4: Determination of ultrasonic pulse velocity*. ISBN 0 580 15139 5. Available from DOI: ConstructionStandard, CS1:2010.
- EUROPEAN COMMITTEE FOR STANDARDIZATION (CEN), 2005. *EN 14580. Natural stone test methods - Determination of static elastic modulus*. ISBN 9780580499364.
- EUROPEAN COMMITTEE FOR STANDARDIZATION (CEN), 2010. *EN 772-1. Methods of test for masonry units. Part 1: Determination of compressive strength*.
- EUROPEAN COMMITTEE FOR STANDARDIZATION (CEN), 2011. *EN 771-1. Specification for masonry units – Part 1: Clay masonry units*.
- EUROPEAN COMMITTEE FOR STANDARDIZATION (CEN), 2013. *EN 12390-13. Testing hardened concrete - Part 13: Determination of secant modulus of elasticity in compression*.
- EUROPEAN COMMITTEE FOR STANDARDIZATION (CEN), 2019. *EN 1015-11. Methods of test for mortar for masonry - Part 11: Determination of flexural and compressive strength of hardened mortar*.
- EWINS, D. J., 2000. *Modal testing : theory, practice, and application*. Research Studies Press. ISBN 0863802184.
- FARSHCHIN, M., 2015. *Frequency Domain Decomposition (FDD)*.
- FEI, W.; HUIYUAN, B.; JUN, Y.; YONGHAO, Z., 2016. Correlation of Dynamic and Static Elastic Parameters of Rock. *Electronic Journal of Geotechnical Engineering*. Vol. 21, no. 04, pp. 1551–1560.

- FERREIRA, T. M.; LOURENÇO, P. B., 2019. Disaster Risk Reduction and Urban Resilience: Concepts, Methods and Applications. In: *Resilient Structures and Infrastructure*. Singapore: Springer Singapore, pp. 453–473. Available from DOI: 10.1007/978-981-13-7446-3_17.
- FERRERO, C.; CAMBIAGGI, L.; VECCHIATTINI, R.; CALDERINI, C., 2020. Damage Assessment of Historic Masonry Churches Exposed to Slow-moving Landslides. *International Journal of Architectural Heritage*, pp. 1–26. ISSN 1558-3058. Available from DOI: 10.1080/15583058.2020.1799259.
- FERRETTI, D.; BAŽANT, Z. P., 2006. Stability of ancient masonry towers: Moisture diffusion, carbonation and size effect. *Cement and Concrete Research*. Vol. 36, no. 7, pp. 1379–1388. ISSN 00088846. Available from DOI: 10.1016/j.cemconres.2006.03.013.
- FÓDI, A., 2011. Effects influencing the compressive strength of a solid, fired clay brick. *Periodica Polytechnica Civil Engineering*. Vol. 55, no. 2, p. 117. ISBN 05536626. ISSN 0553-6626. Available from DOI: 10.3311/pp.ci.2011-2.04.
- FRITSCH, F. N.; CARLSON, R. E., 1980. Monotone Piecewise Cubic Interpolation. *SIAM Journal on Numerical Analysis*. Vol. 17, no. 2, pp. 238–246. ISSN 0036-1429. Available from DOI: 10.1137/0717021.
- GARCÍA, L. E., 2018. *Estudio experimental del comportamiento a compresión de elementos pétreos confinados con materiales compuestos*. Doctoral Thesis. Universitat d'Alacant.
- GARCIA RAMONDA, L.; ISALBERTI, F.; GARCIA ROCA, I.; MARIN GIMENO, X., 2015. *MSc SAHC SA7 PROJECT: Structural evaluation and safety assessment of the monastery's church of Sant Cugat del Vallès*.
- GARNIER, H.; WANG, L., 2008. *Identification of Continuous-time Models from Sampled Data*. London: Springer London. Advances in Industrial Control. ISBN 978-1-84800-160-2. Available from DOI: 10.1007/978-1-84800-161-9.
- GARZÓN-ROCA, J.; ADAM, J. M.; SANDOVAL, C.; ROCA, P., 2013. Estimation of the axial behaviour of masonry walls based on Artificial Neural Networks. *Computers & Structures*. Vol. 125, pp. 145–152. ISSN 00457949. Available from DOI: 10.1016/j.compstruc.2013.05.006.
- GAUDINI, G.; MODENA, C.; CASARIN, F.; BETTIO, C.; LUCCHIN, F., 2008. Monitoring and strengthening interventions on the stone tomb of Cansignorio della Scala, Verona, Italy. In: *Proceedings of the VI International Conference on Structural Analysis of Historic Construction, SAHC08*. CRC Press, pp. 423–432.
- GERCEK, H., 2007. Poisson's ratio values for rocks. *International Journal of Rock Mechanics and Mining Sciences*. Vol. 44, no. 1, pp. 1–13. ISSN 13651609. Available from DOI: 10.1016/j.ijrmm.2006.04.011.
- GIOVINAZZI, S.; LAGOMARSINO, S., 2004. A macroseismic method for the vulnerability assessment of buildings. In: *13th World Conference on Earthquake Engineering*. Vancouver, B.C., Canada.
- GLOBAL SEISMIC HAZARD ASSESSMENT PROGRAM (GSHAP), 1999. *Global Seismic Hazard Map*. Available also from: <http://static.seismo.ethz.ch/GSHAP/global/>.
- GONZÁLEZ, R.; CABALLÉ, F.; DOMENGE, J.; VENDRELL, M.; GIRÁLDEZ, P.; ROCA, P.; GONZÁLEZ, J., 2008. Construction process, damage and structural analysis. Two case studies. In: *Proceedings of the VI International Conference on Structural Analysis of Historic Construction, SAHC08*. CRC Press. Vol. 1, pp. 643–651. ISBN 0415468728. Available from DOI: 10.1201/9781439828229.ch73.
- GONZÁLEZ, R. F., 2006. Utilización de la piedra natural en restauración. *Utilización de rocas y minerales industriales (ed. M. A. García del Cura y J. C. Cañaveras)*. Vol. 2, pp. 155–183. Available also from: <http://scholar.google.com/scholar?hl=en%7B%5C%7DbtnG=Search%7B%5C%7Dq=intitle:Utilizaci?n+de+la+piedra+natural+en+restauraci?n%7B%5C%7D0>.
- HALFPENNY, A., 2008. Data Preprocessing for Damage Detection. In: *Encyclopedia of Structural Health Monitoring*. Chichester, UK: John Wiley & Sons, Ltd. Available from DOI: 10.1002/9780470061626.shm043.
- HEERDEN, W. b., 1987. General relations between static and dynamic moduli of rocks. *International Journal of Rock Mechanics and Mining Sciences & Geomechanics Abstracts*. Vol. 24, no. 6, pp. 381–385. ISSN 01489062. Available from DOI: 10.1016/0148-9062(87)92262-5.
- HEES, R. van; NALDINI, S.; LUBELLI, B., 2009. The development of MDDS-COMPASS. Compatibility of plasters with salt loaded substrates. *Construction and Building Materials*. Vol. 23, no. 5, pp. 1719–1730. ISSN 09500618. Available from DOI: 10.1016/j.conbuildmat.2008.08.010.

- HERAS, V.; STEENBERGHEN, T.; ZÚÑIGA, M.; CARDOSO, F.; VAN BALEN, K., 2012. An information system for heritage documentation management of Cuenca city, Ecuador. *MASKANA*. Vol. 3, no. 1, pp. 51–61. ISSN 13906143. Available from DOI: 10.18537/mskn.03.01.05.
- HERAS, V. C.; WIJFFELS, A.; CARDOSO, F.; VANDESANDE, A.; SANTANA, M.; VAN ORSHOVEN, J.; STEENBERGHEN, T.; BALEN, K. van, 2013. A value-based monitoring system to support heritage conservation planning. *Journal of Cultural Heritage Management and Sustainable Development*. Vol. 3, no. 2, pp. 130–147. ISSN 2044-1266. Available from DOI: 10.1108/JCHMSD-10-2012-0051.
- HEYLEN, W.; LAMMENS, S.; SAS, P., 1998. *Modal analysis theory and testing*. Katholieke Universiteit Leuven, Faculty of Engineering, Dept. of Mechanical Engineering, Division of Production Engineering, Machine Design and Automation. ISBN 907380261X.
- HEYMAN, J.; THRELFALL, B. D., 1976. Inertia forces due to bell-ringing. *International Journal of Mechanical Sciences*. Vol. 18, no. 4, pp. 161–164. ISBN 0020-7403. ISSN 00207403. Available from DOI: 10.1016/0020-7403(76)90020-5.
- HEYMAN, J., 1995. *The Stone Skeleton*. Cambridge University Press. ISBN 9780521472708. Available from DOI: 10.1017/CB09781107050310.
- HORSRUD, P., 2001. Estimating Mechanical Properties of Shale From Empirical Correlations. *SPE Drilling & Completion*. Vol. 16, no. 02, pp. 68–73. ISSN 1064-6671. Available from DOI: 10.2118/56017-PA.
- HUM-HARTLEY, S., 1978. Nondestructive Testing for Heritage Structures. *Bulletin of the Association for Preservation Technology*. Vol. 10, no. 3, p. 4. ISSN 00449466. Available from DOI: 10.2307/1493664.
- INTERNATIONAL COUNCIL ON MONUMENTS AND SITES (ICOMOS), 2003. *ICOMOS charter - Principles for the analysis, conservation and structural restoration of architectural heritage*. Available also from: <https://iscarsah.org/documents/>.
- INTERNATIONAL SCIENTIFIC COMMITTEE ON THE ANALYSIS AND RESTORATION OF STRUCTURES OF ARCHITECTURAL HERITAGE (ISCARSAH), 2005. *Recommendations for the analysis, conservation and structural restoration of architectural heritage*.
- IPCE: INSTITUTO DEL PATRIMONIO CULTURAL DE ESPAÑA (SPANISH INSTITUTE OF CULTURAL HERITAGE), 2012. *Inspección técnica portadas de la Catedral de Palma de Mallorca (Technical inspection of the portal of Palma de Mallorca cathedral)*.
- IVORRA, S.; GIANNOCARO, N. I.; FOTI, D., 2019. Simple model for predicting the vibration transmission of a squat masonry tower by base forced vibrations. *Structural Control and Health Monitoring*. Vol. 26, no. 6, e2360. ISSN 1545-2255. Available from DOI: 10.1002/stc.2360.
- IVORRA, S.; PALLARÉS, F. J.; ADAM, J. M., 2011a. Masonry bell towers: dynamic considerations. *Proceedings of the Institution of Civil Engineers - Structures and Buildings*. Vol. 164, no. 1, pp. 3–12. ISSN 0965-0911. Available from DOI: 10.1680/stbu.9.00030.
- IVORRA, S.; PALLARÉS, F. J.; ADAM, J. M., 2011b. Masonry bell towers: dynamic considerations. *Proceedings of the Institution of Civil Engineers - Structures and Buildings*. Vol. 164, no. 1, pp. 3–12. ISSN 0965-0911. Available from DOI: 10.1680/stbu.9.00030.
- IVORRA, S.; PALOMO, M. J.; VERDÚ, G.; ZASSO, A., 2006. Dynamic forces produced by swinging bells. *Mecanica*. Vol. 41, no. 1, pp. 47–62. ISSN 00256455. Available from DOI: 10.1007/s11012-005-7973-y.
- JOSA, I.; PONS, O.; FUENTE, A. de la; AGUADO, A., 2020. Multi-criteria decision-making model to assess the sustainability of girders and trusses: Case study for roofs of sports halls. *Journal of Cleaner Production*. Vol. 249, p. 119312. ISSN 09596526. Available from DOI: 10.1016/j.jclepro.2019.119312.
- KHOA, N. L. D.; MAKKI ALAMDARI, M.; RAKOTOARIVELO, T.; ANAISSI, A.; WANG, Y., 2018. Structural Health Monitoring Using Machine Learning Techniques and Domain Knowledge Based Features. In: *Human and Machine Learning*. Springer, Cham, pp. 409–435. Available from DOI: 10.1007/978-3-319-90403-0_20.
- KING, M., 1983. Static and dynamic elastic properties of rocks from the Canadian shield. *International Journal of Rock Mechanics and Mining Sciences & Geomechanics Abstracts*. Vol. 20, no. 5, pp. 237–241. ISSN 01489062. Available from DOI: 10.1016/0148-9062(83)90004-9.
- KITA, A.; CAVALAGLI, N.; UBERTINI, F., 2019. Temperature effects on static and dynamic behavior of Consoli Palace in Gubbio, Italy. *Mechanical Systems and Signal Processing*. Vol. 120, pp. 180–202. ISSN 08883270. Available from DOI: 10.1016/j.ymsp.2018.10.021.

- LACY, L. L., 1997. Dynamic Rock Mechanics Testing for Optimized Fracture Designs. In: *SPE Annual Technical Conference and Exhibition*. Society of Petroleum Engineers. Available from DOI: 10.2118/38716-MS.
- LANE, C., 2014. Wave Propagation in Anisotropic Media. In: *The Development of a 2D Ultrasonic Array Inspection for Single Crystal Turbine Blades*, pp. 13–39. ISBN 978-3-319-02516-2. Available from DOI: 10.1007/978-3-319-02517-9_2.
- LAUGIER, P.; HAÏAT, G., 2011. Chapter 2: Introduction to the Physics of Ultrasound. In: *Bone Quantitative Ultrasound*, pp. 29–45. ISBN 9789400700178. ISSN 13514180. Available from DOI: 10.1007/978-94-007-0017-8.
- LAWRANCE, A. J., 1991. Directionality and Reversibility in Time Series. *International Statistical Review / Revue Internationale de Statistique*. Vol. 59, no. 1, p. 67. ISSN 03067734. Available from DOI: 10.2307/1403575.
- LEE, B. J.; KEE, S.-h.; OH, T.; KIM, Y.-y., 2017. Evaluating the Dynamic Elastic Modulus of Concrete Using Shear-Wave Velocity Measurements. *Advances in Materials Science and Engineering*. Vol. 2017, pp. 1–13. ISSN 1687-8434. Available from DOI: 10.1155/2017/1651753.
- LILLIEFORS, H. W., 1967. On the Kolmogorov-Smirnov Test for Normality with Mean and Variance Unknown. *Journal of the American Statistical Association*. Vol. 62, no. 318, p. 399. ISSN 01621459. Available from DOI: 10.2307/2283970.
- LORENZONI, F., 2013. *Integrated methodologies based on Structural Health Monitoring for the protection of Cultural Heritage buildings*. PhD Thesis. University of Trento.
- LORENZONI, F.; CASARIN, F.; CALDON, M.; ISLAMI, K.; MODENA, C., 2016. Uncertainty quantification in structural health monitoring: Applications on cultural heritage buildings. *Mechanical Systems and Signal Processing*. Vol. 66-67, pp. 268–281. ISSN 08883270. Available from DOI: 10.1016/j.ymssp.2015.04.032.
- LORENZONI, F.; CASARIN, F.; MODENA, C.; CALDON, M.; ISLAMI, K.; PORTO, F. da, 2013. Structural health monitoring of the Roman Arena of Verona, Italy. *Journal of Civil Structural Health Monitoring*. Vol. 3, no. 4, pp. 227–246. ISSN 2190-5452. Available from DOI: 10.1007/s13349-013-0065-0.
- LOURENÇO, P. B., 2002. Computations on historic masonry structures. *Progress in Structural Engineering and Materials*. Vol. 4, no. 3, pp. 301–319. ISSN 13650556. Available from DOI: 10.1002/pse.120.
- LOURENÇO, P. B., 1998. Experimental and numerical issues in the modelling of the mechanical behaviour of masonry. In: ROCA, P.; GONZÁLEZ, J.; OÑATE, E.; LOURENÇO, P. (eds.). *Structural analysis of historical constructions II. Possibilities of numerical and experimental techniques*. Barcelona, pp. 57–91. ISBN 84-89925-26-7.
- LYDON, F.; BALENDRAN, R., 1986. Some observations on elastic properties of plain concrete. *Cement and Concrete Research*. Vol. 16, no. 3, pp. 314–324. ISSN 00088846. Available from DOI: 10.1016/0008-8846(86)90106-7.
- MAIA, N. M. M.; MONTALVÃO E SILVA, J. M. (M.), 1997. *Theoretical and experimental modal analysis*. Research Studies Press. ISBN 0863802087.
- MAKOOND, N.; CABANÉ, A.; PELÀ, L.; MOLINS, C., 2020a. Relationship between the static and dynamic elastic modulus of brick masonry constituents. *Construction and Building Materials*. Vol. 259, p. 120386. ISSN 09500618. Available from DOI: 10.1016/j.conbuildmat.2020.120386.
- MAKOOND, N.; PELÀ, L.; MOLINS, C., 2019. Dynamic elastic properties of brick masonry constituents. *Construction and Building Materials*. Vol. 199, pp. 756–770. ISSN 09500618. Available from DOI: 10.1016/j.conbuildmat.2018.12.071.
- MAKOOND, N.; PELÀ, L.; MOLINS, C., 2020. A Risk Index for the Structural Diagnosis of Masonry Heritage (RISDiMaH). **Submitted for publication**.
- MAKOOND, N.; PELÀ, L.; MOLINS, C.; ROCA, P., 2020b. Static structural health monitoring and automated data analysis procedures applied to the diagnosis of a complex medieval masonry monastery. In: ZONTA, D.; HUANG, H. (eds.). *Sensors and Smart Structures Technologies for Civil, Mechanical, and Aerospace Systems 2020*. SPIE. ISBN 9781510635357. Available from DOI: 10.1117/12.2559837.
- MAKOOND, N.; PELÀ, L.; MOLINS, C.; ROCA, P., 2021. Data analysis using ARX models applied to static structural health monitoring of the monastery of Sant Cugat. In: ROCA, P.; PELÀ, L.; MOLINS, C. (eds.). **Accepted for presentation in the 12th International Conference on Structural Analysis of Historical Constructions (SAHC 2020) to be held on September 29-30, and October 1, 2021**.

- MAKOOND, N.; PELÀ, L.; MOLINS, C.; ROCA, P.; ALARCÓN, D., 2020c. Automated data analysis for static structural health monitoring of masonry heritage structures. *Structural Control and Health Monitoring*. ISSN 1545-2255. Available from DOI: 10.1002/stc.2581.
- MANSOR, M. M.; GLONEK, M. E.; GREEN, D. A.; METCALFE, A. V., 2016. Threshold Autoregressive Models for Directional Time Series. In: *Time Series Analysis and Forecasting. Contributions to Statistics*. Springer, Cham, pp. 13–25. Available from DOI: 10.1007/978-3-319-28725-6_2.
- MARASTONI, D.; BENEDETTI, A.; PELÀ, L.; PIGNAGNOLI, G., 2017. Torque Penetrometric Test for the in-situ characterisation of historical mortars: fracture mechanics interpretation and experimental validation. *Construction and Building Materials*. Vol. 157, pp. 509–520. ISSN 09500618. Available from DOI: 10.1016/j.conbuildmat.2017.09.120.
- MARIO AZZARA, R.; DE ROECK, G.; GIRARDI, M.; PADOVANI, C.; PELLEGRINI, D.; REYNDERS, E., 2018. The influence of environmental parameters on the dynamic behaviour of the San Frediano bell tower in Lucca. *Engineering Structures*. Vol. 156, no. March 2017, pp. 175–187. ISSN 01410296. Available from DOI: 10.1016/j.engstruct.2017.10.045.
- MARTÍNEZ-MARTÍNEZ, J.; BENAVENTE, D.; GARCÍA-DEL-CURA, M. A., 2012. Comparison of the static and dynamic elastic modulus in carbonate rocks. *Bulletin of Engineering Geology and the Environment*. Vol. 71, no. 2, pp. 263–268. ISSN 1435-9529. Available from DOI: 10.1007/s10064-011-0399-y.
- MASCIOTTA, M.-G.; RAMOS, L. F.; LOURENÇO, P. B.; MATOS, J. A. C., 2016a. Development of Key Performance Indicators for the Structural Assessment of Heritage Buildings. In: *8th European Workshop on Structural Health Monitoring (EWSHM 2016), 5-8 July 2016, Bilbao, Spain*, pp. 5–8.
- MASCIOTTA, M.-G.; RAMOS, L. F.; LOURENÇO, P. B., 2017. The importance of structural monitoring as a diagnosis and control tool in the restoration process of heritage structures: A case study in Portugal. *Journal of Cultural Heritage*. Vol. 27, pp. 36–47. ISSN 12962074. Available from DOI: 10.1016/j.culher.2017.04.003.
- MASCIOTTA, M.-G.; ROQUE, J. C.; RAMOS, L. F.; LOURENÇO, P. B., 2016b. A multidisciplinary approach to assess the health state of heritage structures: The case study of the Church of Monastery of Jerónimos in Lisbon. *Construction and Building Materials*. Vol. 116, pp. 169–187. ISSN 09500618. Available from DOI: 10.1016/j.conbuildmat.2016.04.146.
- MASHINSKY, E. I., 2003. Differences between static and dynamic elastic moduli of rocks: Physical causes. *Russian Geology and Geophysics*. Vol. 44, no. 9, pp. 953–959.
- MATHWORKS, [n.d.]. *MATLAB R2017b Documentation* [online] [visited on 2018-07-30]. Available from: <https://es.mathworks.com/help/releases/R2017b/index.html>.
- MEEUS, J.; SAVOIE, D., 1992. The history of the tropical year. *Journal of the British Astronomical Association*. Vol. 102, pp. 40–42. Available also from: <http://adsabs.harvard.edu/abs/1992JBAA...102...40M>.
- MILES, L. D., 1972. *Techniques of Value Analysis and Engineering*. 2nd ed. McGraw-Hill. ISBN 0070419264.
- MOLINS, C., 2018. *Evaluation of the structural state of Torre Lloberola and proposal of intervention measures (in Catalan - Avaluació de l'estat actual de l'estructura de la torre de Lloberola (Biosca) i proposta d'intervenció)*.
- MOLINS, C.; ROCA, P., 1998. Capacity of Masonry Arches and Spatial Frames. *Journal of Structural Engineering*. Vol. 124, no. 6, pp. 653–663. ISSN 0733-9445. Available from DOI: 10.1061/(ASCE)0733-9445(1998)124:6(653).
- MOLINS, C.; ROCA, P., 2018. *Analysis of the structural cracks of the church of Santa Maria of Guimerà (in Catalan - Anàlisi de les lesions estructurals de l'església de Santa Maria de Guimerà)*.
- MORÉ, J. J., 1978. The Levenberg-Marquardt algorithm: Implementation and theory. In: WATSON, G. A. (ed.). *Numerical Analysis*. Springer, Berlin, Heidelberg, pp. 105–116. Available from DOI: 10.1007/BFb0067700.
- MOROPOULOU, A.; KAROGLU, M.; AGAPAKIS, I.; MOUZAKIS, C.; ASIMAKOPOULOS, S.; PANTAZIS, G.; LAMBROU, E., 2019. Structural health monitoring of the Holy Aedicule in Jerusalem. *Structural Control and Health Monitoring*. Vol. 26, no. 9. ISSN 1545-2255. Available from DOI: 10.1002/stc.2387.
- NAJIBI, A. R.; GHAFOORI, M.; LASHKARIPOUR, G. R.; ASEF, M. R., 2015. Empirical relations between strength and static and dynamic elastic properties of Asmari and Sarvak limestones, two main oil reservoirs in Iran. *Journal of Petroleum Science and Engineering*. Vol. 126, pp. 78–82. ISSN 09204105. Available from DOI: 10.1016/j.petrol.2014.12.010.

- NATIONAL INSTRUMENTS, 2016. *LabVIEW 2016 Help*.
- NAVARRO, I. J.; YEPES, V.; MARTÍ, J. V., 2019. A Review of Multicriteria Assessment Techniques Applied to Sustainable Infrastructure Design. *Advances in Civil Engineering*. Vol. 2019, pp. 1–16. ISSN 1687-8086. Available from DOI: 10.1155/2019/6134803.
- NAZARCHUK, Z.; SKALSKYI, V.; SERHIYENKO, O., 2017. Chapter 2: Propagation of Elastic Waves in Solids. In: *Acoustic Emission*. Springer International Publishing. Vol. i, pp. 29–73. ISBN 978-3-319-49348-0. Available from DOI: 10.1007/978-3-319-49350-3.
- NEVILLE, A. M., 2011. *Properties of concrete*. 5th Editio. Pearson. ISBN 0273755803.
- NICHOLS, J. M.; TOTOEV, Y. Z., 1997. Experimental determination of the dynamic Modulus of Elasticity of masonry units. In: *15th Australian Conference on the Mechanics of Structures and Materials (ACMSM)*.
- OLIVEIRA, D. V.; LOURENÇO, P. B.; ROCA, P., 2007. Cyclic behaviour of stone and brick masonry under uniaxial compressive loading. *Materials and Structures*. Vol. 39, no. 2, pp. 247–257. ISSN 1359-5997. Available from DOI: 10.1617/s11527-005-9050-3.
- OLIVEIRA, D. V., 2000. *Mechanical Characterization of Stone and Brick Masonry (Report 00-DEC/E-4)*.
- OLIVEIRA, D. V.; LOURENÇO, P. B.; ROCA, P., 2000. Experimental Characterization of the Behaviour of Brick Masonry Subjected to Cyclic Loading. In: *12th international Brick/Block Masonry Conference*, pp. 1–8. No. May 2014.
- ORTEGA, J.; VASCONCELOS, G.; RODRIGUES, H.; CORREIA, M., 2019. A vulnerability index formulation for the seismic vulnerability assessment of vernacular architecture. *Engineering Structures*. Vol. 197, p. 109381. ISSN 18737323. Available from DOI: 10.1016/j.engstruct.2019.109381.
- ORTIZ, R.; ORTIZ, P., 2016. Vulnerability Index: A New Approach for Preventive Conservation of Monuments. *International Journal of Architectural Heritage*. Vol. 10, no. 8, pp. 1078–1100. ISSN 1558-3058. Available from DOI: 10.1080/15583058.2016.1186758.
- OTTONI, F.; BLASI, C., 2015. Results of a 60-Year Monitoring System for Santa Maria del Fiore Dome in Florence. *International Journal of Architectural Heritage*. Vol. 9, no. 1, pp. 7–24. ISSN 1558-3058. Available from DOI: 10.1080/15583058.2013.815291.
- PAGANI, M.; GARCIA-PELAEZ, J.; GEE, R.; JOHNSON, K.; POGGI, V.; STYRON, R.; WEATHERILL, G.; SIMIONATO, M.; VIGANÒ, D.; DANCIU, L.; MONELLI, D., 2018. *Global Earthquake Model (GEM) Seismic Hazard Map*. Available from DOI: 10.13117/GEM-GLOBAL-SEISMIC-RISK-MAP-2018.
- PALAU, R. M.; HÜRLIMANN, M.; BERENQUER, M.; SEMPERE-TORRES, D., 2020. Influence of the mapping unit for regional landslide early warning systems: comparison between pixels and polygons in Catalonia (NE Spain). *Landslides*. Vol. 17, no. 9, pp. 2067–2083. ISSN 1612-510X. Available from DOI: 10.1007/s10346-020-01425-3.
- PAOLINI, A.; VAFADARI, A.; CESARO, G.; SANTANA QUINTERO, M.; VAN BALEN, K.; VILEIKIS, O.; FAKHOURY, L., 2012. *Risk management at heritage sites : a case study of the Petra world heritage site*. UNESCO. ISBN 978-92-3-001073-7.
- PEETERS, B., 2000. *System Identification and Damage Detection in Civil Engineering*. ISBN 9056822748. Available also from: https://www.researchgate.net/profile/Bart%7B%5C_%7DPeeters3/publication/238331491. PhD Thesis. KU Leuven.
- PEETERS, B.; DE ROECK, G., 1999. Reference-based stochastic subspace identification for output-only modal analysis. *Mechanical Systems and Signal Processing*. Vol. 13, no. 6, pp. 855–878. ISBN 0888-3270. ISSN 08883270. Available from DOI: 10.1006/mssp.1999.1249.
- PEETERS, B.; DE ROECK, G., 2001a. One-year monitoring of the Z24-Bridge: environmental effects versus damage events. *Earthquake Engineering & Structural Dynamics*. Vol. 30, no. 2, pp. 149–171. ISSN 0098-8847. Available from DOI: 10.1002/1096-9845(200102)30:2<149::AID-EQE1>3.0.CO;2-Z.
- PEETERS, B.; DE ROECK, G., 2001b. Stochastic System Identification for Operational Modal Analysis: A Review. *Journal of Dynamic Systems, Measurement, and Control*. Vol. 123, no. 4, p. 659. ISBN 0022-0434. ISSN 00220434. Available from DOI: 10.1115/1.1410370.

- PELÀ, L.; ROCA, P.; APRILE, A., 2016. Comparison of MDT techniques for mechanical characterization of historical masonry. In: *Structural Analysis of Historical Constructions: Anamnesis, diagnosis, therapy, controls - Proceedings of the 10th International Conference on Structural Analysis of Historical Constructions, SAHC 2016*. Leuven: CRC Press/Balkema, pp. 769–775. ISBN 9781138029514. Available from DOI: 10.1201/9781315616995-104.
- PELÀ, L.; BOURGEOIS, J.; ROCA, P.; CERVERA, M.; CHIUMENTI, M., 2016a. Analysis of the Effect of Provisional Ties on the Construction and Current Deformation of Mallorca Cathedral. *International Journal of Architectural Heritage*. Vol. 10, no. 4, pp. 418–437. ISSN 1558-3058. Available from DOI: 10.1080/15583058.2014.996920.
- PELÀ, L.; CANELLA, E.; APRILE, A.; ROCA, P., 2016b. Compression test of masonry core samples extracted from existing brickwork. *Construction and Building Materials*. Vol. 119, pp. 230–240. ISSN 09500618. Available from DOI: 10.1016/j.conbuildmat.2016.05.057.
- PELÀ, L.; CERVERA, M.; ROCA, P., 2011. Continuum damage model for orthotropic materials: Application to masonry. *Computer Methods in Applied Mechanics and Engineering*. Vol. 200, no. 9-12, pp. 917–930. ISSN 00457825. Available from DOI: 10.1016/j.cma.2010.11.010.
- PELÀ, L.; CERVERA, M.; ROCA, P., 2013. An orthotropic damage model for the analysis of masonry structures. *Construction and Building Materials*. Vol. 41, pp. 957–967. ISSN 09500618. Available from DOI: 10.1016/j.conbuildmat.2012.07.014.
- PELÀ, L.; ROCA, P.; APRILE, A., 2018. Combined In-Situ and Laboratory Minor Destructive Testing of Historical Mortars. *International Journal of Architectural Heritage*. Vol. 12, no. 3, pp. 334–349. ISSN 15583066. Available from DOI: 10.1080/15583058.2017.1323247.
- PELÀ, L.; ROCA, P.; BENEDETTI, A., 2015. Mechanical Characterization of Historical Masonry by Core Drilling and Testing of Cylindrical Samples. *International Journal of Architectural Heritage*. Vol. 10, no. 2-3: Special issue on SAHC 2014 Conference, pp. 360–374. ISSN 1558-3058. Available from DOI: 10.1080/15583058.2015.1077906.
- PHILILEO, R. E., 1955. Comparison of Results of Three Methods for Determining Young's Modulus of Elasticity of Concrete. *ACI Journal Proceedings*. Vol. 51, no. 1, pp. 461–470. ISSN 0002-8061. Available from DOI: 10.14359/11690.
- PIÑERO, I.; SAN-JOSÉ, J. T.; RODRÍGUEZ, P.; LOSÁÑEZ, M. M., 2017. Multi-criteria decision-making for grading the rehabilitation of heritage sites. Application in the historic center of La Habana. *Journal of Cultural Heritage*. Vol. 26, pp. 144–152. ISSN 12962074. Available from DOI: 10.1016/j.culher.2017.01.012.
- POPOVIC, S., 1975. Verification of relationships between mechanical properties of concrete-like materials. *Matériaux et Constructions*. Vol. 8, no. 3, pp. 183–191. ISSN 0025-5432. Available from DOI: 10.1007/BF02475168.
- PROCEQ, 2014. *PUNDIT PL-200 Operating Instructions*.
- RAMESH, M.; AZENHA, M.; LOURENÇO, P. B., 2019. Study of Early Age Stiffness Development in Lime–Cement Blended Mortars. In: *RILEM Bookseries*. Springer Netherlands. Vol. 18, pp. 397–404. Available from DOI: 10.1007/978-3-319-99441-3_42.
- RAMOS, L.; MARQUES, L.; LOURENÇO, P.; DE ROECK, G.; CAMPOS-COSTA, A.; ROQUE, J., 2010. Monitoring historical masonry structures with operational modal analysis: Two case studies. *Mechanical Systems and Signal Processing*. Vol. 24, no. 5, pp. 1291–1305. ISBN 0888-3270. ISSN 08883270. Available from DOI: 10.1016/j.ymsp.2010.01.011.
- RAMOS, L. F., 2007. *Damage identification on masonry structures based on vibration signatures*. Available also from: <http://repositorium.sdum.uminho.pt/handle/1822/7380>. PhD Thesis. Universidade do Minho.
- REYNDERS, E., 2012. System Identification Methods for (Operational) Modal Analysis: Review and Comparison. *Archives of Computational Methods in Engineering*. Vol. 19, no. 1, pp. 51–124. ISBN 1134-3060. ISSN 11343060. Available from DOI: 10.1007/s11831-012-9069-x.
- REYNDERS, E.; ROECK, G. D., 2008. Reference-based combined deterministic-stochastic subspace identification for experimental and operational modal analysis. *Mechanical Systems and Signal Processing*. Vol. 22, no. 3, pp. 617–637. ISBN 0888-3270. ISSN 08883270. Available from DOI: 10.1016/j.ymsp.2007.09.004.

- REYNDERS, E.; SCHEVENELS, M.; DE ROECK, G., 2011. *MACEC 3.2 User's Manual*. K.U.Leuven. No. February.
- REYNDERS, E.; WURSTEN, G.; ROECK, G. de, 2014. Output-only structural health monitoring in changing environmental conditions by means of nonlinear system identification. *Structural Health Monitoring*. Vol. 13, no. 1, pp. 82–93. ISBN 1475921713. ISSN 14759217. Available from DOI: 10.1177/1475921713502836.
- ROCA, P.; MARTÍNEZ, G.; CASARIN, F.; MODENA, C.; ROSSI, P.; RODRÍGUEZ, I.; GARAY, A., 2007. Monitoring of long-term damage in long-span masonry constructions. In: *Learning from Failure*. WIT Press, pp. 125–152. Available from DOI: 10.2495/978-1-84564-057-6/06.
- ROCA, P.; CERVERA, M.; GARIUP, G.; PELÀ, L., 2010. Structural Analysis of Masonry Historical Constructions. Classical and Advanced Approaches. *Archives of Computational Methods in Engineering*. Vol. 17, no. 3, pp. 299–325. ISBN 1183101090. ISSN 1134-3060. Available from DOI: 10.1007/s11831-010-9046-1.
- ROCA, P.; CERVERA, M.; PELÀ, L.; CLEMENTE, R.; CHIUMENTI, M., 2013. Continuum FE models for the analysis of Mallorca Cathedral. *Engineering Structures*. Vol. 46, pp. 653–670. ISSN 01410296. Available from DOI: 10.1016/j.engstruct.2012.08.005.
- ROCA, P.; CLAPÉS, J.; CASELLES, O.; VENDRELL, M.; GIRÁLDEZ, P.; SÁNCHEZ-BEITA, S., 2008. Contribution of inspection techniques to the assessment of historical structures. In: *RILEM Symposium on On Site Assessment of Concrete, Masonry and Timber Structures - SACoMaTiS 2008*, pp. 621–632.
- ROSE, J. L., 1999. *Ultrasonic Waves in Solid Media*. Cambridge University Press. ISBN 0521548896.
- ROSE, J. L., 2014. *Ultrasonic Guided Waves in Solid Media*. New York: Cambridge University Press. ISBN 9781107273610. Available from DOI: 10.1017/CB09781107273610.
- ROSSI, P. P.; ROSSI, C., 2015. Monitoring of Two Great Venetian Cathedrals: San Marco and Santa Maria Gloriosa Dei Frari. *International Journal of Architectural Heritage*. Vol. 9, no. 1, pp. 58–81. ISSN 1558-3058. Available from DOI: 10.1080/15583058.2013.793435.
- RUIZ-JARAMILLO, J.; MUÑOZ-GONZÁLEZ, C.; JOYANES-DÍAZ, M. D.; JIMÉNEZ-MORALES, E.; LÓPEZ-OSORIO, J. M.; BARRIOS-PÉREZ, R.; ROSA-JIMÉNEZ, C., 2019. Heritage risk index: A multi-criteria decision-making tool to prioritize municipal historic preservation projects. *Frontiers of Architectural Research*. ISSN 20952635. Available from DOI: 10.1016/j.foar.2019.10.003.
- RUSSO, S., 2013. On the monitoring of historic Anime Sante church damaged by earthquake in L'Aquila. *Structural Control and Health Monitoring*. Vol. 20, no. 9, pp. 1226–1239. ISSN 15452255. Available from DOI: 10.1002/stc.1531.
- RUSSO, S.; SPOLDI, E., 2020. Damage assessment of Nepal heritage through ambient vibration analysis and visual inspection. *Structural Control and Health Monitoring*. ISSN 1545-2255. Available from DOI: 10.1002/stc.2493.
- SAATY, T. L., 1990. How to make a decision: The analytic hierarchy process. *European Journal of Operational Research*. Vol. 48, no. 1, pp. 9–26. ISSN 03772217. Available from DOI: 10.1016/0377-2217(90)90057-I.
- SAISI, A.; GENTILE, C.; RUCCOLO, A., 2016. Pre-diagnostic prompt investigation and static monitoring of a historic bell-tower. *Construction and Building Materials*. Vol. 122, pp. 833–844. ISSN 09500618. Available from DOI: 10.1016/j.conbuildmat.2016.04.016.
- SALOUSTROS, S.; CERVERA, M.; PELÀ, L., 2019. *Archives of Computational Methods in Engineering*. Vol. 26, Challenges, Tools and Applications of Tracking Algorithms in the Numerical Modelling of Cracks in Concrete and Masonry Structures. No. 4. ISBN 0123456789. ISSN 18861784. Available from DOI: 10.1007/s11831-018-9274-3.
- SÁNCHEZ, A. R.; MELI, R.; CHÁVEZ, M. M., 2015. Structural Monitoring of the Mexico City Cathedral (1990–2014). *International Journal of Architectural Heritage*. Vol. 10, no. 2-3, p. 15583058.2015.1113332. ISSN 1558-3058. Available from DOI: 10.1080/15583058.2015.1113332.
- SANGIORGIO, V.; UVA, G.; ADAM, J. M., 2020. Integrated Seismic Vulnerability Assessment of Historical Masonry Churches Including Architectural and Artistic Assets Based on Macro-element Approach. *International Journal of Architectural Heritage*, pp. 1–14. ISSN 1558-3058. Available from DOI: 10.1080/15583058.2019.1709916.
- SAPIC, 1996. *Works to consolidate Baroque chapels and restore the south facade of the church of the monastery of Sant Cugat dels Vallès (Obres de consolidació de les capelles barroques i restauració de la façana sud de l'església del monestir de Sant Cugat dels Vallès)*.

- SATHIPARAN, N.; RUMESHKUMAR, U., 2018. Effect of moisture condition on mechanical behavior of low strength brick masonry. *Journal of Building Engineering*. Vol. 17, no. February, pp. 23–31. ISSN 23527102. Available from DOI: 10.1016/j.jobee.2018.01.015.
- SCHULLER, M. P., 2003. Nondestructive testing and damage assessment of masonry structures. *Progress in Structural Engineering and Materials*. Vol. 5, no. 4, pp. 239–251. ISSN 1365-0556. Available from DOI: 10.1002/pse.160.
- SEGURA, J.; APONTE, D.; PELÀ, L.; ROCA, P., 2020. Influence of recycled limestone filler additions on the mechanical behaviour of commercial premixed hydraulic lime based mortars. *Construction and Building Materials*. Vol. 238, p. 117722. ISSN 09500618. Available from DOI: 10.1016/j.conbuildmat.2019.117722.
- SEGURA, J.; PELÀ, L.; ROCA, P.; CABANÉ, A., 2019. Experimental analysis of the size effect on the compressive behaviour of cylindrical samples core-drilled from existing brick masonry. *Construction and Building Materials*. Vol. 228, p. 116759. ISSN 09500618. Available from DOI: 10.1016/j.conbuildmat.2019.116759.
- SEVIERI, G.; GALASSO, C.; D'AYALA, D.; DE JESUS, R.; ORETA, A.; GRIO, M. E. D. A.; IBABAO, R., 2020. A multi-hazard risk prioritisation framework for cultural heritage assets. *Natural Hazards and Earth System Sciences*. Vol. 20, no. 5, pp. 1391–1414. ISSN 1684-9981. Available from DOI: 10.5194/nhess-20-1391-2020.
- SHI, H.; WORDEN, K.; CROSS, E. J., 2016. A nonlinear cointegration approach with applications to structural health monitoring. *Journal of Physics: Conference Series*. Vol. 744, no. 1. ISSN 17426596. Available from DOI: 10.1088/1742-6596/744/1/012025.
- SMITH, G., 2012. Simple Regression. In: *Essential Statistics, Regression, and Econometrics*. Elsevier, pp. 219–258. Available from DOI: 10.1016/B978-0-12-382221-5.00008-8.
- SOHN, H., 2007. Effects of environmental and operational variability on structural health monitoring. *Philosophical Transactions of the Royal Society A: Mathematical, Physical and Engineering Sciences*. Vol. 365, no. 1851, pp. 539–560. ISBN 1364-503X. ISSN 1364-503X. Available from DOI: 10.1098/rsta.2006.1935.
- STONE CONTACT, INTERNATIONAL BUILDERS MARKETPLACE, 2017. *Piedra de Vinaixa - Beige Sandstone - StoneContact.com* [<https://www.stonecontact.com/piedra-de-vinaixa/s8745>]. (Accessed on 10/10/2017).
- SWAMY, R. N.; BANDYOPADHAY, A. K., 1975. The elastic properties of structural lightweight concrete. *Proceedings of the Institution of Civil Engineers*. Vol. 59, no. 3, pp. 381–394. ISSN 1753-7789. Available from DOI: 10.1680/iicep.1975.3671.
- TAKABAYASHI, T., 1954. Comparison of dynamic Young's modulus and static Young's modulus for concrete. *RILEM international symposium on nondestructive testing of materials and structures*. Vol. 1, no. Paris, pp. 34–44.
- TENA, M.; LEÓN, J., 2016. Base management heritage system: Methods of structural qualification and maintenance costs estimated over time. In: *Structural Analysis of Historical Constructions: Anamnesis, diagnosis, therapy, controls - Proceedings of the 10th International Conference on Structural Analysis of Historical Constructions, SAHC 2016*. Leuven: CRC Press, pp. 193–200. ISBN 9781138029514. Available from DOI: 10.1201/9781315616995-25.
- TOLL, D. G.; ABEDIN, Z.; BUMA, J.; CUI, Y.; OSMAN, A. S.; PHOON, K., 2012. *The impact of changes in the water table and soil moisture on structural stability of buildings and foundation systems : systematic review CEE10-005 (SR90)*. Available also from: <http://dro.dur.ac.uk/18298/>.
- TOTOEV, Y. Z.; NICHOLS, J. M., 1997. A Comparative Experimental Study of the Modulus of Elasticity of Bricks and Masonry. In: *11th International Brick/Block Masonry Conference*. No. October.
- ULGEN, K., 2002. Experimental and theoretical investigation of effects of wall's thermophysical properties on time lag and decrement factor. *Energy and Buildings*. Vol. 34, no. 3, pp. 273–278. ISSN 03787788. Available from DOI: 10.1016/S0378-7788(01)00087-1.
- UNITED NATIONS GENERAL ASSEMBLY, 2016. *Report of the open-ended intergovernmental expert working group on indicators and terminology relating to disaster risk reduction*.

- VALLUZZI, M. R.; CESCATTI, E.; CARDANI, G.; CANTINI, L.; ZANZI, L.; COLLA, C.; CASARIN, F., 2018. Calibration of sonic pulse velocity tests for detection of variable conditions in masonry walls. *Construction and Building Materials*. Vol. 192, pp. 272–286. ISSN 09500618. Available from DOI: 10.1016/j.conbuildmat.2018.10.073.
- VAN BALEN, K., 2017. Challenges that Preventive Conservation poses to the Cultural Heritage documentation field. In: *ISPRS - International Archives of the Photogrammetry, Remote Sensing and Spatial Information Sciences, XLII-2/W5*, pp. 713–717. ISSN 2194-9034. Available from DOI: 10.5194/isprs-archives-XLII-2-W5-713-2017.
- VAN BALEN, K., 1996. Expert system for evaluation of deterioration of ancient brick masonry structures. *Science of The Total Environment*. Vol. 189-190, pp. 247–254. ISSN 00489697. Available from DOI: 10.1016/0048-9697(96)05215-1.
- VAN GENECHTEN, B.; SANTANA QUINTERO, M.; DE BRUYNE, M.; POELMAN, R.; HANKAR, M.; BARNES, S.; CANER, H.; BUDEI, L.; HEINE, E.; REINER, H.; LERMA GARCÍA, J. L.; BIOSCA TARONGER, J. M., 2008. *Theory and practice on Terrestrial Laser Scanning: Training material based on practical applications*. Universidad Politecnica de Valencia Editorial. ISBN 978-84-8363-312-0.
- VASANELLI, E.; COLANGIULI, D.; CALIA, A.; SBARTAĬ, Z.-M.; BREYSSE, D., 2017. Combining non-invasive techniques for reliable prediction of soft stone strength in historic masonries. *Construction and Building Materials*. Vol. 146, pp. 744–754. ISSN 09500618. Available from DOI: 10.1016/j.conbuildmat.2017.04.146.
- VELASQUEZ, M.; HESTER, P. T., 2013. An Analysis of Multi-Criteria Decision Making Methods. *International Journal of Operations Research*. Vol. 10, no. 2, pp. 56–66. ISSN 1813-713X.
- VERBEKE, S.; AUDENAERT, A., 2018. Thermal inertia in buildings: A review of impacts across climate and building use. *Renewable and Sustainable Energy Reviews*. Vol. 82, no. September 2017, pp. 2300–2318. ISSN 13640321. Available from DOI: 10.1016/j.rser.2017.08.083.
- VICENTE, R.; PARODI, S.; LAGOMARSINO, S.; VARUM, H.; SILVA, J. A. R. M., 2011. Seismic vulnerability and risk assessment: case study of the historic city centre of Coimbra, Portugal. *Bulletin of Earthquake Engineering*. Vol. 9, no. 4, pp. 1067–1096. ISSN 1570-761X. Available from DOI: 10.1007/s10518-010-9233-3.
- WESCHE, K.; MANN, W., 1970. Résultats d'une enquête internationale sur la détermination du module d'élasticité du béton en compression. *Matériaux et Constructions*. Vol. 3, no. 3, pp. 179–196. ISSN 0025-5432. Available from DOI: 10.1007/BF02478969.
- WITZANY, J.; CEJKA, T.; ZIGLER, R., 2010. The Effect of Moisture on Significant Mechanical Characteristics of Masonry. *Engineering Structures and Technologies*. Vol. 2, no. 3, pp. 79–85. ISSN 2029-882X. Available from DOI: 10.3846/skt.2010.11.
- WORDEN, K.; FARRAR, C. R.; MANSON, G.; PARK, G., 2007. The fundamental axioms of structural health monitoring. *Proceedings of the Royal Society A: Mathematical, Physical and Engineering Sciences*. Vol. 463, no. 2082, pp. 1639–1664. ISSN 14712946. Available from DOI: 10.1098/rspa.2007.1834.
- YOON, K. P.; HWANG, C. L., 1995. *Sage University Paper series on Quantitative Applications in the Social Sciences*. Multiple Attribute Decision Making: An Introduction. Thousand Oaks, CA: Sage. ISBN 9780803954861.
- ZEMAN, J.; NOVÁK, J.; ŠEJNOHA, M.; ŠEJNOHA, J., 2008. Pragmatic multi-scale and multi-physics analysis of Charles Bridge in Prague. *Engineering Structures*. Vol. 30, no. 11, pp. 3365–3376. ISSN 01410296. Available from DOI: 10.1016/j.engstruct.2008.05.012.
- ZIMMERMAN, R. W., 1985. The effect of microcracks on the elastic moduli of brittle materials. *Journal of Materials Science Letters*. Vol. 4, no. 12, pp. 1457–1460. ISSN 0261-8028. Available from DOI: 10.1007/BF00721363.

II

Publications

Dynamic elastic properties of brick masonry constituents

Nirvan Makoond · Luca Pelà · Climent Molins

Accepted manuscript in *Construction and Building Materials*.

Submitted: 07 September 2018

Revised: 08 November 2018

Accepted: 13 December 2018

Dynamic elastic properties of brick masonry constituents

Nirvan Makoond*, Luca Pelà, Climent Molins

Department of Civil and Environmental Engineering, Universitat Politècnica de Catalunya (UPC-BarcelonaTech), Jordi Girona 1-3, 08034 Barcelona, Spain

Abstract

When subjected to dynamic loading, materials can exhibit a mechanical behaviour quite different from its static counterpart. The evaluation of dynamic properties is thus very useful in the assessment of existing masonry structures. This paper presents results of an experimental campaign to determine both the dynamic Young's modulus and the shear modulus of brick masonry constituents through two non-destructive testing methods. Following a discussion on the reliability of the methods, a robust procedure is described and tested on a variety of samples. The results show that the techniques can be successfully applied to provide reliable estimates of the dynamic elastic properties of brick masonry constituents.

Keywords: Brick masonry, Non-destructive testing (NDT), Impulse excitation of vibration (IEV), Ultrasonic pulse velocity (UPV), Elastodynamics, Young's modulus, Shear modulus, Poisson's ratio

Link to formal publication: <https://doi.org/10.1016/j.conbuildmat.2018.12.071>

1. Introduction

Static elastic properties of masonry constituents are in general well understood. Indeed, a considerable amount of information is available in literature on the determination and estimation of such properties. For instance, the European Committee for Standardisation (CEN) has approved a European Standard on the determination of the static elastic modulus for natural stone since 2005 [1]. Tests to determine static elastic properties rely mainly on measuring deformations while applying controlled loading. Hence, the modified application of recommendations from standards designed for other materials such as concrete is, at least in theory, relatively straightforward. As a consequence, several authors such as Binda et al. [2–5], Oliveira et al. [6–8] and Pelà et al. [9] have explored testing procedures to determine these properties for masonry constituents and assemblages. Many of these studies have shown that although the theory behind the evaluation of static elastic properties is well understood, the scatter of results in experimental studies remains high in many cases, often due to the difficulties related to measuring deformations in the elastic range of brittle materials such as those typically used as constituents in brick masonry constructions. Nevertheless, a considerable amount of information is still available, not only on best testing practices, but also on the range of expected results for different types of bricks and mortar, as well as on the effects which can influence the estimates of static elastic properties for brick masonry constituents.

Dynamic elastic properties refer to the constants that define a material's behaviour in the elastic range under vibratory conditions. When subjected to dynamic loading, experiments have shown that materials can feature a mechanical behaviour quite different from its static counterpart. A possible physical cause of this empirically known inequality between measured static and dynamic elastic moduli may be found in the different inelastic contributions to stress-strain which behave as a function of strain amplitude and frequency (energy and strain rate) [10]. Most of the studies available in literature focus on the relation between static and dynamic elastic properties of rocks in a geophysical context [11–14]. As such, although some authors, notably Totoev and Nichols [15, 16], have explored this relationship for specific types of bricks, it is still not

*Corresponding author

Email addresses: nirvan.makoond@upc.edu (Nirvan Makoond), luca.pela@upc.edu (Luca Pelà), climent.molins@upc.edu (Climent Molins)

25 well understood.

The evaluation of elastic dynamic mechanical properties can prove to be very useful for the safety assessment of structures exposed to dynamic loading conditions. These properties can be calculated using data obtained from vibration tests or from the measured velocity of stress waves passing through the material. 30 The American Society for Testing Materials (ASTM) approved two of the most relevant existing standards on test methods that can be used to evaluate these properties, namely:

- A standard on the evaluation of the dynamic Young's Modulus, Shear Modulus and Poisson's ratio by Impulse Excitation of Vibration (IEV) for homogeneous elastic materials [17].
- A standard for the determination of the propagation velocity of ultrasonic longitudinal stress waves 35 through concrete which can be related to the material's dynamic elastic properties [18].

Since dynamic properties are not evaluated directly but computed based on assumptions derived from the known behaviour of materials under specific conditions, the application of recommendations from standards is not so straightforward, particularly when they have been designed for different materials. The parameters being measured (wave travel time, frequency of vibration) often rely on many conditions which need to be 40 understood and controlled carefully. This operation is necessary to be able to use the expressions relating measured parameters to material constants.

The aforementioned work by Totoev and Nichols [15, 16] includes the evaluation of the dynamic Young's modulus for specific types of bricks. However, the range of experimental techniques as well as the range 45 of different constituents tested is rather limited, particularly when compared to the information available on static properties. Notably, the dynamic Young's modulus was only evaluated through means of longitudinal vibration tests and traditional ultrasonic pulse velocity (UPV) testing with longitudinal stress waves (P-waves). In such studies, the dynamic Poisson's ratio is assumed as being invariant from the quasi-static one, and no procedure is described for the experimental determination of the dynamic Poisson's ratio or shear modulus through torsional vibration tests. Although this is most likely a reasonable assumption, there is not sufficient information available in literature for this relationship to be well-established. In fact, studies available in literature involving the determination of dynamic Poisson's ratio or shear moduli, such as [19] and [20], have only focused on very specific types of constituents. Moreover, although Totoev and Nichols [15, 16] mention that UPV measurements can provide information on the isotropy of bricks, no 50 detailed information is provided on the validity or correct interpretation of P-wave travel time readings for anisotropic cases. In such cases, wave propagation is not necessarily governed by the same simplified laws as in isotropic media and therefore evaluation of the dynamic modulus of elasticity using P-wave velocities alone can be quite unreliable. Finally, in order to carry out the longitudinal vibration tests, the specimens are cut from whole bricks so that each resulting specimen has a greater ratio between the lateral dimensions 60 and the length. Thus the non-destructive nature of the vibrational tests is not fully exploited.

The main aim of this research is to assess the applicability of a combined procedure based on two non-destructive techniques to experimentally determine both the dynamic Young's modulus and shear modulus of brick masonry constituents. The two chosen methods are UPV testing with P-waves and IEV testing. 65 The theory behind these two methods, as well as the respective procedures for the estimation of the dynamic elastic properties, are described in Section 2. The two techniques were selected not only because of the simplicity and speed of their application, but also because they make use of equipment that is nowadays widely used in the construction industry and hence relatively accessible. UPV testing with P-wave transducers is commonly used for non-destructive quality control of concrete while accelerometers and data acquisition 70 systems required for IEV testing are used for dynamic response testing and monitoring of many structures, such as bridges and towers. Moreover, the research also aims to test whole brick specimens since this would allow these methods to be applied to recently manufactured bricks as well as to those extracted from existing constructions. Mortar samples tested as part of this research were cast in moulds having dimensions of a standard brick ($290 \times 140 \times 40 \text{ mm}^3$).

75 Different types of bricks and mortars were explored in order to derive useful ranges of results for different masonry typologies. Although an effort has been made to include specimens of varied quality and porosity in the sample set to appropriately validate testing protocols and analysis procedures, explicitly defining the relationship between porosity or chemical composition of the materials to the dynamic elastic properties is

beyond the scope of this research. Previous studies available in literature such as [21] and [22] address these relationships more directly for specific types of materials (alumina ceramics and specific stones).

As a result, a robust methodology, combining information from both UPV and IEV testing, for the determination of dynamic elastic properties of typical brick masonry constituents is proposed.

2. Background & theory

This section introduces the theory behind the two main testing techniques employed as part of this research. It highlights important concepts that are essential to the correct interpretation of results from IEV and UPV testing.

2.1. Impulse excitation of vibration (IEV) testing

It is known that specimens of elastic materials possess specific mechanical resonant frequencies that are determined by the elastic properties, mass, geometry of the test specimen and boundary conditions imposed by the test set-up. The dynamic elastic properties of a material can therefore be computed if the geometry, mass, and mechanical resonant frequencies of a suitable test specimen of that material can be measured. Test set-ups that isolate specific resonance modes together with the processing of recorded vibration signals, allow these resonant frequencies to be determined. Specifications on specimen dimensions, test set-ups, expressions relating identified resonant frequencies to dynamic properties as well as other considerations are described thoroughly in the Standard Test Method for Dynamic Young's Modulus, Shear Modulus, and Poissons Ratio by Impulse Excitation of Vibration released by ASTM [17].

The dynamic Young's modulus can be determined using the resonant frequency in either the flexural or the longitudinal mode of vibration. For the purpose of this study, the dynamic Young's modulus was only evaluated using the resonant frequency in the flexural mode because the ratios of dimensions of typical bricks means that the resonant frequency of the longitudinal mode would be much higher than that of the flexural mode. Since these frequencies were found to already be relatively high in the flexural mode, a quick estimate of the expected frequencies to be measured for the same Young's modulus in the longitudinal mode revealed that this frequency would fall outside the range that could be accurately measured by the data acquisition system. The dynamic shear modulus, or modulus of rigidity, is found using torsional resonant vibrations. To isolate the flexural mode of vibration, the ASTM standard [17] states that the rectangular specimen should be supported along the width at a distance of $(0.224 \times Length)$ from either end of the length, as shown in Figure 1(a). On the other hand, to isolate the torsional mode, the rectangular specimen should be supported along the midpoints across the width and length as shown in Figure 1(b). Figure 1 also shows the recommended impact and sensor locations for each test. An important recommendation from the ASTM standard [17] is to place any direct contact transducers along the nodal lines which ensures minimal interference with the free-vibration of the specimen.

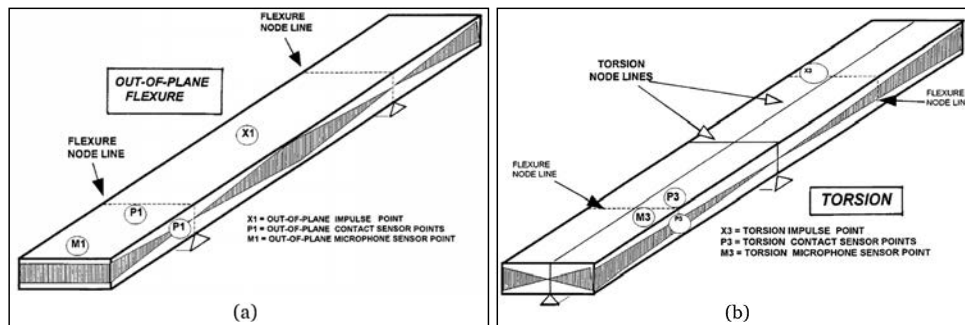


Figure 1: Impulse Excitation of Vibration: Specified test set-up, sensor and impact locations for the flexural mode(a) and torsional mode(b) according to [17].

For the fundamental flexure frequency of a rectangular bar, the dynamic Young's modulus can be evaluated using Equation (1), whilst for the fundamental torsional frequency, the dynamic shear modulus can be computed using Equation (2).

$$E = 0.9465 \left(\frac{m f_f^2}{b} \right) \left(\frac{L^3}{t^3} \right) T_1 \quad (1)$$

$$G = \frac{4Lmf_t^2}{bt} [B/(1+A)] \quad (2)$$

Where E is the dynamic Young's modulus (Pa), m is the mass of the bar (g), b is the width of the bar (mm), L is the length of the bar (mm), t is the thickness of the bar (mm), f_f is the resonant frequency in flexure (Hz), T_1 is a correction factor dependent on Poisson's ratio as well as t and L , G is the dynamic shear modulus (Pa), f_t is the resonant frequency in torsion (Hz), B and A are correction factors dependent on b and t .

As we can see from Equation (2), the computation of the dynamic shear modulus from the measured torsional resonant frequency does not require knowledge of the dynamic Poisson's ratio. However, this unknown parameter is required for the evaluation of the T_1 parameter in Equation (1). If isotropy is assumed, there exists a well known relationship between the Poisson's ratio, the Young's modulus and the shear modulus. Hence, for the isotropic case, the iterative procedure shown in Figure 2 can be used to find a suitable Poisson's ratio that will satisfy this relationship. In order for the iterative procedure to converge, a reasonable initial Poisson's ratio (ν_0) has to be selected. For all the specimens tested as part of this research, a ν_0 of 0.2 proved to be a good initial value to attain convergence.

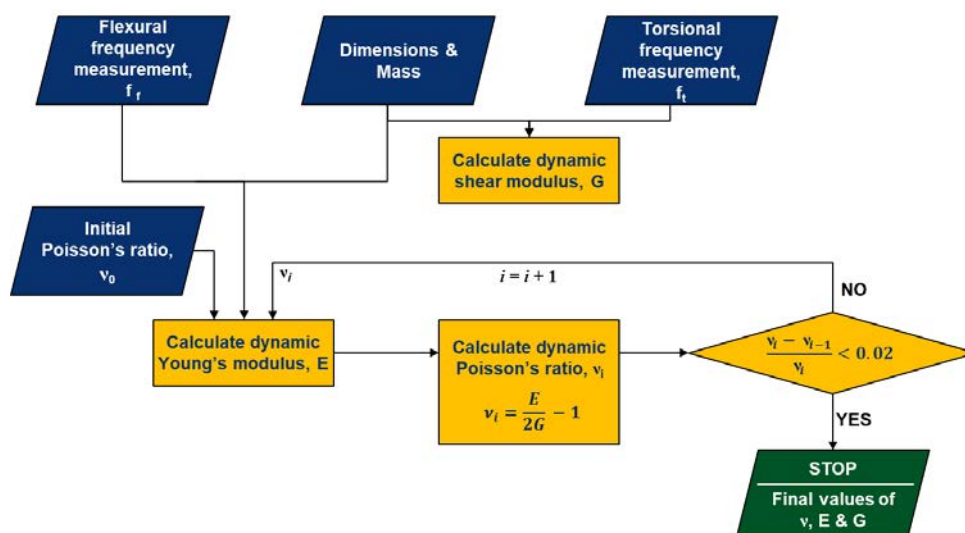


Figure 2: Impulse Excitation of Vibration: Procedure for estimating dynamic Young's modulus, shear modulus and Poisson's ratio according to [17].

2.2. Ultrasonic pulse velocity (UPV) testing

Research on wave propagation in elastic solid materials dates back to the early 19th century [23]. UPV testing makes use of elastic (or acoustic) waves which are in fact mechanical vibrations that propagate in gases, liquids and solids. Ultrasound corresponds to mechanical waves propagating at frequencies above the range of human hearing (conventionally 20 kHz) [24].

Although many different patterns of vibrational motion exist at the atomic level, in solids it can be said that two modes of bulk wave propagation exist that are most relevant to ultrasonic testing in the context of this research, namely:

- **Longitudinal waves:** Waves with particle displacement in the direction of wave propagation. These waves travel the fastest and are also known as compression waves or P-waves. The most accessible and commonly used electro-acoustical transducers in the construction industry produce waves primarily of this type [25].
- **Shear waves:** Also known as transverse waves, the direction of vibrations in these waves is normal to the direction of wave propagation [26]. Note that the direction of particle vibration is referred to as the polarization.

2.2.1. Wave propagation in isotropic media

The micro-structure of many engineering materials is formed from many randomly oriented grains which results in the mechanical properties being independent of direction on the macroscopic scale. These materials are therefore isotropic. In the case of ultrasonic wave propagation, when the ultrasonic wavelength is much greater than the grain size, isotropic assumptions are quite valid [27]. Under these circumstances, bulk waves propagate with equal velocity in every direction. Hence, in an infiniteⁱ isotropic material, wave energy may only propagate in two modes: longitudinal or shear. The equation of motion for an elastic isotropic solid can be decomposed into the following two wave equations relating the velocity of propagation of a longitudinal wave (c_l) and of a shear wave (c_s) to the material density ρ and the two constants used in Hooke's law for an elastic isotropic material (Young's Modulus E and Poisson's ratio ν) [27, 29].

$$c_l = \left(\frac{E(1-\nu)}{\rho(1+\nu)(1-2\nu)} \right)^{\frac{1}{2}} \quad (3)$$

$$c_s = \left(\frac{E}{2\rho(1+\nu)} \right)^{\frac{1}{2}} \quad (4)$$

However, if a wave encounters a boundary separating two media with different properties, part of the disturbance is reflected and part is transmitted into the second medium [23]. Similarly, if a body has a finite cross-section which is comparable to the wavelength of the disturbance, waves can bounce back and forth between the bounding surfaces. Such circumstances can significantly increase the complexity of analysing the recorded wave signals and relating dynamic elastic properties of the material to travel time measurements. This extra layer of complexity can be avoided by selecting the frequency of the signal generated by the ultrasonic transducer, as described in detail in Section 3.3.1.

2.2.2. Standard test methods

As previously mentioned, UPV testing in the construction industry has traditionally been limited to P-wave measurements mainly used for inspection and quality control. As such, the most relevant standards for the purpose of this investigation only cover determination of the propagation velocity of ultrasonic longitudinal waves in hardened concrete (EN 12504-4:2004 [30] and ASTM C597 [18]). Although the ASTM standard presents the relationship shown in Equation (3), it clearly states that the method should not be considered an adequate test for establishing compliance of the modulus of elasticity of field concrete with that assumed in the design. One of the reasons for this is that the relationship described in Equation (3) requires knowledge of the dynamic Poisson's ratio to determine the dynamic Young's modulus from the pulse velocity. Since the ASTM C597 standard is concerned only with determination of the velocity, it provides no indication of how to determine the Poisson's ratio.

The standard test method makes use of a pulse generator, a pair of electro-acoustical transducers, an amplifier, a time measuring circuit and a time display unit as shown in Figure 3.

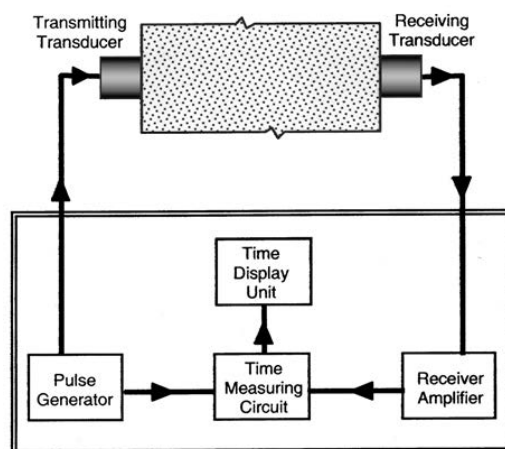


Figure 3: Ultrasonic Pulse Velocity: Test set-up according to ASTM C597 [18]

ⁱNote that in this context, infinite media means that boundaries have no influence on wave propagation [28].

It is stated that for best results, the transducers should be located directly opposite each other. The distance between centres of transducer faces must be measured, and the pulse velocity can then be calculated by dividing this distance by the pulse transit time measured using the apparatus as shown in Figure 3.

2.2.3. Wave propagation in anisotropic media

Previous research indicates that bricks formed by extrusion can exhibit a significant level of anisotropy [31]. Wave propagation in anisotropic media is substantially different from the isotropic case. The most significant difference is that elastic waves propagate with a velocity that depends on direction [27]. Moreover, the number of independent constants which define the elastic behaviour of the material itself will be greater than 2 and will depend on the symmetry class or type of anisotropy assumed. Assuming an orthotropic material will result in 9 independent elastic constants while assuming transverse isotropy (material with a plane of isotropy) will result in 5. Furthermore, unlike the isotropic case, the wave modes are not necessarily pure modes as the particle vibration is neither parallel nor perpendicular to the propagation direction [27]. In practice however, the anisotropic modes do show similarities to the isotropic modes and in these cases are referred to as quasi-longitudinal and quasi-shear. The quasi-shear modes are distinguished further by whether they are primarily horizontally (SH-waves) or vertically (SV-waves) polarized.

Christoffel's equations can be used to relate measured ultrasonic pulse velocities to the elastic constants. These expressions and related experimental procedures are not discussed here but a thorough description is given in [29]. However, because the propagation of a wave along a specific plane does not depend on all the elastic constants used in the material definition, the experimental procedure has to include measurements across different planes. Moreover, the velocities of three wave modes (P-waves, SH-waves and SV-waves) need to be measured across each of these planes in order to determine the elastic constants. Hence, the full elastic characterisation of an anisotropic material cannot be directly determined using P-wave velocity measurements alone.

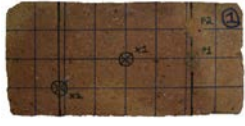
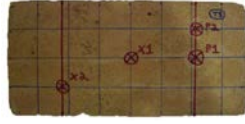



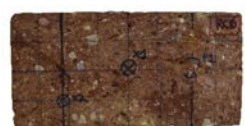

3. Experimental program

The experimental campaign was carried out at the Laboratory of Technology of Structures and Building Materials of the Universitat Politècnica de Catalunya (UPC-BarcelonaTech). This section presents information about the material components, the preparation of the specimens and the testing procedures.

3.1. Materials tested

7 different groups of solid bricks were tested in order to investigate different types of materials, both used in existing and new constructions. 5 of these groups (I(a), I(b), III, V(a) and V(b)) consisted of handmade bricks formed by moulding. Of these, 2 groups (I(a) and I(b)) consisted of solid terracotta bricks, tested after production, before use in any construction project. On the other hand, group III bricks have been extracted from an industrial complex built in the early 20th Century, part of Barcelona's industrial heritage. Bricks from group V(a) and V(b) were extracted from a typical residential building located in Rambla de Catalunya, a street in the centre of Barcelona. It should be noted that the UPV testing procedure for specimens from group V(b) consisted of less measurements (more detail is given in Section 3.3.3). The 2 groups of solid bricks manufactured using a conventional extrusion process (II and IV) were both tested before use in any construction project. The type of bricks from group II have been used to build timber vaults in an ongoing construction project in Barcelona. Finally, bricks from group IV are manufactured using an automated process and are compliant with the EN 771-1:2011 standard [32]. A brief summary of the different groups tested is given in Table 1.

Table 1: Groups of brick types tested.

Group	Specimen labels	Manufacturing	Year	f_{cn}^* [MPa]	Avg. Mass [g]	Average measured dimensions [mm ³]	Sample view
I(a)	1 - 7	Handmade in moulds	2017	17.4	3,212	40 × 147 × 306	
I(b)	T1 - T6	Handmade in moulds	2015	17.4 [†]	3,136	40 × 146 × 306	
II	SF1 - SF5	Conventional extrusion	2016	40.0	2,549	38 × 141 × 291	
III	FC1 - FC3	Handmade in moulds	1903	18.8	2,900	43 × 144 × 294	
IV	A1 - A6	Conventional extrusion	2018	52.7	2,423	40 × 132 × 272	
V(a)	RC6,RC8	Handmade in moulds	1930	10.7 [‡]	2,907	40 × 145 × 291	
V(b)	W2L1 - W2L5, W2L7	Handmade in moulds	1930	10.7	3,134	43 × 145 × 294	




* Reference normalised compressive strength for corresponding brick type obtained by testing bricks in accordance with the European standard EN 772-1 [33].

[†] Same reference normalised compressive strength shown as bricks from group I(a). Bricks from group I(b) were produced with the same raw materials and using the same manufacturing technique as bricks from group I(a).

[‡] Same reference normalised compressive strength shown as bricks from group V(b). Bricks from group V(a) were extracted from the same wall as bricks from group V(b).

Two different types of mortar, which can be considered as being at either end of the range of stiffness encountered in brick masonry structures, were prepared and tested, i.e. a weakened hydraulic lime mortar (MB and MIIB specimen groups) and a cement mortar (MC). The M5 hydraulic lime was weakened by the addition of an inert limestone filler so that it would be more representative of weaker mortars found in historical constructions. Specimens from group MB were uncast after 5 days and tested after 28 days since initial casting. Since specimens from group MB were found to be still relatively fragile at the time of uncasting, MIIB mortar specimens were uncast after 14 days. These specimens were also tested 28 days after initial casting. Finally, the cement mortar specimens were uncast after 1 day and tested 14 days after casting. Table 2 provides a summary of the most important characteristics of the different mortar specimen groups tested.

Table 2: Groups of mortar types tested.

Group	Specimen labels	Mix proportions	f_{cn}^* (28 days) [MPa]	Avg. Mass [g]	Average measured dimensions [mm ³]	Sample view
MB	MB1 - MB5	Lime : filler : water 1 : 0.64 : 0.37	2.3	2,930	41 × 139 × 290	
MIIB	MIIB1 - MIIB8	Lime : filler : water 1 : 0.64 : 0.37	2.0	3,237	42 × 139 × 290	
MC	MC1 - MC5	Cement : sand : water 1 : 3 : 0.5	49.3	3,632	41 × 139 × 291	

* Reference normalised compressive strength for corresponding mortar type obtained by testing prismatic specimens in accordance with the European standard EN 1015-11 [34].

3.2. Impulse excitation of vibration testing

3.2.1. Testing equipment

For each IEV test, a suitable data acquisition system able to record the vibrations of the specimen was required so that the resonant frequency could then be extracted from the resulting acceleration-time history. The data acquisition system designed for these tests consisted of a lightweight (25 g) triaxial integrated circuit piezoelectric accelerometer, a signal conditioner (PCB 482A16) and an embedded real-time controller (cRIO-9064) equipped with a vibration input module (NI-9234). During testing, the real-time controller was connected to a laptop equipped with a program specifically created for these acquisitions using the LabVIEW 2016 programming environment from National Instruments [35].

3.2.2. Specimen preparation

It is clear from Equation (1) that the accuracy of the estimated dynamic elastic modulus is highly dependent on the regularity of the specimen and the uncertainty related to its dimensions. For instance, since the thickness and length variables in the modulus equation have an exponent of 3, an error of 1% in these dimensions would result in an error of 3% in the estimated modulus. Hence, in order to reduce the variations in dimensions within each specimen, the surfaces of brick specimens were polished in order to regularise the faces.

It is important to note that moisture content of the specimens can have an effect on the observed resonant frequency and hence on the estimated dynamic elastic properties. In order to control this parameter, all specimens were dried at 120 °C in a drying oven until the mass was constant as recommended in [36] before the execution of any tests.

Preparation of specimens also entailed marking the lines along which each specimen should be supported during testing to isolate the fundamental flexural and torsional modes. Finally, the impact and sensor locations were also marked as shown in Figure 4 in order to facilitate mounting of the sensor and ensure consistent impulse excitations.

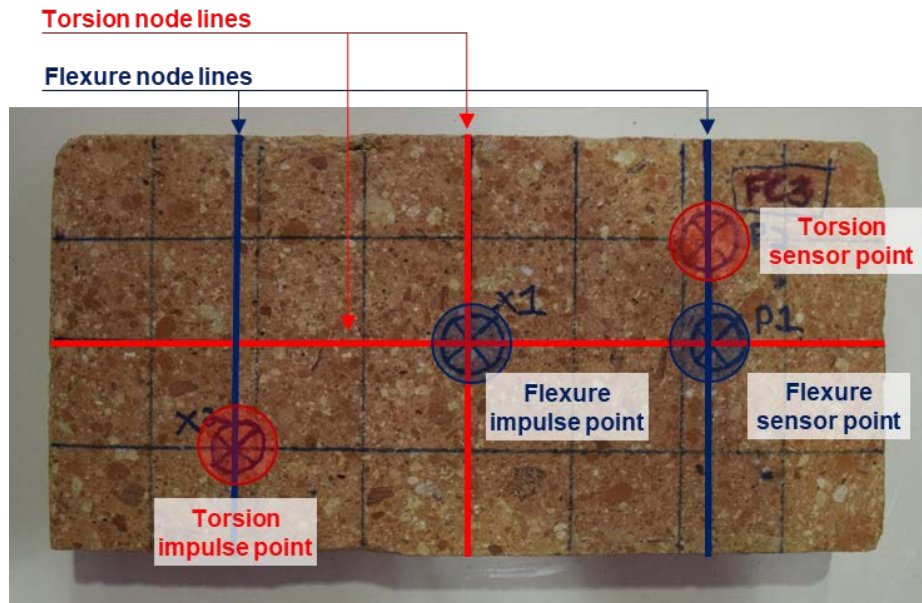


Figure 4: Markings made on every specimen prior to IEV testing.

3.2.3. Test set-up

Simple custom rigid supports were fabricated in order to isolate the flexural and torsional modes. For all tests, the supports were placed on isolation pads in order to prevent ambient vibrations from being picked up by the accelerometer. The supports were metallic and had a sharp edge in contact with the specimen along the nodal lines. The supports can be seen in Figure 5 which also shows the test set-ups used for flexural (a) and torsional (b) IEV tests on whole bricks.

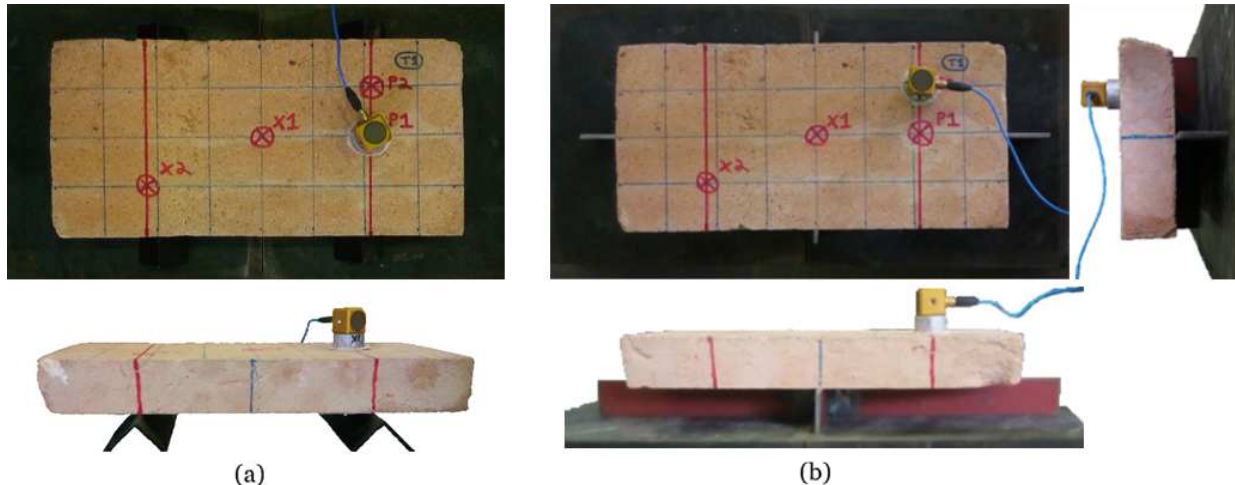


Figure 5: (a) Test set-up for flexural IEV test (view from top and front). (b) Test set-up for torsional IEV test (view from top, front and side).

For all tests on bricks, the accelerometer was fixed using an adhesive mounting technique via a lightweight (18 g) aluminium mounting plate fixed to the brick's surface using a 2-component cold curing superglue. This ensured adequate vibration transmissibility while also reducing any mass loading effects (see Figure 5). Although this technique proved to impart very little damage on most bricks, removal of the mounting plate did cause some loss of material from the surface of many bricks. This loss of material proved to be quite significant in the case of the fragile MB Mortars. Since one of the secondary aims of this research campaign is to keep the specimens as intact as possible for further testing, a less intrusive mounting method was desirable, particularly for the more fragile lime mortar specimens. Hence, a different mounting technique was tested which involved fixing the accelerometer on the surface of the specimen using scrim-backed adhesive tape as shown in Figure 6. Naturally, this technique further reduces any mass loading effects since the mass of

the adhesive tape is much lower than that of the mounting plate. However, since it is a less commonly used mounting technique than the aforementioned one, the adequacy of its vibration transmissibility had to be verified for the purpose of these tests. In order to achieve this, a comparative study was carried out between the two mounting methods on all the specimens from the MB mortar group. The observed resonant frequency was found to differ by less than 1.2% across all the specimens. Hence, the mounting technique with the scrim-backed adhesive tape was used to test all mortar specimens to avoid any further damage to the specimens.

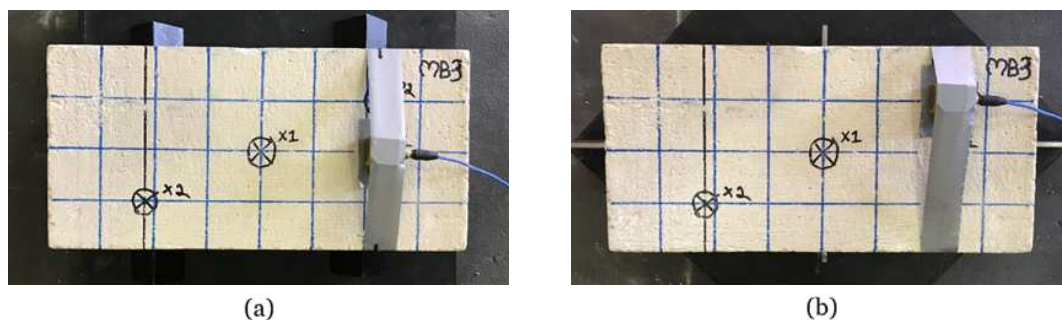


Figure 6: Accelerometer mounting using scrim-backed adhesive tape for (a) flexural test set-up and (b) torsional test set-up of IEV tests.

Another important consideration before testing any specimens involves selecting an appropriate sampling frequency to be used for all the tests. Based on the capabilities of every element of the data acquisition system, a sufficiently high sampling frequency must be chosen to prevent any aliasing. This requires an estimation of the expected resonant frequencies that need to be measured. In the case of the specimens tested for this research campaign, the observed resonant frequencies varied from 586 Hz to 1794 Hz for the flexural tests and from 746 Hz to 2099 Hz for the torsional tests. A sampling frequency of 20 kHz was used for all the IEV tests.

3.2.4. Testing procedure

Before actually executing the vibration tests, the mass and dimensions of each specimen had to be determined accurately for consequent computation of the dynamic elastic properties. The mass was determined using an electronic balance with a precision of 0.5 g, satisfying the 0.1% of specimen mass requirement stipulated in the ASTM standard [17] for all specimens tested. Each dimension was taken as the average of multiple readings along each of them at the locations shown in Figure 7. These measurements were taken with a Vernier caliper with a precision of 0.02 mm. The multiple measurements were not only used to compute the average dimensions but also to quantify the variation in dimensions of the specimens. The coefficients of variation of all dimensions of all specimens were found to be less than 2% except for 6 specimens which had coefficients of variations of less than 4% for the measured thickness dimensions.

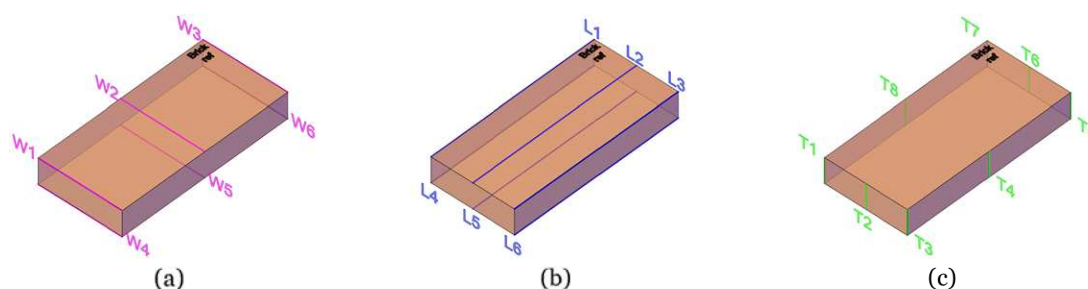


Figure 7: Locations of the 20 measurements taken with a Vernier caliper for every specimen tested under IEV. (a) 6 measurements of the length taken for every specimen. (b) 6 measurements of the width taken for every specimen. (c) 8 measurements of the thickness taken for every specimen.

Once the set-ups described in the previous section have been prepared, the IEV tests simply involve applying an impulse at the specified location using an impact tool which satisfies the requirements stated in [17]. In practice, the size and geometry of the tool depends on the size and weight of the specimen and the force needed to produce vibration. In the case of the bricks, one of the most important considerations

was to ensure that the impact was not too strong for the higher amplitudes of the recorded signals not to fall outside the measurable range of the accelerometer (± 5 g).

For each IEV test, the vibration signals were recorded whilst the specimen was impacted several times (see Figure 8). An appropriate feature extraction procedure needed to be implemented in order to extract the resonant frequency from the acceleration-time histories. It should be noted that one of the requirements from the ASTM standard [17] is to determine the resonant frequency as the average of five consecutive readings which lie within 1% of each other. Because of this requirement, it was essential to be able to estimate the resonant frequency during testing itself. Hence, the Frequency Domain Decomposition (FDD) technique was used, because it does not only allow fast estimation of the resonant frequency but also exploits the data recorded from the 3 channels of the tri-axial accelerometer for improved accuracy. A custom script for processing the files generated by the LabVIEW acquisition program and subsequently carrying out FDD analysis was created in the MATLAB[®] computing environment [37] by modifying the original FDD script by [38]. This process is summarised in Figure 8.

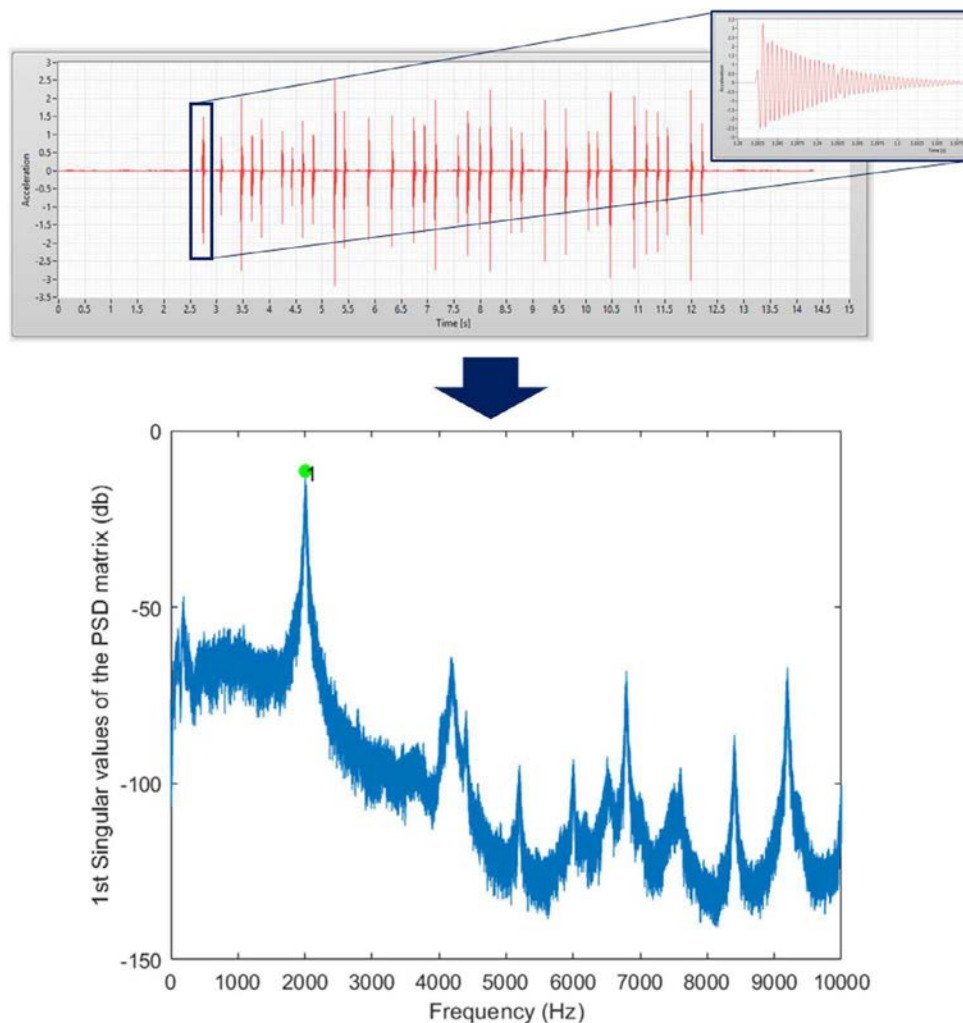


Figure 8: Top: Acceleration-time history for a single IEV test (with a zoom-in of a single impulse shown). Bottom: Selection of peak during FDD process.

Once the resonant frequencies were extracted, Equations (1) and (2) could be used to estimate the dynamic Young's modulus and shear modulus respectively. The iterative procedure described in Section 2.1 was used to estimate the dynamic Poisson's ratio and update the dynamic Young's modulus accordingly.

3.3. Ultrasonic pulse velocity testing

3.3.1. Testing equipment

320 The ultrasonic pulse travel times were recorded using a PROCEQ Pundit[®] PL-200 [39] commercial ultrasonic testing instrument. This equipment incorporates a pulse generator, receiver amplifier and time measuring circuit into one unit with a touch-screen display that can be used to view the waveform of recorded signals and pulse travel time in real-time. Different transducers can be used with this instrument, each of which is better suited for different applications.

325 The selection of the appropriate transducer is largely dependent on grain size and on the dimensions of the test object. The frequency of the transducer should be chosen so that the resulting ultrasonic pulse has a wavelength smaller than the minimum lateral dimension of the test specimen but at least twice as large as the grain size [39]. Since the wavelength is dependent on the velocity of propagation (wavelength equals velocity divided by frequency), the selection of an appropriate transducer before testing the material is not so straightforward. It is known that the ultrasonic pulse velocity in concrete ranges from 3000 m/s to 5000 m/s [39]. Most materials tested as part of this campaign are characterised by lower velocities. In fact, the observed velocities vary from 1132 m/s (Type V(b) brick) to 4270 m/s (CM Mortar). A pair of 250 kHz transducers was used for all the UPV tests carried out as part of this research, resulting in wavelengths ranging from 5 mm to 17 mm. These wavelengths are all smaller than 38 mm, the smallest thickness encountered across all specimens. Although this range of wavelengths can also be considered as being greater than the average grain size of the materials under test, in some cases, the specimens contained significant heterogeneities such as voids or aggregates that are larger than the aforementioned wavelength range. Moreover, the specimens characterised by lower ultrasonic pulse velocities also turn out to be the most heterogeneous. This results in a greater likelihood of scattering affecting the reliability of the results for these specimens, since the wavelengths of the ultrasonic pulses are smaller while the effective grain size can be considered as being larger due to the heterogeneities. Taking multiple readings at different locations can help to improve the reliability of results in such cases.

3.3.2. Treatment of specimens

345 Besides using a coupling gel between the transducers and the material during testing, the surfaces of the bricks were polished beforehand to ensure a smooth surface and hence prevent excessive loss of signal due to inadequate acoustic coupling. Since all the mortar specimens were cast in specifically designed moulds, their surfaces were adequately smooth and no further polishing was carried out.

350 As is the case for IEV tests, moisture content of the specimens is another factor that can influence UPV results. Hence, to control this parameter, all measurements were made on oven-dried specimens which had been allowed to stabilise to room temperature.

355 The final preparation step before executing the UPV tests involved marking the locations through which the velocity will be measured in order to be able to accurately position the transducers and measure the corresponding path lengths. A 4×8 grid of equal divisions on the largest faces of each specimen was used to locate all path lengths across the length, width and thickness (see Figure 4).

3.3.3. Testing procedure

360 Before any UPV tests were carried out, the mass and dimensions measured for the IEV tests were used to compute the density of the specimen which is required to evaluate the dynamic Young's modulus using Equation (3).

365 All measurements of pulse transit times were carried out using direct transmission with the transducers arranged directly opposite each other, widely considered as the optimum configuration for accurate pulse velocity determination. Using the UPV evaluated in this way into Equation (3) can be considered as giving a very localised estimate of the elastic properties since the velocity is only representative of the path along which the pulse travelled. Since it is known that many types of brick masonry constituents can have a significant level of heterogeneity, and even anisotropy in some cases, it is important to determine the pulse velocity at multiple locations and even across different directions before utilising them to evaluate the elastic constants describing the overall material behaviour. For the purpose of this research, three different variables were defined to describe the elastic moduli computed from multiple pulse velocities evaluated across the three different directions of each brick-sized specimen (length, width and thickness). They will hereafter

be referred to as $E_{UPV,L}$, $E_{UPV,W}$ and $E_{UPV,T}$.

375 For the UPV tests across the length and width of specimens, the reported pulse transit time at a single location was taken as the average of five consecutive readings with a coefficient of variation of less than 2% to reduce the effect of any measurement errors. The pulse transit time was measured at 3 locations across the length as shown in Figure 9 and 3 locations across the width as shown in Figure 10. The path lengths at these locations were measured using a Vernier caliper and the pulse velocity was computed by dividing
 380 the path length by the transit time. $E_{UPV,L}$ was then computed from Equation (3) using the average of the computed velocities from the 3 length locations specified and the Poisson's ratio estimated from the IEV tests. $E_{UPV,W}$ was computed using exactly the same procedure but using the velocities computed from the transit times and path lengths measured across the width.

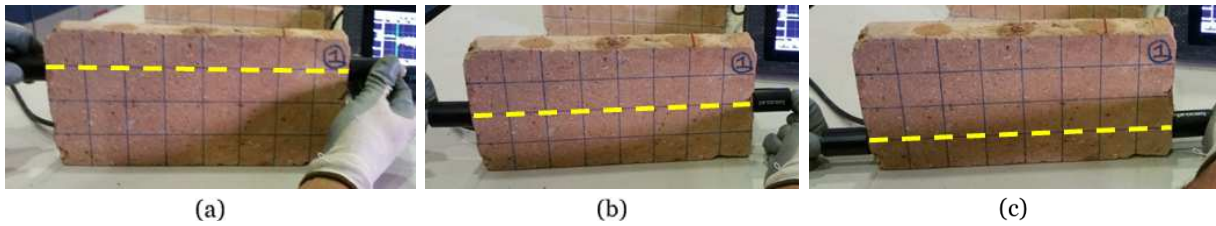


Figure 9: Locations of ultrasonic pulse travel time measurements across length: (a) Top quarter, (b) Middle, (c) Bottom quarter.

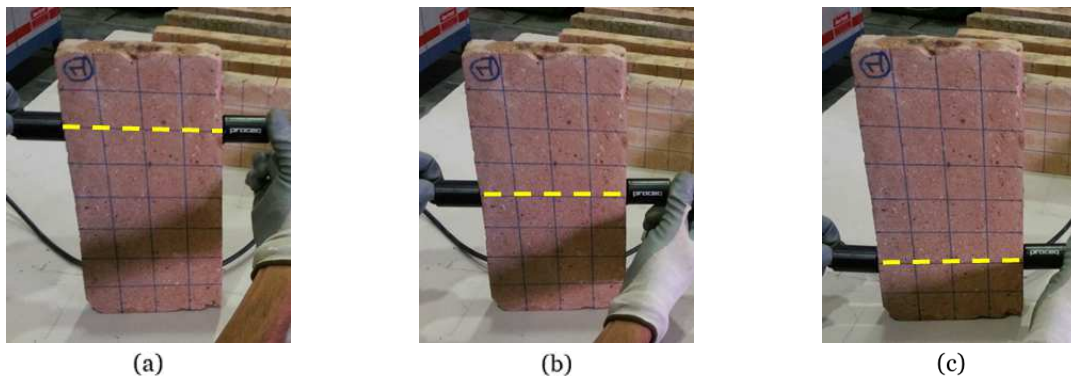


Figure 10: Locations of ultrasonic pulse travel time measurements across width: (a) Top quarter, (b) Middle, (c) Bottom quarter

Specimens from group V(b) were tested before the methodology described herein had been developed.
 385 As such, for specimens from group V(b), the transit time was only measured at the middle location across the length and the width. Moreover, no measurements of pulse transit times were taken across the thickness of specimens from this group.

For all other specimens, the procedure used for computing $E_{UPV,T}$ differed from that used for $E_{UPV,L}$
 390 and $E_{UPV,W}$. Due to the shorter distance of the path length, it was expected that the effect of heterogeneities and scattering would be more significant. As such, the pulse transit time across the thickness was measured at 32 different locations on the face of each specimen as shown in Figure 11. The 32 measurements were used to generate travel time contour maps which could also be used to assess the heterogeneity of each specimen. In order to minimise the effect of any measurement errors, two consecutive sets of 32 readings were taken for
 395 each specimen and corresponding readings that differed by more than 2% were eliminated from any further computation. Since taking 32 measurements of path length was both time-consuming and impractical (parts at the centre of specimens were difficult to access to measure accurately), the pulse velocity was computed by dividing the average of the 8 thickness measurements taken as part of the IEV procedure by the average of the 32 measurements of pulse transit times. $E_{UPV,T}$ was then computed for each specimen from this
 400 computed velocity and using the Poisson's ratio estimated from IEV testing.

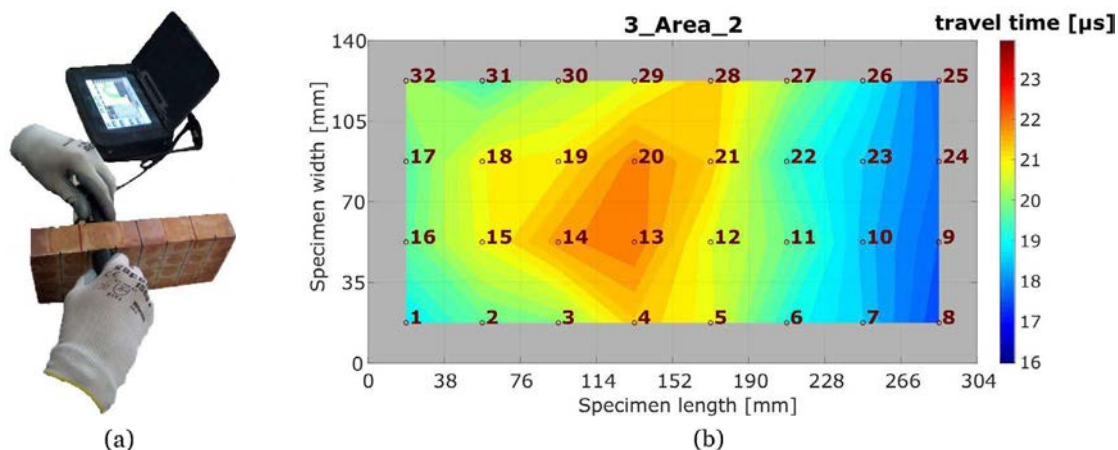


Figure 11: (a) Measurement of ultrasonic pulse transit time across thickness. (b) Example of an ultrasonic travel time colour map generated from 32 measurements over the face of each specimen.

4. Results and discussion

As described in Section 2.1, the dynamic Young's modulus (E_{IEV}), shear modulus (G_{IEV}) and Poisson's ratio (ν_{IEV}) for each specimen were computed from the measured mass, dimensions and fundamental frequencies by direct application of Equations (1) and (2) through the procedure described in Figure 2. The

405

average of these results for each specimen group are presented in Table 3.

Table 3: Final estimated dynamic elastic properties from IEV testing.

Specimen Group	No. of specimens tested	Average values					
		E_{IEV} [MPa]	coeff. of variation	G_{IEV} [MPa]	coeff. of variation	ν_{IEV} [MPa]	coeff. of variation
35		Units					
I(a)	7	7,882	15%	3,530	15%	0.12	14%
I(b)	6	7,931	17%	3,628	17%	0.09	41%
II	5	18,313	1%	7,240	1%	0.26	7%
III	3	7,107	13%	3,309	10%	0.07	31%
IV	6	15,505	1%	5,733	1%	0.35	5%
V(a)	2	5,475	8%	2,525	5%	0.08	31%
V(b)	6	4,068	30%	1,965	29%	0.03	70%
21		Mortar					
MB	5	3,987	10%	1,811	9%	0.10	16%
MIIB	8	4,269	6%	1,886	6%	0.12	24%
MC	8	28,954	5%	11,417	3%	0.27	8%

As can be expected, in the case of bricks, the specimens produced by extrusion (groups II and IV) have higher values of dynamic Young's and shear moduli. This is because they are generally of higher quality and less porous than the bricks handmade in moulds and therefore exhibit a more stiff elastic behaviour. Similarly, the more modern cement mortar specimens appear to be much more stiff than the weaker lime mortars.

410

In addition to the estimates of the dynamic properties from IEV tests, dynamic Young's moduli for every specimen were also computed using Equation (3) from the average ultrasonic pulse velocity across different directions, derived as described in Section 3.3. This results in three estimates of the dynamic Young's modulus from UPV tests for every specimen, corresponding to its three main dimensions ($E_{UPV,L}$, $E_{UPV,W}$ and $E_{UPV,T}$). The average of these results for each specimen group are presented in Table 4.

415

Table 4: Estimated dynamic Young's modulus from UPV measurements across different directions.

Specimen Group	No. of specimens tested	Average values					
		$E_{UPV,L}$ [MPa]	coeff. of variation	$E_{UPV,W}$ [MPa]	coeff. of variation	$E_{UPV,T}$ [MPa]	coeff. of variation
35		Units					
I(a)	7	7,837	18%	8,241	19%	5,764	20%
I(b)	6	7,938	13%	8,189	15%	5,979	17%
II	5	13,756	4%	15,199	4%	8,924	5%
III	3	7,305	2%	8,717	7%	8,016	15%
IV	6	9,157	8%	7,109	8%	12,035	8%
V(a)	2	5,498	4%	6,336	7%	5,754	14%
V(b)	6	4,604	35%	5,538	22%	-	-
21		Mortar					
MB	5	4,527	6%	5,686	7%	6,230	7%
MIIB	8	4,887	16%	6,486	4%	6,123	2%
MC	8	28,601	4%	30,125	6%	29,236	4%

One of the most useful applications of the estimated dynamic Young's moduli across different directions is to evaluate if the specimens are actually isotropic. As such, a comparison of the relative scatters between these estimated properties for every specimen group is summarised in Table 5. The scatters are normalised to $E_{UPV,L}$ which can be considered the most reliable estimate from UPV tests carried out as part of this research. This is due to the fact that it is computed from the pulse velocity determined across the largest dimension of the specimens, hence minimising the effects of localised heterogeneities as well as those of measurement errors.

As described in Section 3.3.3, the 32 measurements of pulse transit time across the thickness cover almost the whole area over the two largest opposing faces of each specimen. Hence, for each set of readings, the maximum variation of the pulse transit times measured across the thickness ($\Delta t_T = t_{T,max} - t_{T,min}$) can provide an indication of the level of heterogeneity for each specimen. As mentioned in Section 3.3.3, two consecutive sets of readings were taken for each specimen. Therefore the representative maximum variation of each specimen ($\Delta t_{T,spec}$) was taken as the average of $\Delta t_{T,1}$ and $\Delta t_{T,2}$. Similarly, the representative average measured pulse transit time of each specimen ($\bar{t}_{T,spec}$) was taken as the average of $\bar{t}_{T,1}$ and $\bar{t}_{T,2}$. In order to allow adequate comparisons between specimens, a unitless heterogeneity measure for each specimen (HM_{spec}) was computed as follows:

$$HM_{spec} = \frac{\Delta t_{T,spec}}{\bar{t}_{T,spec}} \quad (5)$$

Subsequently, the heterogeneity measure for a specimen group (HM_{Group}) was computed as the average of the HM_{spec} values of all specimens belonging to that group. These values are presented in the last column of Table 5.

Table 5: Comparison of dynamic Young's modulus from UPV measurements across different directions and heterogeneity measure for each specimen group.

Specimen Group	No. of specimens tested	Average values			HM_{Group}
		$\frac{E_{UPV,L} - E_{UPV,W}}{E_{UPV,L}}$	$\frac{E_{UPV,L} - E_{UPV,T}}{E_{UPV,L}}$	$\frac{E_{UPV,W} - E_{UPV,T}}{E_{UPV,L}}$	
35		Units			
I(a)	7	-5%	26%	32%	24%
I(b)	6	-3%	25%	28%	22%
II	5	-10%	35%	46%	10%
III	3	-19%	-10%	10%	26%
IV	6	22%	-31%	-54%	8%
V(a)	2	-15%	-5%	11%	26%
V(b)	6	-20%	-	-	-
21		Mortar			
MB	5	-26%	-38%	-12%	16%
MIIB	8	-33%	-25%	7%	11%
MC	8	-5%	-2%	3%	9%

The comparisons in Table 5 reveal that the bricks produced by extrusion (groups II and IV) display a higher level of anisotropy since the relative scatters between estimated dynamic Young's moduli for different directions were consistently greater for specimens from these two groups. It should be noted that the average values of the relative scatters between the estimated dynamic Young's moduli for specific directions also appear to be significant for some of the other specimen groups tested (I(a), I(b), MB, MIIB). However, there are much greater variations in these relative scatters among individual specimens from these groups when compared to the variations among the specimens from groups II and IV. This can be expected due to the greater homogeneity of the bricks manufactured by extrusion, confirmed by the significantly lower group heterogeneity measures (see Table 5). It is clear to see that although the comparison of estimated dynamic Young's moduli from ultrasonic P-wave velocities in different directions can provide some information on the inherent anisotropy of the material, it can be misleading and hence requires very careful interpretation. Moreover, as described in Section 2.2.3, the wave modes are not necessarily pure modes in anisotropic media. Therefore, the ratios of the estimated dynamic moduli from P-wave velocities between different directions do not necessarily reflect the actual ratios between elastic constants of the material. In fact, for the anisotropic case, estimating the dynamic elastic modulus from traditional ultrasonic P-wave testing alone can be considered unreliable.

Comparing the dynamic Young's modulus evaluated from IEV testing with that evaluated from UPV testing with P-waves across the length of the specimens can be considered a more robust way of evaluating the reliability of the results from UPV testing. In theory, the stresses developed during testing with these two methods should be resisted across the same material direction as illustrated in Figure 12.

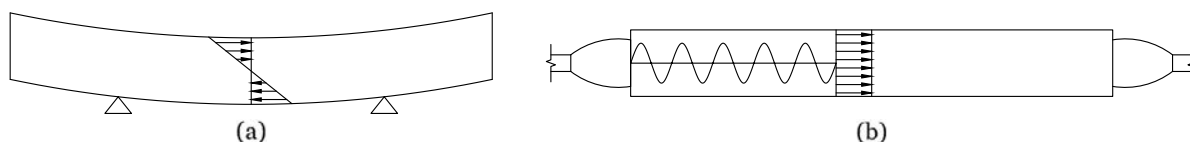


Figure 12: Schematic representation of (a) stresses in material during flexural IEV test, (b) stresses in material during UPV testing across length.

Table 6 presents the relative scatter between E_{IEV} and $E_{UPV,L}$ for each specimen group.

Table 6: Comparison of dynamic Young's modulus from IEV and UPV measured across length.

Specimen Group	No. of specimens tested	Average values				
		E_{IEV} [MPa]	coeff. of variation	$E_{UPV,L}$ [MPa]	coeff. of variation	$\frac{E_{IEV} - E_{UPV,L}}{E_{IEV}}$
35		Units				
I(a)	7	7,882	15%	7,837	18%	1%
I(b)	6	7,931	17%	7,938	13%	-0.1%
II	5	18,313	1%	13,756	4%	25%
III	3	7,107	13%	7,305	2%	-3%
IV	6	15,505	1%	9,157	8%	41%
V(a)	2	5,475	8%	5,498	4%	-0.4%
V(b)	6	4,068	30%	4,604	35%	-13%
21		Mortar				
MB	5	3,987	10%	4,527	6%	-14%
MIIB	8	4,269	6%	4,887	16%	-14%
MC	8	28,954	5%	28,601	4%	1%

From Table 6, it is clear that the differences between E_{IEV} and $E_{UPV,L}$ are significantly greater for specimens from group II and IV when compared to the differences for specimens from any other group of constituent materials tested. This suggests that values of dynamic Young's modulus evaluated from UPV testing only with P-waves is unreliable for bricks produced by extrusion due to their apparent anisotropy. Hence, the comparison of E_{IEV} and $E_{UPV,L}$ has brought us to the same conclusion as the comparison of the dynamic Young's moduli estimated from ultrasonic compression wave velocities across different directions. However, in this case, the disagreement between E_{IEV} and $E_{UPV,L}$ is much more apparent and the

465 comparison does not lend itself to misinterpretation.

From a more general perspective, it is clear that the bricks manufactured through an extrusion process (groups II and IV) show the smallest coefficients of variation. As previously discussed, one of the main reasons for this is that they are characterised by greater homogeneity.

470

For results from IEV testing, the estimates of dynamic Poisson's ratio generally have greater coefficients of variation, indicating that the evaluation of this parameter is more sensitive to heterogeneities and to changes in testing conditions (see Table 3). Nevertheless, for specimens characterised by a more marked isotropic behaviour, it can be said that IEV testing can provide reliable estimates of the dynamic Poisson's ratio. In fact, most specimen groups have a coefficient of variation of 31% or less for this parameter with the exception of groups I(b) and V(b). Even so, it should be noted that the average estimated value of the dynamic Poisson's ratio was quite low for both these groups of specimens. Hence, the 41% and 70% coefficients of variation among specimens from group I(b) and V(b) respectively, relate to variations of only 0.04 and 0.02 respectively in the estimated Poisson's ratio. The value of the dynamic Poisson's ratio determined for the cement mortar is significantly higher than that of the lime mortar and of the brick specimens handmade in moulds.

480

One of the main advantages of being able to determine the dynamic Poisson's ratio reliably using IEV testing, is that it can provide a value for a previously unknown parameter in Equation (3), used to compute the dynamic Young's modulus from the experimentally evaluated ultrasonic compression wave velocity. In order to evaluate the benefit gained from this information, a sensitivity study was carried out between the assumed dynamic Poisson's ratio and the evaluated dynamic Young's modulus for all brick specimens. If no information is known on the dynamic Poisson's ratio, it can be assumed that this value can fall anywhere within the range of values determined from IEV testing across all brick specimens tested as part of this research. Hence, the sensitivity study includes Poisson's ratios ranging from 0.01 to 0.37. The results of this study for $E_{UPV,L}$ are shown first only for bricks from group I(a) (Figure 13) and subsequently for all brick specimen groups (Figure 14).

490

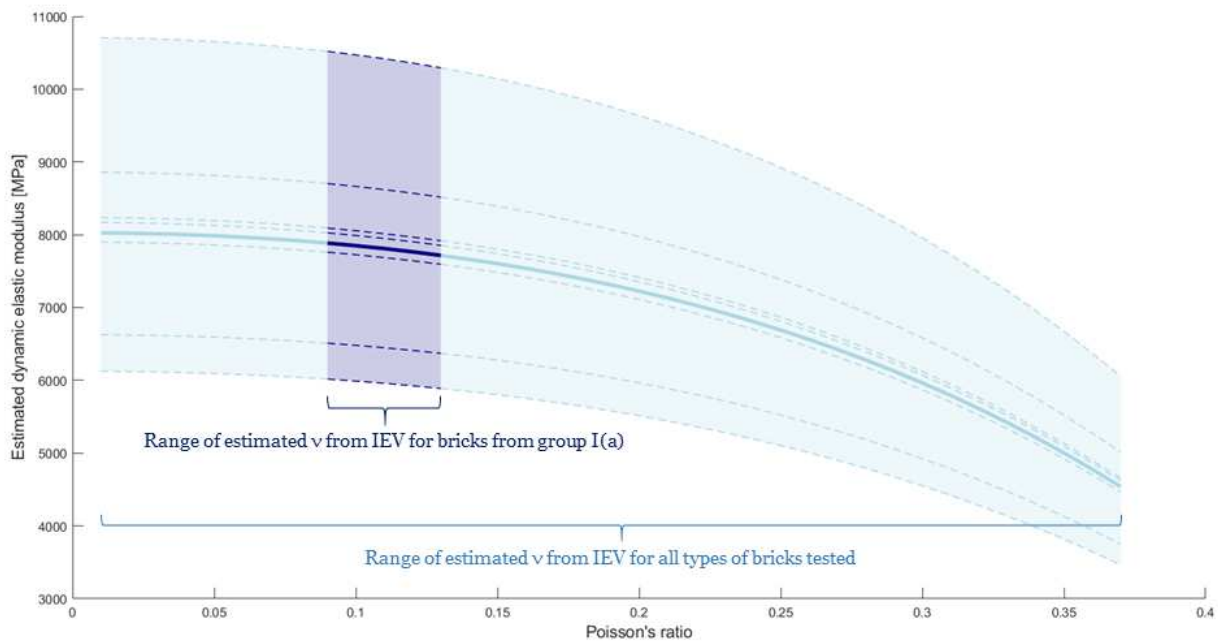


Figure 13: Variation of estimation of $E_{UPV,L}$ with ν for bricks from group I(a).

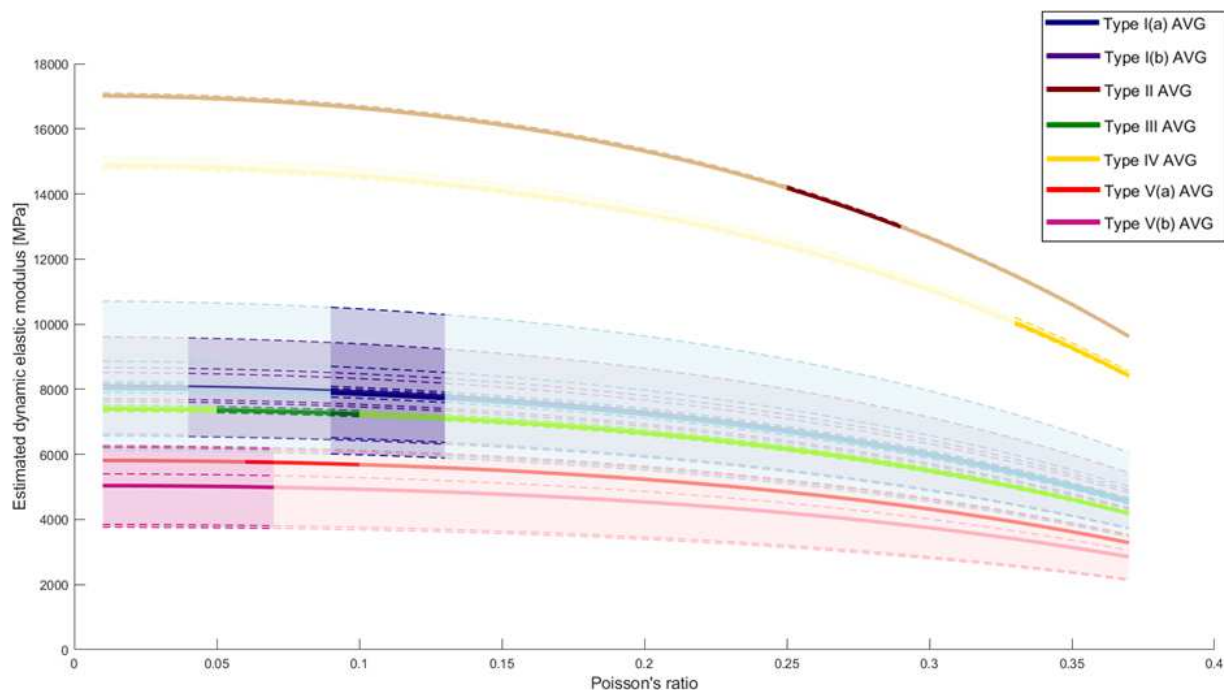


Figure 14: Variation of estimation of $E_{UPV,L}$ with ν for all bricks tested as part of this experimental campaign. Areas shaded with a lighter colour refer to the range of estimated ν across all the types of bricks tested. Areas shaded with a darker colour refer to the range of estimated ν for a specific group. (For interpretation of the references to colour in this figure, the reader is referred to the web version of this article.)

A similar trend across an equivalent range of values as shown for $E_{UPV,L}$ was observed for the sensitivity studies of $E_{UPV,W}$ and $E_{UPV,T}$. It is clear to see that using the information on the dynamic Poisson's ratio obtained from IEV testing can contribute to a significant improvement in the estimation of the dynamic Young's modulus from UPV testing. In fact, the sensitivity study revealed that using the Poisson's ratios only within the range estimated from IEV testing for each specific brick specimen group reduced the maximum variation in the estimated dynamic Young's modulus from 50% to a maximum of 3.6%.

It should be noted that although the coefficients of variation for the computed Poisson's ratio are lowest for the bricks produced by extrusion (see Table 3), the estimated values of this parameter for these types of bricks are unreliable. The main reason for this is that bricks manufactured from an extrusion process usually exhibit a certain level of anisotropy. As previously discussed, results from the tests carried out as part of this research confirm this anisotropic character. Since a fundamental assumption behind the analytical expression used for the computation of Poisson's ratio from IEV results is isotropy, these values cannot be considered reliable estimates. Nevertheless, the values of dynamic shear modulus evaluated from the torsional IEV tests do not depend on Poisson's ratio and therefore still provide a good representation of how the material behaves in the orientation in which it was tested. Although the expression relating the measured flexural resonant frequency to the dynamic Young's modulus (Equation (1)) contains a correction factor dependent on Poisson's ratio, the final estimated value is very insensitive to changes in Poisson's ratio. In fact, a simple sensitivity study showed that this parameter has a maximum variation of less than 1.74% for any specimen over the whole range of estimated Poisson's ratios across all specimen groups. Hence, it can be said that IEV testing also provides a good representation of the dynamic Young's modulus of anisotropic bricks when acting against out-of-plane flexural loads.

5. Proposed analysis procedure

Based on all the experimental methods described in detail in Sections 3.2 and 3.3, a summary of the recommended analysis procedure for obtaining reliable estimates of the dynamic elastic properties of brick masonry constituents is shown in Figure 15.

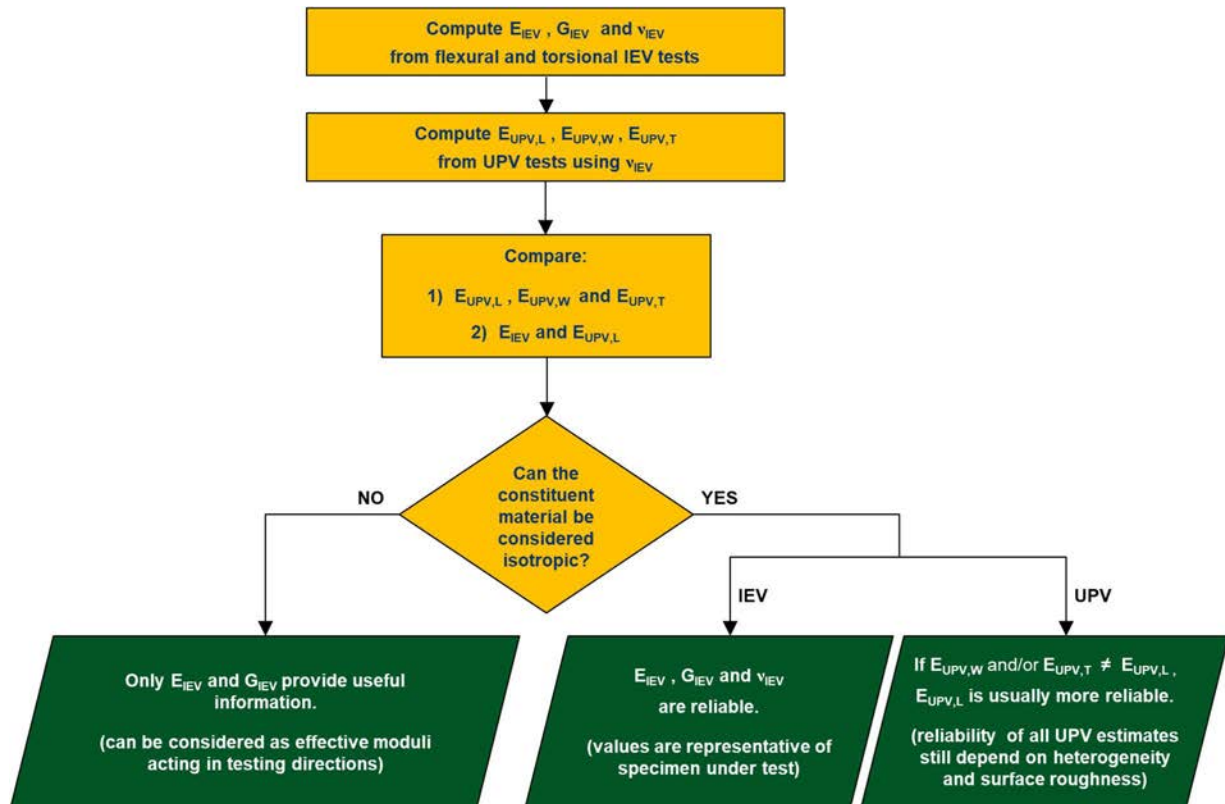


Figure 15: Summary of the proposed procedure for determining dynamic elastic properties of brick masonry constituents.

As can be seen from Figure 15, the first step of the analysis process involves computing E_{IEV} , G_{IEV} and ν_{IEV} from the results of IEV tests conducted as described in Section 3.2. Following this, the resulting ν_{IEV} is used in the computation of $E_{UPV,L}$, $E_{UPV,W}$ and $E_{UPV,T}$ from ultrasonic pulse velocities measured across different dimensions of each specimen as described in Section 3.3. The average values for each group of specimens representing a particular type of brick or mortar can then be obtained. All subsequent analysis can be carried out with these representative average values. Once these values have been obtained, it is important to assess if any of the brick or mortar types being tested exhibit a significant level of anisotropy in order to evaluate the reliability of the obtained results. If there are significant relative scatters ($>30\%$) between $E_{UPV,L}$, $E_{UPV,W}$ and $E_{UPV,T}$ as well as a significant relative scatter ($>20\%$) between E_{IEV} and $E_{UPV,L}$ then the type of brick or mortar under test can be said to be anisotropic. If this is the case, only the dynamic Young's modulus (E_{IEV}) and the dynamic shear modulus (G_{IEV}) computed from results of IEV testing provide a good representation of the behaviour of the material in the respective testing orientations. On the other hand, if the material exhibits a predominantly isotropic behaviour, in theory, all the dynamic elastic material properties evaluated from IEV and UPV testing can be considered reliable. However, since the reliability of UPV estimates depend strongly on heterogeneity and surface roughness, if $E_{UPV,W}$ and/or $E_{UPV,T}$ differ from $E_{UPV,L}$, the latter parameter can be considered as being more reliable in most cases.

The application of this analysis process can be illustrated with two simple examples. Taking the case of the cement mortar tested as part of this research (group MC), the relative scatters between $E_{UPV,L}$, $E_{UPV,W}$ and $E_{UPV,T}$ are all of 5% or less and the relative scatter between E_{IEV} and $E_{UPV,L}$ is of only 1%. In this case, it is clear that the material is isotropic and all the estimated dynamic elastic properties can be considered reliable. On the contrary, for the type of bricks belonging to group II, the relative scatter between $E_{UPV,L}$ and $E_{UPV,T}$ is 35% while that between $E_{UPV,W}$ and $E_{UPV,T}$ is 46%. Furthermore, the relative scatter between E_{IEV} and $E_{UPV,L}$ turned out to be 25%. For these bricks, all properties estimated from UPV tests as well as the value of ν_{IEV} cannot be considered reliable. Nevertheless, E_{IEV} is still representative of the dynamic Young's modulus when out-of-plane flexural loads are acting on this type of brick while G_{IEV} still provides a good representation of the response of bricks of this type to torsional loads (in the same orientation as the bricks were tested).

6. Conclusions and future work

The research has proposed a robust procedure based on the synergy of two approaches, namely Impulse
550 Excitation of Vibration (IEV) and Ultrasonic Pulse Velocity (UPV) testing for the determination of the dy-
namic elastic properties of brick masonry constituents. The influence of testing conditions and other factors
specific to brick masonry constituents have been evaluated to assess the applicability of these techniques.
At the same time, methods to mitigate possible sources of error have been explored and as a result, clear
practical provisions have been given concerning every step of the procedure from testing protocols to the
555 interpretation of results. Moreover, in order to derive meaningful ranges of results for different masonry
typologies, the experimental program has explored different types of bricks and mortars. The tests have
considered hydraulic lime mortar, cement mortar, new bricks manufactured using either hand-made mould-
ing or extrusion, and existing bricks extracted from heritage buildings in Barcelona, Spain.

The proposed methodology can be applied to whole brick specimens as well as to specifically-cast mortar
560 specimens. In the case of whole brick specimens, these can be recently manufactured or extracted from
existing constructions. In the latter scenario, the methods described in this paper cannot be considered as
being fully non-destructive since they implicitly require the extraction of bricks from the structure. Never-
theless, both methods can be used to test extracted bricks without causing any further significant damage
565 to the material, allowing the same bricks to be re-used or to undergo further testing. In the case of mor-
tar specimens, since they have to be cast to specific dimensions, the proposed testing procedures are not
suitable for testing mortar already present in existing masonry structures. Nevertheless, the procedures can
be applied to test freshly-cast mortar either for use in new constructions or intended for repair works. The
results obtained from the present investigation show that the two methods (IEV and UPV) can provide
570 reliable estimates of the actual dynamic elastic properties of typical brick masonry constituents.

For isotropic constituent materials, one of the main advantages of the proposed procedure lies in using
the dynamic Poisson's ratio derived from IEV tests to improve the accuracy of the dynamic Young's modulus
575 evaluated from conventional UPV tests based on the transmission of P-waves. Since UPV tests are simpler
and faster to execute when compared to IEV tests, a possible application of this procedure could involve
determination of the dynamic Poisson's ratio using IEV testing on a selected number of specimens together
with characterisation of the dynamic Young's modulus using UPV testing on a larger sample size. In the
case of existing single-leaf walls, this procedure may even be extended to in situ UPV tests on bricks.

The results reveal that bricks produced by a conventional extrusion procedure exhibit a significant level
580 of anisotropy. In this case, the estimation of the dynamic Young's modulus from traditional UPV tests is
not reliable since the propagation of ultrasonic waves is not governed by the same simplified rules as in
isotropic media. The procedure involving the combined information from flexural and torsional IEV tests
to evaluate the dynamic Poisson's ratio is also not applicable to such bricks since it relies on the fundamen-
585 tal assumption of isotropy. Nevertheless, IEV tests can still provide estimates of effective dynamic elastic
moduli which define the behaviour of brick specimens when subjected to flexural or torsional loading.

An extension of the research presented herein may explore testing procedures involving ultrasonic shear
590 wave transducers to better characterise the dynamic elastic behaviour of anisotropic bricks. Theoretically,
such transducers could also be used to directly evaluate the dynamic Poisson's ratio of isotropic constituents.
However, it should be noted that accurately determining the arrival time of the shear wave can prove to
be especially difficult, particularly when testing brick-sized specimens of materials with significant hetero-
geneities and rough surfaces.

595 One of the most important implications of this work is that it provides a means of better understanding
the relationship between static and dynamic elastic properties for brick masonry constituents. This relation-
ship is as of yet not well understood. Additional laboratory investigations are currently being carried out at
the Universitat Politècnica de Catalunya to correlate the static and dynamic elastic properties in different
masonry components.

Conflicts of interest

The authors confirm that there are no known conflicts of interest associated with this publication.

Acknowledgements

This research has received the financial support from the MINECO (Ministerio de Economía y Competitividad of the Spanish Government) and the ERDF (European Regional Development Fund) through the MULTIMAS project (Multiscale techniques for the experimental and numerical analysis of the reliability of masonry structures, ref. num. BIA2015-63882-P). Support from the AGAUR agency of the Generalitat de Catalunya, in the form of a predoctoral grant awarded to the corresponding author is also gratefully acknowledged.

References

- [1] European Committee for Standardization (CEN), EN 14580:2005. Natural stone test methods - Determination of static elastic modulus (2005).
- [2] L. Binda, C. Tiraboschi, G. Mirabella Roberti, G. Baronio, G. Cardani, Measuring masonry material properties: detailed results from an extensive experimental research Part I: Tests on masonry components. (Report 5.1 Politecnico di Milano), Tech. rep., Politecnico di Milano (1996).
- [3] L. Binda, C. Tiraboschi, S. Abbaneo, Experimental Research to Characterise Masonry Materials, Masonry International. URL <https://www.masonry.org.uk/downloads/experimental-research-to-characterise-masonry-materials/>
- [4] L. Binda, C. Tedeschi, P. Condoleo, Characterisation of Materials Sampled From Some My S'on Temples, in: 7th International Congress on Civil Engineering, 2006.
- [5] G. Baronio, L. Binda, C. Tedeschi, C. Tiraboschi, Characterisation of the materials used in the construction of the Noto Cathedral, Construction and Building Materials 17 (8) (2003) 557–571. doi:10.1016/j.conbuildmat.2003.08.007.
- [6] D. V. Oliveira, Mechanical Characterization of Stone and Brick Masonry (Report 00-DEC/E-4), Tech. rep., University of Minho (2000).
- [7] D. V. Oliveira, P. B. Lourenço, P. Roca, Experimental Characterization of the Behaviour of Brick Masonry Subjected to Cyclic Loading, in: 12th international Brick/Block Masonry Conference, no. May 2014, 2000, pp. 1–8.
- [8] D. V. Oliveira, P. B. Lourenço, P. Roca, Cyclic behaviour of stone and brick masonry under uniaxial compressive loading, Materials and Structures/Materiaux et Constructions 39 (286) (2006) 247–257. doi:10.1617/s11527-005-9050-3.
- [9] L. Pelà, E. Canella, A. Aprile, P. Roca, Compression test of masonry core samples extracted from existing brickwork, Construction and Building Materials 119 (2016) 230–240. doi:10.1016/j.conbuildmat.2016.05.057.
- [10] E. I. Mashinsky, Differences between static and dynamic elastic moduli of rocks: Physical causes, Russian Geology and Geophysics 44 (9) (2003) 953–959.
- [11] M. Ciccotti, F. Mulargia, Differences between static and dynamic elastic moduli of a typical seismogenic rock, Geophysical Journal International 157 (1) (2004) 474 – 477.
- [12] J. Martínez-Martínez, D. Benavente, M. A. García-del Cura, Comparison of the static and dynamic elastic modulus in carbonate rocks, Bulletin of Engineering Geology and the Environment 71 (2) (2012) 263–268. doi:10.1007/s10064-011-0399-y.
- [13] A. R. Najibi, M. Ghafoori, G. R. Lashkaripour, M. R. Asef, Empirical relations between strength and static and dynamic elastic properties of Asmari and Sarvak limestones, two main oil reservoirs in Iran, Journal of Petroleum Science and Engineering 126 (2015) 78–82. doi:10.1016/j.petrol.2014.12.010. URL <http://dx.doi.org/10.1016/j.petrol.2014.12.010>
- [14] W. Fei, B. Huiyuan, Y. Jun, Z. Yonghao, Correlation of Dynamic and Static Elastic Parameters of Rock, Electronic Journal of Geotechnical Engineering 21 (04) (2016) 1551–1560.
- [15] Y. Z. Totoev, J. M. Nichols, A Comparative Experimental Study of the Modulus of Elasticity of Bricks and Masonry, in: 11th International Brick/Block Masonry Conference, no. October, 1997.
- [16] J. M. Nichols, Y. Z. Totoev, Experimental determination of the dynamic Modulus of Elasticity of masonry units, in: 15th Australian Conference on the Mechanics of Structures and Materials (ACMSM), 1997.
- [17] ASTM, E 1876 - Standard Test Method for Dynamic Young's Modulus, Shear Modulus, and Poisson's Ratio by Impulse Excitation of Vibration (2002). doi:10.1520/E1876-09.responsibility.

-
- [18] ASTM, C597 - Standard Test Method for Pulse Velocity Through Concrete (2010). doi:10.1520/C0597-09.
- [19] V. Brotons, R. Tomás, S. Ivorra, A. Grediaga, Relationship between static and dynamic elastic modulus of calcarenite heated at different temperatures: The San Julián's stone, *Bulletin of Engineering Geology and the Environment* 73 (3) (2014) 791–799. doi:10.1007/s10064-014-0583-y.
- [20] S. Dimter, T. Rukavina, K. Minažek, Estimation of elastic properties of fly ash-stabilized mixes using nondestructive evaluation methods, *Construction and Building Materials* 102 (2016) 505–514. doi:10.1016/j.conbuildmat.2015.10.175.
- [21] M. Asmani, C. Kermel, A. Leriche, M. Ourak, Influence of porosity on Young's modulus and Poisson's ratio in alumina ceramics, *Journal of the European Ceramic Society* 21 (8) (2001) 1081–1086. doi:10.1016/S0955-2219(00)00314-9.
- [22] L. E. García, Estudio experimental del comportamiento a compresión de elementos pétreos confinados con materiales compuestos, Doctoral thesis, Universitat d'Alacant (2018).
- [23] J. D. Achenbach, *Wave propagation in elastic solids*, Vol. 16, 1973. arXiv:arXiv:1011.1669v3, doi:10.1002/zamm.19920720607.
- [24] P. Laugier, G. Haïat, Chapter 2: Introduction to the Physics of Ultrasound, in: *Bone Quantitative Ultrasound*, 2011, pp. 29–45. arXiv:arXiv:1011.1669v3, doi:10.1007/978-94-007-0017-8.
- [25] J. H. Bungey, S. G. Millard, M. G. Grantham, *Testing of Concrete in Structures*, 1996.
- [26] Z. Nazarchuk, V. Skalskyi, O. Serhiyenko, Chapter 2: Propagation of Elastic Waves in Solids, in: *Acoustic Emission*, Vol. i, Springer International Publishing, 2017, pp. 29–73. doi:10.1007/978-3-319-49350-3. URL <http://link.springer.com/10.1007/978-3-319-49350-3>
- [27] C. Lane, *Wave Propagation in Anisotropic Media*, in: *The Development of a 2D Ultrasonic Array Inspection for Single Crystal Turbine Blades*, 2014, pp. 13–39. doi:10.1007/978-3-319-02517-9_2. URL http://link.springer.com/10.1007/978-3-319-02517-9_{_}2
- [28] J. L. Rose, *Ultrasonic Guided Waves in Solid Media*, Cambridge University Press, New York, 2014. doi:10.1017/CB09781107273610. URL <http://ebooks.cambridge.org/ref/id/CB09781107273610>
- [29] J. L. Rose, *Ultrasonic Waves in Solid Media*, Cambridge University Press, 1999.
- [30] European Committee for Standardization (CEN), EN 12504-4:2004. *Testing concrete Part 4: Determination of ultrasonic pulse velocity* (2004). doi:ConstructionStandard,CS1:2010.
- [31] A. Fódi, Effects influencing the compressive strength of a solid, fired clay brick, *Periodica Polytechnica Civil Engineering* 55 (2) (2011) 117–128. doi:10.3311/pp.ci.2011-2.04.
- [32] European Committee for Standardization (CEN), EN 771-1:2011+A1:2015. *Specification for masonry units Part 1: Clay masonry units* (2015).
- [33] European Committee for Standardization (CEN), EN 772-1. *Methods of test for masonry units. Part 1: Determination of compressive strength* (2010).
- [34] European Committee for Standardization (CEN), EN 1015-11. *Methods of test for mortar for masonry - Part 11: Determination of flexural and compressive strength of hardened mortar* (2007).
- [35] National Instruments, *LabVIEW 2016 Help* (2016).
- [36] ASTM, C 1259 - Standard Test Method for Dynamic Young's Modulus, Shear Modulus, and Poisson's Ratio for Advanced Ceramics by Impulse Excitation of Vibration (2001). doi:10.1520/E1875-08.2.
- [37] MathWorks, *MATLAB R2017b Documentation*. URL <https://es.mathworks.com/help/releases/R2017b/index.html>
- [38] M. Farshchin, *Frequency Domain Decomposition (FDD)* (2015).
- [39] PROCEQ, *PUNDIT PL-200 Operating Instructions* (2014).

Relationship between the static and dynamic elastic modulus of brick masonry constituents

Nirvan Makoond · Albert Cabané · Luca Pelà · Climent Molins

Accepted manuscript in *Construction and Building Materials*.

Submitted: 09 March 2020

Revised: 18 May 2020

Accepted: 25 July 2020

Relationship between the static and dynamic elastic modulus of brick masonry constituents

Nirvan Makoond*, Albert Cabané, Luca Pelà, Climent Molins

Department of Civil and Environmental Engineering, Universitat Politècnica de Catalunya (UPC-BarcelonaTech), Jordi Girona 1-3, 08034 Barcelona, Spain

Abstract

Different brick masonry typologies have been and are still widely used in construction worldwide. Despite being a fundamental deformation property, experimentally determining the static elastic modulus in compression for brick masonry constituents remains a challenging task. Static modulus estimates usually show much larger dispersion than those involved in determining the dynamic elastic modulus. Although the static property is preferred for common structural verifications, the relationship between the two is yet to be well understood. In light of the above, this paper provides an empirical expression to estimate the static elastic modulus of brick masonry constituents from its dynamic counterpart.

Keywords: Brick masonry, Young's modulus, Compression, Strain measurement, Non-destructive testing (NDT), Impulse excitation of vibration (IEV), Ultrasonic pulse velocity (UPV), Elastodynamics

Link to formal publication: <https://doi.org/10.1016/j.conbuildmat.2020.120386>

1. Introduction

The elastic modulus of a material is a fundamental property that is crucial for characterising the deformation behaviour of structural elements whether it is with respect to the design of new structures or for the assessment of existing ones. Since typical brick masonry constituents usually have negligible or very low tensile strengths, the elastic modulus in compression is often the most relevant material property related to elastic deformation.

Experimental techniques that can be used to evaluate this property may be classified as static or dynamic. The former involves directly loading a specimen and measuring the corresponding change in strain. The static elastic modulus (E_{st}) is then computed by evaluating the slope of the experimental stress-strain curve in the elastic deformation range. On the other hand, the dynamic elastic modulus (E_{dy}) can be derived from the measured resonant frequency of a specimen in a specific vibration test or from the measured velocity of a stress wave passing through the material. It is now well known that E_{st} can differ significantly from E_{dy} , with the latter generally being greater. It can be envisaged that this empirically known inequality arises mainly due to the fact that E_{dy} is measured at almost negligible stress levels compared to its static counterpart [1]. However, studies have shown that this discrepancy is also due to the inherent heterogeneity of materials causing them to respond differently under cyclic or vibratory loading conditions [1–5].

*Corresponding author

Email addresses: nirvan.makoond@upc.edu (Nirvan Makoond), albert.cabane@upc.edu (Albert Cabané), luca.pela@upc.edu (Luca Pelà), climent.molins@upc.edu (Climent Molins)

For brittle materials, such as most typical brick masonry constituents, the static methods present significant challenges. Firstly, they are often very time consuming since they require gradually loading carefully prepared cylindrical or prismatic samples [6]. Secondly, deformation magnitudes in the elastic range tend to be very low and can change relatively abruptly during loading due to the nature of the material [7–10]. Moreover, brick masonry constituents can contain noticeable heterogeneities that can significantly skew estimates of the deformation [11]. Finally, most transducers that can be used to measure surface strains of such materials tend to be very sensitive to machine-specimen surface interaction [12]. As such, it can be very difficult to obtain reliable measurements that reflect the actual elastic deformation of the material and the scatter of results is usually high, as evidenced in [7–10, 13].

Contrarily, the dynamic methods are much faster to execute and have the added benefit of being non-destructive. In addition, they do not suffer from the same limitation related to the difficulty of accurately capturing representative deformations. As a result, most of the scatter in experimental results from such tests can usually be attributed to heterogeneity of the sample set rather than experimental error [11]. However, for most common structural calculations, the statically determined modulus is preferred over that obtained by dynamic methods since the former is more representative of actual loading conditions. Given this fact, it is understandable why the correlation of these two parameters for brittle materials has received considerable attention, most notably for Portland cement concrete and for rocks.

Due to its widespread use as a construction material during the 20th century, a substantial research effort has been dedicated to better understanding the relationship between E_{dy} and E_{st} for concrete. In fact, in 1972, the empirical relationship shown below was even included in the now superseded British code of practice for the structural use of concrete [14].

$$E_{st} = 1.25E_{dy} - 19 \quad (1)$$

Where E_{st} and E_{dy} refer respectively to the static and the dynamic elastic modulus expressed in GPa .

It should be noted that this expression is not applicable for concretes with a cement content greater than 500 kg/m^3 or for lightweight concrete [1]. To address this limitation, some researchers proposed the following expression for the latter [15].

$$E_{st} = 1.04E_{dy} - 4.1 \quad (2)$$

A simpler general empirical relationship for concrete has also been proposed [16]:

$$E_{st} = 0.83E_{dy} \quad (3)$$

As previously mentioned, the inherent material heterogeneity of concrete affects the two moduli (E_{st} and E_{dy}) in different ways. As such, studies have also been carried out in order to better understand how different material properties, such as compressive strength (f_c) or density (ρ_c), can influence the relationship between E_{st} and E_{dy} . As a result of this effort, it has been found that for concrete, the ratio of E_{st} to E_{dy} usually increases with increasing f_c [1, 17, 18]. Many researchers have also attempted to develop empirical relationships between E_{st} and E_{dy} that also incorporate other physical parameters. Although many of those ended up having a relatively limited range of applicability, one of the most useful expressions proposed for concrete does indeed suggest that the relation between E_{st} and E_{dy} is a function of density [19]:

$$E_{st} = \frac{446.09 \cdot E_{dy}^{1.4}}{\rho_c} \quad (4)$$

Where E_{st} and E_{dy} are once again to be specified in GPa and ρ_c is the density of hardened concrete in kg/m^3 .

Because of its relevance in the field of geomechanics, the relation between the static and dynamic elastic

modulus of rocks has also received considerable attention [6, 20–30]. However, the empirical relationships proposed by most authors are either applicable to only certain types of rocks or are valid for a limited elastic modulus range that tends to be greater than the elastic moduli of most typical brick masonry constituents. Of the several empirical relations available for rocks in the scientific literature, the following one proposed by Eissa and Kazi [6] could possibly lend itself to the case of brick masonry constituents since it was derived from a sample containing one of the most diverse set of rocks. Similarly to the expression proposed by Popovics for concrete (Equation (4)), the bulk density is also included as an explanatory variable in this relation.

$$\log_{10} E_{st} = 0.77 \log_{10}(\rho_r E_{dy}) + 0.02 \quad (5)$$

E_{st} and E_{dy} refer to the static and dynamic moduli of the rock in *GPa* while ρ_r refers to its bulk density in g/cm^3 .

Although the sample set used for the derivation of Equation (5) consists of a very diverse set of rocks, the compiled data used for the analysis also come from a wide variety of sources. It could therefore not be ensured that testing conditions have been kept constant for all specimens included in the analysis. It is well known that testing conditions can have a significant effect on the final estimated static or dynamic elastic modulus. A more recent study [30], based on a dedicated experimental campaign on 33 specimens coming from 8 different igneous, sedimentary and metamorphic rock types, proposes the following relationship instead.

$$E_{st} = 11.531 \rho_r^{-0.457} E_{dy}^{1.251} \quad (6)$$

With the static and elastic moduli expressed in *GPa* and the bulk density expressed in kg/m^3 .

The same authors also propose additional correlation models that incorporate total porosity and compressive strength of the rocks as additional explanatory variables. They report improved goodness of fit metrics with increasing level of complexity [30].

In spite of the many empirical relationships proposed for concrete and rock, and despite the widespread use of brick masonry in construction, there exists very little research that attempts to explore this relationship for the case of brick masonry constituents. Totoev and Nichols do compare the static and dynamic moduli for some brick types [31, 32], but no relationship is proposed for practical applications. As such, the relationship is still not well understood for the case of brick masonry constituents.

The main aim of this research is thus to propose an expression that can be used to estimate the static elastic modulus of typical brick masonry constituents from the dynamic one for practical applications. The experimental study includes different types of bricks and mortars so that useful ranges of results for different brick masonry typologies could be derived. First, the procedures used for the experimental determination of the elastic moduli of all the specimens are presented. The static elastic moduli are then compared to the dynamic ones evaluated for the same specimens. Finally, the suitability of several of the empirical expressions developed for rocks and concrete are assessed before proposing one to be used for typical brick masonry constituents.


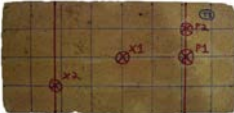





2. Experimental program

The experimental campaign was carried out at the Laboratory of Technology of Structures and Building Materials of the Universitat Politècnica de Catalunya (UPC-BarcelonaTech). This section presents information about the material components and the procedures employed for the experimental determination of the static and dynamic elastic moduli.

2.1. Materials tested

Seven different groups of solid bricks and two different types of mortar were tested as part of the experimental campaign. Five of the seven brick groups were made up of handmade bricks formed by moulding (I(a), I(b), III, V(a), and V(b)). Groups I(a) and I(b) consisted of new solid terracotta bricks while bricks from groups III, V(a) and V(b) were extracted from existing structures in Barcelona. Specifically, group III bricks were acquired from an early 20th Century industrial complex while bricks from groups V(a) and V(b) were extracted from a typical residential building [11]. The remaining 2 brick groups (II and IV) consisted of new solid bricks manufactured using a conventional extrusion process. All brick specimens used for the static tests consisted of $40 \times 40 \times 80 \text{ mm}^3$ prisms cut out from whole bricks (see Section 2.2.1). A brief summary of the different groups of bricks tested is given in Table 1.

Table 1: Groups of brick types tested.



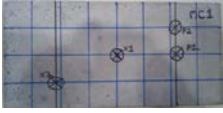
Group	Number of bricks	Number of specimens	Manufacturing	Year	f_{cn}^* [MPa]	Average bulk density [kg/m ³]	Sample view
I(a)	7	42	Handmade in moulds	2017	$16.1 \pm 16\%$	$1,781 \pm 1\%$	
I(b)	6	36	Handmade in moulds	2015	$17.0 \pm 15\%$	$1,768 \pm 3\%$	
II	5	15	Conventional extrusion	2016	$40.0 \pm 16\%$	$1,655 \pm 0.3\%$	
III	3	18	Handmade in moulds	1903	$8.0 \pm 17\%$	$1,598 \pm 5\%$	
IV	6	18	Conventional extrusion	2018	$53.2 \pm 8\%$	$1,673 \pm 0.4\%$	
V(a)	2	11	Handmade in moulds	1930	$8.3 \pm 43\%$	$1,720 \pm 1\%$	
V(b)	6	16	Handmade in moulds	1930	$10.7 \pm 15\%$	$1,718 \pm 1\%$	

* Reference normalised compressive strength for corresponding brick type obtained by testing bricks as prescribed in the European standard EN 772-1 [33].

The mechanical properties of the two types of mortar considered differed significantly. The first mortar type consisted of a hydraulic lime weakened by adding recycled limestone filler to the mixture in order to match mechanical properties more representative of mortars found in historical constructions (MB and

115 MIIB) [34]. For both mortars MB and MIIB, 50% of the powder volume was replaced by the limestone
 filler. The main difference between specimens from these two groups is that those from group MB were
 un moulded 5 days after initial casting whereas those from group MIIB were un moulded after 14 days. This
 change was implemented because specimens from group MB were found to be too fragile at the time of
 un moulding [11]. Specimens from group MB were tested 32 days after initial casting while MIIB specimens
 120 were tested after 27 days. The second mortar type considered consisted of a typical cement mortar used in
 new constructions (MC). This type of mortar was chosen because it can serve as a good control sample, not
 only due to the many studies that have been carried out on the properties of Portland cement mixes, but
 also because it is relatively easy to prepare homogeneous and isotropic specimens from this material. Since
 several studies [35, 36] reveal that such mixes have usually already gained between 85-90% of their stiffness
 125 after just 4 days, it was deemed suitable to test MC specimens after 14 days. All mortar specimens for the
 static tests have been prepared in standard $40 \times 40 \times 160 \text{ mm}^3$ moulds. Key characteristics of the different
 mortar specimen groups tested are summarised in Table 2.

Table 2: Groups of mortar types tested.

Group	Number tested	Mix proportions (by weight)	f_{cn}^* (28 days) [MPa]	Average bulk density [kg/m ³]	Sample view
MB	3	Lime : filler : water 1 : 0.64 : 0.37	$2.3 \pm 6\%$	$1,776 \pm 2\%$	
MIIB	3	Lime : filler : water 1 : 0.64 : 0.37	$2.0 \pm 12\%$	$1,932 \pm 1\%$	
MC	6	Cement : sand : water 1 : 3.2 : 0.33	$48.8 \pm 5\%$	$2,183 \pm 1\%$	

* Reference normalised compressive strength for corresponding mortar type obtained by testing prismatic specimens (cured for 28 days) in accordance with the European standard EN 1015-11 [37].

Some additional information on the brick and mortar specimen groups are presented in [11] which describes the procedure used to obtain the dynamic elastic moduli compared to the static ones in this study.
 130 With respect to mortar specimens, the procedure described in [11] consisted of non-destructive tests carried out on specifically moulded brick-shaped specimens, while the static tests were carried out on specimens cast at the same time in separate standard prismatic moulds. As for the bricks, the procedure described in [11] consisted of non-destructive tests executed on whole brick specimens, whilst the static tests were carried out on small specimens cut out from the same bricks. It should be noted that the average compressive strength
 135 (f_{cn}) listed in [11] for some brick specimen groups differs from the one shown in Table 1. This difference mainly arises from the fact that the f_{cn} reported in [11] was derived from other different bricks of the same type but not from the actual specimens tested during the experimental campaign. However, as described in Section 2.2.1, the f_{cn} reported in Table 1 were derived from specimens cut out from the same bricks as the ones used to determine the static and dynamic elastic modulus.

140 2.2. Experimental determination of static modulus

2.2.1. Specimen preparation for static tests

Static tests from which the elastic moduli are to be evaluated involve fixing the applied stress at lower levels than the compressive strength for fixed intervals during testing. Hence, prior knowledge of the ap-

proximate compressive strengths of the specimens from each group is required before executing the tests.

145

Before cutting out any prisms from bricks to perform static tests, the two opposing largest faces of the bricks were polished so that each brick had a uniform thickness of 40 mm. Since handmade bricks formed by moulding can be reasonably approximated as being isotropic [11, 38], it can be assumed that for each specimen group, the average compressive strength evaluated across the brick lengths should correspond to that evaluated across the widths. As such, for specimen groups I(a), I(b), III and V(a), a $40 \times 40 \times 80$ mm³ prism across the width was cut out from each brick to estimate the compressive strength according to the procedure in [33] (see (c) in Figure 1). The reference compressive strength (f_{cn}) for each group was then taken as the average of the ones estimated from these prisms. As shown in Figure 1, three more $40 \times 40 \times 80$ mm³ prisms were cut out across the width of each remaining brick to evaluate the static elastic modulus across the width ($E_{st,W}$), while three equally sized prisms were cut across the length to evaluate the modulus in that direction ($E_{st,L}$).

155

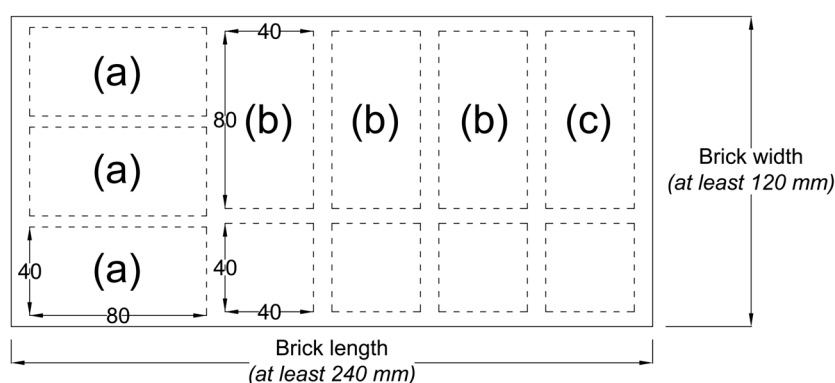


Figure 1: Specimens cut from each handmade brick. (a) Specimens used for estimating static elastic modulus across length. (b) Specimens used for estimating static elastic modulus across width. (c) Specimen used for estimating compressive strength.

160

165

It should be noted that one of the prisms across the width of a brick from group V(a) was damaged and therefore only 2 specimens could be used to evaluate $E_{st,W}$ for that particular brick. Furthermore, although bricks from group V(b) were also formed by moulding, the same specimens shown in Figure 1 were not cut out from each brick. This is due to the fact that $40 \times 100 \times 100$ mm³ prisms had already been cut from these bricks to evaluate their compressive strengths according to [33] as part of a previous experimental campaign. Naturally, the compressive strength evaluated from the previous campaign was taken as the representative strength for each brick from this group. However, this meant that less remaining area was available from each brick to extract specimens for the evaluation of elastic moduli. As such, only $40 \times 40 \times 80$ mm³ prisms across the length were cut from each brick. Although the number of specimens that could be cut out from each brick varied, it was ensured that at least 2 were extracted from each to calculate $E_{st,L}$.

170

As described in greater detail in Section 2.3, only the dynamic elastic modulus across the length is available for bricks produced by extrusion (groups II and IV). Hence, only $E_{st,L}$ is included in this study for these bricks. These were also derived from tests carried out on $40 \times 40 \times 80$ mm³ specimens cut out across the length of each brick.

175

Given that bricks are most often loaded in compression across their thickness, the choice of investigating the relationship between static and dynamic modulus across the width and length of bricks might appear counter-intuitive. Particularly when the procedure described in [11] allows for the estimation of dynamic elastic moduli of bricks handmade in moulds across their thickness. However, since this study mainly aims to better understand the relationship between static and dynamic moduli, this choice was made to ensure that only reliable estimates that reflect the actual material behaviour are compared. As stated in Section 1, for typical brittle brick materials, measuring surface strains in the elastic range can be a very challenging

task with several possible sources of error. The impact of these errors on the final estimated value of the static elastic modulus is likely to be significantly greater if the strains are measured over a shorter gauge length. Since the polished bricks tested as part of this research were at most 40 mm thick, only very short gauge lengths were available to measure strains across this dimension. In fact, the coefficients of variation of static elastic moduli estimated from strain measurements across the lengths and widths of bricks already proved to be significantly greater than those estimated from dynamic methods (see Section 3), despite the fact that they allowed strain measurements over a longer gauge length. Moreover, the dynamic modulus across the thickness is not available for the anisotropic bricks produced by extrusion. As such, elastic moduli estimated across the thickness of bricks were not included in this study.

Before testing, the surfaces of all the cut prismatic brick specimens were polished and regularised to ensure uniform loading and to reduce possible sources of error in deformation measurements. Since moisture content of the specimens can alter the deformation behaviour of these materials, all specimens were dried at 120 °C in a drying oven until the mass was constant prior to testing.

In the case of the mortar specimen groups, standard 40 × 40 × 160 mm³ prismatic specimens were prepared and tested to evaluate both the compressive strength and the static elastic modulus. These were cast and tested at the same time as the brick-shaped specimens used for dynamic testing in [11].

2.2.2. Experimental procedure for static tests

The stress-strain relationship of brittle materials, such as typical brick masonry constituents, usually reveals a certain degree of non-linearity even at stress levels well below their ultimate strength. This can be attributed to microcracks [39] and creep effects [1]. Due to this inherent non-linearity, different definitions of the static elastic modulus have been proposed for such materials depending on how the latter is calculated. It is possible to find a *tangent modulus* at any point on the stress-strain curve, but this will only apply to loading levels in the vicinity of the point at which the modulus was calculated and is therefore of little practical significance. The *chord modulus* taken as the slope of the line connecting two specific points on the stress-strain curve is usually preferred since it is more representative of the material behaviour under actual loading conditions of interest. It should be noted that since the first point used for the computation of the chord modulus is usually at a very low stress level, some books [1], articles [7, 9] and even standards [40] have come to refer to it as a *secant modulus*.

Naturally, since the secant modulus will depend on the two points chosen to compute it, it is important to select them carefully. To the best of the authors' knowledge, no standards exist for the determination of the static elastic modulus of brick masonry constituents. However, some guidance for the selection of appropriate nominal stress levels can be found from the European Standards for the determination of the static moduli of elasticity of concrete (EN 12390-13:2013) [40] and natural stone (EN 14580:2005) [41], as well as in the standard for the determination of the compressive strength of masonry (EN 1052-1:1998) [42]. All these standards recommend to use a nominal upper stress level at a third of the estimated compressive strength (f_c). However, they differ in their recommendation for the nominal lower stress level at which the strain should be evaluated for the computation of the static elastic modulus. Whilst the standard for concrete recommends a nominal lower level between 10% and 15% of f_c , that for natural stone recommends one corresponding to approximately 2% of f_c . Based on these recommendations, for the static tests carried out as part of this research, the nominal upper stress level (σ_b) was set as approximately equal to 30% of the representative compressive strength for each specimen group. The nominal lower stress level (σ_a) was set as approximately equal to 10% of the representative compressive strength for each group. The latter value was chosen because the measured strains at lower stress values approached the minimum resolution of the strain transducer for some of the specimens with low compressive strengths.

To eliminate some of the creep effects and to allow the extension pieces of the transducers to settle at fixed points on the material, it is vital to subject each specimen to cycles of pre-loading up to the nominal upper stress level. Standards [40] and [41] suggest to carry out three loading cycles and to determine the

stabilised secant modulus based on the third cycle. This procedure was thus adopted for all the tests carried out to determine the static elastic modulus of the brick masonry constituents, resulting in the loading scheme shown in Figure 2. As shown, the load was held constant for 60 s at the nominal upper and lower stress levels. The final increasing branch of the loading scheme after the third cycle was implemented to verify the continuity of the slope of the stress-strain curve beyond σ_b .

235

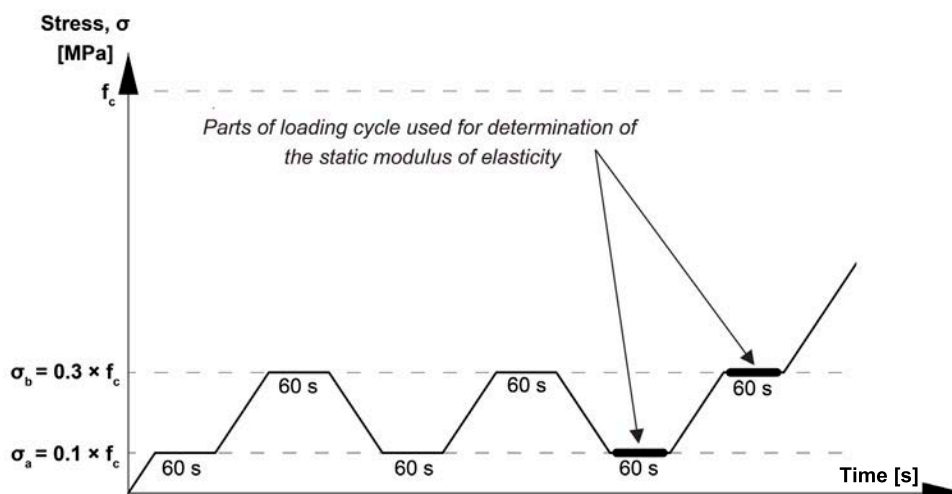


Figure 2: Loading scheme employed for tests to determine the static elastic modulus of specimens.

It should be noted that specimens from group I(a) were tested before the final testing protocol was developed. For tests on these specimens, σ_a was set at 5% of f_c instead of 10%.

The experimental procedure thus involved applying a compressive load according to the loading scheme shown in Figure 2 while recording vertical strain measurements across the surface of three faces using a gauge length of 50 mm as shown in Figure 3. The remaining face of each specimen was equipped with a transducer to record horizontal strains during testing for a different study. A custom adjustable frame was designed and built to quickly and securely hold all the transducers in position without inhibiting their measuring ability.

240

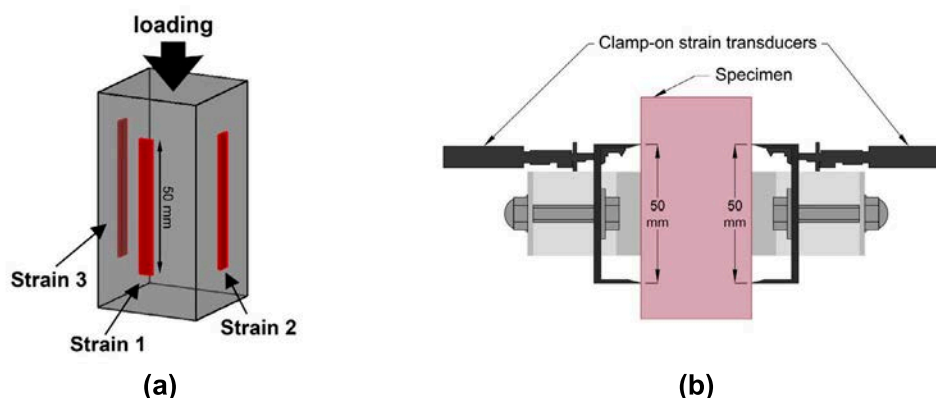


Figure 3: (a) Schematic diagram showing locations at which strain was measured during testing of each specimen. (b) Cross-section across clamp-on strain transducers placed on opposing faces of a specimen.

245

All tests were carried out with load control while measurements were recorded with a sampling rate of 5 Hz. A load cell with a maximum compression force of 200 kN was used for all tests except for those on lime mortar specimens. These were tested using a load cell with a maximum capacity of 10 kN. During

the cyclic loading procedure, loads were applied with a constant velocity of 0.25 kN/s in between successive nominal levels. As shown in Figure 3, clamp-on strain transducers with an effective minimum resolution of approximately $0.013 \mu\text{m}/\text{mm}$ were used to measure strains during all tests.

2.2.3. Derivation of static elastic modulus from raw data

Once the experiments were completed, the compression loads recorded during each test were converted to stresses through division by the cross-sectional area of the specimen. Data points corresponding to the parts of the third loading cycle held at the nominal lower (σ_a) and upper (σ_b) stress levels were then extracted from all the stress and strain measurements. In order to ensure that there were no inconsistencies during loading and that the stresses were effectively held at the nominal levels, the coefficients of variation among extracted data points corresponding to each specific level were verified. Since they never exceeded 0.25%, the loading of all the specimens was deemed as being consistent with the scheme shown in Figure 2 and the mean stress recorded during the period for which the loading was held at a nominal level was taken as the central tendency.

Similarly, each representative measured strain value corresponding to a nominal stress level was computed as the mean of the strains recorded during the period for which the stress was held at that level. However, since surface strain measurements of brittle materials are prone to error, two important verifications were carried out to ensure erroneous measurements were not included in the computation of the elastic modulus. First, measurements from a specific strain transducer for a particular test were discarded if the magnitude of the mean strain for a nominal stress level was lower than the minimum resolution of the transducer ($0.013 \mu\text{m}/\text{mm}$). Measurements smaller than this hardware limitation can actually be considered as being equivalent to not registering any strain. Second, measurements from a specific strain transducer for a particular test were also discarded if the coefficient of variation among extracted data points corresponding to the same nominal level exceeded 1%. This requirement was established to identify apparent sudden changes of strain that were recorded while the applied load was kept constant, such as the one shown in Figure 4.

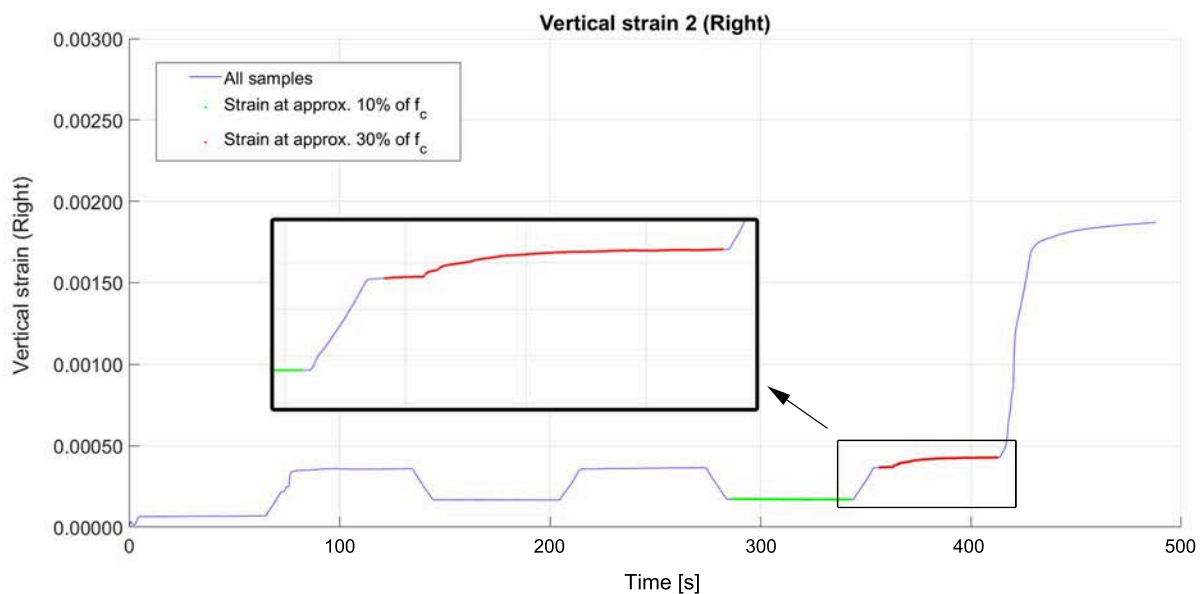


Figure 4: Example of an unsteady strain measurement deemed as being erroneous.

This cross-check of the experimental readings is introduced in this research as it proves to be of paramount importance in experimental tests evaluating the deformation characteristics of masonry components. Identifying and eliminating such erroneous values, mostly due to possible contact problems between the strain

transducer and the specimen's surface, can have a significant effect on the accuracy of the final estimates of the static elastic modulus. In this case, as a result of the filtering procedure described in the previous paragraph, out of the 168 specimens tested, at least one strain measurement was discarded from 22 specimens.

280

Once these erroneous strain values were eliminated, the strain difference between the nominal upper and lower stress levels was computed for each strain transducer for every test. The mean of the three vertical strain changes measured across different faces of each specimen then needs to be computed before E_{st} can be estimated. Naturally, in case one or more of the strain measurements across a particular face had been deemed to be erroneous, they have to be excluded from the computation of the mean strain change. However, before proceeding with the estimation of E_{st} , for some of the specimens still left with three non-erroneous strain measurements, a clear outlier could be identified as shown in Figure 5. These outliers most likely occurred due to the presence of very localised heterogeneities close to the surface across which the strain was being measured and are therefore not representative of the true material behaviour. Hence, although the treatment of outliers is rarely straightforward, in this particular case, it can be deemed that a better estimate of the actual E_{st} can be obtained by excluding such outliers from the data set.

290

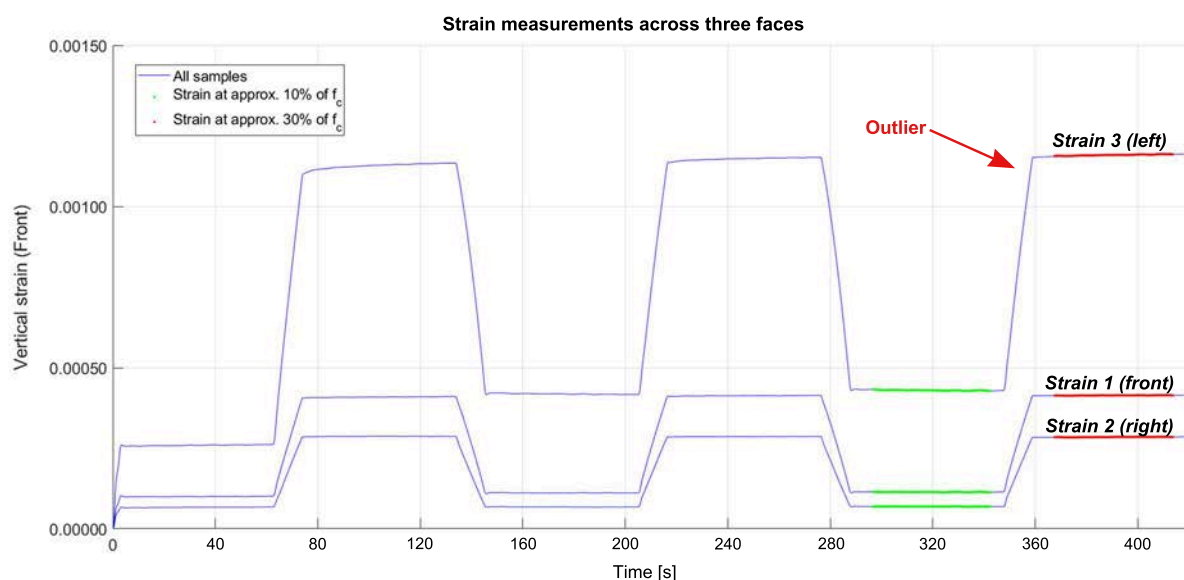


Figure 5: Example of an outlier among 3 strain measurements across different faces of a specimen.

Although there exists several statistical procedures to deal with outliers in data sets, many of them are not effective when only a small number of observations are available. As such, most common methods would not perform well for the case of the measured strain changes since only 3 observations are available.

295

However, a well-known procedure, known as Dixon's Q test [43], has been developed specifically for such cases. It relies on the computation of a Q ratio for each observation as follows:

$$Q = \frac{x_n - x_{n-1}}{\omega} \quad (7)$$

Where x_n is the observation for which the Q ratio is being computed, x_{n-1} is the nearest neighbour of x_n and ω is the range of the set of observations defined as the difference between the largest and the smallest observation.

300

The conventional implementation of the Q test involves excluding observations with Q ratios greater than tabulated rejection thresholds corresponding to a specific confidence level assuming a normally distributed population. As can be seen from Equation (7), the Q ratio is normalised by the range which is considered as

one of the most efficient measures of dispersion for a small number of observations [43]. It is therefore based solely on the relative distances between observations irrespective of the magnitude of the range. As a result, the test tends to penalise outliers more strictly in a less dispersed sample. This is a disadvantage in the case of the measured strain changes since the desired outcome is to exclude an outlier that differs significantly from the other measurements in terms of magnitude rather than excluding one that differs relatively more than the others within a small range. To overcome this limitation, for each set of measured strain changes, the magnitude of the dispersion (measured by the range) was compared to the magnitude of the central tendency (measured by the mean). If the range was found to be greater than 75% of the mean value, the observation with the greatest Q ratio, computed as shown in Equation (7), was excluded from the data set. Using this procedure, a single outlying value for the strain change was excluded for 10 of the 168 specimens tested as part of this research.

Subsequently, the static elastic modulus E_{st} of each tested specimen was computed using the following expression:

$$E_{st} = \frac{\overline{\sigma_b} - \overline{\sigma_a}}{\epsilon_{diff}^*} \quad (8)$$

Where $\overline{\sigma_a}$ and $\overline{\sigma_b}$ refer to the mean stresses recorded during the third loading cycle at the lower and upper nominal levels respectively while ϵ_{diff}^* refers to the mean strain change measured between the two nominal stress levels across 3 different specimen faces excluding any identified outliers or erroneous values.

2.3. Experimental determination of dynamic modulus

The complete procedure to obtain reliable estimates of the dynamic elastic properties of brick masonry constituents, as well as an extensive discussion on the factors that can influence them, has already been presented in a previous publication [11] and will not be reiterated in this article. However, a brief summary of the relevant processes employed to estimate the dynamic elastic moduli compared to static ones is provided in this section.

As described in [11], the most reliable estimate of the dynamic elastic modulus across a brick's length can be obtained through Impulse Excitation of Vibration (IEV) testing. This test method relies on identifying natural frequencies corresponding to specific resonant modes that are isolated through particular test set-ups. Basically, the tests consist of applying an impulse at a particular location on a specimen constrained by specific boundary conditions such as the ones shown in Figure 6(a). At the same time, the resulting acceleration of the specimen is recorded using a lightweight accelerometer fixed along nodal lines to minimise mass loading effects. The resonant frequency corresponding to each isolated mode of vibration is then extracted from the acquired vibration signatures using Frequency Domain Decomposition (FDD). Analytical expressions exist that relate specific resonant frequencies to the elastic properties of the material and the mass and dimensions of the specimen under test. Hence, once the required resonant frequencies are identified, dynamic elastic properties can be estimated by making use of the analytical expressions. The dynamic elastic modulus across a brick's length is related to the flexural vibration mode which can be isolated and identified using the test set-up shown in Figure 6(a). This method was also used to estimate the dynamic moduli of the mortar specimens compared to the static ones in this study.

In order to estimate the elastic modulus across a brick's width, Ultrasonic Pulse Velocity (UPV) testing with compression waves was used instead. This method relies on measuring the travel time of an ultrasonic compression wave across a known length of the material. Because there exist analytical expressions relating the velocity of mechanical waves to elastic properties of the material, the measured travel time can be used to compute the velocity of the pulse and subsequently to estimate the elastic modulus across a brick's length. The procedure employed in [11] involves measuring the travel time and computing the corresponding pulse velocity at the three locations shown in Figure 6(b). The average of these three velocities is then used for the estimation of the dynamic elastic modulus across the width of each brick. It is important to note that material isotropy is a fundamental assumption of the analytical expressions employed. As such, no estimates

of the dynamic elastic modulus across the width could be obtained for bricks produced by extrusion (groups II and IV) since they presented a clearly anisotropic character [11].

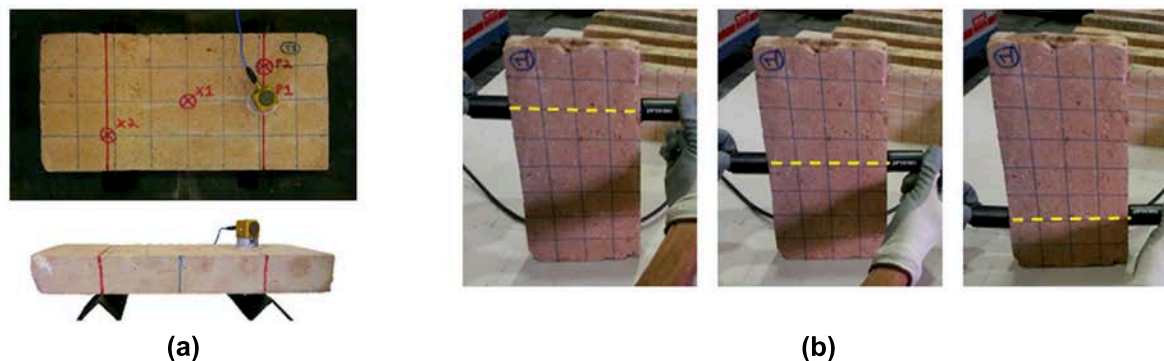


Figure 6: (a) Flexural test set-up used for the estimation of the dynamic elastic modulus of mortars and across the length of bricks through Impulse Excitation of Vibration (IEV) testing. (b) Locations at which the travel time was measured for the estimation of the dynamic elastic modulus across the width of bricks using Ultrasonic Pulse Velocity (UPV) tests [11].

3. Experimental results

For each brick, the average value of static elastic moduli of specimens extracted across the brick length was taken to represent the static elastic modulus of the brick across its length ($E_{st,L}$). Similarly, the average static elastic modulus of specimens extracted across a brick's width was taken as the static elastic modulus of the brick across its width ($E_{st,W}$). Each one of these values were compared to the most reliable corresponding dynamic elastic modulus (E_{dy}) of the same brick, which had previously been estimated using impulse excitation of vibration (IEV) or ultrasonic pulse velocity (UPV) methods [11]. As described in [11], estimates of the dynamic elastic modulus obtained using IEV are more reliable and representative of the elastic modulus of the entire specimen when compared to UPV estimates. Hence, values estimated using IEV were utilised for the comparison of elastic moduli across a brick's length and for mortar specimens. Nevertheless, it is worth mentioning that there is generally a good agreement between UPV and IEV estimates for isotropic constituent materials as described in [11]. Since the IEV methods utilised cannot provide estimates for the dynamic elastic modulus across a brick's width [11], UPV estimates were used for comparison to $E_{st,W}$.

For all specimen groups consisting of handmade bricks formed in moulds, except group V(b) (see Section 2.2.1), both $E_{st,L}$ and $E_{st,W}$ were computed. Due to their anisotropic nature, no dynamic elastic modulus across the width of bricks produced by extrusion was available for comparison (specimen groups II and IV) [11]. Therefore, $E_{st,W}$ of these bricks could not be used to better understand the relationship between E_{st} and E_{dy} . This resulted in a data set containing 35 pairs of E_{st} and E_{dy} estimates across brick lengths and 18 across brick widths. The average values of $E_{st,L}$ and $E_{st,W}$ for each specimen group are summarised in Tables 3 and 4 along with the average dynamic modulus values corresponding to the same specimen group and material direction.

Table 3: Comparison of average static ($E_{st,L}$) and dynamic (E_{IEV}) elastic modulus measured across brick lengths for each specimen group.

Specimen group	Static		Dynamic*		$\frac{E_{st}}{E_{dy}}$
	$E_{st,L}$ [MPa]	coeff. of variation	E_{IEV} [MPa]	coeff. of variation	
I(a)	6,287	27%	7,882	15%	0.798
I(b)	7,920	22%	7,931	17%	0.999
II	16,081	7%	18,313	1%	0.878
III	5,996	22%	7,107	13%	0.844
IV	13,249	16%	15,505	1%	0.855
V(a)	5,572	7%	5,475	8%	1.018
V(b)	4,736	28%	4,068	30%	1.164

* Determined according to the procedure reported in [11].

Table 4: Comparison of average static ($E_{st,W}$) and dynamic ($E_{UPV,W}$) elastic modulus measured across brick widths for each specimen group.

Specimen group	Static		Dynamic*		$\frac{E_{st}}{E_{dy}}$
	$E_{st,L}$ [MPa]	coeff. of variation	$E_{UPV,W}$ [MPa]	coeff. of variation	
I(a)	5,504	23%	8,241	19%	0.668
I(b)	7,563	21%	8,189	15%	0.924
II	-	-	-	-	-
III	6,051	18%	8,717	7%	0.694
IV	-	-	-	-	-
V(a)	5,389	23%	6,336	7%	0.851
V(b)	-	-	-	-	-

* Determined according to the procedure reported in [11].

In contrast, for mortars, a single average E_{st} is taken from all the tested prisms belonging to a specimen group. Thus only 3 new pairs of E_{st} and E_{dy} estimates are added to the data set containing 53 pairs of estimates from different brick specimens. The E_{st} values are shown together with the dynamic elastic modulus for the corresponding mortar type in Table 5.

Table 5: Comparison of average static (E_{st}) and dynamic (E_{IEV}) modulus of mortar specimen groups.

Specimen group	Static		Dynamic*		$\frac{E_{st}}{E_{dy}}$
	$E_{st,L}$ [MPa]	coeff. of variation	E_{IEV} [MPa]	coeff. of variation	
MB	2,696	8%	3,987	10%	0.676
MIIB	2,666	29%	4,269	6%	0.625
MC	27,167	8%	28,954	5%	0.938

* Determined according to the procedure reported in [11].

380

As can be expected, the coefficient of variation (CV) of E_{st} is significantly greater than that of the corresponding E_{dy} for almost all specimen groups. Nonetheless, the CV between specimens for E_{dy} can be seen to be marginally greater than that of E_{st} in 3 cases, namely for MB mortars and for groups V(a) and V(b) when the modulus is evaluated across brick lengths. In these cases, the CV of E_{dy} tends to be only 1%

or 2% higher than that of E_{st} . It should also be noted that many specimens from these particular groups were found to have a relatively high level of heterogeneity and much of the dispersion between estimated moduli values can be attributed to this [11]. In contrast, for the remaining specimen groups, the coefficients of variation among specimens for E_{st} are twice as large on average as those for E_{dy} . In fact, the greatest relative difference between these coefficients of variation occurs for one of the most homogeneous specimen groups (group IV). This is a clear indication of the increased difficulty and propensity for error of the static tests.

In terms of the magnitudes of the elastic moduli, with the exception of $E_{st,L}$ for specimen groups V(a) and V(b), the representative static elastic modulus of a specimen group is found to be always lower than its dynamic counterpart. This is in agreement with the trend generally observed in previous studies of this relationship for rocks and concrete, as already described in Section 1. In fact, for both group V(a) and group V(b), the relative difference between E_{st} and E_{dy} is smaller than the coefficient of variation associated to either value. This shows that the estimate of the difference between the two material properties is smaller than the dispersion related to the measurement of either one. As such, although exceptional observations for which $\frac{E_{st}}{E_{dy}}$ ratios greater than 1 have been reported for the case of rocks [6], in this case, it can be said that these occurrences cannot be deemed significant and do not reflect the true relationship between these two properties.

If individual specimens are analysed, the estimated static elastic modulus is greater than the dynamic one for 11 of the 56 pairs of E_{st} and E_{dy} available for comparison. However, it should be noted that 7 of the 11 specimens are from group V(a) or V(b). Moreover, it should be noted that, even for individual specimens, the ratio $\frac{E_{st}}{E_{dy}}$ is very close to 1 for most cases.

Based on the 42 pairs of E_{st} and E_{dy} values available for handmade bricks formed by moulding, simple linear regression with the intercept fixed at 0 reveals that 0.85 is a reasonable estimate of the $\frac{E_{st}}{E_{dy}}$ ratio for such bricks. The same procedure reveals that 0.87 is a good estimate of this ratio for bricks produced by extrusion based on the 11 data points available. These preliminary observations suggest that a suitable relationship can be found for both bricks produced by extrusion and for those handmade in moulds. As such, they were analysed as a single data set in an attempt to better understand the underlying relationship between static and dynamic elastic moduli for such materials. The 2 pairs of E_{st} and E_{dy} values available for lime mortar specimens suggest an average $\frac{E_{st}}{E_{dy}}$ ratio of 0.65 for this material. On the other hand, MC specimens tested as part of this research suggest a $\frac{E_{st}}{E_{dy}}$ ratio of 0.94, which is in good agreement with findings from previous studies on Portland cement-based mixes [15]. The two available data points for lime mortars and the single one of cement mortar certainly cannot be used for in-depth studies specifically on these respective material types. However, it was deemed beneficial to evaluate how well they agree with a general relationship for brittle constituent materials typically used in brick masonry constructions. As such, they were also included in the data set analysed in the following section.

4. Comparison and discussion

Previous studies [6, 19, 27, 30] have already established that including material compressive strength, density and even porosity can lead to improved prediction capability of correlation models. However, given the variability of the sample set in terms of chemical composition and manufacturing process, it is unclear as to whether or not including them as explanatory variables can limit the range of practical applications significantly. Hence, in order to evaluate this, a correlation study was carried out between different combinations of explanatory variables that can be included in the prediction model (see Tables 6 and 7). Such a study was also carried out previously in order to assess which combinations of material density and dynamic modulus to use for the prediction of the static elastic moduli of rocks [6]. It is achieved by computing the Pearson correlation coefficient ($R_{X,Y}$) between different combinations of dependent and explanatory variables, as shown in Equation (9). This coefficient is a dimensionless measure of linear dependence that can

vary between -1 and +1, with absolute values closer to unity indicating a better correlation. The sign of the coefficient indicates the type of correlation. A negative sign indicates that an increase of one parameter leads to a decrease of the other whereas a positive sign indicates that the increase of one leads to an increase of the other.

$$R_{X,Y} = \frac{cov(X,Y)}{\sigma_X \cdot \sigma_Y} \quad (9)$$

Where $R_{X,Y}$ is the Pearson correlation coefficient between the variables X and Y , $cov(X,Y)$ is the covariance between them and σ_X and σ_Y are their respective standard deviations.

First, the same explanatory variable combinations explored in [6] for rocks were tested on the sample set of brick masonry constituents. As shown in Table 6, this involves various combinations of the material density (ρ) and the dynamic elastic modulus (E_{dy}).

Table 6: Correlation matrix for various combinations of static (E_{st}) and dynamic (E_{dy}) moduli and density (ρ) of brick masonry constituents.

Variables	E_{dy}	$\log_{10} E_{dy}$	ρ	$\rho\sqrt{E_{dy}}$	ρE_{dy}	$\sqrt{\rho E_{dy}}$	$\log_{10} \rho E_{dy}$	$\rho \log_{10} E_{dy}$	$\frac{E_{dy}}{\rho}$	$\sqrt{\frac{E_{dy}}{\rho}}$
E_{st}	0.97	0.89	0.10	0.94	0.96	0.95	0.89	0.70	0.94	0.92
$\log_{10} E_{st}$	0.92	0.92	-0.05	0.88	0.88	0.91	0.91	0.60	0.92	0.93

Previous studies have shown that the compressive strength of the material can influence the relation between static and dynamic elastic moduli for concrete ([1, 17, 18]) and rocks [30]. It was therefore deemed relevant to assess the suitability of including it as an explanatory variable for the case of brick masonry constituents. As such, as shown in Table 7, a correlation study was also carried out involving the same configurations as shown in Table 6 but substituting the material density with its compressive strength (f_c).

Table 7: Correlation matrix for various combinations of static (E_{st}) and dynamic (E_{dy}) moduli and compressive strength (f_c) of brick masonry constituents.

Variables	E_{dy}	$\log_{10} E_{dy}$	f_c	$f_c\sqrt{E_{dy}}$	$f_c E_{dy}$	$\sqrt{f_c E_{dy}}$	$\log_{10} f_c E_{dy}$	$f_c \log_{10} E_{dy}$	$\frac{E_{dy}}{f_c}$	$\sqrt{\frac{E_{dy}}{f_c}}$
E_{st}	0.97	0.89	0.84	0.90	0.93	0.93	0.87	0.86	-0.32	-0.32
$\log_{10} E_{st}$	0.92	0.92	0.85	0.87	0.87	0.91	0.92	0.85	-0.43	-0.42

Since some researchers [30] have reported improved correlation for some rock types when increasing levels of complexity are added to the prediction expressions, the suitability of including both ρ and f_c was also carried out. This was achieved by substituting ρ with $\rho \cdot f_c$ in all the configurations tested in [6] before calculating the correlation coefficients. The outcome is summarised in Table 8.

Table 8: Correlation matrix for various combinations of static (E_{st}) and dynamic (E_{dy}) moduli with density (ρ) and compressive strength (f_c) of brick masonry constituents.

Variables	E_{dy}	$\log_{10} E_{dy}$	$\rho \cdot f_c$	$\rho \cdot f_c \sqrt{E_{dy}}$	$\rho \cdot f_c \cdot E_{dy}$	$\sqrt{\rho \cdot f_c \cdot E_{dy}}$	$\log_{10} (\rho \cdot f_c \cdot E_{dy})$	$(\rho \cdot f_c) \log_{10} E_{dy}$	$\frac{E_{dy}}{\rho \cdot f_c}$	$\sqrt{\frac{E_{dy}}{\rho \cdot f_c}}$
E_{st}	0.97	0.89	0.87	0.93	0.94	0.94	0.87	0.89	-0.33	-0.33
$\log_{10} E_{st}$	0.92	0.92	0.86	0.87	0.85	0.91	0.92	0.86	-0.43	-0.41

As can be seen from Tables 6, 7 and 8, of all the explored combinations, the strength of the linear correlation is strongest directly between E_{st} and E_{dy} . Although it is clear that there is still a relatively

strong linear correlation between f_c and E_{st} or $\rho \cdot f_c$ and E_{st} , none of the explored combinations with E_{dy} contribute to strengthening its linear correlation with E_{st} . As previously mentioned, this is most likely due to the variability of the sample set which reflects the diversity of typical brick masonry constituents. Different mortars have distinct chemical compositions and can harden through different setting reactions. Bricks can differ greatly according to the manufacturing process and ingredients from which they are made. Given this variability, and recognising that the heterogeneity of materials affect the static and dynamic moduli in different ways, it cannot be expected that there exists a single relation between the two moduli based on physical behaviour. However, the high value of the correlation coefficient between E_{st} and E_{dy} is a promising indicator that there exists a linear empirical relationship between the two that could be useful for many practical applications.

As such, simple linear regression was carried out between measured values of E_{st} and E_{dy} to identify the unknown parameters of the relationship between the two. To prevent the proposed model from predicting zero or negative values of the static elastic modulus from positive measured values of the dynamic one, the intercept was fixed as 0. This left the slope as the only unknown parameter to be identified through the regression. As a result of this procedure, the following expression is proposed to estimate the static elastic modulus of brick masonry constituents from measurements of the dynamic one.

$$E_{st} = 0.87E_{dy} \quad (10)$$

Where E_{st} and E_{dy} refer to the static and dynamic moduli measured in consistent units.

Despite the simplistic nature of the proposed expression, the measured data are in very good agreement with its predictions. In fact, although the sample of measured dynamic elastic moduli ranges more than 26 *GPa* (from 2.7 *GPa* to 29 *GPa*), the entire 95% prediction interval of the proposed relation spans only 4.6 *GPa* (see Figure 7). In spite of this, it is worth noting that specifically for the weakened hydraulic lime mortar used as part of this study, using a $\frac{E_{st}}{E_{dy}}$ ratio of 0.65 is recommended instead of the general proposed relationship.

It is clear to see that the proposed relationship is extremely close to one of the simplest and oldest empirical expressions proposed for concrete [16]. This relation suggests that the static modulus is approximately equivalent to $0.83E_{dy}$. As such, although it is unlikely that a single relation between E_{st} and E_{dy} for brittle materials can be developed based on physical behaviour, it is undeniable that there are many similarities in the relation of these properties for such materials. Hence, several existing relationships proposed for concrete and rocks were tested on the data set containing 56 pairs of measured E_{st} and E_{dy} for various brick masonry constituents. Most of these are shown in Figure 7.

Although several metrics were used to assess the accuracy of the models, the standard error of the estimate (σ_e) is probably the one that is most easily interpreted since it is expressed in the units of the measurements. This parameter indicates approximately how large prediction errors are for your data set and is computed as follows.

$$\sigma_e = \sqrt{\frac{\sum_{i=1}^n (Y_i - Y_i')^2}{n - k - 1}} \quad (11)$$

Where Y_i refer to actual measurements of E_{st} while Y_i' refer to model predictions. With n equal to the number of data sample points and k equal to the number of explanatory variables used in the model, $n - k - 1$ represents the number of degrees of freedom available for the computation of the error metric.

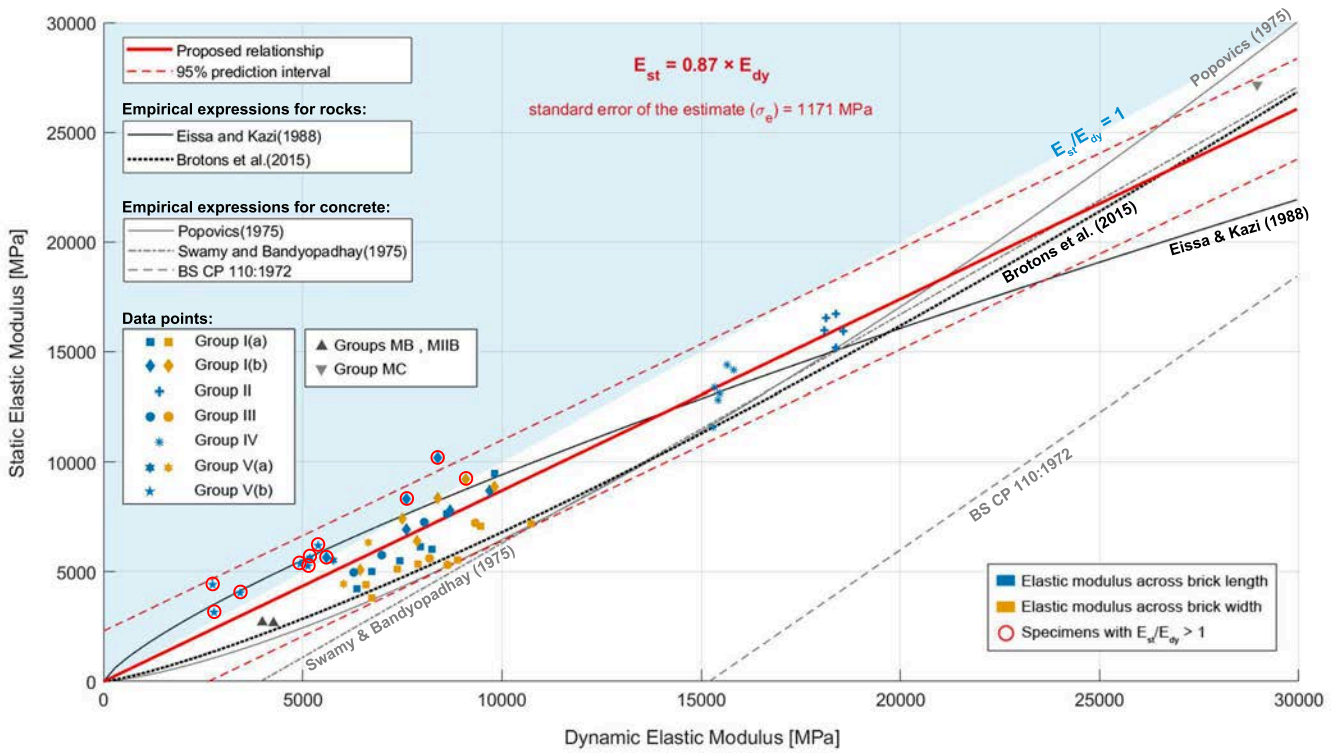


Figure 7: Prediction of static elastic modulus (E_{st}) from dynamic elastic modulus (E_{dy}).

495 The final standard prediction errors for the different models used to predict E_{st} from E_{dy} are shown in Figure 8.

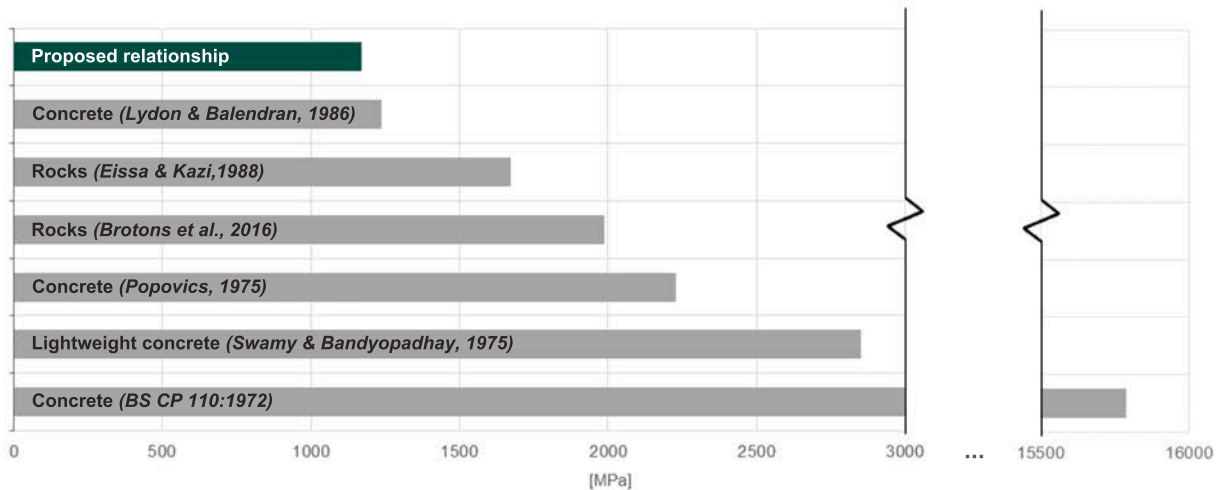


Figure 8: Prediction errors of various existing expressions for estimating E_{st} from E_{dy}

It can be seen that the proposed simple empirical expression results in the smallest error. The second most accurate model is clearly that proposed by Lydon and Balendran (1986) [16]. This is expected since it has the same form as the proposed single-parameter model with only a slight variation in the magnitude of the parameter. However, having been developed for concrete, the expression proposed by Lydon and

Balendran was estimated from specimens with much higher stiffness. The closeness of the two identified models thus suggests that these simple expressions have a large range of applicability which can be very useful for practical applications. The least well-performing models appear to be linear ones developed for concrete that include a non-zero intercept. Although these work well for specific types of concrete, they are clearly not suitable for lower stiffness brittle materials such as the ones tested as part of this research. That being said, specifically for the cement mortar tested as part of this research, the expression proposed by Swamy and Bandyopadhyay (1975) for lightweight concrete [15] provides a better estimate of the measured static elastic modulus when compared to the proposed relationship. Although the nonlinear models that incorporate density are able to better represent the relation between E_{st} and E_{dy} for some small ranges of stiffness, it is clear that over the entire range of specimens tested, they are less accurate than the simpler proposed model. Finally, the nonlinear models developed for rocks appear to be more applicable to the case of brick masonry constituents than the one developed for concrete. This is most likely due to the fact that the variability usually encountered in a sample of rocks more closely matches the variability of typical brick masonry constituents than that of concrete.

5. Conclusions

The research has proposed an empirical expression that can be used to estimate the static elastic modulus of typical brick masonry constituents from the dynamic modulus. Since the estimation of the latter parameter can be executed more quickly and reliably, the proposed expression can be used in a wide range of practical applications. To ensure that the expression would be meaningful for different masonry typologies, the tests have considered hydraulic lime and cement mortar, new bricks manufactured either by hand-made moulding or extrusion and bricks extracted from heritage buildings in Barcelona, Spain.

Several combinations of explanatory variables were investigated before selecting the final model. However, simply expressing the static elastic modulus as a ratio of the dynamic one appears to be most effective over the range of materials tested. This most probably arises due to the large variability of brick masonry constituents in terms of isotropy, heterogeneity as well as chemical composition and manufacturing process. It is undeniable that incorporating other explanatory variables such as density or compressive strength would lead to more accurate models for specific types of brick masonry constituents. However, the proposed expression has proven to be applicable to a wide range of constituent materials with sufficient accuracy for many practical applications.

The most useful application of the proposed expression is that it provides a means to obtain very quick estimates of the static elastic modulus from whole bricks in a laboratory setting with minimal specimen preparation. This can save considerable time when compared to the tedious and lengthy cyclic static tests usually required to estimate this property. For bricks handmade in moulds, the study also revealed that the same expression can be applied to estimate the static elastic modulus across both the length or the width of bricks. Hence, although tests across other dimensions were not explicitly included in this study, it is deemed reasonable to assume that the proposed expression can be used together with appropriate dynamic tests to quickly estimate the static elastic modulus across the thickness of bricks formed by moulding. In addition, for the case of single-leaf brick masonry walls, the proposed relationship can be used together with ultrasonic pulse velocity (UPV) testing to quickly estimate the static modulus of elasticity of bricks in-situ. In fact, the same procedure would even allow the estimation of the static elastic modulus of mortar in-situ if some very thick joints can be identified. Since conventional UPV testing with compression waves is not valid for anisotropic material, such an in-situ procedure cannot be directly extended to the case of walls built with bricks produced by extrusion.

The proposed empirical expression has been calibrated based on an accurate control over the measurements of the static modulus, as they usually exhibit higher scattering due to the relevant technical complexity of the tests. Although the applicability of the same suggested empirical expression cannot be ensured

550 for materials differing significantly from those included in this research, the study has provided a general experimental methodology that may be replicated in the laboratory to derive alternative relationships.

Conflicts of interest

The authors confirm that there are no known conflicts of interest associated with this publication.

Acknowledgements

This research has received the financial support from the Ministry of Science, Innovation and Universities of the Spanish Government (MCIU), the State Agency of Research (AEI), as well as that of the ERDF (European Regional Development Fund) through the SEVERUS project (Multilevel evaluation of seismic vulnerability and risk mitigation of masonry buildings in resilient historical urban centres, ref. num. RTI2018-099589-B-I00). The corresponding author gratefully acknowledges the AGAUR agency of the Generalitat de Catalunya, and the second author gratefully acknowledges the AEI and the European Social Found (ESF), for the financial support of their predoctoral grants.

References

- [1] A. M. Neville, *Properties of concrete*, 5th Edition, Pearson, 2011.
- [2] R. E. Philleo, Comparison of Results of Three Methods for Determining Young's Modulus of Elasticity of Concrete, *ACI Journal Proceedings* 51 (1) (1955) 461 – 470. doi:10.14359/11690.
- [3] K. Wesche, W. Manns, Résultats d'une enquête internationale sur la détermination du module d'élasticité du béton en compression, *Matériaux et Constructions* 3 (3) (1970) 179–196. doi:10.1007/BF02478969.
- [4] K. J. Bastgen, V. Hermann, Experience made in determining the static modulus of elasticity of concrete, *Matériaux et Constructions* 10 (6) (1977) 357–364. doi:10.1007/BF02473733.
- [5] E. I. Mashinsky, Differences between static and dynamic elastic moduli of rocks: Physical causes, *Russian Geology and Geophysics* 44 (9) (2003) 953–959.
- [6] E. Eissa, A. Kazi, Relation between static and dynamic Young's moduli of rocks, *International Journal of Rock Mechanics and Mining Sciences & Geomechanics Abstracts* 25 (6) (1988) 479–482. doi:10.1016/0148-9062(88)90987-4.
- [7] L. Binda, C. Tiraboschi, S. Abbaneo, Experimental Research to Characterise Masonry Materials, *Masonry International* 10 (1997).
URL <https://www.masonry.org.uk/downloads/experimental-research-to-characterise-masonry-materials/>
- [8] L. Binda, C. Tedeschi, P. Condoleo, Characterisation of Materials Sampled From Some My S'on Temples, in: *7th International Congress on Civil Engineering*, 2006.
- [9] G. Baronio, L. Binda, C. Tedeschi, C. Tiraboschi, Characterisation of the materials used in the construction of the Noto Cathedral, *Construction and Building Materials* 17 (8) (2003) 557–571. doi:10.1016/j.conbuildmat.2003.08.007.
- [10] D. V. Oliveira, P. B. Lourenço, P. Roca, Cyclic behaviour of stone and brick masonry under uniaxial compressive loading, *Materials and Structures* 39 (2) (2007) 247–257. doi:10.1617/s11527-005-9050-3.
- [11] N. Makoond, L. Pelà, C. Molins, Dynamic elastic properties of brick masonry constituents, *Construction and Building Materials* 199 (2019) 756–770. doi:10.1016/j.conbuildmat.2018.12.071.
- [12] L. Binda, M. Facchini, G. Mirabella Roberti, C. Tiraboschi, Electronic speckle interferometry for the deformation measurement in masonry testing, *Construction and Building Materials* 12 (5) (1998) 269–281. doi:10.1016/S0950-0618(98)00009-9.
- [13] L. Pelà, E. Canella, A. Aprile, P. Roca, Compression test of masonry core samples extracted from existing brickwork, *Construction and Building Materials* 119 (2016) 230–240. doi:10.1016/j.conbuildmat.2016.05.057.

-
- [14] British Standards Institution (BSI), BS CP 110-1:1972; Code of practice for the structural use of concrete; Part 1: Design, materials and workmanship (1972).
URL <http://shop.bsigroup.com/en/ProductDetail/?pid=000000000010197621>
- [15] R. N. Swamy, A. K. Bandyopadhyay, The elastic properties of structural lightweight concrete, *Proceedings of the Institution of Civil Engineers* 59 (3) (1975) 381–394. doi:10.1680/iicep.1975.3671.
- [16] F. Lydon, R. Balendran, Some observations on elastic properties of plain concrete, *Cement and Concrete Research* 16 (3) (1986) 314–324. doi:10.1016/0008-8846(86)90106-7.
- [17] T. Takabayashi, Comparison of dynamic Young's modulus and static Young's modulus for concrete, *RILEM international symposium on nondestructive testing of materials and structures 1 (Paris) (1954)* 34–44.
- [18] B. J. Lee, S.-h. Kee, T. Oh, Y.-y. Kim, Evaluating the Dynamic Elastic Modulus of Concrete Using Shear-Wave Velocity Measurements, *Advances in Materials Science and Engineering* 2017 (2017) 1–13. doi:10.1155/2017/1651753.
- [19] S. Popovics, Verification of relationships between mechanical properties of concrete-like materials, *Matériaux et Constructions* 8 (3) (1975) 183–191. doi:10.1007/BF02475168.
- [20] M. King, Static and dynamic elastic properties of rocks from the Canadian shield, *International Journal of Rock Mechanics and Mining Sciences & Geomechanics Abstracts* 20 (5) (1983) 237–241. doi:10.1016/0148-9062(83)90004-9.
- [21] W. b Heerden, General relations between static and dynamic moduli of rocks, *International Journal of Rock Mechanics and Mining Sciences & Geomechanics Abstracts* 24 (6) (1987) 381–385. doi:10.1016/0148-9062(87)92262-5.
- [22] B. Chararas, F. Auger, E. Mosse, Determination of the moduli of elasticity of rocks. Comparison of the ultrasonic velocity and mechanical resonance frequency methods with direct static methods, *Materials and Structures* 27 (4) (1994) 222–228. doi:10.1007/BF02473036.
- [23] L. L. Lacy, Dynamic Rock Mechanics Testing for Optimized Fracture Designs, in: *SPE Annual Technical Conference and Exhibition*, Society of Petroleum Engineers, 1997. doi:10.2118/38716-MS.
- [24] P. Horsrud, Estimating Mechanical Properties of Shale From Empirical Correlations, *SPE Drilling & Completion* 16 (02) (2001) 68–73. doi:10.2118/56017-PA.
- [25] M. Ciccotti, F. Mulargia, Differences between static and dynamic elastic moduli of a typical seismogenic rock, *Geophysical Journal International* 157 (1) (2004) 474 – 477.
- [26] J. Martínez-Martínez, D. Benavente, M. A. García-del Cura, Comparison of the static and dynamic elastic modulus in carbonate rocks, *Bulletin of Engineering Geology and the Environment* 71 (2) (2012) 263–268. doi:10.1007/s10064-011-0399-y.
- [27] V. Brotons, R. Tomás, S. Ivorra, A. Grediaga, Relationship between static and dynamic elastic modulus of calcarenite heated at different temperatures: the San Julián's stone, *Bulletin of Engineering Geology and the Environment* 73 (3) (2014) 791–799. doi:10.1007/s10064-014-0583-y.
- [28] A. R. Najibi, M. Ghafoori, G. R. Lashkaripour, M. R. Asef, Empirical relations between strength and static and dynamic elastic properties of Asmari and Sarvak limestones, two main oil reservoirs in Iran, *Journal of Petroleum Science and Engineering* 126 (2015) 78–82. doi:10.1016/j.petrol.2014.12.010.
- [29] W. Fei, B. Huiyuan, Y. Jun, Z. Yonghao, Correlation of Dynamic and Static Elastic Parameters of Rock, *Electronic Journal of Geotechnical Engineering* 21 (04) (2016) 1551–1560.
- [30] V. Brotons, R. Tomás, S. Ivorra, A. Grediaga, J. Martínez-Martínez, D. Benavente, M. Gómez-Heras, Improved correlation between the static and dynamic elastic modulus of different types of rocks, *Materials and Structures* 49 (8) (2016) 3021–3037. doi:10.1617/s11527-015-0702-7.
- [31] Y. Z. Totoev, J. M. Nichols, A Comparative Experimental Study of the Modulus of Elasticity of Bricks and Masonry, in: *11th International Brick/Block Masonry Conference*, no. October, 1997.
- [32] J. M. Nichols, Y. Z. Totoev, Experimental determination of the dynamic Modulus of Elasticity of masonry units, in: *15th*

Australian Conference on the Mechanics of Structures and Materials (ACMSM), 1997.

- [33] European Committee for Standardization (CEN), EN 772-1. Methods of test for masonry units. Part 1: Determination of compressive strength (2010).
- [34] J. Segura, D. Aponte, L. Pelà, P. Roca, Influence of recycled limestone filler additions on the mechanical behaviour of commercial premixed hydraulic lime based mortars, *Construction and Building Materials* 238 (2020) 117722. doi:10.1016/j.conbuildmat.2019.117722.
- [35] C. Boulay, S. Staquet, M. Azenha, A. Deraemaeker, M. Crespini, J. Carette, J. Granja, B. Delsaute, C. Dumoulin, G. Karaiskos, Monitoring elastic properties of concrete since very early age by means of cyclic loadings , ultrasonic measurements , natural resonant frequency of composite beam (EMM-ARM) and with smart aggregates, in: VIII International Conference on Fracture Mechanics of Concrete and Concrete Structures, FraMCoS-8, no. March, 2013.
- [36] M. Ramesh, M. Azenha, P. B. Lourenço, Study of Early Age Stiffness Development in Lime–Cement Blended Mortars, in: RILEM Bookseries, Vol. 18, Springer Netherlands, 2019, pp. 397–404. doi:10.1007/978-3-319-99441-3_42.
- [37] European Committee for Standardization (CEN), EN 1015-11. Methods of test for mortar for masonry - Part 11: Determination of flexural and compressive strength of hardened mortar (2019).
- [38] A. Fódi, Effects influencing the compressive strength of a solid, fired clay brick, *Periodica Polytechnica Civil Engineering* 55 (2) (2011) 117. doi:10.3311/pp.ci.2011-2.04.
- [39] R. W. Zimmerman, The effect of microcracks on the elastic moduli of brittle materials, *Journal of Materials Science Letters* 4 (12) (1985) 1457–1460. doi:10.1007/BF00721363.
- [40] European Committee for Standardization (CEN), EN 12390-13. Testing hardened concrete - Part 13: Determination of secant modulus of elasticity in compression (2013).
- [41] European Committee for Standardization (CEN), EN 14580. Natural stone test methods - Determination of static elastic modulus (2005).
- [42] European Committee for Standardization (CEN), EN 1052-1. Methods of test for masonry - Part 1: Determination of compressive strength (1998).
- [43] R. B. Dean, W. J. Dixon, Simplified Statistics for Small Numbers of Observations, *Analytical Chemistry* 23 (4) (1951) 636–638. doi:10.1021/ac60052a025.

Automated data analysis for static structural health monitoring of masonry heritage

Nirvan Makoond · Luca Pelà · Climent Molins · Pere Roca · Daniel Alarcón

Accepted manuscript in *Structural Control and Health Monitoring*.

Submitted: 09 August 2019

Revised: 01 April 2020

Accepted: 12 May 2020

RESEARCH ARTICLE

Automated data analysis for static structural health monitoring of masonry heritage structures

Nirvan Makoond¹ | Luca Pelà¹ | Climent Molins¹ | Pere Roca¹ | Daniel Alarcón¹

¹Universitat Politècnica de Catalunya (UPC-BarcelonaTech)

Correspondence

Nirvan Makoond, Department of Civil and Environmental Engineering, Universitat Politècnica de Catalunya (UPC-BarcelonaTech), Jordi Girona 1-3, 08034, Barcelona, Spain
Email: nirvan.makoond@upc.edu

Funding information

Ajuntament de Sant Cugat through a project aimed at monitoring the Monastery of Sant Cugat, ref. num. C-10764.

Ministry of Education, Culture and Sports of the Spanish Government through a project aimed at studying the structural condition of Mallorca Cathedral, ref. num. 2/131400106ca - 5/030300592 EF.

AGAUR agency of the Generalitat de Catalunya and European Social Fund, through a predoctoral grant awarded to the corresponding author.

Ministry of Science, Innovation and Universities of the Spanish Government and European Regional Development Fund through the SEVERUS project, ref. num. RTI2018-099589-B-100.

Summary

Masonry heritage structures are often affected by slow irreversible deterioration mechanisms that can jeopardise structural stability in the foreseeable future. Static structural health monitoring (SHM), aimed at the continuous measurement of key slow-varying parameters, has the potential to identify such mechanisms at a very early stage. This can greatly facilitate the implementation of adequate preventive and remedial measures which can be critical to ensure that such structures are preserved for generations to come. However, since monitored parameters usually experience reversible seasonal variations of the same order of magnitude as changes caused by active mechanisms, identification of the latter is often a difficult task. This paper presents a fully integrated automated data analysis procedure for complete static SHM systems utilising dynamic linear regression models to filter out the effects caused by environmental variations. The method does not only produce estimated evolution rates but also classifies monitored responses in pre-defined evolution states. The procedure has successfully been used to identify vulnerable areas in two important medieval heritage structures in Spain, namely the cathedral of Mallorca and the church of the monastery of Sant Cugat.

Keywords

masonry, heritage, medieval structures, environmental effects, dynamic linear models, ARX

Link to formal publication: <https://doi.org/10.1002/stc.2581>

1 | INTRODUCTION

A large number of the established cultural heritage sites worldwide are made of masonry and the common responsibility to safeguard them for future generations is now widely recognized. Although many of these old buildings prove their structural soundness by surviving to the present time in relatively good condition, many have suffered from considerable damages caused either by natural or man induced events throughout their history. In order to ensure their survival, an accurate evaluation of their current structural condition is often of paramount importance. However, recurrent uncertainties regarding material properties and the complex interaction among structural elements often makes the evaluation of their structural safety challenging, despite recent advances in structural analysis, inspection, testing and monitoring techniques.

Structural health monitoring (SHM), which aims to gain knowledge of the integrity of in-service structures by monitoring damage sensitive features, can prove to be a very useful tool to better comprehend underlying causes of damage in structures. This is particularly true for heritage structures since the extraction of a comprehensive set of samples for laboratory testing is often not feasible due to the heritage value of the structure. Moreover, excessive extensive interventions are undesirable in such cases due to the need to respect authenticity and “a correct diagnosis is [thus] indispensable for a proper evaluation of

safety and for rational decisions on any treatment measures to be adopted"¹. Data from SHM can thus prove to be extremely valuable, particularly when ongoing deterioration mechanisms are still present.

In general, monitoring strategies to be applied can be categorised as static or dynamic. Dynamic monitoring is oriented to the characterisation and control of dynamic properties such as natural frequencies, mode shapes and damping ratios²⁻⁷. Static monitoring is aimed at the continuous measurement of slow-varying parameters over a long period⁸. Due to the slow progression of parameters of interest and because the data is largely influenced by seasonal cycles, monitoring periods of at least 2 years are usually required for meaningful conclusions to be derived from the data when it comes to static monitoring. In fact, due to the inability of commonly used analysis techniques to consider several factors and quantify uncertainties related to the analysis, longer monitoring periods are often required to establish a satisfactory level of confidence on resulting conclusions. Although recent research has focused more on data analysis for dynamic monitoring⁹⁻¹⁴, presumably due to the fact that this monitoring strategy enables the extraction of useful information about the structure as a whole in a short time period, it must be said that masonry heritage structures are most often affected by slow ongoing deterioration mechanisms that are not easily identifiable. As such, static monitoring appears to be particularly appealing.

Since unreinforced masonry is characterised by a very low tensile strength, cracking is probably the most common pathology visible in masonry structures of the built cultural heritage. Because structural integrity can be impaired if cracks remain active, crack monitoring has emerged as one of the most important basic parameters in long-term heritage SHM systems¹⁵. Since lateral displacements or rigid rotations of key elements can also severely compromise structural performance, the inclination of such elements and distances between them are the other structural parameters that are most often also of interest.

In the case of static SHM, it is essential to remove any anomalies present in the data that are not caused by a physical phenomena related to structural behaviour before any further analysis can be carried out. These often appear as "spikes" in sensor data¹⁶ and can originate from several sources such as capacitive or inductive noise in the analog signal path, communication errors¹⁷ or undesired external interactions with the sensor. The initial interpretation task then involves the identification of either a stationary or an evolutionary condition from the recorded data of each monitored response. Although this might appear simple in theory, in actual practice it proves to be difficult¹⁸, given that features monitored for their sensitivity to damage are also sensitive to changes caused by environmental and operational conditions. In fact, it can even be said that this is a major issue prohibiting the extension of SHM technologies to structures in operation in the real world¹⁹.

Nevertheless, there exists a number of data normalisation techniques that can be used to separate measurements relevant to structural damage from those associated with the environmental variation of the system²⁰. In fact, there are several examples of static monitoring systems applied to masonry cultural heritage structures as shown in Table 1.

TABLE 1 Some notable examples of static SHM systems installed in masonry cultural heritage structures.

Structure	Monitoring start	No. of years*	No. of instruments	Combined with dynamic tests?
Santa Maria del Fiore (<i>Opera del Duomo system</i>) ^{21;22}	1955	54	22	No
Santa Maria del Fiore (<i>ISMES system</i>) ^{21;22}	1987	20	150	No
Basilica of San Marco ²³	1991	3.5	23	No
Metropolitan Cathedral in Mexico City ²⁴	1994	10	38	Yes
Basilica S. Maria Gloriosa dei Frari ²³	2003	3.6	11	No
Cathedral of Modena ²⁵	2003	9	22	No
"Regina Montis Regalis" Basilica of Vicoforte ²⁶	2004	10	133	No
Monastery of Jerónimos ²⁷	2005	9	10	Yes
Roman Arena of Verona ²⁸	2011	> 4	24	Yes
Church of the Major Seminary of Comillas ²⁹	2012	5	67	No

* Minimum number of monitoring years (as reported in literature).

As shown, some recent static SHM systems have also been used in conjunction with ambient vibration testing (AVT) and/or dynamic monitoring. Examples of structures where such systems have been used include the monastery of Jerónimos in Lisbon²⁷, the Roman Arena²⁸ and the stone tomb of Cansignorio

della Scala³⁰ in Verona as well as the Anime Sante church in L'Aquila³¹.

Many of the above-mentioned investigations have relied on two basic procedures for the analysis and interpretation of the data collected from the static monitoring system. The first of which involves carrying out a simple linear regression from the recorded evolution of structural parameters such as crack widths and inclinations (response variables). If an underlying trend is found, the slope of the trend line allows the rate at which the phenomena in question is progressing to be estimated. The second procedure involves examining the correlation between temperature variations and the evolution of each response variable. In certain cases^{21;23}, analyses have attempted to remove the underlying periodicity present in crack width evolutions by examining the autocorrelation function of the signal and subtracting a sinusoidal function containing the signal's main period. Although it is true that a periodic sinusoid component fitted to the data is likely to contain the main seasonal behaviour, this theoretical formulation does not explicitly address the effect that measured environmental parameters (predictors) such as temperature or humidity have on the variation of monitored structural parameters. As such, careful implementation is required to avoid components not necessarily caused by seasonal variations from also being removed from the original signal during this processing step. Moreover, in this era of climate change, seasonal variations are becoming less predictable. Therefore it can no longer be assumed that their effects can always be accurately modelled by a regular periodic function.

In order to provide a systematic way of dealing with seasonal changes, a simple method based on the evaluation of reference quantities was proposed¹⁸. In fact, this method can be considered as one aiming to solve the well-studied problem of identifying directionality from a time series, whereby directionality is defined as asymmetry in time³². As such, although it has been successfully applied to analyse data in a few heritage structures^{18;33}, like many methods developed to detect directionality in other fields of study³⁴, it cannot explicitly consider the effect of measured predictors on the response parameters.

Some authors have intentionally searched for methods that do not require the measurement of environmental variables, arguing that with approaches having this requirement, all factors influencing the parameters of interest must also be monitored and understood in order to have reasonable confidence in any model prediction capability³⁵. As a consequence, a method based on finding a stationary linear combination among monitored responses, known as cointegration, has been successfully applied to eliminate the adverse influence of environmental changes from dynamic SHM data whilst maintaining sensitivity to structural damage³⁵. However, although such combinations can often be found between two identified natural frequencies, the local nature of response variables in static SHM systems means that finding such combinations can be difficult. Recently, an enhancement of the cointegration approach has been proposed making it more suitable to confronting cases when nonlinear relations between system responses exist⁹. However, since it is based on a Bayesian machine learning approach known as Gaussian process regression, it requires a training period that does not contain any data corresponding to damage⁹. In fact, this is also a requirement of many other sophisticated analysis methods that have been applied to damage detection in the presence of environmental variability from dynamic SHM data. These include negative selection¹⁰, other machine learning techniques^{11;19} as well as those based on linear and kernel principal component analysis (PCA)^{12;13;36} or on the Mahalanobis squared-distance¹⁴. This is a difficult requirement when it comes to static SHM systems for masonry heritage structures since the damage phenomena of interest very often relate to very slow and long processes which have begun long before any decision on monitoring could be taken. Moreover, for such cases, previous studies have shown that temperature is clearly one of the most influential environmental factors contributing to the seasonal variations of the local response parameters being monitored. As such, since temperature monitoring can easily be included in any modern monitoring system with very little additional cost, the current research will focus on a method which takes advantage of measured predictors.

One of the simplest approaches which explicitly takes measured environmental variables into consideration was used for filtering out the effect of temperature from crack widths monitored as part of the static monitoring system in the dome of Santa Maria del Fiore²². The method attempts to remove the periodicity of the response variable caused by the predictor by simply subtracting the corresponding effect from the identified general linear trend found between the two. A key assumption behind this method is that a linear relationship exists between the selected structural and environmental parameters even if this is not always an adequate representation. Moreover, it can be assumed that due to the thermal inertia of the material, among other factors, the crack width at any point in time will in fact depend not

only on the current temperature but also on previous ones. Another limitation of this method is that only a single predictor can be used to filter out the environmental variability of the response variable.

Nevertheless, meaningful conclusions on the state of the structure in question could still be derived from the data of all the previously mentioned static monitoring systems. Indeed, these examples show that static SHM can prove to be a powerful tool with respect to the diagnosis of heritage structures. It must be said however, that in every case, expertise and previous experience of the interpreter still play a vital role in the ability to draw conclusions from the processed data. Moreover, most of the procedures that have been applied to the analysis of data from static SHM systems of heritage structures provide no means of adequately quantifying the uncertainties or understanding the confidence levels associated to the estimated trends.

Utilising statistical black box models could prove to be an appealing alternative to remove the effects of environmental factors on measurements since they can exploit a large number of observations to reconstruct dependencies between recorded parameters. In particular, dynamic linear regression models able to represent response variables when they depend linearly on their own rate of change, on the rate of change of predictors as well as on the present value of the predictors appear to be ideal. Although there exists some examples³⁷⁻³⁹ which make use of such models to filter out environmental effects on the evolution of natural frequencies extracted from dynamic monitoring systems, application to static SHM systems has been very limited. In fact, one of the only examples available in literature involves application to the monitoring of a crack on frescos present in Battuti Hall of Conegliano cathedral⁴⁰. In this case, a Single Input-Single Output (SISO) model that comprehends an Auto-Regressive output and an eXogenous input (ARX) was used. Unlike the case of simple linear regression, the dynamic nature of these regression models mean that they are well suited to model complex environmental effects such as those due to thermal inertia.

Although the quality criteria presented in previous research^{37;40;41} can facilitate the choice of adequate ARX model orders, a systematic methodological procedure for the implementation of such models to the analysis of data from complete masonry heritage static SHM systems is still missing from literature. Moreover, to the best of the authors knowledge, Multiple Input-Single Output (MISO) ARX models incorporating both interior and exterior temperatures as predictors have not yet been applied to the case of static SHM systems. Utilising such models could theoretically allow the identified models to better represent the environmental variability imposed on the response variables since they would be able to incorporate effects caused by thermal gradients. In addition, it should also be noted that despite the theoretical advantages of this method over some of the more traditional analysis techniques, application to large data sets from whole networks of sensors in complex heritage structures is still lacking in literature. It is only through such applications that a well-defined systematic procedure can be developed to move from the analysis results to the diagnosis of the structure as a whole.

As such, the current research work aims to develop a holistic automated procedure which includes not only steps on how to implement ARX models to filter out environmental variability for entire static SHM systems installed in masonry heritage structures, but also steps to facilitate the interpretation of results from such analyses towards the overall diagnosis of the structure being monitored.

Before presenting the proposed analysis methodology, a series of simple and intuitive methods that have previously been applied to analyse data from static SHM of masonry heritage structures are presented. Every methodology described is then applied to data from two case studies, namely the Cathedral of Mallorca (monitored from 2003 to 2008) and the church of the monastery of Sant Cugat close to Barcelona (ongoing monitoring since 2017). A comparison of the outcomes that can be derived from the proposed procedure to those obtained from the more intuitive methods presented is also carried out. The results reveal that the proposed automated data analysis procedure can greatly facilitate the prognosis of masonry heritage structures.

2 | PREVIOUSLY APPLIED DATA ANALYSIS METHODOLOGIES

2.1 | Linear and nonlinear regression of time-series

The most intuitive analysis methodology applied to static SHM involves fitting each data set to a linear trend line using ordinary least squares regression, as shown in Figure 1. The slope of the identified trend

line is then used as an estimate of the evolution rate of the structural parameter in question. Although this method has been used successfully in the past to assess ongoing damage mechanisms in several heritage structures^{22;24;31;42}, it can easily be biased by asymmetry caused by the position of the monitoring period in relation to seasonal cycles. Moreover, since it involves fitting a straight-line to an evolution which is clearly not linear, it provides no means of assessing the quality of the fit.

A more appropriate approach to the problem involves evaluating the underlying trend of each response variable after subtracting a sinusoidal function containing the signal's main period. Several methods can be used for identifying such a sinusoidal function. In the context of this research, a method previously employed for analysing data from the static SHM system installed in Mallorca cathedral from 2003 to 2008 was employed. The method makes use of the Levenberg-Marquardt algorithm⁴³ to solve the nonlinear least squares problem of fitting the data from each sensor to the following nonlinear function comprising of a periodic component ($A \sin(Pt - \phi)$) and a linear one ($Bt + C$).

$$y = A \sin(Pt - \phi) + Bt + C \quad (1)$$

Where y is the monitored structural parameter of interest, t is time while A , P , ϕ , B and C are unknowns found using the Levenberg-Marquardt algorithm. Note that A , P and $\frac{\phi}{P}$ correspond respectively to the amplitude, period and phase shift of the periodic component of the function while B and C correspond respectively to the slope and y -intercept of the straight line component.

Hence, after the fitting procedure, the evolution of each response variable is modelled by a nonlinear periodic function, as shown in Figure 1. The resulting value of B from Equation (1) is then an estimate of the evolution rate of the monitored structural parameter after removing the identified sinusoidal component containing the signal's main period.

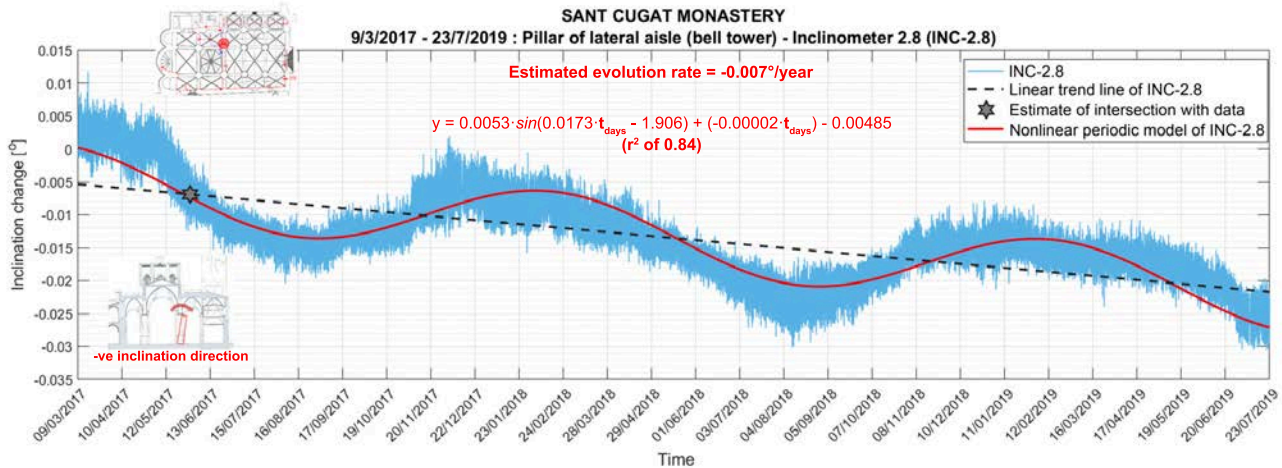


FIGURE 1 Linear and nonlinear periodic model fitted to data. An estimate of the first intersection point of the data with the fitted linear trend is shown in the figure.

However, it must be said that as with many nonlinear fitting algorithms, the Levenberg-Marquardt algorithm is susceptible to converging at a local minimum rather than a global one. Hence, particularly when dealing with large data sets acquired over long time periods, adequate convergence was found to rely heavily on setting appropriate initial estimates of the unknown parameters. In this case, a good initial estimate of the amplitude can be obtained directly from the data while the main period can be expected to relate to the duration of a tropical year (approximately 365.24 days⁴⁴). Initial estimates of the remaining parameters can be obtained using results from the linear regression procedure. A summary of adequate initial estimates for all the unknown parameters in Equation (1) is given in Table 2.

As shown, the initial value of the coefficient related to phase shift relies on an estimate of the position of the first intersection point with the straight line fit. This was obtained by subtracting the identified linear trend from the raw data and identifying the first two points between which there was a change of sign. Linear interpolation between these two points provided an estimate of the time to the first intersection point. In order to avoid intersection points caused by higher frequency fluctuations not representative of the seasonal period, this procedure was carried out after removing higher frequency

components from the data using a multi-level wavelet decomposition with Symlet Wavelets^{45;46}. An example of the estimated intersection point is shown in Figure 1.

TABLE 2 Summary of initial estimates specified for each response variable for the nonlinear fitting procedure.

Parameter in Eqn. (1)	Initial estimate
A	$A_0 = \frac{\max(y_i) - \min(y_i)}{2}$, where y_i refers to the vector containing all the values of the response variable recorded over the whole monitoring period.
P	$P_0 = \frac{2\pi}{365.242}$, if the 24 h day is used as the base unit of the duration vector.
ϕ	$\phi_0 = P_0 \times$ Estimated position of the first intersection point of data with straight line fit (see Figure 1)
B	$B_0 =$ Slope of trendline identified from linear regression
C	$C_0 =$ y-intercept of trendline identified from linear regression

A significant improvement of this method compared to linear regression lies in the fact that it attempts to model the actual nonlinear behaviour of the response variable. Selected metrics can thus be used to assess the quality of the fit and to reject trend estimates when the nonlinear periodic model cannot represent the evolution of the structural parameter. Two simple metrics were found to be particularly useful for this purpose. The first one being the well-known coefficient of determination (r^2)⁴⁷, which ranges from 0 to 1, with a value closer to 1 indicating a better fit. Based on results from the case studies forming part of this research, it is recommended to dismiss evolution rates when the method yields a coefficient of determination lower than 0.6. The other useful metric was found to be the percentage by which the final identified period differs from 365.24 days. The rationale being that since seasonal cycles rely on the movement of the sun, if the periodic component is to represent them, it should have a period close to the duration of a tropical year. As such, if the final identified period is found to differ by more than 25% from 365.24, the estimated evolution trend should be rejected.

Despite this improvement, the method still fails to explicitly assess the effect that measured environmental parameters have on the measured structural parameters. As such, the estimates can be significantly biased by underlying trends or irregular changes in environmental parameters. Once again, this makes it difficult to decide which thresholds reflect an actual evolutionary or stationary condition.

2.2 | Preliminary evaluation of correlation with monitored environmental parameters

It is clear that variations of environmental parameters, notably changes in temperature, are the root cause of reversible seasonal changes experienced by most masonry structures. Since some of these parameters can easily be monitored, taking advantage of such measurements to filter-out their effect from the evolution of structural parameters can definitely provide an improvement on the method presented in Section 2.1.

Before attempting any procedure using actual measurements of environmental parameters, it is important to determine which ones have the greatest influence on the evolution of each response. This can be achieved by computing the Pearson correlation coefficient⁴⁷ ($R_{X,Y}$) between measured environmental and structural parameters. This coefficient can be understood as a normalised version of covariance between two random variables and hence represents a dimensionless measure of their linear dependence. It can vary between -1 and +1 with absolute values closer to unity indicating a better correlation. The sign of the coefficient indicates the type of correlation. A negative sign means that an increase of one parameter leads to a decrease of the other while a positive one signals the opposite. Hence, following this preliminary evaluation, monitored environmental parameters showing the strongest influence on structural ones can be chosen for the subsequent analyses presented in the following sections.

2.3 | Filtering environmental effects using linear regression with selected predictors

One method which explicitly considers measured environmental parameters (predictors) relies on the assumption that their effect on responses can be represented by a perfectly linear model. The two unknown parameters of such a model can be identified through simple linear regression between recorded values

of each response and the chosen predictor as shown in Figure 2. Due to the simplistic nature of the assumed relationship, it is clear that effects caused by structural mechanisms of interest can influence the identified linear models. Hence, one can argue that using data only from a single seasonal cycle for the regressions will provide the most suitable models. On the other hand, since the relationship between some predictors and responses change over several seasonal cycles, it can also be argued that data from the entire monitoring period can better represent their dependency. Hence, models are identified for both cases (listed below) and the results are then compared. In fact, the differences between them are used in the proposed classification procedure to evaluate the evolutionary state of monitored responses.

1. **Linear filter (i):** Linear regression between selected predictor and response variable using data from the entire monitoring period.
2. **Linear filter (ii):** Linear regression between selected predictor and response variable using data only from a full calendar year (this period will hereafter be referred to as the estimation phase).

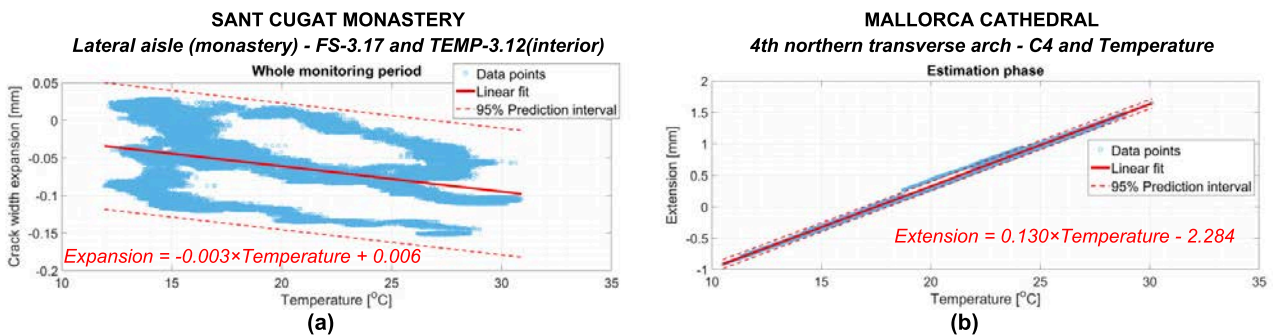


FIGURE 2 (a) Example of linear regression between crack width expansion and temperature over whole monitoring period. (b) Example of linear regression between the monitored span of an arch and temperature over an estimation phase of one year.

Following the regression procedure, measured values of each selected predictor are substituted into the corresponding linear model to simulate changes of the structural parameter caused by the environmental one. Since variations experienced by structural parameters can be considered as the result of a series of phenomena, the actual measurements of the latter are then filtered by simply subtracting the simulated effect, as shown in Figure 3. Estimates of the underlying annual evolution rates ($ER_{lin(i)}$ and $ER_{lin(ii)}$) are then obtained by carrying out simple regressions of these filtered residuals.

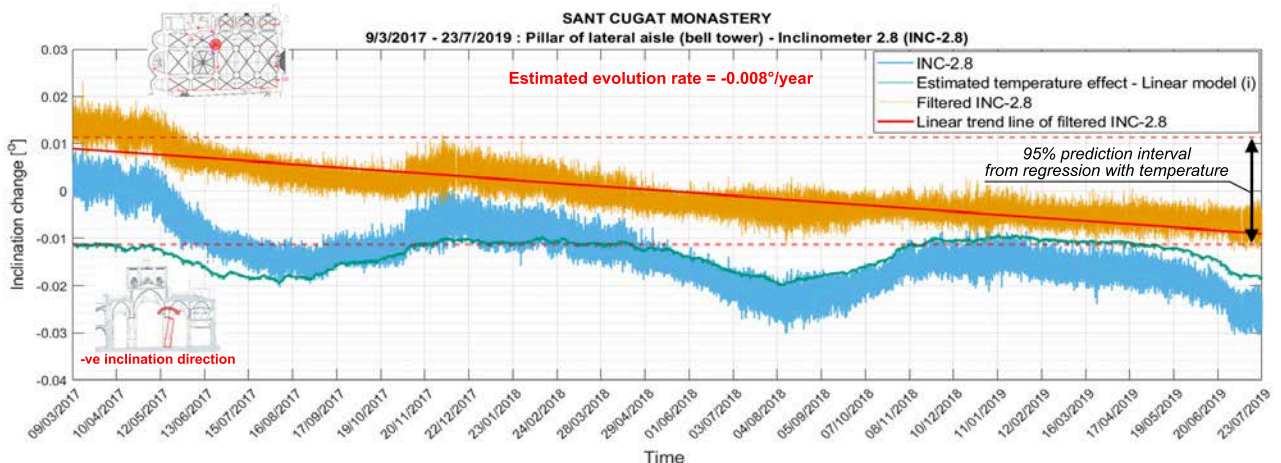


FIGURE 3 Filtering of temperature effect based on identified general linear trend. (For interpretation of the references to colour in this figure, the reader is referred to the web version of this article)

A significant advantage of this method when compared to the previous two is that it explicitly uses measured predictors and hence allows an assessment of how well each linear model can predict the relationship between environmental and structural parameters using common error metrics. In fact, if the residuals are assumed to be normally distributed when no significant structural mechanism is present, a prediction interval representing a specific level of confidence can be obtained based on the dispersion of residuals. This can prove extremely useful for the interpretation of results since it is expressed in the

same units as the monitored structural parameter.

3 | PROPOSED ANALYSIS METHODOLOGY

Although it is clear that simple linear models can provide a good representation of the relationship between environmental and structural parameters (Figure 2(b)), in many cases, it fails to represent the relationship adequately (Figure 2(a)). One of the main reasons for this is the fact that the simplistic nature of the model cannot take into consideration certain effects influencing the system it aims to describe, such as those due to thermal inertia.

Hence the proposed automated data analysis methodology developed as part of this research consists of two parts. The first part aims to improve upon the method presented in Section 2.3 by exploiting dynamic regression models to describe the relationship between selected predictors and structural parameters more reliably. The process can be applied to a complete SHM system and includes a procedure for estimating model orders that are best suited for system identification, as well as provisions to deal with irregularly sampled and missing data.

The second part of the methodology aims to facilitate the interpretation of the predicted evolution rates after the filtering process. This is achieved by classifying the state of each monitored structural parameter based on the evaluated underlying trend and the level of uncertainty associated to the models describing its relationship with selected environmental parameters. Since the linear models described in Section 2.3 are clearly adequate for certain cases, the classification procedure also takes advantage of predictions from this method. Hence, a preliminary step to the proposed data analysis procedure involves carrying out all the analysis methods presented in Section 2.

3.1 | Filtering environmental effects using dynamic statistical models (ARX models)

The procedure of utilising ARX models for evaluating any underlying trends present in response variables involves selecting suitable model orders by adopting some quality criteria. The coefficients of the ARX models can then be estimated using QR factorization⁴⁸ based on measurements collected during an estimation phase. In order for the model to capture most of the reversible components caused by environmental effects during a complete seasonal cycle, the estimation phase should ideally span at least 1 full year. Once this model has been estimated and validated, it can be used together with data collected after the estimation phase to simulate responses based on measured predictors. The residuals obtained by subtracting the simulated behaviour from its recorded counterpart then allows changes related to irreversible structural damage to be distinguished from reversible ones caused by varying environmental conditions.

As its name suggests, an **Auto-Regressive with eXogenous input (ARX)** model utilises measured values of past outputs together with those of past and current or delayed predictors to describe the dynamics of a system. The single-input single-output (SISO) form of the ARX model has the following structure:

$$\hat{y}(t) + a_1 y(t-1) + \dots + a_{na} y(t-na) = b_1 x^{env}(t-nk) + \dots + b_{nb} x^{env}(t-nb-nk+1) + e(t) \quad (2)$$

Where $\hat{y}(t)$ is the predicted response at time t , $e(t)$ is the white-noise disturbance value, na and nb are the auto-regressive and exogenous orders of the ARX model, and nk is the delay. Specifically, na and nb refer respectively to the number of past samples of the response and predictor variables used for identification and nk is the number of samples of the predictor variable that occur before the predictor starts influencing the response. Hence $y(t-1)\dots y(t-na)$ refer to the previous responses on which the current one depends, while $x^{env}(t-nk)\dots x^{env}(t-nb-nk+1)$ refer to the previous and delayed predictors on which the current response depends. The multiple-input single-output (MISO) form of an ARX model has the same structure as that described by Equation (2) but with additional parameters to incorporate any number of additional predictors. Therefore, for each new predictor incorporated in the model, a new exogenous order and delay has to be specified.

The first step of the filtering procedure involves selecting which measured environmental variables will be used as predictors for the representation of the dynamic system as an ARX model. Two possible

candidates that are commonly monitored as part of SHM systems are temperature and relative humidity. It can be expected that temperature will have the greatest influence on the evolution of the response variable. Since relative humidity measurements were available in addition to temperature ones for one of the case studies forming part of this research, the results from the preliminary evaluation of correlation described in Section 2.2 were compared. Indeed, the results reveal that for every monitored structural parameter, the linear correlation is stronger with temperature than with relative humidity. In fact, for almost every response investigated as part of the two case studies, the dependency on temperature is clearly visible when examining daily fluctuations. Hence, SISO ARX models with temperature as the sole predictor constitute the most basic ARX model that should be identified for every monitored response. If temperature is recorded at more than one location (for instance in the interior and at the exterior of the structure), the data from the temperature sensor showing the greatest Pearson correlation coefficient with the response should be used as the predictor in the SISO ARX model.

Recent years have been marked by a significant increase in the ability of modern computers to exploit large amounts of data for system identification. As such, in addition to the SISO ARX models described in the previous paragraph, the proposed data analysis methodology also incorporates the use of MISO ARX models to filter out seasonal variations when multiple suitable environmental parameters are monitored. Naturally, the decision of which environmental parameters to include in the models has to be addressed. It is undeniable that the presence of moisture in the masonry fabric can significantly alter its mechanical behaviour⁴⁹⁻⁵¹ and hence influence the response of structures. However, the design of an adequate acquisition protocol for the monitoring of parameters representative of the water absorption phenomena can be a challenging task, particularly for large complex masonry structures⁵². Some authors have attempted to include measured relative humidity on-site as a predictor in a MISO ARX model in an attempt to filter out moisture related effects from natural frequencies being monitored through a dynamic monitoring system³⁸. Although it was clear that water absorption had a notable effect in this case due to observed changes of the natural frequencies at the beginning of rainy seasons, the inclusion of this predictor provided no improvement in the model's ability to describe the environmental variability. This can be attributed to the fact that measurements made by humidity sensors on the exterior of walls actually reflect the level of moisture in the air and not in the masonry. For this reason, the proposed methodology does not include MISO ARX models with relative humidity as a predictor, even if it is good practice to monitor it in most SHM systems. However, it was envisaged that temperature gradients between interior and exterior temperature could significantly influence the dynamics of the system. Since both are often recorded as part of modern SHM systems, it is recommended to utilise MISO ARX models that incorporate both as predictors to characterise the environmental influence on the evolution of monitored structural responses. Nevertheless, the proposed methodology can be extended to include any monitored environmental parameters causing reversible variations of structural responses such as the moisture content in the masonry or the level of water in the foundation soil. The latter can be monitored with piezometers and the former could possibly be monitored by humidity sensors placed at different locations both along the thickness of masonry walls and at different levels of the structure⁵³. However, it should be noted that in some cases, particularly for masonry structures with an interior leaf made of lime concrete, moisture diffusion can produce a redistribution of stresses over several centuries⁵⁴ which can even be the root cause of a slow irreversible deterioration mechanism. Similarly, changes in water table levels can sometimes cause significant differential settlements over long time periods resulting in the activation of a progressive damage mechanism^{55;56}. Under such circumstances, it would be undesirable to include these monitored parameters as predictors in the MISO ARX model at the filtering stage since the trends they induce can be essential for an accurate diagnosis of the structure.

Once predictors to be used in the ARX models have been selected, the next step of the procedure involves extracting data from the estimation phase. This represents the data set for which the errors between the model output and the measured response will be minimised. In most cases it is perfectly adequate to take data collected during the first complete year as the estimation data. However, if there are significant periods for which data is missing during the first year of monitoring, it is recommended to consider any period lasting one year which has the least amount of missing data as the estimation phase.

It is key to adequately condition the estimation phase data before carrying out any system identification. Besides converting raw signals from sensors to meaningful physical units and removing clear anomalies, another procedure which can be useful to implement involves resampling the data. This is

particularly useful to reduce the computational cost of system identification in cases for which the data is sampled at a high rate. Since the damage phenomena of interest typically progresses slowly over many years, if the SHM system samples data at intervals shorter than an hour, noticeable savings in terms of computational cost can be achieved by increasing the sampling interval to an hour without any significant loss of accuracy in terms of the predicted evolution rates. Naturally, after using the ARX models to simulate the environmental effect, the data will have to be upsampled back to the original sampling rate so that the residuals can be computed from the measured values of the response variables in the same way they were for the method described in Section 2.3. Upsampling is a lossless procedure and hence straightforward application of spline interpolation⁵⁷ can safely be used for this purpose. However, for the downsampling procedure, great care has to be taken to prevent aliasing and avoid distorting the original signal excessively. To prevent aliasing, a lowpass anti-aliasing filter should be implemented before the resampling procedure. The question then arises as to which interpolation method will prove to be both robust and accurate in representing the original signal. Three different methods were tested as part of this research: Linear interpolation using 2 neighbouring points as well as piecewise cubic⁵⁸ and spline interpolation⁵⁷, both of which use 4 neighbouring points. Linear interpolation resulted in the smallest maximum and mean errors for data from all the 16 sensors tested. In every case, the mean error was several orders of magnitude smaller than the minimum resolution of the sensor and the maximum error smaller than the greatest daily variation experienced by the sensor. As such, it was concluded that using linear interpolation for downsampling is most adequate. Although most modern data loggers will accurately provide data at a uniformly sampled rate, analysing data collected from more archaic systems could create a need for system identification from irregularly sampled data. Since such data is not easily handled by discrete-time model identification techniques⁵⁹, it is recommended to resample the data to a uniform rate using the same procedure described in this paragraph before carrying out system identification in such cases.

A particular characteristic of ARX models is that the equation error is modelled as being a zero-mean white process with unknown variance⁶⁰. In fact, the noise model is coupled to the identified parameters of the response variable and hence the only unknown parameter related to noise that needs to be solved for during the identification process is the variance of the noise term. Although this means that the noise and the dynamics of the system cannot be modelled independently, the simplicity of the scheme creates no stability problems in optimal predictors and allows unbiased estimates of the parameters by means of least squares. However, it is crucial to remove the mean from both the response and predictor data before carrying out system identification to avoid an offset term in Equation (2). In fact, it is good practice to normalise the input and output data for this system identification task⁴¹. Therefore, for each estimation data set, the result after removing the mean should also be divided by the standard deviation. It is important to store both the means and the standard deviations, since it is instrumental to transform all the identified ARX models back to the engineering units of the original data.

Before carrying out system identification using the normalised data sets, a choice needs to be made on the delay to be specified. If the environmental and structural parameters are acquired simultaneously, it is perfectly adequate to simply assume a delay of 0 in most cases. This is particularly true when the environmental parameter is temperature, as is the case for the recommended ARX models for the static SHM case. However, in some cases, the model could benefit from a short dead time occurring before the first predictor it uses to simulate the current response. In order to evaluate the most suitable delays for each response, the proposed procedure includes a quick delay estimation computation based on the comparison of ARX models with orders of 8, evaluated for different delays spanning from 0 to 48 hours. As can be expected, out of the 44 ARX models estimated for the case studies (28 SISO and 16 MISO models), the delay estimation computation suggested that a delay of 0 was most appropriate for most of the cases. Moreover, only delays of up to 12 hours were suggested for the 12 cases for which it was deemed that a dead time would be suitable.

The last step remaining before estimating the parameters of the ARX models involves specifying appropriate auto-regressive and exogenous model orders. In essence, these control the duration in the past that is considered by each model to predict responses since it defines the number of past samples used for prediction. Choosing the right combination of model orders is no straightforward task but this can greatly influence the quality of the final models. For instance, it is likely that responses being significantly affected by a structural mechanism would benefit more from a higher auto-regressive order while those influenced

by complex environmental phenomena would benefit more from higher exogenous model orders. Hence, a systematic procedure was developed as part of this research to select suitable combinations of model orders for each response from a pre-defined range. The procedure involves dividing the estimation data of each response equally to form an estimation and a validation subset. Models for each of the structures defined by the pre-defined range are then estimated using the estimation subset. The loss functions are then computed for these models when applied to the validation subset. The loss function (V) refers to the error that is minimised by the least-squares method during system identification. As shown by Equation (3), it can be defined as the normalized sum of squared prediction errors.

$$V = \frac{1}{N} \sum_{k=1}^N e_k^2 \quad (3)$$

Where N is the number of measurements, k is the time step and e_k are prediction errors defined as the measured response minus the predicted one.

Following the computation of loss functions, the structure resulting in the lowest error when applied to the validation data set is specified for each response. The parameters of these models with known structures can then be estimated using all the data from the estimation phase. A significant benefit of the order selection procedure is that it relies on loss functions computed on validation subsets and hence the final ARX models already inherently include a process that helps ensure that they are useful not only for the estimation data, but also for new data from subsequent phases of the monitoring period. However, the task of defining the range of model orders that need to be tested still needs to be addressed. Since it was expected that one of the main benefits stemming from the dynamic nature of ARX models would be their ability to consider thermal inertia effects, an investigation was carried out on the required model orders that would theoretically be able to encompass most of the effects of this physical phenomena. In general, the thermal inertia of a building envelope causes two noticeable differences between external and internal temperature fluctuations: a decrement of the amplitude and a time lag between the two⁶¹. Previous research reveals that the duration of these thermal lags rely heavily on the thermophysical properties of wall elements and that lags of approximately 12 hours can be observed from experiments on brick masonry walls with a thickness of less than 30 cm⁶². It can be expected that thermal inertia effects will be substantially different in masonry heritage structures as they can be characterised by massive external walls that are often thicker than 1 m. Based on measurements from one of the case studies, most of the time lags between external and internal temperature appear to last less than a day. However, in some extreme cases, time lags lasting several days could be identified. Based on these observations, the ranges listed in Table 3 were tested as part of this research. If the acquisition was made at a higher rate, the estimation data was resampled to a sampling period of 1 hour.

TABLE 3 Ranges of ARX model orders tested using estimation data with a sampling period of 1 hour.

Corresponding duration [days]		SISO ARX - model orders tested		MISO ARX - model orders tested	
Lower limit	Upper limit	Lower limit	Upper limit	Lower limit	Upper limit
1	4	24	96	24	96
4	6	96	144	96	144
8	10	192	240	192	240
4	10	96	240	96	240
4	15	96	360	-	-
5	20	120	480	-	-
5	25	120	600	-	-

The results from all the ranges tested reveal that it is important to specify a lower limit in the range to prevent the model structure determined by the order selection procedure from being overly dependent on only past responses or predictors. A lower limit corresponding to at least four days is recommended. It was also found that specifying a larger range leads to more accurate final models even if the upper limit of the range is unchanged. For instance, specifying a pre-defined range of 4 to 10 days yielded more accurate models than specifying one of 8 to 10 days. Of course, the final range selected is largely

dependent on the computational expense that can be spared but the maximum ranges listed in Table 3 are recommended for SISO models and MISO ones with 2 predictors.

Once the final models have been identified for each monitored response, they can be used to simulate the expected responses from new measurements of predictors. It is very important to highlight the distinction made between simulation and prediction in the realm of system identification since one of the greatest advantages of using ARX models for the analysis of static SHM systems stems from this difference. It is clear from Equation (2) that both past responses and predictors are used to describe the dynamics of the system. The data from both are therefore used during the estimation phase. However, there are two ways of generating a model response: it can be predicted or simulated. Prediction involves computing the model response at a particular point in time using values of measured predictors and past responses. Simulation on the other hand, involves computing the model response using only measured predictors. Effectively, this means that although the model is able to account for changes that are likely due to structural mechanisms through the parameters associated to past responses, it is also able to exclude those when computing the expected response by only using terms of the model that correspond to predictors. This is ideal for the case of static SHM since it is often impossible to isolate a period of time during which the relationship between environmental predictors and structural responses can be considered as being completely isolated and free from effects caused by active structural mechanisms. Any evolution trend is then estimated by carrying out a regression of the residuals obtained by subtracting the simulated environmental effect of the responses from their measured values.

Two different goodness-of-fit measures were used to compare the effectiveness of the linear, SISO ARX and MISO ARX models in representing the relationship between predictors and responses: the previously described coefficient of determination (r^2) and 1.96 times the standard error of the estimate⁶³ computed from the residuals ($1.96\sigma_e$). The latter can be interpreted as a typical distance of measured data points from model predictions. It was chosen because it is used to define the 95% prediction interval from a normally distributed sample and because it is in the same units as the responses. In all cases, these were computed from the measured and simulated values of responses over the time period used to estimate the model. As will be seen in Section 4, for almost all of the 28 responses monitored as part of the two case studies, the ARX models were able to represent the environmental variation much more accurately than the linear models.

3.2 | Interpretation of results

As a result of the analyses presented in Sections 2.3 and 3.1, an estimated filtered evolution rate is obtained for each response variable. In fact, since these methods aim to directly model the relationship between environmental and structural parameters, the standard error of the estimate computed from residuals for each model over the estimation phase represents a certain level of confidence in the model's ability to predict variations of the response. Since such metrics are in the same units as the response, they can be compared directly to evaluate the level of certainty associated to the estimated filtered evolution rates. In order to provide a systematic way of doing so, the current research proposes a multi-step classification approach based on comparing results obtained from the methods presented in Sections 2.3 and 3.1 through a series of 5 logical tests (see Figure 5). Two key values obtained from the most extensive ARX-based procedure used are employed in every test: the filtered annual evolution rate (ER_{ARX}) and 1.96 multiplied by the standard error of the estimate computed over the estimation phase ($1.96\sigma_{e-ARX}$). The approach can be programmed so that in addition to the predicted rates, a label is automatically assigned to each monitored response. Based on the outcomes of the tests, each response is classified in one of the following four categories:

1. **Stationary:** Monitored parameters showing a clear stationary trend outside reversible variations caused by environmental parameters.
2. **Evolutionary:** Monitored parameters showing a clear evolutionary trend outside reversible variations caused by environmental parameters.
3. **Apparently stationary:** Monitored parameters showing a stationary trend but for which there still is a rather large uncertainty associated to the estimation of the trend.
4. **Apparently evolutionary:** Monitored parameters showing an evolutionary trend but for which there

still is a rather large uncertainty associated to the estimation of the trend.

5. Inconclusive: Monitored parameters for which no clear conclusion can be made on its evolutionary state from the available monitoring data alone.

The first test of the classification procedure aims to identify responses which clearly show a stationary trend. Since classifying a response as stationary when it is experiencing an active trend can have dangerous consequences, relatively strict conditions have been established for this test. Specifically, $1.96\sigma_{e-ARX}$ must be lower than 5 times the minimum effective resolution of the sensors and $2ER_{ARX}$ (the estimated evolution over two years) must be lower than 0.005 units. In addition to these two requirements, this test includes another requirement based on the normality of the residuals. This stems from the understanding of a truly stationary time-series as one that can be represented by a model with Gaussian errors³⁴. Hence, it can be said that if the residuals after the filtering process are normally distributed, the model has been able to capture most of the environmental variability, and the response does not contain any underlying trend caused by active structural mechanisms. Naturally, in order for this requirement to be incorporated in an automated procedure, one has to quantify the degree of normality of the residuals. There exist many different tests to verify if observations are from a normal population and most of them rely on computing a test statistic and a critical value. The latter is usually dependent on the sample size and a chosen significance level. The hypothesis that the sample belongs to a normal population is then rejected or accepted based on the relationship between the test statistic and the critical value. In the case of data from static SHM, the sample size is usually very large since it contains data sampled every hour over several years. Moreover, the dynamics of the system are often very complex making it difficult for any model to eliminate all reversible effects perfectly. As such, the sample set containing residuals will almost always fail to satisfy most established normality tests irrespective of the chosen significance level. Nevertheless, it is clear that in some cases, the residuals can be well represented by a normal distribution (see Figure 4).

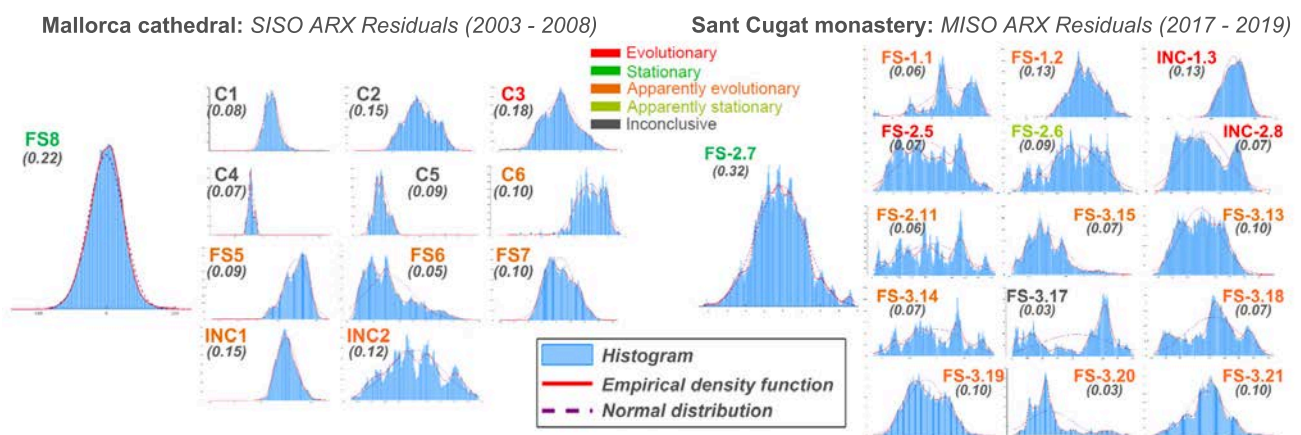


FIGURE 4 Empirical distribution of ARX Residuals for responses forming part of case studies. Values of the adapted Lilliefors ratio for the case of static SHM is also shown. The colour of the sensor name relates to the final estimated condition according to the proposed classification procedure. (For interpretation of the references to colour in this figure, the reader is referred to the web version of this article)

Hence, a modified normality test based on the Lilliefors Test⁶⁴ was developed for this purpose. As is the case for the original test, the test-statistic ($kstat$) is computed by finding the maximum deviation of the empirical cumulative distribution function (CDF) from the CDF of a normal distribution with the same mean and standard deviation as the sample data set. The original test rejects the hypothesis of normality if the test statistic is greater than the critical value. Hence the sample is said to be from a normal distribution if the ratio of the critical value over the test statistic is greater than or equal to 1. In contrast to the original test, the modified one proposes a fixed critical value of 0.005 and requires the computation of an adapted Lilliefors ratio equivalent to $\frac{0.005}{kstat}$. These ratios computed for the residuals obtained from the most extensive ARX-based procedures applied to the responses forming part of the case studies, are shown in Figure 4. Based on these observed ratios, it is suggested that for the case of static SHM, residuals that have an adapted Lilliefors ratio greater than 0.2 can be considered as being

normally distributed. Hence, responses that satisfy this requirement together with the first two presented at the start of this paragraph can be considered as being stationary.

The second test aims to identify responses that clearly show an evolutionary trend. Hence, the estimated evolution rate should be significant in comparison to the error associated to modelling the environmental variation and this error should be sufficiently small. It must be noted that in certain cases, if a structural parameter is particularly responsive to changes in environmental conditions, it can experience large reversible variations. In such cases, even if the ARX model is able to accurately simulate the seasonal variations, the value of $1.96\sigma_{e-ARX}$ might still be significant in comparison to the minimum effective resolution of the sensor. In order to avoid penalising the accuracy of the model in such cases, a small value of $1.96\sigma_{e-ARX}$ was defined as the maximum between 5 times the minimum effective resolution of the sensor and 20% of the average maximum daily variation experienced by all sensors in the SHM system measuring the same type of response. If the residuals satisfy this requirement and $2ER_{ARX}$ is greater than $1.96\sigma_{e-ARX}$, the response is classified as evolutionary.

The subsequent tests are not as rigorous as the first two but intend to utilise most of the useful information obtained from the various proposed analysis procedures to provide an informed estimate of the condition of each structural response being monitored. The third test classifies a response as apparently stationary if $1.96\sigma_{e-ARX}$ is less than 0.05 and $2ER_{ARX}$ is less than $0.4 \times 1.96\sigma_{e-ARX}$. Test 4 relies on three requirements to classify a response as apparently evolutionary: $1.96\sigma_{e-ARX}$ must be less than 0.2, $2ER_{ARX}$ must be greater than $0.4 \times 1.96\sigma_{e-ARX}$ and the Pearson correlation coefficient computed between the response and relevant temperature records must be greater than 0.6. The rationale being that a response is most likely evolutionary if its relationship with temperature can be well represented by a linear approximation and the predicted trend after filtering out simulated environmental effects is significant in relation to the error associated to this simulation. The final test relies on a comparison between the estimated evolution rates from all methods attempting to directly filter out reversible effects caused by measured predictors ($ER_{lin(i)}$, $ER_{lin(ii)}$, $ER_{SISO-ARX}$ and if applicable $ER_{MISO-ARX}$). The test classifies the response as apparently evolutionary if the estimated rates from all these methods agree to within 25% (normalised to the lowest evolution rate for each response) and if $2ER_{ARX}$ is greater than $0.45 \times 1.96\sigma_{e-ARX}$. A greater requirement is imposed on the evolution rate in comparison to Test 4 because there is less physical meaning associated to this test. Although a response can satisfy both Test 4 and Test 5, Test 3 has been designed to be mutually exclusive from these two.

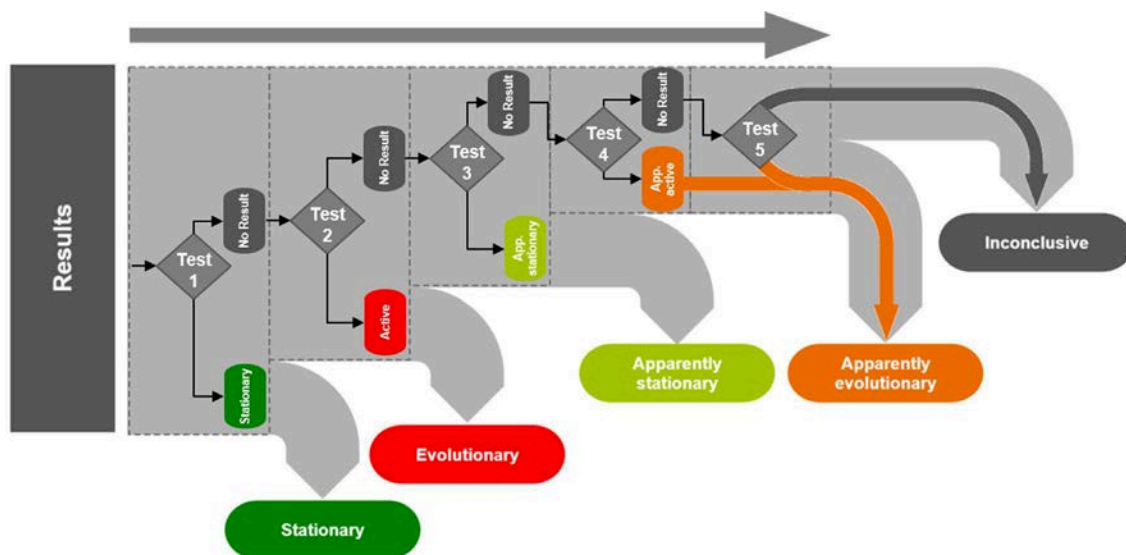


FIGURE 5 Procedure for interpretation of results after filtering effect of environmental variability.

The overall classification procedure is summarised in Figure 5. As can be seen, if Tests 1, 2 or 3 are satisfied, the results related to that particular response does not undergo any further tests since it would already have been assigned a label. If a response fails all tests, it is classified as inconclusive. One of the main advantages of the classification procedure is that it can greatly facilitate how the estimated evolution rates should be prioritised during the prognosis. Basically, the possible underlying mechanisms related to responses classified as "Evolutionary" should be investigated first followed by those labelled

as "Apparently evolutionary" that show the greatest ratio between ER_{ARX} and $1.96\sigma_{e-ARX}$. Responses labelled as "Inconclusive" often require an extended period of monitoring in order to shed more light on their actual state. Of course, longer monitoring periods will also help develop a greater level of certainty on any diagnosis made from the data analysis, particularly if the cause of some estimated trends cannot be explained.

4 | CASE STUDIES

The two case studies forming part of this research consist of medieval churches and cathedrals. Such structures were usually built over very long time periods and still represent some of the most daring and complex examples of masonry design. The first case study, the cathedral of Santa Maria in Palma de Mallorca, was built progressively from the apse to the façade over a period of 300 years, from 1306 to 1600⁶⁵. The cathedral boasts grand proportions and presents many structurally audacious aspects. The most daring of which probably is the slenderness of the columns², reaching a ratio of 14.2 in some areas while the value encountered in other Gothic cathedrals usually ranges from 7 to 9⁶⁶. For all these reasons, it represents one of the most emblematic monuments of the Catalan Gothic Style. The second case study, the monastery of Sant Cugat, is located in Sant Cugat del Vallès, Catalonia. The monastery is composed of a cloister and a church, with the latter being the main focus of the study. The masonry structure at the site today consists of various parts built over different time-periods, mostly from the mid-12th century to the 15th century. The interaction between different parts results in a complex overall structural behaviour, adding to the difficulty of the diagnosis.

4.1 | Mallorca cathedral

4.1.1 | SHM system and results

A five-year monitoring system was installed in the cathedral in 2003 to better understand the complex behaviour of the structure and to identify any active mechanisms possibly contributing to its deterioration. In addition to temperature and humidity sensors, the system consisted of 6 convergence extensometers monitoring changes in the distance between two points, four crackmeters monitoring changes in crack widths and two inclinometers monitoring changes of inclination of key elements. The convergence extensometers and crackmeters had a resolution of 0.01 mm while the inclinometers had an effective resolution of 0.001°. Table 4 describes the location of every sensor monitoring a structural parameter and the total duration of useful data collected by each one over the five-year monitoring period. The predicted evolution rates from methods based on directly fitting time series to selected models are also shown in Table 4. The location of the sensors together with the final estimated evolutionary condition are also shown in Figure 7.

TABLE 4 Summary of structural sensors used in the SHM system installed in Mallorca cathedral and estimated evolution rates from methods based on directly fitting time series to selected models.

Sensor	Location	Years of data	Type	Units	Evolution rate [unit/year]	
					Linear regression	Nonlinear regression
C1	4th central transverse arch	1.2	Extensometer	mm	0.17	-
C2	4th central transverse arch	4.9	Extensometer	mm	0.05	-
C3	4th southern transverse arch	4.8	Extensometer	mm	0.10	0.09
C4	4th northern transverse arch	3.7	Extensometer	mm	0.12	0.06
C5	8th southern longitudinal arch	2.8	Extensometer	mm	0.02	0.05
C6	8th northern longitudinal arch	4.2	Extensometer	mm	0.07	0.06
FS5	Southern wall - 8th bay	4.2	Crackmeter	mm	0.01	0.01
FS6	Southern wall - 8th bay	4.2	Crackmeter	mm	-0.05	-0.04
FS7	Central nave - 6th bay	4.2	Crackmeter	mm	0.06	0.08
FS8	Central nave - 7th bay	4.2	Crackmeter	mm	0.00	0.00
INC1	4th pillar (central nave - south)	2.3	Inclinometer	°	0.000	0.013
INC2	Interior main façade	1.9	Inclinometer	°	0.036	0.034

The evolution rate predicted for convergence extensometer C1 from the periodic model was disregarded because the identified period varied by more than 45% from the duration of a tropical year. On the other hand, that of convergence extensometer C2 was disregarded because it had a very poor correlation with the data (coefficient of determination of 0.19) indicating that the evolution of the data could clearly not be well represented by the nonlinear periodic model. Despite the greater sophistication of the nonlinear model, it can be seen that the estimated evolution rates between these two methods are in good agreement for certain cases, notably for convergence extensometers C3 and C6, for crackmeter FS5 and for inclinometer INC2.

Before discussing the estimated evolution rates predicted by the methods presented in Sections 2.3 and 3.1, a comparison of how well the linear and ARX models are able to represent the relationship between responses and predictors is presented in Figure 6. It is clear that the ARX models are better suited to represent the environmental variation in almost every case.

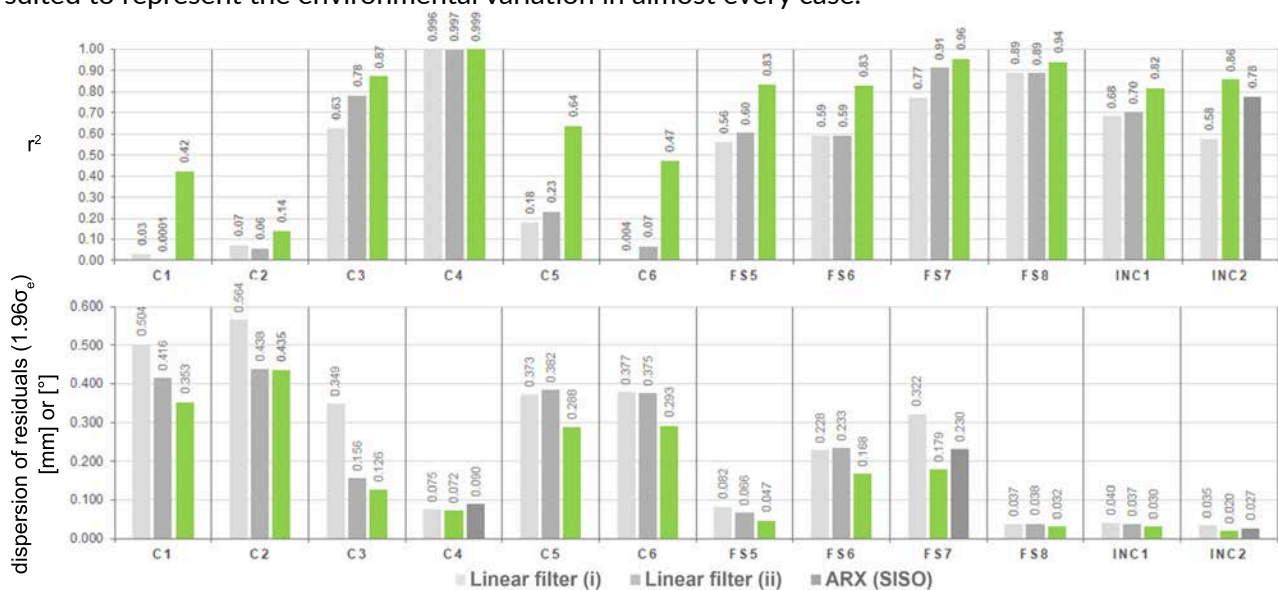


FIGURE 6 Coefficient of determination (r^2) and dispersion of residuals ($1.96\sigma_e$) between simulated and measured responses in Mallorca cathedral.

The evolution rates estimated after filtering the simulated environmental effect using linear and ARX models are presented in Table 5. The estimated condition of each response using the procedure described in Section 3.2 is also shown in the table and illustrated in Figure 7.

TABLE 5 Comparison of estimated evolution rates for monitored structural parameters of Mallorca cathedral from methods filtering out simulated effect of measured environmental parameters.

Sensor	Units	Estimate of annual evolution rate [unit/year]			Estimated condition
		Linear filter (i)	Linear filter (ii)	SISO ARX filter	
C1	mm	0.123	0.163	0.056	Inconclusive
C2	mm	0.055	0.054	0.057	Inconclusive
C3	mm	0.081	0.088	0.077	Evolutionary
C4	mm	0.017	0.016	0.002	Inconclusive
C5	mm	0.007	0.003	0.014	Inconclusive
C6	mm	0.074	0.068	0.068	App. Evolutionary
FS5	mm	0.010	0.009	0.011	App. Evolutionary
FS6	mm	-0.036	-0.036	-0.040	App. Evolutionary
FS7	mm	0.083	0.082	0.050	App. Evolutionary
FS8	mm	0.002	0.002	0.002	Stationary
INC1	°	0.007	0.007	0.007	App. Evolutionary
INC2	°	0.028	0.026	0.031	App. Evolutionary

The results indicate that the convergence extensometer placed across the southern transverse arch of

the 4th bay is clearly experiencing an increasing trend of approximately 0.08 mm/year. The simpler methods considered also predict rates which are in good agreement with this. It can also be observed that the crackmeter placed across a crack in the vault of the central nave in the 7th bay is clearly stationary outside cyclic seasonal variations. Although there is a greater level of uncertainty associated to other estimated trends, the apparent evolutionary trend shown by the inclinometer monitoring the inclination of the front façade (INC2) deserves particular attention because despite being the sensor with the shortest duration of useful data (1.2 years), it shows a significant trend after the effect of temperature has been filtered out and the residuals from the models used for the filtering process have a relatively low scatter. In fact, it very nearly satisfies the condition to be classified as "Evolutionary" according to the procedure described in Section 3.2. Once again, evolution rates predicted by simpler methods are also in good agreement with the final one. The trend exhibited by this sensor corresponds to an outward inclination of the façade.

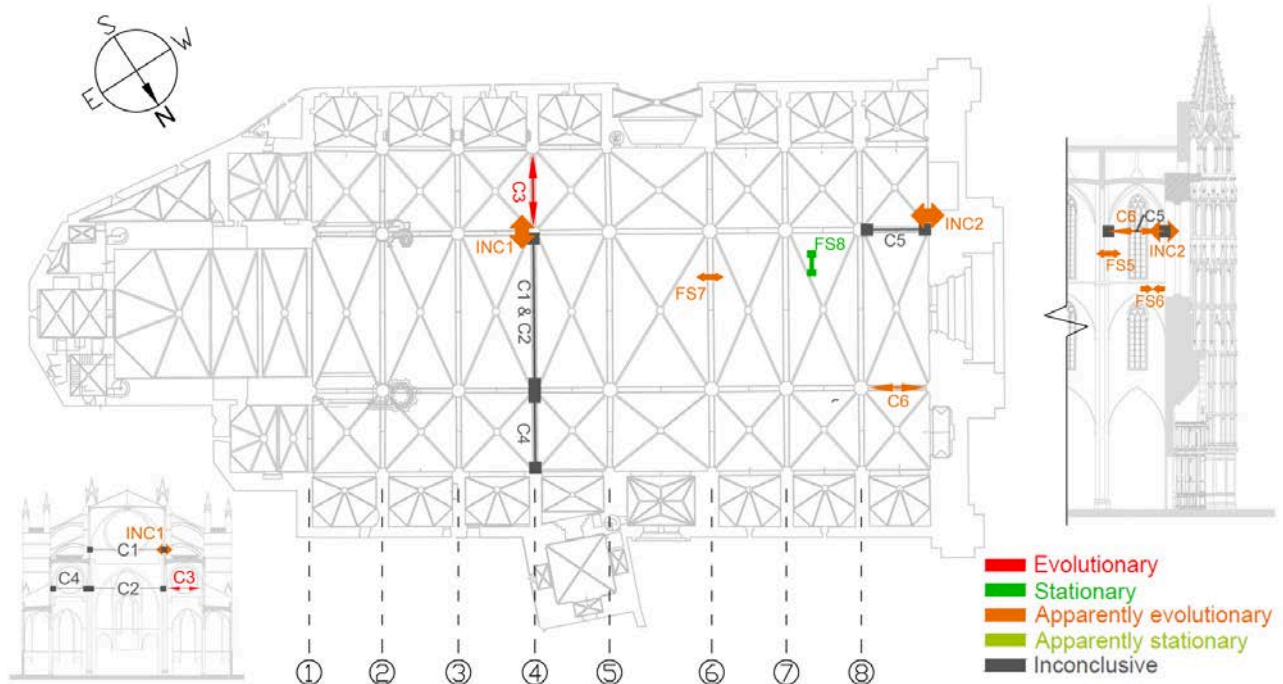


FIGURE 7 Main outcomes from analysis of static SHM data of Mallorca cathedral. (For interpretation of the references to colour in this figure, the reader is referred to the web version of this article)

4.1.2 | Prognosis

The opening trend across the southern transverse arches of Mallorca cathedral has been addressed in a previous study⁶⁵ and can be attributed to a slow ongoing deformation caused by an unbalanced thrust during the construction process. The study, based on a time-dependent finite element analysis able to account for the creep behaviour of masonry, showed that the use of temporary ties during the construction process could clearly contribute to the structure's stability. The model used to represent the creep behaviour of masonry was calibrated based on a deformation rate of 0.1 mm/year between 543 and 548 years after construction (corresponding to the monitoring period) and concluded that under such conditions, this deformation would not have stabilised for a long period of time after construction. However, the research did indicate that if the model was calibrated for lower deformation rates, it could be shown that the phenomena would stabilise in a shorter time period.

The analysis of the monitoring data also reveals that the façade could be experiencing an outward inclination. The structure has already historically faced problems related to the main façade since the previous one was dismantled and reconstructed during the 19th century due to a worrying inclination. In fact, the out-of-plumb of the previous façade is recorded to have increased by 10 cm from the mid-17th century to the beginning of the 19th century. It should also be mentioned that a technical report based on an inspection carried out by the Spanish Institute of Cultural Heritage in 2012⁶⁷ reports the presence of transverse cracks across the vault of the main entrance. Such damage would be consistent with problems related to the detachment of the façade. Moreover, an outward tilting of the façade would

also be consistent with the apparent evolutionary trends derived for the convergence extensometer C6 and the crackmeters FS5 and FS7. However, it must also be said that it is unlikely that the entire façade is tilting outward as a rigid block because the magnitude of the estimated evolution rate is relatively high and hence such a phenomenon would have become clearly visible at a much earlier stage. It is more likely that only the upper part of the façade is experiencing an outward rotation with a rotating centre at a height between sensors FS5 and FS6. This would also explain the apparent underlying closing trend revealed for the crack monitored by FS6. These observations suggest that the façade is still being affected by an active mechanism and that further investigation could definitely shed more light on its true nature.

4.2 | Monastery of Sant Cugat

4.2.1 | SHM system and results

In order to investigate the root cause of several visible structural pathologies, a long-term static SHM system consisting of 14 crackmeters, 2 inclinometers, 3 thermistors and 3 humidity sensors was installed in the church of the monastery, as shown in Figure 9. Most of the sensors have been installed since March 2017 except the two crackmeters placed beneath the rose window (installed in December 2017) and the one placed in the lintel of the main entrance (installed in April 2018). In this case, the crackmeters and inclinometers have minimum resolutions of 0.003 mm and 0.002° respectively. A summary of all the structural sensors of the system is given in Table 6. Although the system is still actively collecting data, the results presented in this paper were based on the data collected up to 22/06/2019. As such, Table 6 also shows the duration of useful data collected by each sensor up to this date.

TABLE 6 Summary of structural sensors used in the SHM system installed in Sant Cugat monastery together with the total duration of useful data collected up to 22/06/2019 and estimated evolution rates from methods based on directly fitting time series to selected models.

Sensor	Location	Years of data	Type	Units	Evolution rate [unit/year]	
					Linear regression	Nonlinear regression
FS-1.1	Fourth aisle	2.3	Crackmeter	mm	0.085	0.078
FS-1.2		2.3	Crackmeter	mm	-0.002	-0.001
INC-1.3	Bell tower	2.3	Inclinometer	°	0.000	-0.002
FS-2.5	Sacristy	2.3	Crackmeter	mm	0.020	0.017
FS-2.6		2.3	Crackmeter	mm	-0.006	-0.004
FS-2.7	Lateral aisle (bell tower)	2.3	Crackmeter	mm	-0.001	0.000
INC-2.8	Central nave	2.3	Inclinometer	°	-0.007	-0.007
FS-2.11		2.3	Crackmeter	mm	0.077	0.029
FS-3.15	Central nave (exterior)	2.3	Crackmeter	mm	-0.028	-
FS-3.13	Lateral aisle (monastery)	2.3	Crackmeter	mm	0.012	-0.023
FS-3.14		2.3	Crackmeter	mm	-0.026	-0.052
FS-3.17	Apse	2.3	Crackmeter	mm	-0.044	-0.055
FS-3.18		2.3	Crackmeter	mm	-0.006	0.006
FS-3.19	Interior front façade	1.5	Crackmeter	mm	0.062	0.112
FS-3.20		1.5	Crackmeter	mm	-0.168	-0.229
FS-3.21	Lintel main entrance	1.2	Crackmeter	mm	0.319	0.339

In this case, the evolution rate estimated by the periodic nonlinear model for FS-3.15 was disregarded due to poor correlation with the measured data (coefficient of determination of 0.52). Once again, the predictions from both methods are in good agreement for certain sensors, notably for INC-2.8.

As for the previous case study, a comparison of the errors between measured responses and those simulated from linear and ARX models during their respective estimation phases was carried out in order to evaluate the ability of each model type to represent the dependency of structural parameters on environmental ones (see Figure 8). In this case, it is possible to see the added benefit of using both interior and exterior temperature as predictors in the ARX models since the MISO models outperform the SISO ones for almost all monitored responses despite the fact that they have lower model orders.

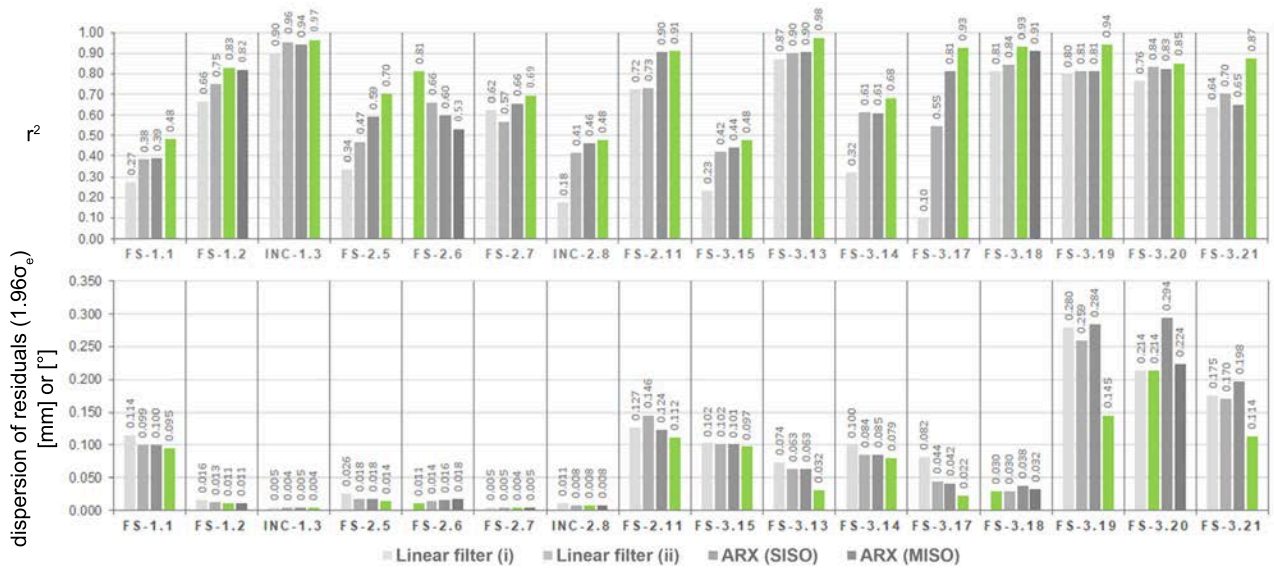


FIGURE 8 Coefficient of determination (r^2) and dispersion of residuals ($1.96\sigma_e$) between simulated and measured responses in Sant Cugat monastery.

Before stating the main conclusions with respect to the diagnosis of the church’s structural condition, the evolution rates estimated using methods described in Sections 2.3 and 3.1 as well as the evolutionary states evaluated from the procedure elaborated in Section 3.2 are summarised in Table 7 and Figure 9.

TABLE 7 Comparison of estimated evolution rates for monitored structural parameters of Sant Cugat monastery from methods filtering out the simulated effect of measured environmental parameters.

Sensor	Units	Estimate of annual evolution rate [unit/year]				Estimated condition
		Linear filter (i)	Linear filter (ii)	SISO ARX filter	MISO ARX filter	
FS-1.1	mm	0.072	0.072	0.073	0.077	App. Evolutionary
FS-1.2	mm	0.003	0.003	0.003	0.003	App. Evolutionary
INC-1.3	°	-0.002	-0.003	-0.002	-0.002	Evolutionary
FS-2.5	mm	0.016	0.016	0.015	0.017	Evolutionary
FS-2.6	mm	-0.001	-0.002	-0.001	0.000	App. Stationary
FS-2.7	mm	0.000	0.000	0.000	0.000	Stationary
INC-2.8	°	-0.008	-0.008	-0.009	-0.010	Evolutionary
FS-2.11	mm	0.045	0.042	0.054	0.040	App. Evolutionary
FS-3.15	mm	-0.037	-0.041	-0.040	-0.038	App. Evolutionary
FS-3.13	mm	-0.023	-0.022	-0.025	-0.025	App. Evolutionary
FS-3.14	mm	-0.038	-0.045	-0.045	-0.047	App. Evolutionary
FS-3.17	mm	-0.048	-0.052	-0.047	-0.063	Inconclusive
FS-3.18	mm	0.004	0.004	-0.002	0.017	App. Evolutionary
FS-3.19	mm	0.033	0.036	0.038	0.099	App. Evolutionary
FS-3.20	mm	-0.188	-0.191	-0.184	-0.156	App. Evolutionary
FS-3.21	mm	0.157	0.148	0.151	0.087	App. Evolutionary

The outcome of the analysis indicates that 3 of the monitored parameters are experiencing significant evolutionary trends outside the cyclic seasonal variations: the inclination of the bell tower (INC-1.3) as well as that of one of the pillars of the cimborio (INC-2.8) on the side of the bell tower towards the south and the opening of the crack in the Sacristy. All methods filtering out the simulated effect of environmental parameters predict very similar rates for these 3 trends. In fact for the inclination of the pillar of the cimborio, which shows the greatest predicted rate out of the two inclinations, methods based solely on fitting the time series to selected models also predict similar rates as those evaluated through the more sophisticated approaches. The same can be said about the crack in the Sacristy. As will be discussed in the next section, it is likely that these trends are being caused by the same phenomenon.

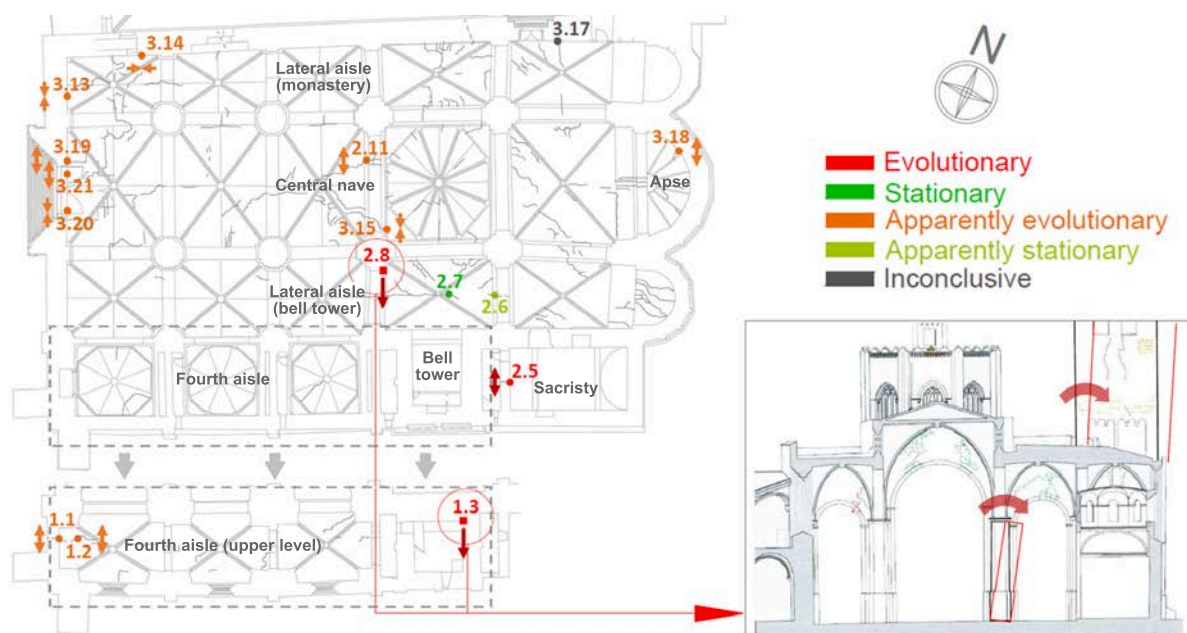


FIGURE 9 Main outcomes from analysis of static SHM data of Sant Cugat monastery. (For interpretation of the references to colour in this figure, the reader is referred to the web version of this article)

The results also reveal that the monitored crack across the vault of the lateral aisle appears to be stationary. It is interesting to note that in both case studies, the monitored parameter showing the most stationary trend corresponds to a crack in a vault. This is most probably due to the flexibility of vaults in comparison to other stiffer structural members and hence their increased ability to deform without suffering significant irreversible damage. It can also be seen that some of the monitored cracks in the lateral aisle on the side of the monastery appear to be experiencing closing trends outside seasonal variations. Since cracks are inherently caused due to the material experiencing tensile stresses, closing trends indicate that the behaviour of the structure has changed since the formation of the crack which initially had to be opening. It is interesting to note that the highest evolutionary rates are predicted for cracks in the interior of the front façade below the rose window. However, the magnitude of the observed trends are comparable to that of the errors associated to the models used to filter out the effect of temperature.

4.2.2 | Prognosis

The first conclusion that can be made from the analysis of the monitoring data so far is related to the effect of the bell tower on the rest of the elements. The measurements of the inclinometer on the wall of the bell tower suggest an outward leaning trend of $0.002^\circ/\text{year}$ outside seasonal variations. The fact that the crack in the western wall of the sacristy appears to be opening at a rate of 0.017 mm/year is consistent with this movement since this wall is intrinsically tied to the bell tower. It also indicates that this outward rotation is most likely starting from a considerably low point (below the point at which the crack is already opening in the sacristy). Moreover, it is likely that the observed outward movement of the pillar supporting the cimborio is linked to this outward movement of the bell tower. All of these observations are consistent with the history of the construction of the structure since most of it was built in the 14th Century while the bell tower was only completed in the 18th Century, when an arch joining the then incomplete bell tower and the cimborio was also dismantled. It appears that the addition of this part of the structure is still having an active effect, even today. The bell tower has a total height of approximately 40m and if this whole part was rotating outwards as a rigid block, the measured inclination would reflect an outward leaning of approximately 1.4cm every 10 years at the top of the tower. In fact, recent topographic and laser scan surveys of the bell tower's geometry reveal that its southern and eastern wall have inclinations of up to 1.5% ⁶⁸ corresponding to a net displacement of 52 cm from the vertical position at the top of the main body of the tower (see Figure 10). This strengthens the findings from the analysis of the monitoring data and suggests that a structural intervention could be required in the future to prevent further deterioration due to this mechanism.

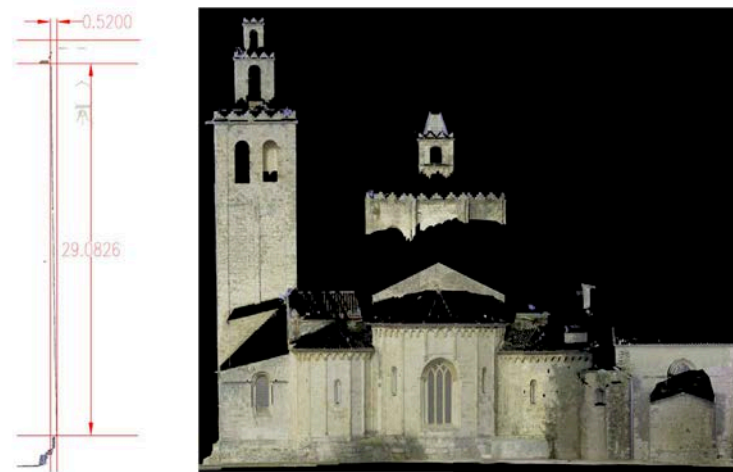


FIGURE 10 Measured inclination of the bell tower of Sant Cugat⁶⁸.

With respect to the apparently evolutionary trends observed for cracks in the lateral aisle on the side of the monastery, these could possibly be caused by complex soil-structure interaction effects. In recent years, a new drainage system around the church has been installed and could help explain some of the closing trends observed for cracks next to the cloister. A longer monitoring period should help to shed more light on the true evolutionary nature and cause of these trends. Finally, the magnitude of the variations experienced by cracks below the rose window indicate that they deserve particular attention. However, since these cracks have been monitored for a shorter period of time and the fact that restoration works were being carried out on this part of the structure during the start of the monitoring period means that an acceptable level of confidence cannot yet be associated to any of the observed trends. Once again, an extended monitoring period is recommended before any suitable conclusions can be made on possible mechanisms affecting this area.

5 | CONCLUSIONS

This research has presented an integrated approach for the data analysis of static SHM of masonry heritage structures. The proposed methodology utilises dynamic linear regression models which can consider multiple predictors to filter out the reversible seasonal variations experienced by most structural parameters of interest. These models are able to attribute components of a current response caused by past ones when estimating the parameters of the model but can then disregard these components when simulating the effect only caused by environmental predictors. This is ideal for the case of static SHM since active structural mechanisms of interest have often begun long before any decision on monitoring could be made and it is thus impossible to define a period of time for which the relationship between structural and environmental parameters are isolated. In fact, the first part of the proposed method could also be used to filter out environmental effects on the evolution of natural frequencies recorded by dynamic monitoring systems. However, it is worth mentioning that in the case of masonry heritage structures, rather than attempting to detect very slow deterioration mechanisms, the dynamic monitoring strategy is most often oriented towards assessing the effectiveness of repairs, identifying significant changes in boundary conditions or towards the early identification of more pronounced damage characterised by a faster evolution rate. The nature of these objectives facilitates the application of several sophisticated analysis procedures because it simplifies the task of defining an adequate training period. As a result, several procedures including machine learning approaches, negative selection and principal component analysis could prove to be more efficient for the analysis of data from dynamic SHM systems.

The static SHM strategy is clearly well suited to identify slow-varying underlying trends in each monitored parameter. However, in most cases, cost and technical limitations only allow a very limited number of parameters to be monitored at specific location points. As a result, it can be very challenging to extract general conclusions on the global structural response. Given this inherent difficulty, one of the main advantages of the proposed methodology over previously applied ones is that it does not only provide estimated evolution rates of the monitored parameters but also evaluates their evolutionary state

and classifies them accordingly. The classification is based on the estimated rates and the errors of the models used to represent the relationship between structural and environmental parameters. This can greatly help to identify areas that should be prioritised during the diagnosis of the structure and to extract meaningful conclusions on the relationship between different monitored parameters. In addition, the entire procedure can be fully automated and once implemented, can provide up to date analysis results as the monitoring period increases. In fact, an extension of the current research would be to assess if the trends of the residuals estimated after the proposed filtering of environmental effects change over longer monitoring periods. If they do, using higher order polynomial models to describe the trend could reveal whether or not a particular evolutionary state is stabilising or not.

The usefulness of the method has clearly been demonstrated through the application to two case studies. In both cases, outcomes of the proposed automatic procedure helped to identify vulnerable areas in important heritage structures. The results also reveal that simpler methods are often able to predict evolution rates rather accurately. This explains why such methods have been used successfully in the past for the accurate diagnosis of structures. However, such methods are not always accurate and provide very little means of assessing the reliability of results, whereas the proposed methodology is more robust and gives clear indications related to the reliability of results.

ACKNOWLEDGEMENTS

This research has received financial support from the City Council of Sant Cugat (Ajuntament de Sant Cugat) through a project aimed at monitoring the church of the Monastery of Sant Cugat (Estudi de monitorització i seguiment de l'estructura de l'Església del Monestir de Sant Cugat, ref. num. C-10764). Additional financial support has also been received from the Spanish Ministry of Education, Culture and Sports through a project aimed at studying the structural condition of Mallorca Cathedral (Estudio, diagnóstico y peritación y en su caso planteamiento de actuaciones sobre el comportamiento constructivo-estructural de la catedral de Santa María, en la ciudad de Palma, isla de Mallorca (Balears), ref. num. 2/131400106ca - 5/030300592 EF). Support from the AGAUR agency of the Generalitat de Catalunya and the European Social Fund, in the form of a predoctoral grant awarded to the corresponding author is also gratefully acknowledged. Finally, the authors gratefully acknowledge the financial support from the Ministry of Science, Innovation and Universities of the Spanish Government, and the European Regional Development Fund through the SEVERUS project (Multilevel evaluation of seismic vulnerability and risk mitigation of masonry buildings in resilient historical urban centres, ref. num. RTI2018-099589-B-I00).

CONFLICT OF INTEREST

The authors declare that they have no conflict of interest.

REFERENCES

1. International Scientific Committee on the Analysis and Restoration of Structures of Architectural Heritage (ISCARSAH). Recommendations for the analysis, conservation and structural restoration of architectural heritage, 2005.
2. Ahmed Elyamani, Oriol Caselles, Pere Roca, and Jaime Clapes. Dynamic investigation of a large historical cathedral. *Structural Control and Health Monitoring*, 24(3):e1885, mar 2017.
3. Fuat Aras and Gulay Altay. Seismic evaluation and structural control of the historical Beylerbeyi Palace. *Structural Control and Health Monitoring*, 22(2):347–364, feb 2015.
4. Elisa Bassoli, Loris Vincenzi, Antonio Maria D'Altri, Stefano de Miranda, Marianna Forghieri, and Giovanni Castellazzi. Ambient vibration-based finite element model updating of an earthquake-damaged masonry tower. *Structural Control and Health Monitoring*, 25(5):e2150, may 2018.
5. Salvador Ivorra, Nicola Ivan Giannoccaro, and Dora Foti. Simple model for predicting the vibration transmission of a squat masonry tower by base forced vibrations. *Structural Control and Health Monitoring*, 26(6):e2360, jun 2019.
6. A. G. El-Attar, A. M. Saleh, and A. H. Zaghw. Conservation of a slender historical Mamluk-style minaret by passive control techniques. *Structural Control and Health Monitoring*, 12(2):157–177, apr 2005.

7. Salvatore Russo and Eleonora Spoldi. Damage assessment of Nepal heritage through ambient vibration analysis and visual inspection. *Structural Control and Health Monitoring*, feb 2020.
8. Filippo Lorenzoni. *Integrated methodologies based on Structural Health Monitoring for the protection of Cultural Heritage buildings*. Phd thesis, University of Trento, 2013.
9. H. Shi, K. Worden, and E. J. Cross. A nonlinear cointegration approach with applications to structural health monitoring. *Journal of Physics: Conference Series*, 744(1), 2016.
10. Alberto Barontini, Maria Giovanna Masciotta, Luís F. Ramos, Paulo Amado Mendes, and Paulo B. Lourenço. Application of a bio-inspired anomaly detection algorithm for unsupervised SHM of a historic masonry church. In *10th International Masonry Conference (10th IMC)*, Milan, Italy, 2018.
11. Nguyen Lu Dang Khoa, Mehrisadat Makki Alamdari, Thierry Rakotoarivelo, Ali Anaissi, and Yang Wang. Structural Health Monitoring Using Machine Learning Techniques and Domain Knowledge Based Features. In *Human and Machine Learning*, pages 409–435. Springer, Cham, 2018.
12. Riccardo Mario Azzara, Guido De Roeck, Maria Girardi, Cristina Padovani, Daniele Pellegrini, and Edwin Reynders. The influence of environmental parameters on the dynamic behaviour of the San Frediano bell tower in Lucca. *Engineering Structures*, 156(March 2017):175–187, feb 2018.
13. Alessandro Cabboi, Carmelo Gentile, and Antonella Saisi. From continuous vibration monitoring to FEM-based damage assessment: Application on a stone-masonry tower. *Construction and Building Materials*, 156:252–265, dec 2017.
14. A. Deraemaeker and K. Worden. A comparison of linear approaches to filter out environmental effects in structural health monitoring. *Mechanical Systems and Signal Processing*, 105:1–15, may 2018.
15. F.J. Baeza, Salvador Ivorra, D. Bru, and F.B. Varona. Structural Health Monitoring Systems for Smart Heritage and Infrastructures in Spain. In Erika Ottaviano, Assunta Pelliccio, and Vincenzo Gattulli, editors, *Mechatronics for Cultural Heritage and Civil Engineering*, volume 92 of *Intelligent Systems, Control and Automation: Science and Engineering*, pages 271–294. Springer International Publishing, 2018.
16. Bram Cornelis and Bart Peeters. Online Bayesian spike removal algorithms for structural health monitoring of vehicle components. In *Eurodyn 2014: Proceedings of the 9th International Conference on Structural Dynamics*, pages 2295–2301, Porto, jul 2014.
17. Andrew Halfpenny. Data Preprocessing for Damage Detection. In *Encyclopedia of Structural Health Monitoring*. John Wiley & Sons, Ltd, Chichester, UK, jan 2008.
18. Simonetta Baraccani, Michele Palermo, Riccardo M. Azzara, Giada Gasparini, Stefano Silvestri, and Tomaso Trombetti. Structural Interpretation of Data from Static and Dynamic Structural Health Monitoring of Monumental Buildings. *Key Engineering Materials*, 747:431–439, jul 2017.
19. Keith Worden, Charles R. Farrar, Graeme Manson, and Gyuhae Park. The fundamental axioms of structural health monitoring. *Proceedings of the Royal Society A: Mathematical, Physical and Engineering Sciences*, 463(2082):1639–1664, 2007.
20. Hoon Sohn. Effects of environmental and operational variability on structural health monitoring. *Philosophical Transactions of the Royal Society A: Mathematical, Physical and Engineering Sciences*, 365(1851):539–560, feb 2007.
21. Gianni Bartoli, Andrea Chiarugi, and Vittorio Gusella. Monitoring Systems on Historic Buildings: The Brunelleschi Dome. *Journal of Structural Engineering*, 122(6):663–673, jun 1996.
22. Federica Ottoni and Carlo Blasi. Results of a 60-Year Monitoring System for Santa Maria del Fiore Dome in Florence. *International Journal of Architectural Heritage*, 9(1):7–24, jan 2015.
23. Pier Paolo Rossi and Christian Rossi. Monitoring of Two Great Venetian Cathedrals: San Marco and Santa Maria Gloriosa Dei Frari. *International Journal of Architectural Heritage*, 9(1):58–81, jan 2015.
24. Abraham R. Sánchez, Roberto Meli, and Marcos M. Chávez. Structural Monitoring of the Mexico City Cathedral (1990-2014). *International Journal of Architectural Heritage*, 10(2-3):15583058.2015.1113332, dec 2015.
25. Simonetta Baraccani, Stefano Silvestri, Giada Gasparini, Michele Palermo, Tomaso Trombetti, Elena Silvestri, Renato Lancellotta, and Alessandro Capra. A Structural Analysis of the Modena Cathedral. *International Journal of Architectural Heritage*, 10(2-3):15583058.2015.1113344, dec 2015.

26. Rosario Ceravolo, Annunziata De Marinis, Marica L. Pecorelli, and Luca Zanotti Fragonara. Monitoring of masonry historical constructions: 10 years of static monitoring of the world's largest oval dome. *Structural Control and Health Monitoring*, 24(10):e1988, oct 2017.
27. Maria-Giovanna Masciotta, João C.A. Roque, Luís F. Ramos, and Paulo B. Lourenço. A multidisciplinary approach to assess the health state of heritage structures: The case study of the Church of Monastery of Jerónimos in Lisbon. *Construction and Building Materials*, 116:169–187, jul 2016.
28. Filippo Lorenzoni, Filippo Casarin, Claudio Modena, Mauro Caldon, Kleidi Islami, and Francesca da Porto. Structural health monitoring of the Roman Arena of Verona, Italy. *Journal of Civil Structural Health Monitoring*, 3(4):227–246, dec 2013.
29. Haydee Blanco, Yosbel Boffill, Ignacio Lombillo, and Luis Villegas. An integrated structural health monitoring system for determining local/global responses of historic masonry buildings. *Structural Control and Health Monitoring*, 25(8):e2196, aug 2018.
30. F. Lucchin G. Gaudini, C. Modena, F. Casarin, C. Bettio. Monitoring and strengthening interventions on the stone tomb of Cansignorio della Scala, Verona, Italy. In *Proceedings of the VI International Conference on Structural Analysis of Historic Construction, SAHC08*, pages 423–432. CRC Press, jun 2008.
31. Salvatore Russo. On the monitoring of historic Anime Sante church damaged by earthquake in L'Aquila. *Structural Control and Health Monitoring*, 20(9):1226–1239, sep 2013.
32. A. J. Lawrance. Directionality and Reversibility in Time Series. *International Statistical Review / Revue Internationale de Statistique*, 59(1):67, apr 1991.
33. Simonetta Baraccani, Tomaso Trombetti, Michele Palermo, Giada Gasparini, Stefano Silvestri, and Antoine Dib. A Methodology of Analysis for a Critique Interpretation of the Data Acquired from Monitoring Systems of Historical Buildings. In *7th European Workshop on Structural Health Monitoring*, 2014.
34. Mahayaudin M. Mansor, Max E. Glonek, David A. Green, and Andrew V. Metcalfe. Threshold Autoregressive Models for Directional Time Series. In *Time Series Analysis and Forecasting. Contributions to Statistics.*, pages 13–25. Springer, Cham, 2016.
35. Elizabeth J. Cross, Keith Worden, and Qian Chen. Cointegration: a novel approach for the removal of environmental trends in structural health monitoring data. *Proceedings of the Royal Society A: Mathematical, Physical and Engineering Sciences*, 467(2133):2712–2732, sep 2011.
36. Edwin Reynders, Gersom Wursten, and Guido de Roeck. Output-only structural health monitoring in changing environmental conditions by means of nonlinear system identification. *Structural Health Monitoring*, 13(1):82–93, 2014.
37. Bart Peeters and Guido De Roeck. One-year monitoring of the Z24-Bridge: environmental effects versus damage events. *Earthquake Engineering & Structural Dynamics*, 30(2):149–171, feb 2001.
38. L.F. Ramos, L. Marques, P.B. Lourenço, G. De Roeck, A. Campos-Costa, and J. Roque. Monitoring historical masonry structures with operational modal analysis: Two case studies. *Mechanical Systems and Signal Processing*, 24(5):1291–1305, jul 2010.
39. Alban Kita, Nicola Cavalagli, and Filippo Ubertini. Temperature effects on static and dynamic behavior of Consoli Palace in Gubbio, Italy. *Mechanical Systems and Signal Processing*, 120:180–202, apr 2019.
40. Filippo Lorenzoni, Filippo Casarin, Mauro Caldon, Kleidi Islami, and Claudio Modena. Uncertainty quantification in structural health monitoring: Applications on cultural heritage buildings. *Mechanical Systems and Signal Processing*, 66-67:268–281, jan 2016.
41. Bart Peeters. *System Identification and Damage Detection in Civil Engineering*. Phd thesis, KU Leuven, 2000.
42. Maria-Giovanna Masciotta, Luis F. Ramos, Paulo B. Lourenço, and José A. C. Matos. Development of Key Performance Indicators for the Structural Assessment of Heritage Buildings. In *8th European Workshop on Structural Health Monitoring (EWSHM 2016), 5-8 July 2016, Bilbao, Spain*, pages 5–8, jul 2016.
43. Jorge J. Moré. The Levenberg-Marquardt algorithm: Implementation and theory. In G. A. Watson, editor, *Numerical Analysis*, pages 105–116. Springer, Berlin, Heidelberg, 1978.
44. J Meeus and D Savoie. The history of the tropical year. *Journal of the British Astronomical Association*, 102:40–42, 1992.
45. Ingrid Daubechies. *Ten Lectures on Wavelets*. Society for Industrial and Applied Mathematics, jan 1992.

46. David L. Donoho and Iain M. Johnstone. Ideal Spatial Adaptation by Wavelet Shrinkage. *Biometrika*, 81(3):425, aug 1994.
47. A. G. Asuero, A. Sayago, and A. G. González. The Correlation Coefficient: An Overview. *Critical Reviews in Analytical Chemistry*, 36(1):41–59, jan 2006.
48. Åke Björck. Solving linear least squares problems by Gram-Schmidt orthogonalization. *BIT*, 7(1):1–21, mar 1967.
49. Amde M Amde, J V Martin, and James Colville. The Effects of Moisture on Compressive Strength and Modulus of Brick Masonry. In *13th International Brick and Block Masonry Conference*, Amsterdam, 2007.
50. Navaratnarajah Sathiparan and Udayakumar Rumeskumar. Effect of moisture condition on mechanical behavior of low strength brick masonry. *Journal of Building Engineering*, 17(February):23–31, may 2018.
51. Jiri Witzany, Tomas Cejka, and Radek Zigler. The Effect of Moisture on Significant Mechanical Characteristics of Masonry. *Engineering Structures and Technologies*, 2(3):79–85, sep 2010.
52. Antonia Moropoulou, Maria Karoglou, Ioannis Agapakis, Charalampos Mouzakis, Simos Asimakopoulos, George Pantazis, and Evangelia Lambrou. Structural health monitoring of the Holy Aedicule in Jerusalem. *Structural Control and Health Monitoring*, 26(9), sep 2019.
53. Luís F Ramos. *Damage identification on masonry structures based on vibration signatures*. Phd thesis, Universidade do Minho, 2007.
54. Daniele Ferretti and Zdeněk P. Bažant. Stability of ancient masonry towers: Moisture diffusion, carbonation and size effect. *Cement and Concrete Research*, 36(7):1379–1388, jul 2006.
55. D. G. Toll, Z. Abedin, J. Buma, Y. Cui, A. S. Osman, and K.K. Phoon. The impact of changes in the water table and soil moisture on structural stability of buildings and foundation systems : systematic review CEE10-005 (SR90). Technical report, Collaboration for Environmental Evidence, 2012.
56. M.J. DeJong. Settlement effects on masonry structures. In *Structural Analysis of Historical Constructions: Anamnesis, diagnosis, therapy, controls - Proceedings of the 10th International Conference on Structural Analysis of Historical Constructions, SAHC 2016*, pages 449–456, 2016.
57. Carl. De Boor. *A Practical Guide to Splines*. Springer-Verlag New York, 1978.
58. F. N. Fritsch and R. E. Carlson. Monotone Piecewise Cubic Interpolation. *SIAM Journal on Numerical Analysis*, 17(2):238–246, apr 1980.
59. Hugues Garnier and Liuping Wang. *Identification of Continuous-time Models from Sampled Data*. Advances in Industrial Control. Springer London, London, 2008.
60. Roberto Diversi, Roberto Guidorzi, and Umberto Soverini. Identification of ARX and ARARX Models in the Presence of Input and Output Noises. *European Journal of Control*, 16(3):242–255, jan 2010.
61. Stijn Verbeke and Amaryllis Audenaert. Thermal inertia in buildings: A review of impacts across climate and building use. *Renewable and Sustainable Energy Reviews*, 82(September 2017):2300–2318, feb 2018.
62. Koray Ulgen. Experimental and theoretical investigation of effects of wall's thermophysical properties on time lag and decrement factor. *Energy and Buildings*, 34(3):273–278, mar 2002.
63. Gary Smith. Simple Regression. In *Essential Statistics, Regression, and Econometrics*, pages 219–258. Elsevier, 2012.
64. Hubert W. Lilliefors. On the Kolmogorov-Smirnov Test for Normality with Mean and Variance Unknown. *Journal of the American Statistical Association*, 62(318):399, jun 1967.
65. Luca Pelà, Julien Bourgeois, Pere Roca, Miguel Cervera, and Michele Chiumenti. Analysis of the Effect of Provisional Ties on the Construction and Current Deformation of Mallorca Cathedral. *International Journal of Architectural Heritage*, 10(4):418–437, may 2016.
66. Pere Roca, Miguel Cervera, Luca Pelà, Roberto Clemente, and Michele Chiumenti. Continuum FE models for the analysis of Mallorca Cathedral. *Engineering Structures*, 46:653–670, jan 2013.
67. IPCE: Instituto del Patrimonio Cultural de España (Spanish Institute of Cultural Heritage). Inspección técnica portadas de la Catedral de Palma de Mallorca (Technical inspection of the portal of Palma de Mallorca cathedral). Technical report, aug 2012.
68. Ajuntament de Sant Cugat (Sant Cugat City Council). Informe tècnic: Comprovació de la verticalitat de la torre del campanar del monestir (Measurement of the inclination of the bell tower of the monastery). Technical report, 2019.